EMERGING INFECTIOUS DISEASES®

CDC
Centers for Disease Control and Prevention

PARASITIC INFECTIONS

June 2022

William C. Campbell (1930–), *Tapeworm Enigma*, 2020. Acrylic with supplemental gel on canvas, 14 in x 18in/35.6 cm x 45.7 cm. Personal Collection, Tom and Bev Kennedy, Waunakee, Wisconsin, USA. Digital image by Tim Fitch Photography.

EMERGING INFECTIOUS DISEASES®

Emerging Infectious Diseases is published monthly by the Centers for Disease Control and Prevention, 1600 Clifton Rd NE, Mailstop H16-2, Atlanta, GA 30329-4027, USA. Telephone 404-639-1960; email, eideditor@cdc.gov

EMERGING INFECTIOUS DISEASES®

Parasitic Infections **June 2022**

On the Cover

William C. Campbell (1930–), *Tapeworm Enigma*, 2020. Acrylic with supplemental gel on canvas, 14 in x 18in/35.6 cm x 45.7 cm. Personal Collection, Tom and Bev Kennedy, Waunakee, Wisconsin, USA. Digital image by Tim Fitch Photography.

Synopses

Research

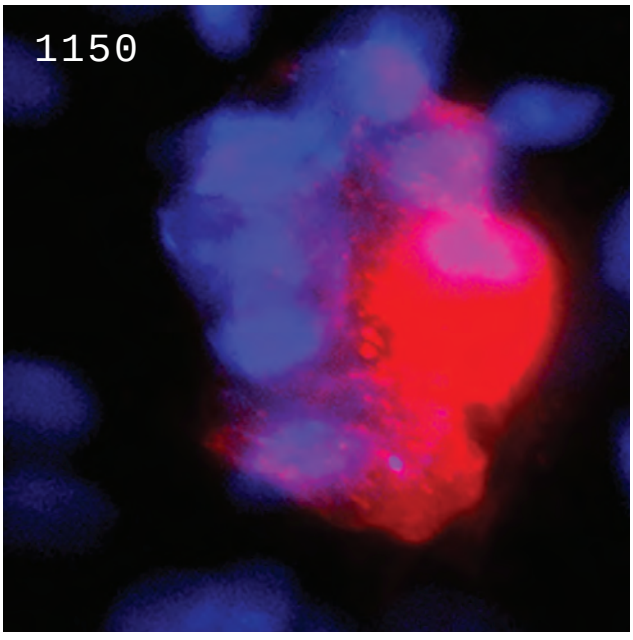

EMERGING INFECTIOUS DISEASES®
June 2022

Dispatches

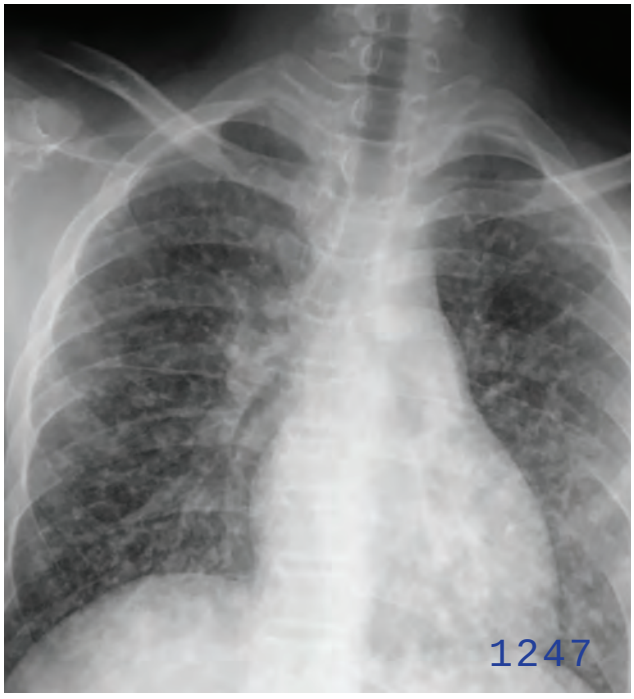

EMERGING INFECTIOUS DISEASES®
June 2022

Comment Letter

Books and Media

About the Cover

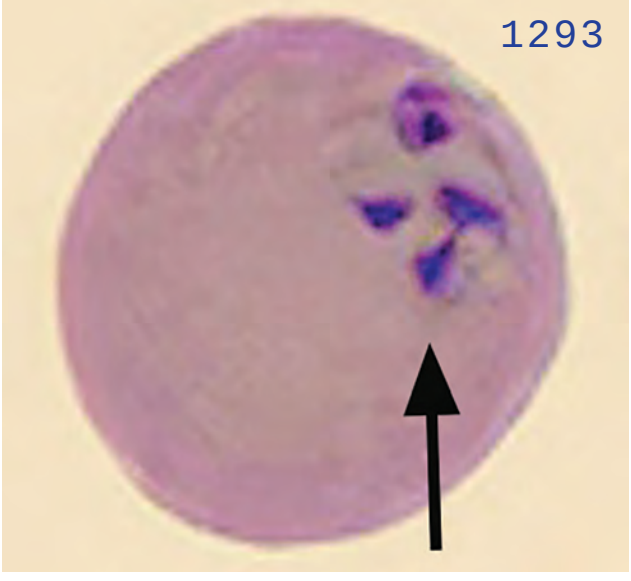

Research Letters

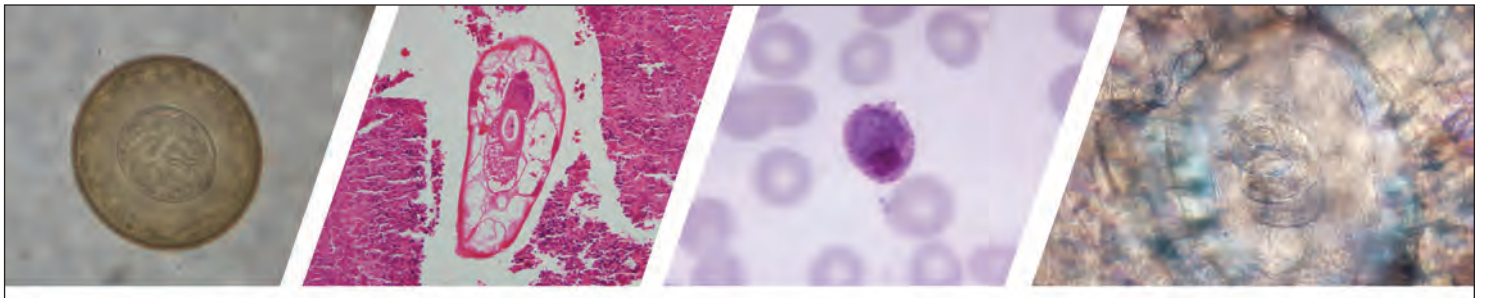

DPDx

Diagnostic Assistance and Training in Laboratory Identification of Parasites

A free service of CDC available to laboratorians, pathologists, and other health professionals in the United States and abroad

- Diagnosis from photographs of worms, histological sections, fecal, blood, and other specimen types
- Expert diagnostic review
- Formal diagnostic laboratory report
- Submission of samples via secure file share

Visit the DPDx website for information on laboratory diagnosis, geographic distribution, clinical features, parasite life cycles, and training via Monthly Case Studies of parasitic diseases.

www.cdc.gov/dpdx
dpdx@cdc.gov

U.S. Department of Health and Human Services
Centers for Disease Control and Prevention

CS272346-DE

Cross-Sectional Study of Clinical Predictors of Coccidioidomycosis, Arizona, USA

Ferris A. Ramadan, Katherine D. Ellingson, Robert A. Canales, Edward J. Bedrick, John N. Galgiani, Fariba M. Donovan

Medscape ACTIVITY EDUCATION

In support of improving patient care, this activity has been planned and implemented by Medscape, LLC and Emerging Infectious Diseases. Medscape, LLC is jointly accredited by the Accreditation Council for Continuing Medical Education (ACCME), the Accreditation Council for Pharmacy Education (ACPE), and the American Nurses Credentialing Center (ANCC), to provide continuing education for the healthcare team.

Medscape, LLC designates this Journal-based CME activity for a maximum of 1.00 ***AMA PRA Category 1 Credit(s)™***. Physicians should claim only the credit commensurate with the extent of their participation in the activity.

Successful completion of this CME activity, which includes participation in the evaluation component, enables the participant to earn up to 1.0 MOC points in the American Board of Internal Medicine's (ABIM) Maintenance of Certification (MOC) program. Participants will earn MOC points equivalent to the amount of CME credits claimed for the activity. It is the CME activity provider's responsibility to submit participant completion information to ACCME for the purpose of granting ABIM MOC credit.

All other clinicians completing this activity will be issued a certificate of participation. To participate in this journal CME activity: (1) review the learning objectives and author disclosures; (2) study the education content; (3) take the post-test with a 75% minimum passing score and complete the evaluation at http://www.medscape.org/journal/eid; and (4) view/print certificate. For CME questions, see page 1310.

Release date: May 16, 2022; Expiration date: May 16, 2023

Learning Objectives

Upon completion of this activity, participants will be able to:

- Describe clinical predictors of coccidiomycosis (CM) in outpatient and inpatient settings, according to an analysis of ≈400 participants with suspected CM prospectively enrolled in 2019
- Determine prediction models for CM for outpatient and inpatient settings, according to an analysis of ≈400 participants with suspected CM prospectively enrolled in 2019
- Identify clinical and public health implications of clinical predictors of CM and prediction models for CM for outpatient and inpatient settings, according to an analysis of 402 participants with suspected CM prospectively enrolled in 2019

CME Editor

Amy J. Guinn, BA, MA, Technical Writer/Editor, Emerging Infectious Diseases. *Disclosure: Amy J. Guinn, BA, MA, has disclosed no relevant financial relationships.*

CME Author

Laurie Barclay, MD, freelance writer and reviewer, Medscape, LLC. *Disclosure: Laurie Barclay, MD, has disclosed the following relevant financial relationships: stocks, stock options, or bonds from AbbVie Inc. (former).*

Authors

Ferris A. Ramadan, MS; Katherine D. Ellingson, PhD; Robert A. Canales, PhD; Edward J. Bedrick, PhD; John N. Galgiani, MD; and ***Fariba M. Donovan, MD/PhD.***

Author affiliations: University of Arizona, Tucson, Arizona, USA (F.A. Ramadan, K.D. Ellingson, E.J. Bedrick); George Washington University, Washington, DC, USA (R.A. Canales); University of Arizona College of Medicine–Tucson, Tucson (J.N. Galgiani, F.M. Donovan)

DOI: https://doi.org/10.3201/eid2806.212311

Demographic and clinical indicators have been described to support identification of coccidioidomycosis; however, the interplay of these conditions has not been explored in a clinical setting. In 2019, we enrolled 392 participants in a cross-sectional study for suspected coccidioidomycosis in emergency departments and inpatient units in *Coccidioides*-endemic regions. We aimed to develop a predictive model among participants with suspected coccidioidomycosis. We applied a least absolute shrinkage and selection operator to specific coccidioidomycosis predictors and developed univariable and multivariable logistic regression models. Univariable models identified elevated eosinophil count as a statistically significant predictive feature of coccidioidomycosis in both inpatient and outpatient settings. Our multivariable outpatient model also identified rash (adjusted odds ratio 9.74 [95% CI 1.03–92.24]; p = 0.047) as a predictor. Our results suggest preliminary support for developing a coccidioidomycosis prediction model for use in clinical settings.

Coccidioidomycosis, colloquially known as cocci or Valley fever, is a fungal infection endemic to the southwestern United States and parts of Central and South America (*1*). Infection occurs through inhalation of an arthroconidium from the dimorphic, soil-dwelling fungi *Coccidioides immitis* and *C. posadasii*. Incidence has increased since 1995, when coccidioidomycosis became a reportable infection (*2*). During 2016–2018, the Centers for Disease Control and Prevention reported a 32% increase in coccidioidomycosis cases (*3*). Epidemiologic studies suggest climate change, more frequent soilborne dust exposures, and a growing population of older adults in endemic regions as possible causes for increased coccidioidomycosis rates (*4*). Despite enhanced surveillance efforts, coccidioidomycosis incidence is underreported (*4*,*5*), and estimates suggest ≥150,000 infections annually in the United States (*6*).

Because of limited ability to prevent *Coccidioides* exposure in the community and no existing vaccine, coccidioidomycosis poses a substantial burden to patients and healthcare systems in endemic areas (*7*,*8*). Most (60%) *Coccidioides* infections are subclinical, but clinical cases produce protracted respiratory conditions (*9*,*10*). Observational studies indicate that 15%–29% of community-acquired pneumonia in endemic areas is caused by coccidioidomycosis (*11*,*12*). Diverse and nonspecific manifestations including fatigue, cough, fever, and rash make diagnosis challenging, and coccidioidomycosis can easily be mistaken for other respiratory illnesses, eczema, or bacterial pneumonia. Thus, misdiagnosis and inappropriate treatments are common, and ≤81% of patients are prescribed an antibacterial drug (*5*,*12*). However, few studies have investigated factors associated with increased coccidioidomycosis incidence to support clinical decision-making (*13*).

Increased incidence and complex clinical manifestations of coccidioidomycosis emphasize the need to improve disease identification in clinical settings. In 2019, we prospectively enrolled participants with suspected coccidioidomycosis to evaluate a novel diagnostic test (*14*). For this study, we used data from our prior study to develop a coccidioidomycosis prediction model based on demographic, clinical, and laboratory factors. We developed independent models for outpatient and inpatient settings.

Methods

Design

During January–December 2019, we collected data from a prospective study that enrolled participants at 2 academic medical centers in southern Arizona, Banner-University Medical Center Tucson, and Banner-University Medical Center Phoenix, and their affiliated outpatient clinics. During that study, we enrolled 402 participants with suspected coccidioidomycosis, which was defined by clinician orders for coccidioidomycosis serologic testing (*14*). Our protocol was consistent with public health recommendations to test for coccidioidomycosis among patients with pneumonia-like symptoms in endemic areas. Patients with alternative clinical manifestations, such as fibrocavitary or disseminated disease, were also evaluated for coccidioidomycosis. Research coordinators were alerted to potential participants via electronic medical record (Cerner, https://www.cerner.com), when clinicians ordered a coccidioidomycosis screening test, or directly by outpatient clinicians (*15*). We excluded persons <18 years of age or with a history of coccidioidomycosis. Consenting participants completed a medical questionnaire and provided an additional blood sample (*14*). The University of Arizona Institutional Review Board provided research approval to enroll participants (project no. 1811085933A011).

Variables

Coccidioidomycosis was our primary outcome of interest, which we defined as confirmatory evidence via positive *Coccidioides* serologic testing, such as ELISA, immunodiffusion, compliment fixation titers >1:2, or a positive culture. We coded indeterminate ELISA and immunodiffusion results as negative. Demographic data collected included age, sex, race, ethnicity, and length of residence in an endemic area. Participants or their designated proxies reported

previous symptoms and length of illness via survey. Laboratory measurements were leukocyte count and differential, hemoglobin, platelet count, serum albumin, and total serum protein. Participants provided an additional blood sample that was used to measure C-reactive protein (CRP), erythrocyte sedimentation rate (ESR), and procalcitonin (PCT) levels. A team of physicians conducted a review of each participant's chart to compile any history of immunocompromised status, such as type 2 diabetes, HIV/AIDS, or immunosuppressive therapies. We identified coccidioidomycosis clinical manifestations by using diagnostic notes and radiographic results.

Analysis

We stratified our analyses by inpatient versus outpatient admission status because of systematic differences in the complexity of clinical presentation and availability of electronic medical record data. We classified race as a binary White or non-White variable because of the low representation of minority racial groups. Continuous variables displayed nonnormal distributions. We used the nonparametric Mann-Whitney U test to evaluate the distribution of continuous variables across groups and Fisher exact test to evaluate categorical variables across groups.

Before model development, we evaluated potential predictor variables for multicollinearity by using variance inflation factors and correlation. We applied a correlation threshold of $r>0.7$ and identified eosinophil percentage as a colinear feature. We omitted eosinophil percentage from our analysis because we considered it to be less clinically relevant in contrast to eosinophil count (Appendix Figures 1, 2, https://wwnc.cdc.gov/EID/article/28/6/21-2311-App1.pdf). All numeric variables exhibited nonnormal distributions and were log transformed. We included clinical features, participant symptoms, and age as binary variables within models, and incorporated length of residence, duration of illness, and laboratory markers as continuous measures. To reduce the loss of sample size, we imputed missing data by Gibbs sampling (*16*,*17*). We evaluated imputed data stability by replicating variable selection methods for 5 distinct completed datasets. In brief, we imputed numeric variables by using predictive mean matching, we imputed binary variables with logistic regression, and we imputed multiclass variables by using Bayesian polytomous regression. An average of 12 (3.1%) observations were missing from each variable; however, ≤63 (16.1%) observations were missing for any single feature. Data with the highest number of missing observations were eosinophil count (16.1%), albumin (13.6%), and total protein (13.6%) (Appendix Table 1). We used imputation methods to retain a sufficient sample size for feature selection; listwise deletion resulted in a loss of 156 (40%) observations.

Variable Selection and Evaluation

First, we developed univariable logistic regression models, reporting all parameter estimates in terms of odds ratios (ORs) on imputed data. We constructed multivariable models by using the semi-automated least absolute shrinkage and selection operator (LASSO) method on imputed data (*18*). In brief, LASSO is a selection technique that uses penalization to shrink

Table 1. Patient characteristics by confirmed *Coccidioides* diagnosis in a cross-sectional study of clinical predictors of coccidioidomycosis, Arizona, USA*

Characteristics	Positive, n = 73	Negative, n = 319	Total, n = 392	p value
Median age, y (range)	55 (18–83)	57 (18–98)	57 (18–98)	**0.038**
Sex, no. (%)				0.514
F	38 (52.8)	152 (47.9)	190 (48.8)	
M	34 (47.2)	165 (52.1)	199 (51.2)	
Race, no. (%)				**0.024**
African American	8 (11.4)	18 (5.8)	26 (6.8)	
American Indian/Alaska Native	6 (8.6)	11 (3.5)	17 (4.5)	
Asian	3 (4.3)	4 (1.3)	7 (1.8)	
White	52 (74.3)	263 (84.8)	315 (82.9)	
Unknown	1 (1.4)	14 (4.5)	15 (3.9)	
Ethnicity, no. (%)				0.882
Hispanic	18 (26.5)	87 (28.1)	105 (27.8)	
Non-Hispanic	50 (73.5)	223 (71.9)	273 (72.2)	
Median length of endemic residence, y (range)	13 (0–78)	21 (0–98)	20 (0–98)	**0.017**
Admission status, no. (%)				
Outpatient	31 (42.5)	49 (15.4)	80 (20.5)	**<0.001**
Inpatient	42 (57.5)	269 (84.6)	311 (79.5)	
Immunocompromised, no. (%)				**0.001**
Y	24 (33.3)	174 (55.1)	198 (51)	
N	48 (66.7)	142 (44.9)	190 (49)	

*Bold text indicates statistical significance.

small regression coefficients to zero. Penalization (lambda) parameters can be selected by using a minimum cross-validated mean squared error (CVMSE) or the CVMSE ≤1 SD of the minimum. We used the mean of these 2 lambda values to penalize our models. We retained variables with nonzero coefficients in each model. We selected LASSO because of its ability to select influential features in a high-dimensional dataset (i.e., a high number of variables relative to the dataset). Other regression methods often suffer degeneracies when the number of predictors exceeds or is close to the number of observations (*19*).

We performed leave-one-out cross-validation to calculate predictive performance of multivariable models and obtain corrected estimates of sensitivity, specificity, and predictive values. This internal validation method provides an out-of-sample performance estimate of each model. We used receiver operating characteristic (ROC) area under the curve (AUC) to evaluate predictive performance of our models. ROC AUC uses a combination of sensitivity and specificity to assess predictive performance. An ROC AUC of 1.0 corresponds to perfect discrimination, whereas 0.50 indicates no predictive ability. We performed sensitivity analyses by using standardized laboratory reference ranges (*20*–*22*) and among participants with and without identifiable immunocompromised conditions. We developed supplemental models to identify alternative laboratory thresholds predictive of coccidioidomycosis. We used R version 3.6.3 (*23*) to conduct analyses and performed multiple imputation by using the mice package (*17*). We conducted LASSO by using the glmnet package in R (*24*). We considered p<0.05 statistically significant with no correction for multiple testing. We report this study according to STrengthening the Reporting of OBservational studies in Epidemiology (STROBE) guidelines (https://www.strobe-statement.org) (Appendix Tables 1–9).

Results

Median participant age was 57 years; 48.8% of participants were female and 51.2% male (Table 1). Participants self-reported as White (82.9%), African American (6.8%), American Indian/Alaskan Native (4.5%), and Asian (1.8%). Only 18.6% of participants tested positive for coccidioidomycosis. The median age for coccidioidomycosis-positive participants was 55 years, and median age for coccidioidomycosis-negative participants was moderately older at 57 years (p = 0.04). Coccidioidomycosis-positive participants had a shorter median length of residence, 13 years, than the 21 years for coccidioidomycosis-negative participants (p = 0.02). A higher proportion of non-White participants had a coccidioidomycosis-positive diagnosis (p = 0.02), but we did not identify statistically significant variations by sex (p = 0.51) or ethnicity (p = 0.88). Coccidioidomycosis-positive participants had significantly lower rates of immunocompromised conditions (33.3%) than did coccidioidomycosis-negative participants (55.1%) (p = 0.001). Positive participants had lower rates for symptoms including fatigue (p = 0.03) and shortness of breath (p = 0.02) than did negative participants, but positive participants had higher rates of rash (36.9%) than did negative participants (12.9%; p<0.001) (Appendix Table 2). Laboratory markers including PCT, CRP, and ESR were significantly lower in coccidioidomycosis-positive than -negative participants (p<0.001). Inversely, hemoglobin (p = 0.008), platelet count (p = 0.01), eosinophil count (p<0.001), and total protein (p = 0.04) levels were higher among coccidioidomycosis-positive participants (Appendix Table 2).

Our initial sample consisted of 392 participants with suspected coccidioidomycosis (Figure). Participants were stratified into outpatient (n = 99) and inpatient groups (n = 293). The outpatient group consisted

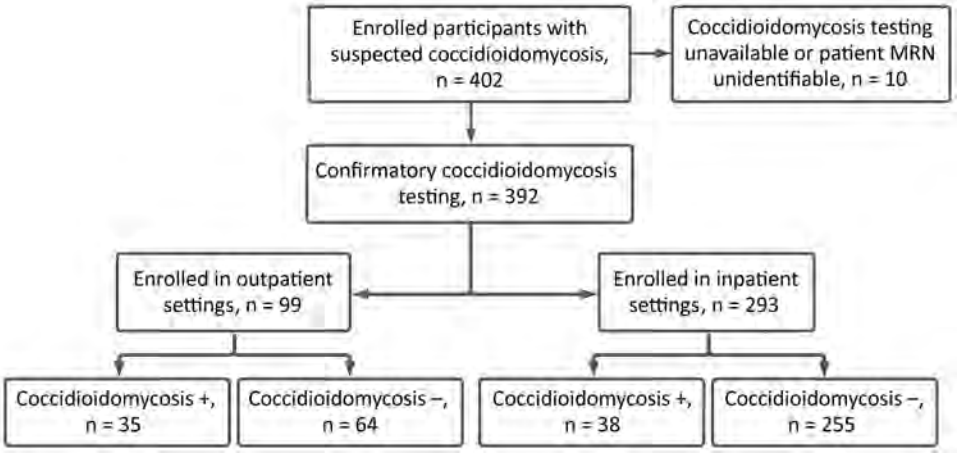

Figure. Stratification diagram for suspected coccidioidomycosis among inpatients and outpatients in a cross-sectional study of clinical predictors of coccidioidomycosis, Arizona, USA. Outpatient participants were recruited from emergency departments and affiliated clinics. Inpatient participants were recruited from among hospitalized patients. MRN, medical record number; +, positive; –, negative.

of 35 coccidioidomycosis-positive participants and 64 coccidioidomycosis-negative participants; our inpatient group consisted of 38 coccidioidomycosis-positive participants and 255 coccidioidomycosis-negative participants (Table 2). The median age for outpatients was 57 years for coccidioidomycosis-positive and 51 years for coccidioidomycosis-negative participants, but we noted no statistical difference in age (p = 0.53) (Table 2).

Table 2. Characteristics of inpatients and outpatients by confirmed *Coccidioides* diagnosis in a cross-sectional study of clinical predictors of coccidioidomycosis, Arizona, USA*

	Outpatient		Inpatient			p value	
Characteristics	Positive, n = 35	Negative, n = 64	Positive, n = 38	Negative, n = 255	Total, n = 392	Outpatient	Inpatient
Median age, y (range)	57 (24–77)	51 (19–93)	45 (18–83)	58 (18–98)	57 (18–98)	0.534	**0.022**
Sex, no. (%)						0.289	1.000
F	20 (58.8)	29 (46)	18 (47.4)	123 (48.4)	190 (48.8)		
M	14 (41.2)	34 (54)	20 (52.6)	131 (51.6)	199 (51.2)		
Race, no. (%)						0.574	**0.018**
African American	2 (5.9)	4 (6.6)	6 (16.7)	14 (5.6)	26 (6.8)		
AI/AN	4 (11.8)	2 (3.3)	2 (5.6)	9 (3.6)	17 (4.5)		
Asian	1 (2.9)	2 (3.3)	2 (5.6)	2 (0.8)	7 (1.8)		
White	27 (79.4)	52 (85.2)	25 (69.4)	211 (84.7)	315 (82.9)		
Unknown	0	1 (1.6)	1 (2.8)	13 (5.2)	15 (3.9)		
Ethnicity, no. (%)						0.808	1.000
Hispanic	8 (25.8)	18 (30)	10 (27)	69 (27.6)	105 (27.8)		
Non-Hispanic	23 (74.2)	42 (70)	27 (73)	181 (72.4)	273 (72.2)		
Median length of endemic residence, y (range)	10 (0–59)	20 (0–88)	19 (0–78)	22 (0–98)	20 (0–98)	0.091	0.331
Immunocompromised, no. (%)†						0.344	0.076
Y	7 (20.6)	20 (31.2)	17 (44.7)	154 (61.1)	198 (51)		
N	27 (79.4)	44 (68.8)	21 (55.3)	98 (38.9)	190 (49)		
Median length of Illness, d (range)	14 (0–300)	14 (0–5,110)	14 (2–365)	14 (1–8,760)	14 (0–8,760)	0.370	0.972
Symptoms, no. (%)‡							
Fatigue	19 (54.3)	39 (60.9)	27 (71.1)	203 (79.9)	288 (73.7)	0.531	0.209
Cough	22 (62.9)	44 (68.8)	26 (68.4)	164 (64.6)	256 (65.5)	0.656	0.718
Fever	12 (34.3)	24 (37.5)	15 (39.5)	128 (50.4)	179 (45.8)	0.829	0.227
Chest pain	13 (37.1)	26 (40.6)	14 (36.8)	82 (32.3)	135 (34.5)	0.831	0.583
Shortness of breath	13 (37.1)	42 (65.6)	25 (65.8)	172 (67.7)	256 (65.5)	**0.011**	0.853
Headache	9 (25.7)	22 (34.4)	13 (34.2)	116 (45.7)	160 (40.9)	0.497	0.221
Night sweats	15 (42.9)	21 (32.8)	13 (34.2)	104 (40.9)	153 (39.1)	0.384	0.481
Muscle aches	13 (37.1)	28 (43.8)	10 (26.3)	122 (47.8)	163 (41.7)	0.670	**0.014**
Joint pain	13 (37.1)	14 (21.9)	7 (18.4)	82 (32.1)	126 (32.2)	0.156	0.051
Rash	16 (45.7)	3 (4.7)	11 (28.9)	38 (15)	68 (17.3)	**<0.001**	**0.037**
Other	11 (31.4)	27 (42.2)	11 (28.9)	74 (29.1)	123 (31.5)	0.388	1.000
Laboratory tests, median (range)							
Procalcitonin, ng/mL	0.05 (0.012–0.27)	0.10 (0.05–11.59)	0.11 (0.05–92.34)	0.165 (0.02–198.5)	0.11 (0.02–198.5)	**<0.001**	0.617
C-reactive protein, mg/L	7.40 (0.7–260)	17.5 (0.6–266.3)	46.0 (1.4–170.2)	68.0 (0.6–557)	49.00 (0.6–557)	0.090	0.066
ESR, mm/h	15.0 (5–76)	26.0 (1–145)	45.0 (6.0–122.0)	46.0 (4–145)	41.0 (1–145)	0.222	0.427
Leukocytes, $\times 10^3$ cells/mm^3	9.8 (4.6–14)	8.9 (3.7–26.5)	9.0 (0.3–24.4)	10.0 (0.1–45.4)	9.90 (0.1–45.4)	0.560	0.481
Hemoglobin, g/dL	13.8 (12.4–15.9)	13.3 (6.9–19.7)	12.0 (7.2–17.4)	12.0 (4.8–18)	12.6 (4.8–19.7)	0.163	0.438
Platelet count, $\times 10^3$/mm^3	312.0 (226–457)	238.0 (94–446)	260 (10–520)	239.0 (5–940)	248.0 (5–940)	**<0.001**	0.676
Eosinophil count, $\times 10^3$/µL	0.39 (0–1.4)	0.1 (0–0.8)	0.2 (0.0–3.0)	0.07 (0.0–4.55)	0.1 (0–4.55)	**<0.001**	**0.015**
Albumin, g/dL	4.05 (2.5–5)	3.9 (1.9–5)	3.0 (1.4–5.0)	3.1 (0.6–6.4)	3.5 (0.6–6.4)	0.483	0.333
Total protein, g/dL	7.3 (6.2–8.7)	7.3 (5.9–9.3)	7.35 (5.4–9.3)	6.95 (2.5–12.0)	7.05 (2.5–12)	0.747	**0.044**

*Inpatient participants were recruited from among hospitalized patients; outpatients were recruited from patients in emergency departments and affiliated clinics. Bold text indicates statistical significance. AI/AN, American Indian/Alaskan Native; ESR, erythrocyte sedimentation rate.
†Immunocompromised status was identified as a participant with a weakened immune system at the time of coccidioidomycosis diagnosis, which included participants with type 2 diabetes, HIV/AIDS, lupus, rheumatoid arthritis, or leukemia, and organ transplant recipients and those receiving chemotherapy agents, corticosteroids, and biologic response modifiers.
‡Symptom counts represent the total number of patients reporting the condition.

Among outpatient participants, coccidioidomycosis status did not differ by sex (p = 0.29) or ethnicity (p = 0.81). Length of residence was 10 years for coccidioidomycosis-positive participants and 20 years for coccidioidomycosis-negative participants (p = 0.09) (Table 2). We did not identify differences in length of illness (p = 0.37) or immunocompromised status (p = 0.34). Coccidioidomycosis-positive participants reported shortness of breath significantly less frequently than did coccidioidomycosis-negative participants (p = 0.01), but positive participants reported rash more frequently (p<0.001). Median PCT was significantly lower among positive participants (0.05 ng/mL, range 0.01–0.27 ng/mL) than among negative participants (0.10 ng/mL, range 0.05–11.6 ng/mL) (p<0.001). Median eosinophil count also was elevated among positive participants (0.39, range 0.0–1.4, interquartile range [IQR] 0.18–0.57) versus negative participants (0.10, range 0.0–0.80, IQR 0.0–0.20) (p<0.001) (Table 2).

Our inpatient population predominantly consisted of coccidioidomycosis-negative participants. Median age was 45 years for coccidioidomycosis-positive and 58 years for coccidioidomycosis-negative inpatient participants (p = 0.02). Coccidioidomycosis diagnosis did not differ for inpatients by sex (p = 1.0) or ethnicity (p = 1.0). Median length of residence was 19 years among positive participants versus 22 years for negative participants (p = 0.33). No difference was identified in median length of illness (p = 0.97). Coccidioidomycosis-positive participants reported muscle aches less frequently than coccidioidomycosis-negative participants (p = 0.01). As we noted in the outpatient population, rash was more frequent among positive participants in the inpatient population (p = 0.04). Median PCT was not statistically lower among positive (0.11 ng/mL, range 0.05–92.3 ng/mL) than negative participants (0.17 ng/mL, range 0.02–198.5 ng/mL) (p = 0.62) (Table 2). We observed lower median CRP levels (46.0 mg/mL, range 1.4–170.2 mg/mL) among positive participants than for negative participants (CRP 68.0 mg/mL, range 0.6–557.0 mg/mL), although the relationship did not meet statistical significance (p = 0.07). Median eosinophil count was elevated ($0.2 \times 10^3/\mu L$, range $0.0–3.0 \times 10^3/\mu L$, IQR $0.0–0.30 \times 10^3/\mu L$) among positive participants compared with negative participants ($0.07 \times 10^3/\mu L$, range $0.0–4.55 \times 10^3/\mu L$, IQR $0.0–0.20 \times 10^3/\mu L$) (p = 0.015). In contrast to outpatient participants, median total protein was moderately elevated among positive (7.4 g/dL, range 5.4–9.3 g/dL) compared with negative inpatient participants (7.0 g/dL, range 2.5–12.0 g/dL) (p = 0.04) (Table 2).

We developed univariable and multivariable LASSO prediction models for coccidioidomycosis stratified by admission status. Within our outpatient univariable models, positivity was significantly associated with rash (p = 0.006), higher eosinophil count (p = 0.012), and a lower PCT concentration (p = 0.039) (Table 3). Univariate models suggested eosinophilia ($>0.50 \times 10^3/\mu L$) is predictive of coccidioidomycosis (Appendix Table 3). Our inpatient univariable models identified higher eosinophil count, higher serum protein, lower age, lower CRP concentration, non-White racial identification, and rash as predictors of coccidioidomycosis, but muscle aches and immunocompromised status were negatively associated with disease (Table 4).

Selected features for our outpatient multivariable model included rash, shortness of breath, PCT, platelet count, and eosinophil count (Table 3); however, only rash was significantly associated with a coccidioidomycosis-positive test result (adjusted OR [aOR] 9.74, 95% CI 1.03–92.24). Outpatient multivariate models did not identify eosinophil count at any level as a predictive marker (Appendix Table 4).

Our inpatient model identified unique predictive characteristics compared with the outpatient model, including age, race, immunocompromised status, and CRP. Within our inpatient multivariable model, we identified a negative association with self-reported muscle aches (aOR 0.38, 95% CI 0.17–0.84). The model identified elevated eosinophil count as a significant predictor of coccidioidomycosis positivity

Table 3. Characteristics of outpatients in univariable and multivariable models in a cross-sectional study of clinical predictors of coccidioidomycosis, Arizona, USA*

Characteristics	Univariable model		Multivariable model	
	OR (95% CI)	p value	aOR (95% CI)	p value
Symptoms				
Rash	19.64 (2.34–164.67)	**0.006**	9.74 (1.03–92.24)	**0.047**
Shortness of breath	0.43 (0.17–1.09)	0.075	0.36 (0.12–1.07)	0.066
Laboratory tests				
Procalcitonin, ng/mL	0.45 (0.21–0.96)	**0.039**	0.59 (0.25–1.38)	0.222
Platelet count, $\times 10^3/mm^3$	1.73 (0.98–3.07)	0.060	1.70 (0.90–3.22)	0.100
Eosinophil count, $\times 10^3/\mu L$	2.18 (1.19–4.01)	**0.012**	1.62 (0.79–3.32)	0.186

*Participants were recruited from among patients in emergency departments and affiliated clinics, including 35 coccidioidomycosis-positive and 64 coccidioidomycosis-negative participants. Bold text indicates statistical significance. aOR, adjusted OR; OR, odds ratio.

Table 4. Characteristics of inpatients in univariable and multivariable models in a cross-sectional study of clinical predictors of coccidioidomycosis, Arizona, USA*

	Univariable model		Multivariable model	
Characteristics	OR (95% CI)	p value	aOR (95% CI)	p value
Demographics				
Age, y	0.70 (0.50–0.98)	**0.035**	0.72 (0.51–1.03)	0.071
Non-White race	2.42 (1.16–5.04)	**0.018**	2.14 (0.51–1.03)	0.061
Symptoms				
Muscle aches	0.45 (0.22–0.94)	**0.034**	0.38 (0.17–0.84)	**0.017**
Rash	2.29 (1.08–4.84)	**0.030**	2.20 (0.97–4.99)	0.060
Clinical feature				
Immunocompromised	0.49 (0.25–0.94)	**0.033**	0.64 (0.31–1.31)	0.220
Laboratory tests				
C-reactive protein, mg/L	0.66 (0.46–0.94)	**0.023**	0.72 (0.49–1.07)	0.100
Eosinophil count, $\times 10^3/\mu L$	1.65 (1.17–2.34)	**0.005**	1.50 (1.02–2.19)	**0.037**
Total protein, g/dL	1.50 (1.08–2.08)	**0.015**	1.30 (0.91–1.87)	0.152

*Participants were recruited from among hospitalized patients, including 38 coccidioidomycosis-positive participants and 255 coccidioidomycosis-negative participants. Bold text indicates statistical significance. Bold text indicates statistical significance. aOR, adjusted odds ratio; OR, odds ratio.

(aOR 1.50, 95% CI 1.02–2.19; p = 0.037) (Table 4). Eosinophilia was not identified as a significant predictive marker of coccidioidomycosis in our inpatient univariable model, but multivariate models applying lower thresholds indicated eosinophil levels ≥0.20 × $10^3/\mu L$ (200 cells/μL) were predictive of coccidioidomycosis (Appendix Table 4).

Using cross-validation, our outpatient model yielded an ROC AUC of 78.2% (95% CI 67.2%–89.1%) with a sensitivity of 72.7% and specificity of 69.5%. Our inpatient model yielded an ROC AUC of 64.3% (95% CI 55.2%–72.8%) with a sensitivity of 34.4% and specificity of 87.5% (Table 5).

Features selected in multivariable models were identical in replicated imputation datasets, suggesting consistency in variable selection. Sensitivity analyses performed by removing 198 immunocompetent outpatient participants similarly identified rash and elevated eosinophil count as predictors of coccidioidomycosis positivity (Appendix Table 5). Specificity in our immunocompetent outpatient model was lower (24.0%) than for the full model (69.5%), but sensitivity modestly improved (86.5%) in contrast to the full outpatient model (72.7%) (Appendix Table 6). After removing immunocompromised participants from our inpatient population, we identified no predictive features in either univariable or multivariable models. Univariable models using clinical breakpoints for laboratory measures were directionally consistent with our main results. Outpatient univariable models identified procalcitonin and eosinophil count as major predictors; however, no laboratory predictors were identified in inpatient models after using standardized reference ranges (Appendix Table 3). Multivariable modeling without stratification by admission status identified a similar feature set compared with our inpatient model because of the large sample size of this group relative to our outpatient population (Appendix Table 7). No predictors were identified for either inpatient or outpatient groups using an immunocompromised-only population. Variables identified in models including participants with acute pulmonary symptoms were directionally consistent with our main findings (Appendix Tables 8, 9).

Discussion

We found preliminary evidence for several markers that could predict coccidioidomycosis based on admission status. Although <40% of outpatient and inpatient participants had rash, our results suggest that rash might support coccidioidomycosis identification better than other symptoms, such as shortness of breath and muscle aches. In outpatient settings, PCT might help differentiate between a bacterial and *Coccidioides* infection. However, for inpatient settings, conventional indicators, including CRP level and immunocompromised status, might be concealed by comorbidities and high inflammatory markers typical to admitted patients and reduce their efficacy as predictive risk factors. Our models suggest elevated eosinophil count could be a viable biomarker to signal coccidioidomycosis in either clinical setting.

Both our univariable analyses and multivariable models among outpatients indicated rash as a major

Table 5. Performance metrics for outpatient and inpatient multivariable model in a cross-sectional study of clinical predictors of coccidioidomycosis, Arizona, USA*

Metric	Outpatient	Inpatient
ROC AUC	78.2	64.3
Sensitivity	72.7	34.4
Specificity	69.5	87.5
Positive predictive value	28.6	11.9
Negative predictive value	93.8	96.4
Prevalence	14.4	4.6
Detection rate	10.5	1.6
Detection prevalence	36.6	13.5
Balanced accuracy	71.1	61.0

*ROC AUC, receiver operating characteristic area under the curve.

predictor of coccidioidomycosis. Our results were likely driven by the low incidence of rash among coccidioidomycosis-negative participants (4.7%) compared with coccidioidomycosis-positive participants (45.7%). This finding might emphasize the utility of rash as a unique marker of coccidioidomycosis, considering the comparatively low occurrence of this symptom in the outpatient population. Our findings are consistent with previous studies suggesting rash is more frequently identified among coccidioidomycosis cases than among cases of other common respiratory infections (*25*). PCT was negatively associated with positive status, but elevated eosinophil count was a predictive marker of coccidioidomycosis. Laboratory markers were not predictive in our multivariable model; however, low serum PCT levels previously have been reported in persons with coccidioidomycosis (*26*). Lower PCT is consistent with the cell-mediated immune response against *Coccidioides* infection because the production of interferon gamma from type-1 T-helper cells impedes PCT upregulation (*27*). Previous studies also have indicated elevated eosinophil counts among persons with coccidioidomycosis (*28*,*29*). Our results substantiate previous recommendations that eosinophilia heightens suspicion of *Coccidioides* infection (*30*).

Our univariable analyses for inpatients identified negative associations with age, muscle aches, immunocompromised status, and CRP with coccidioidomycosis positivity, but non-White racial status, rash, eosinophil count, and total protein were positive predictive markers of disease. Our multivariable model selected an identical feature set, but only lower incidence of muscle aches and a higher eosinophil count remained statistically significant. Some of our null findings could be explained by the high concentration of immunocompromised participants in the inpatient setting, because these patients often have established coccidioidomycosis risk factors at admission. Furthermore, previous evidence suggests that 20%–50% of specimens from immunocompromised persons test false-negative by *Coccidioides* serologies (*31*); thus, false-negative test results among coccidioidomycosis-negative participants might have been artificially inflated in our study. Of note, older age is a well-established coccidioidomycosis risk factor because of the decline in immune function and higher prevalence of chronic diseases among older persons (*32*); substantial evidence also suggests that immunocompromised persons are more susceptible (*33*). Therefore, the predictive capacity of these risk factors might be limited by the intersecting clinical patterns of coccidioidomycosis and other diseases in the inpatient setting. We also identified CRP as a negative predictor for coccidioidomycosis. As a generalized blood test marker, CRP might have detected higher inflammation for other conditions among inpatients. Like our outpatient results, LASSO selection incorporated eosinophil count into our multivariable model, indicating that eosinophil levels $\geq 0.20 \times 10^3/\mu L$ might be predictive of *Coccidioides* infection in inpatient settings. Inpatient models did not identify PCT as a negative predictor of coccidioidomycosis.

Our results differ from risk factors previously identified by Yozwiak et al. (*13*), who developed a model using healthy college-aged students. Although these previously identified risk factors might have practical value for estimating relative risk in a healthy population, the inconsistent feature set with our study suggests previous results have limited transferability to a more diverse clinical population. For example, Yozwiak et al. reported male sex, shorter length of residence in coccidioidomycosis-endemic areas, and shorter duration of symptoms as independent risk factors for coccidioidomycosis, which we did not detect as predictors of disease in our study. Yozwiak et al. further reported higher ESR rates and lower lymphocyte levels were associated with disease. Although eosinophil count was indicative of coccidioidomycosis in our study, we did not identify ESR or other cell types as statistically significant predictive markers.

We describe novel coccidioidomycosis prediction models for inpatient and outpatient clinical settings using an agnostic feature selection technique. We constructed models by using data from our previous cross-sectional study and leveraged these data to substantiate risk factors previously associated with coccidioidomycosis, including clinical, demographic, and laboratory variables. We identified markers that might identify coccidioidomycosis before diagnostic testing and distinctive predictive features based on admission status. We stratified models by inpatient and outpatient groups because of the unique features identified within each clinical setting. Our study identified several clinical features in outpatient and inpatient settings, but screening for *Coccidioides* in endemic settings remains invaluable. Although negative clinical features, such as PCT, muscle aches, or shortness of breath, might be indicative of an alternative diagnosis, we emphasize that the presence of these markers should not deter testing.

Limitations of our study include a reduced sample size used to develop our models, in part due to our stratification, which might have hampered our ability to accurately estimate predictive markers of

coccidioidomycosis. We were further unable to apply clinical breakpoints for laboratory measures because of reduced granularity of binary measures and therefore report the effect of continuous variables. We attempted to minimize feature selection biases by using LASSO to construct models; LASSO offers several benefits over alternative feature selection methods, but our impartial approach might have inappropriately eliminated collinear or other necessary control variables. We additionally recognize that participants with established coccidioidomycosis markers might have been preferentially tested during enrollment, resulting in selection bias, and influencing marker selection. The relative infrequency of identified features further hinders the clinical utility of leveraging these markers to identify coccidioidomycosis and emphasizes the importance of diagnostic testing.

Our study's strengths include that we used a novel multidimensional dataset to evaluate established and suspected coccidioidomycosis risk factors. Stratification reveals substructures within clinical settings that could improve disease identification and diagnosis. Our sensitivity analyses using immunocompetent patients further increases confidence in selected features, because rash and higher eosinophil count were similarly predictive of coccidioidomycosis in the outpatient setting.

Public health recommendations are to test for *Coccidioides* among patients with pneumonialike symptoms in endemic areas. However, the complex and often nonspecific clinical manifestations of coccidioidomycosis indicate a need to improve disease identification. Coupled with the introduction of coronavirus disease in 2019, differentiating between coccidioidomycosis and other pneumonias remains vital for the rapid diagnosis and treatment of disease. The limited accuracy of our models, however, indicate the need for a more robust data source for model development. Replication in a larger clinical study incorporating other endemic regions could provide insight into additional predictive markers for more specific clinical manifestations. Our study identifies surrogate markers in a clinical setting that might provide a developmental framework for future predictive models.

In conclusion, we developed prediction models for multiple clinical settings to support identification of coccidioidomycosis before diagnostic testing. Prediction models could guide the clinical decision-making process to test for coccidioidomycosis, expedite identification of more serious disease complications, and decrease the use of unnecessary diagnostic tests or antimicrobial agents.

This article was preprinted at https://osf.io/qmak3.

This work was supported by the Centers for Disease Control and Prevention (contract no. 75D30118C02899).

About the Author

Mr. Ramadan is a data scientist with the University of Arizona Department of Epidemiology and Biostatistics. His current research interests include application of Mendelian randomization, predictive disease modeling, antimicrobial stewardship, and genetic and infectious disease epidemiology.

References

1. Pappagianis D. Epidemiology of coccidioidomycosis. In: Stevens DA, editor. Coccidioidomycosis: a text. New York: Springer Science+Business Media; 1980. p. 63–85.
2. Centers for Disease Control and Prevention (CDC). Increase in reported coccidioidomycosis—United States, 1998–2011. MMWR Morb Mortal Wkly Rep. 2013;62:217–21.
3. Centers for Disease Control and Prevention. Valley fever statistics 2020 [cited 2021 Jan 20]. https://www.cdc.gov/fungal/diseases/coccidioidomycosis/statistics.html
4. McCotter OZ, Benedict K, Engelthaler DM, Komatsu K, Lucas KD, Mohle-Boetani JC, et al. Update on the epidemiology of coccidioidomycosis in the United States. Med Mycol. 2019;57(Supplement_1):S30–40. https://doi.org/10.1093/mmy/myy095
5. Pu J, Donovan FM, Ellingson K, Leroy G, Stone J, Bedrick E, et al. Clinician practice patterns that result in the diagnosis of coccidioidomycosis before or during hospitalization. Clin Infect Dis. 2021;73:e1587–93. https://doi.org/10.1093/cid/ciaa739
6. Galgiani JN, Ampel NM, Blair JE, Catanzaro A, Johnson RH, Stevens DA, et al.; Infectious Diseases Society of America. Coccidioidomycosis. Clin Infect Dis. 2005;41:1217–23. https://doi.org/10.1086/496991
7. Donovan FM, Wightman P, Zong Y, Gabe L, Majeed A, Ynosencio T, et al. Delays in coccidioidomycosis diagnosis and associated healthcare utilization, Tucson, Arizona, USA. Emerg Infect Dis. 2019;25:1745–7. https://doi.org/10.3201/eid2509.190023
8. Tsang CA, Anderson SM, Imholte SB, Erhart LM, Chen S, Park BJ, et al. Enhanced surveillance of coccidioidomycosis, Arizona, USA, 2007–2008. Emerg Infect Dis. 2010;16:1738–44. https://doi.org/10.3201/eid1611.100475
9. Brown J, Benedict K, Park BJ, Thompson III GR. Coccidioidomycosis: epidemiology. Clin Epidemiol. 2013;5:185–97.
10. Thompson GR III. Pulmonary coccidioidomycosis. Semin Respir Crit Care Med. 2011;32:754–63. https://doi.org/10.1055/s-0031-1295723
11. Chang DC, Anderson S, Wannemuehler K, Engelthaler DM, Erhart L, Sunenshine RH, et al. Testing for coccidioidomycosis among patients with community-acquired pneumonia. Emerg Infect Dis. 2008;14:1053–9. https://doi.org/10.3201/eid1407.070832
12. Valdivia L, Nix D, Wright M, Lindberg E, Fagan T, Lieberman D, et al. Coccidioidomycosis as a common cause of community-acquired pneumonia. Emerg Infect Dis. 2006;12:958–62. https://doi.org/10.3201/eid1206.060028

13. Yozwiak ML, Lundergan LL, Kerrick SS, Galgiani JN. Symptoms and routine laboratory abnormalities associated with coccidioidomycosis. West J Med. 1988;149:419–21.
14. Donovan FM, Ramadan FA, Khan SA, Bhaskara A, Lainhart WD, Narang AT, et al. Comparison of a novel rapid lateral flow assay to enzyme immunoassay results for early diagnosis of coccidioidomycosis. Clin Infect Dis. 2021;73:e2746–53. https://doi.org/10.1093/cid/ciaa1205
15. Lechleitner G, Pfeiffer K-P, Wilhelmy I, Ball M. Cerner millennium: the Innsbruck experience. Methods Inf Med. 2003;42:8–15.
16. Schafer JL. Analysis of incomplete multivariate data. New York: Chapman and Hall/CRC; 1997.
17. van Buuren S, Groothuis-Oudshoorn K. mice: multivariate imputation by chained equations in R. J Stat Softw. 2010;45:1–68. https://doi.org/10.18637/jss.v045.i03
18. Tibshirani R. Regression shrinkage and selection via the Lasso. J R Stat Soc B. 1996;58:267–88. https://doi.org/10.1111/j.2517-6161.1996.tb02080.x
19. Emmert-Streib F, Dehmer M. High-dimensional LASSO-based computational regression models: regularization, shrinkage, and selection. Mach Learn Knowl Extr. 2019;1:359–83. https://doi.org/10.3390/make1010021
20. Algeciras-Schimnich A, Preissner CM, Theobald JP, Finseth MS, Grebe SKG. Procalcitonin: a marker for the diagnosis and follow-up of patients with medullary thyroid carcinoma. J Clin Endocrinol Metab. 2009;94:861–8. https://doi.org/10.1210/jc.2008-1862
21. McPherson RA, Pincus MR. Henry's clinical diagnosis and management by laboratory methods e-book. New York: Elsevier Health Sciences; 2021.
22. Chernecky C, Berger B. Differential leukocyte count (diff)-peripheral blood. In: Chernecky C, Berger B, editors. Laboratory tests and diagnostic procedures. St. Louis (MO): Elsevier Saunders; 2013. p. 440–6.
23. The R Project for Statistical Computing [cited 2020 Nov 2]. https://www.r-project.org
24. Friedman J, Hastie T, Tibshirani R. Regularization paths for generalized linear models via coordinate descent. J Stat Softw. 2010;33:1–22. https://doi.org/10.18637/jss.v033.i01
25. Benedict K, Kobayashi M, Garg S, Chiller T, Jackson BR. Symptoms in blastomycosis, coccidioidomycosis, and histoplasmosis versus other respiratory illnesses in commercially insured adult outpatients—United States, 2016–2017. Clin Infect Dis. 2021;73:e4336–44. https://doi.org/10.1093/cid/ciaa1554
26. Sakata KK, Grys TE, Chang Y-HH, Vikram HR, Blair JE. Serum procalcitonin levels in patients with primary pulmonary coccidioidomycosis. Ann Am Thorac Soc. 2014;11:1239–43. https://doi.org/10.1513/AnnalsATS.201404-180BC
27. Linscheid P, Seboek D, Nylen ES, Langer I, Schlatter M, Becker KL, et al. In vitro and in vivo calcitonin I gene expression in parenchymal cells: a novel product of human adipose tissue. Endocrinology. 2003;144:5578–84. https://doi.org/10.1210/en.2003-0854
28. Schermoly MJ, Hinthorn DR. Eosinophilia in coccidioidomycosis. Arch Intern Med. 1988;148:895–6. https://doi.org/10.1001/archinte.1988.00380040135019
29. Merchant M, Romero AO, Libke RD, Joseph J. Pleural effusion in hospitalized patients with coccidioidomycosis. Respir Med. 2008;102:537–40. https://doi.org/10.1016/j.rmed.2007.11.014
30. Saubolle MA, McKellar PP, Sussland D. Epidemiologic, clinical, and diagnostic aspects of coccidioidomycosis. J Clin Microbiol. 2007;45:26–30. https://doi.org/10.1128/JCM.02230-06
31. Stockamp NW, Thompson GR III. Coccidioidomycosis. Infect Dis Clin North Am. 2016;30:229–46. https://doi.org/10.1016/j.idc.2015.10.008
32. Leake JA, Mosley DG, England B, Graham JV, Plikaytis BD, Ampel NM, et al. Risk factors for acute symptomatic coccidioidomycosis among elderly persons in Arizona, 1996–1997. J Infect Dis. 2000;181:1435–40. https://doi.org/10.1086/315400
33. Galgiani JN, Ampel NM, Blair JE, Catanzaro A, Geertsma F, Hoover SE, et al. 2016 Infectious Diseases Society of America (IDSA) clinical practice guideline for the treatment of coccidioidomycosis. Clin Infect Dis. 2016;63:e112–46. https://doi.org/10.1093/cid/ciw360

Address for correspondence: Ferris A. Ramadan, Department of Epidemiology and Biostatistics, Mel and Enid Zuckerman College of Public Health University of Arizona, Tucson, AZ 85724, USA; email: ferrisr@arizona.edu

Detection of SARS-CoV-2 B.1.351 (Beta) Variant through Wastewater Surveillance before Case Detection in a Community, Oregon, USA

Melissa Sutton, Tyler S. Radniecki, Devrim Kaya, Dana Alegre, Matthew Geniza, Anne-Marie Girard, Katherine Carter, Mark Dasenko, Justin L. Sanders, Paul R. Cieslak, Christine Kelly, Brett M. Tyler

Genomic surveillance has emerged as a critical monitoring tool during the SARS-CoV-2 pandemic. Wastewater surveillance has the potential to identify and track SARS-CoV-2 variants in the community, including emerging variants. We demonstrate the novel use of multilocus sequence typing to identify SARS-CoV-2 variants in wastewater. Using this technique, we observed the emergence of the B.1.351 (Beta) variant in Linn County, Oregon, USA, in wastewater 12 days before this variant was identified in individual clinical specimens. During the study period, we identified 42 B.1.351 clinical specimens that clustered into 3 phylogenetic clades. Eighteen of the 19 clinical specimens and all wastewater B.1.351 specimens from Linn County clustered into clade 1. Our results provide further evidence of the reliability of wastewater surveillance to report localized SARS-CoV-2 sequence information.

Since its emergence in late 2019, more than 481 million COVID-19 cases have been confirmed worldwide (*1*) and >79 million cases reported in the United States (*2*). Numerous variants of the causative virus, SARS-CoV-2, have emerged; variants of concern have demonstrated characteristics of public health concern, including increased transmissibility or clinical severity, reduced vaccine or therapeutic effectiveness, or diagnostic escape (*3*). SARS-CoV-2 genomic surveillance has quickly become an essential tool for tracking transmission and coordinating response (*4*,*5*). Individual-level genomic surveillance relies on the testing of infected persons, which, in turn, requires testing access and acceptance. In the United States, testing access has improved dramatically over the course of the pandemic but remains limited, particularly in disproportionately affected communities (*6*), and testing acceptance remains an obstacle to effective disease mitigation (*7*).

SARS-CoV-2 is shed in feces, and wastewater surveillance has emerged as complementary cost-effective community-level surveillance independent of testing access and acceptance or symptomatic infection (*8*–*10*). Using wastewater testing for SARS-CoV-2 genomic surveillance avoids the testing and symptomatic biases inherent to the sequencing of individual specimens; however, interpreting sequence data from complex mixtures of viruses at a population-level remains challenging (*11*). Multilocus sequence typing (MLST) is a method traditionally used to identify species or variants in environmental samples, including rivers, urban streams, hospital sewage, and wastewater treatment plant influents and effluents (*12*,*13*). MLST is well-suited for the analysis of wastewater RNA because it detects a set of mutations unique to a variant and does not require these mutations to be present on a single molecule of RNA (*12*–*18*).

During the COVID-19 pandemic, Oregon has been among the US states with the lowest cumulative case rates and among those with the highest proportion of cumulative molecular specimens sequenced in the United States (*19*). As of March 31, 2021, a total of 159,455 confirmed cases of COVID-19 had been identified in Oregon, and specimens from 5,674 (3.6%) of the cases had been sequenced and published in the GISAID database (https://www.gisaid.org) (*20*). At that time, the dominant SARS-CoV-2 variant circulating in Oregon was B.1.427/B.1.429 (Epsilon), followed by B.1.2 and B.1.1.7 (Alpha); only 25 B.1.351 (Beta) and 8 P.1 (Gamma) variants had been identified.

Author affiliations: Oregon Health Authority, Portland, Oregon, USA (M. Sutton, P.R. Cieslak); Oregon State University, Corvallis, Oregon (T.S. Radniecki, D. Kaya, D. Alegre, M. Geniza, A.-M. Girard, K. Carter, M. Dasenko, J.L. Sanders, C. Kelly, B.M. Tyler)

DOI: https://doi.org/10.3201/eid2806.211821

On April 19, 2021, Oregon mandated reporting of all SARS-CoV-2 variants of concern to public health authorities; before this, genomic surveillance relied largely on deidentified data submitted to GISAID. Statewide sequencing partners have been asked to submit all individual specimen sequencing results to the State of Oregon phylodynamics resource in GISAID (https://www.gisaid.org/phylodynamics/oregon-usa).

In September 2020, the Oregon Health Authority launched wastewater surveillance in collaboration with the Oregon State University (OSU) Team-Based Rapid Assessment of Community-Level Coronavirus Epidemics (TRACE) project; >40 communities comprising ≈60% of Oregon's population currently participate. Through this program, wastewater samples from the influent of all wastewater treatment facilities are collected at least weekly and sent to OSU for SARS-CoV-2 viral RNA quantification and sequencing of all positive samples with sufficient viral loads. Through this statewide SARS-CoV-2 wastewater surveillance platform, we demonstrate the use of MLST to detect the emergence of the SARS-CoV-2 B.1.351 (Beta) variant in rural Oregon in late March 2021, before its detection in reported cases, illustrating the ability of wastewater-based epidemiology to detect emerging variants of concern.

Methods

Wastewater RNA Extraction

Participating facilities collected wastewater composite samples from Albany(Linn County), Corvallis (Benton County), and Dallas (Polk County), Oregon, USA, during March 26–April 21, 2021, according to routine practice for the Oregon Wastewater Surveillance Program (Table). In brief, 24-hour time-weighted

Table. SARS-CoV-2 variant B.1.351 mutations detected in clinical specimens and wastewater samples in Linn County, Oregon, and surrounding jurisdictions, March-May 2021

			Mutations specific to‡							
			B.1.351			Clade 1			Subclade§	
Sample*	Collection site†	Date	+	–	?	+	–	?	1a	1b
Clinical specimens										
EPI_ISL_1866415	Linn Co.	2021 Mar 29¶	9	0	0	5	1	0	–	–
EPI_ISL_1736521	Linn Co.	2021 Apr 5	9	0	0	6	0	0	+	–
EPI_ISL_1736532	Linn Co.	2021 Apr 5	9	0	0	6	0	0	+	–
EPI_ISL_1737841	Linn Co.	2021 Apr 7	9	0	0	0#	0	0	–	–
EPI_ISL_1964160	Linn Co.	2021 Apr 9	8	0	1	6	0	0	–	+
EPI_ISL_1999265	Linn Co.	2021 Apr 12	9	0	0	5	1	0	–	–
EPI_ISL_2202145	Linn Co.	2021 Apr 16	8	0	1	4	0	2	+	–
EPI_ISL_2139637	Linn Co.	2021 Apr 26	9	0	0	6	0	0	+	–
EPI_ISL_2139638	Linn Co.	2021 Apr 26	9	0	0	6	0	0	+	–
EPI_ISL_2139639	Linn Co.	2021 Apr 26	9	0	0	6	0	0	+	–
EPI_ISL_2139644	Linn Co.	2021 Apr 27	9	0	0	6	0	0	+	–
EPI_ISL_2250177	Linn Co.	2021 Apr 27	8	0	1	6	0	0	–	+
EPI_ISL_2086679	Linn Co.	2021 Apr 28	9	0	0	6	0	0	+	–
EPI_ISL_2086678	Linn Co.	2021 Apr 28	9	0	0	6	0	0	+	–
EPI_ISL_2139636	Linn Co.	2021 Apr 30	9	0	0	6	0	0	+	–
EPI_ISL_2086694	Linn Co.	2021 Apr 30	9	0	0	6	0	0	+	–
EPI_ISL_2339336	Linn Co.	2021 May 10	9	0	0	6	0	0	+	–
EPI_ISL_2382524	Linn Co.	2021 May 12	9	0	0	6	0	0	+	–
EPI_ISL_2382527	Linn Co.	2021 May 14	9	0	0	6	0	0	+	–
Wastewater samples										
ALB-Inf-03-26-21-A	Albany, Linn Co.	2021 Mar 26	7	1	1	3	1	2	–	+
ALB-Inf-03-31-21-A	Albany, Linn Co.	2021 Mar 31	9	0	0	5	0	1	+	+
COR-25th-04-04-21-A	Corvallis, Benton Co.	2021 Apr 4	9	0	0	6	0	0	+	–
COR-26th-04-04-21-A	Corvallis, Benton Co.	2021 Apr 4	6	2	1	5	0	1	–	–
ALB-Inf-04-07-21-A	Albany, Linn Co.	2021 Apr 7	8	1	0	6	0	0	+	+
DAL-Inf-04-19-21-A	Dallas, Polk Co.	2021 Apr 19	9	0	0	6	0	0	–	+
ALB-Inf-04-21-21-A	Albany, Linn Co.	2021 Apr 21	5	3	1	2	3	1	–	–

*Sequences from individual clinical specimens are identified by their GISAID accession numbers (https://www.gisaid.org). Wastewater sequences are identified by their field collection identifier. Co., County; +, mutation detected; –, mutation not detected; ?, inadequate sequence data for a determination.
†Cities where individual clinical specimens were collected are not provided to reduce identifiability of case-patients.
‡Number of mutations matched by the sequences from each sample. Mutations specific to B.1.351 are G174T, A2692T, G5230T, A21801C, 22283Δ9, G22813T, C25904T, C26456T, and C28253T. Mutations specific to clade 1 are A1763G, C5100T, G13045A, C19524T, 28027Δ129, and C29741T.
§A single mutation defines each of clades 1a (A11875G) and 1b (C15928T). Absence of both mutations defines clade 1c in the case of individual specimens; in the case of wastewater samples, determining whether a mutation is truly absent from the RNA molecules present, or if the mutations have simply not been detected, is not possible.
¶This sample was retrospectively identified as B.1.351 late in April 2021 after routine sequencing of historical specimens.
#This specimen falls into clade 2 (Figure 1).

composite wastewater samples were collected weekly from the influent of Albany and Dallas wastewater treatment plants and from wastewater conveyance lines in Corvallis because of micro-sewershed surveillance at a local university. Samples were vacuum-filtered (10–50 mL) onsite through a 0.45-μm pore size, 47-mm diameter mixed cellulose ester electronegative filter (MF-Millipore, https://www.emdmillipore.com). Filters were placed into a 2-mL tube containing garnet (0.5 mm) beads and DNA/RNA Shield (Zymo Research, https://www.zymoresearch.com) to stabilize the RNA during the shipment to OSU for processing.

Upon receipt of the samples, we subjected the filters to bead beating and extracted RNA by using the MagMAX Viral/Pathogen Nucleic Acid Isolation Kit (Thermo Fisher Scientific, https://www.thermofisher.com). We quantified 2 SARS-CoV-2 gene targets (nucleocapsid gene 1 and 2) and a human gene target (ribonuclease P, an internal control) through droplet digital reverse transcription PCR (ddRT-PCR) on a QX200 ddPCR system (Bio-Rad, https://www.bio-rad.com) using the 2019-nCoV CDC ddPCR Triplex Probe Assay (Bio-Rad) and the One-Step RT-ddPCR Advanced Kit for Probes (Bio-Rad), according to the manufacturer's protocols.

Amplicon-Based Sequencing

We performed amplicon-based sequencing to enable high coverage for the length of the genome, except 25 bp at each end. We synthesized cDNA by using the SuperScript IV First-Strand Synthesis System (Thermo Fisher) and sequenced it by using the Swift Amplicon SARS-CoV-2 Panel (Swift Biosciences, https://www.idtdna.com), together with Swift Amplicon Combinatorial Dual indexed adapters (Swift Biosciences), according to the manufacturer's protocols. The Swift Amplicon SARS-CoV-2 Panel spans the SARS-CoV-2 genome with 341 amplicons with an average length of 150 bp. We produced sequences on a HiSeq 3000 or NextSeq 2000 sequencer (Illumina, https://www.illumina.com) to a depth sufficient for confident identification of variants, typically 10–30 million sequence reads per wastewater sample (Appendix, https://wwwnc.cdc.gov/EID/article/28/6/21-1821-App1.pdf).

Bioinformatic Processing of Sequences

We demultiplexed the sequence reads with zero index mismatches by using bcl2fastq2 version 2.20 (Illumina) for samples sequenced on the HiSeq 3000 and BCL Convert version 1.2.1 (Illumina) for the NextSeq 2000, then trimmed them by using BBDuk (BBMap version 38.84 (US Department of Energy Joint Genome Institute, https://jgi.doe.gov). We aligned trimmed reads to the reference sequence (Wuhan-Hu-1, GenBank accession no. NC_045512.2) by using the BWA-MEM algorithm version 0.7.17-r1188 (https://github.com/lh3/bwa) and coordinate-sorted them with SAMtools version 1.10 (Genome Research Limited, https://www.sanger.ac.uk); we then removed primer sequences by using Primerclip version 0.3.8 (Swift BioSciences). We converted reads from sam files to bam files and coordinate-sorted and indexed them using SAMtools. We then used GATK version 4.2.0.0 (Broad Institute, https://www.broadinstitute.org) to identify mutations compared with the reference sequence (Appendix). We used Integrated Genomics Viewer version 2.8.7 (Broad Institute) to manually inspect sequence alignments and mutation calls (*21*,*22*).

Multilocus Sequence Typing

Through the well-established process of MLST (*12*–*18*), we matched sets of mutations unique to known SARS-CoV-2 variants to mutations found in the wastewater sequences to infer the presence of variants in the community's wastewater. Because of the heterogenous nature of wastewater and the potential presence of numerous SARS-CoV-2 variants in wastewater, we used a set of mutations identified as specific to B.1.351 in Oregon to screen for this variant (Table; Appendix Figure 1). To create this unique panel, we screened a set of 22 mutations associated with B.1.351 (H. Tegally et al., unpub. data, https://doi.org/10.1101/2020.12.21.20248640) (Appendix) against a database of mutations associated with individual clinical specimens sequenced in Oregon and deposited into GISAID (*20*) and from published reports of novel variants (*23*–*28*) (I. Ferreira, unpub. data, https://doi.org/10.1101/2021.05.08.443253; X. Deng et al., unpub. data, https://doi.org/10.1101/2021.03.07.212526 47; M.K. Annavajhala et al., unpub. data, https://doi.org/10.1101/2021.02.23.21252259). Of the 22 mutations associated with the B.1.351 variant, 9 were found only in identified B.1.351 sequences from Oregon, 7 were common to >20 variants, and the remaining 6 were shared by 1–3 other variants (Appendix Tables 2–8, Figure 1).

Because wastewater SARS-CoV-2 RNA is derived from a mixture of variants, sequence reads spanning a B.1.351 mutation site would be expected to include reads derived from B.1.351 RNA molecules as well as reads derived from other variants. For a potential positive identification of a B.1.351-associated mutation in wastewater RNA sequences, a lower limit of 5% of sequence reads (with a minimum of 6 total

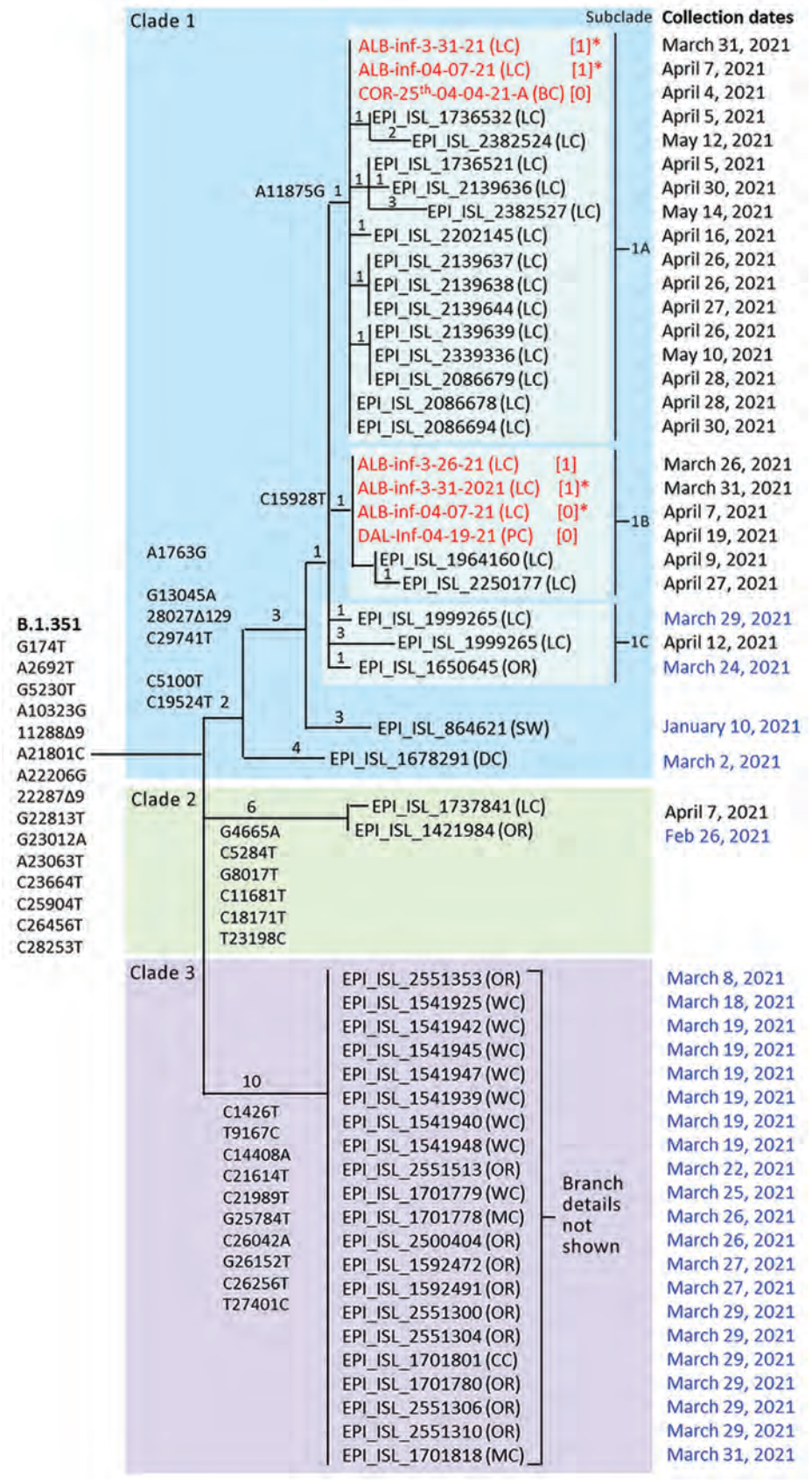

Figure 1. Maximum-parsimony tree demonstrating phylogenetic relationships among SARS-CoV-2 variant B.1.351 clinical specimens and wastewater samples in Linn County, Oregon, USA, and surrounding jurisdictions, March–May 2021. GISAID accession numbers (https://www.gisaid.org) are shown for 19 of 20 B.1.351 specimens identified in Linn County through May 15, 2021, and for 24 additional B.1.351 specimens identified in Oregon through March 31, 2021 (dates in blue). Also included are 2 sequences from outside Oregon (Switzerland and Washington, DC, USA) most closely related to clade 1. Wastewater samples are in red. Exact parsimony trees are shown for clade 1 and 2 sequences, whereas clade 3 sequences are simply listed. Mutations defining B.1.351 and each of the 3 clades, plus subclades 1a and 1b, are shown. Private mutations defining the subbranches of clades 1 and 2 are listed in Appendix Table 9 (https://wwwnc.cdc.gov/EID/article/28/6/21-1821-App1.pdf). Numbers on tree branches indicate the numbers of mutations associated with each branch. Numbers in brackets indicate clade 1 consensus mutations not detected, probably because of poor read coverage. Asterisks indicate samples that appear in both subclades 1a and 1b and are inferred to be a mixture of at ≥2 B.1.351 subtypes. Wastewater sequences ALB-Inf-04-21-21-A and COR-26th-04-04-21-A are not shown because several tracts of those sequences were too uncertain to enable accurate placement on the tree. OR, Oregon; BC, Benton County; CC, Clackamas County; LC, Linn County; MC, Multnomah County; WC, Washington County; DC, Washington, DC; SW, Switzerland.

reads) spanning the mutation site was required. In addition, ≥2 different sites carrying B.1.351 mutations must have been present. The rate of sequence errors produced by the sequencing procedure (a possible source of false-positive reads) was <0.2%.

Ultimately, we used 2 criteria to identify wastewater sample matches to B.1.351: the number of unique mutations present and the normalized proportion of all sequence reads. A minimum of 5 of 9 unique mutations was required for positive identification and we assigned a confidence score as follows: 8–9 matches indicated confident detection, 6–7 matches indicated probable detection, and 5 matches indicated tentative detection. In addition, the normalized proportion of all reads carrying any of the 9 mutations was required to be ≥10% of all reads spanning the 9 mutation sites (Appendix). We reconstructed the putative genome sequences of all variants inferred to be present in wastewater by mapping detected variant-specific mutations onto the reference sequence. We visualized and compared clinical specimen genomes from GISAID and putative viral isolate genomes by using Nextclade version 1.5.2 and used the output to manually construct the maximum-parsimony tree (*29*) (Figure 1). We submitted all wastewater sequences to the National Center for Biotechnology Information Sequence Read Archive (https://www.ncbi.nlm.nih.gov/sra) (*30*).

Phylogenetic Analysis

We constructed phylogenetic trees by using a maximum-parsimony approach (*29*). Because of the simple structure of the Linn County B.1.351 population, we were able to manually construct a single unambiguous tree by using the mutations specific for each clade and subclade together with the mutations private to each clinical sequence (Appendix Table 9). Mutations private to B.1.351 sequences in wastewater could not be reliably identified because of the presence of other variants, so we did not include them in phylogenetic analysis.

The manual approach enabled us to include sequences that had mutation information missing because of poor sequencing quality. We first constructed the tree by using sequences missing no mutations. Then, we added sequences with missing data to the tree on the basis of available mutation data; this approach imputed the presence of the undetected mutations on the basis of the presence of the available mutations. We did not include in the trees sequences that could not be unambiguously placed on the tree due to missing data.

Results

On March 26 and March 31, 2021, routine wastewater surveillance from the city of Albany, Oregon (Linn County), identified 2 samples that contained SARS-CoV-2 RNA exhibiting mutations specific to the B.1.351 lineage in Oregon (Table; Appendix Figure 1). The wastewater sample from March 26 (ALB-Inf-03–26–21-A) exhibited 7 of 9 specific mutations, whereas the wastewater sample from March 31 (ALB-Inf-03–31–21-A) exhibited all 9. At the time of these initial wastewater detections, no cases of B.1.351 in Linn County or adjacent counties had been identified, and only 25 specimens had been identified as B.1.351 through individual-level whole-genome sequencing statewide. On April 23, 2021, the first case of B.1.351 in Linn County was reported to the local public health authority (specimen collection date April 7). During the following month, 15 additional cases were reported. In Linn County, 20 total cases were identified through sequencing of individual clinical specimens collected through May 15 (Figure 2).

Additional community-level evidence in support of the initial detection of B.1.351 in the wastewater of Albany came from wastewater surveillance in 2 nearby cities as well as subsequent wastewater specimens from Albany. On April 4 and April 19, 2021, routine wastewater surveillance and sequencing of samples from the cities of Corvallis (Benton County; samples COR-25th-04-04-21-A and COR-26th-04-04-21-A) and Dallas (Polk County; sample DAL-Inf-04-19-21-A) identified probable (6/9) to confident (9/9) matches to the unique set of B.1.351 mutations referenced previously (Table; Appendix Figure 1), consistent with local circulation of the B.1.351 variant. Subsequent wastewater surveillance in Albany on April 7 (ALB-Inf-04-07-21-A) and April 21 (ALB-Inf-04-21-21-A) contained confident (8/9) and tentative (5/9) matches to the set of nine unique mutations. In sum, 7 wastewater samples matched ≥5 of the 9 mutations unique to the B.1.351 lineage (Table; Appendix Figure 1). In some cases, the lack of confident matches resulted from poor sequence coverage (<6 reads), whereas in other cases, no match was detected despite moderate sequence coverage (Appendix Figure 1).

Individual-level sequencing results were available for 19 of the 20 B.1.351 specimens identified in Linn County through May 15, 2021, in GISAID. Phylogenetic analysis of all 25 Oregon B.1.351 sequences available in GISAID through March 31, 2021, revealed 3 distinct B.1.351 clades in Oregon (Figure 1). Of the 19 Linn County specimens, 18 resided within a single clade (clade 1) defined by 6 unique mutations (A1763G, C5100T, G13045A, C19524T,

28027Δ129, and C29741T), whereas 1 resided within a second clade defined by a distinct set of 6 mutations (clade 2). Two additional mutations divided clade 1 into 3 subclades: subclade 1a (14 sequences, defined by A11875G), subclade 1b (2 sequences, defined by C15928T), and subclade 1c (2 sequences, defined by neither mutation).

To assess the reliability with which B.1.351 was inferred to be present in the wastewater samples, and to genetically relate the wastewater samples to the individual clinical specimens, we searched the wastewater sequences from Albany and the nearby cities of Corvallis and Dallas for matches to the additional mutations identified in the individual specimens. For the 6 mutations defining clade 1, 6 of the 7 wastewater sequences matched ≥3 mutations and 3 matched all 6 mutation sites (Table; Appendix Figure 1). Three wastewater samples matched clade 1a (defined by mutation A11875G), and 4 samples matched clade 1b (defined by mutation C15928T). Two wastewater samples from Albany (ALB-Inf-03-30-21-A and ALB-Inf-04-07-21-A) matched both mutations, suggesting that those samples contained a mixture of SARS-CoV-2 RNA from both subclades. None of the wastewater samples exhibited mutations characteristic of clade 2, which included only 1 individual clinical specimen. The matches of the wastewater sequences to the additional mutations specific to clade 1 found

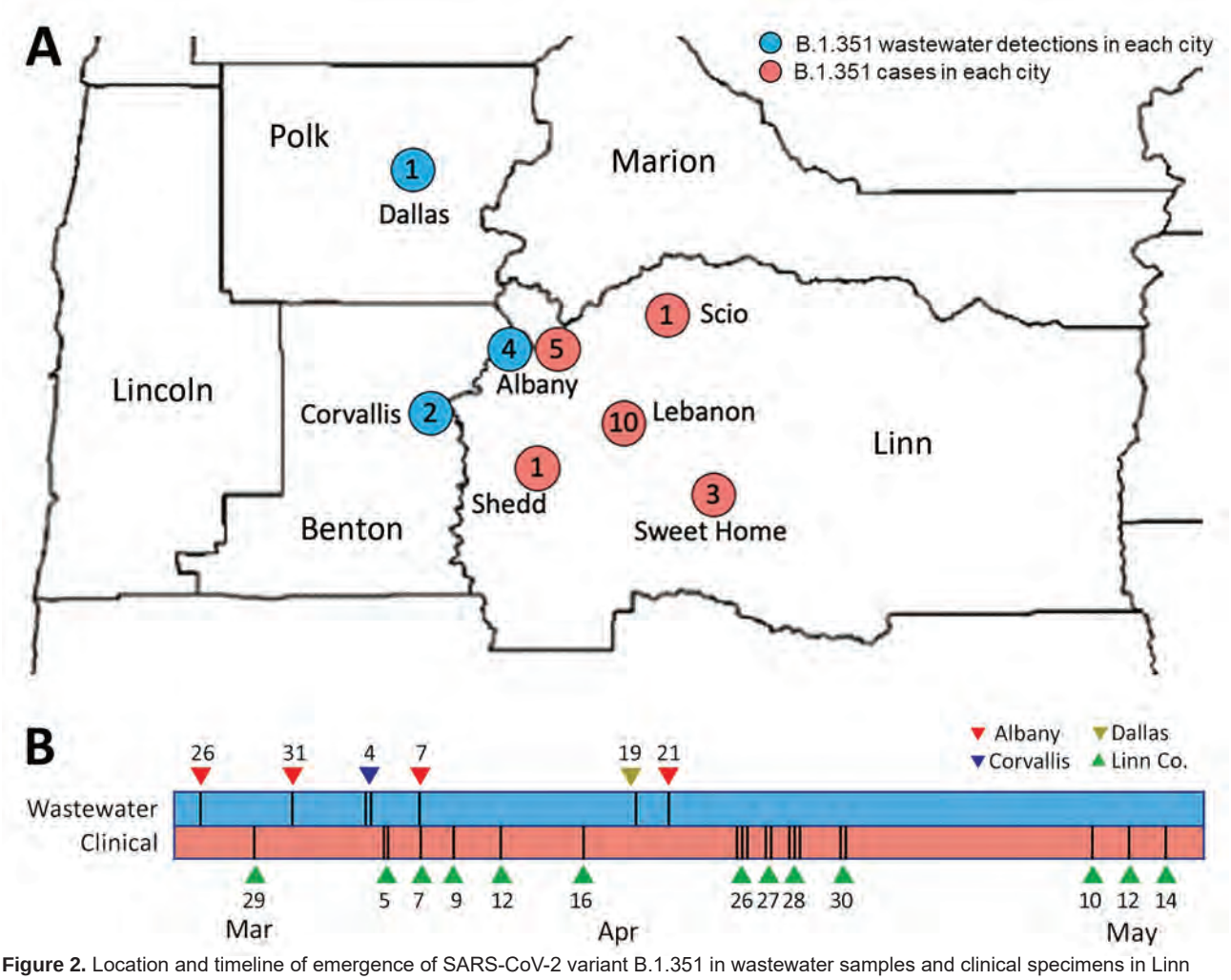

Figure 2. Location and timeline of emergence of SARS-CoV-2 variant B.1.351 in wastewater samples and clinical specimens in Linn County, Oregon, USA, and surrounding jurisdictions, March–May 2021. A) Blue dots represent the sites and numbers of wastewater samples with detections of the B.1.351 variant in Linn County and surrounding jurisdictions. Red dots represent the location and number of individual cases of B.1.351 in Linn County. Initial wastewater samples with evidence of the B.1.351 variant of concern were collected from Albany, Oregon, during March 26–31, 2021, and the first case of B.1.351 infection in Linn County was reported on April 23, 2021 (specimen collection date of April 7, 2021); 18 additional cases were identified through May 15, 2021, including cases with earlier specimen collection dates. B) Timeline of wastewater samples and clinical specimens positive for B.1.351 in Linn County and surrounding jurisdictions. Vertical bars indicate the number of samples or specimens collected on each date. City locations are not given to limit identifiability of individual case-patients.

in most Linn County cases substantially increase the confidence that B.1.351 RNA sequences were correctly identified in the wastewater samples.

We further assessed the sequences of each of the 7 wastewater samples for the presence of 6 additional mutations characteristic of B.1.351 but shared by other variants, including B.1.1.7, B.1.526, and P.1 (Appendix Table 8). To determine if interfering variants were present, we screened the sequences of each wastewater sample for mutations unique to those variants. We did not detect interfering variants in either of the 2 initial wastewater samples (ALB-Inf-03-26-21-A and ALB-03-30-21-A), and both samples exhibited all 6 of the additional shared mutations (Appendix Figure 1). These results provide further evidence for the true identification of B.1.351 in the initial 2 wastewater samples collected in Albany. The remaining 5 wastewater samples from Albany (ALB-Inf-04-07-21-A and ALB-Inf-04-21-21-A), Corvallis (COR-25th-04-04-21-A and COR-26th-04-04-21-A), and Dallas (DAL-Inf-04-19-21-A) demonstrated mutations consistent with B.1.1.7 and, in 1 case, P.1 (Appendix Tables 2–7, Figure 1).

Discussion

In late March 2021, routine sequencing of SARS-CoV-2 wastewater surveillance detected the emergence of the B.1.351 (Beta) variant of concern in rural Linn County, Oregon, before its identification in individual cases. Currently, wastewater surveillance is used to track SARS-CoV-2 transmission trends in several jurisdictions and, in times of minimal transmission, may serve as an early warning system for disease resurgence (*31*). Wastewater surveillance offers local public health authorities and communities actionable data that is independent of symptomatic infection, healthcare access, and testing acceptance and may help in developing vaccination strategy (*32*). Leveraging this surveillance to support genomic surveillance for SARS-CoV-2 offers cost-effective community-level surveillance that may detect not only prevalent circulating variants but emerging variants of concern as well.

Accurate interpretation of wastewater sequencing results faces several challenges. These challenges include the heterogeneous nature of wastewater samples, the fragmentation of viral RNA in wastewater, the need to match wastewater sequences to panels of mutations characteristic of known variants, the variable levels of variant RNA in wastewater samples, the uneven sequence coverage of the viral genome in wastewater sequences, and the sharing of mutations (e.g., N501Y and E484K) across multiple variants. We used the well-established approach of MLST (*13*,*18*) in a novel application to infer the presence of RNA from SARS-CoV-2 variants in community wastewater samples from a statewide wastewater surveillance program.

MLST has been used to detect other pathogens in complex environmental samples, including wastewater. In addition, MLST has been used to analyze fragmented genetic molecules through the rigorous identification of matches to a curated set of mutations (i.e., a mutation panel) (*12*,*13*). Confidence in a detection is based on the proportion of matches to the mutation panel. Amplicon-based sequencing with the Swift Amplicon SARS-CoV-2 Panel is well-suited to MLST, providing excellent coverage of the entire SARS-CoV-2 genome, omitting only 25 bp at each end. With 341 overlapping amplicons of 150 bp on average, this method is robust to most mutations that could disrupt the binding of a primer (i.e., cause primer dropout) (N.L. Washington et al., unpub. data, https://doi.org/10.1101/2020.12.24.20248814).

To establish mutation panels suitable for screening for individual variants, we began with the canonical mutations defining each variant, derived either from the literature (*24*–*27*,*29*,*32*; I. Ferreira, unpub. data; X. Deng et al., unpub. data; M.K. Annavajhala et al., unpub. data) or from the Centers for Disease Control and Prevention (*33*). These sets of mutations were validated through the creation of an expanded panel of mutations identified in statewide individual sequencing data submitted to GISAID. Finally, all mutations shared with known variants were filtered out. This validation step would not be available to an emerging variant for which no local or regional individual-level sequencing data were available, highlighting the complementary properties of individual-level and community-level surveillance.

To address variable levels of variant RNA in the wastewater samples, we conducted in-depth sequencing, producing ≈10–30 million sequence reads per sample, to obtain sufficient sequence data to detect variants comprising as little as 10% of the RNA, even from samples with the lowest levels of viral RNA ($\log_{10}$ gene copies/L of 4.0). To address uneven sequence coverage of the viral genome in wastewater sequences, ranging from <10 to >1,000 reads per amplicon within a single sample, the sequence coverage was normalized to 100 reads per site for mutation sites with coverage of >100 reads. For sites with coverage of <100 reads per site, the actual read numbers were used to assign a proportionately smaller weight to those more poorly sequenced mutation sites.

In this study, we used a panel of 9 mutations identified as specific to B.1.351 to screen for the presence

of this emerging variant of concern. We then used a subsequent panel of 8 additional mutations defining a single clade of B.1.351 sequences identified through statewide individual specimen sequencing to validate the initial set of matches, together with a case-by-case examination of a set of 6 mutations characteristic of B.1.351 but shared with other variants. This 2-step process of screening followed by validation, together with the large number of mutations within the screening and validation panels, rendered the detection of B.1.351 robust to small numbers of mismatches that occurred because of low sequence coverage, low levels of variant RNA, or primer dropout. The ability to compare independent but geographically or temporally related wastewater samples with closely related individual sequences substantially increased confidence in our detection of B.1.351 through wastewater surveillance (Figure 2).

All 7 wastewater sequences and 18 of 19 B.1.351 individual clinical specimen sequences clustered into a single clade (clade 1). The similarity of the sequences and their spatiotemporal proximity suggests a single common origin of the detected viruses. The SARS-CoV-2 sequences most closely related to the sequences in clade 1 were found in Switzerland (Figure 1), suggesting that the Oregon clade 1 cluster in Linn County may have originated from outside the United States. Even though B.1.351 was detected in the wastewater of the nearby cities of Corvallis (Benton County; OSU-25th-04-04-21-A) and Dallas (Polk County; DAL-Inf-04-19-21-A), no cases were identified in Benton or Polk Counties during this period. Thus, the detection of B.1.351 in these 2 counties may have resulted from the transient presence of cases from neighboring counties or may simply reflect insufficient individual-level genomic surveillance to detect B.1.351 in those areas.

Together, the complementary wastewater and clinical data we present clearly support community transmission of the B.1.351 variant in the Linn County region from late March through mid-May 2021. Wastewater sampling detected this emerging variant of concern 12 days before the specimen collection date of the first local case-patient. Wastewater surveillance therefore may be an efficient and reliable means of community-level monitoring for emerging SARS-CoV-2 variants and other human pathogens. Additional studies such as ours must be replicated across rural and urban settings to further understanding of the generalizability and limitations of wastewater surveillance. Scientific consensus regarding methods and minimum thresholds for variant detection in wastewater are urgently needed.

Acknowledgments

This project was conducted in close partnership with the Oregon State University TRACE project (https://trace.oregonstate.edu) and the City of Albany Oregon Public Works Department employees. The authors thank the members of the TRACE leadership team (Benjamin Dalziel, Jeff Bethel, Roy Haggerty, Javier Nieto, Kathryn Higley, Katherine McLaughlin, and Jane Lubchenco) for their support and advice.

Funding for this study came from the National Science Foundation (to T.R. and C.K., award no. 2027679), the David and Lucile Packard Foundation (to the TRACE project), Oregon State University (to the TRACE project, T.R., C.K., and B.M.T.), and the Centers for Disease Control and Prevention (cooperative agreement nos. CK17-1701 and CK-19-1904).

About the Author

Dr. Sutton is medical director of respiratory viral pathogens at Oregon Health Authority. Her research interests include respiratory viral pathogen surveillance, infectious disease epidemiology, and the social determinants of health.

References

1. World Health Organization. WHO coronavirus (COVID-19) dashboard [cited 2022 Mar 29] https://covid19.who.int
2. Centers for Disease Control and Prevention. COVID data tracker weekly review [cited 2022 Mar 29]. https://www.cdc.gov/coronavirus/2019-ncov/covid-data/covidview/index.html
3. Walensky RP, Walke HT, Fauci AS. SARS-CoV-2 variants of concern in the United States—challenges and opportunities. JAMA. 2021;325:1037–8. https://doi.org/10.1001/jama.2021.2294
4. Lo SW, Jamrozy D. Genomics and epidemiological surveillance. Nat Rev Microbiol. 2020;18:478. https://doi.org/10.1038/s41579-020-0421-0
5. Robishaw JD, Alter SM, Solano JJ, Shih RD, DeMets DL, Maki DG, et al. Genomic surveillance to combat COVID-19: challenges and opportunities. Lancet Microbe. 2021;2:e481–4. https://doi.org/10.1016/S2666-5247(21)00121-X
6. Rader B, Astley CM, Sy KTL, Sewalk K, Hswen Y, Brownstein JS, et al. Geographic access to United States SARS-CoV-2 testing sites highlights healthcare disparities and may bias transmission estimates. J Travel Med. 2020;27:taaa076.
7. Contreras S, Dehning J, Loidolt M, Zierenberg J, Spitzner FP, Urrea-Quintero JH, et al. The challenges of containing SARS-CoV-2 via test-trace-and-isolate. Nat Commun. 2021;12:378. https://doi.org/10.1038/s41467-020-20699-8
8. Thompson JR, Nancharaiah YV, Gu X, Lee WL, Rajal VB, Haines MB, et al. Making waves: wastewater surveillance of SARS-CoV-2 for population-based health management. Water Res. 2020;184:116181. https://doi.org/10.1016/j.watres.2020.116181
9. Medema G, Heijnen L, Elsinga G, Italiaander R, Brouwer A. Presence of SARS-Coronavirus-2 RNA in sewage and

correlation with reported COVID-19 prevalence in the early stage of the epidemic in the Netherlands. Environ Sci Technol Lett. 2020;7:511–6. https://doi.org/10.1021/acs.estlett.0c00357
10. Daughton CG. Wastewater surveillance for population-wide Covid-19: The present and future. Sci Total Environ. 2020; 736:139631. https://doi.org/10.1016/j.scitotenv.2020.139631
11. Izquierdo-Lara R, Elsinga G, Heijnen L, Munnink BBO, Schapendonk CME, Nieuwenhuijse D, et al. Monitoring SARS-CoV-2 circulation and diversity through community wastewater sequencing, the Netherlands and Belgium. Emerg Infect Dis. 2021;27:1405–15. https://doi.org/10.3201/eid2705.204410
12. Durigan M, Abreu AG, Zucchi MI, Franco RMB, de Souza AP. Genetic diversity of *Giardia duodenalis*: multilocus genotyping reveals zoonotic potential between clinical and environmental sources in a metropolitan region of Brazil. PLoS One. 2014;9:e115489. https://doi.org/10.1371/journal.pone.0115489
13. Ma J, Feng Y, Hu Y, Villegas EN, Xiao L. Human infective potential of *Cryptosporidium* spp., *Giardia duodenalis* and *Enterocytozoon bieneusi* in urban wastewater treatment plant effluents. J Water Health. 2016;14:411–23. https://doi.org/10.2166/wh.2016.192
14. Ibarz Pavón AB, Maiden MCJ. Multilocus sequence typing. Methods Mol Biol. 2009;551:129–40. https://doi.org/10.1007/978-1-60327-999-4_11
15. Maiden MCJ, Bygraves JA, Feil E, Morelli G, Russell JE, Urwin R, et al. Multilocus sequence typing: a portable approach to the identification of clones within populations of pathogenic microorganisms. Proc Natl Acad Sci U S A. 1998;95:3140–5. https://doi.org/10.1073/pnas.95.6.3140
16. Urwin R, Maiden MC. Multi-locus sequence typing: a tool for global epidemiology. Trends Microbiol. 2003;11:479–87. https://doi.org/10.1016/j.tim.2003.08.006
17. Wang Z-G, Zheng Z-H, Shang L, Li L-J, Cong LM, Feng MG, et al. Molecular evolution and multilocus sequence typing of 145 strains of SARS-CoV. FEBS Lett. 2005;579:4928–36. https://doi.org/10.1016/j.febslet.2005.07.075
18. Charpentier E, Garnaud C, Wintenberger C, Bailly S, Murat J-B, Rendu J, et al. Added value of next-generation sequencing for multilocus sequence typing analysis of a *Pneumocystis jirovecii* pneumonia outbreak. Emerg Infect Dis. 2017;23:1237–45. https://doi.org/10.3201/eid2308.161295
19. Centers for Disease Control and Prevention. COVID data tracker. 2021 [cited 2021 Jul 18]. https://covid.cdc.gov/covid-data-tracker/#datatracker-home.
20. Elbe S, Buckland-Merrett G. Data, disease and diplomacy: GISAID's innovative contribution to global health. Glob Chall. 2017;1:33–46. https://doi.org/10.1002/gch2.1018
21. Robinson JT, Thorvaldsdóttir H, Winckler W, Guttman M, Lander ES, Getz G, et al. Integrative genomics viewer. Nat Biotechnol. 2011;29:24–6. https://doi.org/10.1038/nbt.1754
22. Robinson JT, Thorvaldsdóttir H, Wenger AM, Zehir A, Mesirov JP. Variant review with the Integrative Genomics Viewer. Cancer Res. 2017;77:e31–4. https://doi.org/10.1158/0008-5472.CAN-17-0337
23. Rambaut A, Loman N, Pybus O, Barclay W, Barrett J, Carabelli A, et al. Preliminary genomic characterisation of an emergent SARS-CoV-2 lineage in the UK defined by a novel set of spike mutations. 2020 [cited 2021 Aug 12]. https://virological.org/t/preliminary-genomic-characterisation-of-an-emergent-sars-cov-2-lineage-in-the-uk-defined-by-a-novel-set-of-spike-mutations/563
24. Fujino T, Nomoto H, Kutsuna S, Ujiie M, Suzuki T, Sato R, et al. Novel SARS-CoV-2 variant in travelers from Brazil to Japan. Emerg Infect Dis. 2021;27:1243–5. https://doi.org/10.3201/eid2704.210138
25. Faria NR, Claro IM, Candido D, Franco LM, Andrade PS, Coletti TM, et al. Genomic characterisation of an emergent SARS-CoV-2 lineage in Manaus: preliminary findings. 2021 [cited 2021 Aug 12]. https://virological.org/t/genomic-characterisation-of-an-emergent-sars-cov-2-lineage-in-manaus-preliminary-findings/586
26. Naveca F, Nascimento V, Souza V, Corado A, Nascimento F, Silva G, et al. Phylogenetic relationship of SARS-CoV-2 sequences from Amazonas with emerging Brazilian variants harboring mutations E484K and N501Y in the Spike protein. 2021 [cited 2021 Aug 12]. https://virological.org/t/phylogenetic-relationship-of-sars-cov-2-sequences-from-amazonas-with-emerging-brazilian-variants-harboring-mutations-e484k-and-n501y-in-the-spike-protein/585
27. Zhang W, Davis BD, Chen SS, Sincuir Martinez JM, Plummer JT, Vail E. Emergence of a novel SARS-CoV-2 variant in Southern California. JAMA. 2021;325:1324–6. https://doi.org/10.1001/jama.2021.1612
28. World Health Organization. Weekly epidemiological update on COVID-19, 27 April 2021 [cited 2021 Aug 12]. https://www.who.int/publications/m/item/weekly-epidemiological-update-on-covid-19—27-april-2021
29. Kannan L, Wheeler WC. Maximum parsimony on phylogenetic networks. Algorithms Mol Biol. 2012;7:9. https://doi.org/10.1186/1748-7188-7-9
30. Sayers EW, Barrett T, Benson DA, Bolton E, Bryant SH, Canese K, et al. Database resources of the national center for biotechnology information. Nucleic Acids Res. 2011;39(suppl_1):D38–51. https://doi.org/10.1093/nar/gkq1172
31. Venugopal A, Ganesan H, Sudalaimuthu Raja SS, Govindasamy V, Arunachalam M, Narayanasamy A, et al. Novel wastewater surveillance strategy for early detection of coronavirus disease 2019 hotspots. Curr Opin Environ Sci Health. 2020;17:8–13. https://doi.org/10.1016/j.coesh.2020.05.003
32. Smith T, Cassell G, Bhatnagar A. Wastewater surveillance can have a second act in COVID-19 vaccine distribution. JAMA Health Forum. 2021;2:e201616. https://doi.org/10.1001/jamahealthforum.2020.1616
33. Centers for Disease Control and Prevention. SARS-CoV-2 variant classifications and definitions. 2021 [cited 2021 Aug 12]. https://www.cdc.gov/coronavirus/2019-ncov/variants/variant-info.html

Address for correspondence: Melissa Sutton, Public Health Division, Oregon Health Authority, 800 NE Oregon St, Ste 772, Portland, OR 97232, USA; email: melissa.sutton@dhsoha.state.or.us

Antimicrobial-Resistant *Shigella* spp. in San Diego, California, USA, 2017–2020

Thaidra Gaufin, Jill Blumenthal, Claudia Ramirez-Sanchez, Sanjay Mehta, David T. Pride, Joshua Fierer, Jeffrey D. Jenks

Medscape EDUCATION ACTIVITY

In support of improving patient care, this activity has been planned and implemented by Medscape, LLC and Emerging Infectious Diseases. Medscape, LLC is jointly accredited by the Accreditation Council for Continuing Medical Education (ACCME), the Accreditation Council for Pharmacy Education (ACPE), and the American Nurses Credentialing Center (ANCC), to provide continuing education for the healthcare team.

Medscape, LLC designates this Journal-based CME activity for a maximum of 1.00 ***AMA PRA Category 1 Credit(s)™***. Physicians should claim only the credit commensurate with the extent of their participation in the activity.

Successful completion of this CME activity, which includes participation in the evaluation component, enables the participant to earn up to 1.0 MOC points in the American Board of Internal Medicine's (ABIM) Maintenance of Certification (MOC) program. Participants will earn MOC points equivalent to the amount of CME credits claimed for the activity. It is the CME activity provider's responsibility to submit participant completion information to ACCME for the purpose of granting ABIM MOC credit.

All other clinicians completing this activity will be issued a certificate of participation. To participate in this journal CME activity: (1) review the learning objectives and author disclosures; (2) study the education content; (3) take the post-test with a 75% minimum passing score and complete the evaluation at http://www.medscape.org/journal/eid; and (4) view/print certificate. For CME questions, see page 1311.

Release date: May 17, 2022; Expiration date: May 17, 2023

Learning Objectives

Upon completion of this activity, participants will be able to:

- Evaluate the microbiology of *Shigella* spp.
- Analyze characteristics of patients with infection with *Shigella* spp. in the current study
- Distinguish rates of antimicrobial resistance among *Shigella* spp. in the current study
- Assess risk factors for antibiotic resistance among *Shigella* spp. in the current study.

CME Editor

P. Lynne Stockton Taylor, VMD, MS, ELS(D), Technical Writer/Editor, Emerging Infectious Diseases. *Disclosure: P. Lynne Stockton Taylor, VMD, MS, ELS(D), has disclosed no relevant financial relationships.*

CME Author

Charles P. Vega, MD, Health Sciences Clinical Professor of Family Medicine, University of California, Irvine School of Medicine, Irvine, California. *Disclosure: Charles P. Vega, MD, has disclosed the following relevant financial relationships: served as an advisor or consultant for GlaxoSmithKline; Johnson & Johnson Pharmaceutical Research & Development, L.L.C.*

Authors

Thaidra Gaufin, MD; Jill Blumenthal, MD; Claudia Ramirez-Sanchez, MD; Sanjay Mehta, MD; David T. Pride; Joshua Fierer, MD; and ***Jeffrey D. Jenks, MD, MPH.***

Author affiliations: Sansum Clinic Infectious Diseases, Santa Barbara, California, USA (T. Gaufin); University of California San Diego, La Jolla, California, USA (J. Blumenthal, C. Ramirez-Sanchez, S. Mehta, D.T. Pride, J. Fierer); San Diego Veterans Affairs Medical Center, San Diego (S. Mehta, J. Fierer); Durham County Department of Public Health, Durham, North Carolina, USA (J.D. Jenks)

DOI: https://doi.org/10.3201/eid2806.220131

Annually, *Shigella* spp. cause ≈188 million cases of diarrheal disease globally, including 500,000 cases in the United States; rates of antimicrobial resistance are increasing. To determine antimicrobial resistance and risk factors in San Diego, California, USA, we retrospectively reviewed cases of diarrheal disease caused by *Shigella flexneri* and *S. sonnei* diagnosed during 2017–2020. Of 128 evaluable cases, *S. flexneri* was slightly more common than *S. sonnei*; most cases were in persons who were gay or bisexual cisgender men, were living with HIV, were unhoused, or used methamphetamines. Overall, rates of resistance to azithromycin, fluoroquinolones, ampicillin, and trimethoprim/sulfamethoxazole (TMP/SMX) were comparable to the most recent national data reported from the Centers for Disease Control and Prevention; 55% of isolates were resistant to azithromycin, 23% to fluoroquinolones, 70% to ampicillin, and 83% to TMP/SMX. The rates that we found for TMP/SMX were slightly higher than those in national data.

Shigella bacteria are facultatively anaerobic, nonmotile, gram-negative bacilli and a common global cause of infectious diarrhea, especially in low-income settings (*1*). They are relatively resistant to the high acidity of the stomach and can survive transit into the small intestine, where they multiply and pass into the colon, invading colonic cells and causing diarrhea. As few as 10–100 organisms are capable of causing disease (*2*). This low infectious dose increases transmission by the fecal–oral route or via contaminated food and water. Globally, *Shigella* spp. cause an estimated 188 million cases of diarrheal disease annually and account for 164,000 deaths (*1*), particularly in children.

In the United States, ≈500,000 cases of shigellosis occur annually; 81% are caused by *Shigella sonnei*, followed by *S. flexneri* (12.6%), *S. boydii* (0.2%), and *S. dysenteriae* (0.1%) (*3*). Most transmission occurs via the fecal–oral route, at locations such as daycare centers, but transmission can also occur after ingesting contaminated food or drinking water, after ingesting untreated recreational water (*4*), and among men who have sex with men (MSM). Among MSM, multiple outbreaks have been described in Montreal, Quebec, Canada (*5*,*6*), and Germany (*7*); and in the United States (*8*,*9*), including Minnesota (*10*); the Chicago, Illinois, and Minneapolis-St. Paul, Minnesota, regions (*11*); and New York, New York (*12*).

For children and adults with symptomatic shigellosis, antimicrobial therapy is typically recommended because it shortens symptom duration and decreases the duration of bacterial shedding in adults (*13*) and children (*14*–*17*). For children, antimicrobial therapy should be guided by local resistance profiles. For adults, empiric antimicrobial therapy selection should be guided by local resistance profiles as well as patient demographics. For example, in parts of Asia, widespread resistance to azithromycin, ceftriaxone, and ciprofloxacin has been reported (*18*,*19*). In addition, increasing antimicrobial resistance has been found in certain groups, such as MSM, and has also been associated with travel (*20*), including increasing resistance to first-line agents such as fluoroquinolones (*5*,*7*) and azithromycin (*8*). Last, susceptibilities obtained from culture should be used in the event of treatment failure.

To determine antimicrobial resistance and risk factors in the San Diego, California, USA, area, we investigated cases of symptomatic shigellosis causing diarrheal disease at the University of California San Diego Health System and San Diego Veterans Affairs Medical Center over a 3-year period. The study was approved by the Human Research Protection Program at University of California San Diego Health and the San Diego Veterans Affairs Institutional Review Board.

Methods

We analyzed the electronic health records (EHRs) of persons ≥18 years of age who received care at the University of California San Diego Health System or the San Diego Veterans Affairs Medical Center from March 1, 2017, through May 31, 2020, for diarrhea and a diagnosis of shigellosis. We did not include persons <18 years of age because those data were not accessible in our EHR.

Stool samples from study participants were cultured or tested initially with a multiplex PCR panel ordered by providers at the University of California San Diego Health System or the San Diego Veterans Affairs Medical Center. Isolates that were positive for *Shigella* spp. on multiplex PCR were confirmed by stool culture for *Shigella* spp. on matrix-assisted laser desorption/ionization-time of flight mass spectrometry. Those isolates were then sent to the San Diego County Public Health laboratory to confirm speciation.

For persons for whom *Shigella* spp. isolation from stool culture was confirmed, we collected further information through EHR review. Information included patient ethnicity, race, age at diagnosis, history of travel out of San Diego County within 14 days before diagnosis, housing status, recent methamphetamine use, HIV status, use of highly active antiretroviral therapy (HAART), or use of preexposure prophylaxis (PrEP) for HIV prevention.

The most frequently reported antimicrobial susceptibility panel for *S. flexneri* and *S. sonnei* includes

ampicillin, a fluoroquinolone, and trimethoprim-sulfamethoxazole (TMP/SMX); thus, we included these antimicrobials in the comparative analysis. The specific fluoroquinolone reported at each site differed. Most were ciprofloxacin; however, other fluoroquinolones, such as moxifloxacin or levofloxacin, were reported for a few persons. For the purpose of comparative analysis, we grouped fluoroquinolones together and reported them as either sensitive or resistant; we identified intermediate strains as resistant. We used broth microdilution for susceptibility testing. The standards for resistance were set by the Clinical and Laboratory Standards Institute (CSLI, https://clsi.org). The standards changed in 2022 (*21*), when CSLI began including azithromycin susceptibility, but we did not use these latest guidelines for our study because our data included only time points until May 2020.

We analyzed the data by using SPSS Statistics 27 (IBM, https://www.ibm.com) and descriptive statistics via cross-tabulations with the Fisher exact test and χ^2 by creating a 2-by-2 table comparing different variables: resistance of various antimicrobials cross-tabulated with HIV status, sexual orientation, use of HAART if living with HIV, use of PrEP, being unhoused, or recent use of methamphetamines. We included methamphetamine use because this information was readily available on chart review (based either on positive urine toxicology screen or documented recent use in physician notes). Data associated with other substance use on chart review were not available. We considered $p<0.05$ to indicate statistical significance.

Results

Of the 140 EHRs for patients for whom *Shigella* spp. was isolated from ≥1 stool specimen, we included 128 in our analysis and excluded 12 (for 6, the *Shigella* isolate was not speciated; for 2, *S. boydii* was isolated from stool culture; for 2, there was not enough information to complete the analysis; and for 2, duplicate positive isolates were obtained within a 2-week period). Overall, 55% of *Shigella spp.* isolates were identified as *S. flexneri* and 45% as *S. sonnei*. Patient ages ranged from 15–79 years; mean age was 47 years (Table 1). Eighty-one percent were male. Most patients self-identified as non-Hispanic white. Fifty-six percent identified as gay or bisexual male (GBM), and 3 identified as transgender women who had sex with men. Fifty-one percent were living with HIV, among whom 85% were receiving HAART; for 11%, HIV status was unknown. Twenty-three percent were unhoused, and for 33%, recent methamphetamine use was documented.

S. flexneri infection was more common than *S. sonnei* infection among those who were living with HIV (68% vs. 43%; $p = 0.008$), were not unhoused (92% vs. 60%; $p<0.001$), did not use methamphetamines (77% vs. 54%; $p = 0.006$), and had not recently traveled (63% vs. 24%; $p = 0.008$) (Table 2). Sexual orientation and use of HAART and PrEP were not associated with *S. flexneri* or *S. sonnei* infection.

Of the 128 evaluable isolates, 23% were resistant to fluoroquinolones (11% of *S. flexneri* and 39% of *S. sonnei* isolates). Overall, 70% of *Shigella* spp. isolates were resistant to ampicillin (87% of *S. flexneri* and 47% of *S. sonnei* isolates), and 83% of all isolates were resistant to TMP/SMX (73% of *S. flexneri* and 95% of *S. sonnei* isolates). Only 4 (3%) isolates were susceptible to fluoroquinolones, TMP/SMX, and ampicillin; 38% were resistant to 1 antimicrobial (27% for *S. flexneri* vs. 53% for *S. sonnei*), 38% were resistant to 2 antimicrobials (62% for *S. flexneri* vs. 9% for *S. sonnei*), and 20% were resistant to 3 antimicrobials (7% for *S. flexneri* vs. 37% for *S. sonnei*) (Appendix, https://wwwnc.cdc.gov/EID/article/28/6/22-0131-App1.pdf).

Compared with persons without HIV infection, a higher percentage of *Shigella* isolates from persons with HIV infection and shigellosis were resistant to ≥2 antimicrobials (32% vs. 11%; $p<0.001$), and the rate of ampicillin resistance was higher for persons with than without HIV infection (48% vs. 30%; $p<0.001$). We found no difference between HIV status and fluoroquinolone or TMP/SMX resistance. Rates of *Shigella* resistance to 2 antimicrobials were higher for non-GBM/transgender persons than for GBM/transgender persons (41% vs. 3%; $p<0.003$).

Rates of antimicrobial resistance to 1 (25% vs. 13%; $p = 0.016$) or 2 antimicrobials (34% vs. 4%; $p = 0.009$) were higher for persons with stable housing than for those without stable housing; rates of resistance were higher for ampicillin (60% vs. 9%; $p<0.001$) and TMP/SMX (60% vs. 15%; $p = 0.01$). Compared with recent methamphetamines use, no methamphetamine use was associated with resistance to 2 antimicrobials (30% vs. 8%; $p = 0.021$) and higher rates of ampicillin resistance (51% vs. 19%; $p = 0.042$). Neither history of travel nor use of HAART was associated with increased antimicrobial resistance.

In the antimicrobial susceptibility panels at our sites, ceftriaxone and azithromycin were not commonly tested. Although isolates were not routinely tested against azithromycin, of the 36 isolates tested, 55% were resistant to azithromycin according to MIC breakpoints established by the 2022 CLSI m100 Performance Standards for Antimicrobial Susceptibility Testing for *Shigella* spp. (MIC >16 μg/mL for *S. flexneri*

Table 1. General characteristics of persons with diarrheal disease and *Shigella* spp. isolated from stool culture, San Diego, California, USA, March 1, 2017–May 31, 2020*

Characteristic	Frequency, no. (%)
Shigella spp. infection	
S. flexneri	71 (55)
S. sonnei	57 (45)
Sex	
M	104 (81.3)
F	21 (16.4)
Transgender, male-to-female	3 (2.3)
Ethnicity	
Hispanic/Latin	28 (21.9)
Mixed race/other	16 (12.5)
Native Hawaiian/Pacific Islander	1 (0.8)
Non-Hispanic Black	12 (9.4)
Non-Hispanic White	69 (53.9)
Unknown	2 (1.6)
Sexual orientation	
GBM/transgender	71 (55.5)
Not GBM	20 (15.6)
Unknown	37 (28.9)
HIV status	
Positive	65 (50.8)
Negative	49 (38.3)
Unknown	14 (10.9)
HAART use by persons living with HIV	
Yes	55/65 (84.6)
No	10/65 (15.4)
PrEP use among persons at risk for HIV	
Yes	8/12 (66.7)
No	4/12 (33.3)
Unhoused	
Yes	29/128 (22.7)
No	99/128 (77.3)
Methamphetamine use	
Yes	42/128 (32.8)
GBM/transgender	24/42 (57)
Unhoused	24/42 (57)
HIV positive	23/42 (55)
No	86/128 (67.2)
Travel history (international and domestic travel)	
Yes	20/128 (15.6)
No	67/128 (52.3)
Unknown	41/128 (32.0)

*Patient age range 15–79 y, mean age 47 y. GBM, gay and bisexual man; HAART, highly active antiretroviral therapy; PrEP, preexposure prophylaxis.

and >32 μg/mL for *S. sonnei*) (*21*). Azithromycin started to become more frequently tested at 1 of the sites by August 2019. Of the 128 samples analyzed, ceftriaxone susceptibility was reported for 37% of the cases without any reported resistance.

Discussion

According to our retrospective review, *S. flexneri* and *S. sonnei* caused diarrheal disease in a large number of gender and sexual minorities who were living with HIV, persons of unhoused status, and persons who had recently used methamphetamines. Although the association between MSM and shigellosis has been reported, the rate of concomitant HIV infection and shigellosis in our study was higher than rates previously reported, including in a study of New York, New York, residents, in which 27% with shigellosis infection were living with HIV (*12*). In addition, although methamphetamine use by MSM can increase the risk for HIV and for hepatitis C virus infection (*22*,*23*), to our knowledge only a small number of reports have described an association between methamphetamine use and shigellosis, specifically among MSM (*24*,*25*). Unlike the studies that documented methamphetamine use in MSM living with HIV, we also found high rates among those who were unhoused.

Isolation of *S. flexneri* from 55% of stool specimens in our study is much higher than the national prevalence of 12.6% in 2016 reported by the Centers for Disease Control and Prevention (CDC) (*26*). Other studies have found high rates of *S. flexneri* causing shigellosis in certain populations, including in 34% of sporadic cases in a New York, New York, study

Table 2. Variables associated with *Shigella flexneri* and *Shigella sonnei* Infection, San Diego, California, USA, March 1, 2017–May 31, 2020*

Patient variable	*Shigella flexneri*, no. (%)	*Shigella sonnei*, no. (%)	p value
HIV positive	44 (68)	21 (43)	0.008
Sexual orientation, GBM/transgender woman	45 (85)	26 (68)	0.061
HAART use by persons living with HIV	40 (91)	15 (71)	0.065
PrEP use among HIV-negative	4 (80)	4 (57)	0.408
Unhoused	6 (8)	23 (40)	<0.001
Methamphetamine use	16 (23)	26 (46)	0.006
Travel	11 (15)	9 (20)	0.008

*GBM, gay and bisexual man; HAART, highly active antiretroviral therapy; PrEP, preexposure prophylaxis.

(*12*) and 65% of cases from a cohort of MSM in the United States (*22*). Similarly, we found high rates of *S. flexneri* in GBM/transgender persons, persons living with HIV, and those receiving PrEP. Thus, although overall *S. flexneri* prevalence may be low in the United States, rates may be higher for certain populations, such as those reported here.

Increasing antimicrobial resistance of *Shigella* spp. has been documented globally, including in the United States. Clusters of ciprofloxacin-resistant *S. sonnei* have been reported, suspected to be associated with international travel, and 86% of isolates have been reported to be resistant (*27*). Conversely, in another study of shigellosis in MSM, all isolates were sensitive to ciprofloxacin (*28*). In our cohort, 23% of isolates were resistant to ciprofloxacin. Among MSM, decreasing susceptibility to azithromycin (MIC ≥32 μg/mL) in several *S. sonnei* outbreaks has been documented (*29*), including all isolates either resistant to (*11*) or with detected *mph*A or *erm*B macrolide resistance genes (*8*,*11*,*29*). We also detected a large number of isolates for which susceptibility to azithromycin was reduced.

Rates of antimicrobial resistance among the isolates tested were comparable to those reported in the most recent data from the CDC National Antimicrobial Resistance Monitoring System (NARMS) data (https://wwwn.cdc.gov/narmsnow), which included mostly *S. flexneri* and *S. sonnei* isolates. Among all *Shigella spp*. isolates, 55% of the isolates in our study were resistant to azithromycin compared with 54% from preliminary NARMS estimates from 2021, 23% were resistant to fluoroquinolones compared with 32% from NARMS (ciprofloxacin only), 70% were resistant to ampicillin compared with 79% from NARMS, and 83% were resistant to TMP/SMX compared with 75% from NARMS. We found no resistance to ceftriaxone in our study, which could be reflective of a smaller sample size, although of 28 isolates in 2021, only 1 (3.6%) was resistant to ceftriaxone according to NARMS data. The most recent NARMS data report a rate of 25% of resistance to ampicillin, ciprofloxacin, and TMP/SMX, which is comparable to the resistance rate of 20% to these 3 antimicrobial drugs in our study.

It is unclear why those who are unhoused in San Diego County may be at risk for shigellosis. Of note, a hepatitis A outbreak during 2016–2018 in San Diego County, which was the largest US hepatitis A outbreak in 2 decades, primarily involved persons experiencing unstable housing conditions, those who used drugs in unsanitary settings, or both (*30*). It is possible that unsanitary living conditions and illicit drug use also predispose unhoused persons to shigellosis, although further research would help clarify.

Our first study limitation is including data from only 2 medical centers in San Diego County, California, which means that our findings may not be representative of other locations within the United States or elsewhere globally. The high proportion of GBM/transgender, HIV-infected, unhoused, and methamphetamine-using persons may be unique to our setting and may not be reflective of other settings because it may not be reflective of the general population in San Diego County. Second, isolates were not routinely tested against azithromycin, which would have been helpful because this drug has traditionally been empirically used to treat shigellosis. Regardless, because most of the isolates tested were resistant to azithromycin according to the MICs, resistance to azithromycin in our setting is probably high, indicating that empiric use of azithromycin may not be beneficial. Third, given that the study was a retrospective review of EHRs, inconsistent availability of documentation of HIV status, travel, unhoused status, or methamphetamine use could have led to missing data.

In conclusion, in this retrospective study, we found shigellosis frequently diagnosed for GBM/transgender, HIV-seropositive, and unhoused persons who use methamphetamine; rates of *S. flexneri* prevalence were higher than those in national prevalence data. Overall, we found high rates of resistance to azithromycin, fluoroquinolones, ampicillin, and TMP/SMX, which were comparable to those most recently reported by CDC, except we found slightly

lower resistance rates to ciprofloxacin and slightly higher resistance rates to TMP/SMX. Clinicians should remain aware of the risk for antimicrobial resistance among patients with shigellosis, particularly gender and sexual minorities, those living with HIV, persons of unhoused status, and persons who use methamphetamines.

About the Author

Dr. Gaufin recently completed an infectious diseases fellowship at the University of California San Diego. She currently works in clinical infectious diseases at the Sansum Clinic in Santa Barbara.

References

1. Kotloff KL, Riddle MS, Platts-Mills JA, Pavlinac P, Zaidi AKM. Shigellosis. Lancet. 2018;391:801–12. https://doi.org/10.1016/S0140-6736(17)33296-8g
2. Bennish ML. Potentially lethal complications of shigellosis. Rev Infect Dis. 1991;13(Suppl 4):S319–24. https://doi.org/10.1093/clinids/13.Supplement_4.S319
3. Centers for Disease Control and Prevention. National Enteric Disease Surveillance: *Shigella* annual report [cited 2022 Jan 5]. https://www.cdc.gov/nationalsurveillance/pdfs/LEDS-Shig-2016-REPORT-508.pdf
4. Graciaa DS, Cope JR, Roberts VA, Cikesh BL, Kahler AM, Vigar M, et al. Outbreaks associated with untreated recreational water—United States, 2000–2014. MMWR Morb Mortal Wkly Rep. 2018;67:701–6. https://doi.org/10.15585/mmwr.mm6725a1
5. Gaudreau C, Ratnayake R, Pilon PA, Gagnon S, Roger M, Lévesque S. Ciprofloxacin-resistant *Shigella sonnei* among men who have sex with men, Canada, 2010. Emerg Infect Dis. 2011;17:1747–50. https://doi.org/10.3201/eid1709.102034
6. Gaudreau C, Barkati S, Leduc JM, Pilon PA, Favreau J, Bekal S. *Shigella* spp. with reduced azithromycin susceptibility, Quebec, Canada, 2012–2013. Emerg Infect Dis. 2014;20:854–6. https://doi.org/10.3201/eid2005.130966
7. Hoffmann C, Sahly H, Jessen A, Ingiliz P, Stellbrink HJ, Neifer S, et al. High rates of quinolone-resistant strains of *Shigella sonnei* in HIV-infected MSM. Infection. 2013;41:999–1003. https://doi.org/10.1007/s15010-013-0501-4
8. Heiman KE, Karlsson M, Grass J, Howie B, Kirkcaldy RD, Mahon B, et al.; Centers for Disease Control and Prevention (CDC). Notes from the field: *Shigella* with decreased susceptibility to azithromycin among men who have sex with men—United States, 2002–2013. MMWR Morb Mortal Wkly Rep. 2014;63:132–3.
9. Bowen A, Grass J, Bicknese A, Campbell D, Hurd J, Kirkcaldy RD. Elevated risk for antimicrobial drug-resistant *Shigella* infection among men who have sex with men, United States, 2011–2015. Emerg Infect Dis. 2016;22:1613–6. https://doi.org/10.3201/eid2209.160624
10. Eikmeier D, Talley P, Bowen A, Leano F, Dobbins G, Jawahir S, et al. Decreased susceptibility to azithromycin in clinical *Shigella* isolates associated with HIV and sexually transmitted bacterial diseases, Minnesota, USA, 2012–2015. Emerg Infect Dis. 2020;26:667–74. https://doi.org/10.3201/eid2604.191031
11. Bowen A, Eikmeier D, Talley P, Siston A, Smith S, Hurd J, et al.; Centers for Disease Control and Prevention (CDC). Notes from the field: outbreaks of *Shigella sonnei* infection with decreased susceptibility to azithromycin among men who have sex with men—Chicago and Metropolitan Minneapolis–St. Paul, 2014. MMWR Morb Mortal Wkly Rep. 2015;64:597–8.
12. Murray K, Reddy V, Kornblum JS, Waechter H, Chicaiza LF, Rubinstein I, et al. Increasing antibiotic resistance in *Shigella* spp. from infected New York City residents, New York, USA. Emerg Infect Dis. 2017;23:332–5. https://doi.org/10.3201/eid2302.161203
13. Christopher PR, David KV, John SM, Sankarapandian V. Antibiotic therapy for *Shigella* dysentery. Cochrane Database Syst Rev. 2010;8:CD006784.
14. Haltalin KC, Nelson JD, Ring R III, Sladoje M, Hinton LV. Double-blind treatment study of shigellosis comparing ampicillin, sulfadiazine, and placebo. J Pediatr. 1967;70:970–81. https://doi.org/10.1016/S0022-3476(67)80275-0
15. Haltalin KC, Kusmiesz HT, Hinton LV, Nelson JD. Treatment of acute diarrhea in outpatients. Double-blind study comparing ampicillin and placebo. Am J Dis Child. 1972;124:554–61. https://doi.org/10.1001/archpedi.1972.02110160092010
16. Garcia de Olarte D, Trujillo H, Agudelo N, Nelson JD, Haltalin KC. Treatment of diarrhea in malnourished infants and children. A double-blind study comparing ampicillin and placebo. Am J Dis Child. 1974;127:379–88. https://doi.org/10.1001/archpedi.1974.02110220077011
17. Nelson JD, Haltalin KC. Broad-spectrum penicillins in enteric infections of children. Ann N Y Acad Sci. 1967;145(2 Comparative A):414–22. https://doi.org/10.1111/j.1749-6632.1967.tb50240.x
18. Rahman M, Shoma S, Rashid H, El Arifeen S, Baqui AH, Siddique AK, et al. Increasing spectrum in antimicrobial resistance of *Shigella* isolates in Bangladesh: resistance to azithromycin and ceftriaxone and decreased susceptibility to ciprofloxacin. J Health Popul Nutr. 2007;25:158–67.
19. Holt KE, Thieu Nga TV, Thanh DP, Vinh H, Kim DW, Vu Tra MP, et al. Tracking the establishment of local endemic populations of an emergent enteric pathogen. Proc Natl Acad Sci U S A. 2013;110:17522–7. https://doi.org/10.1073/pnas.1308632110
20. Li YL, Tewari D, Yealy CC, Fardig D, M'ikanatha NM. Surveillance for travel and domestically acquired multidrug-resistant human *Shigella* infections—Pennsylvania, 2006–2014. Health Secur. 2016;14:143–51. https://doi.org/10.1089/hs.2016.0026
21. Clinical and Laboratory Standards Institute. Performance standards for antimicrobial susceptibility testing, 32th ed. Wayne (PA): The Institute; 2022.
22. Kirby T, Thornber-Dunwell M. High-risk drug practices tighten grip on London gay scene. Lancet. 2013;381:101–2. https://doi.org/10.1016/S0140-6736(13)60032-X
23. Gilbart VL, Simms I, Jenkins C, Furegato M, Gobin M, Oliver I, et al. Sex, drugs and smart phone applications: findings from semistructured interviews with men who have sex with men diagnosed with *Shigella flexneri* 3a in England and Wales. Sex Transm Infect. 2015;91:598–602. https://doi.org/10.1136/sextrans-2015-052014
24. Wu HH, Shen YT, Chiou CS, Fang CT, Lo YC. Shigellosis outbreak among MSM living with HIV: a case-control study in Taiwan, 2015–2016. Sex Transm Infect. 2019;95:67–70. https://doi.org/10.1136/sextrans-2017-053410
25. Mitchell H, Hughes G. Recent epidemiology of sexually transmissible enteric infections in men who have sex with men. Curr Opin Infect Dis. 2018;31:50–6. https://doi.org/10.1097/QCO.0000000000000423

26. Centers for Disease Control and Prevention. National Antimicrobial Resistance Monitoring System (NARMS): human isolates surveillance report for 2015 (final report) [cited 2022 Apr 20]. https://www.cdc.gov/narms/pdf/2015-NARMS-Annual-Report-cleared_508.pdf
27. Bowen A, Hurd J, Hoover C, Khachadourian Y, Traphagen E, Harvey E, et al.; Centers for Disease Control and Prevention (CDC). Importation and domestic transmission of *Shigella sonnei* resistant to ciprofloxacin—United States, May 2014–February 2015. MMWR Morb Mortal Wkly Rep. 2015;64:318–20.
28. Hines JZ, Pinsent T, Rees K, Vines J, Bowen A, Hurd J, et al. Notes from the field: shigellosis outbreak among men who have sex with men and homeless persons—Oregon, 2015–2016. MMWR Morb Mortal Wkly Rep. 2016;65:812–3. https://doi.org/10.15585/mmwr.mm6531a5
29. Sjölund Karlsson M, Bowen A, Reporter R, Folster JP, Grass JE, Howie RL, et al. Outbreak of infections caused by *Shigella sonnei* with reduced susceptibility to azithromycin in the United States. Antimicrob Agents Chemother. 2013;57:1559–60. https://doi.org/10.1128/AAC.02360-12
30. Kang M, Horman SF, Taplitz RA, Clay B, Millen M, Sitapati A, et al. Public health role of academic medical center in community outbreak of hepatitis A, San Diego County, California, USA, 2016–2018. Emerg Infect Dis. 2020;26:1374–81. https://doi.org/10.3201/eid2607.191352

Address for correspondence: Thaidra Gaufin, Sansum Clinic Infectious Diseases, 317 W Pueblo St, Santa Barbara, CA 93106, USA; email: tgaufin@gmail.com; Jeffrey Jenks, Durham County Department of Public Health, 414 E Main St, Durham, NC 27701, USA; email: jjenks@dconc.gov

Foodborne Illness Outbreaks Reported to National Surveillance, United States, 2009–2018

Alice E. White, Alexandra R. Tillman, Craig Hedberg, Beau B. Bruce, Michael Batz, Scott A. Seys, Daniel Dewey-Mattia, Michael C. Bazaco, Elaine Scallan Walter

Foodborne outbreaks reported to national surveillance systems represent a subset of all outbreaks in the United States; not all outbreaks are detected, investigated, and reported. We described the structural factors and outbreak characteristics of outbreaks reported during 2009–2018. We categorized states (plus DC) as high (highest quintile), middle (middle 3 quintiles), or low (lowest quintile) reporters on the basis of the number of reported outbreaks per 10 million population. Analysis revealed considerable variation across states in the number and types of foodborne outbreaks reported. High-reporting states reported 4 times more outbreaks than low reporters. Low reporters were more likely than high reporters to report larger outbreaks and less likely to implicate a setting or food vehicle; however, we did not observe a significant difference in the types of food vehicles identified. Per capita funding was strongly associated with increased reporting. Investments in public health programming have a measurable effect on outbreak reporting.

Foodborne diseases remain a major public health challenge in the United States, where 31 known pathogens cause an estimated 9 million illnesses, 56,000 hospitalizations, and 1,300 deaths annually (*1*). Efforts to improve food safety and reduce the burden of foodborne disease rely on data from foodborne disease surveillance and outbreak investigations to help prioritize food safety interventions, policies, and practices. Data from foodborne illness outbreaks reported to the Centers for Disease Control and Prevention (CDC) provide vital information on the foods causing illness and common food–pathogen pairs. Those data are used by the Interagency Food Safety Analytics Collaboration (IFSAC) to inform outbreak-based attribution models that attribute illnesses to specific food categories (*2*,*3*).

Foodborne illness outbreaks are investigated by local, state, and territorial health departments, CDC, the US Food and Drug Administration (FDA), and the Food Safety and Inspection Service of the United States Department of Agriculture and are reported to CDC's Foodborne Disease Outbreak Reporting Surveillance System (FDOSS) through the web-based National Outbreak Reporting System (NORS). Although reported outbreaks are a rich data source, they represent a subset of all outbreaks occurring in the United States; not all outbreaks will be detected, investigated, and reported. Factors influencing which outbreaks are detected, investigated, and reported to CDC include both structural factors associated with the jurisdiction in which the outbreak occurred (e.g., infrastructure and capacity) and characteristics of the outbreak (e.g., size, geographic location, pathogen).

We integrated data from a variety of sources to examine structural factors and describe outbreak characteristics of foodborne outbreaks involving *Salmonella*, Shiga toxin–producing *Escherichia coli* (STEC) O157, norovirus, and bacterial toxins that were reported to national surveillance. In addition, we assessed the effects of state variation in outbreak reporting on the types of food vehicles identified.

Author affiliations: Colorado School of Public Health, Aurora, Colorado, USA (A.E. White, A.R. Tillman, E. Scallan Walter); University of Minnesota, Minneapolis, Minnesota, USA (C. Hedberg); Centers for Disease Control and Prevention, Atlanta, Georgia, USA (B.B. Bruce, D. Dewey-Mattia); US Food and Drug Administration, College Park, Maryland, USA (M. Batz, M.C. Bazaco); US Department of Agriculture Food Safety Inspection Service, Washington, DC, USA (S.A. Seys)

DOI: https://doi.org/10.3201/eid2806.211555

Methods

Foodborne Outbreak Data

We obtained outbreak surveillance data from CDC's FDOSS for 2009–2018, extracted November 22, 2019.

This passive surveillance system receives outbreak reports from state, local, and territorial health agencies using a standard outbreak report form that includes information on the date and location of the outbreak, investigation methods, case demographics, etiology, transmission route, setting, and implicated food, among other variables. Forms have been submitted electronically through NORS since 2009. For this study, we included all single-state foodborne outbreaks (exposures occurred in 1 state) reported to FDOSS by 50 states and Washington, DC. We excluded multistate outbreaks (exposures occurred in multiple states) because there are relatively few multistate outbreaks, and single-state outbreaks are more reflective of individual state resources and capacity. We included city jurisdictions reporting independently in state totals. When categorizing outbreaks by pathogen, we included any outbreaks with a confirmed or suspected etiology of *Salmonella*, STEC O157, norovirus, and bacterial toxins (*Clostridium perfringens*, *Bacillus cereus*, and *Staphylococcus aureus*). Outbreaks associated with other priority IFSAC pathogens, including *Campylobacter* spp. and *Listeria monocytogenes* were not included in pathogen-specific analyses because few outbreaks were reported. We included outbreaks caused by multiple pathogens in all outbreaks and excluded them from pathogen group analysis.

We calculated outbreak reporting rates as the number of single-state foodborne illness outbreaks reported annually per 10 million population for 2009–2018, averaged over time by state. We categorized states by outbreak reporting quintile for all etiologies, then collapsed into high (the highest outbreak reporting quintile), middle (the middle 3 quintiles), or low (the lowest quintile) reporting groups. We compared high, middle, and low outbreak reporting over time and by the structural and outbreak characteristics described using bivariate χ^2, Kruskal-Wallis, or Fisher exact test as appropriate. We analyzed data using SAS version 9.4 (SAS Institute Inc., https://www.sas.com). This analysis did not meet the definition of human subjects research as defined in the US Code of Federal Regulations, Title 45 Part 46, and was not subject to review by an institutional review board.

Structural Characteristics

Structural characteristics related to state reporters were available from a variety of sources and included reporting structure, funding sources, and participation in foodborne or environmental health programs. Reporters were classified as having a centralized surveillance reporting structure, in which state health departments were the primary leaders of surveillance and outbreak investigations, or decentralized structure, in which local health departments were the primary leaders of surveillance and outbreak investigations using the 2014 LawAtlas codebook for state foodborne illness reporting laws and the 2007 Enteric Disease Outbreak Investigation and Surveillance survey (*4*,*5*). Funding sources we examined included the total number of public health full-time employees (FTEs) and state public health revenue by source, available from the Association of State and Territorial Health Officials (ASTHO) Profile of State and Territorial Public Health reports (https://www.astho.org); Epidemiology and Laboratory Capacity for Prevention and Control of Emerging Infectious Diseases (ELC) cooperative-agreement funding for fiscal years 2016–2018, which funded states and territories to detect, respond to, control, and prevent infectious diseases (*6*); and federal foodborne or environmental health programs. ELC-funded state programs for foodborne illness detection and response include the Integrated Food Safety Centers of Excellence (CoE; https://www.cdc.gov/foodsafety/centers), Foodborne Diseases Centers for Outbreak Response Enhancement (FoodCORE; https://www.cdc.gov/foodcore), and OutbreakNet Enhanced (OBNE, https://www.cdc.gov/foodsafety/outbreaknetenhanced).

States can receive funding for multiple programs. For analysis purposes, we assigned states to the program with the highest average funding award per capita (e.g., states with CoE and FoodCORE or OBNE were categorized as CoE). ELC-funded state programs for norovirus included Norovirus Sentinel Testing and Tracking (NoroSTAT, https://www.cdc.gov/norovirus/reporting/norostat). State programs for foodborne illness funded by CDC under the Emerging Infections Program included the Foodborne Diseases Active Surveillance Network (FoodNet; https://www.cdc.gov/foodnet). Environmental health outbreak response programs included FDA Voluntary National Retail Regulatory Food Program Standard 5, state-level meat and poultry inspection, FDA Rapid Response Team, Environmental Health Specialists Network, and the National Environmental Assessment Reporting System; the CIFOR Food Safety Programs Reference Guide contains program descriptions (*7*). We obtained surveillance data for state estimates of *Salmonella* and STEC O157 illnesses from the Laboratory-based Enteric Disease Surveillance (LEDS) system (*8*,*9*) and used them to compare underlying disease rates with outbreak reporting.

Table 1. Single-state foodborne outbreaks reported by US states and Washington, DC, to the Foodborne Disease Outbreak Surveillance System, 2009–2018*

Characteristic	All etiologies	Norovirus	*Salmonella*	Bacterial toxins	STEC O157
No. reporters	51	51	50	46	34
No. outbreaks	8,131	2,798	1,191	617	150
Range by state	9–906	1–357	1–100	1–72	1–14
Total outbreak-associated illnesses	131,525	55,406	21,656	17,110	1,624
Range by state	84–11,242	22–4,755	3–1,717	5–1,771	2–164
Mean annual outbreak rate per 10 million population, by state	28.6	9.2	4.7	2.6	0.9
Range by state	4.7–86.3	0.5–52.1	1.3–11.4	0.1–7.6	0.1–3.2
Outbreaks with confirmed etiology, no. (%)	3,962 (49)	1,529 (55)	1,101 (92)	258 (42)	139 (93)
Range by state, %	21–84	0–100	54–100	0–100	50–100
Outbreaks with food vehicle identified, no. (%)	2,960 (36)	693 (25)	477 (40)	397 (64)	88 (59)
Range by state, %	11–77	0–100	0–80	0–100	0–100
Outbreaks with confirmed etiology and food vehicle identified, no. (%)	1,819 (22)	425 (15)	449 (38)	194 (31)	82 (55)
Range by state, %	0–56	0–40	0–80	0–100	0–80

*All etiologies includes reported outbreaks with multiple etiologies. Bacterial toxins include *Clostridium perfringens*, *Bacillus cereus*, and *Staphylococcus aureus*. STEC, Shiga toxin–producing *Escherichia coli*.

Outbreak Characteristics

We obtained outbreak characteristics from FDOSS. Characteristics included the number of ill cases per outbreak (laboratory-confirmed and probable primary cases); setting identified (yes/no); setting type (restaurant, private residence, institution, or other); food implicated (yes/no); food implicated using food categories defined by IFSAC (*10*); and whether the implicated food was confirmed or suspected. During 2017 and 2018, states reported foods as confirmed or suspected directly to NORS. For outbreaks before 2017, in this analysis we retrospectively classified implicated foods as confirmed or suspected using criteria outlined in the current NORS guidance (https://www.cdc.gov/nors/forms.html).

Results

During 2009–2018, a total of 8,131 single-state outbreaks involving 131,525 outbreak-associated illnesses were reported. Of these, 5,986 (74%) had a confirmed or suspected etiology. Causes of the outbreaks included norovirus (2,798; 47%), *Salmonella* (1,191; 20%), bacterial toxins (617; 10%), and STEC O157 (150; 3%) (Table 1). The etiology was confirmed for 49% of the outbreaks (range across states 21%–84%). The percentage of outbreaks with

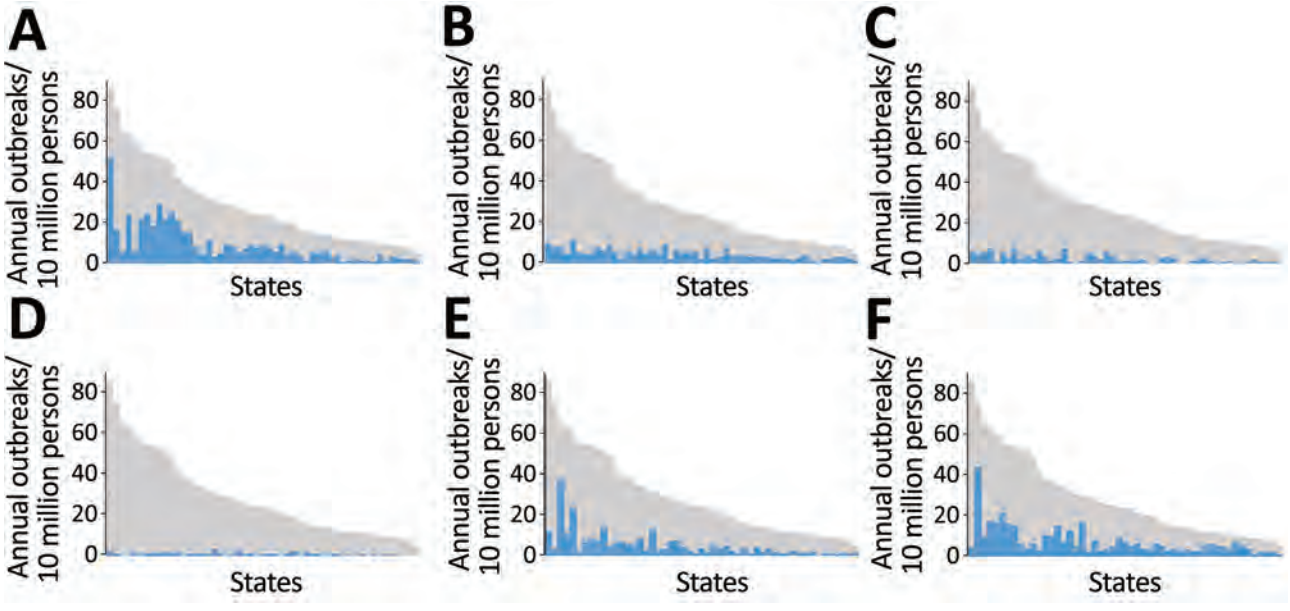

Figure 1. Mean annual rates of foodborne disease outbreaks reported to the Centers for Disease Control and Prevention per 10 million population by etiology and US state (deidentified), Foodborne Disease Outbreak Surveillance System, United States, 2009–2018. Blue bars represent outbreaks reported for the specified etiology. Gray bars represent all outbreaks reported. Blue and gray bars correspond to the same reporting jurisdiction and are ordered by reporting rate for all single-state outbreaks. A) Norovirus; B) *Salmonella*; C) bacterial toxins; D) Shiga toxin–producing *E. coli* O157; E) Other known cause; F) Unknown cause.

a confirmed etiology was higher for *Salmonella* (92%) and STEC (93%) outbreaks than for norovirus (55%) and bacterial toxin (42%) outbreaks. A confirmed or suspected food vehicle was identified for 36% of the total outbreaks (range by state 11%–77%) (Table 1).

Overall, states reported a mean of 29 outbreaks per 10 million population per year (range by state: 5–86 outbreaks) and a mean of 9 (range 0.5–52) norovirus outbreaks, 5 *Salmonella* (range 1–11) outbreaks, 3 (range 0.1–8) bacterial toxin outbreaks, and 0.9 (range

	All outbreaks	Norovirus	*Salmonella*	Bacterial toxins	STEC O157	Other known etiology	Unknown etiology
1	86.3	52.1	9.9	6.1	2.6	11.6	4.0
2	75.8	16.6	8.0	3.8	0.7	3.1	43.6
3	65.8	5.5	8.2	5.5	0.0	37.0	9.6
4	63.5	23.7	4.7	7.6	0.0	10.4	17.1
5	60.0	6.4	11.4	0.7	1.4	23.6	16.4
6	55.5	22.2	5.5	5.5	0.0	1.4	20.8
7	54.2	24.1	4.8	2.8	0.8	6.0	15.7
8	54.1	18.4	4.5	7.3	1.1	7.7	15.0
9	52.6	29.2	8.1	1.8	1.0	7.0	5.5
10	51.4	22.3	6.2	4.0	1.6	14.0	3.4
11	48.6	25.7	8.9	2.5	0.8	4.7	5.9
12	42.3	21.2	5.6	6.3	1.2	5.4	2.6
13	38.2	15.6	1.7	3.5	0.0	6.9	10.4
14	37.8	15.2	5.8	1.2	0.4	5.1	10.0
15	35.1	7.9	4.2	2.2	0.7	5.1	15.0
16	34.5	4.1	7.9	7.2	0.3	8.2	6.8
17	32.2	11.3	4.5	0.9	0.3	2.5	12.7
18	30.4	3.2	6.4	0.0	3.2	12.8	4.8
19	29.8	4.9	3.9	1.2	1.0	2.2	16.5
20	29.0	9.4	9.4	5.5	0.0	2.9	1.9
21	28.1	8.4	2.1	3.6	0.1	6.6	7.3
22	26.3	5.5	6.7	1.8	2.4	7.3	2.4
23	25.3	7.3	5.0	6.0	0.2	3.9	2.9
24	25.1	8.7	5.2	3.4	0.9	2.3	4.6
25	24.0	7.5	6.0	0.8	0.0	0.8	9.0
26	23.6	9.3	2.6	1.2	0.3	3.3	6.9
27	23.5	7.7	7.7	1.4	0.5	1.4	4.8
28	21.3	6.0	2.5	1.5	0.5	5.0	5.8
29	20.3	9.2	3.1	1.7	0.0	3.0	3.3
30	20.2	4.2	7.7	0.1	0.9	4.3	3.0
31	19.6	5.9	3.9	0.0	2.0	2.0	5.9
32	16.0	3.7	4.3	2.7	0.0	0.5	4.8
33	15.4	1.2	3.6	3.6	1.2	3.6	2.4
34	15.0	5.3	3.1	2.3	0.3	0.6	3.5
35	14.3	4.5	3.8	0.0	0.8	3.8	1.5
36	13.8	6.1	3.1	0.0	0.0	1.5	3.1
37	13.2	2.8	3.1	1.3	0.5	3.4	2.2
38	12.0	3.9	2.5	1.4	0.7	1.4	2.1
39	11.9	0.5	2.7	2.7	0.0	0.5	5.4
40	11.6	1.1	2.0	1.2	0.2	1.4	5.8
41	11.4	2.7	1.6	0.1	0.0	2.1	4.9
42	10.9	1.3	2.8	0.7	0.8	0.8	4.5
43	10.5	1.4	4.1	1.0	0.0	1.4	2.7
44	10.3	0.7	1.5	0.1	0.1	1.4	6.5
45	9.7	4.3	0.0	0.0	0.0	0.0	5.4
46	9.1	1.1	2.3	0.9	0.5	0.9	3.4
47	8.9	3.2	2.0	1.9	0.2	0.9	0.7
48	8.8	2.6	3.4	0.5	0.0	0.3	2.1
49	8.1	1.9	3.1	0.4	0.0	1.0	1.7
50	7.5	2.3	2.5	0.5	0.0	0.3	1.8
51	4.7	1.3	1.3	0.3	0.0	1.0	0.7

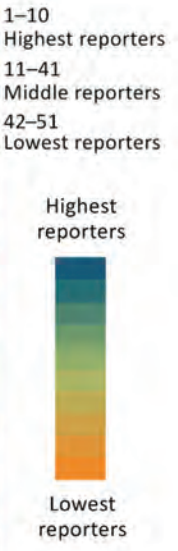

Figure 2. Annual rates of foodborne-illness outbreaks per 10 million population by reporting state and etiology, Foodborne Disease Outbreak Surveillance System, United States, 2009–2018. STEC, Shiga toxin–producing *Escherichia coli.*

Table 2. Outbreak characteristics from high, middle, and low outbreak reporter states, all etiologies, Foodborne Disease Outbreak Surveillance System, United States, 2009–2018*

Characteristic	Highest 10 reporters	Middle 31 reporters	Lowest 10 reporters	p value
Total no. outbreaks	2,416	5,091	624	
Etiology identified	1,897 (78.5)	3,733 (73.3)	356 (57.1)	<0.01
Confirmed etiology‡				<0.01
Norovirus	546 (35.7)	913 (59.7)	70 (4.6)	
Salmonella	245 (22.3)	731 (66.4)	125 (11.4)	
Bacterial toxins†	67 (26.0)	167 (64.7)	24 (9.3)	
STEC O157	44 (31.7)	87 (62.6)	8 (5.8)	
Other known§	257 (27.5)	642 (68.7)	36 (3.9)	
Confirmed or suspected				<0.01
Norovirus	1,036 (37.0)	1,661 (59.4)	101 (3.6)	
Salmonella	264 (22.2)	782 (65.7)	145 (12.2)	
Bacterial toxins†	168 (27.2)	416 (67.4)	33 (5.3)	
STEC O157	48 (32.0)	92 (61.3)	10 (6.7)	
Other known§	381 (31.0)	782 (63.6)	67 (5.4)	
Setting identified	2,310 (95.6)	4,678 (91.9)	457 (73.2)	<0.01
Setting‡¶				<0.01
Restaurant	1,528 (66.2)	2,893 (61.8)	237 (51.9)	
Institution	78 (3.4)	186 (4.0)	31 (6.8)	
Private residence	217 (9.4)	366 (7.8)	45 (9.9)	
Other single setting	119 (5.2)	303 (6.5)	32 (7.0)	
Multiple setting	368 (15.9)	930 (19.9)	112 (24.5)	
Food vehicle confirmed or suspected	879 (36.4)	1,917 (37.7)	164 (26.3)	<0.01
Food‡				<0.01
Multiple	314 (35.7)	704 (36.7)	73 (44.5)	
Aquatic animals	192 (21.8)	335 (17.5)	11 (6.7)	
Land animals	214 (24.4)	522 (27.2)	51 (31.1)	
Plant	138 (15.7)	290 (15.1)	24 (14.6)	
Other#	21 (2.4)	66 (3.4)	5 (3.1)	
Food vehicle confirmed	656 (74.6)	1,440 (75.1)	92 (56.1)	<0.01
Season				0.02
Winter	649 (26.9)	1,306 (25.7)	128 (20.5)	
Spring	639 (26.5)	1,481 (29.1)	195 (31.3)	
Summer	613 (25.4)	1,282 (25.2)	166 (26.6)	
Autumn	515 (21.3)	1,022 (20.1)	135 (21.6)	
Sex of case-patients unknown	196 (8.1)	443 (8.7)	79 (12.7)	<0.01
No. cases, median (IQR)**	6 (11)	8 (13)	10 (20)	<0.01††

*Values are no. (%) except as indicated. The highest reporter states were the highest outbreak reporting quintile, middle reporters the middle 3 quintiles, and low reporters the lowest quintile, based on number of outbreaks reported per 10 million population. p values are from χ^2 test results compared across the 3 reporting tiers. STEC, Shiga toxin–producing *Escherichia coli*.
†Bacterial toxin outbreaks include *Clostridium perfringens*, *Bacillus cereus*, *Staphylococcus aureus.*
‡Among outbreaks with characteristic identified.
§Includes outbreaks associated with multiple pathogens.
¶Restaurant setting includes caterer, banquet hall; Institution includes daycares, hospitals, long-term care facilities/nursing homes/assisted living facilities, prison/jails, and school/college/universities; Other setting category includes camp, fair, festival, other temp or mobile services, farm/dairy, grocery store, hotel/motel, office/indoor workplace, other, religious facility, ship/boat.
#Includes foods that were unclassifiable or invalid using food categories defined by the Interagency Food Safety Analytics Collaboration (*8*).
**Laboratory-confirmed and probable primary cases.
††By Kruskal-Wallis test.

0.1–3) STEC O157 outbreaks per 10 million population per year (Table 1; Figure 1). The 10 states with the highest number of reported outbreaks (high reporters) averaged 62 outbreaks per 10 million population per year, whereas the 10 states with the fewest number of reported outbreaks (low reporters) averaged 9 and the remaining 30 states (middle reporters) 24 outbreaks per 10 million population per year (Figure 2). Outbreak reporting quintiles were mostly consistent across pathogens, with the exception of STEC O157 (Figure 2). Among outbreaks with a known etiology other than norovirus, *Salmonella*, bacterial toxins, and STEC O157, the most common etiologies were fish toxins (433 outbreaks, 33%) and *Campylobacter* (294 outbreaks, 22%).

During 2009–2018, low reporters reported less than one third the number of outbreaks (624) reported by high reporters (2,416) (Table 2). This pattern was similar over time except in 2017–2018, when the number of outbreaks reported by low reporters more than doubled as a result of changes in reporting practices in a single large-population state (Figure 3, panels A, B). Low reporters were significantly less likely than middle and high reporters to report outbreaks with an identified etiology (57% low, 73% middle, 79% high) and reported fewer norovirus outbreaks (5% low, 60% middle, 36% high). Low reporters were also less likely to identify a setting (73% low, 92% middle, 96% high) and less likely to implicate (26% low, 38% middle, 36%

high) or confirm (56% low, 75% middle, 75% high) a food vehicle. Low reporters were more likely to report the sex of case-patients as unknown (low 13%, 9% middle, 8% high). Low reporters were also more likely to report larger outbreaks (median for low, 10 cases; middle, 8 cases; high, 6 cases) (Table 2). These trends were similar across all pathogen groups.

We found no apparent associations between reporting structure and reporting group (Table 3). The percentage of state agency finance received from federal sources was similar across reporting groups, and although high reporters (27%) were more likely than middle reporters (21%) and low reporters (15%) to have received federal funding from CDC, the difference was not statistically significant. Per capita ELC funding was, however, significantly associated with reporting group; high reporters received more funding ($1.30 per capita) than middle reporters ($0.81) and low reporters ($0.44) ($p<0.01$). Receiving funding for foodborne programs was not statistically significantly associated with reporting group, but all reporters in the highest funding tiers (CoE, FoodCORE) were high or middle reporters, and only 1 of the 15 states receiving no foodborne program funding was a high reporter. Reporters receiving OBNE funding were equally distributed across reporting groups. Similarly, differences between reporters based on whether they receive funding for NoroSTAT or FoodNet were not statistically significant across tiers, but all states receiving funding were high or middle reporters. We saw no association between participation in environmental health outbreak response programs and reporting (Table 3). We observed similar trends for outbreak and structural characteristics across reporters for outbreaks caused by 4 pathogens (Appendix Tables 1–4, https://wwwnc.cdc.gov/EID/article/28/6/21-1555-App1.pdf). The average *Salmonella* incidence rate as reported to LEDS was consistent across reporting groups (Appendix Table 2), whereas high reporters of STEC O157 outbreaks also reported a higher average STEC incidence rate (4.9 illnesses per 100,000 population) compared with middle (2.4) and low (2.6) reporters ($p = 0.04$) (Appendix Table 4).

The distribution of implicated foods categorized by Level 1 IFSAC overarching food category (i.e., land animals, aquatic animals, plant), multiple, or other differed substantially by reporting group for all etiologies and other known etiologies, but not for norovirus, *Salmonella*, bacterial toxin, and STEC O157 outbreaks (Table 4). We saw slightly more variation across reporters when implicated foods were classified by more detailed level 2 food type categories (e.g., fish, shellfish, dairy, meat and poultry, eggs, produce, grains and beans); the low reporters reporting fewer produce outbreaks for norovirus, *Salmonella*, and STEC O157 etiology outbreaks, and more meat and poultry outbreaks for STEC O157 and outbreaks of unknown etiology (Figure 4).

Discussion

Several factors may affect outbreak reporting. NORS is a passive, voluntary system, and reporting depends on state and local capacity to detect, investigate, and report outbreaks. We found considerable variation across states in the number and types of foodborne outbreaks reported through NORS. The top 10 states reported 4 times more outbreaks per 10 million population than the lowest 10 states reported. The widest gap in outbreak reporting rates was for norovirus outbreaks; the highest reporter reported >40 times as many outbreaks as the lowest one. We also found

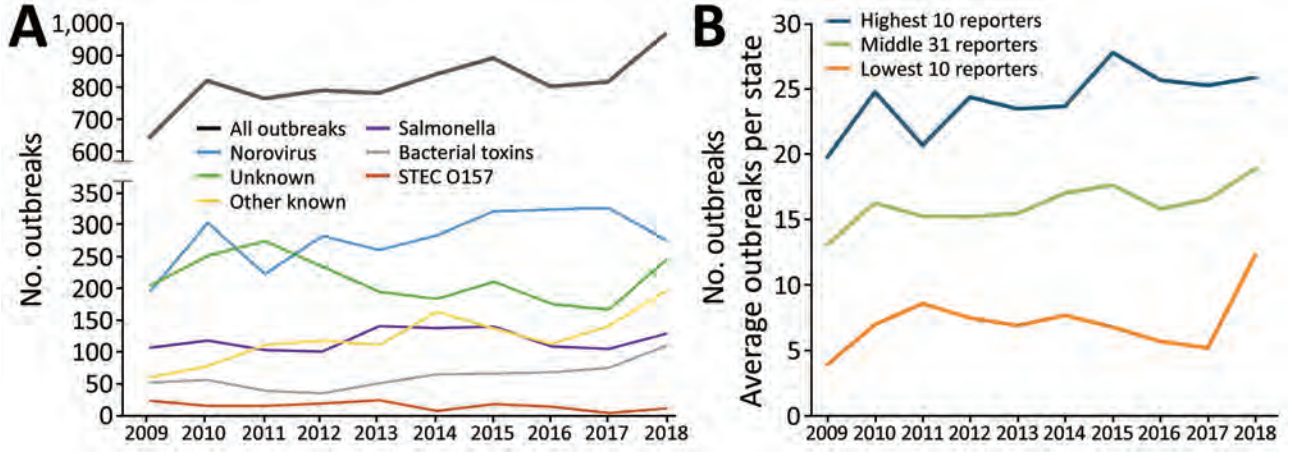

Figure 3. Foodborne outbreaks reported through the Foodborne Disease Outbreak Surveillance System, by etiology and reporting group, United States, 2009–2018. A) Single-state foodborne outbreaks by etiology. B) Average outbreaks per state by reporting group (high, middle, low). STEC, Shiga toxin–producing *Escherichia coli.*

Table 3. State structural characteristics from all outbreak reporter states, Foodborne Disease Outbreak Surveillance System, United States, 2009–2018*

Characteristic	Highest 10 reporters	Middle 31 reporters	Lowest 10 reporters	p value
Reporting structure				0.61
No. centralized (%)	5 (50.0)	10 (32.3)	4 (40)	
No. decentralized (%)	5 (50.0)	21 (67.7)	6 (60)	
State agency finance, median (IQR)†				
% State funds	26.9 (22.5–32.6)	29.2 (21.7–47.3)	19.7 (12.9–23.7)	0.11
% Federal funds	54.3 (39.9–63.1)	51.1 (43.8–61.4)	49.4 (39.7–69.0)	0.96
% CDC federal funds	26.7 (23.6–36.5)	20.6 (15–33.3)	14.8 (14.2–28.3)	0.14
Median ELC funding per capita, US$‡	$1.30 ($0.91-2.12)	$0.81 ($0.45–1.49)	$0.44 ($0.34–0.59)	<0.01
State agency workforce				
FTEs per 10,000 population, median (IQR)†	2.7 (2.2–4.9)	2.2 (1.2–5.1)	4.8 (2.6–6.8)	0.37
CDC ELC-funded foodborne programs§				0.35
CoE	3 (30.0)	3 (9.7)	0	
FoodCORE	1 (10.0)	4 (12.9)	0	
OBNE	5 (50.0)	15 (48.4)	5 (50.0)	
None	1 (10.0)	9 (29.3)	5 (50.0)	
NoroSTAT¶	3 (30.0)	9 (29.3)	0	0.18
FoodNet#	3 (30.0)	7 (22.6)	0	0.21
Food safety environmental health programs				
FDA standard 5**	4 (40.0)	15 (48.4)	3 (30.0)	0.63
State-level meat and poultry inspection	4 (40.0)	19 (61.3)	5 (50.0)	0.46
RRT	4 (40.0)	16 (51.6)	4 (40.0)	0.79
EHS-Net	2 (20.0)	3 (9.7)	0	0.36
NEARS	5 (50.0)	15 (48.4)	4 (40.0)	0.93

*Values are no. (%) except as indicated. The highest reporter states were the highest outbreak reporting quintile, middle reporters the middle 3 quintiles, and low reporters the lowest quintile, based on number of outbreaks reported per 10 million population. p values are from Kruskal-Wallis tests for continuous variables and Fisher exact test for categorical variables. CoE, Center of Excellence; ELC, Epidemiology and Laboratory Capacity for Prevention and Control of Emerging Infectious Diseases; FDA, Food and Drug Administration; FTE, full-time employee; NEARS, National Environmental Assessment Reporting System; OBNE, OutbreakNet Enhanced; RRT, FDA Rapid Response Team.
†Association of State and Territorial Health Officials Profile of State and Territorial Public Health volume 4.
‡ELC funding per capita, fiscal years 2016–18. Excludes supplemental Zika virus funding for fiscal years 2016–20.
§ELC-funded foodborne programs: Integrated Food Safety Centers of Excellence, Foodborne Diseases Centers for Outbreak Response Enhancement (FoodCORE), OBNE. States with multiple programs were categorized into the category with more funding (e.g., states with CoE and FoodCORE were counted only in CoE) such that program categories are mutually exclusive.
¶Norovirus Sentinel Testing and Tracking (NoroSTAT).
#Foodborne Diseases Active Surveillance Network.
**State agency participation in FDA Voluntary National Retail Regulatory Food Program Standard 5 (Foodborne Illness and Food Defense Preparedness and Response) as of most recent assessment or audit.

variation in the types of outbreaks reported by states; low reporters were more likely to report larger outbreaks caused by reportable conditions (e.g., *Salmonella*, STEC O157) and less likely to implicate a setting or food vehicle in an outbreak.

Some differences in outbreak reporting may be due to differences in underlying incidence of disease. For example, most outbreaks associated with fish toxins are inherently regional, occurring in coastal states (*11*), and they tend to be smaller (*12*). In this study, aquatic animal outbreaks were mostly associated with norovirus and were more likely to occur in coastal states. We found that states that reported more STEC O157 outbreaks also reported a higher incidence of STEC to LEDS than middle and low reporters. However, although regional variation is substantial in reported *Salmonella* cases by population overall and among serotypes (*13*), we did not find *Salmonella* outbreak reporting to be correlated with incidence. Despite variation in outbreak reporting across states, we did not identify substantial differences over time or in the foods reported, which suggests that national outbreak surveillance is stable and a reliable source for monitoring relative trends in foodborne illness, including estimating food source attribution.

The structural characteristic most closely associated with outbreak reporting rates was per capita ELC funding. High reporters received ≈3 times as much funding as low reporters. These estimates included funding for nonfoodborne infectious disease program areas, such as healthcare-associated infections and vectorborne disease, suggesting that increasing funding has a positive effect overall on public health department capacity. In foodborne outbreak investigations, epidemiologists work directly on or collaborate with waterborne, animal contact, and other communicable disease programs, especially in local public health agencies. We observed that states that were high reporters were high reporters across multiple pathogen groups, including pathogens detected primarily through reportable disease surveillance (*Salmonella*, STEC O157) and pathogens detected primarily through

nonreportable, or complaint-based, surveillance (norovirus, bacterial toxins).

The ability of states to detect outbreaks varies and depends on type of surveillance systems, interview questionnaires, cluster and outbreak tracking systems, case definitions, and laboratory testing capacity. Previous work found a correlation between the number of consumer complaints received by an agency and outbreak reporting rates; however, complaint systems range from no system, to localized systems that do not communicate across jurisdictions, to fully centralized systems (*14*). Jones et al. found that outbreak reporting was higher in states requiring submission of all *Salmonella* isolates to state laboratories and in states that routinely perform molecular subtyping of all isolates (*15*), which has since become standard practice.

Once an outbreak is detected, investigators determine whether they have the resources to proceed with an investigation. Most jurisdictions prioritize investigations associated with pathogens that may cause more severe illness (e.g., STEC O157); however, many lack the personnel to investigate outbreaks of less severe illness or may intentionally deprioritize norovirus outbreaks that are more likely to spread person-to-person, such as in congregate settings (*16*). Furthermore, outbreak investigations are costly (*17*,*18*), requiring time, resources, and commitment among competing priorities (*19*), and some jurisdictions may be less willing to divert personnel and resources from other public health activities or may prioritize outbreaks on the basis of the likelihood of finding actionable information. Cross-disciplinary and interagency collaboration is crucial to successful outbreak investigations; states reporting more outbreaks also reported more collaboration with other states and federal partners (*15*). Finally, states differentially interpret foodborne outbreak and cluster case definitions and report inconsistency and ambiguity in how these definitions are applied for national reporting (*19*).

Although overall ELC funding was associated with increased reporting, we did not find a statistically significant association between reporting and participation in CDC ELC-funded foodborne (CoE, FoodCORE, OBNE) and norovirus (NoroSTAT) programs, CDC foodborne programs funded through other mechanisms (FoodNet), or environmental health programs. This finding could be caused by a delay in observing effects of the funding award. Average funding awards vary within programs, and data on funding for specific foodborne programs were not readily accessible. For example, the average annual award for FoodCORE is $190,000–$510,000 per site, depending on population size and individual work plans (*20*). Funding is awarded through an application process, so awards may reflect capacity and support in the jurisdiction applying, whereas states with less capacity may be less likely to apply for or receive supplemental ELC grant funding. ELC funding awards are competitive and could be an indication of the underlying capacity of public health agencies to conduct surveillance, rather than a specific cause for high reporting of foodborne disease outbreaks.

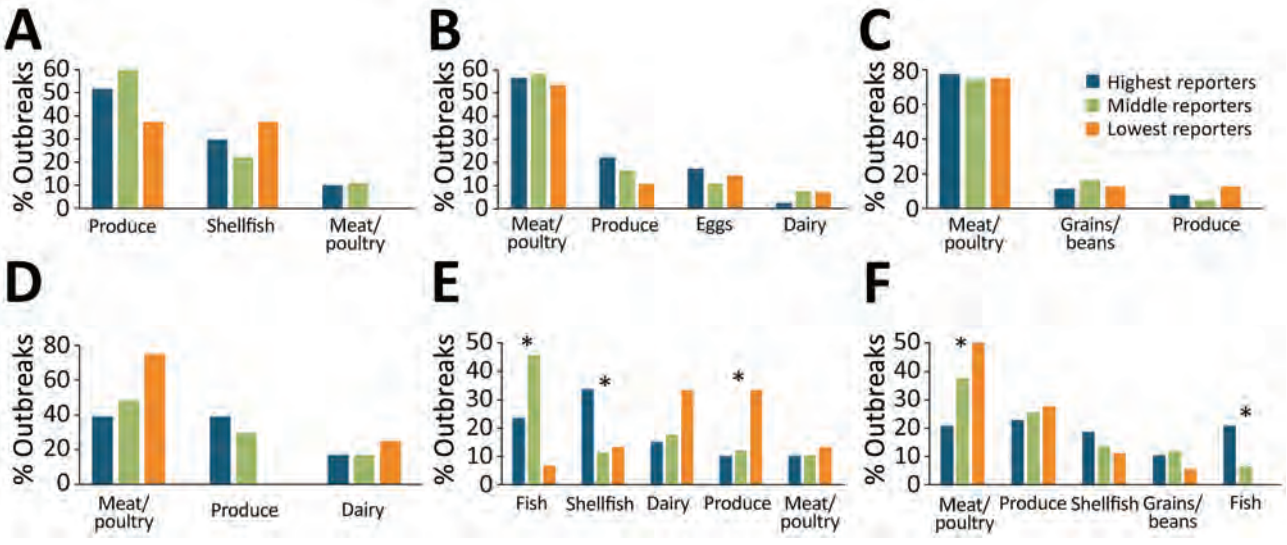

Figure 4. Most common foods implicated in foodborne illness, by detailed food category, Foodborne Disease Outbreak Surveillance System, United States, 2009–2018. Asterisks (*) indicate statistical significance (p<0.05 by Fisher exact test). Data are shown for (A) norovirus, 216 cases; (B) *Salmonella*, 321 cases; (C) bacterial toxins, 209 cases; D) Shiga toxin–producing *Escherichia coli* O157, 76 cases; (E) illness of other known etiology, 715 cases; (F) illness of unknown etiology, 191 cases.

Table 4. Overarching food categories of implicated food vehicles in outbreaks reported to Foodborne Disease Outbreak Surveillance System, United States, 2009–2018*

Characteristic	Land animals	Aquatic animals	Plants	Unassignable†	Other‡	p value
All etiologies						<0.01
Highest reporters	214 (24.4)	192 (21.8)	138 (15.7)	314 (35.7)	21 (2.4)	
Middle reporters	522 (27.2))	335 (17.5)	290 (15.1)	704 (36.7)	66 (3.4)	
Lowest reporters	51 (31.1)	11 (6.7)	24 (14.6)	73 (44.5)	5 (3.1)	
Norovirus						0.26
Highest reporters	16 (6.5)	27 (10.9)	55 (22.2)	136 (54.8)	14 (5.7)	
Middle reporters	15 (3.5)	31 (7.3)	85 (20.0)	261 (61.4)	33 (7.8)	
Lowest reporters	1 (5.0)	3 (15.0)	4 (20.0)	12 (60.0)	0	
Salmonella						0.61
Highest reporters	63 (52.5)	1 (0.8)	18 (15.0)	36 (30.0)	2 (1.7)	
Middle reporters	165 (52.6)	10 (3.2)	41 (13.1)	88 (28.0)	10 (3.2)	
Lowest reporters	22 (51.2)	3 (7.0)	4 (9.3)	12 (27.9)	2 (4.7)	
Bacterial toxins§						0.89
Highest reporters	45 (42.9)	1 (1.0)	10 (9.5)	49 (46.7)	0	
Middle reporters	115 (41.8)	3 (1.1)	31 (11.3)	121 (44.0)	5 (1.8)	
Lowest reporters	6 (35.3)	0	3 (17.7)	8 (47.1)	0	
STEC O157						0.65
Highest reporters	11 (50.0)	0	7 (31.8)	4 (18.2)	0	
Middle reporters	37 (61.7)	1 (1.7)	16 (26.7)	6 (10.0)	0	
Lowest reporters	5 (83.3)	0	0	1 (16.7)	0	
Other known						0.01
Highest reporters	67 (24.5)	143 (52.2)	31 (11.3)	32 (11.7)	1 (0.4)	
Middle reporters	137 (25.6)	265 (49.4)	68 (12.7)	57 (10.6)	9 (1.7)	
Lowest reporters	7 (30.4)	3 (13.0)	7 (30.4)	5 (21.7)	1 (4.4)	
Unknown						0.06
Highest reporters	12 (10.9)	20 (18.2)	17 (15.5)	57 (51.8)	4 (3.6)	
Middle reporters	53 (17.3)	25 (8.1)	49 (16.0)	171 (55.7)	9 (2.9)	
Lowest reporters	10 (18.2)	2 (3.6)	6 (10.9)	35 (63.6)	2 (3.6)	

*Values are no. (%) except as indicated. p values are determined by χ^2 test.
†A food or foods were implicated, but the contaminated ingredient was not determined so a food category could not be assigned or >1 food category was implicated using the Interagency Food Safety Analytics Collaboration categorization scheme (*10*).
‡Includes foods that were unclassifiable using food categories defined by the Interagency Food Safety Analytics Collaboration.
§Bacterial toxin outbreaks include *Clostridium perfringens*, *Bacillus cereus*, *Staphylococcus aureus.*

Outbreak investigations provide critical information on the epidemiology of foodborne diseases and the foods that cause illness. Opportunities to improve outbreak response and reporting are ample, and improvements could further our understanding of what causes foodborne illnesses. Funding is not the only investment needed to improve capacity. Funding must be targeted and flexible (*15*). Peer, community, and cross-jurisdictional support, as fostered by the CoE within the 5 CoE regions (https://www.cdc.gov/foodsafety/centers), are potential mechanisms for improving capacity. Continuing education, workforce engagement, and ongoing evaluation and quality improvement using standardized metrics are all components of increasing public health capacity. Targeted CDC-led funding programs; expansion of CoE-led regional training, mentorship, and technical assistance programs; and opportunities for state- and local-level collaboration via peer networks appear to be useful for improving outbreak surveillance and response. Evaluation using standardized metrics (*7*,*20*) can identify evidence-based practices to continue to make the system more efficient and effective.

Despite variability in reporting, this study found the food categories reported across groups were similar, which supports the use of outbreak data in food source attribution estimates. IFSAC, a collaboration across 3 federal agencies (CDC, FDA, and USDA-FSIS), produces annual estimates of the most common food categories responsible for illnesses caused by pathogens based on national surveillance data for foodborne outbreaks (*2*). However, the extent to which the distribution of food vehicles and locations of preparation implicated in outbreaks reflect the same vehicles and locations as sporadic foodborne illnesses is unknown (10). Most foodborne illnesses are not associated with a known outbreak, and the use of outbreak data for attribution may be limited if reported outbreaks are not representative of all foodborne outbreaks (*3*). Our study found that although there is variation in the number and types of outbreaks reported by states as well as an overall low proportion of outbreaks with an implicated food, there was not substantial variation in the foods reported, suggesting the IFSAC approach of using outbreak data for national food source attribution estimates is not biased by state reporting practices. This finding is consistent

with other work that found similar characteristics of sporadic and outbreak-associated foodborne illnesses and continues to be an active focus for IFSAC (*21*).

The first limitation of our study is that no data are readily available to identify and describe outbreaks that were detected and investigated but not reported. Some jurisdictions may be more likely to report outbreaks with an identified etiologic agent or food vehicle. Furthermore, in focusing on reporting, this study did not capture other improvements in completeness and timeliness of outbreak response activities. For example, FoodCORE metrics demonstrate improved completeness and timeliness of outbreak investigations (*20*), and this study did not assess the effects of intermediary metrics on national reporting. Limited data were available on state structural characteristics, and our study did not incorporate factors such as laboratory testing metrics, surveillance and investigation practices, and other state or local level established practices. Relevant survey data sources have not been updated in the past decade, including surveys used by Jones, et al., such as the Council of State and Territorial Epidemiologists Food Safety Capacity Assessment and the Association of Public Health Laboratories national PulseNet survey (*22*,*23*), which limited our ability to compare the effects of structural factors over time. Finally, participation in specific foodborne surveillance programs, which we did not find to be significantly associated with reporting, changed over the course of the study period, and our methods did not adjust for changes in participation over time. Specifically, the CoE program was started in 2012, and OBNE was started in 2015.

Future projects should include national surveys that further explore the association between structural factors and detecting, investigating, and reporting foodborne outbreaks. Some data were from different years; for example, ELC funding was only publicly available for 2016–2018. This analysis focused only on reported outbreaks with foodborne transmission, and states likely have different practices for reporting different transmission routes. Finally, this study focused on state-level outbreak reporting. However, most outbreak investigations occur at local public health agencies. Expertise, interest, and preparedness vary dramatically within states, particularly decentralized ones, to respond to foodborne outbreaks. Results from this study did not indicate a relationship between state legal structure and reporting, but this variable does not capture the nuance and diversity of the responsibility of investigating foodborne outbreaks. However, this finding could affect how federal funders such as CDC can target funding to improve communicable disease surveillance and public health preparedness.

In conclusion, this study demonstrates that investments in public health programming produce large benefits and measurable impact on national surveillance. Other studies have shown that robust surveillance systems improve health and decrease overall healthcare costs (*24*). Because individual state characteristics do not appear to bias our detection of which foods are associated with outbreaks, improving outbreak surveillance will also improve food attribution efforts.

Acknowledgments

We thank members of the Interagency Food Safety Analytics Collaboration for their critical reading of the manuscript and helpful comments.

This work was funded in part by the Colorado and Minnesota Integrated Food Safety Centers of Excellence, which are supported by the Epidemiology and Laboratory Capacity for Infectious Disease Cooperative Agreement through the Centers for Disease Control and Prevention.

About the Author

Ms. White is a senior research instructor in the department of epidemiology at the Colorado School of Public Health. Her primary research interests are public health surveillance and the epidemiology of foodborne diseases.

References

1. Scallan E, Hoekstra RM, Angulo FJ, Tauxe RV, Widdowson MA, Roy SL, et al. Foodborne illness acquired in the United States—major pathogens. Emerg Infect Dis. 2011;17:7–15. https://doi.org/10.3201/eid1701.P11101
2. Interagency Food Safety Analytics Collaboration. Foodborne illness source attribution estimates for *Salmonella*, *Escherichia coli* O157, *Listeria monocytogenes*, and *Campylobacter* using multi-year outbreak surveillance data, United States. Atlanta and Washington: US Department of Health and Human Services; 2020.
3. Painter JA, Hoekstra RM, Ayers T, Tauxe RV, Braden CR, Angulo FJ, et al. Attribution of foodborne illnesses, hospitalizations, and deaths to food commodities by using outbreak data, United States, 1998-2008. Emerg Infect Dis. 2013;19:407–15. https://doi.org/10.3201/eid1903.111866
4. Katz R. State foodborne illness reporting laws, 2011–2013. Inter-university Consortium for Political and Social Research. 2014 [cited 2022 Apr 15]. https://www.icpsr.umich.edu/web/HMCA/studies/34935
5. Keene BK, Kanwat CP. Enteric disease outbreak investigation and surveillance survey. Presented at: Council for State and Territorial Epidemiologists 2007 Annual Conference; June 24–28, 2007; Atlantic City, NJ, USA.
6. Centers for Disease Control and Prevention. Epidemiology and Laboratory Capacity for Prevention and Control of Emerging Infectious Diseases (ELC). 2021 [cited 2021 May 19]. https://www.cdc.gov/ncezid/dpei/epidemiology-laboratory-capacity.html

7. Hedberg C. Guidelines for foodborne disease outbreak response. 3rd edition. Atlanta: Council to Improve Foodborne Outbreak Response; 2020 [cited 2021 May 19]. https://cifor.us/downloads/clearinghouse/CIFOR-Guidelines-Complete-third-Ed.-FINAL.pdf
8. Centers for Disease Control and Prevention. National *Salmonella* surveillance annual report, 2016. Atlanta: US Department of Health and Human Services; 2018.
9. Centers for Disease Control and Prevention. National Shiga toxin–producing *Escherichia coli* (STEC) surveillance annual report, 2016. Atlanta: US Department of Health and Human Services; 2018.
10. Richardson LC, Bazaco MC, Parker CC, Dewey-Mattia D, Golden N, Jones K, et al. An updated scheme for categorizing foods implicated in foodborne disease outbreaks: a tri-agency collaboration. Foodborne Pathog Dis. 2017;14:701–10. https://doi.org/10.1089/fpd.2017.2324
11. Barrett KA, Nakao JH, Taylor EV, Eggers C, Gould LH. Fish-associated foodborne disease outbreaks: United States, 1998–2015. Foodborne Pathog Dis. 2017;14:537–43. https://doi.org/10.1089/fpd.2017.2286
12. Dewey-Mattia D, Manikonda K, Hall AJ, Wise ME, Crowe SJ. Surveillance for foodborne disease outbreaks—United States, 2009–2015. MMWR Surveill Summ. 2018;67:1–11. https://doi.org/10.15585/mmwr.ss6710a1
13. Centers for Disease Control and Prevention. An atlas of *Salmonella* in the United States, 1968–2011: laboratory-based enteric disease surveillance. Atlanta: US Department of Health and Human Services; 2013.
14. Li J, Shah GH, Hedberg C. Complaint-based surveillance for foodborne illness in the United States: a survey of local health departments. J Food Prot. 2011;74:432–7. https://doi.org/10.4315/0362-028X.JFP-10-353
15. Jones TF, Rosenberg L, Kubota K, Ingram LA. Variability among states in investigating foodborne disease outbreaks. Foodborne Pathog Dis. 2013;10:69–73. https://doi.org/10.1089/fpd.2012.1243
16. Marsh Z, Shah MP, Wikswo ME, Barclay L, Kisselburgh H, Kambhampati A, et al. Epidemiology of foodborne norovirus outbreaks—United States, 2009–2015. Food Saf (Tokyo). 2018;6:58–66. https://doi.org/10.14252/foodsafetyfscj.2017028
17. Ailes E, Budge P, Shankar M, Collier S, Brinton W, Cronquist A, et al. Economic and health impacts associated with a *Salmonella* Typhimurium drinking water outbreak—Alamosa, CO, 2008. PLoS One. 2013;8:e57439. https://doi.org/10.1371/journal.pone.0057439
18. Thomas MK, Vriezen R, Farber JM, Currie A, Schlech W, Fazil A. Economic cost of a *Listeria monocytogenes* outbreak in Canada, 2008. Foodborne Pathog Dis. 2015;12:966–71. https://doi.org/10.1089/fpd.2015.1965
19. Murphree R, Garman K, Phan Q, Everstine K, Gould LH, Jones TF. Characteristics of foodborne disease outbreak investigations conducted by Foodborne Diseases Active Surveillance Network (FoodNet) sites, 2003–2008. Clin Infect Dis. 2012;54(Suppl 5):S498–503. https://doi.org/10.1093/cid/cis232
20. Biggerstaff GK; FoodCORE Team. Improving response to foodborne disease outbreaks in the United States. J Public Health Manag Pract. 2015;21:E18–26. https://doi.org/10.1097/PHH.0000000000000115
21. Ebel ED, Williams MS, Cole D, Travis CC, Klontz KC, Golden NJ, et al. Comparing characteristics of sporadic and outbreak-associated foodborne illnesses, United States, 2004–2011. Emerg Infect Dis. 2016;22:1193–200. https://doi.org/10.3201/eid2207.150833
22. Boulton ML, Rosenberg LD. Food safety epidemiology capacity in state health departments—United States, 2010. MMWR Morb Mortal Wkly Rep . 2011;60:1701–4.
23. Association of Public Health Laboratories. PulseNet on the frontlines of foodborne disease surveillance: national molecular subtyping network for foodborne pathogens. APHL Public Health Laboratory Issues in Brief. April 2013 [cited 2022 Apr 17]. https://www.aphl.org/aboutAPHL/publications/Documents/FS_2013April29_PulseNet-on-the-Front-Lines-of-Foodborne-Disease-Surveillance.pdf
24. Scharff RL, Besser J, Sharp DJ, Jones TF, Peter GS, Hedberg CW. An economic evaluation of PulseNet: a network for foodborne disease surveillance. Am J Prev Med. 2016;50(Suppl 1):S66–73. https://doi.org/10.1016/j.amepre.2015.09.018

Address for correspondence: Alice White, Department of Epidemiology, Colorado School of Public Health, 13001 East 17th Pl, Mailstop B119, Aurora, CO 80045, USA; email: alice.white @cuanschutz.edu

Characterization of Healthcare-Associated and Community-Associated *Clostridioides difficile* Infections among Adults, Canada, 2015–2019

Tim Du,[1] Kelly B. Choi,[1] Anada Silva, George R. Golding, Linda Pelude, Romeo Hizon, Ghada N. Al-Rawahi, James Brooks, Blanda Chow, Jun C. Collet, Jeannette L. Comeau, Ian Davis, Gerald A. Evans, Charles Frenette, Guanghong Han, Jennie Johnstone, Pamela Kibsey, Kevin C. Katz, Joanne M. Langley, Bonita E. Lee, Yves Longtin, Dominik Mertz, Jessica Minion, Michelle Science, Jocelyn A. Srigley, Paula Stagg, Kathryn N. Suh, Nisha Thampi, Alice Wong, Susy S. Hota

We investigated epidemiologic and molecular characteristics of healthcare-associated (HA) and community-associated (CA) *Clostridioides difficile* infection (CDI) among adult patients in Canadian Nosocomial Infection Surveillance Program hospitals during 2015–2019. The study encompassed 18,455 CDI cases, 13,735 (74.4%) HA and 4,720 (25.6%) CA. During 2015–2019, HA CDI rates decreased by 23.8%, whereas CA decreased by 18.8%. HA CDI was significantly associated with increased 30-day all-cause mortality as compared with CA CDI (p<0.01). Of 2,506 isolates analyzed, the most common ribotypes (RTs) were RT027, RT106, RT014, and RT020. RT027 was more often associated with CDI-attributable death than was non-RT027, regardless of acquisition type. Overall resistance *C. difficile* rates were similar for all drugs tested except moxifloxacin. Adult HA and CA CDI rates have declined, coinciding with changes in prevalence of RT027 and RT106. Infection prevention and control and continued national surveillance are integral to clarifying CDI epidemiology, investigation, and control.

Clostridioides difficile is a major cause of infectious nosocomial diarrhea in high-income countries (*1*). Disease severity ranges from asymptomatic colonization to fulminant colitis, sometimes leading to colectomy and death (*2*). Healthcare costs attributed to *C. difficile* infection (CDI) are estimated to be $4.8 billion in the United States and €3 billion in Europe (*3*). A study in Canada estimated 38,000 annual CDI cases and conservative estimated costs of CDN $280 million resulting from extended hospital stays and rehospitalization (*4*).

The epidemiology of *C. difficile* has evolved markedly in the past decade (*1*). Whereas CDI was once

Author affiliations: National Microbiology Laboratory, Winnipeg, Manitoba, Canada (T. Du, G.R. Golding, R. Hizon); Public Health Agency of Canada, Ottawa, Ontario, Canada (K.B. Choi, A. Silva, L. Pelude, J. Brooks); British Columbia Children's Hospital, Vancouver, British Columbia, Canada (G.N. Al-Rawahi); Alberta Health Services, Calgary, Alberta, Canada (B. Chow); BC Children's & Women's Hospitals, Vancouver (J.C. Collet, J.A. Srigley); Dalhousie University, Halifax, Nova Scotia, Canada (J.L. Comeau); Queen Elizabeth II Health Sciences Centre, Halifax (I. Davis); Kingston Health Sciences Centre, Kingston, Ontario, Canada (G.A. Evans); McGill University Health Centre, Montréal, Quebec, Canada (C. Frenette); Provincial Infection Control Network, Vancouver (G. Han); Sinai Health, Toronto, Ontario, Canada (J. Johnstone); Royal Jubilee Hospital, Victoria, British Columbia, Canada (P. Kibsey); North York General Hospital, Toronto (K.C. Katz); IWK Health Centre, Halifax (J.M. Langley); Stollery Children's Hospital, Edmonton, Alberta, Canada (B.E. Lee); Jewish General Hospital, Montréal (Y. Longtin); Hamilton Health Sciences, Hamilton, Ontario, Canada (D. Mertz); Regina General Hospital, Regina, Saskatchewan, Canada (J. Minion); The Hospital for Sick Children, Toronto (M. Science); Western Memorial Regional Hospital, Corner Brook, Newfoundland and Labrador, Canada (P. Stagg); The Ottawa Hospital, Ottawa (K.N. Suh); Childrens Hospital of Eastern Ontario, Ottawa (N. Thampi); Royal University Hospital, Saskatoon, Saskatchewan, Canada (A. Wong); University Health Network, Toronto (S.S. Hota)

DOI: https://doi.org/10.3201/eid2806.212262

[1]These authors contributed equally to this article.

believed to be mostly healthcare-associated (HA), increased evidence points to transmission in community settings (*5*,*6*). An estimated 40% of patients with community-associated (CA) CDI require hospitalization; 20% experience treatment failure, and 28% have recurrent CDI episodes (*7*).

Several international studies have reported changes in molecular and epidemiologic characteristics of CDI in healthcare and community settings (*8*–*13*); we investigated changes in adult CA CDI epidemiology in Canada. The Canadian Nosocomial Infection Surveillance Program (CNISP) collects standardized epidemiologic and laboratory-linked data from sentinel hospitals across Canada, currently representing 30% of all acute care beds. We previously reported a decrease in HA CDI rates during 2009–2015, associated with a reduction in ribotype (RT) 027 (*1*). Here, we describe findings of a multicenter study evaluating incidence, patient characteristics, outcomes, RT prevalence, and antimicrobial resistance rates for HA and CA CDI identified during 2015–2019 in hospitals participating in CNISP. We also assessed associations between predominant RTs and all-cause and CDI-attributable deaths.

Methods

Case Definition

We used previously described case definitions for primary CDI (*14*) (Appendix, https://wwnc.cdc.gov/EID/article/28/6/21-2262-App1.pdf). A case of HA CDI was defined on the basis of laboratory confirmation of CDI and a compatible clinical syndrome developing ≥72 hours after admission, or <72 hours after admission if the patient had a previous admission to the hospital and was discharged within the previous 4 weeks. CA CDI was defined as clinical manifestation of CDI symptoms ≤72 hours before admission with no history of hospitalization or healthcare exposure, including outpatient healthcare exposures, within the previous 12 weeks.

Severe outcomes were defined as CDI-attributable admission to an intensive care unit (ICU), colectomy, or death ≤30 days after admission. All deaths were reviewed by an infectious disease physician or medical microbiologist by using clinical judgement to determine whether deaths were CDI-attributable.

Data Sources and Collection

CNISP has conducted prospective surveillance for HA CDI in hospitalized patients in Canada since 2007, and CA CDI surveillance was added in 2015. By 2019, CNISP included a network of 76 acute care hospitals across 10 provinces and 1 territory (Appendix Table 1). We analyzed data collected during 2015–2019 from adult and mixed (adult and pediatric) hospitals. The Canadian Network for Public Health Intelligence collected and verified clinical and laboratory surveillance data to ensure accuracy, as previously described (*14*).

Bacterial Culture and Molecular Characterization

We performed *C. difficile* isolation by using an ethanol shock treatment method, then selected for *C. difficile* on *Clostridium difficile* Moxalactam Norfloxacin agar (Oxoid, https://www.oxoid.com), as previously described (*15*,*16*). We prepared DNA for PCR analysis and ribotyping by using InstaGene Matrix (Bio-Rad, https://www.bio-rad.com), as previously described (*17*). We performed multiplex PCR targeting toxin A (*tcdA*), toxin B (*tcdB*), binary toxin (*cdtB*), negative regulator of toxin production (*tcdC*), and triose phosphate isomerase (*tpi*) housekeeping gene, as previously described (*15*,*18*,*19*), with slight modifications. We substituted an in-house A3B primer (5′-ACCATCAATCTCGAAAAGTCCAC-3′) for the tcd-R reverse primer for detecting *tcdA* (420 bp amplicon) and the detection of *tcdA* deletion variants (147 bp amplicon).

PCR Ribotyping

We performed capillary gel electrophoresis–based ribotyping targeting the 16S-23S intergenic spacer region, as previously described (*17*). We assigned RTs by comparing query profiles to those of a reference set of RTs used in a previous multicenter international study (*17*).

Antimicrobial Susceptibility Testing

We used Etest strips (bioMérieux, https://www.biomerieux.com) to perform susceptibility testing for metronidazole, clindamycin, vancomycin, rifampin, moxifloxacin, and tigecycline, as previously described (*16*,*20*). We interpreted antimicrobial resistance in accordance with Clinical and Laboratory Standards Institute guidelines (*20*).

Statistical Analysis

We calculated HA CDI incidence rates as number of cases per 10,000 patient-days and CA CDI incidence rates as number of cases per 1,000 patient admissions. We used the Cochran-Armitage test for categorical variables and the Mann-Kendall test for continuous variables to assess statistically significant trends over time for patient characteristics and outcome results. To compare characteristics of patients with HA CDI versus CA CDI, we used the χ^2 test for categorical variables and the Student *t* test or Wilcoxon rank sum test for continuous variables.

We used multivariable logistic regression to model the association between RTs and outcomes (i.e., 30-day all-cause and 30-day CDI-attributable mortality) and adjusted for a priori–selected confounders of age, sex, severe CDI cases (albumin level <30 g/L, leukocyte count ≥15 $\times 10^9$/L, or both), and CDI case types (i.e., HA vs. CA CDI). We used 2-tailed statistical tests and considered $p \leq 0.05$ statistically significant. We performed all analyses in SAS version 9.4 (SAS Institute Inc., https://www.sas.com).

Results

Our analysis included a total of 18,455 adult inpatient cases of primary CDI from participating hospitals during 2015–2019. HA CDI accounted for 74.4% (n = 13,735) of cases and CA for 25.6% (n = 4,720). The number of hospitals participating in HA CDI surveillance each year ranged from 58–64, and 46–54 hospitals participated in CA CDI surveillance (Appendix Table 1). We also completed a sensitivity analysis to restrict hospitals that conducted both HA and CA CDI surveillance but observed no stastically significant differences in results (data not shown).

During 2015–2019, HA CDI rates decreased by 23.8%, from 4.74 to 3.61 cases/10,000 patient-days (p<0.02), and CA CDI rates decreased by 18.8%, from 1.33 to 1.08 cases/1,000 admissions (p<0.33) (Figure 1). Regionally, HA CDI rates decreased significantly in the central (p<0.02) and western (p<0.02) regions of Canada, but rates fluctuated in the eastern region (p = 0.62), peaking at 4.06 cases/10,000 patient-days in 2019. Despite a decline, CA CDI infection rates remained highest in the central region, at 1.53 cases/1,000 admissions in 2019. Of the 64 hospitals for which data were available for adult CDI surveillance, 58 (91%) reported data for the entire 5-year period of surveillance. After restricting our analyses to these 58 hospitals, interpretation of our results did not change. Incidence rates for HA CDI decreased by 22.8%, CA CDI incidence decreased by 18.0%, and rates were consistent with those reported and generated with data from 64 hospitals.

We aggregated patient characteristics and outcomes by case type (Table 1). Compared with HA CDI patients, CA CDI patients were younger (median age 67.0 vs. 70.0 years; p<0.01), and more CA CDI patients were female (56.0% vs. 49.1% male; p<0.01).

Clinical Manifestations

Of the 18,455 cases, 3,084 had clinical and outcome data available; these data are collected during a 2-month targeted surveillance period (March–April) each year. Overall, 10.4% (316/3,033) of patients with CDI died, and 2.9% (86/3,019) of deaths were CDI-attributable (Table 1). Of 316 deaths among patients with CDI, 27.2% (86/316) were CDI-attributable. Patients with HA CDI had significantly higher 30-day all-cause mortality than patients with CA CDI (11.4% vs. 7.3%; p<0.01). Of 3,073 patients with CDI, 207 (6.8%) required ICU admission, 27.5% (57/207) of whom were admitted because of CDI complications, and 1.9% (57/3,073) all patients with CDI were admitted to the ICU because of CDI complications. We observed no statistically significant differences in ICU admission by acquisition type.

During 2015–2019, ICU admission data were available for 2,340 HA CDI patients (433–507 patients annually). ICU admissions decreased significantly among HA CDI cases, from 9.1% (46/507) in 2015 to 5.9% (26/442) in 2019 (p<0.02). We saw no statistically significant trends for age, sex, or 30-day outcomes for all-cause or CDI-attributable deaths (Appendix Table 2).

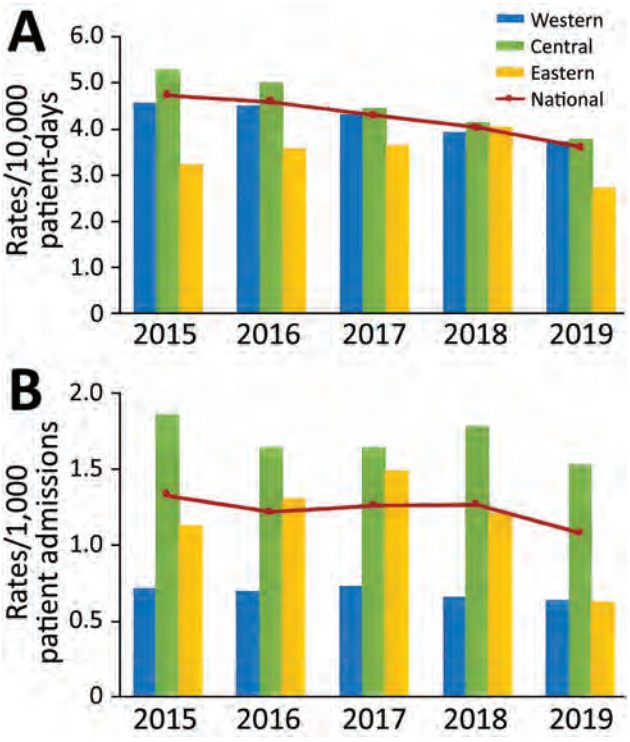

Figure 1. National and regional healthcare-associated (A) and community-associated (B) *Clostridioides difficile* infection rates among adults, Canada, 2015–2019. Western region is British Columbia, Alberta, Saskatchewan, and Manitoba; Central region is Ontario and Quebec; Eastern region is Nova Scotia, New Brunswick, Prince Edward Island, and Newfoundland and Labrador.

Ribotyping Analysis

Of the 18,455 cases, a total of 3,189 stool samples were received for *C. difficile* isolation at the National

Table 1. Clinical and molecular characteristics of healthcare-associated and community-associated *Clostridioides difficile* infection among adults, Canada, 2015–2019*

Characteristics	Healthcare-associated	Community-associated	All cases	p value
Routine surveillance, no. (%)†	13,735 (74.4)	4,720 (25.6)	18,455	
Patient characteristics				
Age, y				
Mean (SD)	68.3 (16.9)	64.4 (18.4)	67.3 (17.4)	**<0.001**
Median (IQR)	70.0 (59.0–81.0)	67.0 (54.0–79.0)	70.0 (58.0–80.0)	**<0.001**
Sex, no. (%)				
F	6,747 (49.1)	2,645 (56.0)	9,392 (50.9)	**<0.001**
M	6,988 (50.9)	2,075 (44.0)	9,063 (49.1)	
Targeted surveillance, no. (%)‡	2,350 (76.2)	734 (23.8)	3,084	
Clinical results and outcomes				
Median (IQR) leukocyte count, × 10^9 cells/L	10.9 (23.0–33.0)	10.6 (6.9–15.7)	10.8 (7.1–16.0)	NS
Median (IQR) albumin, g/L	26.0 (22.0–31.0)	28.0 (23.0–33.0)	27.0 (22.0–32.0)	**0.0232**
FMT, no. positive/no. tested (%)§	11/3,645 (0.3)	4/1,557 (0.3)	15/5,202 (0.3)	NS
Colectomy, no. positive/no. tested (%)	30/2,255 (1.3)	15/725 (2.1)	45/2,980 (1.5)	NS
Loop ileostomy, no. positive/no. tested (%)	2/798 (0.3)	3/270 (1.1)	5/1,068 (0.5)	NS
ICU admission, no. (%)	n = 2,340	n = 733	n = 3,073	
All cause	156 (6.7)	51 (7.0)	207 (6.8)	NS
Due to complications of CDI	46 (2.0)	11 (1.5)	57 (1.9)	NS
30-d mortality, no. (%)	n = 2,302	n = 731		
Death, all causes	263 (11.4)	53 (7.3)	316/3,033 (10.4)	**0.0001**
Death, attributable to CDI	69 (3.0)	17 (2.3)	86/3,019 (2.9)	NS

*Missing or unknown values were excluded from the analysis. χ^2 test was used to assess statistical significance for categorical variables; Student *t* test, or the Wilcoxon rank sum test was used for continuous variables. CDI, *Clostridiodes difficile* infection; FMT, fecal microbiota transplantation; ICU, intensive care unit; IQR, interquartile range; NS, not significant.
†Patient characeristics data collected year-round.
‡Clinical results and outcome data are collected during a 2-month targeted surveillance period (March–April) each year except FMT where the data were collected year-around.
§FMT data collection started in 2018.

Microbiology Laboratory (Winnipeg, Manitoba, Canada), and 2,506 samples met inclusion criteria. Of samples tested, 1,887 (75.3%) were HA CDI and 619 (24.7%) were CA CDI. We performed capillary gel electrophoresis ribotyping and antimicrobial susceptibility testing to further characterize isolates.

Among 1,887 HA CDI isolates characterized during the study period, we noted 170 unique PCR RTs (Figure 2). The most common RTs among HA CDI were RT027 (16.0%), RT106 (11.5%), RT014 (8.6%), RT020 (6.4%), and RT002 (5.7%). The 15 most prevalent RTs accounted for 69.6% of isolates tested (Appendix Table 3). The prevalence of RT027 in HA CDI cases decreased from 24.6% in 2015 to 9.4% in 2019 (p<0.01), but the incidence of RT106 increased from 7.3% in 2015 to 18.1% in 2019 (p<0.01).

Of 619 CA CDI isolates, we noted 115 unique RTs, of which RT106 (12.3%), RT020 (8.4%), RT014 (8.1%), RT027 (7.9%), and RT056 (5.0%) were the most prevalent. For CA CDI, the 15 most prevalent RTs

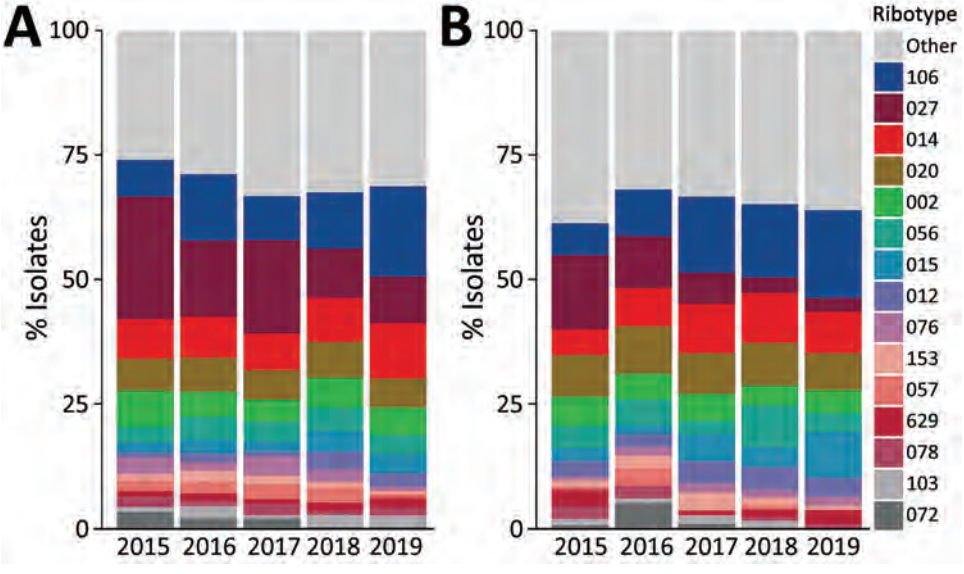

Figure 2. Prevalence of *Clostridioides difficile* ribotypes detected each year from healthcare-associated (A) and community-associated (B) infections among adults, Canada, 2015–2019.

accounted for 66.1% of isolates tested (Appendix Table 3). As for HA CDI, we noted a decrease in prevalence of RT027, from 14.8% in 2015 to 2.8% in 2019 (p<0.01) and RT106 increased from 6.5% in 2015 to 17.6% in 2019 (p<0.01). Despite a steady decline in prevalence over the study period, RT027 remained the most commonly isolated strain type with an overall combined prevalence of 14.0% (351/2,506 isolates).

RT078 and RT126 are livestock-associated strains that correlate with increased virulence and disease severity and have been identified in human CDIs. RT078 and RT126 prevalence among HA CDI cases averaged 2.4% (range 2.0%–3.2%), but for CA CDI, RT078 and RT126 prevalence averaged 1.9% (range 0.8%–3.2%) (Appendix Table 4).

All-Cause and CDI-Attributable Deaths

Among patients with reported 30-day all-cause mortality (n = 316) and 30-day CDI-attributable mortality (n = 86), most were HA CDI: 80.2% (263/316) of all-cause and 83.7% (69/86) of CDI-attributable deaths. In addition, more deaths occurred among female patients, who made up 55.4% (175/316) of all-cause and 57.0% of CDI-attributable (49/86) deaths, and more patients ≥65 years of age, who comprised 79.8% (252/316) of all-cause and 83.7% of CDI-attributable deaths (72/86).

After multivariable analysis, patient characteristics significantly associated with 30-day all-cause mortality and 30-day CDI-attributable mortality were age ≥65 years and severe CDI (Table 2). The adjusted odds ratio of 30-day all-cause mortality among patients with HA CDI was 1.83 (95% CI 1.23–2.72) times more than for patients with CA CDI (p<0.01). Similarly, the adjusted odds ratio of 30-day CDI-attributable mortality was 1.25 (95% CI 0.67–2.35) times higher among HA CDI than CA CDI, but this difference was not statistically significant.

Analysis of RT027 and RT106 Outcomes

Among 2,320 case-patients with available data on 30-day all-cause mortality, 316 (13.6%) were reported to have died (Appendix Table 5). Of 235 deaths among patients with associated ribotyping data, 44 (18.7%) deaths were associated with RT027 and 30 (12.8%) deaths with RT106. Among RT027 cases, a significantly higher proportion of 30-day all-cause mortality was associated with HA CDI cases than with CA CDI cases (p = 0.01). We saw no statistically significant difference in 30-day all cause mortality between HA and CA CDI cases associated with RT106. We also saw no statistically significant difference in CDI-attributable deaths when stratified by HA and CA CDI cases for RT027 and RT106.

Table 2. Univariable and multivariable analysis of 30-day all-cause and *Clostridioides difficile*–attributable mortality, Canada, 2015–2019*

	Univariable analysis		Multivariable analysis	
Characteristics	Odds ratio (95% CI)	p value	Adjusted odds ratio (95% CI)	p value
All-cause mortality				
Sex				
M	Referent		Referent	
F	1.15 (0.91–1.45)	0.2484	1.26 (0.93–1.70)	NS
Age group, y				
<65	Referent		Referent	
≥65	**2.66 (2.00–3.53)**	**<0.0001**	**3.63 (2.45–5.39)**	**<0.0001**
Severe CDI†	**2.53 (1.90–3.36)**	**<0.0001**	**2.66 (1.90–3.73)**	**<0.0001**
CDI case type				
Community-associated	Referent		Referent	
Healthcare-associated	**1.65 (1.21–2.24)**	**0.0014**	**1.83 (1.23–2.72)**	**0.0028**
RT027 vs. non-RT027	**1.48 (1.04–2.10)**	**0.0289**	1.10 (0.74–1.63)	NS
RT106 vs. non-RT106	1.09 (0.73–1.63)	0.6804	NA	
CDI-attributable mortality				
Sex				
M	Referent		Referent	
F	1.22 (0.79–1.87)	0.3776	1.33 (0.81–1.19)	NS
Age group, y				
<65	Referent		Referent	
≥65	**3.28 (1.84–5.85)**	**<0.0001**	**3.44 (1.73–6.82)**	**0.0004**
Severe CDI†	**2.40 (1.45–4.0)**	**0.0006**	**2.25 (1.28–3.94)**	**0.0050**
CDI case type				
Community-associated	Referent		Referent	
Healthcare-associated	1.29 (0.76–2.22)	0.3476	1.25 (0.67–2.35)	NS
RT027 vs. non-RT027	**3.17 (1.89–5.29)**	**<0.0001**	**2.85 (1.64–5.00)**	**0.0002**
RT106 vs. non-RT106	0.95 (0.45–2.00)	0.8830	NA	

*Bold text indicates statistical significance. CDI, *Clostridioides difficile* infection; NA, not applicable; NS, not significant; RT, ribotype.
†Severe CDI defined as albumin level <30 g/L, leukocyte count ≥15 × 10^9 cells/L, or both.

Of 162 cases with severe outcomes for which ribotype analysis was available in the HA CDI population, 33 (11.7%) were associated with RT027 and 10 (4.8%) were associated with RT106 (p<0.01). We also noted a small number of severe outcomes associated with RT027 (n = 2) and RT106 (n = 3) in CA CDI cases; however, we noted no statistically significant differences between HA and CA CDI.

Multivariate analysis found RT027 was significantly associated with 30-day CDI-attributable mortality (adjusted odds ratio [aOR] 2.85, 95% CI 1.64–5.00) compared with non-RT027 cases (p<0.01). However, the association of RT027 with the outcome of 30-day all-cause mortality did not remain statistically significant compared with non-RT027 cases when controlling for other factors within the multivariate model (aOR 1.10, 95% CI 0.74–1.63). When compared with non-RT106 cases, RT106 was not significantly associated with either 30-day all-cause (p = 0.68) or CDI attributable (p = 0.88) mortality in the univariate model.

Antimicrobial Susceptibility

We conducted antimicrobial resistance testing for HA and CA CDI isolates collected during 2015–2019 (Figure 3; Appendix Tables 6, 7). During the study years, HA CDI resistance was 21.7% to moxifloxaxin, 31.0% to clindamycin, and 1.9% to rifampin and CA CDI resistance was 12.4% to moxifloxacin, 33.6% to clindamycin, and 1.5% to rifampin. Of note, HA CDI resistance to moxifloxacin decreased from 34.3% in 2015 to 13.5% in 2019. Similarly, CA CDI resistance to moxifloxacin declined from 18.7% in 2015 to 11.1% in 2019. Resistance to clindamycin was more variable in both study populations, overall resistance was 32.3% (range 19%–54%) (Figure 3).

RT027 accounted for 60.2% (293/487) of identified moxifloxacin-resistant isolates. Of note, 83.5% (293/351) of all RT027 isolates examined were moxifloxacin-resistant, of which 97.3% (285/293) had MICs ≥32 μg/mL. Among RT027 isolates, resistance was higher in HA CDI (85.4%; 258/302) than CA CDI (71.4%; 35/49) cases. In contrast, RT106, the second most prevelant strain type (11.7%), accounted for 6.0% of all moxifloxacin-resistant isolates. Fluoroquinolone resistance in RT106 isolates was much lower (9.9%; 29/293), and resistance values were similar for both HA (10.6%) and CA settings (7.9%).

RT027 strains also were more likely to be associated with resistance to ≥1 antimicrobial drug. Of 172 isolates resistant to both moxifloxacin and clindamycin, 79 (45.9%) were RT027. Of 22 isolates found to be resistant to moxifloxacin, clindamycin, and rifampin, 68.2% (15/22) were RT027; of these, 12 were from HA CDI cases and 3 were from CA CDI cases. No other RT strain exhibited resistance to ≥1 drug with a prevalence >5%.

We did not observe resistance for metronidazole, vancomycin, or tigecycline for any study year in either HA or CA CDI populations. One adult patient with HA CDI in 2019 had intermediate susceptibility to vancomycin (MIC 6 μg/mL) but sensitivity to all other drugs tested.

Discussion

Using 5 years of CDI surveillance data from acute care hospitals across Canada, we observed a decline in rates of HA and CA CDI that coincided with a marked change in the prevalence of predominant circulating ribotypes. The epidemiologic and molecular characterization of HA and CA CDI revealed differences in patient characteristics and select clinical outcomes, with associations to predominant ribotypes.

The decline in CDI rates in Canada follows a parallel trend observed globally, despite rates being higher in North America (*10*,*21*). We previously reported HA CDI rates ranging from 2.1 to 6.6 cases/10,000 inpatient days during 2011–2016 but showing a decreasing trend over time (*13*). We noted an increase in CA CDI rates in that study, but in this study, we found that rates of CA CDI have decreased since 2015. Although the precise reasons for decreased CDI incidence in Canada are unclear, enhanced infection control and antimicrobial stewardship measures combined with improved surveillance methods might have contributed to the overall decline (*22*). Furthermore, patients with mild to moderate CA CDI might not be admitted to or tested in a hospital, resulting in underestimation of the true burden of CA CDI.

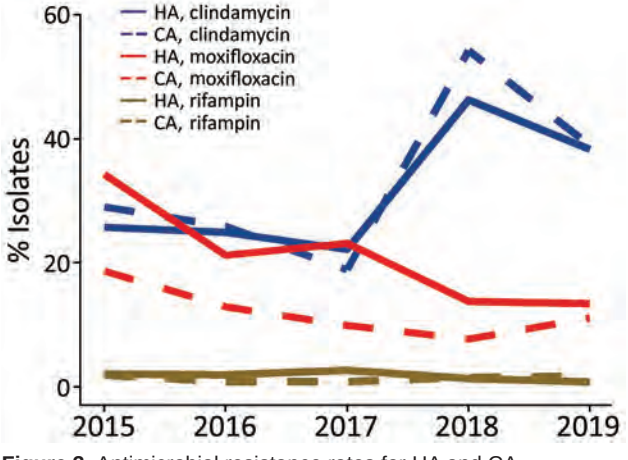

Figure 3. Antimicrobial resistance rates for HA and CA *Clostridioides difficile* infections among adults, Canada, 2015–2019. CA, community-associated; HA, healthcare-associated.

Although molecular surveillance of CDI in Canada revealed a dynamic and heterogeneous RT population, the predominant circulating types were RT027, RT106, RT020, and RT014. Similar to findings in this study, RT027 has been reported to be decreasing in prevalence in North America, the United Kingdom, and elsewhere; however, RT027 remains a major cause of CDI (*1*,*23*–*26*). In Canada, the dramatic decrease in RT027 prevalence in HA CDI has continued since its initial reporting (*1*). Declining trends observed among HA (−15.2%) and CA (−12.0%) CDI during 2015–2019 in Canada are also consistent with trends in the United States, where HA CDI rates declined from 21% to 15% and CA CDI declined from 17% to 6% during 2012–2017 (*25*).

Although RT027 prevalence in Canada decreased during 2015–2019, RT106 greatly increased during the same period, from 7.3% to 18.1% in healthcare settings and from 6.5% to 17.6% in community settings. Identified in the United Kingdom in 1999 (*27*), RT106 is now found worldwide and is one of the most predominant strains in the United States (*28*). Studies indicate that RT106 has enhanced spore-producing and biofilm formation capabilities that enable greater persistence in the environment and hospital settings, possibly leading to increased infection rates (*28*,*29*). In addition, studies report that patients infected with RT106 are more likely to experience multiple episodes of relapse (*28*,*30*).

C. difficile RT078 and RT126, which have demonstrated epidemic potential in other countries (*31*–*33*), appear to be uncommon in patients hospitalized with CDI in Canada. Our surveillance shows a small increase in RT078 and RT126 prevalence since a previous report showed rates of 2.4% in HA and 1.9% CA CDI populations (*14*).

Similar to previous findings, our study showed that CA CDI patients were more likely to be younger and female (*10*,*34*–*36*). In addition, this study found that HA CDI is associated with an increased risk for 30-day all-cause mortality compared with CA CDI; however, this association did not remain significant for CDI-attributable deaths. Hospitalized patients with CDI possibly are exposed to other risks and complications during their hospital stay or have underlying conditions that increase their risk for all-cause death. Our findings agree with previously published studies assessing all-cause and CDI-attributable death (*34*,*37*).

We further analyzed the effects of RT027 and RT106, the 2 most prevalent *C. difficile* strains, on all-cause and CDI-attributable death. We previously showed a significant association between RT027 and attributable mortality (*1*). In this study, we concluded that RT027 is a significant predictor of CDI-attributable death even after adjusting for case type (HA or CA CDI). We noted no association between RT106 and all-cause and CDI-attributable deaths.

We found that *C. difficile* antimicrobial resistance is less common in Canada than in the United States or globally (*38*). Stratified by case type, HA and CA CDI isolates revealed no significant difference in resistance, except for moxifloxacin resistance, which was 21.7% for HA and 12.4% for CA CDI, consistent with previously reported findings (*30*). In addition, diverse RT populations observed in both HA and CA CDI might be predicative of lower resistance rates observed because RT heterogeneity has been shown to be inversely correlated with antimicrobial resistance as measured by cumulative resistance scores (*12*,*39*).

Our study's first limitations is that hospital participation in HA and CA CDI surveillance varied by year and might have affected trends over time. Furthermore, hospitals self-select whether to participate in both HA and CA CDI surveillance, which might have influenced the comparison of HA and CA CDI patients. To mitigate this limitation, we conducted a sensitivity analysis restricted to hospitals that conducted both HA and CA CDI surveillance. Second, although CDI diagnostic testing methods were collected throughout the study period, data completeness was not consistent from year to year, limiting the inferences we could make regarding the effect of CDI diagnostic testing methods on adult CDI rates over time. Third, for CA CDI surveillance, our study captured data from patients admitted to a CNISP hospital and requiring medical intervention for CDI symptoms or other underlying conditions. The features and outcomes of these patients might not be relevant to patients with CA CDI who do not require hospital care. Finally, although a qualified physician determined the cause of death in patients with CDI, attribution of death is difficult and could be subjective.

In conclusion, rates of HA and CA CDI in Canada declined during 2015–2019, coinciding with a decrease in prevalence of RT027 and increased prevalence of RT106. HA CDI was associated with higher rates of all-cause death than was CA CDI, and RT027 was a major predictor of CDI-attributable death, irrespective of location of acquisition. We noted major decreases in antimicrobial resistance to moxifloxacin in both HA and CA CDI populations, concordant with an overall decrease in prevalence of RT027. Despite declining rates, CDI continues to be a major health burden in Canada. To ensure continued success in combatting this global health threat, robust national surveillance and infection prevention and control programs are integral to clarifying CDI epidemiology, investigation, and control.

Acknowledgment

We gratefully acknowledge the physicians, epidemiologists, infection control practitioners, and laboratory staff at each participating hospital for their contributions. We thank the staff at the Public Health Agency of Canada, especially Joelle Cayen, Sean Ahmed, and Jennifer Campbell.

This work was supported by the Public Health Agency of Canada.

Canadian Nosocomial Infection Surveillance Program hospitals provided expertise in the development of protocols in addition to epidemiological data and laboratory isolates. National Microbiology Laboratory staff and epidemiologists from Public Health Agency of Canada were responsible for the conception, analysis, interpretation, drafting, and revision of the paper.

About the Authors

Dr. Du is a biologist with the Public Health Agency of Canada in Winnipeg, Manitoba, Canada. His primary research interests include the epidemiology of *Clostridioides difficile* in addition to antimicrobial resistance in hospital acquired infections. Dr. Choi is an epidemiologist with Canadian Nosocomian Infection Surveillance Program, Public Health Agency of Canada, Ottawa, Ontario, Canada. Her primary research interest is antimicrobial-resistant infections, including *C. difficile* infection and surgical site infections.

References

1. Katz KC, Golding GR, Choi KB, Pelude L, Amaratunga KR, Taljaard M, et al.; Canadian Nosocomial Infection Surveillance Program. The evolving epidemiology of *Clostridium difficile* infection in Canadian hospitals during a postepidemic period (2009–2015) [cited 2021 May 7]. CMAJ. 2018;190:E758–65. https://doi.org/10.1503/cmaj.180013
2. Gravel D, Miller M, Simor A, Taylor G, Gardam M, McGeer A, et al.; Canadian Nosocomial Infection Surveillance Program. Health care-associated *Clostridium difficile* infection in adults admitted to acute care hospitals in Canada: a Canadian Nosocomial Infection Surveillance Program Study. Clin Infect Dis. 2009;48:568–76. https://doi.org/10.1086/596703
3. Bouza E. Consequences of *Clostridium difficile* infection: understanding the healthcare burden. Clin Microbiol Infect. 2012;18:5–12. https://doi.org/10.1111/1469-0691.12064
4. Levy AR, Szabo SM, Lozano-Ortega G, Lloyd-Smith E, Leung V, Lawrence R, et al. Incidence and costs of *Clostridium difficile* infections in Canada. Open Forum Infect Dis. 2015;2:ofv076. https://doi.org/10.1093/ofid/ofv076
5. Zanichelli V, Garenc C, Villeneuve J, Moisan D, Frenette C, Loo V, et al.; Québec C.difficile Infection Surveillance Program (SPIN-CD). Increased community-associated *Clostridioides difficile* infections in Quebec, Canada, 2008–2015. Emerg Infect Dis. 2020;26:1291–4. https://doi.org/10.3201/eid2606.190233
6. Gupta A, Khanna S. Community-acquired *Clostridium difficile* infection: an increasing public health threat. Infect Drug Resist. 2014;7:63–72.
7. Khanna S, Pardi DS, Aronson SL, Kammer PP, Baddour LM. Outcomes in community-acquired *Clostridium difficile* infection. Aliment Pharmacol Ther. 2012;35:613–8. https://doi.org/10.1111/j.1365-2036.2011.04984.x
8. Lee J-H, Lee Y, Lee K, Riley TV, Kim H. The changes of PCR ribotype and antimicrobial resistance of *Clostridium difficile* in a tertiary care hospital over 10 years. J Med Microbiol. 2014;63:819–23. https://doi.org/10.1099/jmm.0.072082-0
9. Thornton CS, Rubin JE, Greninger AL, Peirano G, Chiu CY, Pillai DR. Epidemiological and genomic characterization of community-acquired *Clostridium difficile* infections. BMC Infect Dis. 2018;18:443. https://doi.org/10.1186/s12879-018-3337-9
10. Kotila SM, Mentula S, Ollgren J, Virolainen-Julkunen A, Lyytikäinen O. Community-and healthcare-associated *Clostridium difficile* infections, Finland, 2008–2013. Emerg Infect Dis. 2016;22:1747–53. https://doi.org/10.3201/eid2210.151492
11. Snydman DR, McDermott LA, Jenkins SG, Goldstein EJC, Patel R, Forbes BA, et al. Epidemiologic trends in *Clostridioides difficile* isolate ribotypes in United States from 2011 to 2016. Anaerobe. 2020;63:102185. https://doi.org/10.1016/j.anaerobe.2020.102185
12. Freeman J, Vernon J, Pilling S, Morris K, Nicolson S, Shearman S, et al.; Pan-European Longitudinal Surveillance of Antibiotic Resistance among Prevalent Clostridium difficile Ribotypes' Study Group. Five-year pan-European, longitudinal surveillance of *Clostridium difficile* ribotype prevalence and antimicrobial resistance: the extended ClosER study. Eur J Clin Microbiol Infect Dis. 2020;39:169–77. https://doi.org/10.1007/s10096-019-03708-7
13. Xia Y, Tunis MC, Frenette C, Katz K, Amaratunga K, Rhodenizer Rose S, et al. Epidemiology of *Clostridioides difficile* infection in Canada: a six-year review to support vaccine decision-making. Can Commun Dis Rep. 2019;45:191–211. https://doi.org/10.14745/ccdr.v45i78a04
14. Canadian Nosocomial Infection Surveillance Program. Healthcare-associated infections and antimicrobial resistance in Canadian acute care hospitals, 2014–2018. Canada Commun Dis Rep. 2020;46:99–112. https://doi.org/10.14745/ccdr.v46i05a01
15. Miller M, Gravel D, Mulvey M, Taylor G, Boyd D, Simor A, et al. Health care-associated *Clostridium difficile* infection in Canada: patient age and infecting strain type are highly predictive of severe outcome and mortality. Clin Infect Dis. 2010;50:194–201. https://doi.org/10.1086/649213
16. Lynch T, Chong P, Zhang J, Hizon R, Du T, Graham MR, et al.; Canadian Nosocomial Infection Surveillance Program (CNISP). Characterization of a stable, metronidazole-resistant *Clostridium difficile* clinical isolate. PLoS One. 2013;8:e53757. https://doi.org/10.1371/journal.pone.0053757
17. Fawley WN, Knetsch CW, MacCannell DR, Harmanus C, Du T, Mulvey MR, et al. Development and validation of an internationally-standardized, high-resolution capillary gel-based electrophoresis PCR-ribotyping protocol for *Clostridium difficile*. PLoS One. 2015;10:e0118150. https://doi.org/10.1371/journal.pone.0118150
18. Lemee L, Dhalluin A, Testelin S, Mattrat MA, Maillard K, Lemeland JF, et al. Multiplex PCR targeting *tpi* (triose phosphate isomerase), *tcdA* (Toxin A), and *tcdB* (Toxin B) genes for toxigenic culture of *Clostridium difficile*. J Clin Microbiol. 2004;42:5710–4. https://doi.org/10.1128/JCM.42.12.5710-5714.2004
19. Spigaglia P, Mastrantonio P. Comparative analysis of *Clostridium difficile* clinical isolates belonging to different

genetic lineages and time periods. J Med Microbiol. 2004;53:1129–36. https://doi.org/10.1099/jmm.0.45682-0
20. Clinical and Laboratory Standards Institute. Methods for antimicrobial susceptibility testing of anaerobic bacteria, 9th edition. CLSI standard M11. Wayne (PA): The Institute; 2018.
21. Ho J, Wong SH, Doddangoudar VC, Boost MV, Tse G, Ip M. Regional differences in temporal incidence of *Clostridium difficile* infection: a systematic review and meta-analysis. Am J Infect Control. 2020;48:89–94. https://doi.org/10.1016/j.ajic.2019.07.005
22. Pereira JA, McGeer A, Tomovici A, Selmani A, Chit A. Incidence and economic burden of *Clostridioides difficile* infection in Ontario: a retrospective population-based study. CMAJ Open. 2020;8:E16–25. https://doi.org/10.9778cmajo.20190018
23. Jassem AN, Prystajecky N, Marra F, Kibsey P, Tan K, Umlandt P, et al. Characterization of *Clostridium difficile* strains in British Columbia, Canada: a shift from NAP1 majority (2008) to novel strain types (2013) in one region. Can J Infect Dis Med Microbiol. 2016;2016:8207418. https://doi.org/10.1155/2016/8207418
24. Karlowsky JA, Zhanel GG, Hammond GW, Rubinstein E, Wylie J, Du T, et al. Multidrug-resistant North American pulsotype 2 *Clostridium difficile* was the predominant toxigenic hospital-acquired strain in the province of Manitoba, Canada, in 2006–2007. J Med Microbiol. 2012;61:693–700. https://doi.org/10.1099/jmm.0.041053-0
25. Centers for Disease Control and Prevention. 2018 Annual report for the Emerging Infections Program for *Clostridioides difficile* infection [cited 2021 Jun 25]. https://www.cdc.gov/hai/eip/Annual-CDI-Report-2017.html.
26. Public Health England. *Clostridium difficile* Ribotyping Network (CDRN) for England and Northern Ireland, 2015–2018. London: Public Health England; 2019.
27. Stubbs SLJ, Brazier JS, O'Neill GL, Duerden BI. PCR targeted to the 16S-23S rRNA gene intergenic spacer region of *Clostridium difficile* and construction of a library consisting of 116 different PCR ribotypes. J Clin Microbiol. 1999;37:461–3. https://doi.org/10.1128/JCM.37.2.461-463.1999
28. Carlson TJ, Blasingame D, Gonzales-Luna AJ, Alnezary F, Garey KW. *Clostridioides difficile* ribotype 106: A systematic review of the antimicrobial susceptibility, genetics, and clinical outcomes of this common worldwide strain. Anaerobe. 2020;62:102142. https://doi.org/10.1016/j.anaerobe.2019.102142
29. Roxas BAP, Roxas JL, Claus-Walker R, Harishankar A, Mansoor A, Anwar F, et al. Phylogenomic analysis of *Clostridioides difficile* ribotype 106 strains reveals novel genetic islands and emergent phenotypes. Sci Rep. 2020;10:22135. https://doi.org/10.1038/s41598-020-79123-2
30. Suárez-Bode L, Barrón R, Pérez JL, Mena A. Increasing prevalence of the epidemic ribotype 106 in healthcare facility-associated and community-associated *Clostridioides difficile* infection. Anaerobe. 2019;55:124–9. https://doi.org/10.1016/j.anaerobe.2018.12.002
31. Keessen EC, Harmanus C, Dohmen W, Lipman LJA, Kuijper EJ. *Clostridium difficile* infection associated with pig farms. Emerg Infect Dis. 2013;19:1032–4. https://doi.org/10.3201/eid1906.121645
32. Mulvey MR, Boyd DA, Gravel D, Hutchinson J, Kelly S, McGeer A, et al. Hypervirulent *Clostridium difficile* strains in hospitalized patients, Canada. Emerg Infect Dis. 2010;16:678–81. https://doi.org/0.3201/eid1604.091152
33. Knetsch CW, Kumar N, Forster SC, Connor TR, Browne HP, Harmanus C, et al. Zoonotic transfer of *Clostridium difficile* harboring antimicrobial resistance between farm animals and humans. J Clin Microbiol. 2018;56:e01384-17. https://doi.org/10.1128/JCM.01384-17
34. Kwon SS, Gim JL, Kim MS, Kim H, Choi JY, Yong D, et al. Clinical and molecular characteristics of community-acquired *Clostridium difficile* infections in comparison with those of hospital-acquired *C. difficile*. Anaerobe. 2017;48:42–6. https://doi.org/10.1016/j.anaerobe.2017.06.014
35. Tan XQ, Verrall AJ, Jureen R, Riley TV, Collins DA, Lin RT, et al. The emergence of community-onset *Clostridium difficile* infection in a tertiary hospital in Singapore: a cause for concern. Int J Antimicrob Agents. 2014;43:47–51. https://doi.org/10.1016/j.ijantimicag.2013.09.011
36. Fellmeth G, Yarlagadda S, Iyer S. Epidemiology of community-onset *Clostridium difficile* infection in a community in the South of England. J Infect Public Health. 2010;3:118–23. https://doi.org/10.1016/j.jiph.2010.07.002
37. Crobach MJT, Notermans DW, Harmanus C, Sanders IMJG, De Greeff SC, Kuijper EJ. Community-onset *Clostridioides difficile* infection in hospitalized patients in the Netherlands. Open Forum Infect Dis. 2019;6:ofz501. https://doi.org/10.1093/ofid/ofz501
38. Peng Z, Jin D, Kim HB, Stratton CW, Wu B, Tang YW, et al. Update on antimicrobial resistance in *Clostridium difficile*: resistance mechanisms and antimicrobial susceptibility testing. J Clin Microbiol. 2017;55:1998–2008. https://doi.org/10.1128/JCM.02250-16
39. Freeman J, Vernon J, Morris K, Nicholson S, Todhunter S, Longshaw C, et al.; Pan-European Longitudinal Surveillance of Antibiotic Resistance among Prevalent Clostridium difficile Ribotypes' Study Group. Pan-European longitudinal surveillance of antibiotic resistance among prevalent *Clostridium difficile* ribotypes. Clin Microbiol Infect. 2015;21:248.e9–16. https://doi.org/10.1016/j.cmi.2014.09.017

Address for correspondence: George Golding, Surveillance, Reference and Science Directorate of the National Microbiology Laboratory Branch, One Health Division, Antimicrobial Resistance and Nosocomial Infections, National Microbiology Laboratory, 1015 Arlington St, Winnipeg, MB R3E 3R2, Canada; email: george.golding@phac-aspc.gc.ca

Divergent Rabies Virus Variant of Probable Bat Origin in 2 Gray Foxes, New Mexico, USA

Rene E. Condori, Adam Aragon, Mike Breckenridge, Kendra Pesko, Kerry Mower, Paul Ettestad, Sandra Melman, Andres Velasco-Villa, Lillian A. Orciari, Pamela Yager, Daniel G. Streicker, Crystal M. Gigante, Clint Morgan, Ryan Wallace, Yu Li

In the Western Hemisphere, bat-associated rabies viruses (RABVs) have established independent transmission cycles in multiple mammal hosts, forming genetically distinct lineages. In New Mexico, USA, skunks, bats, and gray foxes are rabies reservoir hosts and represent a public health risk because of encounters with humans. During 2015 and 2019, two previously undescribed RABVs were detected in 2 gray foxes (*Urocyon cinereoargenteus*) in Lincoln County, New Mexico. Phylogenetic analysis of the nucleoprotein gene indicated that the isolates are a novel RABV variant. These 2 cases probably represent repeated spillover events from an unknown bat reservoir to gray foxes. Molecular analysis of rabies cases across New Mexico identified that other cross-species transmission events were the result of viral variants previously known to be enzootic to New Mexico. Despite a robust rabies public health surveillance system in the United States, advances in testing and surveillance techniques continue to identify previously unrecognized zoonotic pathogens.

Rabies is a viral zoonotic disease that infects the central nervous system of mammals and causes a highly lethal acute encephalitis. *Rabies lyssavirus* is the most prevalent of the 17 recognized species of the genus *Lyssavirus* and is genetically grouped within the phylogroup I (*1*,*2*). Rabies virus (RABV) is distributed worldwide and has an estimated human rabies death toll of >59,000 annually. Most human rabies deaths are associated with dog-mediated rabies, predominantly in Asia, Africa, and several countries in the Western Hemisphere (*3*). Rabies is commonly transmitted through direct contact with the saliva of rabid animals; humans or any susceptible mammal usually become infected through a bite. After potential exposure to RABV, if postexposure prophylaxis (PEP) is not administered before symptom onset, the outcome will nearly always be fatal (*4*).

In the Western Hemisphere, 2 genetic lineages of RABV have been identified: Cosmopolitan Dog lineage and New World lineage. The Cosmopolitan Dog lineage was introduced during European colonization; dog-to-dog transmission and host switching to other terrestrial mesocarnivores enabled this lineage to spread and establish across the Americas and some Caribbean islands. The New World lineages circulate mainly within bat populations, with several exceptions of lineages that shifted to terrestrial mesocarnivores (*5*,*6*).

The United States recognized dog and wildlife rabies as a problem and organized large-scale public health efforts to control the disease as early as 1944 (https://wwwn.cdc.gov/nndss/conditions/rabies-animal), the year in which a consensus agreement was reached to consider rabies a reportable disease (*7*). Interrupting the chain of dog-to-dog transmission thorough immunization led to the milestone of eliminating rabies circulating in dogs (*8*). According to the most recent annual surveillance reports, since 2015, bats have become the most commonly reported rabies reservoir species in the continental United States (*9*,*10*). RABVs circulating in bat populations are incredibly diverse.

Monoclonal antibodies (mAbs) provide evidence of antigenic differences among RABVs,

Author affiliations: Centers for Disease Control and Prevention, Atlanta, Georgia, USA (R.E. Condori, A. Velasco-Villa, L.A. Orciari, P. Yager, C.M. Gigante, C. Morgan, R. Wallace, Y. Li); New Mexico Department of Health, Albuquerque, New Mexico, USA (A. Aragon, M. Breckenridge, K. Pesko, P. Ettestad, S. Melman); New Mexico Department of Game and Fish, Santa Fe, New Mexico, USA (K. Mower); University of Glasgow, Glasgow, Scotland, UK (D.G. Stricker)

DOI: https://doi.org/10.3201/eid2806.211718

and mAbs patterns form the basis for determining conventional RABV variant nomenclature (*11*). However, RABV variant identification by using mAbs might not be able to provide appropriate resolution because of genetic variation, particularly when applied to the highly diverse bat RABV. Therefore, a comprehensive genetic analysis is frequently used to understand transmission dynamics and explore genetic differences (*12*). In the United States, RABV variants are often named on the basis of the presumptive reservoir host (e.g., *Tadarida brasiliensis* bats); ≥18 different recognized bat-specific variants have been identified (*13*,*14*). Detailed genetic studies have suggested several instances in which RABV circulating in bats has shifted to terrestrial mammals. Enzootic cycles of RABV from bat origin have been established by host shift events separately in raccoons (*Procyon lotor*) and skunks (*Mephitis mephitis*) (*15*).

Host shift events are rare, and the factors that lead to a successful host shift are poorly understood. Some studies have linked such events to ecologic, viral, or host factors that might contribute to long-term establishment (*16*–*18*). Circulation of novel RABV variants in wildlife species can remain unnoticed unless there is an outbreak or an event that leads to an infected animal reported the National Rabies Surveillance System (https://www.healthypeople.gov), in which testing and additional virus characterization can detect unexpected virus–host infections (*19*,*20*). Laboratory-based surveillance using molecular tools is useful to identify genetic changes and explore relatedness at a more refined level, which can help to identify novel RABV variants (*21*).

New Mexico is known to have ≥3 RABV enzootic cycles represented by skunks (south-central skunk variant), gray foxes (Arizona gray fox variant), and numerous variants associated with bats. During 2000–2020, the state surveillance system detected 275 rabies cases in wildlife species and 14 cases in domestic animals (https://nmhealth.org/about/erd/ideb/zdp/rab). In 2015, a woman in Lincoln County was attacked by a gray fox and appropriate PEP was given; a sample showed positive results for rabies, but preliminary antigenic and molecular analysis did not align with known RABV variants. In 2019, a second isolate collected from a gray fox that bit a man in the same county, but in a different city, showed a similar genetic pattern. The purpose of this study was to characterize these divergent RABV isolates from gray foxes in Lincoln County and investigate potential reservoir host species.

Materials and Methods

RABV Samples

All samples were collected as part of routine public health surveillance activities, and no animal sampling was performed for this study. Of the 289 samples tested that were positive for RABV in New Mexico during 2000–2020, a total of 90 were available for molecular characterization (Appendix 1 Table 1, https://wwwnc.cdc.gov/EID/article/28/6/21-1718-App1.xlsx). Of the 90 samples, 58 were analyzed by the Scientific Laboratory Division Department of Health of New Mexico (SLD-NM) and 32 were submitted for rabies virus characterization to the National Rabies Reference Laboratory (NRRL), Division of Global Migration and Quarantine, National Center for Emerging and Zoonotic Infectious Diseases, Centers for Disease Control and Prevention (CDC) (Appendix 2 Table, https://wwwnc.cdc.gov/EID/article/28/6/21-1718-App2.pdf). Five isolates from gray foxes collected by the surveillance system in Arizona and 3 archived isolates from *Lasiurus intermedius* bats from Florida were also included. In addition, from the batch of isolates submitted to CDC, we tested isolates A15-0755 and A19-2238 from gray foxes collected in Lincoln County during 2015 and 2019 by using a panel of RABV nucleoprotein mAbs (*22*) and obtained the whole genomes.

RNA Extraction and Reverse Transcription PCR Amplification

We extracted total RNA from brain tissue by using either TRIzol (Invitrogen, https://www.thermofisher.com) or the Direct-zol RNA MiniPrep Kit (Zymo Research, https://www.zymoresearch.com) according to the manufacturer's instructions. We performed traditional reverse transcription PCR to produce partial and full nucleoprotein gene amplicons by using overlapping nucleoprotein gene primers described (*19*). To obtain the whole RABV genome for isolates A15-0755 and A19-2238, we synthesized cDNA by using specific primer LN34 forward (*23*) with avian myeloblastosis virus reverse transcriptase (Roche, Sigma-Aldrich, https://www.sigmaaldrich.com). PCR amplicons suitable to cover the entire genome were generated by using 6 overlapping pair of primers (Appendix 1 Table 2) and Takara long amplicon Taq polymerase (Takara Bio USA, https://www.takarabio.com).

Nucleotide Sequencing and Phylogenetic Analysis

We obtained partial and complete nucleoprotein gene sequences by using overlapping primers with the BigDye Terminator v1.1 Cycle Sequencing Kit

(Thermo Fisher). We sequenced the amplicons in a 3730 DNA Analyzer (Applied Biosystems, (Thermo Fisher) by using standard Sanger sequencing method (*19*). SADB119 (GenBank accession no. M31046) sequence was used as a reference to assemble the partial and full nucleoprotein gene and the whole genome. Nucleoprotein gene sequences were edited by using Bioedit software (*24*). We included high-throughput sequencing to obtain whole genome sequences for isolates A15-0755 and A19-2238. We generated amplicons >2 kb by using specific primers (Appendix 1 Table 2) and pooled and fragmented all amplicons for each isolate to 500 bp by using Covaris S220 (https://www.covaris.com).

We quantified DNA by using a Qubit instrument (Thermo Fisher), performed library preparation by using the Accel-NGS 2S plus DNA Library Kit (Swift Biosciences, https://www.idtdna.com), and obtained sequence reads in a MiSeq Instrument (Illumina, https://www.illumina.com). We assembled genomes by using CLC Genomics Workbench version 20 (https://digitalinsights.qiagen.com), trimmed reads with a quality limit of 0.05, then mapped to reference JQ685895 to generate a majority draft consensus. We generated final genomes by mapping reads back to draft genomes and extracting consensus sequences with minimum 50× read depth; we inserted ambiguous bases with a noise threshold of 10%. We submitted sequences generated in this study to GenBank (accession nos. OM202982–3049).

We aligned sequences generated in this study by using ClustalW in Geneious 10.2.2 (https://www.geneious.com). We conducted phylogenetic analysis by using a Bayesian approach in the BEAST v1.10.4 package (*25*). To estimate the time since the most recent common ancestor of fox-associated viruses and other bat and carnivore-associated RABVs, we analyzed 141 nucleoprotein gene sequences (Appendix 1 Table 2). Preliminary analyses used iqTree to compare substitution models and obtain a maximum-likelihood topology without a molecular clock assumption (*26*).

We used the most likely substitution model according to the corrected Akaike Information (generalized time reversible plus finite sites plus invariant sites plus gamma 4) in subsequent analyses. We checked for temporal signal in our sequence data by correlating sampling time with root-to-tip divergence by applying TempEst (*27*) to the maximum-likelihood tree estimated in iqTree (*28*). We subsequently performed Bayesian phylogenetic analyses in duplicate by using the relaxed lognormal molecular clock and the Bayesian skyline demographic model with BEAST (*25*,*29*). We partitioned codon positions 1 and 2 separately from codon position 3 and applied the generalized time reversible plus invariant sites plus gamma substitution model to both partitions. We modeled 1 year of uncertainty around each sampling date. We performed each analysis for 100 million generations, sampling trees, and parameters every 5,000 steps and checked chains for convergence within and between runs in Tracer (https://beast.community/trac). We combined trees and log files in LogCombiner (https://beast.community/logcombiner) after removing 10 million generations as burn-in; we further thinned tree files to be sampled every 10,000 steps. This strategy led to effective sample size values >200 for all parameters. We visualized all the phylogenetic trees by using Fig Tree v1.4.0 (*30*).

We calculated genetic distance in Geneious and visualized rabies distribution across New Mexico by exporting partial nucleoprotein gene Bayesian tree into ArcGIS desktop v10.7.1 (https://www.esri.com). We sourced administrative boundaries (Figure 1) from GADM version 4 (Database of Global Administrative Areas; www.gadm.org) and specific imagery from Maxar Technologies Inc. (https://www.maxar.com) accessed from ESRI World Imagery.

Results

During 2015 and 2019, two persons in Lincoln County were bitten by rabid gray foxes. Initially, we compared the full nucleoprotein gene sequence of the 2015 isolate, A15-0755, with sequences available in GenBank. The most similar sequence was the RABV isolate collected in Canada from a *Myotis lucifugus* bat (GenBank accession no. AF351837) and characterized as silver-haired bat RABV variant (*Lasionycteris noctivagans* bats) with a sequence identity of 93.25%. A15-0755 showed an atypical reaction pattern with mAbs 2 and 11; a similar reaction pattern was observed in a historic isolate from a northern yellow bat (*Lasiurus intermedius)* collected in Florida and archived at CDC. During 2019, a second isolate, A19-2238, from a second rabid gray fox from the same county was identified in SLD-NM and was further characterized at CDC. A full nucleoprotein gene sequence showed a single nucleotide mismatch with the 2015 isolate. A19-2238 produced a Mab reaction pattern similar to a RABV variant circulating in hoary bats (*Lasiurus cinereus*).

Phylogenetic Analysis

Bayesian phylogenetic inference of partial and complete nucleoprotein genes in BEAST showed consistent tree topologies, grouping the New Mexico isolates into 3 major clades. The first clade of bat RABV variants included isolates from bats and

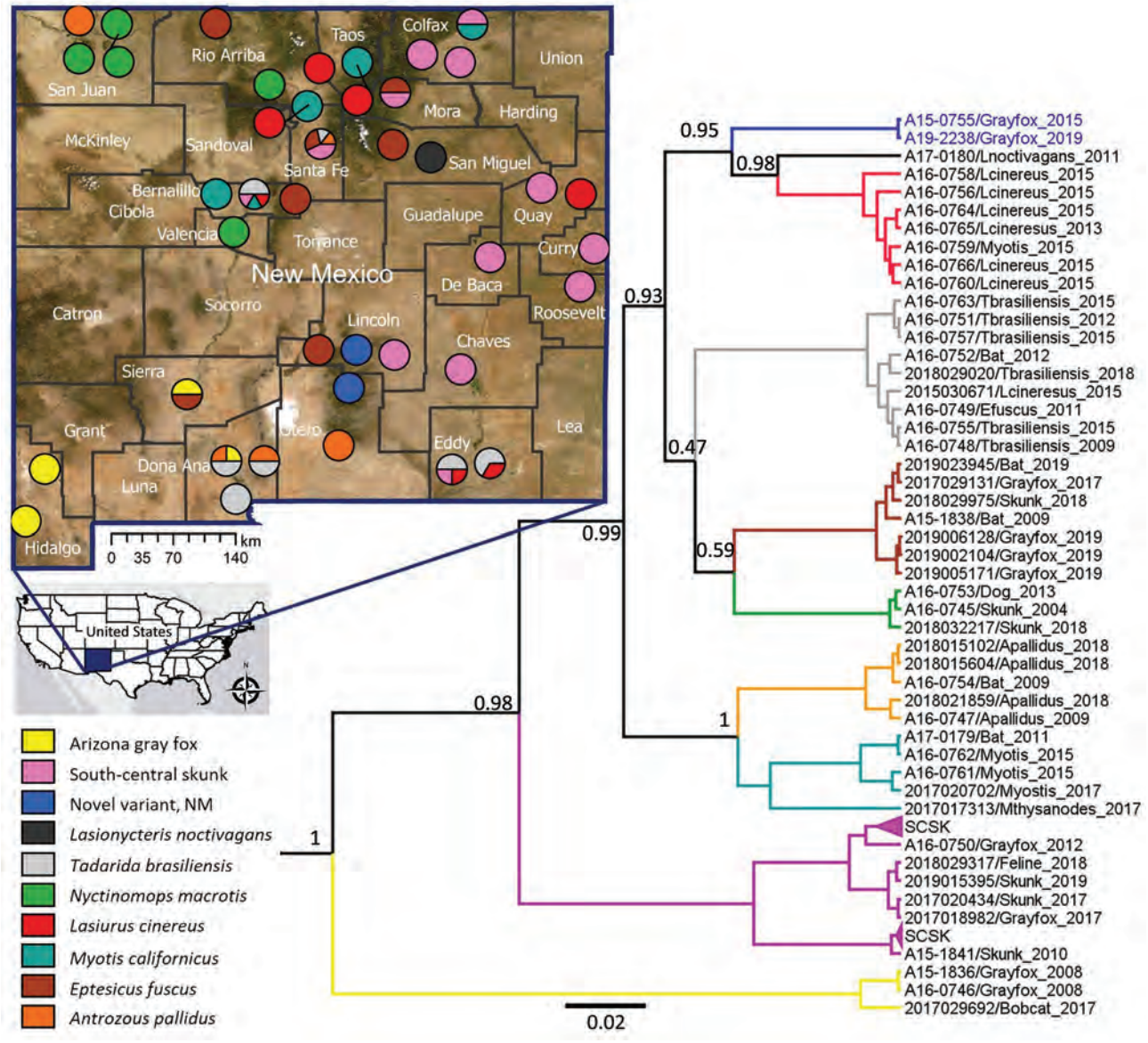

Figure 1. Phylogenetic tree based on partial nucleoprotein gene (348 bp) sequences and geographic distribution of rabies virus (RABV) variants, New Mexico, USA. The tree was constructed by using representative isolates and only posterior values leading to the RABV variants are included on the tree nodes. Three major clades were identified in New Mexico. The RABV variants are displayed in distinct colors in the tree and map according to the legend included in the figure. Blue indicates novel RABV isolates collected from gray fox in Lincoln County. Accuracy of the location in the map is at city level; for samples that did not have city information, the location was randomly assigned within the county. Numbers along branches are bootstrap values. Scale bar indicates nucleotide substitutions per site.

terrestrial carnivores that were presumed to be the result of cross-species transmission (Figure 1). Within this clade, 7 previously known RABV genetic variants were identified. Isolates A15-0755 and A19-2238 formed an independent branch. Phylogenetic analysis did not identify a close relationship with any RABV sequences available in GenBank. Both isolates were most closely related to, but still highly divergent from (mean ± SD identity 95.85% ± 2.21%), the branches containing RABVs detected in *Lasiurus cinereus* bats and *L. noctivagans* bats. The third RABV isolate from a gray fox in Lincoln County (A15-1838) clustered within a branch that contained isolates from *Eptesicus fuscus* bats, which indicated a spillover event of a bat RABV variant to a terrestrial mammal.

We also identified other spillover events from bats to terrestrial mammals (Appendix 2 Table). The

variant commonly circulating among *E. fuscus* bats was detected in gray foxes and skunks, and a RABV variant circulating in *Nycintomops macrotis* bats was found in a skunk isolate (A16-0745) from San Juan County and a dog isolate (A16-0753) from Valencia County. The second clade containing isolates identified as south-central skunk RABV variant included isolates collected from gray foxes, coyotes, and domestic cats. The third clade identified as Arizona gray fox contained 2 isolates from gray foxes and 2 from bobcats. Circulation of variants A16-0745 and A16-0753 in terrestrial mammals was consistent with previous reports (Figure 1) (*31*,*32*). Bat virus variants were found throughout the state but showed no notable epidemiologic pattern.

Phylogenetic inferences including all 32 nucleoprotein gene sequences from New Mexico generated at CDC and representative sequences retrieved from GenBank produced a phylogenetic tree with similar topologies to the partial nucleoprotein gene (Figure 1). Gray fox isolates A15-0755 and A19-2238 formed a unique branch high posterior support (*1*); the most similar isolate available on GenBank (accession no. AF351837) clustered separately within the *Perimyotis subflavus* and *Lasionyteris noctivagans* bat RABV variants (Figure 2).

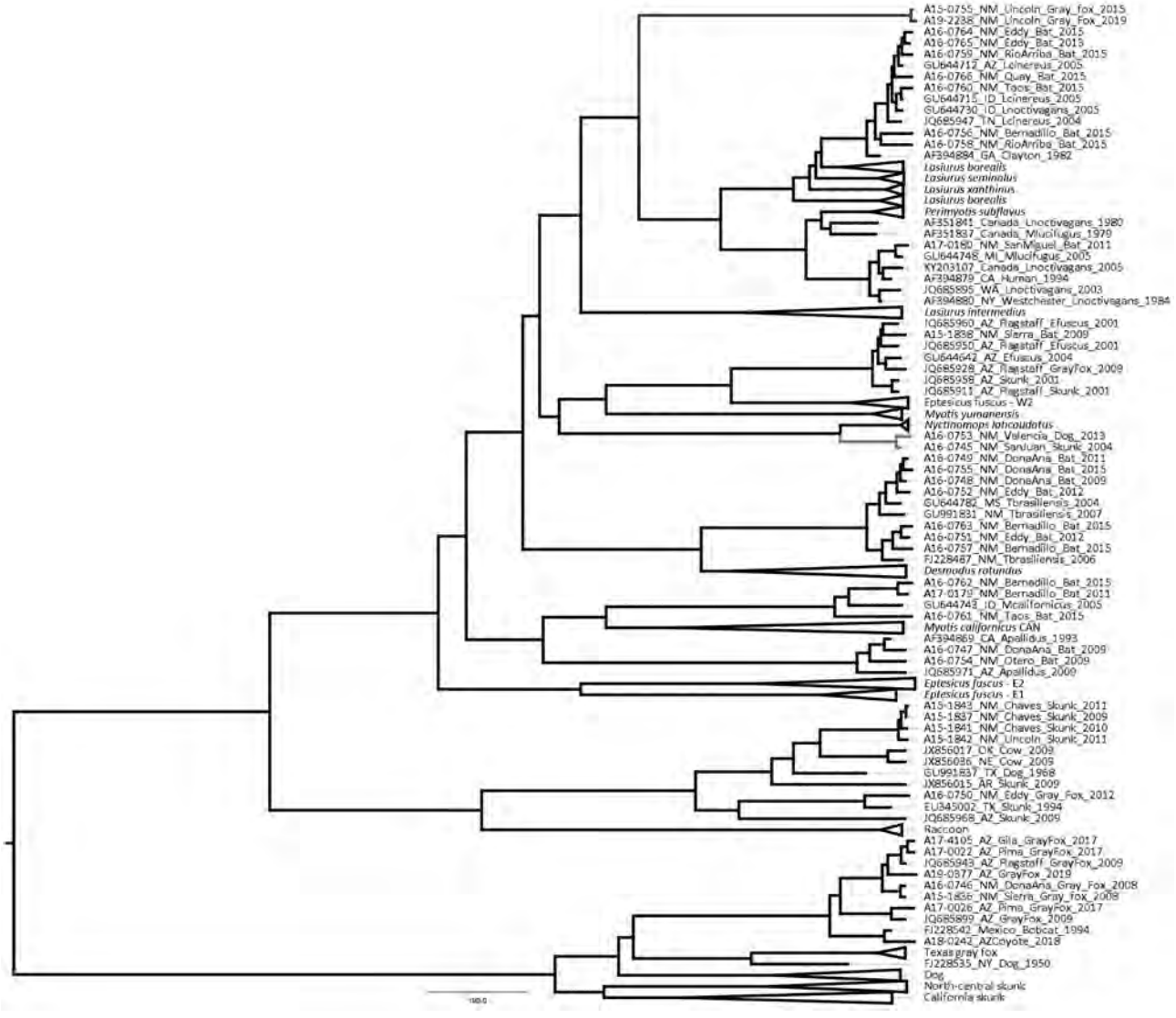

Figure 2. Maximum clade credibility tree using full nucleoprotein gene sequences of RABV variants identified in New Mexico, USA, and representative sequences from RABV variants in the Western Hemisphere. Values in the nodes indicate estimates for the posterior clade probability for each RABV variants. Branch in blue indicates novel RABV variant that includes the 2 isolates from Lincoln County, and branch in green indicates RABV associated with *Nyctinomops macrotis* bats. Scale bar indicates nucleotide substitutions per site. RABV, rabies virus.

Novel Gray Fox Isolates

The substitution rate along the branch leading to the 2 gray fox isolates identified as a novel RABV variant was 1.6×10^{-4} substitutions/site/year (95% highest posterior density 9.2×10^{-5}–2.4×10^{-4} substitutions/site/year). The substitution rate across the entire tree was 1.7×10^{-4} substitutions/site/year (95% highest posterior density (1.2×10^{-4}–2.2×10^{-4} substitutions/site/year), indicating a similar rate of evolution. The nucleoprotein gene genetic distance between RABV variants examined showed that the highest identity to isolate A15-0755 was 93.19% for isolate AF351837 (silver-haired bat variant), and the identity for isolate A19-2238 was 93.11% (Appendix 1 Table 3). We conducted a BLAST (https://blast.ncbi.nlm.nih.gov/Blast.cgi) search of the glycoprotein gene from the 2 novel RABV variant isolates in GenBank; isolate KJ174682 from an *E. fuscus* bat and described as EF-W3 had the closest glycoprotein gene identity (90.42% nt). Nucleotide comparison across the entire genome of isolates A15-0755 and A19-2238 showed 99.78% identity.

The nucleoprotein gene, which is highly conserved and a target for laboratory diagnosis, showed a single synonymous substitution at nt position 333. The glycoprotein gene, which induces production of virus-neutralizing antibodies that provide immunologic protection, showed a nonsynonymous substitution at nt position 554, resulting in a substitution of the amino acid tyrosine at position 184 by serine (Y184S). Phylogenetic analysis using a reduced set of glycoprotein gene sequences placed isolates A15-0755 and A19-2238 in an independent branch, closely related to *L. noctivagans* and *P. subflavus* bats, that has well-supported posterior values (Appendix 2 Figure).

Other Isolates

Two other isolates A16-0745 (skunk 2004) and A16-0753 (dog 2013) were compared with available sequences in GenBank. The partial nucleoprotein (244 bp) of a skunk isolate (A16-0745) showed 100% identity with RABV isolate AY960093 from GenBank, previously detected in an *N. macrotis* bat in Colorado, and 99.5% to isolate AY170304 from GenBank, detected in Arizona. The full nucleoprotein gene showed 98.0% (A16-0745) and 97.8% (A16-0753) identities with a RABV (GenBank accession no. KM594034) found in *N. laticaudatus* bats from Brazil. In the phylogenetic analysis using the full nucleoprotein gene, we found that both isolates branched independently and contained only these 2 terrestrial mammals (Figure 2).

Cross-Species Transmission

Of the 49 bat clade samples that had sequencing results, 11 (22.4%) instances of bat-to-terrestrial cross species transmission were detected. Of 37 isolates with the south-central skunk RABV variant, 9 (24.3%) were cross-species transmissions to nonskunk species, and 2 (50%) of the 4 gray fox RABV variant isolates were cross-species transmissions. There were no instances of a terrestrial RABV variant found in a bat.

Discussion

In the United States, 7 unique RABV variants are defined on the basis of unique mAbs patterns, each associated with a specific terrestrial host species in terrestrial mammals (arctic fox, gray fox, striped skunk, raccoon, and mongoose) (*13*). Based on patterns of the specific mAbs used, the standard panel can differentiate ≥15 RABV variants (*33*). Robust rabies surveillance systems and regular virus characterization are used to not only define the geographic distribution of variants but also detect RABV spillover into nonreservoir wildlife or domestic species that might reflect changes in rabies epidemiology and affect human or animal health. This study was conducted after the New Mexico Department of Health confirmed human RABV exposures to confirmed rabid foxes and pursued additional laboratory-based methods to determine if these cases represented a shift in the epidemiology of rabies in the state. As a result of this investigation, a novel RABV variant was identified. Detection of this novel variant in 2 gray foxes, separated by 5 years, probably represents independent cross-species transmission events from a cryptic transmission cycle among a species of bats.

Available data for the United States show that the distribution of terrestrial RABV variants is geographically delimited; in contrast, the distribution of bat RABV variants is broader, and these variants show an abundant diversity, each variant associated with specific species (*9*,*14*). For example, according to the National Rabies Surveillance System, during 2008–2018, at least 17,700 rabid bats were detected in 39 different bat species, but 54.9% of rabid bats were not identified to species, and 63% did not undergo variant typing (antigenic or molecular) (*34*,*35*). Given these apparent gaps in characterizing rabid bats in the United States, it should be no surprise that novel RABV variants are still being discovered. As characterization methods and bat identification guides (*36*) become more accessible, it is expected that a wider diversity of bat RABV variants will be detected. Furthermore, public health surveillance is biased toward animals with human or domestic

animal exposures, potentially masking detection of RABV variants in species not commonly found near inhabited areas.

RABV isolates from New Mexico included in this study were derived from bats and terrestrial mammals collected in different locations spanning over 20 years. The phylogenetic inferences (Figure 1) clearly show 3 major clades supported that have high posterior values. All isolates were closely associated with RABV variants already described in New Mexico (*14*,*37*), except for the 2 isolates from gray foxes collected during 2015 and 2019 in Lincoln County. An extensive analysis of full nucleoprotein and glycoprotein genes supported the uniqueness of the isolates as an unrecognized RABV variant. Nucleotide analysis of the glycoprotein gene of the novel RABV variant had a specific glycoprotein gene mutation that is located in the antigenic site II, which is involved in stimulating the antibody response (*38*). Although the current rabies vaccine is effective in protecting against all lyssaviruses from phylogroup I, monitoring the nucleotide mutation across the glycoprotein gene on emergent RABVs in domestic and wild animals might help to predict if the vaccine will still be effective against these new viruses (*39*). This single mutation is not believed to lead to an escape from current RABV biologics, as shown by the lack of development of rabies in the 2 persons exposed to this virus after they received PEP.

On the basis of phylogenetic analysis, we reason that the reservoir of this novel RABV variant is most likely a bat from the group commonly referred to as migratory tree bats, including the genera *Lasiurus* and *Lasionycteris*. The isolates identified probably represent repeated spillover events from a bat reservoir into gray foxes in Lincoln County. This hypothesis is supported by the low frequency of detection of the variant (2 cases in 5 years), which might be expected because bats and wild terrestrial mammals have limited contact with humans and other terrestrial mammals unless they are sick or injured (*40*). On the basis of available data and analysis, we cannot provide enough evidence to prove that this variant represents a host shift from bat RABV variants into gray foxes; however, the question will remain open until the reservoir is determined. After rabies was recognized in the gray fox during 2015, an active surveillance program was enacted in Lincoln County and surrounding counties; however, no rabid terrestrial animals were detected during this 6-month effort. To increase the robustness of this analysis, isolates from additional rabid foxes or bats either in Lincoln County or neighboring areas are clearly needed. In nature, bats inhabit diverse ecologic niches (*41*). Migratory tree bats usually travel long distances, which opens the possibility that this novel RABV variant might be present in other states or countries (*42*).

Although migratory tree bats are a major rabies reservoir in the United States, other species of migratory bats, such as *N. macrotis* (big free-tailed bats), commonly travel long distances, covering a range from South America to North America (*43*). Detecting rabies in *N. macrotis* bats is uncommon, and the availability of genetic data in GenBank is limited to 2 partial nucleoprotein gene sequences (300 bp): AY170304 (Arizona) and AY960093 (Colorado). The surveillance system in the United States detected 18 rabid *N. macrotis* bats during 2008–2018; the highest incidences were in 2015 (n = 9) and 2010 (n = 4) (*10*,*34*,*44*–*46*).

In this study, we found an *N. macrotis* bat RABV variant in a domestic dog and a skunk separated by 11 years. Analysis of the full nucleoprotein gene provided high posterior support that the RABV variant detected in United States shared a recent ancestor with a RABV variant found in Brazil in *N. laticaudatus* bats (*47*). The finding of a relatively rare RABV variant in a migratory bat species represents a reminder that RABVs can be carried long distances by reservoir species and could represent a method of introduction of exotic RABVs into the United States, yet another example of the need for adequate surveillance, routine species identification, and RABV characterization (*48*).

Antigenic characterization is useful to rapidly identify the common RABV variants in the United States (*49*). The antigenic patterns of the isolates from Lincoln County gave conflicting results; the isolates showed different patterns, despite having 99.9% genetic similarity. These discrepancies in the interpretation of the mAb results demonstrate the limitation of that method to differentiate RABVs within certain bat species. In comparison, the amplicon sequences generated by the LN34 assay (*50*), which target a highly conserved lead sequence of RABV genome, are able to confirm the distinct sequences for this novel RABV. This study highlights the need for RABV characterization when there are concerns about epidemiologic shifts to inform public health and animal health interventions. Despite extensive surveillance systems in the United States for RABV, virus characterization is not routinely performed. As genetic virus characterization becomes more routine, additional cryptic RABV transmission cycles probably will be recognized.

Acknowledgments

We thank Ashutosh Wadhwa, Yoshinori Nakazawa, and Mary Reynolds for supporting this study, and the public health personnel of the New Mexico Department of Health for their laborious work on rabies surveillance.

D.G.S. was supported by a Wellcome Trust Senior Research Fellowship (grant 217221/Z/19/Z).

About the Author

Mr. Condori is a microbiologist in the National Center for Emerging and Zoonotic Infectious Diseases, Centers for Disease Control and Prevention, Atlanta, GA. His primary research interest is public health laboratory-based surveillance for rabies viruses.

References

1. Rupprecht C, Kuzmin I, Meslin F. Lyssaviruses and rabies: current conundrums, concerns, contradictions and controversies. F1000 Res. 2017;6:184. https://doi.org/10.12688/f1000research.10416.1
2. Hu SC, Hsu CL, Lee MS, Tu YC, Chang JC, Wu CH, et al. Lyssavirus in Japanese Pipistrelle, Taiwan. Emerg Infect Dis. 2018;24:782–5. https://doi.org/10.3201/eid2404.171696
3. Hampson K, Coudeville L, Lembo T, Sambo M, Kieffer A, Attlan M, et al.; Global Alliance for Rabies Control Partners for Rabies Prevention. Estimating the global burden of endemic canine rabies. PLoS Negl Trop Dis. 2015;9:e0003709. https://doi.org/10.1371/journal.pntd.0003709
4. Jackson AC. Current and future approaches to the therapy of human rabies. Antiviral Res. 2013;99:61–7. https://doi.org/10.1016/j.antiviral.2013.01.003
5. Velasco-Villa A, Mauldin MR, Shi M, Escobar LE, Gallardo-Romero NF, Damon I, et al. The history of rabies in the Western Hemisphere. Antiviral Res. 2017;146:221–32. https://doi.org/10.1016/j.antiviral.2017.03.013
6. Franka R, Constantine DG, Kuzmin I, Velasco-Villa A, Reeder SA, Streicker D, et al. A new phylogenetic lineage of rabies virus associated with western pipistrelle bats (*Pipistrellus hesperus*). J Gen Virol. 2006;87:2309–21. https://doi.org/10.1099/vir.0.81822-0
7. Steele JH, Tierkel ES. Rabies problems and control. Public Health Rep. 1949;64:785–96. https://doi.org/10.2307/4586998
8. Velasco-Villa A, Escobar LE, Sanchez A, Shi M, Streicker DG, Gallardo-Romero NF, et al. Successful strategies implemented towards the elimination of canine rabies in the Western Hemisphere. Antiviral Res. 2017;143:1–12. https://doi.org/10.1016/j.antiviral.2017.03.023
9. Ma X, Monroe BP, Cleaton JM, Orciari LA, Li Y, Kirby JD, et al. Rabies surveillance in the United States during 2017. J Am Vet Med Assoc. 2018;253:1555–68. https://doi.org/10.2460/javma.253.12.1555
10. Birhane MG, Cleaton JM, Monroe BP, Wadhwa A, Orciari LA, Yager P, et al. Rabies surveillance in the United States during 2015. J Am Vet Med Assoc. 2017;250:1117–30. https://doi.org/10.2460/javma.250.10.1117
11. Wiktor TJ, Koprowski H. Antigenic variants of rabies virus. J Exp Med. 1980;152:99–112. https://doi.org/10.1084/jem.152.1.99
12. Bonnaud EM, Troupin C, Dacheux L, Holmes EC, Monchatre-Leroy E, Tanguy M, et al. Comparison of intra- and inter-host genetic diversity in rabies virus during experimental cross-species transmission. PLoS Pathog. 2019;15:e1007799. https://doi.org/10.1371/journal.ppat.1007799
13. Wallace RM, Gilbert A, Slate D, Chipman R, Singh A, Cassie Wedd, et al. Right place, wrong species: a 20-year review of rabies virus cross species transmission among terrestrial mammals in the United States. PLoS One. 2014;9:e107539. https://doi.org/10.1371/journal.pone.0107539
14. Streicker DG, Turmelle AS, Vonhof MJ, Kuzmin IV, McCracken GF, Rupprecht CE. Host phylogeny constrains cross-species emergence and establishment of rabies virus in bats. Science. 2010;329:676–9. https://doi.org/10.1126/science.1188836
15. Troupin C, Dacheux L, Tanguy M, Sabeta C, Blanc H, Bouchier C, et al. Large-scale phylogenomic analysis reveals the complex evolutionary history of rabies virus in multiple carnivore hosts. PLoS Pathog. 2016;12:e1006041. https://doi.org/10.1371/journal.ppat.1006041
16. Mollentze N, Biek R, Streicker DG. The role of viral evolution in rabies host shifts and emergence. Curr Opin Virol. 2014;8:68–72. https://doi.org/10.1016/j.coviro.2014.07.004
17. Chan JF, To KK, Tse H, Jin DY, Yuen KY. Interspecies transmission and emergence of novel viruses: lessons from bats and birds. Trends Microbiol. 2013;21:544–55. https://doi.org/10.1016/j.tim.2013.05.005
18. Fleischmann WR Jr., Baron S, editors. Viral genetics. In: Fleischmann WR Jr, Baron S, editors. Medical microbiology, 4th ed. Galveston (TX): University of Texas Medical Branch at Galveston; 1996. Chapter 43.
19. Condori-Condori RE, Streicker DG, Cabezas-Sanchez C, Velasco-Villa A. Enzootic and epizootic rabies associated with vampire bats, Peru. Emerg Infect Dis. 2013;19:1463–9. https://doi.org/10.3201/eid1909.130083
20. Aréchiga-Ceballos N, Velasco-Villa A, Shi M, Flores-Chávez S, Barrón B, Cuevas-Domínguez E, et al. New rabies virus variant found during an epizootic in white-nosed coatis from the Yucatan Peninsula. Epidemiol Infect. 2010;138:1586–9. https://doi.org/10.1017/S0950268810000762
21. Pieracci EG, Brown JA, Bergman DL, Gilbert A, Wallace RM, Blanton JD, et al. Evaluation of species identification and rabies virus characterization among bat rabies cases in the United States. J Am Vet Med Assoc. 2020;256:77–84. https://doi.org/10.2460/javma.256.1.77
22. Smith JS. Monoclonal antibody studies of rabies in insectivorous bats of the United States. Rev Infect Dis. 1988;10(Suppl 4):S637–43. https://doi.org/10.1093/clinids/10.Supplement_4.S637
23. Wadhwa A, Wilkins K, Gao J, Condori RE, Gigante CM, Zhao H, et al. A pan-lyssavirus Taqman real-time RT-PCR assay for the detection of highly variable rabies virus and other lyssaviruses. PLoS Negl Trop Dis. 2017;11:e0005258. https://doi.org/10.1371/journal.pntd.0005258
24. Hall TA. BioEdit: a user-friendly biological sequence alignment editor and analysis program for Windows 95/98/NT. Nucleic Acids Symp Ser. 1999;41:95–8.
25. Drummond AJ, Suchard MA, Xie D, Rambaut A. Bayesian phylogenetics with BEAUti and the BEAST 1.7. Mol Biol Evol. 2012;29:1969–73. https://doi.org/10.1093/molbev/mss075
26. Nguyen L-T, Schmidt HA, von Haeseler A, Minh BQ. IQ-TREE: a fast and effective stochastic algorithm for estimating maximum-likelihood phylogenies. Mol Biol Evol. 2015;32:268–74. https://doi.org/10.1093/molbev/msu300
27. Rambaut A, Lam TT, Max Carvalho L, Pybus OG. Exploring the temporal structure of heterochronous sequences using TempEst (formerly Path-O-Gen). Virus Evol. 2016;2:vew007. https://doi.org/10.1093/ve/vew007

28. Streicker DG, Lemey P, Velasco-Villa A, Rupprecht CE. Rates of viral evolution are linked to host geography in bat rabies. PLoS Pathog. 2012;8:e1002720. https://doi.org/10.1371/journal.ppat.1002720
29. Drummond AJ, Rambaut A, Shapiro B, Pybus OG. Bayesian coalescent inference of past population dynamics from molecular sequences. Mol Biol Evol. 2005;22:1185–92. https://doi.org/10.1093/molbev/msi103
30. Rambaut A. FigTree Version1.4.0. 2012 [cited 2022 Mar 13]. http://tree.bio.ed.ac.uk/software/figtree
31. Velasco-Villa A, Reeder SA, Orciari LA, Yager PA, Franka R, Blanton JD, et al. Enzootic rabies elimination from dogs and reemergence in wild terrestrial carnivores, United States. Emerg Infect Dis. 2008;14:1849–54. https://doi.org/10.3201/eid1412.080876
32. Davis R, Nadin-Davis SA, Moore M, Hanlon C. Genetic characterization and phylogenetic analysis of skunk-associated rabies viruses in North America with special emphasis on the central plains. Virus Res. 2013;174:27–36. https://doi.org/10.1016/j.virusres.2013.02.008
33. Rupprecht CE, Fooks AR, Abela-Ridder B. Laboratory techniques in rabies. 5th ed. Geneva: World Health Organization; 2018.
34. Ma X, Monroe BP, Cleaton JM, Orciari LA, Gigante CM, Kirby JD, et al. Public veterinary medicine: public health: rabies surveillance in the United States during 2018. J Am Vet Med Assoc. 2020;256:195–208. https://doi.org/10.2460/javma.256.2.195
35. Blanton JD, Robertson K, Palmer D, Rupprecht CE. Rabies surveillance in the United States during 2008. J Am Vet Med Assoc. 2009;235:676–89. https://doi.org/10.2460/javma.235.6.676
36. Morgan CN, Ammerman LK, Demere KD, Doty JB, Nakazawa YJ, Mauldin MR. Field identification key and guide for bats of the United States of America. Lubbock (TX): Natural Science Research Laboratory Museum of Texas Tech University; 2019.
37. Kuzmin IV, Shi M, Orciari LA, Yager PA, Velasco-Villa A, Kuzmina NA, et al. Molecular inferences suggest multiple host shifts of rabies viruses from bats to mesocarnivores in Arizona during 2001–2009. PLoS Pathog. 2012;8:e1002786. https://doi.org/10.1371/journal.ppat.1002786
38. Evans JS, Selden D, Wu G, Wright E, Horton DL, Fooks AR, et al. Antigenic site changes in the rabies virus glycoprotein dictates functionality and neutralizing capability against divergent lyssaviruses. J Gen Virol. 2018;99:169–80. https://doi.org/10.1099/jgv.0.000998
39. Brookes SM, Healy DM, Fooks AR. Ability of rabies vaccine strains to elicit cross-neutralising antibodies. Dev Biol (Basel). 2006;125:185–93.
40. Paterson BJ, Butler MT, Eastwood K, Cashman PM, Jones A, Durrheim DN. Cross sectional survey of human-bat interaction in Australia: public health implications. BMC Public Health. 2014;14:58. https://doi.org/10.1186/1471-2458-14-58
41. Schipper J, Chanson JS, Chiozza F, Cox NA, Hoffmann M, Katariya V, et al. The status of the world's land and marine mammals: diversity, threat, and knowledge. Science. 2008;322:225–30. https://doi.org/10.1126/science.1165115
42. Fleming TH. Bat migration. In: Choe J, editor. Encyclopedia of animal behavior; 2019. New York: Elsevier. p. 605–10.
43. Mora JM, Espinal MR, Ruedas LA, Lopez LI. The big free-tailed bat, *Nyctinomops macrotis* (Gray, 1839), in central America. Mastozool Neotrop. 2016;23:551–6.
44. Dyer JL, Yager P, Orciari L, Greenberg L, Wallace R, Hanlon CA, et al. Rabies surveillance in the United States during 2013. J Am Vet Med Assoc. 2014;245:1111–23. https://doi.org/10.2460/javma.245.10.1111
45. Ma X, Monroe BP, Cleaton JM, Orciari LA, Yager P, Li Y, et al. Rabies surveillance in the United States during 2016. J Am Vet Med Assoc. 2018;252:945–57. https://doi.org/10.2460/javma.252.8.945
46. Shankar V, Orciari LA, De Mattos C, Kuzmin IV, Pape WJ, O'Shea TJ, et al. Genetic divergence of rabies viruses from bat species of Colorado, USA. Vector Borne Zoonotic Dis. 2005;5:330–41. https://doi.org/10.1089/vbz.2005.5.330
47. Oliveira RN, Freire CC, Iamarino A, Zanotto PM, Pessoa R, Sanabani SS, et al. Rabies virus diversification in aerial and terrestrial mammals. Genet Mol Biol. 2020;43:e20190370. https://doi.org/10.1590/1678-4685-gmb-2019-0370
48. Marston DA, Banyard AC, McElhinney LM, Freuling CM, Finke S, de Lamballerie X, et al. The lyssavirus host-specificity conundrum-rabies virus-the exception not the rule. Curr Opin Virol. 2018;28:68–73. https://doi.org/10.1016/j.coviro.2017.11.007
49. Smith JS, Reid-Sanden FL, Roumillat LF, Trimarchi C, Clark K, Baer GM, et al. Demonstration of antigenic variation among rabies virus isolates by using monoclonal antibodies to nucleocapsid proteins. J Clin Microbiol. 1986;24:573–80. https://doi.org/10.1128/jcm.24.4.573-580.1986
50. Condori RE, Niezgoda M, Lopez G, Matos CA, Mateo ED, Gigante C, et al. Using the LN34 pan-lyssavirus real-time RT-PCR assay for rabies diagnosis and rapid genetic typing from formalin-fixed human brain tissue. Viruses. 2020;12:120. https://doi.org/10.3390/v12010120

Address for correspondence: Ryan Wallace, Centers for Disease Control and Prevention, 1600 Clifton Rd NE, Atlanta, GA 30329-4027, USA; email: euk5@cdc.gov

Effects of Acute Dengue Infection on Sperm and Virus Clearance in Body Fluids of Men

Joffrey Mons, Dominique Mahé-Poiron, Jean-Michel Mansuy, Hélène Lheureux, Delphine Nigon, Nathalie Moinard, Safouane Hamdi, Christophe Pasquier, Nathalie Dejucq-Rainsford, Louis Bujan

We investigated the effects of dengue virus (DENV) on semen using samples collected 7, 15, 30, 60, and 90 days after symptom onset from 10 infected volunteers on Réunion Island. We assessed characteristics of semen and reproductive hormones and isolated motile spermatozoa from semen. We assayed semen for DENV using reverse transcription PCR and searched for DENV RNA by virus isolation in Vero E6 cell cultures. Four volunteers had ≥1 DENV RNA-positive semen samples; 2 volunteers had DENV RNA–positive semen at day 15 and 1 at day 30. No motile sperm were DENV positive. After exposure to positive semen, few Vero E6 cells stained positive for DENV antigens, indicating low levels of replicative virus. We found DENV had shorter duration in semen than in blood. These findings support the possibilities that DENV is sexually transmissible for a short period after acute dengue illness and that acute dengue induces reversible alterations in sperm.

Dengue is a mosquitoborne viral disease common in regions with tropical climates. Worldwide annual dengue incidence is estimated at ≈100 million diagnosed and ≈300 million asymptomatic infections. To date, it is estimated that >55% of the population worldwide is exposed to dengue virus (DENV), an RNA virus from the genus *Flavivirus* of the Flaviviridae family. The disease represents a global health issue because it is endemic in >100 countries and the World Health Organization listed dengue as a top 10 disease threat in 2019 (https://www.who.int/news-room/spotlight/ten-threats-to-global-health-in-2019). Climate change and increased circulation of *Aedes albopictus* mosquitoes in temperate countries mean that dengue incidence is being forecast to increase and extend to regions not previously affected.

Most dengue-infected persons are asymptomatic or develop a mild form of the disease with common signs and symptoms resembling those of influenza, such as fever, retroocular pain, headache, rash, muscle and joint pain, nausea, vomiting, and fatigue. However, a small proportion of infections progress to severe illness that can cause rapid onset of capillary leakage leading to bleeding, thrombocytopenia, and rapid shock. Severe dengue can be fatal, and it is often impossible to predict the progression from mild infection to severe dengue (*1*).

Dengue virus (DENV), which has 4 antigenically distinct genotypes (1–4), is transmitted to humans by bites from female *Aedes* mosquitoes, usually *Ae. aegypti* and *Ae. albopictus*. In addition, like Zika virus (ZIKV), DENV transmission by routes other than mosquitoes has been documented. Vertical transmission of DENV from pregnant women to fetuses, associated with increased rates of preterm birth, low birthweight, and miscarriage, has been reported (*2*–*5*). DENV has been found in breast milk, and transmission to infants through breast-feeding has been reported (*6*). Transmission has also been reported through blood products by mucocutaneous contact or needlestick injury during patient care or laboratory work (*7*,*8*) and by blood transfusion (*9*,*10*) or organ (*11*) or blood stem cell (*12*) transplants.

Sexual transmission of DENV was recently reported in a male patient returning to Spain from Cuba and Puerto Rico who developed dengue symptoms at the time of arrival, 7–10 days after having unprotected sexual intercourse with a male partner, who also developed dengue (*13*). Reverse transcription PCR (RT-PCR) testing of semen samples found

Author affiliations: Groupe Hospitalier Sud Réunion, St. Pierre, France (J. Mons, H. Lheureux); Institut National de la Santé et de la Recherche Médicale, Rennes, France (D. Mahé-Poiron, N. Dejucq-Rainsford);–Centre Hospitalier-universitaire, Toulouse, France (J.-M. Mansuy, N. Moinard, S. Hamdi, C. Pasquier, L. Bujan); Institut National de la Santé et de la Recherche Médicale, Toulouse-Montpellier, France (N. Moinard, S. Hamdi, L. Bujan)

DOI: https://doi.org/10.3201/eid2806.212317

identical genomic DENV viral sequences in both partners. Probable woman-to-man sexual transmission of DENV in South Korea was reported elsewhere (*14*). Two studies on DENV in semen have yielded discrepant results. A case report described detection of DENV RNA in semen 9, 24, and 37 days after symptom onset, but viral isolation using cell culture was unsuccessful (*15*). In contrast, another study documented failure to detect DENV RNA in semen from 5 DENV-infected men studied 3–5 days after fever onset (*16*). We conducted a prospective longitudinal study to investigate the relationships between whole blood, serum, urine, and semen DENV RNA viral loads over time, to identify characteristics of DENV in semen and within the different semen compartments, and to determine semen characteristics and reproductive hormone levels up to 90 days after infection to research the effects of DENV infection on human reproductive function.

Methods

Study Design and Subjects

For the study, we included men 18–45 years of age in France's overseas department of Réunion Island (located in the Indian Ocean) who had diagnosed DENV-2 infection (DENV RNA detected in blood serum). We excluded men who had other acute illnesses, were unable to provide a semen sample ≥1.5 mL, had an ejaculation disorder, or tested negative for DENV RNA in serum or urine. Patients attended follow-up visits 7, 15, 30, 60, and 90 days after symptom onset (Appendix, https://wwwnc.cdc.gov/EID/article/28/6/21-2317-App1.pdf). We collected whole blood, serum, urine, and semen samples at each visit.

After a press information campaign in Réunion Island, 12 male patients with clinical symptoms of acute dengue virus infection were recruited through physicians and underwent a DENV RNA test in serum. Of these 12 men, we excluded 1 with a negative DENV RNA test and 1 with very low semen volume. We enrolled the remaining 10 men, who were diagnosed with acute symptomatic DENV infection and were positive for DENV RNA, in Saint-Pierre University Hospital, Réunion Island. This area has been an officially designated DENV-2 outbreak area since the beginning of 2018.

The study was registered at ClinicalTrials.gov (NCT03612609) and approved by the institutional ethics review board (CPP Sud-Méditerranée II). All volunteers gave written informed consent and received compensation (€400) for their participation. At each visit, participants completed a questionnaire about any unusual events since their previous visit to the laboratory.

Specimen Collection and Analysis

Volunteers provided 46 semen samples by masturbation after a recommended 3–6 d abstinence period. We processed the samples within 1 h after ejaculation for analysis. We centrifuged the samples at 600 × *g* and obtained seminal plasma and whole semen cells from a 200 µL semen aliquot and froze the products at −80°C. We performed semen analysis according to World Health Organization guidelines (Appendix).

At 7 and 15 days after symptoms began, we processed an aliquot of semen to isolate spermatozoa cell populations (80% fraction and swim-up fraction) according to methods used for HIV-infected men, published elsewhere (*17*) (Appendix). We performed DENV RNA searches on 40% and 80% fractions obtained from DENV RNA-positive seminal plasma or semen cells samples. We collected morning urine, whole blood, and serum samples at Saint-Pierre University Hospital, Réunion Island, and froze the samples until DENV RT-PCRs were performed at Toulouse University Hospital (Toulouse, France).

Hormonal Analyses

We assessed serum AMH (anti-Müllerian hormone), FSH (follicle-stimulating hormone), LH (luteinizing hormone), and testosterone levels using Cobas 8000e602 automated immunoassay (Roche Diagnostics, https://www.roche.com). We quantified serum inhibin B levels in duplicate using a manual ELISA assay (Ansh Labs, https://www.anshlabs.com) with a quantification limit of 4.6 pg/mL.

Virologic Methods—DENV RNA Detection

We extracted RNA from whole blood, serum, urine, and semen fractions with the MagNA Pure 96 instrument using the DNA and viral NA small volume kit (Roche Diagnostics) with 200 µL input and 100 µL output minimum volumes. For semen cell fractions, we adjusted input volume to 2×10^6 cells. We detected DENV RNA using a homemade 1-step real-time RT-PCR triplex protocol to specifically detect DENV, ZIKV, or chikungunya (CHIKV) RNA (*18*). We added 15 µL of extracted RNA to a 45 µL amplification containing 140 nmol/L of each primer; 100 nmol/L each of GAPDH-LC670, DENV-LC610, and ZIKV-FAM TaqMan probes; 45 nmol/L of CHIKV-Cyan500 TaqMan probe; and 1 µL of enzyme (Superscript III Platinum One-step RT-PCR kit, ThermoFisher Scientific, https://www.thermofisher.com). We used a LightCycler 480 Thermocycler (Roche Diagnostics) for

amplification and detection with reverse transcription at 52°C for 20 min, melting at 95°C for 2 min, followed by 45 cycles with denaturation at 95°C for 15 s, hybridization at 55°C for 45 s, elongation at 68°C for 20 s, and finally, cooling at 40°C for 30 s.

Virological Methods—Isolation of Infectious DENV

We incubated semen samples from the 2 donors with the highest DENV RNA levels in seminal plasma, cell fractions, or both, or from an uninfected donor on subconfluent Vero cells, as described elsewhere (*19*), with some modifications. We incubated 200 µL seminal plasma diluted 5-fold in culture medium or cell pellets diluted in 900 µL medium for 5 h with subconfluent Vero E6 cells cultured onto glass coverslips in 24-well plates (250 µL diluted seminal plasma/well or 300 µL diluted cells/well). We washed out seminal plasma and cell pellets and cultured Vero cells with fresh medium for 6 d. We submitted Vero cells from this first passage to immunofluorescence using the flavivirus group antigen antibody, clone D1-4G2-4-15 (Millipore Sigma, https://www.emdmillipore.com), to search for DENV-positive cells, as described elsewhere (*20*). We observed no labeling in Vero cells incubated with uninfected or infected semen samples. We performed a second passage by adding 800 µL of supernatants collected from the first passage (i.e., Vero cells cultured for 6 d after direct contact with semen fractions) to fresh Vero cells, which we also cultured for 7 d. At the end of this second round of amplification, we submitted Vero cells to immunofluorescence using the 4G2 antibody. The negative controls (i.e., mock-exposed Vero cells and Vero cells exposed to semen from uninfected donors) showed no labeling, ensuring the specificity of DENV detection. We transferred all frozen samples to the Germethèque biobank (BB-0033-00081; https://www.chu-toulouse.fr/-germetheque-centre-de-ressources-biologiques) and centralized data from case report forms at Toulouse University Hospital.

Statistical Analysis

Data are presented as medians and interquartile ranges, quartiles 1–3, and as boxplots for graphic representation. We recorded differences between day 7 after symptom onset and days 15, 30, 60, and 90 for sperm characteristics using the Wilcoxon signed rank-sum test and for hormone values. Because there were multiple comparisons, we used a Bonferroni correction with $p<0.0125$ considered significant. We considered $p<0.05$ significant if there was no Bonferroni correction. We used Stata IC15 software (StataCorp, LLC, https://www.stata.com) to perform statistical analyses.

Results

We included 10 DENV-2–positive men in the study. Mean age was 33.4 [SD 6.1] years; 7 of the men were Creole and 3 were White. All were RNA-negative for ZIKV and CHIKV in blood. All 10 patients reported febrile episodes, muscle aches, joint pain, and asthenia; 9 reported headaches, and 5 had skin rash or conjunctivitis. However, all disease signs and symptoms were mild, and no patient was hospitalized. We found no clinical signs of orchitis. We did not explore sexual function in this study, and no patient spontaneously reported sexual dysfunction.

Four men had no children, and 6 had 1–3 children. Only 1 man had previously provided a sperm sample for fertility investigation. No patient had a history of genital infection or previous genital surgery. One patient had diabetes and 1 had Crohn's disease. All patients experienced a febrile episode with a median duration of 4 days (range 3–5 days). Two patients were moderate smokers (3 and 10 cigarettes/d). All patients worked but we identified no occupational risk to fertility. We prospectively followed 9 patients for 90 days; 1 patient withdrew after his first visit on Day 7 (no reason given). We included in our statistical analysis only data from the 9 patients who attended all visits.

DENV RNA Detection

During follow-up, we found that all but 1 volunteer had a DENV RNA-positive result in ≥1 body fluid sample. Among whole blood samples, 25/46 (54.3%) were DENV RNA-positive (Ct range 27.95–42.89), but the number of volunteers with positive whole blood samples decreased over time. Only 1 volunteer had a positive whole blood sample at 90 days (Figure 1; Appendix Table). Four volunteers had DENV RNA-positive urine specimens from ≥1 visit and a total of 7/46 (15.2%) urine specimens were DENV RNA-positive (Ct range 32.66–38.33). One volunteer had a positive urine specimen at day 30 but no volunteer tested positive after day 30.

Among the 10 volunteers supplying seminal plasma or semen samples at day 7, a total of 4 (40%) had ≥1 DENV RNA-positive result. We never detected DENV RNA in semen or its fractions in 6 (60%) volunteers, including 1 tested only on Day 7. We found DENV RNA in both seminal plasma and semen cell samples from 2 volunteers and only in seminal plasma samples from 2 others. We systematically confirmed all RNA detections by retesting the samples (Ct range 33.9–41.6); 3/30 (10%) semen cell samples and 6/30 (20%) seminal plasma samples were DENV RNA-positive. Two of 9 volunteers had

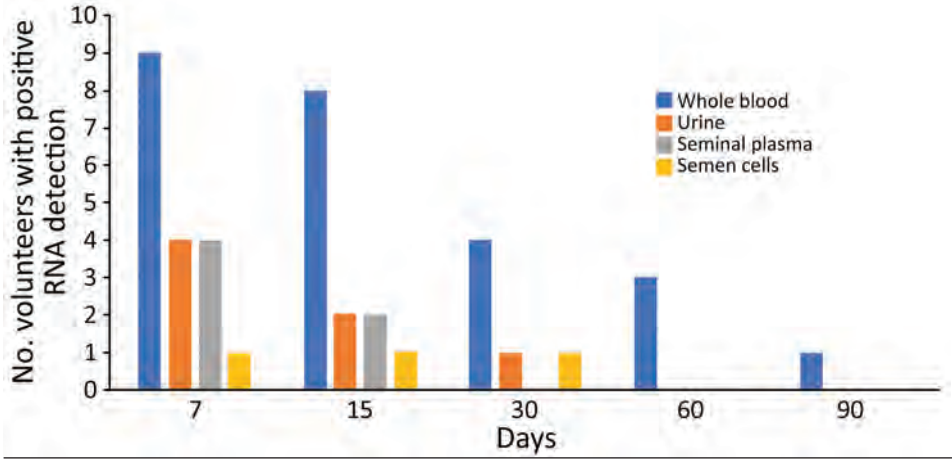

Figure 1. Frequency of dengue virus RNA detection in different fluids in 9 volunteers from Réunion Island with dengue virus infection in a study of virus clearance and effects on reproductive function, according to time points (days) after onset of signs and symptoms.

positive seminal plasma and semen cells samples at day 15 and 1/9 had a positive semen cell result at day 30. We isolated spermatozoa fractions from all but 2 semen samples at day 7 and from all semen samples at day 15. We found no 80% fractions containing only spermatozoa positive for DENV RNA and two 40% fractions among 12 samples tested that were DENV RNA-positive.

DENV Isolation

We attempted to isolate DENV from semen samples displaying the highest viral loads: whole semen cells from patient 3 and seminal plasma and 40% fractions obtained from patient 6 after isolation from semen. We detected a few DENV-positive Vero E6 cells after exposure to semen samples using immunocytofluorescence against the viral envelope (Figure 2). However, we detected no DENV RNA in the supernatants of the semen-exposed Vero E6 cultures (data not shown).

Median sperm count, total sperm count, and total motile sperm count significantly decreased by day 30 ($p<0.0125$); median sperm count was only 15% and total sperm count only 19% of sperm production at day 7. The percentage of normal sperm was lowest at day 30 but this decrease did not reach statistical significance, probably because of the small number of volunteers studied (Table 1; Figure 3). We found no statistical differences between results at the different follow-up times for any of the hormones studied; however, the testosterone/LH ratio was significantly lower at day 7 than at days 15 and 30 ($p<0.0125$) (Table 2).

Discussion

Our prospective study provides results from a longitudinal assessment of different biologic samples (whole blood, urine, and semen) and reports semen and reproductive hormones characteristics after acute DENV infection in men. We also document the detection and clearance of DENV RNA in different semen fractions and the presence of replicative virus, including in motile spermatozoa fractions, generally used in assisted reproductive procedures.

Ten symptomatic patients provided first samples 7 days after symptom onset. We recruited these patients after they were diagnosed with DENV infection through positive results from molecular testing during the 2018–2019 dengue epidemic on Réunion Island. Whole blood samples were DENV RNA-positive for all but 1 patient, who was negative at days 7 and 15 after symptom onset. Viremia remained in 2 patients at day 60 and in 1 at day 90 after symptom onset. The duration of DENV viremia has been estimated at ≈9.1 days (95% CI 4.4–13.9 days) (*21*). DENV RNA detection was more sensitive and the diagnostic window was probably longer for whole blood than serum samples (*22*). Prolonged viremia of 18–80 days has been reported in hematopoietic stem cell transplant recipients with hematological malignancies (*23*). However, the patient with the longest duration of viremia in our study had no disease. We detected DENV RNA less frequently in urine than in whole blood; only 40% of patients had a positive urine result. One urine sample was DENV RNA-positive at day 30 in a patient whose whole blood sample was positive at the same time, but no later urine samples were positive.

Two previous studies looked for DENV in semen from infected men, with discrepant results. In a case report of a man returning from Thailand, DENV-2 RNA was detected in semen (Ct 24–31.8) 9, 24, and 37 days after dengue symptom onset, but no infectious virus could be detected (*15*). In contrast, in another study from Singapore of 5 DENV-infected men, DENV RNA was not detected in semen 3–5 days after fever (*16*). In our study, 4 (40%) of the 10 infected men tested had ≥1 DENV RNA-positive

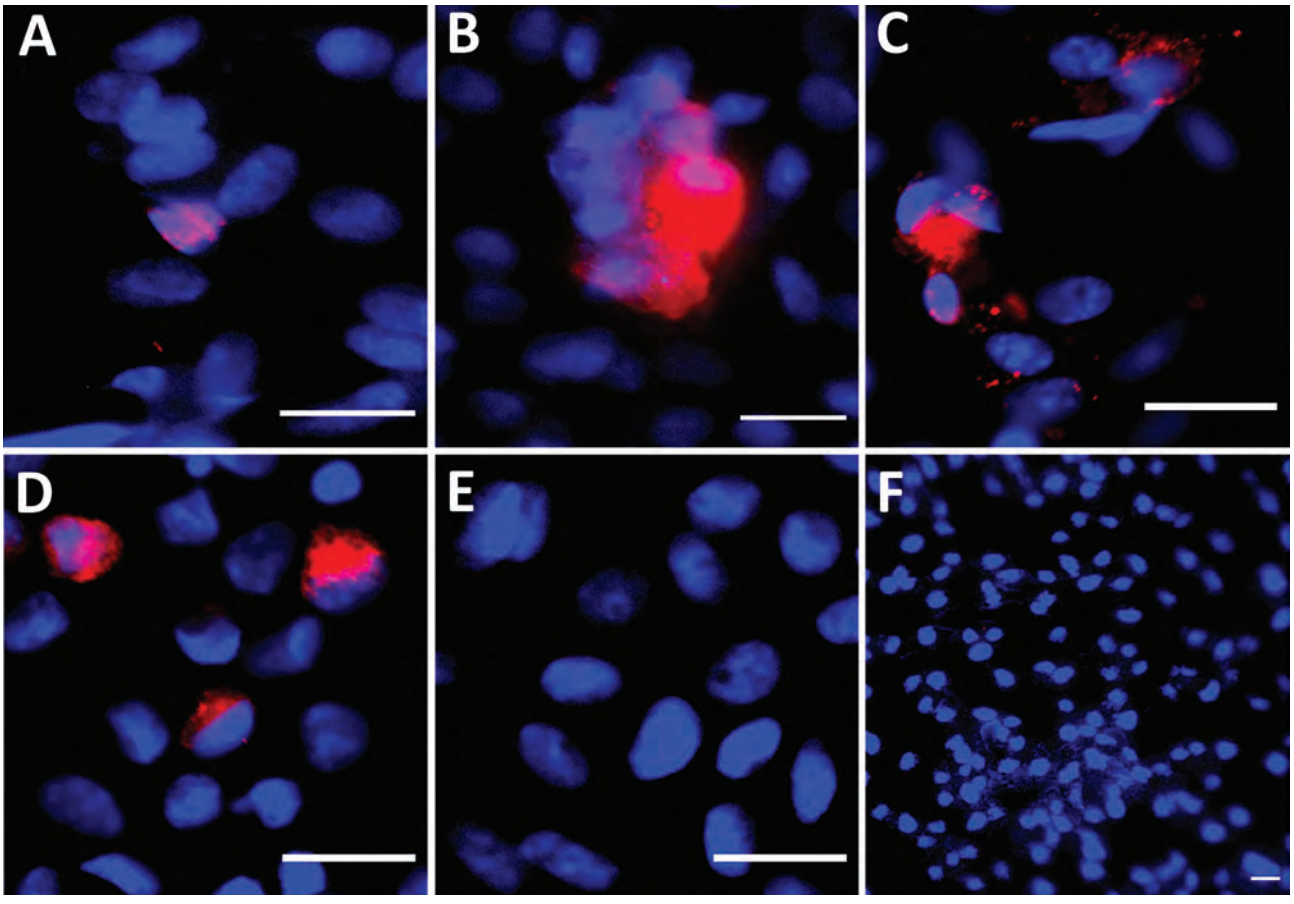

Figure 2. Immunofluorescent images from Vero E6 cells exposed to semen samples obtained at day 7 after symptom onset from volunteers from Réunion Island with dengue virus (DENV) infection in a study of virus clearance and effects on reproductive function. A) Seminal plasma (patient 6); B) whole semen cells (patient 3); C) cells from 40% fraction obtained after semen preparation (patient 6); D) DENV-1 infected Vero E6 cells (positive control) (multiplicity of infection 0.01 for 3 days); E) noninfected Vero E6 cells; F) Vero E6 cells inoculated with noninfected semen (negative controls). VeroE6 cells were inoculated with the semen fractions indicated from DENV-infected (A, B, C) or uninfected patients (E) and cultured for 7 days (first passage). Images were made after detection of DENV envelope protein (DENV-E) from a second passage on VeroE6 of culture supernatants collected after the first passage. Red indicates DENV-E, blue indicates DAPI staining. Scale bars indicate 20 μm.

semen samples. Seminal plasma was more often positive than semen cell pellets. Positivity in semen was independent of results from urine, suggesting that infection of these fluids originated in different tissues. However, unlike in some other viruses, such as ZIKV (*19*), DENV positivity in semen was always associated with whole-blood positivity in our study. Of note, semen was DENV positive 30 days after symptom onset in our study, a duration similar to that reported elsewhere (*15*).

Table 1. Semen characteristics of 9 dengue virus–infected volunteers according to time points after symptom onset, Réunion Island*

Characteristic	Median value (interquartile range)				
	Day 7	Day 15	Day 30	Day 60	Day 90
Volume, mL	1.8 (1.7–2.2)	3 (2–6)	2.2 (1.6–2.5)	2.5 (2–3.8)	2.4 (1.8–2.9)
Sperm count, millions/mL	60 (46–72)	55 (13–70)	9 (6–20)†	25 (20–49)	54 (22–80)
Total sperm count, millions/ejaculate	108 (96–403.2)	78 (27.3–189)	20.7 (16.8–22.5)†	96 (34–142.1)	97.2 (81.4–273.6)
Total motile sperm count, millions/ejaculate	53.76 (48.96–193.54)	34.32 (8.51–75.6)	6.53 (4.76–9.75)†	47.52 (18.36–68.16)	55.35 (49.92–120.38)
Progressive motility, %	47 (45–55)	43 (40–44)	34 (26–37)	53 (45–59)	53 (50–67)
Vitality, %	86 (75–91)	80 (71–83)	81 (75–88)	87 (84–90)	87 (83–91)
Normal, %	15 (10–17)	14 (11–19)	10 (9–14)	15.5 (11–18)	16.5 (11.5–20)

*Ten volunteers were recruited, but only 9 completed follow-up.
†p<0.0125 between day 7 and days 15, 30, 60, 90.

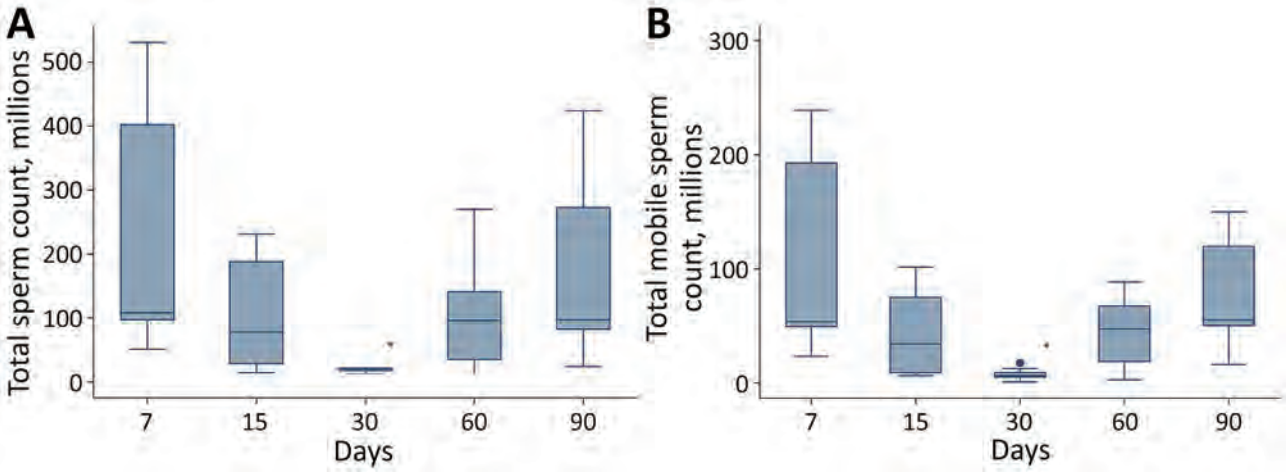

Figure 3. Semen characteristics of 9 dengue virus–infected volunteers from Réunion Island at specific time points (days) after onset of signs and symptoms from dengue virus infection. A) Total sperm count (millions/ejaculate); B) total motile sperm count (millions/ejaculate). Horizontal lines within boxes indicate medians; box tops and bottoms indicate interquartile ratios; error bars indicate minimums and maximums. Significant value (*p<0.0125) between day 7 and subsequent days

Other flaviviruses, such as hepatitis C virus or ZIKV, have been found in semen (*19*,*24*). Although DENV is a more widespread flavivirus than ZIKV, data on the tropism and effects of DENV in the male genital tract are scarce. Four cases of acute scrotal edema associated with DENV infection have been reported, but their mechanisms were not elucidated (*25*,*26*). Although ZIKV actively replicates in the human testis ex vivo and persists in this organ (*20*,*27*), it is unknown whether DENV can infect the human testis, an established viral reservoir (*28*). In vitro DENV was able to infect a human Sertoli cell line, but less efficiently than ZIKV (*29*). In nonhuman primates infected with DENV, viral proteins were observed in the seminal vesicles and prostate but not in the testis (*30*). The origin of DENV in semen requires further studies. Because detection of DENV RNA in semen does not imply that semen is infectious, we attempted to isolate replication-competent virus from semen using Vero E6 cells. Only a few Vero E6 cells positive for DENV envelope were observed after contact with seminal plasma or cell pellets (40% fraction), suggesting a low level of replicative virions in those samples. This finding is in line with a relatively low level of DENV RNA in semen, as suggested by the Ct values in the range of 33.9 to 41.6. DENV RNA detection was negative in the Vero E6 culture supernatants, which might be because of a replication level below the detection limit. Further studies will be needed to confirm the isolation of replication-competent virus in semen from DENV-infected men.

Although dengue is a common infection worldwide, only 2 cases of sexually transmitted DENV have been reported (*13*,*15*), unlike ZIKV, for which sexual transmission has been reported in 14 countries outside the epidemic area. Those results may reflect a lower viral load in semen for DENV. In addition, some evidence supports a shorter duration of DENV excretion in semen compared with ZIKV; ZIKV RNA has been detected in semen up to 414 days after symptom onset (*31*), and replicative virus has been shown to persist in seminal cells up to 90 days (*27*), whereas for this study we detected DENV RNA in semen no longer than 30 days after symptom onset.

Table 2. Hormone values in serum samples of 9 dengue virus–infected volunteers at different time points after symptom onset, Réunion Island*

	Median value (interquartile range)				
Hormones†	Day 7	Day 15	Day 30	Day 60	Day 90
LH, IU/L	5.1 (4.2–6.7)	3.8 (3.3–7.3)	4 (2.9–5.3)	3.8 (3.4–4.8)	5 (3.6–6.6)
FSH, IU/L	3.6 (2.5–5)	3.5 (2.6–6)	3.9 (2–4.7)	3.0 (2.1–4.1)	3.3 (2–4.8)
Inhibin, pg/mL	157 (141–230)	163 (133–249)	179 (147–270)	167 (135–215)	179 (160–204)
AMH, ng/mL	6.4 (5.5–6.6)	5.9 (5.5–6.4)	6.9 (6.1–7.8)	7.1 (6.6–9.4)	7.6 (5.5–8.8)
Testosterone, ng/dL	333 (321–403)	479 (353–645)	507 (312–570)	438 (302–557)	450 (394–511)
Testosterone/LH ratio	72 (20–106)	114 (56–191)‡	113 (61–181)‡	106 (47–199)	89 (49–162)

*Ten volunteers were recruited, but only 9 completed follow-up; AMH, anti-Müllerian hormone; FSH, follicle-stimulating hormone; LH, luteinizing hormone.
†Normal range values: LH, 1.7–8.6UI/l; FSH, 1.5–12.4 IU/l; inhibin, 152–174 pg/mL; testosterone, 260–1,000 ng/dL.
‡p<0.0125 between day 7 and days 15, 30, 60, and 90.

Moreover, infectious virus was readily detected in the semen from ZIKV-infected persons, unlike for DENV patients, in whom we observed only sparse counts of infected reporter Vero E6 cells, suggesting a low level of infectious virions in the semen samples.

To better identify the location of DENV within semen, we submitted the collected semen to a density gradient process, which separates the different fractions of semen and isolates sperm cell fractions. Semen pellets (sperm and nonsperm cells) and seminal plasma from our patients were positive for DENV RNA, but not motile spermatozoa cell fractions, indicating that either DENV was not associated with motile spermatozoa or the viral load was below the detection threshold. The sperm processing methods used for assisted reproductive technology therefore seem to be effective for isolating spermatozoa free of DENV virus as they do for several other viruses. Nevertheless, this finding remains to be demonstrated in cases of high DENV shedding in semen, because this technique was not sufficient to remove infectious spermatozoa from the semen of ZIKV-infected men with a high semen viral load (*19*).

In this prospective study, we found that sperm production decreased 30 days after symptom onset. Although we found no significant changes in reproductive hormones, the significant decrease in the testosterone/LH ratio might reflect subtle Leydig cell dysfunction at day 7 after symptom onset. These transient sperm alterations could have resulted from the viral infection itself, from fever, or from both, because all patients self-reported febrile episodes. Although the precise origins of such alterations after DENV infection still need to be identified, it is noteworthy that increased sperm DNA fragmentation has been observed after testicular or epididymal hyperthermia (*32*).

One limitation of our prospective study was the relatively low number of patients and the absence of a control group of noninfected men for the study of semen and hormonal characteristics. Also, this study included men with slight or mild symptoms of dengue infection; no data were available on the effects in men with asymptomatic or severe dengue.

In conclusion, this study provides a longitudinal assessment of the detection and clearance of DENV in different body compartments. We demonstrate that DENV RNA is detected in whole blood longer than in serum and urine and show that DENV RNA was found in semen up to 30 days after symptom onset but was not associated with motile sperm cells. Development of knowledge about the interactions between DENV and the reproductive tract is currently in its infancy. These findings emphasize the need for further studies in this field and also have implications for public health policy, such as contributing to increased diagnostic efficiency and limiting sexual transmission of DENV. Finally, our findings provide information relevant to counseling DENV-infected patients and couples who wish to conceive a child.

Acknowledgments

The authors thank all volunteers for their participation in the study. Many thanks to Annie Laurent, Catherine Louerat, Eva Passal, and Karin Farreyrol, technicians involved in the project. Thanks also to Vincent Ehinger for sample collection management and administrative support during this study. We acknowledge Laurence Thauvin, Noéline Merle, Melanie Boussard, for the management of samples in the Germethèque biobank and Celia Bettiol for her help on data management. Finally, the authors thank Amandine Pauze for administrative support and Nina Crowte, in particular, for text editing.

This study was supported by a grant from the Agence de la Biomédecine. It was sponsored by the University Hospital of Toulouse for regulatory and ethical submission. The funding source had no involvement in study design, the collection, analysis, and interpretation of data, the writing of the report, or the decision to submit the paper for publication. The work undertaken in the laboratory of Nathalie Dejucq-Rainsford was supported by ANR (project ANR21-CE15-0021-01), Inserm, and Rennes University and performed in part using Biosit platforms.

About the Author

Dr. Mons is a medical doctor working in the assisted reproductive laboratory of the university hospital in Réunion Island, France. His main interest area is reproductive biology.

References

1. Nedjadi T, El-Kafrawy S, Sohrab SS, Desprès P, Damanhouri G, Azhar E. Tackling dengue fever: current status and challenges. Virol J. 2015;12:212. https://doi.org/10.1186/s12985-015-0444-8
2. Chye JK, Lim CT, Ng KB, Lim JM, George R, Lam SK. Vertical transmission of dengue. Clin Infect Dis. 1997;25:1374–7. https://doi.org/10.1086/516126
3. Thaithumyanon P, Thisyakorn U, Deerojnawong J, Innis BL. Dengue infection complicated by severe hemorrhage and vertical transmission in a parturient woman. Clin Infect Dis. 1994;18:248–9. https://doi.org/10.1093/clinids/18.2.248
4. Paixão ES, Teixeira MG, Costa MDCN, Rodrigues LC. Dengue during pregnancy and adverse fetal outcomes: a systematic review and meta-analysis. Lancet Infect Dis. 2016;16:857–65. https://doi.org/10.1016/S1473-3099(16)00088-8

5. Pouliot SH, Xiong X, Harville E, Paz-Soldan V, Tomashek KM, Breart G, et al. Maternal dengue and pregnancy outcomes: a systematic review. Obstet Gynecol Surv. 2010;65:107–18. https://doi.org/10.1097/OGX.0b013e3181cb8fbc
6. Barthel A, Gourinat AC, Cazorla C, Joubert C, Dupont-Rouzeyrol M, Descloux E. Breast milk as a possible route of vertical transmission of dengue virus? Clin Infect Dis. 2013;57:415–7. https://doi.org/10.1093/cid/cit227
7. Chen LH, Wilson ME. Nosocomial dengue by mucocutaneous transmission. Emerg Infect Dis. 2005;11:775. https://doi.org/10.3201/eid1105.040934
8. de Wazières B, Gil H, Vuitton DA, Dupond JL. Nosocomial transmission of dengue from a needlestick injury. Lancet. 1998;351:498. https://doi.org/10.1016/S0140-6736(05)78686-4
9. Sabino EC, Loureiro P, Lopes ME, Capuani L, McClure C, Chowdhury D, et al.; International Component of the NHLBI Recipient Epidemiology and Donor Evaluation Study-III. Transfusion-transmitted dengue and associated clinical symptoms during the 2012 epidemic in Brazil. J Infect Dis. 2016;213:694–702. https://doi.org/10.1093/infdis/jiv326
10. Stramer SL, Linnen JM, Carrick JM, Foster GA, Krysztof DE, Zou S, et al. Dengue viremia in blood donors identified by RNA and detection of dengue transfusion transmission during the 2007 dengue outbreak in Puerto Rico. Transfusion. 2012;52:1657–66. https://doi.org/10.1111/j.1537-2995.2012.03566.x
11. Rosso F, Pineda JC, Sanz AM, Cedano JA, Caicedo LA. Transmission of dengue virus from deceased donors to solid organ transplant recipients: case report and literature review. Braz J Infect Dis. 2018;22:63–9. https://doi.org/10.1016/j.bjid.2018.01.001
12. Punzel M, Korukluoğlu G, Caglayik DY, Menemenlioglu D, Bozdag SC, Tekgündüz E, et al. Dengue virus transmission by blood stem cell donor after travel to Sri Lanka; Germany, 2013. Emerg Infect Dis. 2014;20:1366–9. https://doi.org/10.3201/eid2008.140508
13. ECDC. Rapid risk assessment—sexual transmission of dengue in Spain. 2019 [cited on 2019 Nov 18]. https://www.ecdc.europa.eu/en/publications-data/rapid-risk-assessment-sexual-transmission-dengue-spain
14. Lee C, Lee H. Probable female to male sexual transmission of dengue virus infection. Infect Dis (Lond). 2019;51:150–2. https://doi.org/10.1080/23744235.2018.1521004
15. Lalle E, Colavita F, Iannetta M, Gebremeskel Teklè S, Carletti F, Scorzolini L, et al. Prolonged detection of dengue virus RNA in the semen of a man returning from Thailand to Italy, January 2018. Euro Surveill. 2018;23:18–00197. https://doi.org/10.2807/1560-7917.ES.2018.23.18.18-00197
16. Molton JS, Low I, Choy MMJ, Aw PPK, Hibberd ML, Tambyah PA, et al. Dengue virus not detected in human semen. J Travel Med. 2018;25:25. https://doi.org/10.1093/jtm/tay023
17. Bujan L, Daudin M, Matsuda T, Righi L, Thauvin L, Berges L, et al. Factors of intermittent HIV-1 excretion in semen and efficiency of sperm processing in obtaining spermatozoa without HIV-1 genomes. AIDS. 2004;18:757–66. https://doi.org/10.1097/00002030-200403260-00006
18. Mansuy JM, Lhomme S, Cazabat M, Pasquier C, Martin-Blondel G, Izopet J. Detection of Zika, dengue and chikungunya viruses using single-reaction multiplex real-time RT-PCR. Diagn Microbiol Infect Dis. 2018;92:284–7. https://doi.org/10.1016/j.diagmicrobio.2018.06.019
19. Joguet G, Mansuy JM, Matusali G, Hamdi S, Walschaerts M, Pavili L, et al. Effect of acute Zika virus infection on sperm and virus clearance in body fluids: a prospective observational study. Lancet Infect Dis. 2017;17:1200–8. https://doi.org/10.1016/S1473-3099(17)30444-9
20. Matusali G, Houzet L, Satie AP, Mahé D, Aubry F, Couderc T, et al. Zika virus infects human testicular tissue and germ cells. J Clin Invest. 2018;128:4697–710. https://doi.org/10.1172/JCI121735
21. Busch MP, Sabino EC, Brambilla D, Lopes ME, Capuani L, Chowdhury D, et al.; International Component of the NHLBI Recipient Epidemiology and Donor Evaluation Study-III (REDS-III). Duration of dengue viremia in blood donors and relationships between donor viremia, infection incidence and clinical case reports during a large epidemic. J Infect Dis. 2016;214:49–54. https://doi.org/10.1093/infdis/jiw122
22. Waggoner JJ, Stittleburg V, Natrajan MS, Paniagua-Avila A, Bauer D, Olson D, et al. Sensitive and prolonged detection of dengue virus RNA in whole blood. Am J Trop Med Hyg. 2021;104:1734–6. https://doi.org/10.4269/ajtmh.20-1497
23. de Souza Pereira BB, Darrigo Junior LG, de Mello Costa TC, Felix AC, Simoes BP, Stracieri AB, et al. Prolonged viremia in dengue virus infection in hematopoietic stem cell transplant recipients and patients with hematological malignancies. Transpl Infect Dis. 2017;19:19. https://doi.org/10.1111/tid.12721
24. Pasquier C, Daudin M, Righi L, Berges L, Thauvin L, Berrebi A, et al. Sperm washing and virus nucleic acid detection to reduce HIV and hepatitis C virus transmission in serodiscordant couples wishing to have children. AIDS. 2000;14:2093–9. https://doi.org/10.1097/00002030-200009290-00004
25. Shamim M, Naqvi SZG. Dengue fever associated with acute scrotal oedema: two case reports. J Pak Med Assoc. 2011;61:601–3.
26. Sharda M, Soni A, Nigam H, Singh A, Sharma N. Acute scrotal edema: an atypical manifestation of dengue. J Assoc Physicians India. 2016;64:103–4.
27. Mahé D, Bourgeau S, Frouard J, Joguet G, Pasquier C, Bujan L, et al. Long-term Zika virus infection of non-sperm cells in semen. Lancet Infect Dis. 2020;20:1371. https://doi.org/10.1016/S1473-3099(20)30834-3
28. Le Tortorec A, Matusali G, Mahé D, Aubry F, Mazaud-Guittot S, Houzet L, et al. From ancient to emerging infections: the odyssey of viruses in the male genital tract. Physiol Rev. 2020;100:1349–414. https://doi.org/10.1152/physrev.00021.2019
29. Siemann DN, Strange DP, Maharaj PN, Shi PY, Verma S. Zika virus infects human Sertoli cells and modulates the integrity of the *In vitro* blood-testis barrier model. J Virol. 2017;91:e00623–17. https://doi.org/10.1128/JVI.00623-17
30. Prabandari SA, Arifin E, Saepuloh U, Iskandriati D, Pamungkas J. Dengue virus type 3 (DENV-3) distribution in tissues of pig-tailed macaque (*Macaca nemestrina*) post infection using immunohistochemistry technique. Int J Sci Basic Appl Res. 2017;33:1–9.
31. Bujan L, Mansuy JM, Hamdi S, Pasquier C, Joguet G. 1 year after acute Zika virus infection in men. Lancet Infect Dis. 2020;20:25–6. https://doi.org/10.1016/S1473-3099(19)30678-4
32. Sergerie M, Mieusset R, Croute F, Daudin M, Bujan L. High risk of temporary alteration of semen parameters after recent acute febrile illness. Fertil Steril. 2007;88:970e1–7.

Address for correspondence: Louis Bujan, Inserm 1203 and CECOS, Hôpital Paule de Viguier, CHU Toulouse, 330 avenue de Grande Bretagne, F-31059 Toulouse CEDEX, France; email: bujan.l@chu-toulouse.fr

Risk Factors for SARS-CoV-2 Infection and Illness in Cats and Dogs[1]

Dorothee Bienzle, Joyce Rousseau, David Marom, Jennifer MacNicol, Linda Jacobson, Stephanie Sparling, Natalie Prystajecky, Erin Fraser, J. Scott Weese

We tested swab specimens from pets in households in Ontario, Canada, with human COVID-19 cases by quantitative PCR for SARS-CoV-2 and surveyed pet owners for risk factors associated with infection and seropositivity. We tested serum samples for spike protein IgG and IgM in household pets and also in animals from shelters and low-cost neuter clinics. Among household pets, 2% (1/49) of swab specimens from dogs and 7.7% (5/65) from cats were PCR positive, but 41% of dog serum samples and 52% of cat serum samples were positive for SARS-CoV-2 IgG or IgM. The likelihood of SARS-CoV-2 seropositivity in pet samples was higher for cats but not dogs that slept on owners' beds and for dogs and cats that contracted a new illness. Seropositivity in neuter-clinic samples was 16% (35/221); in shelter samples, 9.3% (7/75). Our findings indicate a high likelihood for pets in households of humans with COVID-19 to seroconvert and become ill.

SARS-CoV-2 originated in horseshoe bats and probably reached humans through an unidentified intermediary host (1). The virus is aerosolized and highly transmissible among humans; new variants have arisen and spread in successive waves across the world since late 2019. Since a report of SARS-CoV-2 infection in a dog in March 2020 (2), an ever-increasing range of species has been shown to be susceptible to infection, including household cats, dogs, ferrets, and hamsters (3–10).

Author affiliations: Ontario Veterinary College, Guelph, Ontario, Canada (D. Bienzle, J. Rousseau, D. Marom, J. MacNicol, J.S. Weese); Toronto Humane Society, Toronto, Ontario, Canada (L. Jacobson); Toronto Animal Services, Toronto (S. Sparling); BC Centre for Disease Control Public Health Laboratory, Vancouver, British Columbia, Canada (N. Prystajecky); University of British Columbia, Vancouver (N. Prystajecky); Communicable Disease and Immunization Service, BC Centre for Disease Control, Vancouver (E. Fraser); University of British Columbia School of Population and Public Health, Vancouver (E. Fraser)

DOI: https://doi.org/10.3201/eid2806.220423

Companion animals have closest contact with humans, creating ample opportunity for exposure. Experimental infections have suggested that most companion animals are infected only transiently, as indicated by PCR positivity or virus isolation (11,12). Conversely, detection of antibodies by ELISA or neutralizing antibody assay suggests infection rates of 0.2%–43.9% related to factors such as the likelihood and frequency of interaction with infected humans (13–16). Infections in animals are typically subclinical or associated with transient respiratory or gastrointestinal disease (17,18). In rare cases, death has been attributed to SARS-CoV-2 infection; however, defining the contribution of SARS-CoV-2 to death in animals with underlying conditions such as cancer, bacterial pneumonia, or obesity is challenging. On the other hand, minks are highly susceptible to infection and pneumonia, and mortality rates of 35%–55% caused by SARS-CoV-2 infection were reported from outbreaks among farmed mink in Utah (19). Captive minks also contracted viruses with a unique amino acid substitution in the spike (S) protein that were subsequently retransmitted to humans and to community cats and dogs, around mink farms in the Netherlands (5,20). Similarly, infected pet Syrian hamsters may also retransmit SARS-CoV-2 to humans (21). More than 30% of free-ranging white-tailed deer tested in Ohio were SARS-CoV-2 positive by PCR, and a similarly high proportion of white-tailed deer in Texas and other North America locations had neutralizing antibodies (22,23). Experimentally, white-tailed deer transmitted SARS-CoV-2 to other deer vertically and horizontally by direct contact (24). It has not yet been determined if infected deer experience illness or have increased illness and death rates or if transmission is sustained among wild deer populations. However, such high

[1]Preliminary results from this study were presented at the 30th (September 23–25, 2020) and 31st (July 9–12, 2021) European Congress of Clinical Microbiology and Infectious Diseases.

prevalence suggests SARS-CoV-2 may become endemic in some deer populations in North America.

SARS-CoV-2 is transmitted predominantly via aerosols, aided by proximity of infected and susceptible hosts, the degree of host susceptibility, and the concentration of infectious virions in air. Although most infections in animals originate from humans, neither risk factors for zoonotic transmission from humans to pets nor the frequency and nature of clinical illness in pets are well defined. We report the frequency of SARS-CoV-2 seropositivity in cohorts of pets from households, low-cost neuter clinics, and animal shelters in Ontario, Canada, and analyze household risk factors associated with seropositivity. The University of Guelph (Ontario, Canada) approved the studies by Animal Utilization Protocol 4411 and Research Ethics Board Protocol 20-04-002.

Methods

Swab Samples

Pet owners who had a diagnosis of SARS-CoV-2 infection or symptoms compatible with COVID-19 in the previous 3 weeks were invited to have their pet swabbed by study veterinarians during April 24, 2020–August 31, 2021. Dogs, cats, and ferrets of any age and clinical status were eligible for testing; the only exclusion criterion was medical or behavioral issues that precluded safe sampling. We obtained swab samples from the distal nares, oropharynx, and rectum, whenever possible. We placed swabs in inactivating media (PrimeStore; Longhorn Vaccines and Diagnostics, https://lhnvd.com) for a minimum of 12 hours, extracted RNA using Galvens Viral RNA Extraction (Montreal Biotech, https://www.montrealbiotech.com), and eluted into water.

We performed quantitative reverse transcription PCR to amplify SARS-CoV-2 cDNA with primers and probe in the viral N1 gene (Appendix 1, https://wwwnc.cdc.gov/EID/article/28/6/22-0423-App1.pdf). We submitted samples with positive results for amplification of segments of the envelope (E) and RNA-dependent RNA polymerase (RdRp) genes and whole-genome sequencing in additional laboratories.

Serum Samples

During June 8, 2020–November 30, 2021, we invited owners of pets who received a diagnosis of SARS-CoV-2 infection 2 weeks–3 months previously to have a blood sample of their pet analyzed for SARS-CoV-2 antibodies.

Veterinarians or veterinary technicians at Toronto Humane Society (THS) collected blood samples from cats and dogs admitted to the shelter during June 18–November 28, 2020. Any animal that did not have health and behavioral reasons for exclusion was eligible for the study, regardless of origin (surrender, seizure, stray) or known history of SARS-CoV-2 exposure. Similarly, we collected samples through Toronto Animal Services (TAS) from unowned and owned cats admitted to a low-cost neuter clinic during January 21–July 6, 2021. We centrifuged all blood samples on site and shipped serum samples to Ontario Veterinary College (Guelph, Ontario, Canada). Serum samples were frozen in aliquots until batch analysis.

We constructed ELISA assays for the detection of cat and dog IgG and IgM to SARS-CoV-2 S protein (Appendix 1). Positive controls were from a SARS-CoV-2–experimentally-infected cat and 2 dogs with high titers; negative controls were cat and dog serum samples collected before 2019.

We tested the initial 42 serum samples and a subsequent 70 samples with IgG optical density (OD) >1.4 with the surrogate virus neutralization test (sVNT; GenScript, https://www.genscript.com) to determine blocking of the interaction of the receptor-binding domain (RBD) of SARS-CoV-2 with the ACE2 receptor. Following manufacturer instructions, we interpreted inhibition >20% relative to the kit positive control as indicating the presence of neutralizing antibodies.

Survey

We asked owners of household pets to complete an online 20-question survey concerning household demographics, the nature of the interaction with their pets, and the development of new illness in pets (Appendix 2, https://wwwnc.cdc.gov/EID/article/28/6/22-0423-App2.pdf). We also administered a questionnaire to owners of cats brought to the low-cost neuter clinic (Appendix 3, https://wwwnc.cdc.gov/EID/article/28/6/22-0423-App3.pdf). Questionnaires were not administered for unowned cats.

Statistical Analysis

For household cats, factors associated with PCR positivity were not evaluated because of the small sample size and low prevalence. We evaluated factors associated with seropositivity by univariable analysis using $\chi 2$, Fisher exact, or Wilcoxon tests as appropriate for the data. We categorized neuter-clinic cats by age: cats <6 months of age were kittens and cats >6 months adults. We calculated odds ratios and 95% CI. We did not perform multivariable analysis because of limitations in sample size.

We compared differences in seropositivity among different pet cohorts with Mann-Whitney tests. We

Table 1. Serology results from dogs and cats whose owners had received a diagnosis of SARS-CoV-2 infection or had symptoms compatible with COVID-19 in the previous 3 weeks, Ontario, Canada*

Test result	IgG	IgM	IgG and IgM	IgG or IgM
Dogs, n = 59				
>3 SD	26 (44)	26 (44)	21 (36)	31 (53)
>6 SD	22 (37)	16 (27)	16 (27)	24 (41)
Cats, n = 48				
>3 SD	29 (60)	29 (60)	22 (46)	35 (73)
>6 SD	23 (48)	13 (27)	11 (23)	25 (52)

*Values are no. (%). Results were >3 or >6 SD above the mean result for negative controls.

calculated correlation of ELISA OD with sVNT results using Prism version 9.3.1 (GraphPad, https://www.graphpad.com); $p<0.05$ was considered significant.

Results

PCR

We collected a total of 283 swab specimens from 65 cats, 49 dogs, and 6 ferrets: 70 nasal, 90 oral, 107 rectal and 16 fur (dorsum) samples. Samples from 5 (7.7%) cats and 1 (2.0%) dog had positive PCR results. Each N1 PCR positive result (Ct <35.99) was confirmed by amplification with E, R, or RdRp primers. For all 6 animals testing positive, the nasal swab samples were positive; oral swab samples were positive from 2 of 3 tested, and rectal swab samples were positive from 1 of 3 tested. Swab samples from an additional 10 (15%) cats, 3 (6.1%) dogs, and 3 (50%) ferrets had nonnegative results. N1 PCR Ct values for those 16 samples were 36.00–39.00. Testing of other targeted regions at additional laboratories yielded similar nonnegative results.

One cat with an initial Ct of 21.56 was retested weekly 5 times after the first positive result and had positive results during the first 3 weeks. Another cat with an initial Ct of 24.11 tested positive again 1 week later (Ct 36.19) and negative thereafter.

We derived whole-genome sequences (>99.3% coverage) from 2 positive cats. Phylogenetic analysis assigned the sequences to Pangolin lineage A.23.1 and B.1.2, which had the highest similarity to human SARS-CoV-2 sequences derived in that time period from the corresponding geographic region.

Serology

Household Pets

We collected serum samples from 59 dogs and 48 cats from 77 households and 1 animal shelter (from recently surrendered cats). Median number of samples per household was 1 (range 1–4). We collected 7 samples from the humane society; those 7 samples were excluded from risk factor analysis because of the potential clustering effect and the lack of metadata about these animals. Dogs were a median of 5 years of age (range 5 months–14 years of age), and cats were a median of 6 years of age (range 1–19 years of age).

Seropositivity for IgG and IgM was 42%–62% using >3 SD above the mean of the negative control samples as a cutoff and 25%–48% at >6 SD (Table 1). At >6 SD, all IgM positive dogs were also IgG positive, whereas 12/48 (25%) cats were IgG positive but IgM negative.

For statistical analysis, we defined seropositivity as >3 SD for IgG, IgM, or both. We observed a significant association between seropositivity and owner-reported onset of new respiratory disease in dogs at the time of the owner's infection ($p = 0.04$), but not in cats (Table 2). Association of seropositivity and owner-reported new onset of clinical signs (respiratory, gastrointestinal, or systemic signs such as lethargy) approached significance in dogs ($p = 0.06$).

Not all risk factor data were available for all animals. Univariable risk factor analysis did not identify risk factors for dogs, but sleeping in the owner's bed was a risk factor for seropositivity in cats (OR 5.8, 95% CI 1.1–29.4) We determined no effect from the presence of multiple pets in the household (dogs $p = 0.33$, cats $p = 0.70$) or the number of persons with confirmed (dogs $p = 0.77$, cats $p = 0.64$) or confirmed and suspected (dogs $p = 0.92$, cats $p = 0.47$) COVID-19. We did not see an association between time the animal typically spent per day with the infected owner for either dogs ($p = 0.71$) or cats ($p = 0.53$).

When we defined seropositivity as >6 SD above the mean of negative controls, we saw no significant association between seropositivity and owner-reported

Table 2. Association of seropositivity for SARS-CoV-2 in pets with household risk factors and development of new illness, Ontario, Canada*

	Dogs, n = 59			Cats, n = 48		
Variable	Seropositive*	Seronegative	p value	Seropositive	Seronegative	p value
Kissed by owner	16/25 (64)	16/27 (59)	0.73	16/27 (59)	3/13 (30)	0.15
Licked hands/face of owner	19/25 (64)	22/25 (81)	0.63	13/27 (48)	3/13 (30)	0.46
Slept in/on bed	17/24 (68)	15/27 (56)	0.36	23/27 (85)	5/10 (50)	0.04
New respiratory signs	9/29 (31)	2/27 (7.4)	0.04	8/29 (28)	2/10 (20)	1.00
New clinical signs	12/29 (41)	5/27 (19)	0.06	12/29 (41)	2/10 (20)	0.28

*Seropositivity is defined by IgG, IgM or both against viral S protein. Results were positive if optical density is >3 SD above the mean of negative controls.

Table 3. Association of seropositivity for SARS-CoV-2 in pets with household risk factors and development of new illness, Ontario, Canada*

Variable	Dogs, n = 59			Cats, n = 48		
	Seropositive	Seronegative	p value	Seropositive	Seronegative	p value
Multiple pets	9/24 (38)	15/19 (44)	0.79	15/27 (56)	12/19 (63)	0.61
Kissed by owner	13/20 (65)	19/32 (59)	0.69	11/19 (58)	8/18 (44)	0.52
Licked hands/face of owner	16/20 (80)	25/32 (78)	1.00	10/19 (53)	6/18 (33)	0.32
Slept in/on bed	13/20 (65)	19/32 (59)	0.69	17/19 (76)	11/18 (61)	0.06
New respiratory signs	7/23 (30)	4/33 (12)	0.17	8/21 (38)	2/18 (11)	0.07
New clinical signs	11/23 (48)	6/33 (18)	0.018	12/21 (57)	2/18 (11)	0.006

*Seropositivity is defined by IgG, IgM or both against viral S protein. Results were positive if optical density is >6 SD above the mean of negative controls.

onset of new respiratory disease in the pet at the time of the owner's infection for dogs (Table 3). However, we observed a significant association of seropositivity and owner-reported new onset of clinical respiratory, gastrointestinal, or systemic signs such as lethargy in the pet. We found the same association in cats.

Univariable risk factor analysis did not identify an association of seropositivity with risk factors (Table 3). We saw no association between time the animal typically spent per day with the infected owner for either dogs (p = 0.73) or cats (p = 0.35). However, cats that spent <2 hours per day with their owner were significantly less likely to be seropositive (1/7 [16%] vs. 18/30 [67%]; p = 0.04). We did not see the same result for dogs (p = 0.51). We saw no effect from the presence of multiple pets in the household (dogs p = 0.61, cats p = 0.69) or the number of persons per household with confirmed (dogs p = 0.83, cats p = 0.74) or confirmed or suspected (dogs p = 0.84, cats p = 0.82) COVID-19. Overall, >1 animal was seropositive in 3 (16%) of the 19 households where >1 animal was sampled: 2 households in which 2 dogs were seropositive and 1 in which a dog and cat were seropositive.

We performed sVNT on 53 samples from household pets. Of those, 30/41 (76%) that were positive for IgG and/or IgM (6 SD) were also positive on sVNT compared with 0/12 IgG/IgM negative samples (p<0.0001). Despite the smaller sample size, we repeated risk factor analysis using the samples tested by sVNT. For dogs, licking hands or face of owners was associated with seropositivity (OR 10.5 95% CI 1.5–73; p = 0.017). In addition, we noticed an association between positivity and dogs spending 19–24 hours with owners (OR 13.3, 95% CI 1.3–135; p = 0.033). For cats, the association between positivity and being kissed by owners was significant (OR 18.7, 95% CI 1.6–223; p = 0.020).

Neuter-Clinic Cats

We collected serum samples from 221 cats during January–June 2021. Full animal information and history were not available for all cats. The median age of the 184 (83%) cats for which age was reported or estimated was 1.5 years (interquartile range 3.25 years). We classified 32/184 (17%) cats as kittens and 152 (83%) as adults (Table 4). COVID contact status was known for 103 cats. We detected S IgG (>6 SD) in 35/221 (16%) cats. Monthly seropositivity rate was 0%–40%; we identified a significant association between month and seropositivity (p<0.0001) (Figure 1).

Univariable analyses were performed excluding animals whose exposure to persons with COVID-19 was unknown (Table 4). We identified animal source as a risk factor for seropositivity. Compared with cats originating from households, cats that were in a shelter, rescue or foster facility cats were 3.6 times as likely to be seropositive (95% CI 1.5–8.8; p = 0.005). We found no significant difference between feral and household cats or feral and shelter/rescue/foster cats.

Humane Society Animals

Of 67 cat and 8 dog samples from THS, 7/75 (9.3%) overall and 7/67 (10%) of cat samples were seropositive (>6 SD). We did not perform risk factor analysis because limited metadata were available.

Correlation of ELISA with sVNT

We identified a significant difference in the mean OD between household samples and those from both THS

Table 4. Characteristics of 221 cats at a neuter clinic tested for the presence of SARS-CoV-2 serum antibodies and univariable analysis results, Ontario, Canada

Characteristic	Seropositive, no. (%)	p value
Categorical age		0.12
Kitten	2/32 (6.3)	
Adult	27/152 (18)	
Sex		1.0
M	16/106 (15)	
F	12/78 (15)	
Not reported	7/37 (19)	
Animal source		0.01
Household pet	7/93 (8)	
Shelter/rescue/foster	23/102 (23)	
Feral	5/26 (19)	
Exposure to person with COVID		0.59
Yes	2/13 (15)	
No	6/90 (6.7)	
Unknown or declined to answer	27/118 (23)	

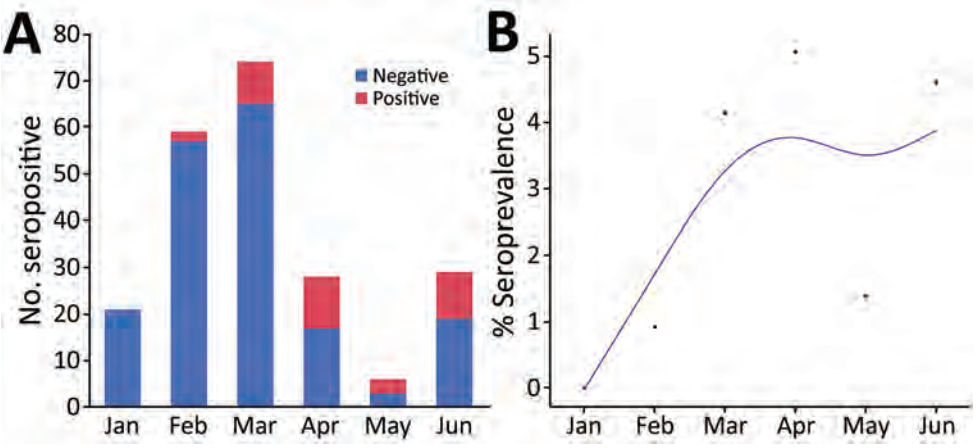

Figure 1. Seropositivity for SARS-CoV-2 in cats brought for care to a low-cost spay/neuter clinic during January – June 2021, Ontario, Canada. A) Test results for 221 cats shown by month. B) Positivity rate per month. The points indicate the proportion of positive test results among all test results over time. Blue line indicates the smoothed rate of seropositivity. The association between month and the change in seropositivity was significant (p<0.0001).

and TAS. Differences between THS and TAS were not significant (Figure 2).

In addition to ELISA testing, we also assessed a subset of 112 serum samples (53 household and 59 from shelter and spay/neuter clinic) with the sVNT. We found a significant correlation between the ELISA OD and neutralization of virus binding (ρ = 0.4188, 95% CI 0.2529–0.5608; p<0.0001) (Figure 3, panel A). The correlation between ELISA and sVNT results was higher for cats than dogs (Figure 3, panel B).

Discussion

Our findings suggest that transmission of SARS-CoV-2 from infected humans to their pets as indicated by seroconversion is common. PCR-based detection of SARS-CoV-2 in pets was uncommon within 3 weeks from owners being symptomatic or having a diagnosis of COVID-19, which may reflect genuine brevity of infection in pets, as noted experimentally in cats (12).Other factors are variations in time intervals between owner infection and pet sampling and the challenge of obtaining representative samples from the nose in cats (12). Other studies of infection of cats from households of persons with COVID-19 had similarly low PCR-based prevalence (16,25–28). The timeframe required for owners to be diagnosed, contact the study team, and arrange a household visit likely resulted in false negative PCR results from samples being collected too late relative to onset of infection. The definition of COVID-19 symptoms and access to PCR testing for sick persons was limited early in the pandemic, and it is possible that pets in this study were infected concurrently or immediately after their owners but swabbed only after they had eliminated infection. Kittens 4–5 months old experimentally infected with 1×106 TCID50 of SARS-CoV-2 intranasally and orally had detectable viral RNA for 10 days in nasopharyngeal swabs, 7 days in oropharyngeal swabs, and 14 days in rectal swabs, but such high viral challenge may not simulate typical human–cat household interactions (12). Subtle pulmonary lesions and viral RNA detectable until 6 days postinfection in experimentally infected cats suggest that, even with high viral inoculates, cats rarely get sick and can clear infection relatively quickly (29).

Longitudinal samples were rarely available; however, serial sampling for 1 cat revealed prolonged PCR positivity. That cat had chronic upper respiratory disease; whether the condition played a role in the prolonged PCR positivity is unclear. Despite the duration of PCR positivity, it is unlikely that the cat was infectious because the relatively high PCR Ct values would be consistent with low-level shedding of viral nucleic acids. Similar prolonged PCR positivity

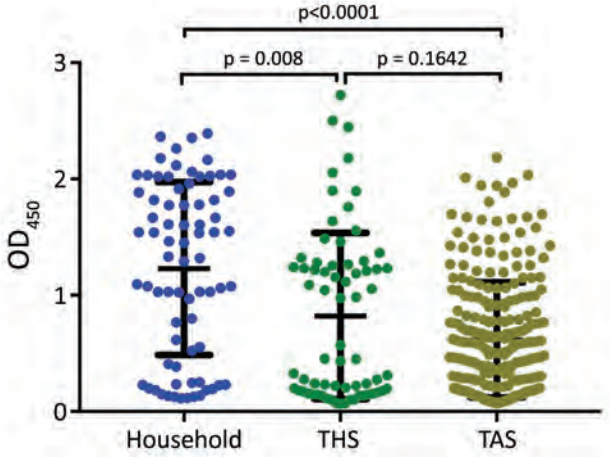

Figure 2. Mean serum SARS-CoV-2 spike protein IgG as measured by ELISA for samples from household cats, from cats in a shelter (THS), and from cats brought to a spay/neuter clinic for care (TAS), Ontario, Canada. The mean and SD are indicated. Differences were significant for household vs. shelter cats and household vs. clinic cats, but not for shelter vs. clinic cats. OD450, optical density at 450 nm; THS, Toronto Humane Society; TAS, Toronto Animal Services.

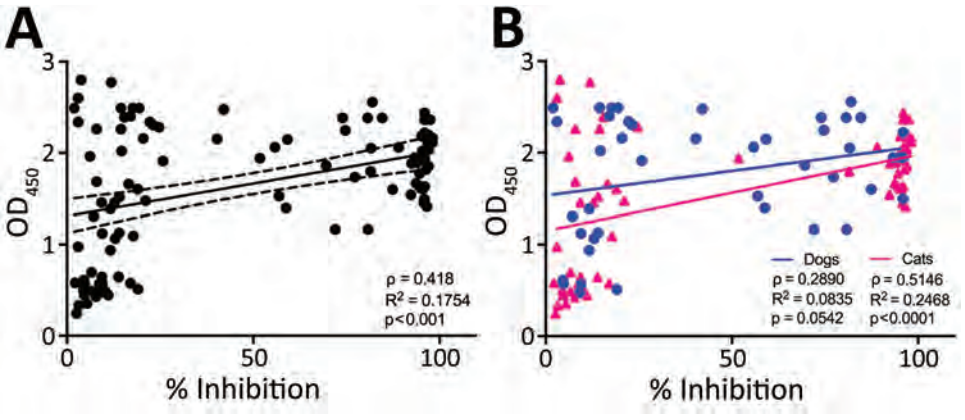

Figure 3. Results of IgG ELISA in relation to percentage inhibition of binding of the SARS-CoV-2 receptor binding domain (RBD) to the ACE2 receptor in cat and dog serum samples measured with a surrogate virus neutralization assay, Ontario, Canada. A) Surrogate virus neutralization test results correlated with IgG ELISA results. B) Percentage of inhibition for dog (blue circles) and cat (pink triangles) samples. The solid line shows correlation and dashed lines 95% CI. Correlation is higher for cat than dog samples. OD450, optical density at 450 nm.

has been reported for a cat exposed in a retirement home (30) and for tigers and lions in zoos (31). More data regarding the duration of positivity in naturally infected dogs and cats, and whether infectious virus is shed, are needed.

Seroprevalence was much higher than PCR positivity. We expected this finding because serologic data represent historical exposure and there is not a need to sample animals within a narrow infection window. Seroprevalence detected in other studies was 0.4%–30% or higher; in most instances such variability could be attributed to the extent of pets' exposure to infected humans (6,9,32–34).

Without broadly accepted definitions, the parameters and interpretation of serologic assays for SARS-CoV-2 vary widely (13,28,35–37). We designed traditional ELISAs detecting IgG and IgM for S protein. We used a range of negative serum samples from before 2019, as well as serum from cats with feline infectious peritonitis caused by enteric α coronavirus. The negative controls yielded consistently low ODs for S protein IgG and IgM; we interpreted results from exposed animals at 3 SD and 6 SD above the mean of the least diluted negative controls to enable comparison with other studies (12,13). A relatively high proportion of dogs and cats had antibodies to S protein, which could indicate infection or exposure. Results of the sVNT, most likely to reflect infection, correlated with S protein ELISA results in this and other studies (38). Some serum samples had high S antibodies despite lack of neutralization; this pattern could indicate exposure rather than infection or postinfection persistence of antibodies broadly reactive with S protein but not neutralizing RBD binding. The cause of the discrepant results cannot be determined from samples collected at a single time point that was potentially days or weeks postexposure. Furthermore, development of antibodies to SARS-CoV-2 is affected by host age, immunocompetence, and comorbidities, which could not be controlled in this surveillance study (36); even experimentally infected young cats had inconsistent antibody responses (12).

Risk factor analyses identified plausible associations presumably linked to the duration and closeness of human–animal contact. Limited risk factor information for dogs and cats has been reported (16, 28,37,39); however, association of seropositivity and proximity or sleeping with infected owners has been reported for dogs (16) and in a study where canine and feline data were combined (40). In our study, the same risk factors were not identified when using different serologic cutoffs or tests, which was likely a result of small sample sizes.

The substantially higher seroprevalence in cats exposed to infected persons gives more credence to the seropositivity data. Yet, the prevalence of seropositivity was still moderately high in cats with no known exposure to infected people. The lack of metadata makes this challenging to interpret, because it is possible that cats from the humane society or neuter clinic had previously been exposed to infected humans (28).

PCR positivity rate was too low for robust comparison of sample sites. However, all positive animals had positive nasal swab specimens, despite the challenges that can be encountered collecting good nasal swabs, especially from cats. Adding oral, rectal, or fur swab specimens did not increase diagnostic yield. Further study of sampling sites under field conditions would identify sampling approaches that maximize diagnostic yield while minimizing the number of sites that must be sampled. These data are preliminary but support the

importance of collecting nasal swab specimens as part of or all of the sample set.

Our study's first limitation was sample size; enrollment was hampered by low human COVID-19 infection rates in the study region throughout the main sampling times and by difficulties identifying exposed households in an appropriate timeframe. Lack of a coordinated One Health approach concurrently investigating human and animal exposures was a problem; local or provincial public health agencies had little interest in leading research or performing a joint study. The timing of sampling also affected PCR results. More complete validation of the specificity of serologic assays with a samples from animals with diverse other infectious and inflammatory conditions remains to be done. Ideally, the timeframe for sampling would have been more condensed to focus testing on animals whose owners were more recently infected (e.g., 1–2 weeks after the onset of the owner's infection).

These data indicate relatively common transmission of SARS-CoV-2 from humans to animals and that certain human–animal contacts (e.g., kissing the pet, pet sleeping on the bed) appear to increase the risk. We inferred that infections in dogs and cats reflect direct transmission from humans to animals, given the pandemic nature of this virus in humans and limited contact of most household pets with other animals (41). Intra-household transmission cannot be ruled out as a cause of some infections; however, multiple seropositive animals were only identified in 3/19 (16%) households where multiple animals were tested. We did not specifically investigate whether this relates to differences in individual animal susceptibility or animal–owner contact.

The relevance of human–pet transmission of SARS-CoV-2 needs further study. We observed an association between infection and clinical disease in both dogs and cats; in most cases, disease was very mild and self-limiting. Clinical data from this study are consistent with other studies indicating limited overall health risk to otherwise healthy dogs and cats (17,18,42). The zoonotic risk posed by dogs is probably low based on the lower infection rate and lack of evidence of transmission experimentally (43). Risk is probably higher for cats; cat–cat transmission has been identified, but the actual risk for cat–human transmission is unknown (44). Our findings support the occurrence of human–dog and human–cat transmission and highlight the need for further study of the animal and human health consequences of spillback of this zoonotic pathogen into animals.

Acknowledgments

We thank the animal owners who provided samples and information for this study, and the veterinarians and veterinary technicians who assisted with sample procurement.

Funding was provided by the Ontario Ministry of Agriculture via the Ontario Animal Health Network and by the University of Guelph.

About the Author

Dr. Bienzle is a professor of veterinary pathology at Ontario Veterinary College. Her research interests include infectious diseases of companion animals.

References

1. Koopmans M, Daszak P, Dedkov VG, Dwyer DE, Farag E, Fischer TK, et al. Origins of SARS-CoV-2: window is closing for key scientific studies. Nature. 2021;596:482–5. https://doi.org/10.1038/d41586-021-02263-6
2. Almendros A, Gascoigne E. Can companion animals become infected with COVID-19? Vet Rec. 2020;186:419–20. https://doi.org/10.1136/vr.m1322
3. Bosco-Lauth AM, Root JJ, Porter SM, Walker AE, Guilbert L, Hawvermale D, et al. Peridomestic mammal susceptibility to severe acute respiratory syndrome coronavirus 2 infection. Emerg Infect Dis. 2021;27:2073–80. https://doi.org/10.3201/eid2708.210180
4. Decaro N, Vaccari G, Lorusso A, Lorusso E, De Sabato L, Patterson EI, et al. Possible human-to-dog transmission of SARS-CoV-2, Italy, 2020. Emerg Infect Dis. 2021;27:1981–4. https://doi.org/10.3201/eid2707.204959
5. van Aart AE, Velkers FC, Fischer EAJ, Broens EM, Egberink H, Zhao S, et al. SARS-CoV-2 infection in cats and dogs in infected mink farms. Transbound Emerg Dis. 2021.
6. van der Leij WJR, Broens EM, Hesselink JW, Schuurman N, Vernooij JCM, Egberink HF. Serological screening for antibodies against SARS-CoV-2 in Dutch shelter cats. Viruses. 2021;13:1634. https://doi.org/10.3390/v13081634
7. Shou S, Liu M, Yang Y, Kang N, Song Y, Tan D, et al. Animal models for COVID-19: hamsters, mouse, ferret, mink, tree shrew, and non-human primates. Front Microbiol. 2021;12:626553. https://doi.org/10.3389/fmicb.2021.626553
8. Hobbs EC, Reid TJ. Animals and SARS-CoV-2: species susceptibility and viral transmission in experimental and natural conditions, and the potential implications for community transmission. Transbound Emerg Dis. 2021;68:1850–67. https://doi.org/10.1111/tbed.13885
9. Patterson EI, Elia G, Grassi A, Giordano A, Desario C, Medardo M, et al. Evidence of exposure to SARS-CoV-2 in cats and dogs from households in Italy. Nat Commun. 2020;11:6231–5. https://doi.org/10.1038/s41467-020-20097-0
10. Zoccola R, Beltramo C, Magris G, Peletto S, Acutis P, Bozzetta E, et al. First detection of an Italian human-to-cat outbreak of SARS-CoV-2 Alpha variant—lineage B.1.1.7. One Health. 2021;13:100295. https://doi.org/10.1016/j.onehlt.2021.100295
11. Gaudreault NN, Carossino M, Morozov I, Trujillo JD, Meekins DA, Madden DW, et al. Experimental re-infected cats do not transmit SARS-CoV-2. Emerg Microbes Infect. 2021;10:638–50. https://doi.org/10.1080/22221751.2021.1902753

12. Gaudreault NN, Trujillo JD, Carossino M, Meekins DA, Morozov I, Madden DW, et al. SARS-CoV-2 infection, disease and transmission in domestic cats. Emerg Microbes Infect. 2020;9:2322–32. https://doi.org/10.1080/22221751.2020.1833687
13. Zhao S, Schuurman N, Li W, Wang C, Smit LAM, Broens EM, et al. Serologic screening of severe acute respiratory syndrome coronavirus 2 infection in cats and dogs during first coronavirus disease wave, the Netherlands. Emerg Infect Dis. 2021;27:1362–70. https://doi.org/10.3201/eid2705.204055
14. Stevanovic V, Tabain I, Vilibic-Cavlek T, Mauric Maljkovic M, Benvin I, Hruskar Z, et al. The emergence of SARS-CoV-2 within the dog population in Croatia: host factors and clinical outcome. Viruses. 2021;13:1430. https://doi.org/10.3390/v13081430
15. Hamer SA, Ghai RR, Zecca IB, Auckland LD, Roundy CM, Davila E, et al. SARS-CoV-2 B.1.1.7 variant of concern detected in a pet dog and cat after exposure to a person with COVID-19, USA. Transbound Emerg Dis. 2021 May 6 [Epub ahead of print]. https://doi.org/10.1111/tbed.14122
16. Goryoka GW, Cossaboom CM, Gharpure R, Dawson P, Tansey C, Rossow J, et al. One Health investigation of SARS-CoV-2 infection and seropositivity among pets in households with confirmed human COVID-19 cases—Utah and Wisconsin, 2020. Viruses. 2021;13:1813. https://doi.org/10.3390/v13091813
17. Rotstein DS, Peloquin S, Proia K, Hart E, Lee J, Vyhnal KK, et al. Investigation of SARS-CoV-2 infection and associated lesions in exotic and companion animals. Vet Pathol. 2022;1:3009858211067467. https://doi.org/10.1177/03009858211067467
18. Carpenter A, Ghai RR, Gary J, Ritter JM, Carvallo FR, Diel DG, et al. Determining the role of natural SARS-CoV-2 infection in the death of domestic pets: 10 cases (2020–2021). J Am Vet Med Assoc. 2021;259:1032–9. https://doi.org/10.2460/javma.259.9.1032
19. Eckstrand CD, Baldwin TJ, Rood KA, Clayton MJ, Lott JK, Wolking RM, et al. An outbreak of SARS-CoV-2 with high mortality in mink (Neovison vison) on multiple Utah farms. PLoS Pathog. 2021;17:e1009952. https://doi.org/10.1371/journal.ppat.1009952
20. Lu L, Sikkema RS, Velkers FC, Nieuwenhuijse DF, Fischer EAJ, Meijer PA, et al. Adaptation, spread and transmission of SARS-CoV-2 in farmed minks and associated humans in the Netherlands. Nat Commun. 2021;12:6802. https://doi.org/10.1038/s41467-021-27096-9
21. Yen H-L, Sit THC, Brackman CJ, Chuk SSY, Cheng SMS, Gu H, et al. Transmission of SARS-CoV-2 delta variant (AY.127) from pet hamsters to humans, leading to onward human-to-human transmission: a case study. Lancet. 2022;399:1070–78. https://doi.org/10.1016/S0140-6736(22)00326-9
22. Hale VL, Dennis PM, McBride DS, Nolting JM, Madden C, Huey D, et al. SARS-CoV-2 infection in free-ranging white-tailed deer. Nature. 2022;602:481–6. https://doi.org/10.1038/s41586-021-04353-x
23. Palermo PM, Orbegozo J, Watts DM, Morrill JC. SARS-CoV-2 neutralizing antibodies in white-tailed deer from Texas. Vector Borne Zoonotic Dis. 2022;22:62–4.
24. Cool K, Gaudreault NN, Morozov I, Trujillo JD, Meekins DA, McDowell C, et al. Infection and transmission of ancestral SARS-CoV-2 and its alpha variant in pregnant white-tailed deer. Emerg Microbes Infect. 2022;11:95–112. https://doi.org/10.1080/22221751.2021.2012528
25. Barrs VR, Peiris M, Tam KWS, Law PYT, Brackman CJ, To EMW, et al. SARS-CoV-2 in quarantined domestic cats from COVID-19 households or close contacts, Hong Kong, China. Emerg Infect Dis. 2020;26:3071–4. https://doi.org/10.3201/eid2612.202786
26. Krafft E, Denolly S, Boson B, Angelloz-Pessey S, Levaltier S, Nesi N, et al. Report of one-year prospective surveillance of SARS-CoV-2 in dogs and cats in France with various exposure risks: confirmation of a low prevalence of shedding, detection and complete sequencing of an Alpha variant in a cat. Viruses. 2021;13:1759. https://doi.org/10.3390/v13091759
27. de Carvalho OV, Ristow LE, Rodrigues DDS, Farias CKDS, Maia RCC. Retrospective surveillance of severe acute respiratory syndrome coronavirus 2 in pets from Brazil. Vet World. 2021;14:2803–8. https://doi.org/10.14202/vetworld.2021.2803-2808
28. Spada E, Vitale F, Bruno F, Castelli G, Reale S, Perego R, et al. A pre- and during pandemic survey of SARS-CoV-2 infection in stray colony and shelter cats from a high endemic area of northern Italy. Viruses. 2021;13:618. https://doi.org/10.3390/v13040618
29. Patania OM, Chiba S, Halfmann PJ, Hatta M, Maemura T, Bernard KA, et al. Pulmonary lesions induced by SARS-CoV-2 infection in domestic cats. Vet Pathol. 2021:3009858211066840. https://doi.org/10.1177/03009858211066840
30. Schulz C, Martina B, Mirolo M, Müller E, Klein R, Volk H, et al. SARS-CoV-2–specific antibodies in domestic cats during first COVID-19 wave, Europe. Emerg Infect Dis. 2021;27:3115–8. https://doi.org/10.3201/eid2712.211252
31. Bartlett SL, Diel DG, Wang L, Zec S, Laverack M, Martins M, et al. SARS-CoV-2 infection and longitudinal fecal screening in Malayan tigers (Panthera tigris Jacksoni), Amur tigers (Panthera tigris Altaica), and African lions (Panthera Leo Krugeri) at the Bronx Zoo, New York, USA. J Zoo Wildl Med. 2021;51:733–44. https://doi.org/10.1638/2020-0171
32. Cossaboom CM, Medley AM, Spengler JR, Kukielka EA, Goryoka GW, Baird T, et al. Low SARS-CoV-2 seroprevalence and no active infections among dogs and cats in animal shelters with laboratory-confirmed COVID-19 human cases among employees. Biology (Basel). 2021;10:898. https://doi.org/10.3390/biology10090898
33. Michelitsch A, Hoffmann D, Wernike K, Beer M. Occurrence of antibodies against SARS-CoV-2 in the domestic cat population of Germany. Vaccines (Basel). 2020;8:772. https://doi.org/10.3390/vaccines8040772
34. Schulz C, Wylezich C, Wernike K, Gründl M, Dangel A, Baechlein C, et al. Prolonged SARS-CoV-2 RNA shedding from therapy cat after cluster outbreak in retirement home. Emerg Infect Dis. 2021;27:1974–6. https://doi.org/10.3201/eid2707.204670
35. Semmler G, Traugott MT, Graninger M, Hoepler W, Seitz T, Kelani H, et al. Assessment of S1-, S2-, and NCP-specific IgM, IgA, and IgG antibody kinetics in acute SARS-CoV-2 infection by a microarray and twelve other immunoassays. J Clin Microbiol. 2021;59:e02890-20. https://doi.org/10.1128/JCM.02890-20
36. Pallett SJ, Jones R, Abdulaal A, Pallett MA, Rayment M, Patel A, et al. Variability in detection of SARS-CoV-2-specific antibody responses following mild infection: a prospective multicentre cross-sectional study, London, United Kingdom, 17 April to 17 July 2020. Euro Surveill. 2022;27:2002076. https://doi.org/10.2807/1560-7917.ES.2022.27.4.2002076
37. Fritz M, Rosolen B, Krafft E, Becquart P, Elguero E, Vratskikh O, et al. High prevalence of SARS-CoV-2 antibodies in pets from COVID-19+ households.

One Health. 2020;11:100192. https://doi.org/10.1016/j.onehlt.2020.100192
38. Perera RAPM, Ko R, Tsang OTY, Hui DSC, Kwan MYM, Brackman CJ, et al. Evaluation of a SARS-CoV-2 surrogate virus neutralization test for detection of antibody in human, canine, cat, and hamster sera. J Clin Microbiol. 2021;59:e02504-20. https://doi.org/10.1128/JCM.02504-20
39. Barroso R, Vieira-Pires A, Antunes A, Fidalgo-Carvalho I. Susceptibility of pets to SARS-CoV-2 infection: lessons from a seroepidemiologic survey of cats and dogs in Portugal. Microorganisms. 2022;10:345. https://doi.org/10.3390/microorganisms10020345
40. Calvet GA, Pereira SA, Ogrzewalska M, Pauvolid-Corrêa A, Resende PC, Tassinari WS, et al. Investigation of SARS-CoV-2 infection in dogs and cats of humans diagnosed with COVID-19 in Rio de Janeiro, Brazil. PLoS One. 2021;16:e0250853. https://doi.org/10.1371/journal.pone.0250853
41. Yaglom HD, Hecht G, Goedderz A, Jasso-Selles D, Ely JL, Ruberto I, et al. Genomic investigation of a household SARS-CoV-2 disease cluster in Arizona involving a cat, dog, and pet owner. One Health. 2021;13:100333. https://doi.org/10.1016/j.onehlt.2021.100333
42. Hosie MJ, Epifano I, Herder V, Orton RJ, Stevenson A, Johnson N, et al.; COVID-19 Genomics UK (COG-UK) consortium. Detection of SARS-CoV-2 in respiratory samples from cats in the UK associated with human-to-cat transmission. Vet Rec. 2021;188:e247. https://doi.org/10.1002/vetr.247
43 Shi J, Wen Z, Zhong G, Yang H, Wang C, Huang B, et al. Susceptibility of ferrets, cats, dogs, and other domesticated animals to SARS-coronavirus 2. Science. 2020;368:1016–20. https://doi.org/10.1126/science.abb7015
44. Halfmann PJ, Hatta M, Chiba S, Maemura T, Fan S, Takeda M, et al. Transmission of SARS-CoV-2 in domestic cats. N Engl J Med. 2020;383:592–4. https://doi.org/10.1056/NEJMc2013400

Address for correspondence: Dorothee Bienzle, Department of Pathobiology, University of Guelph, Rm 3822, Bldg 89 419 Gordon St, Guelph, ON, N1G2W1, Canada; email: dbienzle@uoguelph.ca

Angiostrongylus cantonensis Nematode Invasion Pathway, Mallorca, Spain

Sofia Delgado-Serra,[1] Jessica Sola, Nieves Negre, Claudia Paredes-Esquivel[1]

Neural angiostrongyliasis is an emerging zoonosis caused by the rat lungworm, *Angiostrongylus cantonensis*. In humans, infection with this nematode often results in eosinophilic meningitis and other severe disorders of the central nervous system. Europe was deemed a nonendemic region until 2018, when *A. cantonensis* worms were detected on the Mediterranean island of Mallorca, Spain, a tourism hotspot. Since that time, a sentinel surveillance system and a molecular approach have been used to follow the invasion path of the rat lungworm on the island. *A. cantonensis* worms have been found in animals from 8 locations on the island over 3 consecutive years. Our preliminary results show a recognizable pattern of clinical signs in infected hedgehogs and a single mitochondrial haplotype circulating in Mallorca. We present strong evidence confirming that the rat lungworm has successfully established and colonized an island in Europe and discuss observations and possible strategies for its early detection across continental Europe.

The rat lungworm, *Angiostrongylus cantonensis*, infects animals and humans. Although this nematode species is recognized as the main etiologic agent of eosinophilic meningitis (*1*), infection might result in other central nervous system disorders (*2*). Clinical manifestations are aggravated by movement and subsequent death of the worms in the central nervous system, causing physical lesions and inflammation in accidental hosts (*3*). In humans, severe headache, neck stiffness, paresthesia, convulsions, urinary failure, visual impairment, and other symptoms, occasionally leading to coma and death, have been reported (*1*,*4*).

Author affiliations: University of the Balearic Islands, Palma, Spain (S. Delgado-Serra; C. Paredes-Esquivel); Consorci per a la Recuperació de la Fauna de les Illes Balears, Santa Eugènia, Spain (J. Sola, N. Negre)

DOI: https://doi.org/10.3201/eid2806.212344

The life cycle of *A. cantonensis* worms includes rats as definitive and gastropods as intermediate hosts; crustaceans, planarians, amphibians, reptiles, and fish might act as paratenic hosts (*2*). More than 20 vertebrate species, including humans, have been reported as *A. cantonensis* lungworm accidental hosts (*5*). This long list of vertebrate hosts includes nonhuman primates (*6*), marsupials (*7*), bats (*8*), horses (*9*), dogs (*10*), birds (*11*), and more recently, hedgehogs (*12*). The role of hedgehogs in the transmission of this parasite remains to be clarified.

A. cantonensis worms were detected in Canton, China, infecting the lungs of rats (*13*) and a decade later, in the cerebrospinal fluid of a person from Taiwan (*14*). For decades, disease-endemic areas were limited to the Pacific basin and Southeast Asia, but this parasite has spread to new territories at an alarming rate (*1*). The invasion of *A. cantonensis* lungworms has been associated with unintended importation of infected rats and gastropods on ships (*2*,*15*). Almost 3,000 cases of human neuroangiostrongyliasis have been reported (*16*) from 30 territories (*3*), although the prevalence might be higher (*17*).

Europe was considered to be nonendemic for *A. cantonensis* worms until 2018 when the parasite was reported infecting the brains of 2 hedgehogs on the Mediterranean island of Mallorca (*12*). Although the rat lungworm had been previously reported on Tenerife, a subtropical, non-European overseas oceanic island (*18*), its detection in Mallorca is an indisputable indication of its presence in Europe (*5*). Mallorca is a major Mediterranean tourism hotspot, highly interconnected with continental Europe. After the detection, the question remained whether *A. cantonensis* nematodes could survive the temperate winters of Europe. The purpose of this study was to use sentinel surveillance for symptomatic fauna to confirm whether the rat lungworm has been successfully established on Mallorca.

[1]These authors contributed equally to this article.

Methods

Surveillance Strategy

We conducted sentinel surveillance of hedgehogs that had signs of disease during 2018–2020 for early detection of *A. cantonensis* lungworm–positive animals on Mallorca. Availability of animals was contingent on local citizens providing injured, ill, or orphaned North African hedgehogs (*Atelerix algirus*) to the Consorci per a la Recuperació de la Fauna de les Illes Balears wildlife hospital. Animals showing neurologic clinical signs were hospitalized, and their behavior was observed daily.

When possible, a blood sample was obtained from the animal's jugular vein and sent to an external laboratory (Laboratorio Echevarne S.A., https://laboratorioechevarne.com) for hematologic and clinical chemistry analyses. Blood extraction was not always possible in severely ill or dehydrated hedgehogs. We euthanized critically ill animals to avoid suffering and then subjected them to necropsy, performed in a BioSafety Level 2 facility, according to the regulations of the University of the Balearic Islands. We kept lungs, heart, and head frozen for further analysis.

Detection and Morphologic Identification

We opened preserved skulls by using a scalpel and making 2 parallel incisions along the frontal and parietal bones to access the brain underneath. We completely removed the brain and macroscopically examined the interior of the skull and the subarachnoid space of the brain by using a stereomicroscope (magnification ×10–40). We conducted external examination of the lungs, heart and pulmonary arteries according to the same procedure. We collected nematodes from the brain and the skull's inner surface.

During 2018, we detected parasites macroscopically, During 2019 and 2020, we changed the method approach and used a tissue digestion technique after the visual inspection. When worms were present, we tentatively identified them as *A. cantonenisis* nematodes by their typical barber's pole appearance, which results from spiral disposition of the blood-filled intestine and the white uterine tubes in fully developed female worms. This characteristic can be observed in other *Angiostrongylus* species. Using the morphologic keys of Chen (*13*) and Kinsella (*19*), we also identified male nematodes on the basis of characteristics of the copulatory bursa, with a small dorsal ray, shorter than the externodorsal ones, and by the presence of long spicules (1–1.4 μm). We identified female worms on the basis of the form of their ventrally curved posterior end. We distinguished adults from larvae by their body size and development of the sexual apparatus.

Molecular Identification and Phylogenetic Analysis

We conducted molecular analysis to confirm the morphologic identifications. We extracted genomic DNA by using an NZY Tissue gDNA Isolation Kit (Nzytech, https://www.nzytech.com) and amplified a fragment of the cytochrome c oxidase subunit I (COI) gene region by PCR using primers COI forward, 5′-TTTTTTGGGCATCCTGAGGTTTAT-3′, and COI reverse, 5′-TAAAGAAAGAACATAATGAAAATG-3′ (*20*). The 50-μL PCR contained 2 μL of genomic DNA, 2 μL of each primer (10 mmol/L), 2 μL of 50 mmol/L $MgCl_2$, 25 μL of Taq Master Mix (Supreme NZY*Taq*II 2x Green Master Mix; Nzytech), and 17 μL of water. We performed PCRs in a Verity Thermo Cycler (Applied Biosystems, https://www.thermofisher.com) as follows: 1 cycle of initial denaturation at 95°C for 3 min; followed by 35 cycles at 95°C for 30 s, 50°C for 30 s, and 72°C for 1 min; and a final extension at 72°C for 10 min.

We visualized PCR products by electrophoresis on a 2% agarose gel containing Pronasafe Nucleic Acid Stain (Conda Laboratories, https://www.condalab.com). We purified samples by using an NZYGelpure Purification Kit (Nzytech) according to manufacturer specifications. We performed Sanger sequencing by Sistemas Genómicos S.L. (https://www.sistemasgenomicos.com). One *A. cantonensis* specimen/infected hedgehog was sequenced.

We conducted BLAST analysis (https://blast.ncbi.nlm.nih.gov) of the resulting sequences and used the GenBank database to confirm the identification of the parasites. We retrieved the top 78 hits corresponding with COI sequences of *A. cantonensis* nematodes for further phylogenetic analysis. We aligned retrieved sequences from GenBank and those obtained in this study by using CodonCode Aligner version 9.0.1 (CodonCode Co., https://www.codoncode.com). We inferred a maximum-likelihood phylogenetic tree by using MEGAX software (https://www.megasoftware.net) with Kimura 2-parameter and 500 bootstrap replicates.

Results

In a 3-year period, 8 animals that had signs of disease were rescued by local citizens from different parts of Mallorca. These animals had clinical signs compatible with a neurologic disease: astasia, pelvic limb ataxia, atonia, asthenia, paresis, and behavioral decay. Five of these animals were females (3 adults, 2 juveniles) and 3 were males (2 adults, 1 juvenile). The age of the

hedgehogs was calculated according to Garcia-Salguero et al. (*21*). The first 2 hedgehogs received were reported previously (*12*). The common clinical signs in infected hedgehogs were astasia, defined as the inability to stand and walk; lateral recumbency (present in all examined hedgehogs), defined as lying on their side; and bicycling movement (present in 6/8 hedgehogs), defined as a consistent, synchronized movement of the limbs (Video, https://wwwnc.cdc.gov/EID/article/28/6/21-2344-V1.htm). Bicycling often resulted in skin lacerations.

Infected hedgehogs were found in 8 localities from 7 of municipalities in Mallorca (Table; Figure 1). These locations varied from typical coastal places (hedgehogs AaAL1 and AaAN1) (the abbreviation Aa indicates the name of the hedgehog species [*A. algirus*]), in which tourism is the most prominent economic activity, to traditional inland rural areas dedicated to farmland (hedgehogs AaSP1 and AaSM1) (Figure 1). With the exception of hedgehog AaSN1, all specimens were found in municipalities located at the foot of the eastern foothills of the Tramuntana Mountain range. Two hedgehogs showed positive results during 2018 and 2019, and 4 hedgehogs showed positive results during 2020. All positive hedgehogs harbored *A. cantonensis* adults. None of the female worms had eggs.

Infected hedgehogs were found during autumn to early winter, specifically during September, October, and December (Table). None of the *A. cantonensis* specimens were found in the lungs or hearts of infected hedgehogs. All but 2 positive hedgehogs were co-infected with the lungworm *Crenosoma striatum*. Hematologic analysis could only be conducted for 2 infected hedgehogs. Hedgehog AaSP1 had a blood eosinophil count of 4% and an absolute blood count of 0.836×10^3 cells/μL, and hedgehog AaAL1 had a blood eosinophil count of 2% and an absolute blood count of 0.208×10^3 cells/μL.

DNA Assessment

After ClustalW alignment (https://www.ebi.ac.uk), we obtained a 389-bp sequence of the COI gene region. DNA extraction was not successful for parasites from hedgehog AaAL1. All remaining DNA sequences resulted in the same CI haplotype, the same one that was reported by our group in 2019 (*12*). We subjected the haplotype sequence to BLAST analysis against the GenBank database. The top 78 hits corresponded with COI sequences of *A. cantonensis* nematodes; the first 5 sequences showed 100% identity. Maximum-likelihood analysis resulted in a phylogenetic tree lacking strong bootstrap support values at deeper nodes (Figure 2). Specimens from Mallorca

Table. Details and clinical information for *Angiostrongylus cantonensis* lungworm–infected hedgehogs hospitalized at the Consorci per a la Recuperació de la Fauna de les Illes Balears wildlife hospital, Mallorca, Spain

Hedgehog specimen	Location	Date	Clinical manifestations	No. lungworms recovered		Helminth co-infections
				On skull	In brain	
AaAN1*	Camp de Mar (Andratx)	2018 Oct 13	Pelvic limb ataxia, atonia, asthenia, behavioral decay, lateral recumbency	0	1	None
AaPA1*	Son Castelló (Palma)	2018 Oct 23	Pelvic limb ataxia, atonia, behavioral decay, lateral recumbency	0	5	None
AaSP1	Sa Pobla	2019 Nov 11	Asthenia, astasia, bicycling movements, lateral recumbency, skin lacerations	1 male	0	*Crenosoma striatum* (lungs)
AaAL1	Alcúdia	2019 Dec 23	Astasia, bicycling movements, lateral recumbency	0	2 female, 2 male, 4 damaged specimens	*Crenosoma striatum* (lungs)
AaSM1	Santa Maria del Camí	2020 Jan 28	Astasia, bicycling movements, lateral recumbency	0	11 female, 191 male, 7 damaged specimens	None
AaIN1	Inca	2020 Oct 28	Astasia, bicycling movements, skin lacerations, lateral recumbency	0	6 female, 3 male, 9 damaged specimens	*Crenosoma striatum* (lungs)
AaPA2	Establiments (Palma)	2020 Nov 26	Astasia, bicycling movements, lateral recumbency	2 female, 1 male, 1 damaged specimen	33 female, 20 male, 11 damaged specimens	*Crenosoma striatum* (lungs)
AaSN1	Calonge (Santanyí)	2020 Dec 28	Astasia, repetitive cycling movements, lateral recumbency	0	2 female	*Crenosoma striatum* (lungs)

*Infected hedgehogs previously reported (*12*).

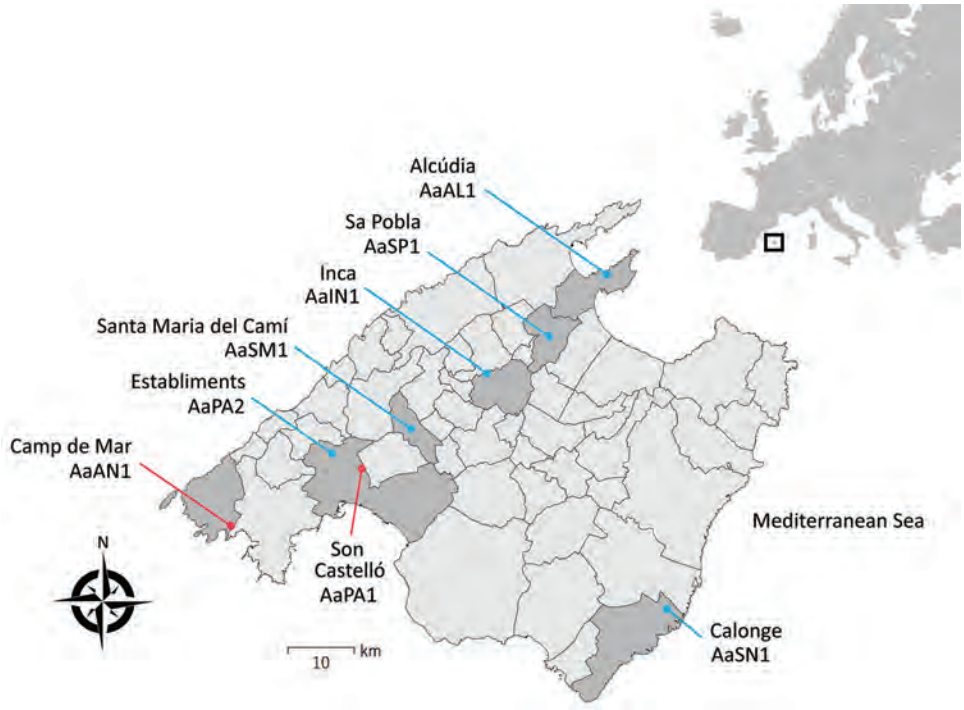

Figure 1. Geographic location of hedgehogs infected by *Angiostrongylus cantonensis* rat lungworms, Mallorca, Spain, 2018–2020. Blue indicates new cases reported in this study (see Table for details), and red indicates cases reported previously (*12*). Inset shows location of Mallorca off the coast of southwestern Europe.

were clustered in the same clade as those from Tenerife (Canary Islands, Spain), Australia, Taiwan, and New Orleans, Louisiana, USA.

Discussion

This study showed that the invasive neurotropic parasite *A. cantonensis*, the rat lungworm, is the main cause of neurologic disease in North African hedgehogs on the Mediterranean island of Mallorca. The rat lungworm has been found in hedgehogs from 8 locations in Mallorca over 3 consecutive years, indicating that this parasite is spreading and has successfully established in this territory of Europe since 2018.

Sentinel surveillance of hedgehogs that had signs of disease has resulted in a powerful and inexpensive public health monitoring tool to follow invasion of *A. cantonensis* lungworms in Mallorca. Hedgehogs are ubiquitous in Europe, and they have been reported as the most common mammal admitted to wildlife hospitals in Europe, where their clinical signs can be monitored closely (*21*,*22*). Despite the proven utility of this strategy, sentinel surveillance is often underused for detecting emerging pathogens (*23*).

Other mammals have been proposed as sentinels for early detection and understanding of the dynamics of *A. cantonensis* transmission: for example, the tawny frogmouth *Podargus strigoides* in Australia (*24*) because of its abundance and ubiquity (*25*), and dogs because of their clear clinical manifestations (*26*). We found a high (100%) prevalence of *A. cantonensis* worms in animals showing neurologic signs. In positive hedgehogs, the most predictive signs were astasia, lateral recumbency, and bicycling movement. These clinical manifestations might be used for presumptive diagnosis of an *A. cantonensis* infection in wildlife hospitals in Europe. More studies are necessary to validate these observations.

Characteristic neurologic signs of *A. cantonensis* infection have also been observed in tawny frogmouths. Ma et al. detected the parasite in 80% of symptomatic birds, in which paresis/paralysis affecting the hind limbs was the most common clinical manifestation (*25*). Progressive ascending paralysis of the limbs has also been observed in dogs (*27*). The gastropod-borne nematode *C. striatum* was present in most rat lungworm–positive hedgehogs in our study. This finding is not surprising because the prevalence of this lungworm in Mallorca is high (S. Delgado-Serra, unpub. data) but indicates that both parasites can co-infect the lungs of these mammals. Conversely, eosinophil count was unremarkable. The absence of eosinophilia in peripheral blood has also been observed in other animals (*28*) and humans (*29*) positive for this infection.

We found preliminary evidence of an apparent seasonality of neural angiostrongyliasis in Mallorca; all cases were detected in autumn and early winter (October–December). This seasonal pattern has also been observed in dogs in eastern Australia (*26*).

However, cases in tawny frogmouths, also in eastern Australia, occur in late summer and autumn (*25*). Instead of seasonality, prevalence of neural angiostrongyliasis might reflect periods of increased precipitation because this increase has a direct effect on the availability of snails and slugs (*30*).

Mallorca is an endemic foci of the rat lungworm in Europe; however, intermediate hosts in this region remain to be determined. To date, Egypt and Mallorca are the only rat lungworm–endemic territories in the Mediterranean Basin. Although none of the intermediate hosts reported in Egypt are present in Mallorca, the snail species *Theba pisana* and *Cornu aspersum*, reported in the Canary Islands (*31*) are also present in Mallorca. Both species are widely distributed in continental Europe.

All lungworms we sequenced had the same haplotype and were 100% congruent with those reported in Australia, New Orleans, Taiwan, and Tenerife. The single haplotype found in all specimens might be explained by recent range expansion of this parasite and might be the result of a single colonization event. However, more studies are needed to investigate the invasion origin of this parasite species.

Some open questions and limitations of this study should be discussed. First, we cannot know the exact locations where the parasite is circulating in Mallorca because the extent of the home range of North African hedgehogs can be >90 hectares/day (*32*). Surveillance should then include rats, which have smaller home ranges (*33*), or gastropods, especially because these hosts are far more abundant and widespread than hedgehogs. Second, the data presented do not reflect the real status of neural angiostrongyliasis in hedgehogs in Mallorca because we have only examined animals rescued by citizens. Third, the role of hedgehogs within the living cycle of the parasite is unknown. In 2018, our group found a gravid *A. cantonensis* female worm in the brain of a hedgehog (*12*), indicating that the parasite might reach sexual maturity in this host. However, we found no gravid female subsequently. Whether hedgehogs act as definitive hosts requires further research.

The heavy traffic of ships between the Balearic Islands and continental Europe might have already resulted in the introduction of infected rats to the mainland, and *A. cantonensis* lungworms might be more widely distributed on the continent than previously believed (*5*). Furthermore, the Mediterranean region confronts its own challenges in relation to the arrival of the rat lungworm. Snails are a major part of the Mediterranean diet, which has resulted in an increase of snail farms in the region (*34*). Food

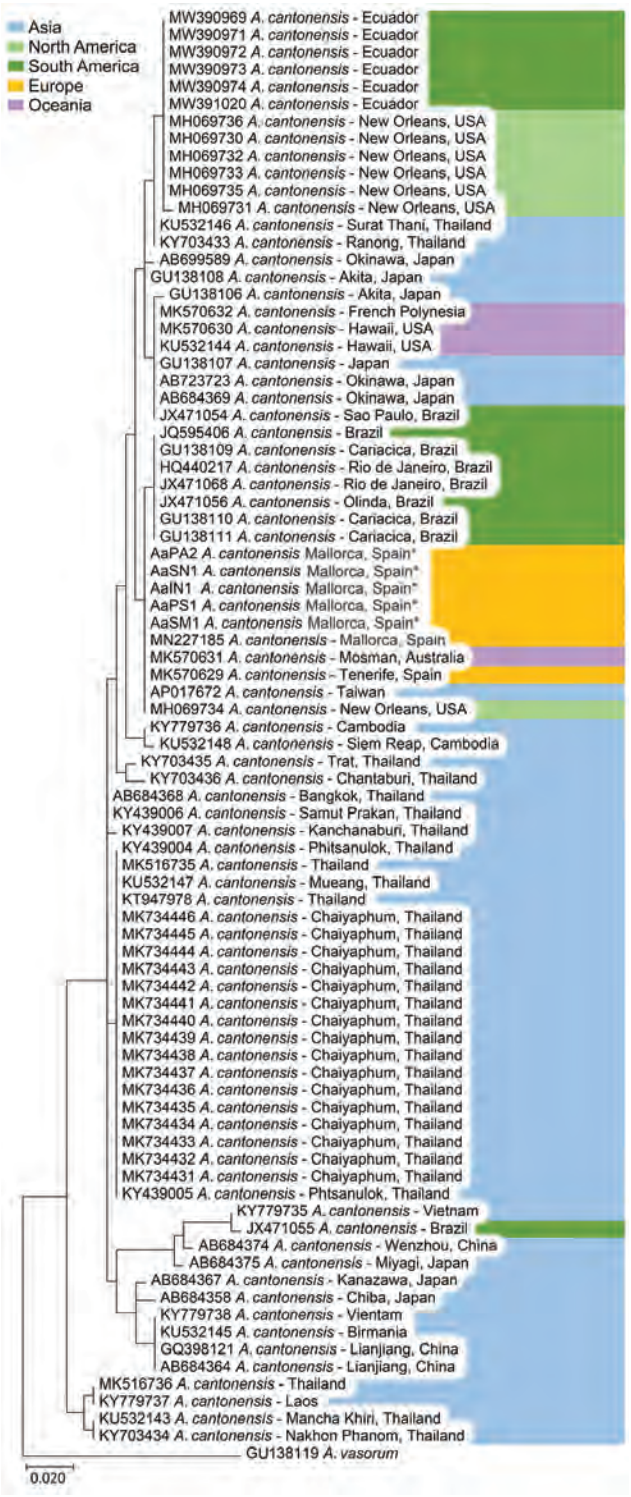

Figure 2. Maximum-likelihood tree showing the phylogenetic position of *Angiostrongylus cantonensis* rat lungworm cytochrome c oxidase subunit I gene fragments generated in study of infected hedgehogs in Mallorca, Spain, 2018–2020 (asterisks), and reference sequences retrieved from GenBank (accession numbers shown).

safety agencies on the continent might be aware of the increasing challenges for this industry because of possible introduction of the rat lungworm. The first detections of these worms in nonendemic areas often occur after the report of fatal human cases (*35*–*37*). In other regions, infections in wild, domestic, and captive animals have preceded those in humans (*28*), providing the ideal sequence of events to raise early public awareness and to establish early prevention strategies. A delay in the diagnosis and treatment for patients often results in worse prognosis. We recommend adopting a sentinel surveillance and One Health approaches similar to the one we provide in this study for the early detection of the rat lungworm in wildlife hospitals across Europe. However, this strategy should not replace the traditional means of detecting the rat lungworm. Further efforts should include increasing public and medical awareness of neuroangiostrongyliasis and conducting systematic surveillance of rats and gastropods (*38*) in areas across the continent where the rat lungworm is already established or could potentially become established.

Acknowledgments

We thank all wildlife hospital staff at Consorci per a la Recuperació de la Fauna de les Illes Balears for providing invaluable contributions to establishment of a One Health approach, Sebastià Jaume Ramis for providing help in transport of specimens, and the University of the Balearic Islands for providing support in the establishment of a Biosafety Level 2 laboratory.

This study was partially supported by the Govern de les Illes Balears (grants BIA0920-2 and PDR2020/61).

About the Author

Ms. Delgado-Serra is a doctoral student in the Applied Zoology and Animal Conservation Research Group at the University of the Balearic Islands, Palma, Spain. Her primary research interests are the molecular epidemiology of parasites and their vectors in the Mediterranean region.

References

1. McAuliffe L, Fortin Ensign S, Larson D, Bavaro M, Yetto J, Cathey M, et al. Severe CNS angiostrongyliasis in a young marine: a case report and literature review. Lancet Infect Dis. 2019;19:e132–42. https://doi.org/10.1016/S1473-3099(18)30434-1
2. Wang QP, Lai DH, Zhu XQ, Chen XG, Lun ZR. Human angiostrongyliasis. Lancet Infect Dis. 2008;8:621–30. https://doi.org/10.1016/S1473-3099(08)70229-9
3. Cowie RH. Biology, systematics, life cycle, and distribution of *Angiostrongylus cantonensis*, the cause of rat lungworm disease. Hawaii J Med Public Health. 2013;72(Suppl 2):6–9.
4. Sawanyawisuth K, Kitthaweesin K, Limpawattana P, Intapan PM, Tiamkao S, Jitpimolmard S, et al. Intraocular angiostrongyliasis: clinical findings, treatments and outcomes. Trans R Soc Trop Med Hyg. 2007;101:497–501. https://doi.org/10.1016/j.trstmh.2006.07.010
5. Morgan ER, Modry D, Paredes-Esquivel C, Foronda P, Traversa D. Angiostrongylosis in animals and humans in Europe. Pathogens. 2021;10:1236. https://doi.org/10.3390/pathogens10101236
6. Kim DY, Stewart TB, Bauer RW, Mitchell M. *Parastrongylus* (=*Angiostrongylus*) *cantonensis* now endemic in Louisiana wildlife. J Parasitol. 2002;88:1024–6. https://doi.org/10.1645/0022-3395(2002)088[1024:PACNEI]2.0.CO;2
7. McKenzie RA, Green PE, Wood AD. *Angiostrongylus cantonesis* infection of the brain of a captive Bennett's wallaby (*Macropus rufogriseus*). Aust Vet J. 1978;54:86–8. https://doi.org/10.1111/j.1751-0813.1978.tb00354.x
8. Barrett JL, Carlisle MS, Prociv P. Neuro-angiostrongylosis in wild black and grey-headed flying foxes (*Pteropus* spp) Aust Vet J. 2002;80:554–8. https://doi.org/10.1111/j.1751-0813.2002.tb11039.x
9. Costa LR, McClure JJ, Snider III TG, Stewart TB. Verminous meningoencephalomyelitis by *Angiostrongylus* (=*Parastrongylus*) *cantonensis* in an American miniature horse. Equine Vet Educ. 2000;12:2–6. https://doi.org/10.1111/j.2042-3292.2000.tb01754.x
10. Mason KV, Prescott CW, Kelly WR, Waddell AH. Letter: granulomatous encephalomyelitis of puppies due to *Angiostrongylus cantonensis*. Aust Vet J. 1976;52:295. https://doi.org/10.1111/j.1751-0813.1976.tb00124.x
11. Monks DJ, Carlisle MS, Carrigan M, Rose K, Spratt D, Gallagher A, et al. *Angiostrongylus cantonensis* as a cause of cerebrospinal disease in a yellow-tailed black cockatoo (*Calyptorhynchus funereus*) and two tawny frogmouths (*Podargus strigoides*). J Avian Med Surg. 2005;19:289–93. https://doi.org/10.1647/2004-024.1
12. Paredes-Esquivel C, Sola J, Delgado-Serra S, Puig Riera M, Negre N, Miranda MÁ, et al. *Angiostrongylus cantonensis* in North African hedgehogs as vertebrate hosts, Mallorca, Spain, October 2018. Euro Surveill. 2019;24:1900489. https://doi.org/10.2807/1560-7917.ES.2019.24.33.1900489
13. Chen HT. A new pulmonary nematode of rats, *Pulmonema cantonensis* ng, nsp from Canton. Ann Parasitol. 1935;13:312–7. https://doi.org/10.1051/parasite/1935134312
14. Beaver PC, Rosen L. Memorandum on the first report of *Angiostrongylus* in man, by Nomura and Lin, 1945. Am J Trop Med Hyg. 1964;13:589–90. https://doi.org/10.4269/ajtmh.1964.13.589
15. Martín-Carrillo N, Feliu C, Abreu-Acosta N, Izquierdo-Rodriguez E, Dorta-Guerra R, Miquel J, et al. A peculiar distribution of the emerging nematode *Angiostrongylus cantonensis* in the Canary Islands (Spain): recent introduction or isolation effect? Animals (Basel). 2021;11:1267. https://doi.org/10.3390/ani11051267
16. Cowie RH. *Angiostrongylus cantonensis*: agent of a sometimes fatal globally emerging infectious disease (rat lungworm disease). ACS Chem Neurosci. 2017;8:2102–4. https://doi.org/10.1021/acschemneuro.7b00335
17. Diao Z, Yin C, Qi H, Wang J. International symposium on *Angiostrongylus* and angiostrongyliasis, 2010. Emerg Infect Dis. 2011;17:e1.
18. Foronda P, López-González M, Miquel J, Torres J, Segovia M, Abreu-Acosta N, et al. Finding of *Parastrongylus cantonensis* (Chen, 1935) in *Rattus* in Tenerife, Canary Islands (Spain). Acta Trop. 2010;114:123–7. https://doi.org/10.1016/j.actatropica.2010.02.004

19. Kinsella JM. *Angiostrongylus schmidti* sp. n. (Nematoda: Metastrongyloidea) from the rice rat, *Oryzomys palustris*, in Florida, with a key to the species of *Angiostrongylus* Kamensky, 1905. J Parasitol. 1971;57:494–7. https://doi.org/10.2307/3277901
20. Monte TC, Simões RO, Oliveira AP, Novaes CF, Thiengo SC, Silva AJ, et al. Phylogenetic relationship of the Brazilian isolates of the rat lungworm *Angiostrongylus cantonensis* (Nematoda: Metastrongylidae) employing mitochondrial *COI* gene sequence data. Parasit Vectors. 2012;5:248. https://doi.org/10.1186/1756-3305-5-248
21. Garcia-Salguero A, Delgado-Serra S, Sola J, Negre N, Miranda MA, Paredes-Esquivel C. Combined morphology and DNA-barcoding to identify *Plagiorhynchus cylindraceus* cystacanths in *Atelerix algirus.* Parasitol Res. 2019;118:1473–8. https://doi.org/10.1007/s00436-019-06299-6
22. Molony SE, Dowding CV, Baker PJ, Cuthill IC, Harris S. The effect of translocation and temporary captivity on wildlife rehabilitation success: an experimental study using European hedgehogs (*Erinaceus europaeus*). Biol Conserv. 2006;130:530–7. https://doi.org/10.1016/j.biocon.2006.01.015
23. Halliday JE, Meredith AL, Knobel DL, Shaw DJ, Bronsvoort BM, Cleaveland S. A framework for evaluating animals as sentinels for infectious disease surveillance. J R Soc Interface. 2007;4:973–84. https://doi.org/10.1098/rsif.2007.0237
24. Spratt M, Neuroangiostrongyliasis disease in wildlife and humans. Microbiol Aust. 2005;26:63. https://doi.org/10.1071/MA05063
25. Ma G, Dennis M, Rose K, Spratt D, Spielman D. Tawny frogmouths and brushtail possums as sentinels for *Angiostrongylus cantonensis*, the rat lungworm. Vet Parasitol. 2013;192:158–65. https://doi.org/10.1016/j.vetpar.2012.11.009
26. Lunn JA, Lee R, Smaller J, MacKay BM, King T, Hunt GB, et al. Twenty two cases of canine neural angiostrongylosis in eastern Australia (2002–2005) and a review of the literature. Parasit Vectors. 2012;5:70. https://doi.org/10.1186/1756-3305-5-70
27. Mason KV. Canine neural angiostrongylosis: the clinical and therapeutic features of 55 natural cases. Aust Vet J. 1987;64:201–3. https://doi.org/10.1111/j.1751-0813.1987.tb15181.x
28. Duffy MS, Miller CL, Kinsella JM, de Lahunta A. *Parastrongylus cantonensis* in a nonhuman primate, Florida. Emerg Infect Dis. 2004;10:2207–10. https://doi.org/10.3201/eid1012.040319
29. Hiraoka T, Cuong NC, Hamaguchi S, Kikuchi M, Katoh S, Anh LK, et al. Meningitis patients with *Angiostrongylus cantonensis* may present without eosinophilia in the cerebrospinal fluid in northern Vietnam. PLoS Negl Trop Dis. 2020; 14:e0008937. https://doi.org/10.1371/journal.pntd.0008937
30. Gelis S, Spratt DM, Raidal SR. Neuroangiostrongyliasis and other parasites in tawny frogmouths (*Podargus strigoides*) in south-eastern Queensland. Aust Vet J. 2011; 89:47–50. https://doi.org/10.1111/j.1751-0813.2010.00660.x
31. Martin-Alonso A, Abreu-Yanes E, Feliu C, Mas-Coma S, Bargues MD, Valladares B, et al. Intermediate hosts of *Angiostrongylus cantonensis* in Tenerife, Spain. PLoS One. 2015;10:e0120686. https://doi.org/10.1371/journal.pone.0120686
32. García-Rodríguez S, Puig-Montserrat X. Algerian hedgehog (*Atelerix algirus* Lereboullet, 1842) habitat selection at the northern limit of its range. Galemys Spanish Journal of Mammalogy. 2014;26:49–56. https://doi.org/10.7325/Galemys.2014.A5
33. Byers KA, Lee MJ, Patrick DM, Himsworth CG. Rats about town: a systematic review of rat movement in urban ecosystems. Front Ecol Evol. 2019;7:13. https://doi.org/10.3389/fevo.2019.00013
34. Segade P, García-Estévez J, Arias C, Iglesias R. Parasitic infections in mixed system-based heliciculture farms: dynamics and key epidemiological factors. Parasitology. 2013;140:482–97. https://doi.org/10.1017/S0031182012001795
35. Lindo JF, Waugh C, Hall J, Cunningham-Myrie C, Ashley D, Eberhard ML, et al. Enzootic *Angiostrongylus cantonensis* in rats and snails after an outbreak of human eosinophilic meningitis, Jamaica. Emerg Infect Dis. 2002;8:324–6. https://doi.org/10.3201/eid0803.010316
36. Al Hammoud R, Nayes SL, Murphy JR, Heresi GP, Butler IJ, Pérez N. *Angiostrongylus cantonensis* meningitis and myelitis, Texas, USA. Emerg Infect Dis. 2017;23:1037–8. https://doi.org/10.3201/eid2306.161683
37. Flerlage T, Qvarnstrom Y, Noh J, Devincenzo JP, Madni A, Bagga B, et al. *Angiostrongylus cantonensis* eosinophilic meningitis in an infant, Tennessee, USA. Emerg Infect Dis. 2017;23:1756–8. https://doi.org/10.3201/eid2310.170978
38. Stockdale Walden HD, Slapcinsky JD, Roff S, Mendieta Calle J, Diaz Goodwin Z, Stern J, et al. Geographic distribution of *Angiostrongylus cantonensis* in wild rats (*Rattus rattus*) and terrestrial snails in Florida, USA. PLoS One. 2017; 12:e0177910. https://doi.org/10.1371/journal.pone.0177910

Address for correspondence: Claudia Paredes-Esquivel, Applied Zoology and Animal Conservation Research Group, University of the Balearic Islands; Carretera de Valldemossa km 7.5, 07122 Palma, Balearic Islands, Spain; email: claudia.paredes@uib.es

Economic Burden of Reported Lyme Disease in High-Incidence Areas, United States, 2014–2016

Sarah A. Hook, Seonghye Jeon, Sara A. Niesobecki, AmberJean P. Hansen, James I. Meek, Jenna K.H. Bjork, Franny M. Dorr, Heather J. Rutz, Katherine A. Feldman, Jennifer L. White, P. Bryon Backenson, Manjunath B. Shankar, Martin I. Meltzer, Alison F. Hinckley

Approximately 476,000 cases of Lyme disease are diagnosed in the United States annually, yet comprehensive economic evaluations are lacking. In a prospective study among reported cases in Lyme disease–endemic states, we estimated the total patient cost and total societal cost of the disease. In addition, we evaluated disease and demographic factors associated with total societal cost. Participants had a mean patient cost of ≈$1,200 (median $240) and a mean societal cost of ≈$2,000 (median $700). Patients with confirmed disseminated disease or probable disease had approximately double the societal cost of those with confirmed localized disease. The annual, aggregate cost of diagnosed Lyme disease could be $345–968 million (2016 US dollars) to US society. Our findings emphasize the importance of effective prevention and early diagnosis to reduce illness and associated costs. These results can be used in cost-effectiveness analyses of current and future prevention methods, such as a vaccine.

Lyme disease is a bacterial illness caused primarily by infection with *Borrelia burgdorferi*, transmitted by the bite of infected *Ixodes scapularis* and *I. pacificus* ticks in the United States. Early symptoms can include a rash known as erythema migrans and influenza-like symptoms (*1*). Disseminated infection can cause neurologic, musculoskeletal, and cardiac complications; in rare cases, cardiac involvement can be fatal (*1*–*4*). Most patients will experience a full recovery after antibiotic treatment, although a minority may continue to experience symptoms related to disease sequelae (*1*).

Lyme disease case numbers consistently rank in the top 10 among all nationally notifiable conditions, and it is the most commonly reported vector-borne disease in the United States (*4*,*5*). Annually, >30,000 cases are reported to the Centers for Disease Control and Prevention (*4*), but recent studies have demonstrated that the annual number of diagnosed cases is ≈476,000 (*6*). This figure represents a substantial disease burden, but the total economic cost to US society is unknown (*7*).

Economic evaluations for Lyme disease have limitations (*7*). Most studies report direct medical costs but lack data on nonmedical costs and losses in productivity (*8*–*11*). Several studies were conducted >2 decades ago in a few Maryland counties where Lyme disease was emerging (*9*,*11*,*12*); however, this limited scope prevents generalizability to other areas in which the disease is endemic, and results might not be representative of today's costs because of changes in disease management and healthcare structures. More recent studies have used diagnosis codes (e.g., International Classification of Diseases, 9th Revision, Clinical Modification) to identify Lyme disease patients from insurance claims databases. However, the low sensitivity and specificity of these codes in identifying actual cases (*13*,*14*) might lead to incorrect estimates of direct medical costs attributable to the disease. The few studies that provide more comprehensive cost estimates of Lyme disease were conducted in Europe under healthcare systems with financing structures different from those of the United States (*15*–*17*). As such, updated estimates of the total

Author affiliations: Centers for Disease Control and Prevention, Fort Collins, Colorado, USA (S.A. Hook, A.F. Hinckley); Centers for Disease Control and Prevention, Atlanta, Georgia, USA (S. Jeon, M.B. Shankar, M.I. Meltzer); Connecticut Emerging Infections Program, Yale School of Public Health, New Haven, Connecticut, USA (S.A. Niesobecki, A.P. Hansen, J.I. Meek); Minnesota Department of Health, St. Paul, Minnesota, USA (J.K.H. Bjork, F.M. Dorr); Maryland Department of Health, Baltimore, Maryland, USA (H.J. Rutz, K.A. Feldman); New York State Department of Health, Albany, New York, USA (J.L. White, P.B. Backenson)

DOI: https://doi.org/10.3201/eid2806.211335

societal cost of Lyme disease, including direct and indirect costs, are needed in the United States (*7*).

We aimed to address current research gaps by conducting a prospective cost-of-illness study to estimate the economic burden of reported Lyme disease in high-incidence areas of the United States. The main objectives of this study were to estimate the patient cost and the societal cost per participant. The secondary objective was to evaluate the association of select disease and demographic factors with the societal cost per participant. Results can be used by public health officials and communities to assess the cost-effectiveness of interventions to reduce the incidence of Lyme disease.

Methods

Study Design

This study was conducted as part of TickNET, a public health network of researchers who collaborate on tickborne disease research and surveillance (*18*). We conducted a prospective cost-of-illness study to estimate total costs per patient caused by Lyme disease in 4 high-incidence states: Connecticut, Maryland, Minnesota, and New York. We used an incidence-based design, measuring the cost of illness from onset to conclusion (*19*,*20*). We analyzed these costs from the patient perspective (i.e., costs incurred by the patient) and the societal perspective (i.e., costs incurred by the patient, healthcare system, or third-party payer) (*21*,*22*). Cost categories included direct medical costs (clinician visits, procedures, diagnostic testing, therapy, hospitalization, emergency department visits, or other relevant costs); direct nonmedical costs (roundtrip travel costs for healthcare visits and amount paid for assistance with self-care, dependent care, or house or yard maintenance because of Lyme disease); and indirect costs, which are the cost of productivity losses (time taken off work or school because of symptoms or healthcare visits) (Appendix Table 1, https://wwwnc.cdc.gov/EID/article/28/6/21-1335-App1.pdf) (*23*). Henceforth, we will refer to direct medical costs as either patient medical costs (for medical costs borne by the patient) or societal medical costs (for total medical costs borne by the patient, healthcare system, and third-party payer); in addition, we will refer to direct nonmedical costs as nonmedical costs.

Study Population

The source population included pediatric and adult patients with clinician-diagnosed Lyme disease reported to public health surveillance authorities in Connecticut and Minnesota and in select counties in Maryland and New York (Appendix Table 2). Eligible patients met the national surveillance case definition for confirmed or probable disease during the study period and were referred by surveillance authorities to study personnel upon case classification (*24*). To ensure enrollment of incident cases only, we excluded the following cases: probable cases with no symptoms reported by the clinician, cases with a previous Lyme disease diagnosis within 2 calendar years of current diagnosis date, and cases with a diagnosis date >12 months before date of enrollment. Non–English-speaking patients were not enrolled because of limited resources for interpreters.

We classified eligible patients into 3 disease categories. Those with confirmed Lyme disease were divided into 2 groups: confirmed localized disease (i.e., those with erythema migrans) and confirmed disseminated disease (i.e., those with arthritis, lymphocytic meningitis, cranial neuritis or facial palsy, radiculoneuropathy, encephalomyelitis, or second- or third-degree heart block) (*24*). The third category included probable cases with symptoms reported by a clinician. To ensure enrollment of participants with a range of disease severity, we stratified recruitment by disease category and, using quota sampling, aimed to recruit approximately equal numbers of participants in each category each month. This strategy also enabled us to enroll participants as close to their diagnosis date as possible to reduce participant recall error regarding costs. Each state aimed to enroll a minimum of 50 participants per disease category; the overall minimum enrollment goal was 150 total participants per state. Recruitment and enrollment occurred during September 2014–January 2016.

Data Collection

Participants consented to data collection for either patient costs or societal costs. Study coordinators conducted introductory telephone-based surveys with participants (or legal guardians for pediatric participants) to collect data on age, sex, annual household income, insurance coverage, and disease onset date. Patient cost data were collected at the introductory survey and then approximately monthly by using the IBM SPSS Data Collection Web Interviews survey program (IBM, https://www.ibm.com). We collected the following data on all surveys: dates for Lyme disease–related healthcare visits, clinician contact information, patient medical costs, nonmedical costs, and productivity losses. Surveys ceased when participants reported no Lyme disease–related expenses

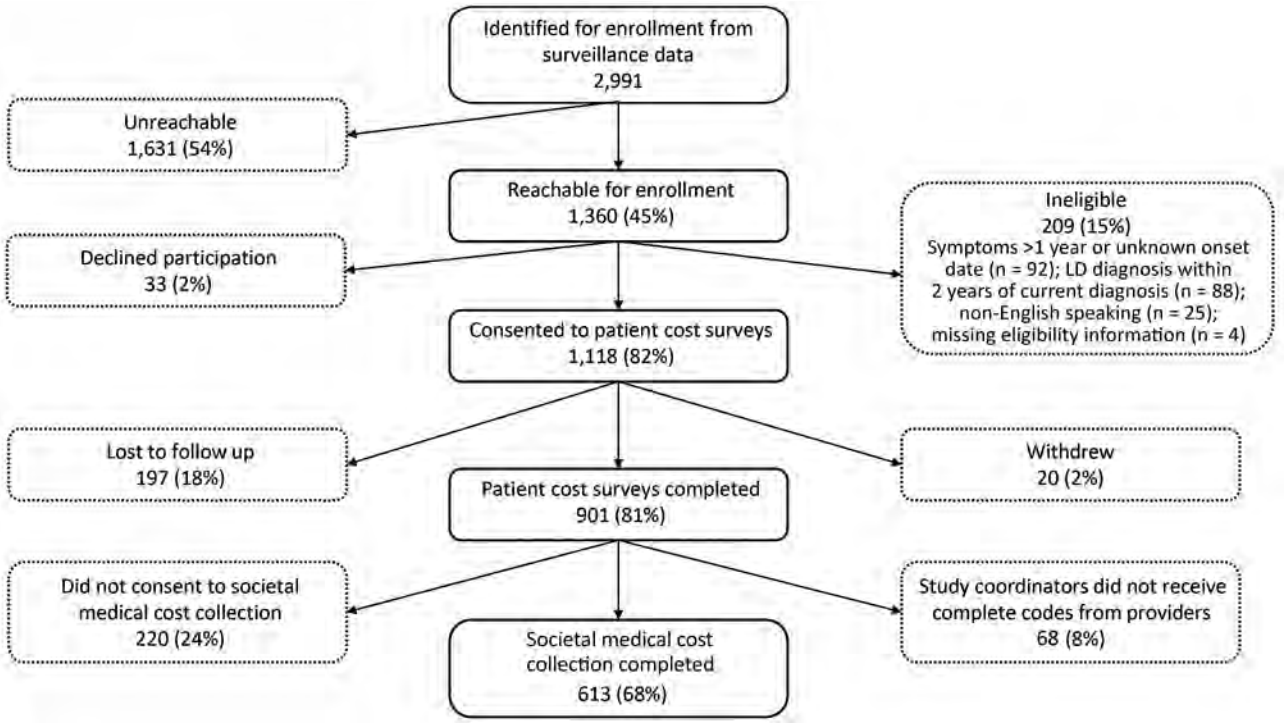

Figure 1. Flowchart of enrollment and completion by participants in study of economic burden of reported Lyme disease in high-incidence areas, United States, 2014–2016. LD, Lyme disease.

for 2 consecutive surveys or when they completed the maximum of 12 surveys.

To calculate societal medical costs, we requested billing codes (i.e., Current Procedural Terminology [CPT], 4th Edition) directly from participants' clinicians. We requested codes from 1 month before the self-reported disease onset date to the date of the final survey. We used a date range instead of individual visit dates reported by the participant in the event participants had incorrectly reported dates. We extracted mean reimbursement for each CPT code collected for participants with private insurance from IBM MarketScan Research Databases (IBM), which include national medical claims data for privately insured persons ≤65 years of age and their dependents, and reimbursements for CPT codes collected for non-privately insured participants from the Physician Fee Schedule from the Centers for Medicare and Medicaid Services (*25*). We extracted the costs of reimbursements according to state, year, and inpatient versus outpatient status (Appendix).

Analysis

To provide an overall weighted mean and median set of reimbursements and costs, disease category sampling probabilities were estimated from disease category proportions derived from surveillance data (*4*) to approximate stratified random sampling. We then used the inverse of the sampling probabilities to weight the data for all analyses described. We excluded participants who did not complete 3 consecutive surveys from all analyses. We adjusted medical costs to 2016 US dollars by using the Consumer Price Index for medical care and the general Consumer Price Index for nonmedical costs and costs of productivity losses (*26*). We estimated the mean, median, 10th and 90th percentiles, and SDs of patient costs, societal medical costs, and total societal costs per participant. We used the Kruskal-Wallis rank-sum test to evaluate differences in cost among the 3 disease categories (confirmed localized, confirmed disseminated, probable).

To estimate the patient cost, we summed self-reported patient medical costs, nonmedical costs, and cost of productivity losses over all surveys per participant (Appendix). To calculate the societal medical costs, we summed the mean cost per CPT code collected for each participant (Appendix). Finally, we calculated the societal cost by summing the societal medical costs, patient nonmedical costs, and cost of productivity losses per participant.

We conducted multivariable linear regression analysis by using the weighted dataset to evaluate associations between the societal cost per participant and the following independent variables: disease

Table 1. Demographic characteristics of 901 participants in study of economic burden of reported Lyme disease in high-incidence areas, United States, 2014–2016

Characteristic	No. participants	Unweighted %	Weighted %
Disease category*			
Confirmed localized	402	44.6	54.5
Confirmed disseminated	238	26.4	21.2
Probable	261	29.0	24.2
Age group, y			
<18	259	28.7	28.4
18–45	145	16.1	16.1
46–65	326	36.2	36.1
>65	171	19.0	19.4
Sex			
F	385	42.7	43.1
M	516	57.3	56.9
Race			
Non-White	59	6.5	6.4
White	842	93.5	93.6
State			
Connecticut	225	25.0	23.7
Maryland	239	26.5	26.8
Minnesota	268	29.7	29.6
New York	169	18.8	20.0
Income†			
≤$60,000	238	29.2	28.8
>$60,000	576	70.8	71.2
Insurance			
Private	632	70.1	70.2
Other	269	29.9	29.8

*Disease categories were derived from the surveillance case definition for Lyme disease (*24*). Those with confirmed Lyme disease were divided into 2 groups: confirmed localized disease (i.e., those with erythema migrans) and confirmed disseminated disease (i.e., those with arthritis, lymphocytic meningitis, cranial neuritis or facial palsy, radiculoneuropathy, encephalomyelitis, or 2nd or 3rd degree heart block). Those classified as probable met the probable case definition, plus had ≥1 symptom reported by a clinician.
†Participants were not required to provide information on income; n = 814.

category (confirmed localized, confirmed disseminated, probable), age group (<18, 18–45, 46–65, >65 years of age), sex (male, female), and state (Connecticut, Maryland, Minnesota, New York). We controlled for insurance status (private or nonprivate insurance), income (<$60,000 or ≥$60,000, which was the approximate median household income for participating states in 2015) (*27*), and study year (2014, 2015, 2016). As is typical for healthcare cost data, the distribution of societal cost was highly skewed, resulting in heteroskedasticity of the residuals in the model (*28*). Therefore, we transformed societal cost per participant by using natural logarithms and conducted sampling-weighted least squares regression (Appendix).

We obtained research approval from institutional review boards at Centers for Disease Control and Prevention, Connecticut Department of Public Health, Maryland Department of Health, Minnesota Department of Health, New York State Department of Health, and Yale University. We conducted analyses using SAS version 9.4 (SAS Institute, https://www.sas.com) and R version 3.5.2 (*29*–*34*).

Results

During the enrollment period, we identified 2,991 Lyme disease patients who were classified as having confirmed cases or probable cases with symptoms reported (Figure 1). Of the 1,360 (45%) patients we were able to contact, 1,118 (82%) consented to patient cost surveys; we included 901 (81%) participants with complete survey data in the patient cost analysis. Last, 613 (68%) of these participants also had complete societal medical cost data, and we included them in the societal cost analysis.

The study population included 402 (55%) confirmed localized, 238 (21%) confirmed disseminated, and 261 (24%) probable cases (Table 1). Overall, 36% of participants were 46–65 years of age, 57% were

Table 2. Clinician visits and duration of costs incurred, by Lyme disease category, in high-incidence areas, United States, 2014–2016

Characteristic	All	Lyme disease category		
		Confirmed localized	Confirmed disseminated	Probable
Median provider visits (range)	2 (1–47)	2 (1–25)	3 (1–45)	2 (1–47)
Median surveys* (range)	3 (1–12)	2 (1–12)	3 (1–12)	4 (1–12)

*Participants began taking surveys at study enrollment and continued at approximately 1-month intervals until they reported no Lyme disease–related expenses for 2 consecutive surveys or when they completed the maximum of 12 surveys. The following were collected on all surveys: dates for Lyme disease–related healthcare visits, clinician contact information, patient medical costs, nonmedical costs, and productivity losses.

Table 3. Patient perspective of cost of Lyme disease per participant, by disease category, in high-incidence areas, United States, 2014–2016

Disease category	No. participants	Patient perspective, cost per participant,* 2016 US dollars					
		Median	Mean	SD	10th percentile	90th percentile	Range
All†	901	244	1,252	2,972	29	3,139	0–30,628
Confirmed localized	402	170	1,070	4,164	27	2,535	1–26,686
Confirmed disseminated	238	358	1,692	7,323	32	4,116	2–30,628
Probable	261	315	1,277	4,629	34	3,987	0–18,833

*Cost per participant according to the patient perspective represents the sum of patient medical costs, nonmedical costs, cost of productivity losses, and other related costs as reported by each participant on all surveys.
†Estimates for the overall population use the sample-weighted data except the range.

men, and 94% were white. Most had income >$60,000 (71%) and private health insurance (70%). Demographic distributions were similar for the 613 participants who completed both patient cost surveys and societal medical cost collection (Appendix Table 3).

Participants reported a median of 2 provider visits and completed a median of 3 surveys (Table 2). Those with confirmed disseminated disease had the highest number of provider visits, reflecting the highest healthcare use, whereas those with probable disease had the highest number of surveys completed, reflecting the longest duration of costs incurred. Forty (4%) participants were still reporting symptoms and 25 (3%) were still incurring costs at survey 12.

Overall, the patient cost per participant ranged from $0.46 to $30,628. The median cost was $244 and the mean cost $1,252, reflecting a highly positively skewed distribution (Table 3). Participants with confirmed disseminated Lyme disease had the highest median cost ($358) and mean cost ($1,692), followed by those with probable disease (median $315 and mean $1,277), then participants with confirmed localized disease (median $170 and mean $1,070).

We calculated the median and mean cost per component of the patient cost by disease category (Figure 2; Appendix Table 4). For all disease categories, productivity losses had the highest mean cost of all cost components: $727 for those with confirmed disseminated disease, $627 for those with probable disease, and $540 for those with confirmed localized disease. However, the median cost of productivity losses for all disease categories was $0. Medical bills had the next highest cost: a median of $83 and a mean of $628 for those with confirmed disseminated disease, a median of $83 and a mean of $389 for those with probable disease, and a median of $42 and a mean of $314 for those with confirmed localized disease. All other cost components for all disease categories had median costs <$22 and mean costs <$80.

We collected 9,679 CPT codes to estimate societal medical costs. The most common codes were for office visits (17%) and routine venipuncture (6%) (Appendix Table 6). Overall, the societal medical cost per participant ranged from $50 to $121,869, for a median of $478 and mean of $1,333 (Table 4). Participants with confirmed disseminated disease had the highest median and mean societal medical cost ($696 and $2,537), followed by those with probable disease ($612 and $1,804), then confirmed localized disease ($374 and $668).

Overall, the societal cost of Lyme disease per participant ranged from $54 to $122,766; the median was $690 and the mean $2,032 (Table 5). Participants with confirmed disseminated disease had the highest median and mean societal cost ($1,081 and $3,251), followed by those with probable disease ($940 and $2,620), then confirmed localized disease ($493 and $1,307) (Appendix Table 7). Applying these per participant societal costs to estimates of the number of Lyme disease cases diagnosed each year (*6*), the aggregate cost to US society annually would be ≈$345 million using median costs and ≈$968 million using mean costs (2016 US dollars; Appendix Tables 9, 10).

In multivariable linear regression analysis, disease category, age, and state were associated with societal cost per participant (Table 6; Appendix Table 8). Costs for participants with confirmed disseminated disease were 120% higher than costs for participants with confirmed localized disease ($p<0.001$); participants with probable disease had costs that were 59% higher than for those with confirmed localized disease. Participants 18–45 and 46–65 years of age had costs that were 96% and 108% higher, respectively, than those <18 years of age ($p<0.001$); however, those >65 years of age did not have significantly different costs. Minnesota residents had 75% higher costs than did Connecticut residents, but Maryland and New York residents did not have significantly different costs from those for Connecticut residents.

Discussion

In this study, persons with confirmed or probable Lyme disease had an average patient cost of ≈$1,200 (median cost ≈$240) and an average societal cost of ≈$2,000 (median cost ≈$700). In stratified analyses by disease category, those with confirmed disseminated

or probable disease had double or more the societal cost per participant than those with confirmed localized disease, highlighting the importance of early and accurate diagnosis. Having disseminated or probable disease, being 18–65 years of age, and residing in Minnesota had the greatest effects on the societal cost of Lyme disease. Although median societal costs were typically ≤$1,000 for all disease categories, mean costs were substantially higher, indicating that most patients have low costs, but some experience very high costs related to this disease. Similarly, the low median number of provider visits and hours of lost productivity suggest that Lyme disease illness is manageable for most patients, but for a minority, it can be highly disruptive. Approximately 476,000 cases of Lyme disease are diagnosed each year in the United States, so the aggregate cost to society annually could be $345–968 million (2016 US dollars). This substantial economic burden underscores the need for effective prevention methods, such as a vaccine.

Classification of a reported case as probable means a clinician has diagnosed Lyme disease in a patient and laboratory evidence of infection exists. However, any reported symptoms are typically

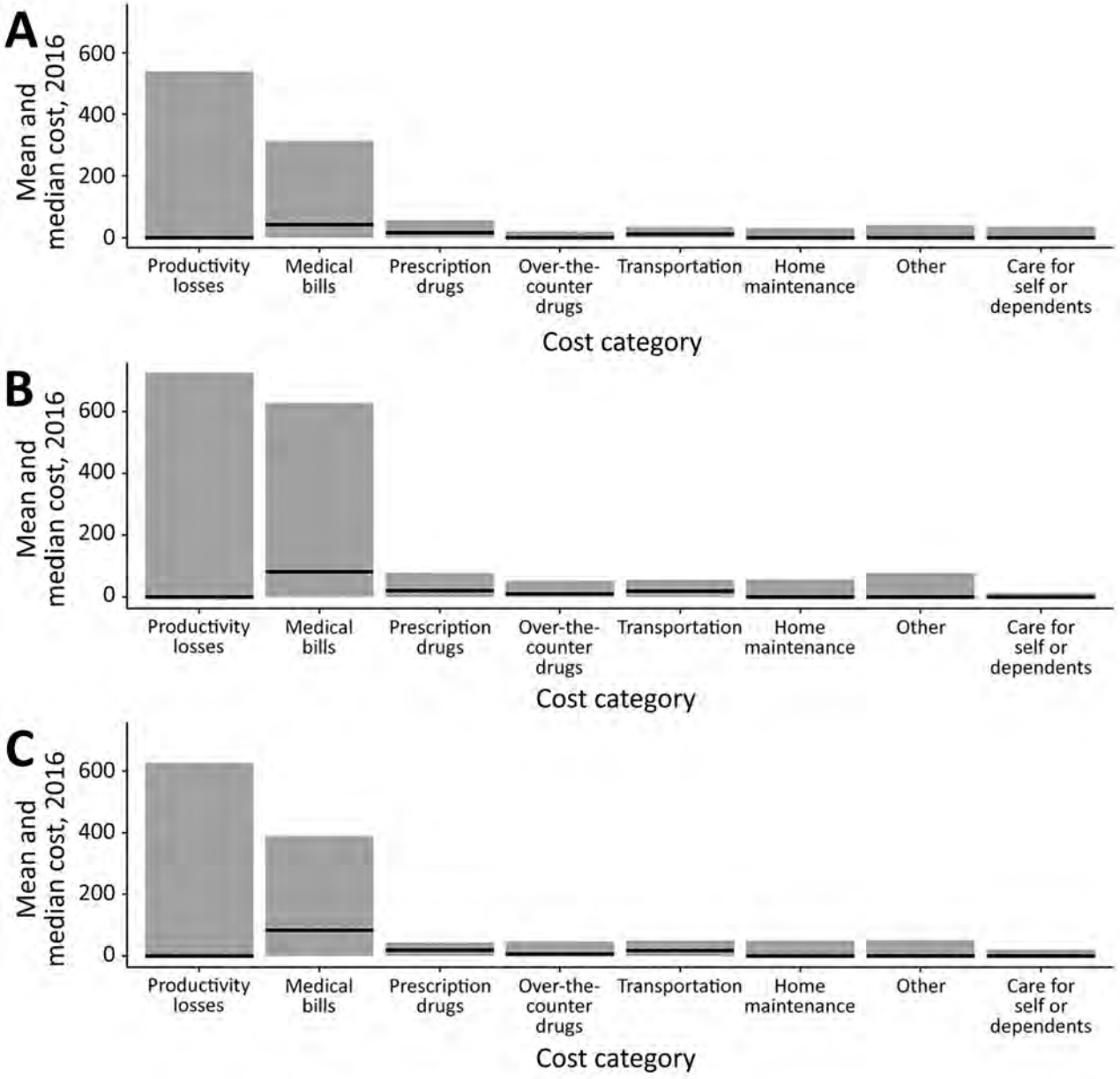

Figure 2. Mean and median cost per participant, by Lyme disease category and cost category of the total patient cost in high-incidence areas of the United States, 2014–2016. A) Confirmed localized disease; B) confirmed disseminated disease; C) probable disease. Black lines indicate median cost.

Table 4. Societal perspective of medical cost of Lyme disease per participant, by disease category, in high-incidence areas, United States, 2014–2016

Disease category	No. participants	Societal perspective, medical cost per participant,* 2016 US dollars					
		Median	Mean	SD	10th percentile	90th percentile	Range
All†	613	478	1,333	5,690	164	1,932	50–121,869
Confirmed localized	273	374	668	1,715	136	1,224	50–13,050
Confirmed disseminated	154	696	2,537	20,220	259	4,366	147–121,869
Probable	186	612	1,804	15,188	237	2,454	124–105,494

*Societal medical cost per participant excludes Current Procedural Terminology (CPT) codes deemed unrelated to Lyme disease as determined by a physician subject matter expert (Appendix Table 5, https://wwwnc.cdc.gov/EID/article/28/6/21-1335-App1.pdf).
†Estimates for the overall population use the sample-weighted data except the range.

nonspecific and do not meet clinical criteria for a confirmed case (*24*). Further, laboratory evidence of infection includes single-tier IgG immunoblot seropositivity, which might indicate past, rather than current, infection. As such, the increased costs for probable cases might result from higher healthcare use for disease unrelated to Lyme disease, which highlights the need for improvements in Lyme disease diagnosis and clinician education.

In a geographically limited study of Lyme disease patients residing on the eastern shore of Maryland during 1998–2001, Zhang et al. (*9*) reported mean total costs of $3,494 and median total costs of $500 (2016 US dollars) per patient attributable to this disease. However, their case definition differed from ours in its inclusion of patients with early, late, and suspected disease, as well as those with tick bite and other related complaints, as identified using diagnosis codes in medical records. Therefore, these figures might not be directly comparable to our mean and median societal costs ($2,032 and $690). Zhang et al. reported mean and median total costs of $2,275 and $689 (2016 US dollars) for participants with clinically defined early disease, which are higher than what we found for confirmed localized disease (mean $1,307 and median $493). However, in regression analyses, Zhang et al. found that disease category and age, but not sex, were significantly associated with societal medical costs, similar to our findings for societal cost. In another US study using nationwide commercial insurance claims data to compare cases with matched controls during 2006–2010, Adrion et al. (*8*) estimated an increase of $3,009 (2016 US dollars) in societal medical costs attributable to Lyme disease over a 12-month period. That cost is higher than our overall mean societal medical cost ($1,333), likely because of study population differences, but is similar to that found for our participants with confirmed disseminated disease ($2,537). In a recent study in the Netherlands, Van den Wijngaard et al. (*17*) used a societal perspective to estimate a total cost of $137 for patients with erythema migrans only and $6,398 (2016 US dollars) for those with disseminated Lyme borreliosis. These costs are lower than those for our societal results for confirmed localized disease ($1,307) and higher than those for our societal results for confirmed disseminated disease ($3,251). These cost differences might result from different healthcare financing systems in the United States versus Europe or from variations in clinical manifestations resulting from infection with different *B. burgdorferi* sensu lato strains (*15*–*17*).

Our study adds to the scarce literature on the economic burden of Lyme disease and provides a comprehensive estimate of its costs to both the patient and society. In addition, our prospective collection of all patient costs, including nonmedical costs and productivity losses, enables more accurate and more comprehensive cost estimates compared with previous studies in the United States. Further, these results provide estimates of the cost savings per case averted, which can be used in cost-benefit analyses of prevention interventions, such as a potential vaccine.

The first limitation of our study is that our estimates might be affected by recall error, either by

Table 5. Societal perspective of total cost of Lyme disease per participant, by disease category, in high-incidence areas, United States, 2014–2016

Disease category	No. participants	Societal perspective, total cost per participant,* 2016 US dollars					
		Median	Mean	SD	10th percentile	90th percentile	Range
All†	613	690	2,032	6,091	203	4,201	54–122,766
Confirmed localized	273	493	1,307	3,559	154	2,678	54–18,322
Confirmed disseminated	154	1,081	3,251	20,908	297	6,238	216–122,766
Probable	186	940	2,620	15,533	316	5,021	130–105,500

*Total cost per participant according to the societal perspective includes societal medical costs, patient nonmedical costs, and cost of productivity losses. Patient medical costs were not added because they are already included in societal medical costs.
†Estimates for the overall population use the sample-weighted data except the range.

Table 6. Impact of disease category, age group, sex, and state on total societal cost of Lyme disease per participant, United States, 2014–2016 (n = 613)*

Variable	% Difference	Total cost difference, 2016 US dollars (95% CI)
Baseline cost†	NA	305 (206–451)
Lyme disease category		
Confirmed, localized	Referent	Referent
Confirmed, disseminated	120	367 (188–545)
Probable	59	181 (71–291)
Age group, y		
<18	Referent	Referent
18–45	96	293 (107–479)
46–65	108	331 (175–486)
>65	27	84 (−28 to 195)
Sex		
F	Referent	Referent
M	11	35 (−26 to 95)
State		
Connecticut	Referent	Referent
Maryland	0	0 (−76 to 76)
Minnesota	75	229 (114–345)
New York	−6	−19 (−119 to 82)

*Results from sample-weighted multivariable linear regression analysis. The model includes independent variables of interest (i.e., disease category, age group, sex, and state), while controlling for insurance status, income, and study year (Appendix, https://wwwnc.cdc.gov/EID/article/28/6/21-1335-App1.pdf). Adjusted R^2 = 0.19.
†Baseline cost represents a patient with confirmed localized Lyme disease, female, <18 years of age, residing in Connecticut, without private insurance, with income <$60,000, in the study year of 2014.

participants or providers, although we attempted to mitigate such error by enrolling patients as close to disease onset as possible, by surveying them monthly to capture ongoing costs, and by requesting codes from providers for a date range instead of for individual visits. However, by requesting codes over a date range, some billing codes unrelated to Lyme disease (e.g., for other comorbidities) might have been included despite our excluding codes definitively unrelated to Lyme disease, potentially leading to overestimates. Information bias might have occurred in our measure of association between disease category and cost because those with milder disease might be more likely to forget some costs than those with more severe disease, with a potential bias away from null. In addition, although the use of quota sampling to recruit reported cases was necessary to enroll patients near disease onset, this nonprobability sampling method limits our ability to meet assumptions for calculating sampling error. Use of surveillance data to weight responses by disease category was intended to ensure representativeness by disease category. Nevertheless, in surveillance data, confirmed localized cases are likely underreported, resulting in confirmed disseminated cases representing an artificially large proportion of cases; therefore, our overall cost might be overestimated (*35*,*36*). Finally, this study did not include costs related to deaths from Lyme disease, because no enrolled participants died. Although very rare, death from Lyme carditis has been reported (*2*,*3*), and associated productivity losses would greatly increase cost estimates.

Our results reflect the costs of diagnosed cases meeting the Lyme disease surveillance case definition in high-incidence states (*24*); as such, these costs likely reflect that of actual infections. However, we were not able to evaluate whether our estimates accurately represent the cost of diagnosed but unreported Lyme disease, cases that reflect some proportion of overdiagnosis (*6*). Further, our results might not reflect costs in states with emerging or low incidence of Lyme disease. Therefore, our results for extrapolation of costs to an estimated ≈476,000 diagnosed cases nationally per year should be interpreted with caution. Last, our results do not include costs for suspected Lyme disease (e.g., consultation and prophylactic treatment for tick bite, negative diagnostic tests), undiagnosed disease, or nonacute disease (e.g., patients experiencing long-term symptoms). These costs would further increase the total economic burden attributable to Lyme disease. Future efforts should include cost-effectiveness analyses of current and future prevention methods, such as a vaccine, in addition to economic evaluations of unreported, suspected, and nonacute disease.

In conclusion, Lyme disease represents a substantial economic burden to individual patients and US society. The aggregate cost of diagnosed Lyme disease could be nearly $1 billion annually, not including suspected, undiagnosed, or nonacute cases. These findings emphasize the importance of early and accurate diagnosis to reduce both illness and its associated personal and societal costs.

Acknowledgments

We thank Nadia Thomas, Shaylee Mehta, David Neitzel, Elizabeth Schiffman, Molly Peterson, Julie Ray, Jamie Sommer, Robert Heimer, Mark Lamias, Craig Mincic, and John Jones for their assistance in conducting this study; Brad Biggerstaff, Zach Weller, and Josh Keller for their statistical advice; and Paul Mead, Jennifer Peel, Jude Bayham, Sheryl Magzamen, and Brooke Anderson for their valuable insights during manuscript preparation.

This work was supported by the Centers for Disease Control and Prevention.

About the Author

Dr. Hook is an epidemiologist in the Bacterial Diseases Branch, Division of Vector-Borne Diseases, National Center for Emerging and Zoonotic Infectious Diseases, Centers for Disease Control and Prevention, Fort Collins, Colorado. Her primary research interests are the epidemiology and prevention of bacterial vector-borne infections.

References

1. Wormser GP, Dattwyler RJ, Shapiro ED, Halperin JJ, Steere AC, Klempner MS, et al. The clinical assessment, treatment, and prevention of Lyme disease, human granulocytic anaplasmosis, and babesiosis: clinical practice guidelines by the Infectious Diseases Society of America. Clin Infect Dis. 2006;43:1089–134. https://doi.org/10.1086/508667
2. Forrester JD, Mead P. Third-degree heart block associated with Lyme carditis: review of published cases. Clin Infect Dis. 2014;59:996–1000. https://doi.org/10.1093/cid/ciu411
3. Forrester JD, Meiman J, Mullins J, Nelson R, Ertel SH, Cartter M, et al.; Centers for Disease Control and Prevention (CDC). Notes from the field: update on Lyme carditis, groups at high risk, and frequency of associated sudden cardiac death—United States. MMWR Morb Mortal Wkly Rep. 2014;63:982–3.
4. Schwartz AM, Hinckley AF, Mead PS, Hook SA, Kugeler KJ. Surveillance for Lyme disease—United States, 2008–2015. MMWR Surveill Summ. 2017;66:1–12. https://doi.org/10.15585/mmwr.ss6622a1
5. Rosenberg R, Lindsey NP, Fischer M, Gregory CJ, Hinckley AF, Mead PS, et al. Vital signs: trends in reported vectorborne disease cases—United States and territories, 2004–2016. MMWR Morb Mortal Wkly Rep. 2018;67:496–501. https://doi.org/10.15585/mmwr.mm6717e1
6. Kugeler KJ, Schwartz AM, Delorey MJ, Mead PS, Hinckley AF. Estimating the frequency of Lyme disease diagnoses, United States, 2010–2018. Emerg Infect Dis. 2021;27:616–9. https://doi.org/10.3201/eid2702.202731
7. Mac S, da Silva SR, Sander B. The economic burden of Lyme disease and the cost-effectiveness of Lyme disease interventions: a scoping review. PLoS One. 2019;14:e0210280. https://doi.org/10.1371/journal.pone.0210280
8. Adrion ER, Aucott J, Lemke KW, Weiner JP. Health care costs, utilization and patterns of care following Lyme disease. PLoS One. 2015;10:e0116767. https://doi.org/10.1371/journal.pone.0116767
9. Zhang X, Meltzer MI, Peña CA, Hopkins AB, Wroth L, Fix AD. Economic impact of Lyme disease. Emerg Infect Dis. 2006;12:653–60. https://doi.org/10.3201/eid1204.050602
10. Strickland GT, Karp AC, Mathews A, Peña CA. Utilization and cost of serologic tests for Lyme disease in Maryland. J Infect Dis. 1997;176:819–21. https://doi.org/10.1086/517311
11. Fix AD, Strickland GT, Grant J. Tick bites and Lyme disease in an endemic setting: problematic use of serologic testing and prophylactic antibiotic therapy. JAMA. 1998;279:206–10. https://doi.org/10.1001/jama.279.3.206
12. Strickland GT, Caisley I, Woubeshet M, Israel E. Antibiotic therapy for Lyme disease in Maryland. Public Health Rep. 1994;109:745–9.
13. Rutz H, Hogan B, Hook S, Hinckley A, Feldman K. Exploring an alternative approach to Lyme disease surveillance in Maryland. Zoonoses Public Health. 2018;65:254–9. https://doi.org/10.1111/zph.12446
14. White J, Noonan-Toly C, Lukacik G, Thomas N, Hinckley A, Hook S, et al. Lyme disease surveillance in New York state: an assessment of case underreporting. Zoonoses Public Health. 2018;65:238–46. https://doi.org/10.1111/zph.12307
15. Lohr B, Müller I, Mai M, Norris DE, Schöffski O, Hunfeld KP. Epidemiology and cost of hospital care for Lyme borreliosis in Germany: lessons from a health care utilization database analysis. Ticks Tick Borne Dis. 2015;6:56–62. https://doi.org/10.1016/j.ttbdis.2014.09.004
16. Joss AW, Davidson MM, Ho-Yen DO, Ludbrook A. Lyme disease—what is the cost for Scotland? Public Health. 2003; 117:264–73. https://doi.org/10.1016/S0033-3506(03)00067-2
17. van den Wijngaard CC, Hofhuis A, Wong A, Harms MG, de Wit GA, Lugnér AK, et al. The cost of Lyme borreliosis. Eur J Public Health. 2017;27:538–47. https://doi.org/10.1093/eurpub/ckw269
18. Mead P, Hinckley A, Hook S, Beard CB. TickNET—a collaborative public health approach to tickborne disease surveillance and research. Emerg Infect Dis. 2015;21:1574–7. https://doi.org/10.3201/eid2109.150301
19. Jo C. Cost-of-illness studies: concepts, scopes, and methods. Clin Mol Hepatol. 2014;20:327–37. https://doi.org/10.3350/cmh.2014.20.4.327
20. Tarricone R. Cost-of-illness analysis. What room in health economics? Health Policy. 2006;77:51–63. https://doi.org/10.1016/j.healthpol.2005.07.016
21. Rice DP. Cost of illness studies: what is good about them? Inj Prev. 2000;6:177–9. https://doi.org/10.1136/ip.6.3.177
22. Rice DP. Estimating the cost of illness. Am J Public Health Nations Health. 1967;57:424–40. https://doi.org/10.2105/AJPH.57.3.424
23. Meltzer MI. Introduction to health economics for physicians. Lancet. 2001;358:993–8. https://doi.org/10.1016/S0140-6736(01)06107-4
24. Centers for Disease Control and Prevention. Lyme disease (Borrelia burgdorferi) 2008 case definition. 2008 [cited 2019 Oct 18]. https://wwwn.cdc.gov/nndss/conditions/lyme-disease/case-definition/2008
25. Centers for Medicare and Medicaid. PFS national payment amount file. 2019 [cited 2019 Nov 6]. https://www.cms.gov/Medicare/Medicare-Fee-for-Service-Payment/PhysicianFeeSched/PFS-National-Payment-Amount-File.html
26. US Bureau of Labor Statistics. Historical consumer price index for all urban consumers (CPI-U) [cited 2019 Jun 27]. https://www.bls.gov/cpi/tables/supplemental-files/historical-cpi-u-201812.pdf
27. Posey KG. Household Income: 2015. 2016 [cited 2022 Feb 1]. https://www.census.gov/content/dam/Census/library/publications/2016/acs/acsbr15-02.pdf
28. Mihaylova B, Briggs A, O'Hagan A, Thompson SG. Review of statistical methods for analysing healthcare resources and

costs. Health Econ. 2011;20:897–916. https://doi.org/10.1002/hec.1653
29. Wickham H. tidyverse: easily install and load the 'Tidyverse.' R package version 1.2.1 ed; 2017 [cited 2022 May 3]. https://cran.r-project.org/web/packages/tidyverse/index.html
30. Freedman GE. srvyr: 'dplyr'-like syntax for summary statistics of survey data. R package version 0.3.4 ed; 2019 [cited 2022 May 3]. https://cran.r-project.org/web/packages/srvyr/index.html
31. Lumley T. Survey: analysis of complex survey samples R package version 3.35–1 ed; 2019 [cited 2022 May 3]. https://cran.r-project.org/web/packages/survey/index.html
32. Long J. jtools: Analysis and presentation of social scientific data. R package version 2.0.1 ed; 2019 [cited 2022 May 3]. https://cran.r-project.org/web/packages/jtools/index.html
33. Wei T, Simko V. R package "corrplot": visualization of a correlation matrix (version 0.84). Version 0.84 ed; 2017 [cited 2022 May 3]. https://www.rdocumentation.org/packages/corrplot/versions/0.84
34. Fox J, Weisberg S. An {R} companion to applied regression, 2nd edition. Thousand Oaks (CA): Sage Publishing; 2011.
35. Naleway AL, Belongia EA, Kazmierczak JJ, Greenlee RT, Davis JP. Lyme disease incidence in Wisconsin: a comparison of state-reported rates and rates from a population-based cohort. Am J Epidemiol. 2002;155:1120–7. https://doi.org/10.1093/aje/155.12.1120
36. Cartter ML, Lynfield R, Feldman KA, Hook SA, Hinckley AF. Lyme disease surveillance in the United States: looking for ways to cut the Gordian knot. Zoonoses Public Health. 2018;65:227–9. https://doi.org/10.1111/zph.12448

Address for correspondence: Sarah Hook, Centers for Disease Control and Prevention, 3156 Rampart Rd, Mailstop P02, Fort Collins, CO, 80521, USA; email: vhx8@cdc.gov

etymologia revisited

Salmonella

[sal''mo-nel'ə]

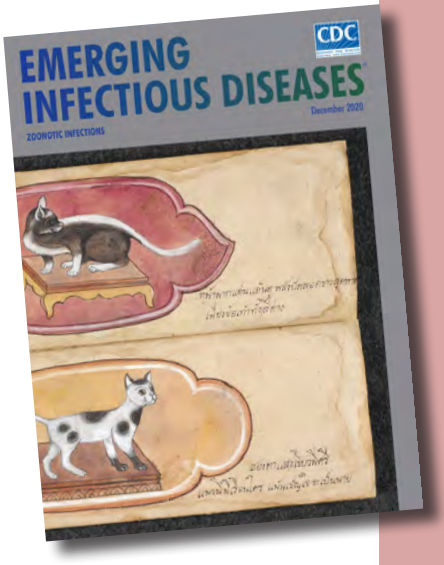

Originally published in December 2020

Named in honor of Daniel Elmer Salmon, an American veterinary pathologist, *Salmonella* is a genus of motile, gram-negative bacillus, nonspore-forming, aerobic to facultatively anaerobic bacteria of the family Enterobacteriaceae. In 1880, Karl Joseph Eberth was the first to observe *Salmonella* from specimens of patients with typhoid fever (from the Greek *typhōdes* [like smoke; delirious]), which was formerly called *Eberthella typhosa* in his tribute. In 1884, Georg Gaffky successfully isolated this bacillus (later described as *Salmonella* Typhi) from patients with typhoid fever, confirming Eberth's findings. Shortly afterward, Salmon and his assistant Theobald Smith, an American bacteriologist, isolated *Salmonella* Choleraesuis from swine, incorrectly assuming that this germ was the causative agent of hog cholera. Later, Joseph Lignières, a French bacteriologist, proposed the genus name *Salmonella* in recognition of Salmon's efforts.

Sources:

1. Dorland's Illustrated Medical Dictionary. 32nd ed. Philadelphia: Elsevier Saunders; 2012.
2. Gossner CM, Le Hello S, de Jong B, Rolfhamre P, Faensen D, Weill FX, et al. Around the world in 1,475 Salmonella geo-serotypes [Another Dimension]. Emerg Infect Dis. 2016;22:1298–302.
3. Issenhuth-Jeanjean S, Roggentin P, Mikoleit M, Guibourdenche M, de Pinna E, Nair S, et al. Supplement 2008-2010 (no. 48) to the White-Kauffmann-Le Minor scheme. Res Microbiol. 2014;165:526–30.
4. Salmon DE. The discovery of the germ of swine-plague. Science. 1884;3:155–8.
5. Su LH, Chiu CH. Salmonella: clinical importance and evolution of nomenclature. Chang Gung Med J. 2007;30:210–9.

https://wwwnc.cdc.gov/eid/article/26/12/et-2612_article

Effect of Recombinant Vesicular Stomatitis Virus–Zaire Ebola Virus Vaccination on Ebola Virus Disease Illness and Death, Democratic Republic of the Congo

Neil Rupani, Mbong Eta Ngole, J. Austin Lee, Adam R. Aluisio, Monique Gainey, Shiromi M. Perera, Lina Kashibura Ntamwinja, Ruffin Mbusa Matafali, Rigo Fraterne Muhayangabo, Fiston Nganga Makoyi, Razia Laghari, Adam C. Levine, Alexis S. Kearney

We conducted a retrospective cohort study to assess the effect vaccination with the live-attenuated recombinant vesicular stomatitis virus–Zaire Ebola virus vaccine had on deaths among patients who had laboratory-confirmed Ebola virus disease (EVD). We included EVD-positive patients coming to an Ebola Treatment Center in eastern Democratic Republic of the Congo during 2018–2020. Overall, 25% of patients vaccinated before symptom onset died compared with 63% of unvaccinated patients. Vaccinated patients reported fewer EVD-associated symptoms, had reduced time to clearance of viral load, and had reduced length of stay at the Ebola Treatment Center. After controlling for confounders, vaccination was strongly associated with decreased deaths. Reduction in deaths was not affected by timing of vaccination before or after EVD exposure. These findings support use of preexposure and postexposure recombinant vesicular stomatitis virus–Zaire Ebola virus vaccine as an intervention associated with improved death rates, illness, and recovery time among patients with EVD.

Ebola virus disease (EVD) has ranked among the deadliest of all infectious diseases since its documented emergence during 1976 in Zaire (now the Democratic Republic of the Congo; DRC) (*1*). Since 1976, there have been 41 EVD outbreaks, most of which have occurred in sub-Saharan Africa. Case-fatality rates have ranged from 25% to 90% in these outbreaks (*2*). EVD is caused by 1 of 5 species of *Ebolavirus* that are known to infect humans. Symptom onset occurs ≈10 days after exposure and commonly includes malaise, myalgias, fever, nausea, vomiting, diarrhea, rash, and bleeding (*1*). EVD is transmitted through body fluids, which enables the disease to spread through direct, close contact (*3*). Historically, supportive care, such as fluid and electrolyte repletion, has been the most effective treatment for EVD (*1*). However, EVD thrives in areas where poverty and inadequate healthcare infrastructure intersect, limiting the ability to rapidly diagnose cases or provide adequate supportive care (*4*).

The deadliest EVD outbreak was the 2014–2016 West Africa outbreak, which had 28,610 cases and 11,308 deaths (*2*). The sheer size and subsequent socioeconomic effect of this outbreak sparked an unprecedented effort to develop and study new treatment and prevention strategies for EVD, including randomized clinical trials of Ebola virus vaccinations (*5*). The recombinant vesicular stomatitis virus–Zaire Ebola virus (rVSV-ZEBOV) vaccine, known commercially as Ervebo, is a live-attenuated recombinant vesicular stomatitis virus vaccine. It is administered as a single-dose intramuscular injection (*6*). It is effective against the species *Zaire ebolavirus* (ZEBOV), but does not protect against other species of *Ebolavirus* (*7*). The

Author affiliations: Brown University, Providence, Rhode Island, USA (N. Rupani, J.A. Lee, A.R. Aluisio, A.C. Levine, A.S. Kearney); International Medical Corps, Goma, Democratic Republic of the Congo (M.E. Ngole, L.K. Ntamwinja, R.M. Matafali, R.F. Muhayangabo, F.N. Makoyi, R. Laghari); Rhode Island Hospital, Providence (M. Gainey); International Medical Corps, Washington, DC, USA (S.M. Perera)

DOI: https://doi.org/10.3201/eid2806.212223

rVSV-ZEBOV vaccine was initially administered in Guinea under emergency use authorization by the US Food and Drug Administration (FDA) and in DRC under compassionate use by the World Health Organization (WHO) (*8*,*9*).

Multiple clinical trials have demonstrated that the rVSV-ZEBOV vaccine is well tolerated without serious adverse events. However, many vaccine recipients report self-limiting systemic symptoms, including fever, headache, myalgias, and fatigue, within the first 24 hours after vaccination. Symptoms caused by reactogenicity mimic the first symptoms of EVD; this reaction is essential to consider, particularly in outbreak settings, because recipients are often vaccinated after a potential EVD exposure. Vaccine recipients have also reported delayed side effects, including polyarthralgia, polyarticular arthritis, and skin eruptions in the first 2–3 weeks after vaccination (*10*–*12*). Clinical trials have demonstrated that the vaccine is highly immunogenic, elicits immune responses that are largely maintained over a 12-month period, and is highly effective at preventing EVD (*10*,*13*–*15*).

On August 1, 2018, the DRC Ministry of Health declared its 10th EVD outbreak, which became the second deadliest in history, resulting in 3,481 cases and 2,299 deaths (*2*,*9*). The *Zaire ebolavirus* species was identified as the cause of the outbreak (*16*). A ring vaccination strategy was implemented to administer rVSV-ZEBOV vaccine during this outbreak, targeting contacts of cases, contacts of contacts, and healthcare workers (*9*). Many persons were vaccinated postexposure. Other persons might have received preexposure vaccination, particularly if they were identified as contacts of contacts. In late 2019, rVSV-ZEBOV vaccine was prequalified by WHO and approved for use in persons ≥18 years of age by the FDA (*17*,*18*). To date, >350,000 persons have received rVSV-ZEBOV vaccine in Guinea and the DRC (*2*). Although studies have demonstrated the vaccine is safe and effective, WHO states that further research is needed to support its full licensure (*19*).

A major remaining question is whether rVSV-ZEBOV vaccine can reduce illness and death for patients who have confirmed EVD, in addition to preventing infection. Other vaccines, such as those directed against pertussis, varicella, and rotavirus, have evidence supporting reduced illness, death, and disease severity in patients experiencing breakthrough infections (*20*,*21*). More recently, vaccination against SARS-CoV-2 with authorized mRNA vaccines has demonstrated reduced viral load, lower risk for febrile symptoms, and shorter duration of symptoms among persons experiencing breakthrough infections (*22*). Furthermore, some vaccines have been shown to provide protection when administered after exposure. Examples include measles, rabies, hepatitis A and B, and varicella vaccines (*20*). The purpose of our study was to determine the effect that vaccination with rVSV-ZEBOV has on clinical characteristics and outcomes among patients with laboratory-confirmed EVD.

Methods

Study Design, Setting, and Population

We conducted a retrospective cohort study of patients who came for care at the International Medical Corps Mangina Ebola Treatment Center (ETC) during the 2018 EVD outbreak in the DRC. The eastern provinces of the DRC (North Kivu and Ituri) served as the main catchment area for the Mangina ETC, located in North Kivu. All persons who came to the Mangina ETC during December 7, 2018–January 29, 2020, who had laboratory-confirmed diagnosis of EVD were eligible for inclusion in this study. Persons were excluded if they did not have a documented EVD outcome (death or survival), if the patient's vaccination status was unknown, or if they did not have a reported date of symptom onset (Figure 1). The Institutional Review Board at Rhode Island Hospital (Lifespan Health System, Providence, RI, USA) provided ethics exemption for this study and waived the requirement to obtain informed consent.

Laboratory Diagnosis

All patients had laboratory testing conducted by the Institut National de Recherche Biomédicale (Kinshasa-Bombe, DRC). The Cepheid GeneXpert Ebola Assay (https://www.cepheid.com) was used for detection of ZEBOV RNAs encoding surface glycoprotein and nucleoprotein. The assay was also used to determine the cycle threshold (Ct), a proxy for viral load (*23*,*24*). The Ct value is inversely proportional to viral load; a Ct value >40 was considered negative for cases. A reverse transcription PCR was used to confirm EVD cases.

Study Procedures

Response teams were deployed to health zones in North Kivu, South Kivu, and Ituri Provinces in the eastern part of DRC to identify suspected, confirmed, or probable cases of EVD. Suspected and confirmed case-patients were isolated and transported to ETCs for further testing and treatment. Patients could also self-present to the ETC. All patients were screened by trained clinical staff to ensure they met the clinical

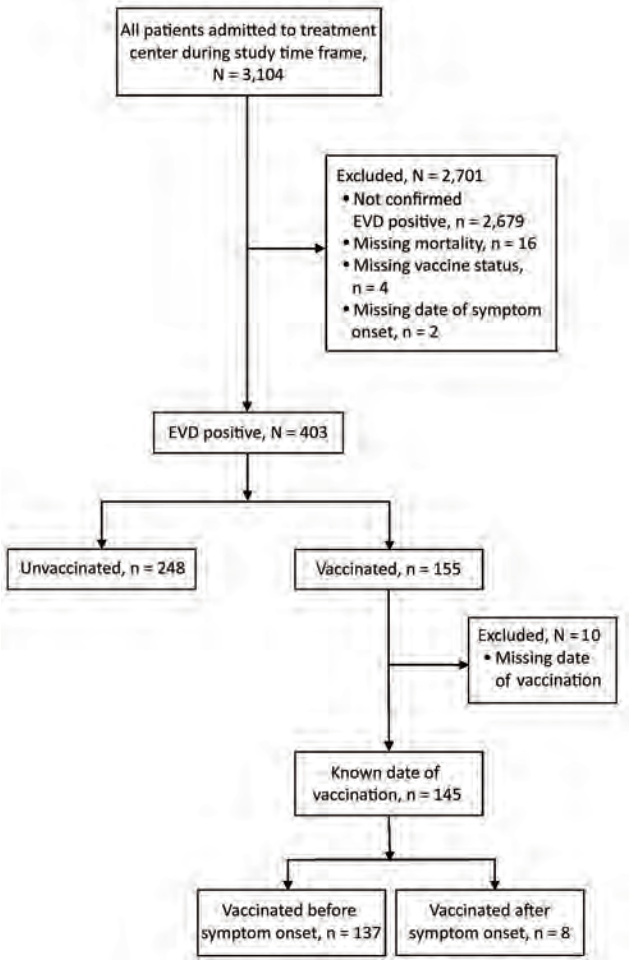

Figure 1. Inclusion/exclusion algorithm and makeup of study sample for study of impact of recombinant vesicular stomatitis virus–Zaire Ebola virus vaccination on EVD illness and death, Democratic Republic of the Congo. EVD, Ebola virus disease.

case definition for suspected or confirmed EVD based on WHO and Médecins Sans Frontières guidelines, in consultation with local health authorities (*25*,*26*). Patients who had a previously confirmed laboratory diagnosis of EVD were directly admitted to the confirmed ward. Patients who met the case definition for suspected EVD were admitted to the ETC suspect ward, in which blood samples were drawn for initial EVD testing. If the initial test result of the patient was negative, they remained in the ETC until 72 hours had passed since symptom onset, at which point a second test was performed. Patients with a positive test result at that point were considered EVD positive and moved to the confirmed ward for further management (*27*,*28*). All patients who died during admission to the suspect ward or were dead on arrival to the ETC had an oral swab specimen taken for PCR testing before being moved to the morgue.

During triage at the ETC, detailed information was collected about each patient on standardized clinical forms, which included demographics, symptoms, potential contact with a suspected or confirmed EVD individual, comorbidities, and self-reported Ebola vaccination status. During ETC admission, protocol based care was provided. Patients were discharged from the ETC after 2 consecutive negative laboratory test results. The Mangina ETC also served as a PALM Trial site (Pamoja Tulinde Maisha [Together Save Lives in Kiswahili]), in which patients were randomized to receive experimental therapeutics (*29*). Additional detailed information about the clinical care provided at the ETC is provided (https://wwwnc.cdc.gov/EID/article/28/6/21-2223-App1.pdf).

Data Management

Data were retrospectively abstracted from clinical documentation by independent trained study personnel blinded to the specific study aims and entered into a standardized digital database. Additional information on data management is provided (Appendix).

Statistical Methods and Variables

We performed data analyses by using R Studio version 4.0.2 (*30*). We used a Pearson χ^2 test and a Fisher exact test to measure association between categorical variables and the Wilcoxon rank-sum test for continuous variables. Significance was established at p value <0.05. We used a case-centered, multivariable logistic regression and the Cox Proportional-Hazards model to examine the association between previous vaccination with rVSV-ZEBOV (exposure of interest) and the primary outcome of facility-based death (*31*). Models controlled for potential confounders including age, sex, time between symptom onset and admission to the ETC, treatment with experimental therapeutic agents, and Ct value (inversely proportional to viral load). We incorporated age^2 into models to control for the quadratic relationship between age and survival for EVD patients (*32*).

One variable included in our models accounted for the experimental therapeutics patients received. Previous research has demonstrated that, of the 4 potential therapeutics administered at the ETC, 2 of these treatments (monoclonal antibody [mAb] 114, a single mAb; and REGN-EB3, a triple mAb) are more effective against EVD than the other 2 treatments (Zmapp, a triple mAb; and Remdesivir, an antiviral agent) (*29*). As a result, this variable was categorized on the basis of whether the patient

received mAb114 or REGN-EB3, Zmapp or Remdesivir, or no therapeutics.

Additional posthoc analysis explored the effect vaccination timing had on deaths. We used the Cox Proportional-Hazards model to analyze this relationship. In previous vaccine efficacy studies, EVD cases with a symptom onset ≥10 days from randomization were included in the analyses. This categorical cutoff was chosen to account for the incubation period for EVD (*33*,*34*), time between symptom onset and laboratory confirmation, and the unknown period of time between vaccination and vaccine-induced protective immunity (*15*). The typical incubation period for EVD is 10 days after exposure to the disease, although data suggest that it might be shorter for children (*33*,*34*). Therefore, in our subanalysis, we used vaccination ≥10 days before symptom onset as the categorical cutoff. We also used vaccination at 7 and 14 days before symptom onset as cutoffs in a sensitivity analysis. In addition, although we excluded persons who were vaccinated after symptom onset from our initial analysis, we conducted a separate sensitivity analysis examining the effect vaccination had on deaths within this smaller group.

Results

Characteristics of Study Participants

Of the 3,104 persons admitted to the Mangina ETC during December 7, 2018–January 29, 2020, a total of 403 patients had laboratory-confirmed EVD. Of those, 385 patients had sufficient data for analysis; 137 (35.6%) had been vaccinated before onset of symptoms. An additional 8 patients were vaccinated after symptom onset; these patients were excluded from the initial analysis (Figure 1).

We outlined the similarities and differences between the unvaccinated and vaccinated groups (Table 1). Among EVD-confirmed case-patients, a larger proportion of unvaccinated persons were female (63.3%) than male (36.7%) (p = 0.018). Vaccinated patients came to the ETC earlier in their disease course than unvaccinated patients (2 vs. 5 days after symptom onset; p<0.001), were older (median age 28.0 years vs. 25.5 years; p = 0.044), and were more likely to have reported contact with a suspected or confirmed EVD-positive person (65.7% vs. 52.4%; p<0.001).

Although the rVSV-ZEBOV vaccine is FDA approved for use in persons ≥18 years of age, some

Table 1. Patient characteristics for study of the effect of recombinant vesicular stomatitis virus–Zaire Ebola virus vaccination on Ebola virus disease illness and death, Democratic Republic of the Congo*

Characteristic	Overall, n = 385	Not vaccinated, n = 248	Vaccinated, n = 137	p value†
Age, y	26.0 (18.0–40.0)	25.5 (12.0–40.0)	28.0 (20.0–40.0)	**0.044**
<5	49 (12.7)	43 (17.3)	6 (4.4)	**0.001**
5–15	34 (8.8)	26 (10.5)	8 (5.8)	
16–25	101 (26.2)	55 (22.2)	46 (33.6)	
26–35	88 (22.9)	54 (21.8)	34 (24.8)	
36–45	38 (9.9)	19 (7.6)	19 (13.9)	
46–55	41 (10.7)	27 (10.9)	14 (10.2)	
>55	34 (8.8)	24 (9.7)	10 (7.3)	
Sex				**0.018**
M	159 (41.3)	91 (36.7)	68 (49.6)	
F	226 (58.7)	157 (63.3)	69 (50.4)	
Province				**0.002**
North Kivu	235 (61.0)	142 (57.3)	93 (67.9)	
Ituri	142 (36.9)	104 (41.9)	38 (27.7)	
Unknown	8 (2.1)	2 (0.8)	6 (4.4)	
Known or suspected Ebola contact				**<0.001**
No	73 (19.0)	62 (25.0)	11 (8.0)	
Yes	220 (57.1)	130 (52.4)	90 (65.7)	
Unknown	92 (23.9)	56 (22.6)	36 (26.3)	
Days between symptom onset and admission, d	4.0 (2.0–6.0)	5.0 (3.0–7.0)	2.0 (1.0–4.0)	**<0.001**
First cycle threshold value	21.6 (18.2–26.2)	20.4 (17.7–24.2)	24.6 (19.9–28.1)	**<0.001**
Therapeutic received				**0.005**
None	65 (16.9)	53 (21.4)	12 (8.8)	
Zmapp or Remdesivir	76 (19.7)	46 (18.5)	30 (21.9)	
mAb114 or REGN-EB3	244 (63.4)	149 (60.1)	95 (69.3)	
Final outcome				**<0.001**
Died	191 (49.6)	157 (63.3)	34 (24.8)	
Survived	194 (50.4)	91 (36.7)	103 (75.2)	
Length of stay among survivors, d	21.0 (18.0–26.0), n = 193	22.0 (19.0–28.5), n = 91	20.0 (17.0–23.8), n = 102	**0.004**

*Values are median (IQR) or no. (%) . IQR, interquartile range; MAb, monoclonal antibody.
†Statistical tests were performed by using the Wilcoxon rank sum test, the Pearson χ^2 test, and the Fisher exact test. Boldface indicates a significant difference (p<0.05).

children received the vaccine through investigative protocols. A larger proportion of vaccinated patients were from North Kivu Province (67.9%) than from Ituri Province (27.7%) (p = 0.002). A total of 16 (10.2%) unvaccinated women were pregnant, and 10 (14.5%) vaccinated women were pregnant. Vaccinated persons were more likely to receive mAb114 or REGN-EB3 than were unvaccinated persons (69.3% vs. 60.1%). We provide additional information about specific anti-EBOV treatments stratified by vaccination timing. (Appendix Table 1).

EVD-Associated Clinical Findings

A greater proportion of unvaccinated patients experienced EVD-associated symptoms than did vaccinated patients. These symptoms included nausea, diarrhea, asthenia, anorexia, abdominal pain, chest pain, myalgia, dyspnea, dysphagia, sore throat, conjunctivitis, and bleeding (Table 2).

Diagnostic Testing and Time to First Negative Test Result

Vaccinated patients had a lower viral load, as indicated by a higher Ct value, than did unvaccinated patients (24.6 vs. 20.4; p<0.001) (Table 1). Among those who survived (n = 144), vaccinated patients cleared the virus more rapidly than did unvaccinated patients; this relationship was statistically significant and persisted when the data were analyzed using the date of symptom onset, first positive test result date, or date of admission to the ETC as the starting point (Figure 2; Appendix Figures 1, 2). Unvaccinated survivors of EVD also spent more time at the ETC than did vaccinated survivors (22.0 days vs. 20.0 days; p = 0.004).

Deaths

Overall, 24.8% of vaccinated patients died, compared with 63.3% of unvaccinated patients (p<0.001). Previous vaccination with rVSV-ZEBOV was associated with decreased likelihood of death compared with those unvaccinated (odds ratio 0.19, 95% CI 0.12–0.30; p<0.001). This relationship persisted after controlling for potential confounders (adjusted odds ratio 0.26, 95% CI 0.15–0.46; p<0.001).

We used the Cox Proportional-Hazards model to determine the relationship between vaccination and death among all patients who had EVD symptom onset. After controlling for potential confounders, we found that vaccination remained a major predictor of reduced deaths for these patients (adjusted hazard ratio [aHR] 0.38, 95% CI 0.25–0.56) (Figure 3).

We also explored the relationship between timing of vaccination and death by using the Cox Proportional-Hazards Model for different subsets of all patients who were vaccinated. Models controlled for potential confounders. Vaccination with rVSV-ZEBOV reduced the risk for death in those vaccinated ≥10 days before symptom onset (aHR 0.41, 95% CI 0.23–0.73; p = 0.002) and in those vaccinated <10 days before symptom onset (aHR 0.34, 95% CI 0.21–0.55; p<0.001)

Table 2. Frequency of symptoms reported by vaccinated and unvaccinated Ebola virus disease–confirmed patients, Democratic Republic of the Congo

Symptom	Not vaccinated, n = 248, No. (%)	Vaccinated, n = 137, no. (%)	p value*
Asthenia†	214 (86.6)	102 (74.5)	0.004
Anorexia	204 (82.3)	80 (58.4)	**<0.001**
Fever	193 (77.8)	99 (72.3)	0.273
Headache†	156 (63.2)	90 (65.7)	0.700
Abdominal pain	152 (61.3)	56 (40.9)	**<0.001**
Nausea	140 (56.5)	50 (36.5)	**<0.001**
Conjunctivitis†	138 (55.9)	49 (35.8)	**<0.001**
Diarrhea†	137 (55.5)	45 (32.8)	**<0.001**
Arthralgia	134 (54.0)	74 (54.0)	1.000
Myalgia	128 (51.6)	54 (39.4)	**0.029**
Chest pain†	89 (36.0)	32 (23.4)	**0.014**
Cough†	75 (30.4)	36 (26.3)	0.466
Bleeding‡	67 (27.1)	14 (10.3)	**<0.001**
Dysphagia	61 (24.6)	17 (12.4)	**0.007**
Sore throat†	52 (21.1)	17 (12.4)	**0.048**
Dyspnea†	47 (19.0)	13 (9.5)	**0.020**
Coma‡	16 (6.5)	2 (1.5)	0.050
Confusion‡	14 (5.7)	2 (1.5)	0.090
Rash‡	14 (5.7)	5 (3.7)	0.540
Hiccup‡	14 (5.7)	3 (2.2)	0.188
Jaundice†	12 (4.9)	2 (1.5)	0.156
Photophobia†	5 (2.0)	1 (0.7)	0.588

*Boldface indicates a significant difference (p<0.05).
†One patient had missing data for this symptom.
‡Two patients had missing data for this symptom.

when compared with those unvaccinated. We developed a Kaplan-Meier curve for these data (Appendix Figure 3). These relationships persisted when using vaccination at ≥7 days and ≥14 days before symptom onset as cutoffs. Moreover, among those vaccinated ≥10 days before symptom onset, the specific number of days between vaccination and symptom onset was not a significant predictor of risk for death. This result was also true for those vaccinated <10 days before symptom onset.

We also explored the relationship between timing of vaccination and death by using the Cox Proportional-Hazards Model for different subsets of all patients who were vaccinated. Models controlled for potential confounders. Vaccination with rVSV-ZEBOV reduced the risk for death in those vaccinated ≥10 days before symptom onset (aHR 0.41, 95% CI 0.23–0.73; p = 0.002) and in those vaccinated <10 days before symptom onset (aHR 0.34, 95% CI 0.21–0.55; p<0.001) when compared with those unvaccinated. We developed a Kaplan-Meier curve for these data (Appendix Figure 3). These relationships persisted when using vaccination at ≥7 days and ≥14 days before symptom onset as cutoffs. Moreover, among those vaccinated ≥10 days before symptom onset, the specific number of days between vaccination and symptom onset was not a significant predictor of risk for death. This result was also true for those vaccinated <10 days before symptom onset.

An additional 8 persons were vaccinated after symptom onset. Although these patients were not included in the larger analysis, we used the Cox Proportional-Hazards model to assess the effect of vaccine administration after symptom onset on death. The association between death and vaccination after symptom onset was not statistically significant (HR 0.22, 95% CI 0.03–1.61; p = 0.138).

Discussion

In this study, we found that both preexposure and postexposure vaccination with rVSV-ZEBOV was associated with a reduction in EVD symptoms and deaths in laboratory-confirmed, EVD-positive patients. Vaccinated patients had a lower viral load upon admission and had fewer EVD-associated symptoms overall than their unvaccinated counterparts. Vaccinated persons were slightly older and more likely to have reported contact with a suspected or confirmed EVD-positive person. Unvaccinated persons were more likely to be female. Vaccinated persons also came to the ETC earlier in their disease course than unvaccinated patients, which might suggest that this population is more able or willing to engage with the

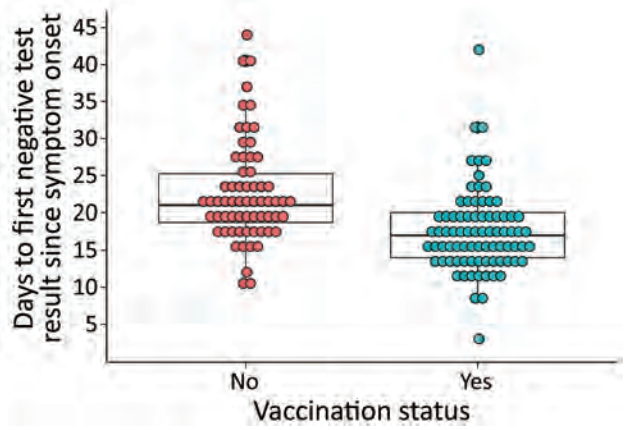

Figure 2. Days to first negative test result since symptom onset among patients who survived, stratified by vaccination status, n = 144, for impact of recombinant vesicular stomatitis virus–Zaire Ebola virus vaccination on Ebola virus disease illness and death, Democratic Republic of the Congo. Horizontal lines within boxes indicate medians; error bars indicate interquartile ranges, p<0.0001, by Wilcoxon rank sum test.

healthcare system or to follow recommended health guidelines. Accepting the vaccine suggests more knowledge about the disease itself and is a positive health-seeking behavior; both of these factors might prompt such a person to seek care earlier. Increased knowledge of a disease has also been associated with increased vaccine uptake for other illnesses, including SARS-CoV-2 (*35*,*36*).

The willingness of vaccinated patients to seek care earlier in the disease course enabled treatment to be initiated earlier, which might have prevented their illness from becoming as severe as it otherwise

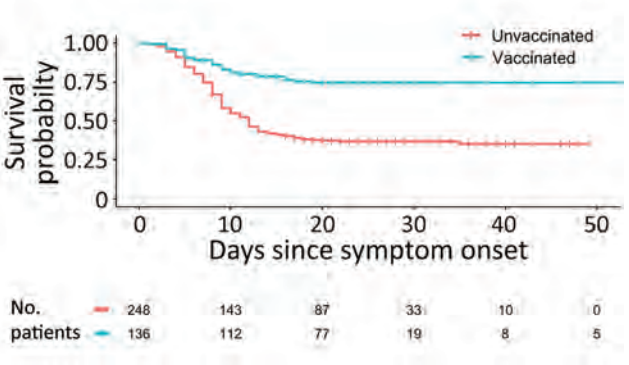

Figure 3. Kaplan-Meier survival plot of patients with Ebola virus disease, stratified by vaccination status, for study of effect of recombinant vesicular stomatitis virus–Zaire Ebola virus vaccination on Ebola virus disease illness and death, Democratic Republic of the Congo. Numbers below chart indicate number of ill patients at that time point, excluding patients who had died or who recovered and were discharged. One patient in the vaccinated group was excluded from this analysis because that patient did not have a reported date of discharge.

might have been. Persons enrolled in the PALM Trial demonstrated similar behavior trends (*29*). Vaccinated persons were more likely to enroll in the trial sooner after the onset of symptoms, which, the authors concluded, might suggest a possible positive relationship between vaccination status and health-seeking behaviors. Data from the PALM Trial also highlight the need for initiation of treatment with mAb114 or REGN-EB3 early in the disease course. The authors observed an 11% increase in the odds of death for each additional day that symptoms persisted before enrollment in the study (*29*). In our study population, vaccinated persons were more likely to receive mAb114 or REGN-EB3 than unvaccinated persons. This finding might also positively impact illness and death. However, after controlling for treatment with experimental therapeutic agents in our model, we found that vaccination remained a major predictor of survival.

Our findings are consistent with results from a previous retrospective cohort study that also examined the impact vaccination had on EVD deaths in eastern DRC (*37*). Those authors concluded that EVD-positive persons who received rVSV-ZEBOV vaccine before admission had reduced viral load and reduced deaths compared with those who did not receive the vaccine. The authors also controlled for known EVD contact in their models. When we included this additional variable in our models, all relationships between the vaccine and deaths were preserved.

Vaccinated persons cleared the virus faster and had a shorter length of stay at the ETC than their unvaccinated counterparts, suggesting that they recovered faster from the disease. Because some patients were directed to the convalescent ward after 2 consecutive negative EVD test results, instead of being discharged to home, length of stay might be increased for the unvaccinated and vaccinated groups. However, we have no reason to believe that either group was preferentially sent to the convalescent ward.

After controlling for potential confounders, we found that vaccination with rVSV-ZEBOV before symptom onset was associated with decreased deaths. This relationship persisted regardless of timing of vaccine administration before onset of symptoms. These results suggest that the vaccine might still be effective days after exposure to EVD and that the extent of its effectiveness against death is not singularly dependent on timing of vaccination before symptom onset. The exact amount of time to complete vaccine-induced immune protection against EVD remains unclear (*38*); however, animal studies conducted in cynomolgus macaques demonstrated complete protection against EVD when the vaccine was administered 7 days before challenge and partial protection when administered 3 days before challenge (*39*). Thus, more aggressive vaccination campaigns in outbreak situations could be beneficial, especially given the observed reduced time to viral load clearance and shortened length of stay for hospitalized patients, in addition to the partial protection afforded by the vaccine in nonhuman primates.

Finally, only a small number of persons were vaccinated after symptom onset (n = 8). One died, and 7 survived. We were unable to conclude whether administration of the vaccine after symptom onset was also protective against EVD-associated illness and death. However, this finding is a potential avenue for future studies. Previous studies have explored the idea of using rVSV-ZEBOV as postexposure prophylaxis. In 1 study, rhesus macaques were infected with ZEBOV and subsequently vaccinated with rVSV-ZEBOV 24 hours postexposure. Results demonstrated that 33%–67% of the vaccinated animals survived infection (*40*). The vaccine has also been used as an experimental postexposure prophylaxis in humans after high-risk occupational exposures. In 1 instance, a person who sustained an accidental needle stick during an animal study at a Biosafety Level 4 facility received the vaccine 48 hours after the injury. No evidence of infection was detected during her hospitalization, and she was discharged from the hospital on day 21 (*41*). The vaccine has also been administered to clinical and nonclinical ETC staff after high-risk exposures; all staff had self-limited symptoms, including fever, after receiving the vaccine, and none showed development of EVD (*42*–*44*).

Further research into the potential role rVSV-ZEBOV might play in EVD treatment protocols is needed. More specifically, additional research is needed to evaluate the potential harmful interaction that could occur with coadministration of rVSV-ZEBOV vaccine, which is designed to elicit a neutralizing immune response to the main EBOV glycoprotein, and therapeutic mAbs, including REGN-EB3, which target the same glycoprotein (*45*). If administration of rVSV-ZEBOV vaccine alone or in combination with other therapeutics is shown to be effective on a larger scale as a treatment modality, this administration might have major implications with respect to the public health response and treatment for EVD outbreaks.

Much of the data used in this study were self-reported by patients, including their symptoms, recent contact with a suspected or confirmed EVD-positive person, and vaccination status. This self-reporting could lead to desirability bias with respect to

vaccination status, as well as recall bias, particularly with respect to date of onset of symptoms and date of vaccination. In addition, there was missing data for a few variables, such as vaccination status, vaccination date, date of symptom onset, and final outcome. Removing patients who had missing data for these variables could lead to potential bias in the estimation of various parameters. Moreover, we used the Ct value as a proxy for viral load in the interpretation of our analysis. Although we attempted to adjust for confounders that might impact death and be associated with vaccination status, there are inevitably additional factors, including health literacy and health-seeking behaviors, which we were not able to adjust for in this study.

In conclusion, our results showed that previous vaccination with rVSV-ZEBOV reduces EVD-associated illness and death. This relationship persists regardless of vaccination timing, provided it is administered before onset of symptoms. This study directly addresses the paucity of scientific research identified by WHO as a limitation to rVSV-ZEBOV vaccine achieving full authorization for use in preventing EVD illness and death.

N.R. was supported by the National Institute of Allergy and Infectious Diseases, National Institutes of Health (grant R25AI140490).

About the Author

Mr. Rupani is an undergraduate student at Brown University, Providence, RI. His primary research interests are public health and the epidemiology of infectious diseases in underserved communities.

References

1. Baseler L, Chertow DS, Johnson KM, Feldmann H, Morens DM. The pathogenesis of Ebola virus disease. Annu Rev Pathol. 2017;12:387–418. https://doi.org/10.1146/annurev-pathol-052016-100506
2. World Health Organization. Ebola virus disease. February 23, 2021 [cited 2021 Sep 26]. https://www.who.int/news-room/fact-sheets/detail/ebola-virus-disease
3. Centers for Disease Control and Prevention. Transmission: Ebola hemorrhagic fever. January 14, 2021 [cited 2021 Sep 26]. https://www.cdc.gov/vhf/ebola/transmission/index.html
4. Forrester JD, Pillai SK, Beer KD, Neatherlin J, Massaquoi M, Nyenswah TG, et al.; Centers for Disease Control and Prevention (CDC). Assessment of Ebola virus disease, health care infrastructure, and preparedness—four counties, southeastern Liberia, August 2014. MMWR Morb Mortal Wkly Rep. 2014;63:891–3.
5. Suder E, Furuyama W, Feldmann H, Marzi A, de Wit E. The vesicular stomatitis virus-based Ebola virus vaccine: From concept to clinical trials. Hum Vaccin Immunother. 2018;14:2107–13. https://doi.org/10.1080/21645515.2018.1473698
6. Merck & Co. ERVEBO® (Ebola Zaire vaccine, live). United States Patent 8,012,489B2. 2019. [cited 2022 Apr 1]. https://www.merck.com
7. Ervebo (Ebola Zaire vaccine, live suspension for intramuscular injection): uses, dosage, side effects, interactions, warning. RxList. 2021 May 25 [cited 2021 Sep 26]. https://www.rxlist.com/ervebo-drug.htm
8. Whitehouse CA, Bavari S, Perkins MD. United States FDA's emergency use authorization of Ebola virus diagnostics: current impact and lessons for the future. Expert Rev Mol Diagn. 2015;15:1231–5. https://doi.org/10.1586/14737159.2015.1077117
9. Aruna A, Mbala P, Minikulu L, Mukadi D, Bulemfu D, Edidi F, et al.; CDC Ebola response. Ebola virus disease outbreak—Democratic Republic of the Congo, August 2018–-November 2019. MMWR Morb Mortal Wkly Rep. 2019;68:1162–5. https://doi.org/10.15585/mmwr.mm6850a3
10. Regules JA, Beigel JH, Paolino KM, Voell J, Castellano AR, Hu Z, et al. rVSVΔG-ZEBOV-GP Study Group. A recombinant vesicular stomatitis virus Ebola vaccine. N Engl J Med. 2017;376:330–41. https://doi.org/10.1056/NEJMoa1414216
11. Agnandji ST, Huttner A, Zinser ME, Njuguna P, Dahlke C, Fernandes JF, et al. Phase 1 trials of rVSV Ebola vaccine in Africa and Europe. N Engl J Med. 2016;374:1647–60. https://doi.org/10.1056/NEJMoa1502924
12. Huttner A, Dayer JA, Yerly S, Combescure C, Auderset F, Desmeules J, et al. VSV-Ebola Consortium. The effect of dose on the safety and immunogenicity of the VSV Ebola candidate vaccine: a randomised double-blind, placebo-controlled phase 1/2 trial. Lancet Infect Dis. 2015;15:1156–66. https://doi.org/10.1016/S1473-3099(15)00154-1
13. Bolay FK, Grandits G, Lane HC, Kennedy SB, Johnson MP, Fallah MP, et al. PREVAIL I Cluster Vaccination Study with rVSVΔG-ZEBOV-GP as part of a public health response in Liberia. J Infect Dis. 2019;219:1634–41. https://doi.org/10.1093/infdis/jiy698
14. Kennedy SB, Bolay F, Kieh M, Grandits G, Badio M, Ballou R, et al. PREVAIL I Study Group. Phase 2 placebo-controlled trial of two vaccines to prevent Ebola in Liberia. N Engl J Med. 2017;377:1438–47. https://doi.org/10.1056/NEJMoa1614067
15. Henao-Restrepo AM, Camacho A, Longini IM, Watson CH, Edmunds WJ, Egger M, et al. Efficacy and effectiveness of an rVSV-vectored vaccine in preventing Ebola virus disease: final results from the Guinea ring vaccination, open-label, cluster-randomised trial (Ebola Ça Suffit!). Lancet. 2017;389:505–18. https://doi.org/10.1016/S0140-6736(16)32621-6
16. Shears P, Garavan C. The 2018/19 Ebola epidemic in the Democratic Republic of the Congo (DRC): epidemiology, outbreak control, and conflict. Infect Prev Pract. 2020;2:100038.
17. World Health Organization. Ebola virus disease vaccines [cited 2021 Sep 26]. https://www.who.int/teams/regulation-prequalification/eul/ebola-vaccines
18. US Food and Drug Administration. First FDA-approved vaccine for the prevention of Ebola virus disease, marking a critical milestone in public health preparedness and response. December 19, 2019 [cited 2021 Sep 26]. https://www.fda.gov/news-events/press-announcements/first-fda-approved-vaccine-prevention-ebola-virus-disease-marking-critical-milestone-public-health
19. World Health Organization. Frequently asked questions: compassionate use of Ebola vaccine in the context of the Ebola outbreak in North Kivu, Democratic Republic of

Congo [cited 2021 Sep 26]. https://www.afro.who.int/publications/frequently-asked-questions-compassionate-use-ebola-vaccine-context-ebola-outbreak
20. Andre FE, Booy R, Bock HL, Clemens J, Datta SK, John TJ, et al. Vaccination greatly reduces disease, disability, death and inequity worldwide. Bull World Health Organ. 2008;86:140–6. https://doi.org/10.2471/BLT.07.040089
21. Schmitt H-J, von König CHW, Neiss A, Bogaerts H, Bock HL, Schulte-Wissermann H, et al. Efficacy of acellular pertussis vaccine in early childhood after household exposure. JAMA. 1996;275:37–41. https://doi.org/10.1001/jama.1996.03530250041024
22. Thompson MG, Burgess JL, Naleway AL, Tyner H, Yoon SK, Meece J, et al. Prevention and attenuation of COVID-19 with the BNT162b2 and mRNA-1273 vaccines. N Engl J Med. 2021;385:320–9. https://doi.org/10.1056/NEJMoa2107058
23. Xpert® Ebola Assay: instructions for use . Solna (Sweden): Cepheid; 2015 [cited 2021 Sep 26]. https://www.fda.gov/media/91944/download
24. Mbala-Kingebeni P, Aziza A, Di Paola N, Wiley MR, Makiala-Mandanda S, Caviness K, et al. Medical countermeasures during the 2018 Ebola virus disease outbreak in the North Kivu and Ituri Provinces of the Democratic Republic of the Congo: a rapid genomic assessment. Lancet Infect Dis. 2019;19:648–57. https://doi.org/10.1016/S1473-3099(19)30118-5
25. World Health Organization. Clinical management of patients with viral haemorrhagic fever: a pocket guide for the front-line health worker. 2014 [cited 2021 Oct 8]. http://apps.who.int/iris/bitstream/10665/130883/2/WHO_HSE_PED_AIP_14.05.pdf
26. Médecins Sans Frontières. Filovirus haemorrhagic fever guideline. 2008 [cited 2021 Oct 8]. https://www.ghdonline.org/uploads/MSF_Ebola_2008.pdf
27. Roshania R, Mallow M, Dunbar N, Mansary D, Shetty P, Lyon T, et al. Successful implementation of a multicountry clinical surveillance and data collection system for Ebola virus disease in West Africa: findings and lessons learned. Glob Health Sci Pract. 2016;4:394–409. https://doi.org/10.9745/GHSP-D-16-00186
28. International Medical Corps. Viral hemorrhagic fever draft guidelines: standard clinical/psychosocial procedures for Ebola treatment unit (ETU) operations [cited 2022 Apr 1]. https://internationalmedicalcorps.org
29. Mulangu S, Dodd LE, Davey RT Jr, Tshiani Mbaya O, Proschan M, Mukadi D, et al.; PALM Writing Group. PALM Consortium Study Team. A randomized, controlled trial of Ebola virus disease therapeutics. N Engl J Med. 2019;381:2293–303. https://doi.org/10.1056/NEJMoa1910993
30. R Studio Team. RStudio: integrated development environment for R. Boston: RStudio, PBC; 2019 [cited 2021 Sep 26]. https://www.rstudio.com
31. Fireman B, Lee J, Lewis N, Bembom O, van der Laan M, Baxter R. Influenza vaccination and mortality: differentiating vaccine effects from bias. Am J Epidemiol. 2009;170:650–6. https://doi.org/10.1093/aje/kwp173
32. Skrable K, Roshania R, Mallow M, Wolfman V, Siakor M, Levine AC. The natural history of acute Ebola virus disease among patients managed in five Ebola treatment units in West Africa: a retrospective cohort study. PLoS Negl Trop Dis. 2017;11:e0005700. https://doi.org/10.1371/journal.pntd.0005700
33. Agua-Agum J, Ariyarajah A, Blake IM, Cori A, Donnelly CA, Dorigatti I, et al.; WHO Ebola Response Team. Ebola virus disease among children in West Africa. N Engl J Med. 2015;372:1274–7. https://doi.org/10.1056/NEJMc1415318
34. Agua-Agum J, Ariyarajah A, Blake IM, Cori A, Donnelly CA, Dorigatti I, et al.; WHO Ebola Response Team. Ebola virus disease among male and female persons in West Africa. N Engl J Med. 2016;374:96–8. https://doi.org/10.1056/NEJMc1510305
35. Kourlaba G, Kourkouni E, Maistreli S, Tsopela CG, Molocha NM, Triantafyllou C, et al. Willingness of Greek general population to get a COVID-19 vaccine. Glob Health Res Policy. 2021;6:3. https://doi.org/10.1186/s41256-021-00188-1
36. Mahmud S, Mohsin M, Khan IA, Mian AU, Zaman MA. Knowledge, beliefs, attitudes and perceived risk about COVID-19 vaccine and determinants of COVID-19 vaccine acceptance in Bangladesh. PLoS One. 2021;16:e0257096. https://doi.org/10.1371/journal.pone.0257096
37. Kasereka MC, Ericson AD, Conroy AL, Tumba L, Mwesha OD, Hawkes MT. Prior vaccination with recombinant vesicular stomatitis virus: Zaire Ebolavirus vaccine is associated with improved survival among patients with Ebolavirus infection. Vaccine. 2020;38:3003–7. https://doi.org/10.1016/j.vaccine.2020.02.044
38. Ebola ça Suffit Vaccination Trial Consortium. The ring vaccination trial: a novel cluster randomised controlled trial design to evaluate vaccine efficacy and effectiveness during outbreaks, with special reference to Ebola. BMJ. 2015;351:h3740.
39. Marzi A, Robertson SJ, Haddock E, Feldmann F, Hanley PW, Scott DP, et al. VSV-EBOV rapidly protects macaques against infection with the 2014/15 Ebola virus outbreak strain. Science. 2015;349:739–42. https://doi.org/10.1126/science.aab3920
40. Marzi A, Hanley PW, Haddock E, Martellaro C, Kobinger G, Feldmann H. Efficacy of vesicular stomatitis virus–Ebola virus postexposure treatment in rhesus macaques infected with Ebola virus Makona. J Infect Dis. 2016;214(suppl 3):S360–6. https://doi.org/10.1093/infdis/jiw218
41. Günther S, Feldmann H, Geisbert TW, Hensley LE, Rollin PE, Nichol ST, et al. Management of accidental exposure to Ebola virus in the biosafety level 4 laboratory, Hamburg, Germany. J Infect Dis. 2011;204(Suppl 3):S785–90. https://doi.org/10.1093/infdis/jir298
42. Wong KK, Davey RT Jr, Hewlett AL, Kraft CS, Mehta AK, Mulligan MJ, et al. Use of postexposure prophylaxis after occupational exposure to Zaire ebolavirus. Clin Infect Dis. 2016;63:376–9. https://doi.org/10.1093/cid/ciw256
43. Cnops L, Gerard M, Vandenberg O, Van den Wijngaert S, Heyndrickx L, Willems E, et al. Risk of misinterpretation of Ebola virus PCR results after rVSV ZEBOV-GP vaccination. Clin Infect Dis. 2015;60:1725–6. https://doi.org/10.1093/cid/civ131
44. Lai L, Davey R, Beck A, Xu Y, Suffredini AF, Palmore T, et al. Emergency postexposure vaccination with vesicular stomatitis virus-vectored Ebola vaccine after needlestick. JAMA. 2015;313:1249–55. https://doi.org/10.1001/jama.2015.1995
45. Tshiani Mbaya O, Mukumbayi P, Mulangu S. Review: insights on current FDA-approved monoclonal antibodies against Ebola virus infection. Front Immunol. 2021;12:721328. https://doi.org/10.3389/fimmu.2021.721328

Address for correspondence: Neil Rupani, Brown University, 69 Brown St, Mail# 9186, Providence, RI 02912, USA; email: neil_rupani@brown.edu

Risk Prediction Score for Pediatric Patients with Suspected Ebola Virus Disease

Alicia E. Genisca,[1] Tzu-Chun Chu,[1] Lawrence Huang, Monique Gainey, Moyinoluwa Adeniji, Eta N. Mbong, Stephen B. Kennedy, Razia Laghari, Fiston Nganga, Rigo F. Muhayangabo, Himanshu Vaishnav, Shiromi M. Perera, Andrés Colubri,[2] Adam C. Levine,[2] Ian C. Michelow[2,3]

Rapid diagnostic tools for children with Ebola virus disease (EVD) are needed to expedite isolation and treatment. To evaluate a predictive diagnostic tool, we examined retrospective data (2014–2015) from the International Medical Corps Ebola Treatment Centers in West Africa. We incorporated statistically derived candidate predictors into a 7-point Pediatric Ebola Risk Score. Evidence of bleeding or having known or no known Ebola contacts was positively associated with an EVD diagnosis, whereas abdominal pain was negatively associated. Model discrimination using area under the curve (AUC) was 0.87, which outperforms the World Health Organization criteria (AUC 0.56). External validation, performed by using data from International Medical Corps Ebola Treatment Centers in the Democratic Republic of the Congo during 2018–2019, showed an AUC of 0.70. External validation showed that discrimination achieved by using World Health Organization criteria was similar; however, the Pediatric Ebola Risk Score is simpler to use.

Ebola virus disease (EVD) is a potentially fatal infectious disease, easily transmitted through direct contact with infected body fluids. Children exhibit a range of nonspecific clinical signs that mirror common endemic febrile diseases, such as malaria and gastroenteritis. Few children experience hemorrhage, and some are afebrile (*1*). The 2014–2016 West Africa Ebola outbreak was the largest EVD epidemic in history; 28,646 cases were suspected, probable, or confirmed, of which nearly 20% occurred in children <15 years of age, and 11,323 case-patients of all ages died (*2*). EVD quickly became a global public health concern as 7 other countries, including the United States, reported cases (*3*). Since then, there have been several outbreaks in the Democratic Republic of the Congo (DRC), the largest of which occurred during 2018–2020 in the North Kivu, Ituri, and South Kivu Provinces.

Our research and that of others previously showed young children to be especially vulnerable and susceptible to EVD; mortality rates exceeded 55% (*1*,*4*). Consequently, there is a critical need to rapidly diagnose EVD in children so they can be appropriately isolated and begin treatment. During EVD outbreaks, triage protocols are typically based on World Health Organization (WHO) criteria for screening children with suspected EVD. According to WHO criteria, a suspected case-patient is defined as anyone, dead or alive, who has been in contact with someone with a suspected, probable, or confirmed EVD case; has sudden onset of fever combined with ≥3 other signs/symptoms; has inexplicable bleeding; or suddenly inexplicably died in the context of an EVD outbreak (*5*). Therefore, we adopted age-dependent case definitions: a fever and 1 other sign/symptom for children <5 years of age, 2 other signs/symptoms for children 5–12 years of age, and >3 signs/symptoms for children >12 years of age (*6*). However, nonspecific signs/symptoms in the early stages of disease impede prompt and accurate identification of cases and result in poor discrimination when applying the WHO broad case definitions. In addition,

Author affiliations: Brown Emergency Medicine, Providence, Rhode Island, USA (A.E. Genisca, H. Vaishnav, A.C. Levine); Alpert Medical School of Brown University, Providence (A.E. Genisca, A.C. Levine, I.C. Michelow); University of Georgia, Athens, Georgia, USA (T.C. Chu); Brown University, Providence (L. Huang, M. Adeniji); Rhode Island Hospital, Providence (M. Gainey); International Medical Corps, Goma, Democratic Republic of the Congo (E.N. Mbong, R. Laghari, F. Nganga, R.F. Muhayangabo); Ministry of Health, Monrovia, Liberia (S.B. Kennedy); International Medical Corps, Washington, DC, USA (S.M. Perera); University of Massachusetts Chan Medical School, Worcester, Massachusetts, USA (A. Colubri)

DOI: https://doi.org/10.3201/eid2806.212265

[1]These authors contributed equally to this article.

[2]These authors contributed equally to this article.

[3]Current affiliation: Pediatric Infectious Diseases & Immunology, Connecticut Children's Medical Center, Hartford, Connecticut, USA.

if EVD-negative children are unnecessarily admitted to Ebola treatment centers (ETCs), they require use of scarce resources and are potentially exposed to EVD case-patients. There is a critical knowledge gap in clinical diagnostics for children with EVD; few published studies focus on the epidemiology and diagnosis of pediatric EVD (*4*,*6*). To our knowledge, 1 study has created a diagnostic predictive score for pediatric EVD (*6*), but those results have not been externally validated.

Although great strides in EVD care have been made with the advent of highly effective vaccines and treatments (*7*–*9*), an accurate predictive clinical diagnostic tool can be helpful for clinicians before molecular test results are available. Such a tool would help streamline the triage process, enhancing the ability of clinicians to rapidly identify children at the highest risk for EVD, initiate time-sensitive treatment, and protect EVD-negative children from nosocomial acquisition of EVD.

With this study, we addressed the knowledge gaps associated with management for children with suspected EVD by developing a predictive diagnostic tool. Ethics approval for this study was exempted by the Rhode Island Hospital Institutional Review Board because it is a secondary analysis of deidentified data.

Materials and Methods

Data Sources

Our retrospective study used data that had been prospectively collected from children at the International Medical Corps (IMC) ETCs in West Africa (West Africa cohort) and the DRC (DRC cohort). The derivation dataset was built from data collected at 5 IMC ETCs in Sierra Leone and Liberia during September 2014–September 2015. The validation dataset was derived from children who were at the IMC Mangina ETC in the DRC during December 2018–December 2019. For the derivation and the validation datasets, we systematically extracted data from paper clinical records, which were scanned by ETC staff onto the IMC secure server. Research staff then transcribed the information into respective databases and removed all personal identifiers before analysis.

Data Quality Audit

For the derivation and validation datasets, all data were deidentified before analysis. To ensure minimal errors during data entry, we took the following steps: used data validation settings in Excel documents; used codebooks to ensure that patient data were standardized; had data entry research coordinators conduct additional audits; and discussed data entry concerns with the principal investigator. We used a random sample of charts to assess the quality of data entered from original patient charts into the database for EVD-positive persons. We selected 19 patients for the derivation dataset and 62 patients for the validation dataset and included them in the data quality audit, in which patient charts were reentered into a second database by using scanned files of the original charts (*10*). After reentry was complete, we compared the original data to the reentered database for each respective cohort and recorded each discrepancy as an error. With results from this audit, we concluded that, overall, 99.8% of data were entered correctly in the derivation dataset and 97.3% of the data in the original database were consistent with information from the scans of patient charts for the validation dataset (*10*).

For additional quality assurance, we compared the validation dataset's more simplified line list database and the EVD-positive database across 145 common variables to check for any inconsistencies. If any fields were flagged, we referenced the paper charts for further clarification and resolved in both databases.

Inclusion and Exclusion Criteria

For the derivation and the validation datasets, all pediatric patients (<18 years of age) with suspected EVD who were admitted to any of the ETCs were eligible for study inclusion. We excluded from analysis patients for whom all clinical sign/symptom data were missing. We also excluded patients who died within the first 24 hours after admission because a diagnostic tool would probably be less useful for severely ill patients whose death was imminent.

EVD Triage and Diagnosis

Trained clinical staff screened all patients at the IMC ETCs according to WHO and Médecins Sans Frontières guidelines (*11*,*12*) as well as individual clinicians' judgment. Patients with a previously confirmed laboratory diagnosis of EVD were directly admitted to the ETC confirmed ward. Otherwise, patients who met the definition of having a suspected case were admitted to the ETC suspected ward, where they had a blood sample drawn for initial EVD testing (Appendix, https://wwwnc.cdc.gov/EID/article/28/6/21-2265-App1.pdf). If the patient's initial test result was negative, the patient remained in the ETC until a second test ruled out EVD. Patients with a second negative test result were considered EVD negative and discharged. Patients with a positive test result were considered EVD positive and moved to the confirmed ward for further management (E.N. Mbong, unpub. data) (*10*,*13*).

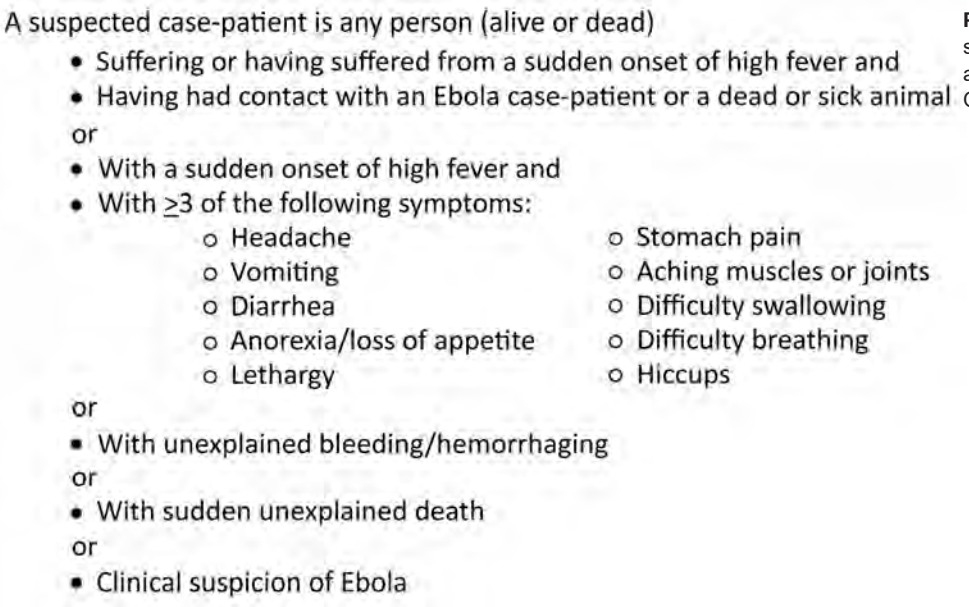

Figure 1. Ebola virus disease suspected case definition according to 2016 World Health Organization guidelines.

West Africa: Liberia and Sierra Leone

In Liberia, ETCs received all patients from the surrounding catchment areas. However, in Sierra Leone, multiple agencies operating in the ETC districts and the government-run District Ebola Response Center determined to which ETCs patients should be sent. In both countries, most patients seen at the ETC had >1 signs/symptoms consistent with EVD but no laboratory confirmation. Some may have had EVD confirmed in community or government-managed holding centers before arrival at the ETC (*10*,*13*).

For Liberia, the US Naval Medical Research Center Mobile Laboratory (Frederick, Maryland, USA) conducted the 1-step quantitative Ebola Zaire real-time reverse transcription PCR (RT-PCR) (Taqman) assay for both IMC ETCs. For this assay, they used a QIAamp Viral RNA Mini Kit (https://www.qiagen.com) to extract RNA from blood samples treated with QIAGEN buffer AVL and ethanol. Using the Applied Biosystems StepOnePlus instrument (https://www.thermofisher.com), they tested the extracted RNA for 2 Ebola virus (EBOV) gene targets (Zaire ebolavirus locus and minor groove binding locus). If both targets were detected, a sample was considered positive for EVD. If only 1 target was detected, the sample was considered indeterminate, and the patient was retested (*10*,*13*).

In Sierra Leone, the Public Health England (PHE) laboratories in Port Loko and Bombali districts performed EVD testing for patients admitted to ETCs in those districts, and the Nigeria laboratory in Kambia District provided RT-PCR testing for patients admitted to the Kambia ETCs with support from the European Union Mobile Laboratory Consortium. The PHE and Nigeria laboratories tested only 1 EBOV gene target (Zaire ebolavirus locus). In February 2015, the PHE laboratories switched from using the commercially available Altona real-time RT-PCR to the in-house Trombley assay (*10*,*13*).

DRC

DRC ETCs received all patients from the surrounding catchment areas, some of whom may have had EVD confirmed by laboratory testing in the community or another test facility before arrival. EVD diagnoses

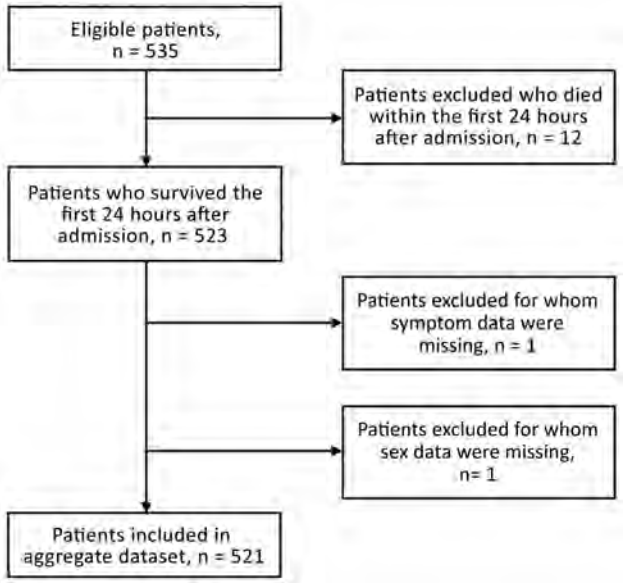

Figure 2. Selection process for West Africa (derivation) dataset during model development for study of risk prediction score for pediatric patients with suspected Ebola virus disease in West Africa.

Table 1. Demographic and clinical characteristics of patients, by EVD status at triage, in West Africa, September 2014 – September 2015*

Characteristics	Total, no (%), n = 521	EVD positive, no. (%), n = 120 (23%)	EVD negative, no. (%), n = 401 (77%)	OR (95% CI)	p value
Sex					
M	261 (50)	53 (44)	208 (52)	0.73 (0.49–1.10)	0.14
F	260 (50)	67 (56)	193 (48)	Referent	
Sign/symptom					
Fever	431 (83)	95 (79)	336 (84)	0.74 (0.44–1.25)	0.24
Headache	268 (51)	54 (45)	214 (53)	0.71 (0.47–1.08)	0.11
Breathlessness	84 (16)	16 (13)	68 (17)	0.75 (0.41–1.33)	0.35
Bone/muscle pain	201 (39)	43 (36)	158 (39)	0.86 (0.56–1.31)	0.48
Asthenia	333 (64)	77 (64)	256 (64)	1.01 (0.67–1.56)	0.95
Abdominal pain	219 (42)	29 (24)	190 (47)	0.35 (0.22–0.56)	**<0.001**
Hiccups	39 (7.5)	5 (4.2)	34 (8.5)	0.47 (0.16–1.13)	0.12
Any bleeding	77 (15)	36 (30)	41 (10)	3.76 (2.26–6.25)	**<0.001**
GI symptoms	355 (68)	73 (61)	282 (70)	0.66 (0.43–1.01)	0.05
Ebola contact					**<0.001**
Yes	218 (42)	104 (87)	114 (28)	31.3 (15.1–76.1)	
No known	56 (11)	9 (7.5)	47 (12)	6.57 (2.33–19.2)	
No	247 (47)	7 (5.8)	240 (60)	Referent	
Malaria					**0.009**
Yes	163 (31)	27 (23)	136 (34)	0.42 (0.24–0.73)	
Missing†	233 (45)	53 (44)	180 (45)	0.63 (0.39–1.02)	
No	125 (24)	40 (33)	85 (21)	Referent	

*Patient median age (interquartile range) = 7 (3–13) y; OR (95% CI) = 1.00 (0.97–1.04); p = 0.80. Boldface indicates statistical significance. EVD, Ebola virus disease; GI, gastrointestinal; OR, odds ratio.
†Missing refers to patients who did not have a rapid diagnostic test completed or results not available.

were made by using a Cepheid GeneXpert Ebola RT-PCR blood assay (https://www.cepheid.com) targeting 2 EBOV genes: glycoprotein and nucleoprotein (*14*,*15*). Laboratory testing was conducted by the Institut National de Recherche Biomédicale (Kinshasa, DRC). All cycle threshold values presented in this study are based on RT-PCR. Cycle threshold values >40 were considered negative for all cases.

Statistical Analyses

We described the demographic and clinical characteristics of the study population according to EVD status by using frequencies with percentages for categorical variables and median values with interquartile ranges (IQRs) for continuous variables. We performed univariate analyses to evaluate associations between candidate predictors and EVD status and reported odds ratios (ORs) with 95% CIs.

The 12 candidate predictors were age, sex, and 10 other epidemiologic and clinical variables based on the current WHO criteria (Figure 1) for identifying suspected Ebola cases (fever, headache, breathlessness, bone or muscle pain, asthenia, abdominal pain, hiccups, unexplained bleeding, gastrointestinal symptoms [vomiting, diarrhea, nausea, anorexia or swallowing problems], and contact with an EVD case-patient [Ebola contact]). Ebola contact was a composite variable consisting of a combination of 11 individual variables associated with potential contact with an EVD case-patient. These variables included contact with a known/suspected EVD case-patient or any sick person in the previous 21 days; contact with the body, body fluids, or potentially contaminated objects or eating utensils; shared living space with an EVD patient/sick person; attendance at a funeral or contact with the infected body at a funeral; travel outside the patient's home/village; hospitalization or visit with a hospitalized patient; consultation with a traditional healer; or direct contact with animals or raw meat (hunting/touching/eating). To use the

Table 2. Ebola diagnostic model and corresponding point risk score in West Africa, September 2014–September 2015

Variable	Regression coefficient (95% CI)	Odds ratio (95% CI)	Risk score
Ebola contact			
No	Referent	Referent	0
Yes	3.55 (2.78 to 4.49)	34.9 (16.1 to 89.2)	3
No known	1.88 (0.81 to 3.00)	6.56 (2.24 to 20.0)	2
Any bleeding			
No	Referent	Referent	0
Yes	2.02 (1.31 to 2.77)	7.51 (3.70 to 16.0)	2
Abdominal pain			
No	Referent	Referent	0
Yes	−1.19 (−1.80 to −0.63)	0.30 (0.17 to 0.53)	−1

Table 3. Performance measures of Pediatric Ebola Risk Score at different cut points and WHO criteria in West Africa cohort, September 2014 – September 2015

Measure	Measure, % (95% CI)					
	Sensitivity	Specificity	PPV	NPV	LR+	LR–
Score						
≥0	98.3 (94.1–99.8)	26.2 (21.9–30.8)	28.5 (24.2–33.1)	98.1 (93.4–99.8)	1.33 (1.25–1.42)	0.06 (0.02–0.25)
≥1	95.8 (90.5–98.6)	52.4 (47.3–57.3)	37.6 (32.1–43.3)	97.7 (94.7–99.2)	2.01 (1.8–2.24)	0.08 (0.03–0.19)
≥2	94.2 (88.4–97.6)	60.1 (55.1–64.9)	41.4 (35.5–47.5)	97.2 (94.3–98.9)	2.36 (2.08–2.68)	0.10 (0.05–0.2)
≥3	79.2 (70.8–86.0)	81.8 (77.7–85.4)	56.6 (48.7–64.2)	92.9 (89.7–95.4)	4.35 (3.47–5.46)	0.25 (0.18–0.36)
≥4	26.7 (19.0–35.5)	98.0 (96.1–99.1)	80.0 (64.4–90.9)	81.7 (78.0–85.1)	13.4 (6.33–28.2)	0.75 (0.67–0.83)
WHO criteria	83.3 (75.4–89.5)	28.9 (24.5–33.6)	26.0 (21.7–30.7)	85.3 (78.2–90.8)	1.17 (1.06–1.30)	0.58 (0.38–0.88)

*LR+, true positive/false positive likelihood ratio; LR–, false negative/true negative likelihood ratio; NPV, negative predictive value; PPV, positive predictive value; WHO, World Health Organization.

complete dataset, we created 3 categories for Ebola contacts: yes, no, or no known.

Derivation of Clinical Diagnostic Model

We entered 12 candidate predictors into a logistic regression model to predict EVD diagnosis by using a forward stepwise regression algorithm with 10-fold cross-validation as previously described (*16*). We modeled clinical symptom predictors as dichotomous variables and Ebola contacts as 2 indicator variables and used no contact as the reference. We explored models with interactions. Age was fitted as a linear variable and as restricted cubic splines with 3 knots located at the 10th, 50th, and 90th quantiles. We selected the model without restricted cubic splines or interaction terms because that model performed the best.

Model Performance and Development of a Risk Score

We assessed the discrimination for the derived model and newly created risk score compared with the WHO criteria. Model discrimination was evaluated by using the area under the receiver operating characteristic curve (AUC) and its 95% CIs at consecutive threshold settings of the predicted probability (*17*,*18*). We developed a point-based risk score (Pediatric Ebola Risk Score; PERS) by converting the regression coefficient of each predictor in the final model to an integer (*19*). We then calculated a total score for each patient by adding these weighted risk scores. The performance of the PERS was also evaluated in the same fashion as the original model. Other performance measures of PERS and WHO criteria at each cut point were also estimated for EVD diagnosis, including sensitivity, specificity, positive predictive value (PPV), negative predictive value (NPV), and positive and negative likelihood ratios.

External Validation and Model Updating

We externally validated our PERS tool with the DRC dataset by using the same inclusion criteria as used for the derivation dataset. We performed bivariate analyses to compare baseline characteristics between the West Africa and DRC cohorts by using χ^2 tests. To assess the performance of PERS versus WHO criteria in the DRC cohort, we calculated the AUC, sensitivity, specificity, PPV, NPV, and positive and negative likelihood ratios. All analyses were conducted by using R version 4.0.3 (R Foundation for Statistical Computing, https://www.r-project.org) and Stata version 16.0 (StataCorp, https://www.stata.com).

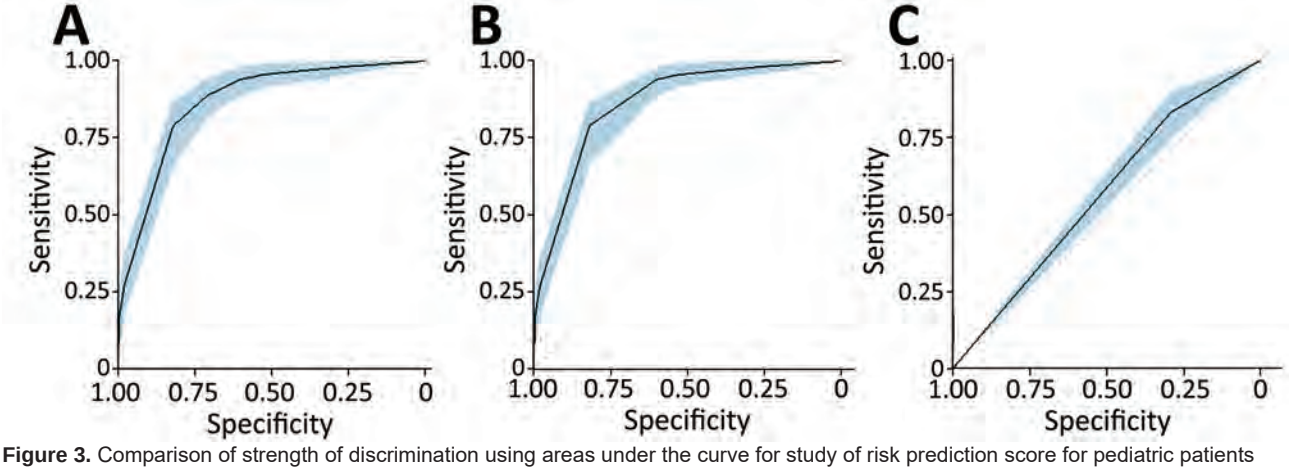

Figure 3. Comparison of strength of discrimination using areas under the curve for study of risk prediction score for pediatric patients with suspected Ebola virus disease in West Africa. A) Ebola diagnostic model; B) Pediatric Ebola Risk Score; C) World Health Organization criteria. The shaded blue regions within each of the panels represent the confidence bands for the areas under the curve.

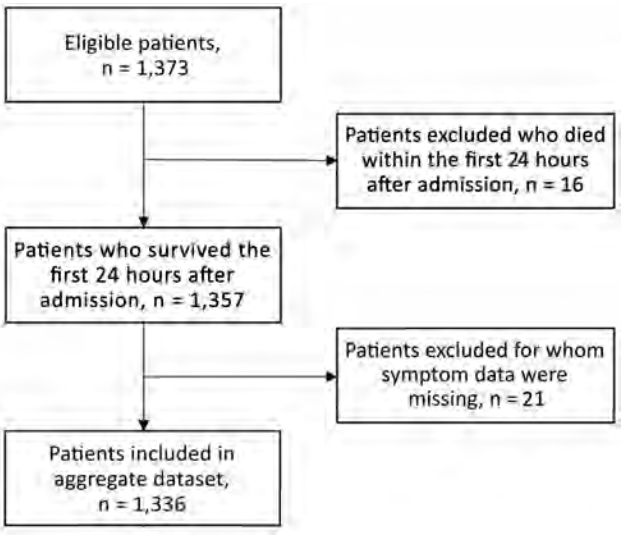

Figure 4. Selection process for Democratic Republic of the Congo (validation) dataset for study of risk prediction score for pediatric patients with suspected Ebola virus disease in West Africa.

Results

Enrollment and Baseline Characteristics

During September 2014–September 2015, a total of 535 patients <18 years of age at IMC West Africa ETCs with suspected EVD were eligible for inclusion. We excluded from analysis 12 patients who died within the first 24 hours after admission, 1 patient for whom sex classification was missing, and 1 patient for whom all sign/symptom data were missing, leaving 521 patients in the final derivation analysis (Figure 2). Median patient age was 7 (IQR 3–13) years, and 261 (50%) patients were male (Table 1).

Derivation of Predictive Diagnostic Model for EVD

Of the 12 candidate predictors included in the bivariate analyses, 3 variables were significantly positively associated with an EVD diagnosis: bleeding (OR 3.76, 95% CI 2.26–6.25), a reported Ebola contact (OR 31.3, 95% CI 15.1–76.1), and no known Ebola contact (OR 6.57, 95% CI 2.33–19.2). Abdominal pain (OR 0.35, 95% CI 0.22–0.56) was negatively associated with an EVD diagnosis (Table 1).

Risk Score Assessment and Validation

Forward stepwise regression yielded a final model consisting of 3 covariates: abdominal pain, any bleeding, and Ebola contact without inclusion of interaction terms. The regression coefficients for each variable were converted into integer scores, producing a 7-point scoring system (Table 2). The sensitivity and specificity of the various score cut points for determining EVD status were calculated; higher score cut points were more specific and less sensitive (Table 3). Model discrimination, measured by using the AUC, was 0.87 (95% CI 0.83–0.90) for EVD diagnostic model and point-based risk score (Figure 3). According to the WHO criteria for this dataset, the AUC is 0.56 (95% CI 0.52–0.60).

External Validation

We included 1,336 patients in the final validation dataset after excluding 16 patients who died within the first 24 hours of admission and 21 for whom any sign/symptom data were missing (Figure 4). For the DRC cohort at triage (Table 4), median age of patients in the validation cohort was 7 (IQR 2–11) years and 52% were male, similar to the West Africa cohort. In

Table 4. Demographic and clinical characteristics of patients, by EVD status at triage, in Democratic Republic of the Congo, December 2018–December 2019*

Characteristic†	Overall, no. (%), n = 1,336	EVD positive, no (%), n = 84 (6%)	EVD negative, no. (%), n = 1,252 (94%)	OR (95% CI)	p value
Sex					
M	690 (52)	32 (38)	658 (53)	0.56 (0.35–0.87)	0.01
F	646 (48)	52 (62)	594 (47)	Referent	
Signs/symptoms					
Fever	818 (61)	72 (86)	746 (60)	4.07 (2.27–7.96)	<0.001
Headache	700 (52)	47 (56)	653 (52)	1.17 (0.75–1.83)	0.50
Breathlessness	93 (7.0)	13 (15)	80 (6.4)	2.68 (1.37–4.90)	0.002
Bone/muscle pain	116 (8.7)	16 (19)	100 (8.0)	2.71 (1.47–4.74)	<0.001
Asthenia	960 (72)	62 (74)	898 (72)	1.11 (0.68–1.87)	0.68
Abdominal pain	458 (34)	34 (40)	424 (34)	1.33 (0.84–2.08)	0.22
Hiccups	16 (1.2)	1 (1.2)	15 (1.2)	0.99 (0.05–4.99)	>0.99
Any bleeding	99 (7.4)	21 (25)	78 (6.2)	5.02 (2.86–8.54)	<0.001
GI symptoms	1,026 (77)	84 (100)	942 (75)	55.7 (3.44–900)	0.005
Ebola contact					
Yes	191 (14)	54 (64)	137 (11)	5.40 (3.03–10.1)	<0.001
No known	910 (68)	14 (17)	896 (71)	0.21 (0.10–0.45)	
No	235 (18)	16 (19)	219 (17)	Referent	

*Age, y, mean (interquartile range): overall, 7 (2–11); EVD positive, 5 (1.4–13); EVD negative, 6 (2.5–11); OR 1.00 (95% CI 0.96–1.04); p = 0.96. EVD, Ebola virus disease; GI, gastrointestinal; OR, odds ratio.
†Malaria was not reported for this cohort because rapid diagnostic tests for malaria were not conducted for all patients at the EVD treatment centers.

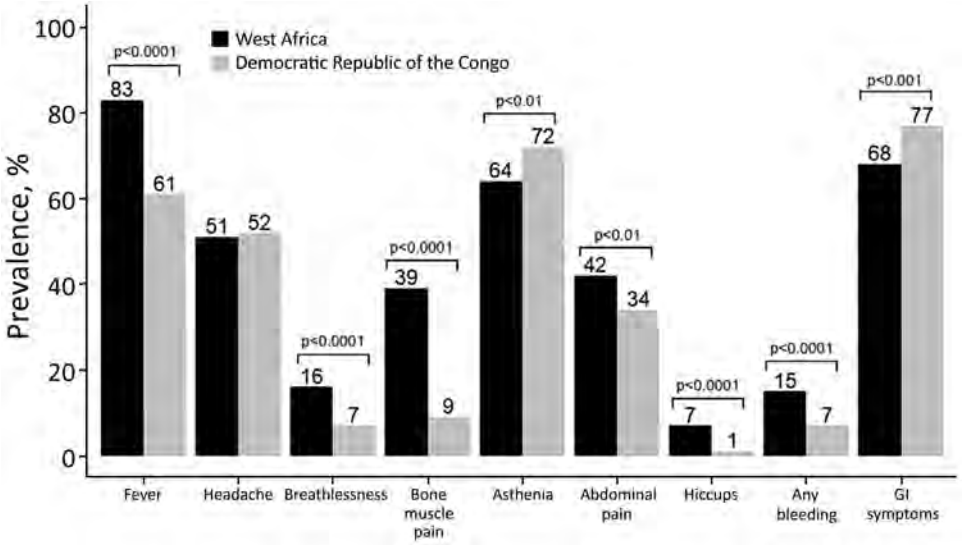

Figure 5. Prevalence of clinical symptoms for pediatric patients with suspected Ebola virus disease in West Africa, September 2014–September 2015, compared with Democratic Republic of the Congo, 2018–2019.

terms of clinical signs/symptoms for patients in the 2 cohorts (Figure 5), prevalence of fever, breathlessness, and bone/muscle pain was significantly higher among those in the West Africa cohort (p<0.0001), and gastrointestinal signs/symptoms were significantly higher among those in the DRC cohort (p<0.001).

The performance characteristics of the various score cut points used to determine EVD status by applying the PERS tool to the DRC cohort demonstrated that higher score cut points were more specific and less sensitive, similar to findings for the West Africa cohort (Table 5). Discrimination of the EVD diagnostic model with and without the no known Ebola contact variable was performed by using the DRC cohort. The measured AUC for each model with the no known Ebola contact variable was 0.70 (95% CI 0.63–0.77) and without the variable was 0.71 (95% CI 0.65–0.78). The WHO criteria performed similarly for these datasets (Figure 6).

Discussion

In this study, we derived and externally validated a predictive diagnostic model and score for children with EVD. An EVD diagnosis for children was associated with unexplained bleeding, known exposure to an EVD case-patient, or not knowing if the child had come into contact with an EVD case-patient. When converted to a score, the score performed well and showed good discrimination. In addition, the model and score performed similarly or better than the WHO criteria for EVD, the score having the advantage of being simpler and more practical for point-of-care use. Contact with an EVD-positive sick person has been shown to be a strong predictor for EVD diagnosis among adults and children (*6*,*20*). In many studies, bleeding has been shown to be a predictor for poor prognosis (*1*) but is not consistently reported for diagnosis and is usually a late sign in the course of the disease. We found that abdominal pain was negatively associated with an EVD diagnosis.

We externally validated this model and scoring system by using data from the outbreak in the DRC. A PERS >3 had a similar NPV (97%) to the WHO criteria and greater specificity (87%) than the WHO criteria (62%). Therefore, PERS, which is derived from 3 variables compared with 12 variables from the WHO criteria, is a convenient and simple point-of-care tool that can be used by caregivers at the time of triage

Table 5. Performance measures of Pediatric Ebola Risk Score at different cut points and World Health Organization criteria in Democratic Republic of the Congo cohort, December 2018–December 2019*

Measure	Measure, % (95% CI)					
	Sensitivity	Specificity	PPV	NPV	LR+	LR–
Score						
≥0	91.7 (83.6–96.6)	4.5 (3.4–5.8)	6.1 (4.8–7.5)	88.9 (78.4–95.4)	0.96 (0.90–1.02)	1.86 (0.88–3.96)
≥1	88.1 (79.2–94.1)	16.3 (14.3–18.5)	6.60 (5.21–8.21)	95.3 (91.6–97.7)	1.05 (0.97–1.14)	0.73 (0.40–1.32)
≥2	79.8 (69.6–87.7)	41.9 (39.1–44.6)	8.43 (6.59–10.6)	96.9 (95.0–98.2)	1.37 (1.22–1.54)	0.48 (0.31–0.74)
≥3	53.6 (42.4–64.5)	87.3 (85.3–89.1)	22.1 (16.6–28.4)	96.6 (95.3–97.5)	4.22 (3.30–5.40)	0.53 (0.42–0.67)
≥4	16.7 (9.42–26.4)	96.4 (95.2–97.4)	23.7 (13.6–36.6)	94.5 (93.1–95.7)	4.64 (2.65–8.10)	0.86 (0.79–0.95)
WHO criteria	77.4 (67.0–85.8)	62.2 (59.5–64.9)	12.1 (9.45–15.1)	97.6 (96.3–98.6)	2.05 (1.79–2.35)	0.36 (0.24–0.54)

*Patients with missing Ebola contact information (n = 910) were assigned with a risk score of no known group. LR, likelihood ratio; NPV, negative predictive value; PPV, positive predictive value; WHO, World Health Organization.

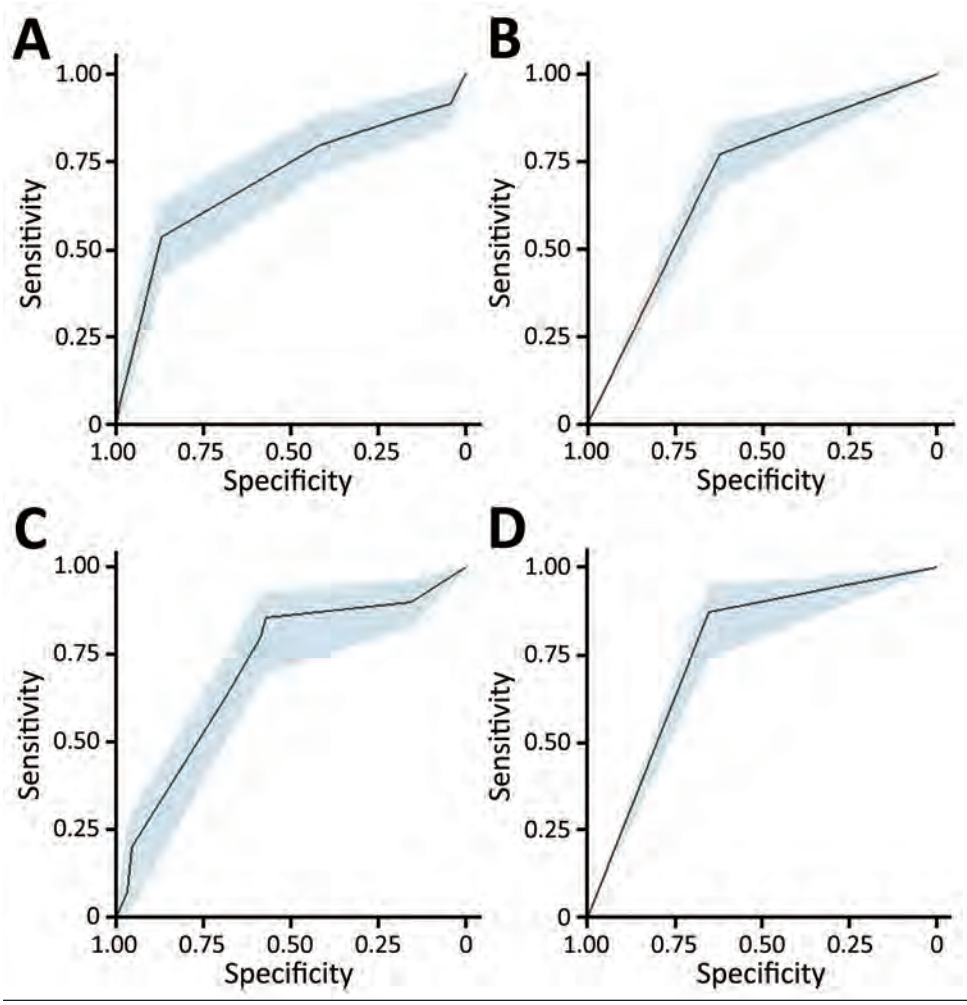

Figure 6. Comparison of strength of discrimination using areas under the curve for Pediatric Ebola Risk Score (PERS) and World Health Organization criteria for study of risk prediction score for pediatric patients with suspected Ebola virus disease in Democratic Republic of the Congo, 2018–2019. A) PERS applied to data including no known Ebola contact (n = 1,336); B) World Health Organization criteria applied to data including no known Ebola contact (n = 1,336); C) PERS applied to data excluding no known Ebola contact (n = 426); and D) World Health Organization criteria applied to data excluding no known Ebola contact (n = 426). The shaded blue regions within each of the panels represent the confidence bands for the areas under the curve.

to rule in EVD and avoid potentially exposing uninfected children to other possible or confirmed EVD case-patients in an ETC. The low PPV of the PERS tool in the DRC probably partly results from a different prevalence of disease (23% in West Africa compared with 6% in DRC). In addition, the percentage of no known Ebola contacts for the DRC cohort (68%) was much larger than that for the West Africa cohort (11%). This finding was a strong diagnostic predictor in the derivation cohort, for which disease prevalence was higher, but it may not have had the same effect in the smaller validation cohort, for which prevalence was lower.

A study limitation is missing epidemiologic and clinical sign/symptom data, which are challenging to collect during an emergency situation, although our data entry error rate was low (after conducting a data quality audit, 99.8% of the West Africa data and 97.3% of DRC re-entry data matched that on the scanned patient charts for patients selected for the data audit) (*10*). In addition, we evaluated only those children who were at the ETCs and met the WHO criteria of having a suspected case. Our findings are not necessarily generalizable to symptomatic children outside this setting.

In summary, using the PERS diagnostic model, we found that Ebola contact status and bleeding were positive predictors of EVD diagnosis, whereas abdominal pain was a negative predictor. The model performed better than the WHO criteria with the West Africa cohort and similarly to WHO criteria with the DRC cohort, yet the PERS model is simpler to use because it requires clinicians to collect only 3 variables rather than 12. Furthermore, using the parsimonious PERS will enable clinicians to promptly triage children with suspected EVD, assign them to cohorts according to their calculated risk for infection, and initiate medical care while awaiting the results of definitive molecular tests. This approach could substantially improve the immediate care of children with suspected EVD and favorably affect their outcomes.

Acknowledgments

We thank the International Medical Corps field team members, who serve tirelessly to provide excellent care to patients with Ebola Virus Disease; Kexin Qu for providing the R codes to implement the model selection; and the Advance Clinical and Translational Research team at Brown University.

This research was supported in part by the Rhode Island Foundation and National Institutes of Health/National Institute of Allergy and Infectious Diseases R25AI140490.

About the Author

Dr. Genisca is an assistant professor of Emergency Medicine and Pediatrics at the Warren Alpert Medical School of Brown University. Her primary research interests are strengthening emergency medical systems in low-resource settings, medical education, and point-of-care ultrasonography.

References

1. Smit MA, Michelow IC, Glavis-Bloom J, Wolfman V, Levine AC. Characteristics and outcomes of pediatric patients with Ebola virus disease admitted to treatment units in Liberia and Sierra Leone: a retrospective cohort study. Clin Infect Dis. 2017;64:243–9. https://doi.org/10.1093/cid/ciw725
2. Hsu CH, Champaloux SW, Keïta S, Martel L, Bilivogui P, Knust B, et al. Sensitivity and specificity of suspected case definition used during West Africa Ebola epidemic. Emerg Infect Dis. 2018;24:9–14. https://doi.org/10.3201/eid2401.161678
3. Centers for Disease Control and Prevention. 2014–2016 Ebola outbreak in West Africa [cited 2021 Aug 24]. https://www.cdc.gov/vhf/ebola/history/2014-2016-outbreak/index.html
4. Chérif MS, Koonrungsesomboon N, Kassé D, Cissé SD, Diallo SB, Chérif F, et al. Ebola virus disease in children during the 2014-2015 epidemic in Guinea: a nationwide cohort study. Eur J Pediatr. 2017;176:791–6. https://doi.org/10.1007/s00431-017-2914-z
5. World Health Organization. Case definition recommendations for Ebola or Marburg virus diseases [cited 2021 Aug 24]. https://apps.who.int/iris/bitstream/handle/10665/146397/WHO_EVD_CaseDef_14.1_eng.pdf
6. Fitzgerald F, Wing K, Naveed A, Gbessay M, Ross JCG, Checchi F, et al. Development of a pediatric Ebola predictive score, Sierra Leone. Emerg Infect Dis. 2018;24:311–9. https://doi.org/10.3201/eid2402.171018
7. Wells CR, Pandey A, Parpia AS, Fitzpatrick MC, Meyers LA, Singer BH, et al. Ebola vaccination in the Democratic Republic of the Congo. Proc Natl Acad Sci U S A. 2019;116:10178–83. https://doi.org/10.1073/pnas.1817329116
8. World Health Organization. Preliminary results on the efficacy of rVSV-ZEBOV-GP Ebola vaccine using the ring vaccinations strategy in the control of an Ebola outbreak in the Democratic Republic of the Congo: an example of integration of research into epidemic response [cited 2021 Aug 24]. https://www.who.int/publications/m/item/preliminary-results-on-the-efficacy-of-rvsv-zebov-gp-ebola-vaccine-using-the-strategy-in-the-control-of-an-ebola-outbreak.
9. Mulangu S, Dodd LE, Davey RT Jr, Tshiani Mbaya O, Proschan M, Mukadi D, et al.; PALM Writing Group; PALM Consortium Study Team. PALM Consortium Study Team. A randomized, controlled trial of Ebola virus disease therapeutics. N Engl J Med. 2019;381:2293–303. https://doi.org/10.1056/NEJMoa1910993
10. Roshania R, Mallow M, Dunbar N, Mansary D, Shetty P, Lyon T, et al. Successful implementation of a multicountry clinical surveillance and data collection system for Ebola virus disease in West Africa: findings and lessons learned. Glob Health Sci Pract. 2016;4:394–409. https://doi.org/10.9745/GHSP-D-16-00186
11. Sterk E. Filovirus haemorrhagic fever guideline. Médecins Sans Frontières [cited 2022 Apr 4]. https://asprtracie.hhs.gov/technical-resources/resource/3490/filovirus-haemorrhagic-fever-guideline
12. World Health Organization. Clinical management of patients with viral haemorrhagic fever: a pocket guide for the front-line health worker [cited 2021 Aug 4]. http://apps.who.int/iris/bitstream/10665/130883/2/ WHO_HSE_PED_AIP_14.05.pdf
13. Skrable K, Roshania R, Mallow M, Wolfman V, Siakor M, Levine AC. The natural history of acute Ebola virus disease among patients managed in five Ebola treatment units in West Africa: a retrospective cohort study. PLoS Negl Trop Dis. 2017;11:e0005700. https://doi.org/10.1371/journal.pntd.0005700
14. Mbala-Kingebeni P, Aziza A, Di Paola N, Wiley MR, Makiala-Mandanda S, Caviness K, et al. Medical countermeasures during the 2018 Ebola virus disease outbreak in the North Kivu and Ituri Provinces of the Democratic Republic of the Congo: a rapid genomic assessment [cited 2021 Jun 21]. https://www.thelancet.com/journals/laninf/article/PIIS1473-3099(19)30118-5/fulltext
15. Xpert Ebola: accurate and reliable detection of Ebola Zaire virus [cited 2021 Sep 28]. https://p.widencdn.net/pesypn/Cepheid-Xpert-Ebola-Brochure-CE-IVD-3058-English
16. Levine AC, Barry MA, Gainey M, Nasrin S, Qu K, Schmid CH, et al. Derivation of the first clinical diagnostic models for dehydration severity in patients over five years with acute diarrhea. PLoS Negl Trop Dis. 2021;15:e0009266. https://doi.org/10.1371/journal.pntd.0009266
17. Royston P, Moons KG, Altman DG, Vergouwe Y. Prognosis and prognostic research: developing a prognostic model. BMJ. 2009;338:b604. https://doi.org/10.1136/bmj.b604
18. Steyerberg EW, Vickers AJ, Cook NR, Gerds T, Gonen M, Obuchowski N, et al. Assessing the performance of prediction models: a framework for traditional and novel measures. Epidemiology. 2010;21:128–38. https://doi.org/10.1097/EDE.0b013e3181c30fb2
19. Sullivan LM, Massaro JM, D'Agostino RB Sr. Presentation of multivariate data for clinical use: the Framingham Study risk score functions. Stat Med. 2004;23:1631–60. https://doi.org/10.1002/sim.1742
20. Levine AC, Shetty PP, Burbach R, Cheemalapati S, Glavis-Bloom J, Wiskel T, et al. Derivation and internal validation of the Ebola prediction score for risk stratification of patients with suspected Ebola virus disease. Ann Emerg Med. 2015;66:285–293.e1. https://doi.org/10.1016/j.annemergmed.2015.03.011

Address for correspondence: Ian C. Michelow, Connecticut Children's Medical Center, 85 Seymour St, Ste 816, Hartford, CT 06106, USA; email: imichelow@connecticutchildrens.org; Alicia E. Genisca, 55 Claverick St, 2nd Fl, Providence, RI 02903, USA; email: alicia.genisca@brownphysicians.org

Retrospective Genomic Characterization of a 2017 Dengue Virus Outbreak, Burkina Faso

Andrew G. Letizia,[1] Catherine B. Pratt,[1] Michael R. Wiley, Anne T. Fox, Mba Mosore, Bright Agbodzi, Clara Yeboah, Selassie Kumordjie, Nicholas Di Paola, Kone Cisse Assana, David Coulidiaty, Casimir Ouedraogo, Joseph H. Kofi Bonney, William Ampofo, Zékiba Tarnagda, Lassana Sangaré

Knowledge of contemporary genetic composition of dengue virus (DENV) in Africa is lacking. By using next-generation sequencing of samples from the 2017 DENV outbreak in Burkina Faso, we isolated 29 DENV genomes (5 serotype 1, 16 serotype 2 [DENV-2], and 8 serotype 3). Phylogenetic analysis demonstrated the endemic nature of DENV-2 in Burkina Faso. We noted discordant diagnostic results, probably related to genetic divergence between these genomes and the Trioplex PCR. Forward and reverse1 primers had a single mismatch when mapped to the DENV-2 genomes, probably explaining the insensitivity of the molecular test. Although we observed considerable homogeneity between the Dengvaxia and TetraVax-DV-TV003 vaccine strains as well as B cell epitopes compared with these genomes, we noted unique divergence. Continual surveillance of dengue virus in Africa is needed to clarify the ongoing novel evolutionary dynamics of circulating virus populations and support the development of effective diagnostic, therapeutic, and preventive countermeasures.

Dengue virus (DENV), the causative agent of dengue fever, is a mosquitoborne single-stranded RNA virus from the genus *Flavivirus*, often defined as 4 related serotypes (DENV-1, DENV-2, DENV-3, and DENV-4) (*1*). Globally, ≈4 billion persons in 128 countries are at risk for dengue fever (*2*). An estimated 390 million infections occur annually, of which 96 million are symptomatic (*3*), making DENV the most prevalent and rapidly spreading mosquitoborne viral disease of human beings (*4*). Clinical manifestations vary from a self-limited, potentially debilitating illness to hypovolemic shock; the mortality rate can be as high as 20% if left untreated (*4*).

An estimated 750 million persons are at risk for acquiring DENV in Africa, and the disease burden is estimated to be nearly equivalent to that of the Americas (*3*,*5*). Many countries in Africa lack a national surveillance system and reporting mechanism (*6*), causing dengue fever cases to be misdiagnosed as malaria (*7*), which might explain why among the 34 countries in Africa to report dengue fever, 12 were not reported by the country where it occurred but by travelers returning to their country of origin (*8*). Travel, particularly to Africa, is emerging as a well-recognized mechanism of intercontinental DENV spread (*9*,*10*).

Less than 1% of all global DENV envelope sequence data, key information for vaccine targets, come from isolates from Africa (*11*). A need exists for additional DENV sequencing, especially in Africa (*12*,*13*). The lack of genomic DENV data from Africa combined with complex transmission dynamics involving urban and sylvatic cycles impairs our understanding of DENV's evolutionary history, transmission and spread (*13*), molecular diagnostics (*14*), antiviral targets (*15*), vector susceptibility (*16*), human immune response (*17*), vaccine development (*17*), and DENV spillover events (*18*). Determining which contemporary genotypes are in circulation is crucial to ensuring effective diagnostics and developing preventive and therapeutic countermeasures (*19*).

Author affiliations: Naval Medical Research Unit TWO, Singapore (A.G. Letizia); University of Nebraska Medical Center, Omaha, Nebraska, USA (C.B. Pratt, M.R. Wiley); Naval Medical Research Unit THREE, Ghana Detachment, Accra, Ghana (A.T. Fox); Noguchi Memorial Institute for Medical Research, Accra (M. Mosore, B. Agbodzi, C. Yeboah, S. Kumordjie, J.H.K. Bonney, W. Ampofo); US Army Medical Research Institute of Infectious Disease, Frederick, Maryland, USA (N. Di Paola); Institut de Recherche en Sciences de la Santé, Bobo-Dioulasso, Burkina Faso (K.C. Assana, Z. Tarnagda); Centre Hospitalier Universitaire Yalgado Ouédraogo, Ouagadougou, Burkina Faso (D. Coulidiaty, C. Ouedraogo, L. Sangaré)

DOI: https://doi.org/10.3201/eid2806.212491

[1]These first authors contributed equally to this article.

Burkina Faso, a country in West Africa with a population of ≈21 million persons, has had documented dengue fever outbreaks since 1925; known subsequent outbreaks occurred in 1982 and 2013 (*20*). In 2016, the World Health Organization declared an outbreak identifying 1,061 probable cases, primarily in the capital of Ouagadougou, population ≈2.5 million persons, in a setting of minimal surveillance and limited diagnostic ability (*21*). A larger outbreak, primarily in the central region that includes Ouagadougou, but involving all 13 health regions, occurred during August–November 2017, when Burkina Faso reported 9,029 suspected cases (*22*). Previous serotyping was conducted on 72 samples and demonstrated DENV-2 (58 cases), DENV-3 (12 cases), and DENV-1 (2 cases) (*23*); co-circulation of 3 serotypes occurred in Ouagadougou. The only published DENV genomes from either of these outbreaks were serotype 2, genotype Cosmopolitan, occurring after exposure during the 2016 outbreak among travelers returning to Japan and France (*24*,*25*).

By using in silico analyses, we determined whether unique DENV molecular divergence is occurring in Burkina Faso and assessed its impact on diagnostic assays and potential efficacy of vaccines and therapeutics. We sequenced DENV genomes from the 2017 outbreak in Burkina Faso to determine the molecular epidemiology of DENV and assess the homogeneity with targets for the US Centers for Disease Control and Prevention (CDC) Trioplex real-time reverse transcription PCR (RT-PCR), Dengvaxia (Sanofi Pasteur (https://www.sanofi.com) and TetraVax-DV-TV003 (Butantan Institute (http://butantan.gov.br) vaccine strains, and DENV antiviral epitopes.

Methods

Sample Processing and Sequencing

We obtained 791 deidentified human serum samples from patients with illness meeting the World Health Organization's clinical case definition of dengue fever during the 2017 DENV outbreak in Burkina Faso (Appendix Table 1, https://wwwnc.cdc.gov/EID/article/28/6/21-2491-App1.pdf). Samples were provided by the Institut de Recherche en Sciences de la Santé (IRSS) in Bobo-Dioulasso and Centre Hospitalier Universitaire Yalgado Ouédraogo in Ouagadougou. We processed the samples at Noguchi Memorial Institute of Medical Research in Accra, Ghana.

We tested each sample by using molecular and serologic techniques, and if any test consistent with acute infection was positive, we selected that sample for genome sequencing (Appendix Figure 1). We conducted molecular-based evaluation for DENV by using the CDC Trioplex assay after extraction with QIAamp viral RNA mini kits (QIAGEN, https://www.qiagen.com) according to the manufacturer's instructions. Serologic analyses included the detection of nonstructural protein 1 (NS1) antigen, DENV IgM, and DENV IgG (SD Bioline Dengue Duo; Abbott, https://www.globalpointofcare.abbott). We sequenced samples on an Illumina MiSeq (https://www.illumina.com) by using an enrichment-based method, as previously described, with modifications to enrich DENV (Appendix).

Phylogenetics and Molecular Clock Analysis

To determine specific DENV genotypes, we aligned the Burkina Faso genomes with all complete genomes obtained from the US National Institutes of Health National Institute of Allergy and Infectious Diseases Virus Pathogen Database and Analysis Resource (http://www.viprbrc.org) and inferred a phylogenetic tree by using FastTree 2.1 (https://bioweb.pasteur.fr/packages/pack@FastTree@2.1.10). For our large-scale phylodynamics analysis, we retained all genomes from Africa and randomly subsampled ≈10% of the remaining genomes. We estimated time-calibrated phylogenies with the Markov chain Monte Carlo method implemented in BEAST 1.10.4 (https://beast.community) (Appendix).

Evaluation of PCR Diagnostics

We mapped primers and probe for the CDC Trioplex assay (patent no. WO2018169550A1), CDC DENV-1–4 RT-PCR (*26*), and Johnson et al. DENV RT-PCR (*27*) to the 29 Burkina Faso genomes in Geneious Prime 2021.0.3 (https://www.geneious.com). We then calculated mismatches within the primer–probe binding sites.

We further mapped the Trioplex forward primer, reverse1 primer, and probe sequences to an alignment of all available DENV genomes. We trimmed alignments to each primer–probe region and calculated the number of mismatches. We retained sequences with country information and calculated the proportion of genomes from each country with ≥1 mismatches. We represented these proportions in a chloropleth map by using ArcGIS Pro 2.8.0 (https://pro.arcgis.com).

Vaccine and Epitope Analysis

We compared our Burkina Faso genomes to the Dengvaxia and TetraVax-DV-TV003 vaccine strains through sequence alignment in Geneious Prime 2021.0.3 by using MAFFT 7.427 (https://mafft.cbrc.jp/alignment/software). We were unable to obtain

genome sequences of the TAK-003 dengue vaccine (Takeda, https://www.takeda.com). For the continental comparison, we downloaded all available DENV genomes from the Virus Pathogen Database and Analysis Resource and grouped them by serotype. We aligned the downloaded genomes to the vaccine strains with MAFFT and trimmed them to the membrane precursor (prM) and envelope (E) gene regions; we then retained and translated all genomes with country of origin. We assigned each represented country to a continent and calculated the proportion of sequences with divergent amino acids compared with the vaccines within each continental alignment.

We performed epitope mapping to compare the amino acid diversity of DENV strains from the 2017 outbreak in Burkina Faso to relevant epitopes that could serve as targets for antiviral human monoclonal antibodies. Appropriate epitopes for DENV-1–3 serotypes have been identified previously; we used an approach previously described comparing those amino acid targets and vaccine components to genomes from Burkina Faso (*28*) (Appendix).

Data Availability

We submitted the consensus sequences that we generated from our Burkina Faso samples to GenBank (accession nos. MT261951–79). Probe sequences used during sequencing, nucleotide and amino acid alignments, and the .xml files are available online (https://github.com/cathrnbp/paper-dengue-2021).

Ethics Considerations

The study protocol was approved by the Naval Medical Research Center's Institutional Review Board (project no. NAMRU3.2018.0001). The study was in compliance with all applicable federal regulations governing the protection of human subjects.

Results

Dengue Virus Diversity in Burkina Faso

Only 31 of the 791 samples had a measurable cycle threshold (Ct), and 20 of these met the criteria to be considered positive for the Trioplex assay (Appendix Table 1). Subsequent serologic tests detected NS1 antigen in 44 samples, DENV IgM in 18 samples, and DENV IgG in 27 samples, resulting in a total of 86 samples positive by PCR, NS1 antigen test, IgM test, or all 3 tests; many samples were positive by >1 test (Appendix Table, Figure 1).

We excluded samples positive only for DENV IgG. In total, we describe 29 DENV genomes with >85% coverage from 65 sequenced samples (Table). Genomic analysis confirmed the presence of serotypes 1–3; we identified no mixed serotype infections. To place these 29 genomes in context, we inferred maximum-likelihood and molecular-clock phylogenies for each serotype. Phylogenetic analysis of the genomes classified them into a single genotype for each serotype (Figure 1).

We sequenced 5 DENV-1 genotype V, 16 DENV-2 Cosmopolitan, and 8 DENV-3 genotype III genomes. The DENV-1 genomes grouped closely with a traveler from France returning from Benin in 2019 (GenBank accession no. MN600714) (*29*) and the DENV-2 genomes with a traveler returning to France from Burkina Faso in 2016 (GenBank accession nos. KY627762/3). The DENV-1 genomes have a most recent common ancestor (MRCA) from July 2016 (95% highest posterior density [HPD] 2016.1–2016.9) (Figure 2) and form a monophyletic clade with other genomes from West Africa sampled during 2015–2019, having a common ancestor from September 2014 (95% HPD 2014.0–2015.3). Our analysis of all complete Africa DENV-1 genomes indicates multiple separate introductions into Africa, followed by localized spread (Figure 2). DENV-1 may have been introduced into West Africa as early as 2010 (95% HPD 2009.9–2011.4), probably from Asia. The phylogenetic tree inferred from all E gene sequences corroborates this conclusion (Appendix Figure 2).

Our DENV-2 genomes form several clusters across a monophyletic Africa clade with a MRCA from May 2015 (95% HPD 2014.8–2015.9) (Figure 3). DENV-2 genomes in this clade have been sequenced from countries across West Africa, and available data suggest the 2017 Burkina Faso variant was probably exported to China (Figure 3), demonstrating the movement of DENV from Africa to Asia. In contrast to DENV-1, DENV-2 genomes share a common ancestor with other genomes from Burkina Faso collected as far back as 1983. The MRCA of the entire monophyletic Africa clade, including 2 outlying genomes from Kenya, was from May 1978 (95% HPD 1975.3–1981.1). The long branch from the early 1980s to 2015 is probably the result of undersampling rather than the absence of human DENV-2 cases. To ensure this long branch was not a result of excluded sequencing data in our complete genome analysis, we inferred phylogenetic trees from all E gene sequences from partial and complete genomes (Appendix Figure 3). We identified partial genomes from an additional 9 Africa countries that clustered within the same clade as these Burkina Faso genomes; only genomes sampled from Indonesia in the 1970s were antecedent. These

data demonstrate that DENV-2 has been circulating across Africa since the late 1970s, when it was probably introduced from Southeast Asia.

The molecular-clock phylogeny for DENV-3 genomes from Burkina Faso cluster into 2 distinct clades within a monophyletic Africa clade (Figure 4). The MRCA for the DENV-3 Burkina Faso clade was from January 2013 (95% HPD 2010.8–2014.9) and the MRCA of all Africa genomes from March 2006 (95% HPD 2004.0–2008.1); these genomes were probably introduced from Asia. When including all E gene genomes in a phylogenetic analysis, we see introductions to 8 additional countries in Africa (Appendix Figure 4). These results provide evidence of widespread dengue virus circulation within Africa with DENV-1 existing for >7 years, DENV-2 for >39 years, and DENV-3 for >11 years.

Trioplex Assay in Africa

Although only 31 of the 791 samples we tested were positive by the Trioplex assay, after sequencing we unexpectedly gained complete genomes from 3 samples that were negative by PCR, indicating concerns with PCR sensitivity. The median Trioplex assay Ct value for DENV-1 genomes was 29.5, for DENV-2 was 37.9, and DENV-3 25.3 (Appendix Figure 5), suggesting that the Trioplex assay was less sensitive against DENV-2 than DENV-1 and DENV-3. This finding is corroborated by the limits of detection reported in the Trioplex package insert, which are stated as 5.82×10^4

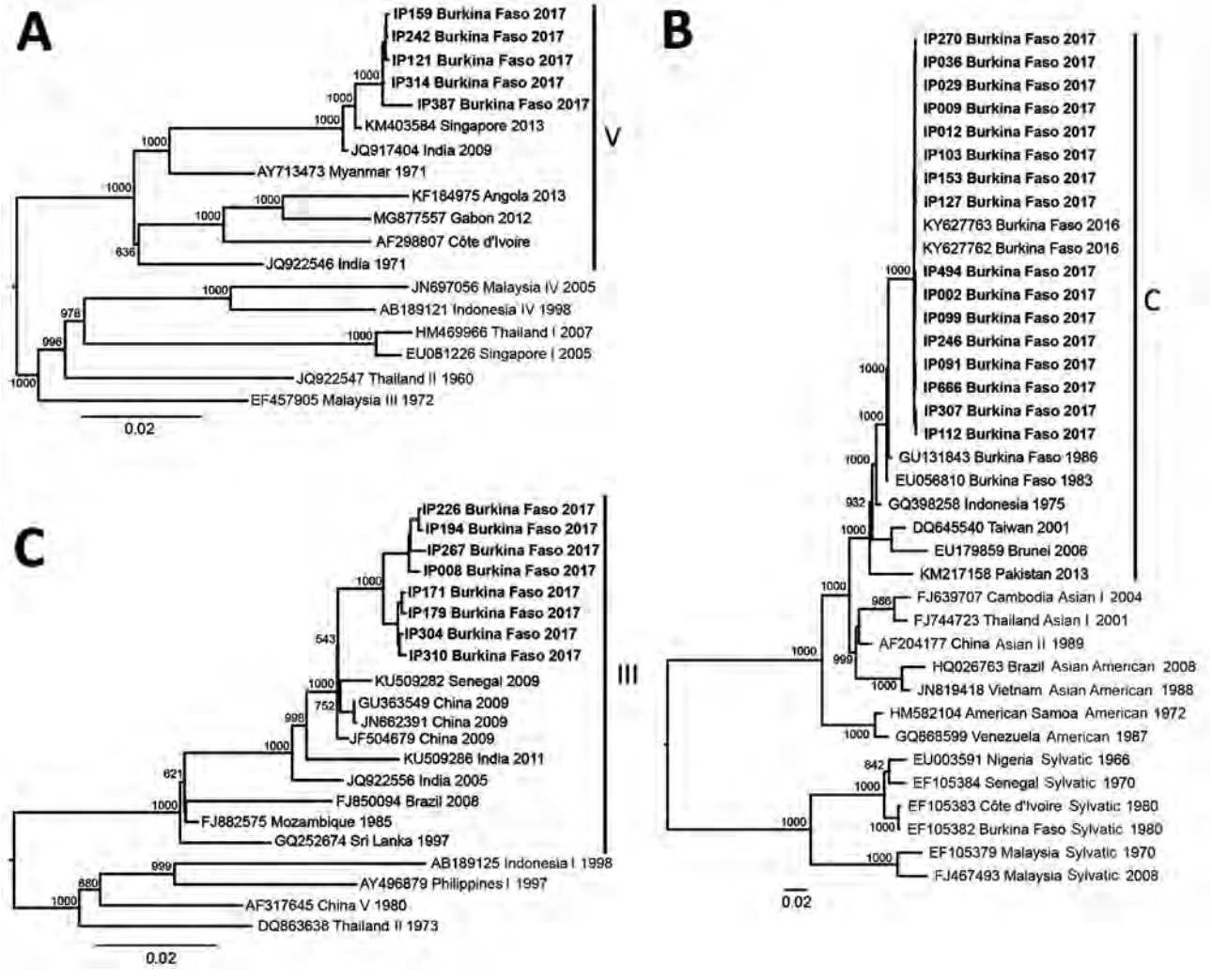

Figure 1. Phylogenetic trees of dengue virus (DENV) serotypes 1 (A), 2 (B), and 3 (C), inferred from an alignment of the 2017 Burkina Faso dengue virus outbreak genomes (boldface) and all other complete genomes from US National Institutes of Health National Institute of Allergy and Infectious Diseases Virus Pathogen Database and Analysis Resource (http://www.viprbrc.org) and pruned to representative genotypes. The Burkina Faso genomes were DENV-1 genotype V, DENV-2 genotype Cosmopolitan, and DENV-3 genotype III. GenBank accession numbers are provided for reference genomes.

Table. Suspected dengue virus–positive samples from the 2017 Burkina Faso dengue virus outbreak, found to be positive by CDC Trioplex real-time RT-PCR or serologic testing, and sequencing results for samples that generated genomes with >85% coverage*

NMIMR laboratory ID	Specimen collection date, 2017	PCR results, Ct	Serologic results			Sequencing results		
			NS1 Ag	IgM	IgG	Serotype	Genome coverage, %	GenBank accession no.
IP-002	Oct 16	UND	+	–	–	DENV-2	99.6	MT261956
IP-008	Oct 16	35.5	+	–	–	DENV-3	99.1	MT261972
IP-009	Oct 16	37.1	+	–	–	DENV-2	99.7	MT261957
IP-012	Oct 16	40.6	+	–	–	DENV-2	87.6	MT261958
IP-029	Oct 17	37.5	+	–	–	DENV-2	98.8	MT261959
IP-036	Oct 17	40.6	+	–	–	DENV-2	99.5	MT261960
IP-091	Oct 26	36	+	–	–	DENV-2	99.8	MT261961
IP-099	Oct 25	40.3	+	–	–	DENV-2	99.6	MT261962
IP-103	Oct 25	34.6	+	–	–	DENV-2	99.7	MT261963
IP-112	Oct 24	39.5	+	–	–	DENV-2	99.7	MT261964
IP-121	Oct 23	29	+	–	–	DENV-1	99.7	MT261951
IP-127	Oct 23	38.2	–	–	–	DENV-2	99.4	MT261965
IP-153	Nov 8	33.7	+	–	–	DENV-2	99.8	MT261966
IP-159	Nov 9	32	+	–	–	DENV-1	99.3	MT261952
IP-171	Nov 9	33.8	+	+	+	DENV-3	94.3	MT261973
IP-179	Nov 13	22.5	+	–	–	DENV-3	94.4	MT261974
IP-194	Nov 17	25.2	–	–	–	DENV-3	99.7	MT261975
IP-226	Oct 4	25.4	–	–	–	DENV-3	99.8	MT261976
IP-242	Oct 9	29.5	–	–	–	DENV-1	99.6	MT261953
IP-246	Oct 9	31.1	–	–	–	DENV-2	99.8	MT261967
IP-267	Oct 12	19.3	–	–	–	DENV-3	99.8	MT261977
IP-270	Oct 12	37.1	–	–	–	DENV-2	99.5	MT261968
IP-304	Oct 27	24.1	+	–	–	DENV-3	99.7	MT261978
IP-307	Oct 30	37.3	–	–	–	DENV-2	99.7	MT261969
IP-310	Nov 2	30.3	+	–	+	DENV-3	95.7	MT261979
IP-314	Nov 2	23.8	+	–	–	DENV-1	99.7	MT261954
IP 387	Dec 12	UND	+	–	–	DENV-1	88.4	MT261955
IP 494	Nov 3	41.2	+	–	–	DENV-2	99.6	MT261970
IP 666	Nov 6	UND	+	–	–	DENV-2	99.6	MT261971

*CDC, US Centers for Disease Control Prevention; Ct, cycle threshold; NMIMR, Noguchi Memorial Institute for Medical Research; NS1 Ag, nonstructural protein 1 antigen; RT-PCR, reverse transcription PCR; UND, undetected; +, positive; –, negative.

genome copies/mL for DENV-1, 8.25×10^4 genome copies/mL for DENV-2, and 4.36×10^4 genome copies/mL for DENV-3.

In addition, we performed an in silico analysis of these assays by mapping the primers and probe to the Burkina Faso genomes and comparing nucleotide homogeneity. The Trioplex primers and probe were identical to the DENV-1 and DENV-3 Burkina Faso genomes, but both the forward and reverse1 primers had a single mismatch when mapped to the DENV-2 genomes. We also investigated the CDC DENV-1–4 RT-PCR (*26*), which had 5 mismatches across the primers and probe for the DENV-1, DENV-2, and DENV-3, and the Johnson et al. RT-PCR (*27*), which had 8 mismatches (Appendix Figure 6).

To determine if these mismatches were specific to Burkina Faso or indicated a more global problem, we mapped the Trioplex primers and probe to all available DENV genomes and calculated the proportion of genomes from each country that exhibited <100% homogeneity to the primers and probe (i.e., had ≥1 mismatch) (Figure 5). Because the Trioplex assay targets the 5′ untranslated region and many genomes lacked coverage in this region, especially for the forward primer, they could not be included. For DENV-1 and DENV-3, we observed almost complete homogeneity between the probe and reverse1 primer within all countries. The forward primer was similarly identical, except for some divergence in Asia and North America. Conversely, for DENV-2, although the probe sequence was almost completely identical to the DENV-2 genomes at its binding site, the forward primer exhibited a single mismatch in every genome included in our analysis. This mismatch is likely the cause of the lowered limit of detection for DENV-2 compared with DENV-1 and DENV- 3, as noted previously. Approximately 95% of genomes from Africa had ≥1 mismatches in the reverse1 primer (and a mismatch in the forward primer) compared with 6% of genomes from South America, 20% from Oceania, and 50% from Asia (Figure 5).

Dengue Vaccines and African Variants

The 29 full genomes from the Burkina Faso 2017 outbreak were compared with the Dengvaxia and TetraVax-DV-TV003 vaccine strains for each serotype (Figure 6). Dengvaxia is based on an immunoprotective serotype-specific prM and E gene region in a

background of yellow fever virus while TetraVax-DV-TV003 uses a different dengue virus serotype. Therefore, the comparison with the full genome sequences focused on the prM and E proteins. Divergent amino acids occurred throughout the prM and E proteins between the vaccine strain and Burkina Faso wild types,

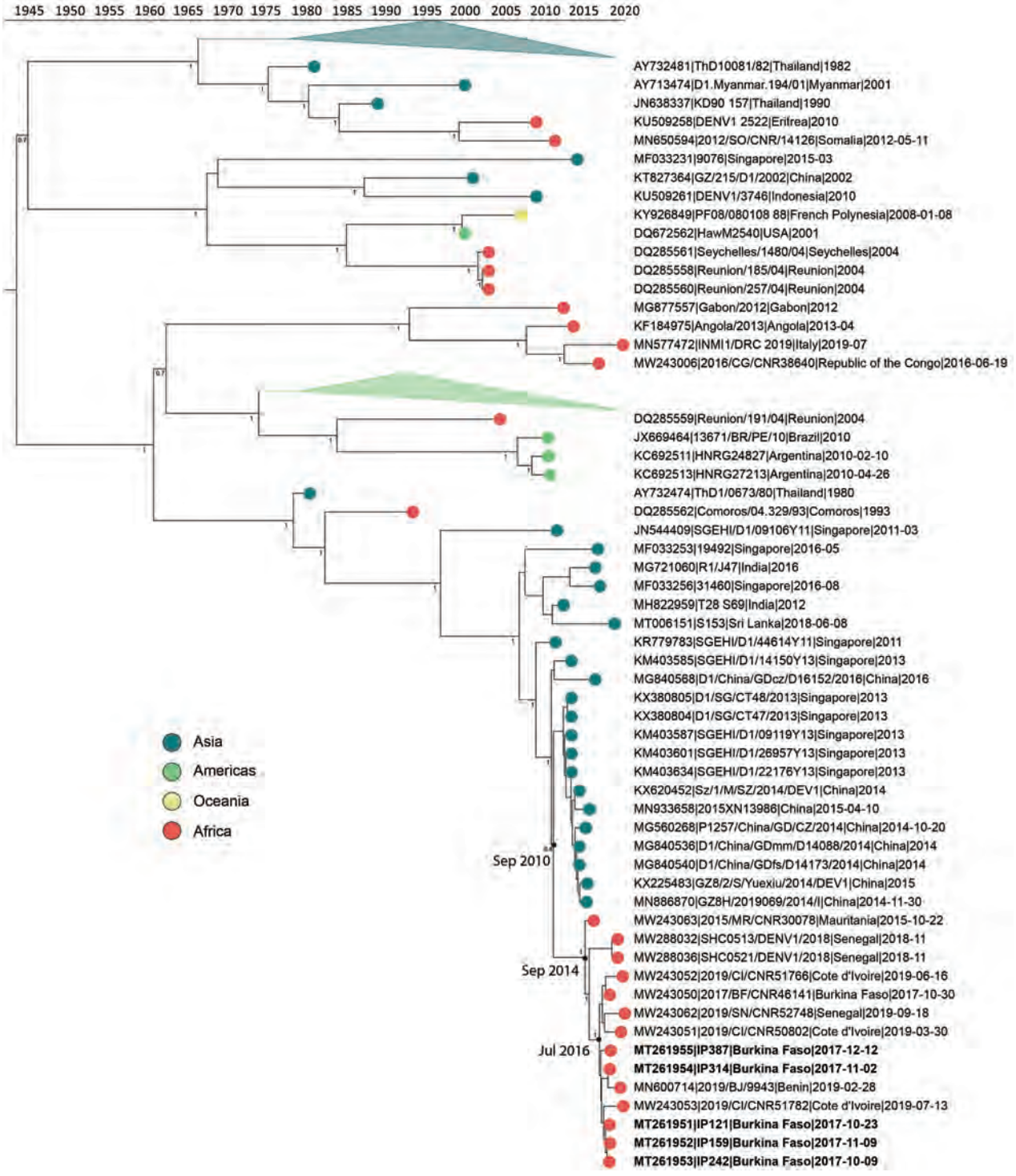

Figure 2. Time-calibrated phylogenetic trees of a subset of global dengue virus 1 genomes and 2017 Burkina Faso dengue virus outbreak genomes (boldface). Colored circles indicate geographic origin. Dates indicate the most recent common ancestor for the 2017 Burkina Faso dengue virus outbreak and all genomes from Africa. Posterior probabilities are indicated at major nodes. GenBank accession numbers are provided for reference genomes.

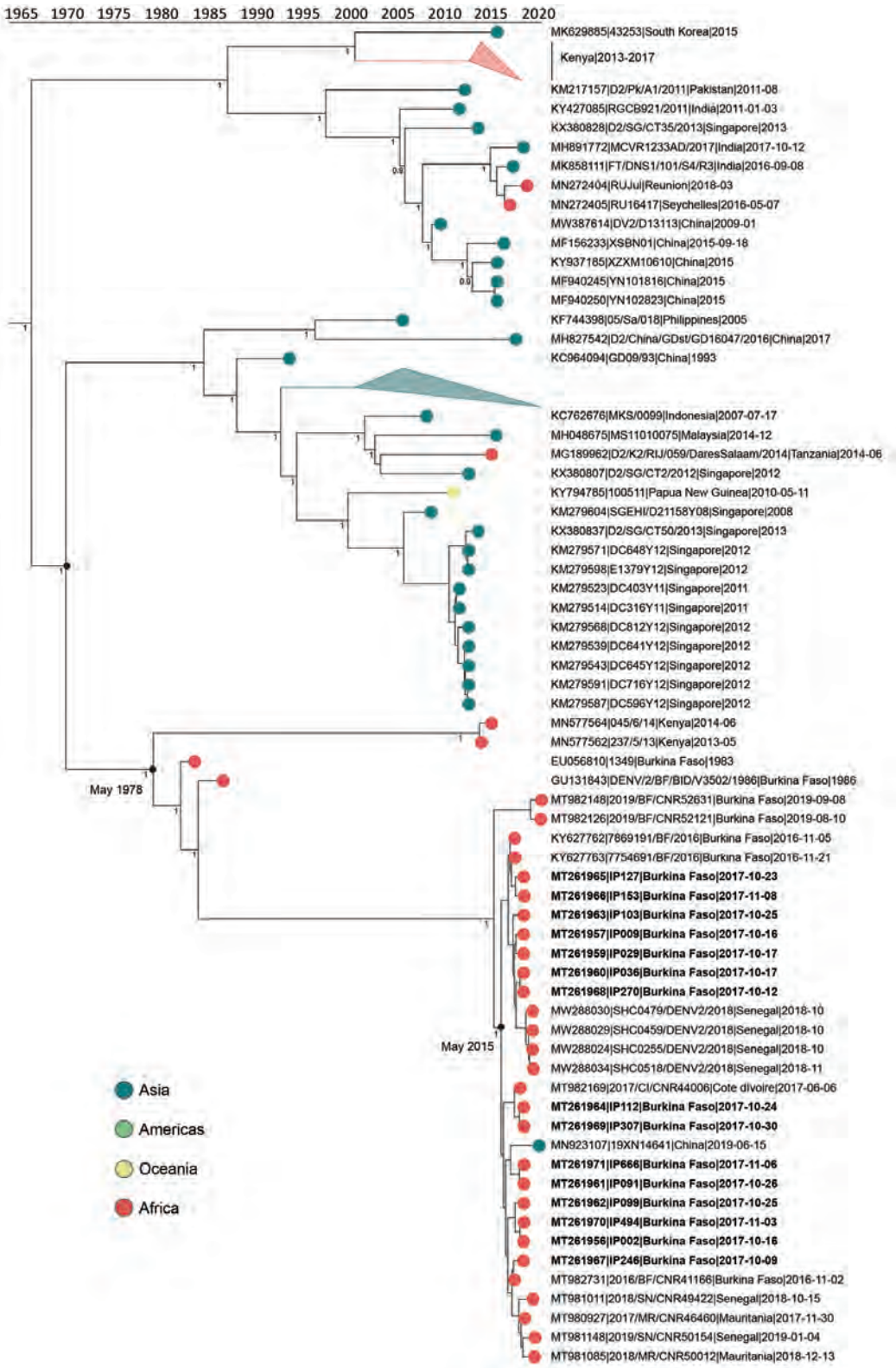

Figure 3. Time-calibrated phylogenetic trees of a subset of global dengue virus 2 genomes and 2017 Burkina Faso dengue virus outbreak genomes (boldface). Colored circles indicate geographic origin. Dates indicate the most recent common ancestor for the 2017 Burkina Faso dengue virus outbreak and all genomes from Africa. Posterior probabilities are indicated at major nodes. GenBank accession numbers are provided for reference genomes.

including 20 substitutions for DENV-1 sequences, 18 for DENV-2, and 17 for DENV-3 when compared with the Dengvaxia vaccine and 18 substitutions for DENV-1, 25 for DENV-2, and 19 for DENV-3 when compared with the TetraVax-DV-TV003 vaccine. None of the discordant amino acids clustered to any particular structural domain.

We compared the Burkina Faso wild type virus sequences with the vaccine strains at 8 B cell epitopes (Figure 7). The noted divergence is similar to that

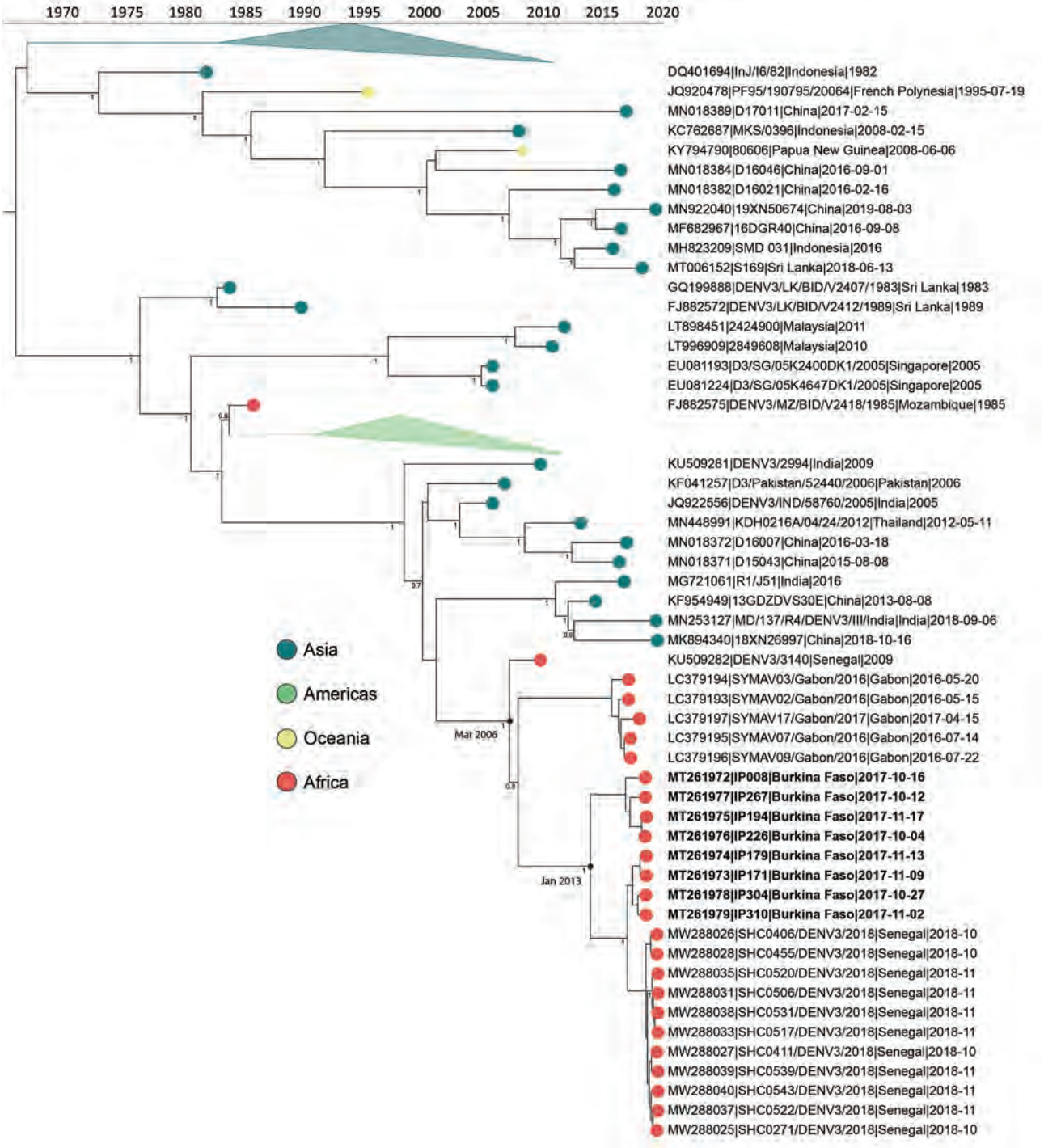

Figure 4. Time-calibrated phylogenetic trees of a subset of global dengue virus 3 genomes and 2017 Burkina Faso dengue virus outbreak genomes indicated (boldface). Colored circles indicate geographic origin. Dates indicate the most recent common ancestor for the 2017 Burkina Faso dengue virus outbreak and all genomes from Africa. Posterior probabilities are indicated at major nodes. GenBank accession numbers are provided for reference genomes.

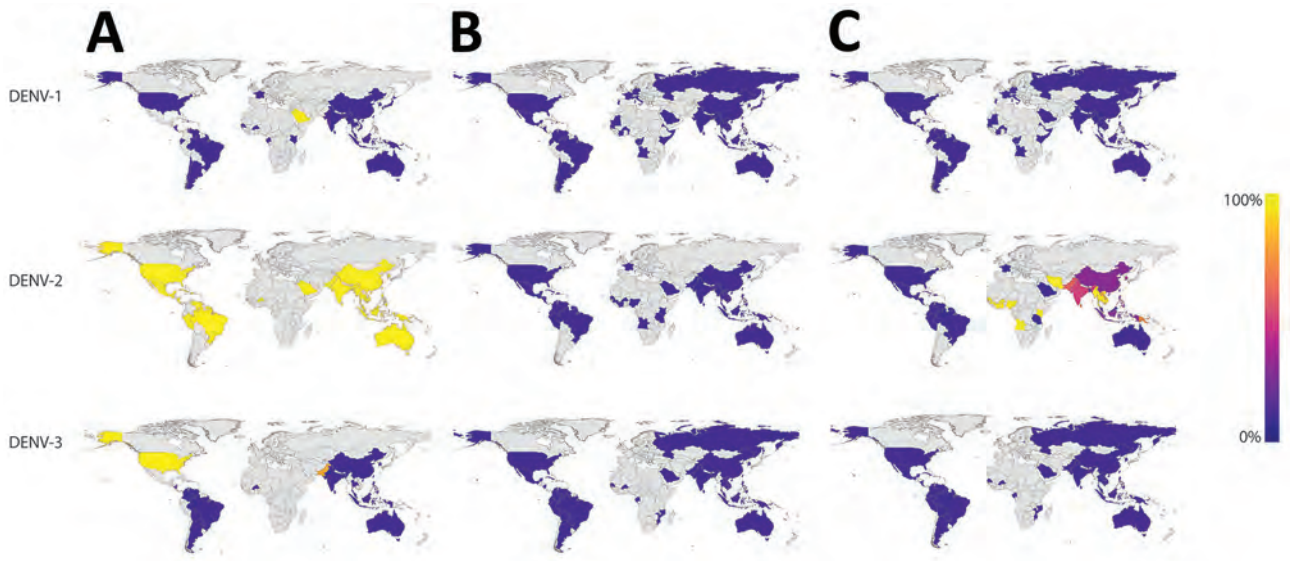

Figure 5. Nucleotide identity between dengue virus molecular diagnostics and all sequenced DENV genomes from the 2017 Burkina Faso dengue outbreak. The map indicates the proportion of genomes from each country with ≥1 mismatches against the Trioplex PCR forward primer (A), probe (B), and reverse1 primer (C). Countries in gray have no data. DENV-1 and DENV-3 have concordant nucleotide identity to the primers and probe, but most DENV-2 forward primer and reverse1 primer in sequences from Africa have a high proportion of genomes with ≥1 mismatches to the Trioplex PCR's primers and probe. DENV-1, dengue virus serotype 1; DENV-2, dengue virus serotype 2; DENV-3, dengue virus serotype 3

seen in Southeast Asia and the Americas and has been previously described at E protein sites 155, 161, and 171 for DENV-1; sites 71 and 149 for DENV-2; and site 124 for DENV-3 (*28*).

Because of the paucity of genomic data from Burkina Faso, we expanded our analysis to the continental scale. We calculated the proportion of genomes within each continental alignment diverging from the vaccine sequence at each amino acid position. Amino acid positions with >5% divergence from the Dengvaxia (Appendix Figure 7) and TetraVax-DV-TV003 (Appendix Figure 8) vaccine strains were retained. In a minimum of 12 amino acid positions across each serotype and vaccine comparison, DENV genomes from Africa had the greatest proportion of genomes divergent from the vaccine strains. DENV genomes circulating in Africa exhibit their own genomic diversity, impairing the potential effectiveness of a DENV vaccine on that continent.

Discussion

We sequenced 29 full DENV genomes from the 2017 outbreak in Burkina Faso, confirming cocirculation of DENV-1, DENV-2, and DENV-3 serotypes. Phylogenetic analysis of DENV-2 genomes show the most similar genomes to those from the DENV 2017 outbreak are also from Burkina Faso, dating from 1983 through 1986. The genetic similarities between DENV-2 strains from 2017 and those from >30 years ago suggest local circulation of DENV-2 genotype Cosmopolitan both within Burkina Faso and in other countries in West Africa and that DENV-2 is endemic to this area. All the genomes from the 2017 outbreak in Burkina Faso were most closely related to strains from Africa or Asia and not those from the Americas. This finding could be attributable to greater trade, travel, and economic-based contact between Burkina Faso and other countries of Africa with Asia as opposed to countries in the Americas.

We obtained 2 complete genomes and 1 partial genome from PCR-negative samples, and the Ct for DENV-2 samples was consistently higher than that for DENV-1 and DENV-3, suggesting a drop in assay sensitivity against DENV-2 genomes. This decrease is probably because of mismatches between the primers and probe and target sequences, or because the samples were too degraded for PCR but not for hybrid capture sequencing, which seems unlikely. An in silico analysis identified mismatches between the primers and probe for the Trioplex assay and DENV-2 genomes, both in our Burkina Faso genomes and across Africa. The Trioplex assay was designed during the 2015–2016 Zika virus epidemic to differentiate between Zika, chikungunya, and DENV infections and has also been made available to international laboratories in a lyophilized format at no charge (*30*). This altruism means that it is a commonly used assay in low-resource laboratories, such as those in many

countries in Africa. The Trioplex assay was validated by using samples collected in Puerto Rico (*30*). In our analyses, genomes from the Americas were most congruent with the Trioplex primers and probe and those from Africa were the least congruent. Further, the target of the Trioplex assay is near the 5′ untranslated region and vulnerable to degradation, which is more likely to occur in low-resource countries, where samples are often transported to a central laboratory under less than ideal conditions for RNA preservation. The CDC developed another PCR with serotype-specific primers and probe, the CDC-DENV-1–4 RT-PCR (*26*), based on the Johnson et al. RT-PCR (*27*), but both of these assays exhibited even less nucleotide homogeneity in silico than the Trioplex assay. The observed genomic divergence, discordance between sequencing and PCR results, and existence of multiple mismatches in the primer binding site within samples from Africa suggest that Africa-specific virus evolution is occurring, probably leading to an underreporting of dengue cases because of insensitive diagnostics. This probability necessitates the development of diagnostics that account for the unique molecular divergence occurring in Africa to have an accurate assessment of the disease burden of DENV and improve patient care.

Because of the threat that DENV poses to Africa, the number of outbreaks, and the lack of countermeasures, it is not too early to consider preventive measures. The Burkina Faso genomes enabled us to perform in silico analyses of DENV vaccine efficacy and assess divergence from known important epitopes. In general, the 3 DENV serotypes circulating during the 2017 outbreak in Burkina Faso were very similar to the vaccine strains used in the CYD- Dengvaxia and TetraVax-DV-TV003 vaccines.

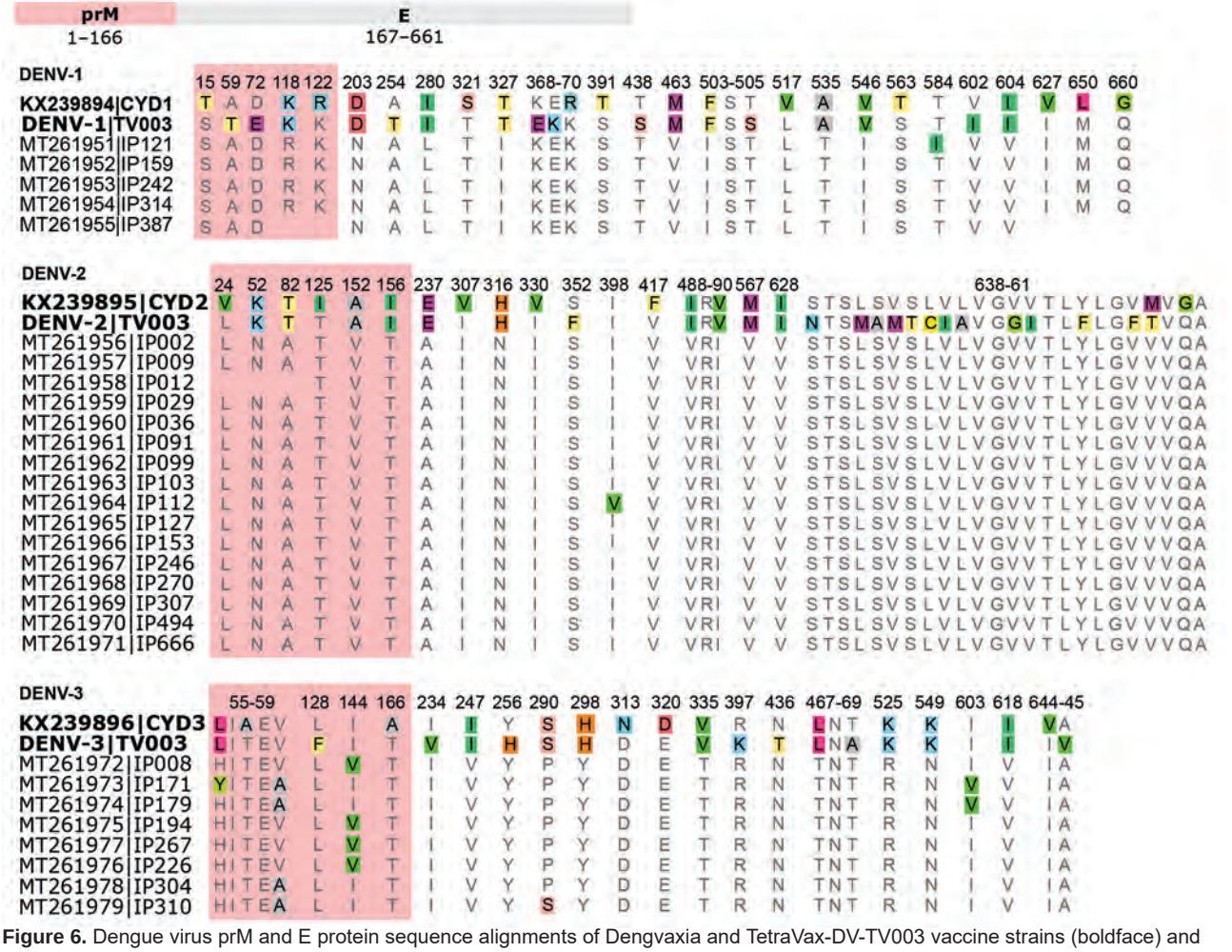

Figure 6. Dengue virus prM and E protein sequence alignments of Dengvaxia and TetraVax-DV-TV003 vaccine strains (boldface) and 2017 Burkina Faso dengue virus outbreak genomes for serotypes 1, 2, and 3. Only amino acid positions with disagreements are shown; single-point disagreements are highlighted. For clarity, prM protein sequences are shaded in red. Numerals represent the prM and E protein amino acid position. CYD, Dengvaxia vaccine; DENV-1, dengue virus serotype 1; DENV-2, dengue virus serotype 2; DENV-3, dengue virus serotype 3; E, envelope; prM, premembrane; TV003, TetraVax-DV-TV003 vaccine.

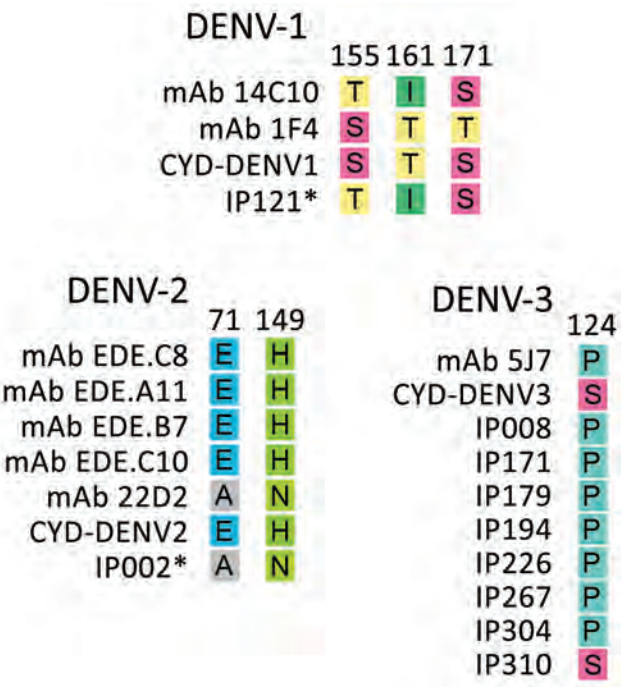

Figure 7. Amino acid mismatch comparison between 2017 Burkina Faso dengue virus outbreak genomes and virus neutralizing human mAbs for the 3 dengue virus serotypes. The amino acid changes presented are expected to disrupt binding between the envelope protein and heavy chain of the monoclonal antibodies. Dengvaxia vaccine amino acid included for comparison. Asterisk indicates all of the 2017 Burkina Faso dengue virus outbreak genomes share the same amino acid at that position. Numerals represent the E protein amino acid position. CYD, Dengvaxia vaccine; DENV-1, dengue virus serotype 1; DENV-2, dengue virus serotype 2; DENV-3, dengue virus serotype 3; E, envelope; mAb, monoclonal antibody.

Although the Dengvaxia vaccine was noted to have decreased efficacy against DENV-2 compared with other serotypes (*31*), it appears to have been more efficacious against the DENV-2 Cosmopolitan genotype than against the Asian 1 genotype (*28*). However, there were key positions in the Dengvaxia and TetraVax-DV-TV003 vaccine sequences where genomes from Africa diverged more often than genomes from other continents, indicating the development of unique diversity within Africa. Further research is needed to understand how various genotypes and subtle differences at the amino acid level of prM and E proteins affect clinical immunity. Additional in vivo testing is necessary to determine if a dengue vaccine could be used in West Africa.

The amino acid prM and E protein sequences from the Burkina Faso DENV outbreak were also very similar to known targets for B cell epitopes. The differences noted have been previously reported in DENV strains from the Americas and Southeast Asia (*28*). However, we observed 2 mismatches at important epitope sites E71 and E149 among all DENV-2 Cosmopolitan samples. Although this discordance is documented in other DENV-2 genotypes, including American, American-Asian, Asian 1, and Asian II genotypes, it is not as well defined in the Cosmopolitan genotype.

A limitation of our study is that ≥1 year had passed since the initial collection of the samples before next-generation sequencing was performed, introducing multiple factors that could have contributed to this low percentage of positive results: sample degradation over time, less than ideal storage, low viremia, poor coverage of the assay, or a combination of these factors. Using further molecular diagnostics may have revealed more DENV-positive samples but were not available in the country at the time of the study. Additional genomes could have increased the probability of detecting unusual genomes or amino acid changes. Assessing the evolutionary patterns of DENV is difficult because so few whole DENV genomes from Africa are available on GenBank to compare with the genomes from Burkina Faso. Finally, donor virus strains other than Dengvaxia and TetraVax-DV-TV003 were not assessed.

Our assessment of DENV whole genomes from Burkina Faso provide information on the molecular epidemiology of this virus and divergence from diagnostics, vaccine strains, and B cell epitopes. Further surveillance of contemporary DENV genotypes in Africa is needed to address the contemporary antigenic and genetic variations within a region. The endemicity of DENV and increasing number of outbreaks in countries like Burkina Faso suggest the need for the development of diagnostics that account for ongoing viral evolution in Africa and consideration for adding countries in Africa to DENV clinical trials to address the emerging public health threat.

Acknowledgments

We thank Steve Whitehead for sharing TetraVax-DV-TV003 genome sequences.

This work was funded by the Armed Forces Health Surveillance Branch and its Global Emerging Infections Surveillance and Response Section (work unit no. ProMIS ID P0142_19_N3). The funder played no role in the design of the study, sample collection, analysis and interpretation of results, or manuscript preparation.

Genomes have been submitted to GenBank. Individual participant data beyond what is available in GenBank will not be available.

All authors declare no competing or conflicts of interest. A.L. and N.D. are military service members or government employees. This work was prepared as part of their official duties. Title 17, U.S.C., §105 provides that copyright protection under this title is not available for any work of the US government. Title 17, U.S.C., §101 defines a US government work as a work prepared by a military service member or employee of the US government as part of that person's official duties. The views expressed in the article are those of the authors and do not necessarily express the official policy and position of the US Navy, the US Department of Defense, the US government, or the institutions affiliated with the authors.

About the Author

Dr. Letizia is the science director at the Naval Medical Research Unit TWO in Singapore and is a board-certified infectious disease physician on active duty in the US Navy. His research interest is in emerging infectious diseases, including dengue virus.

References

1. Simmons CP, Farrar JJ, Nguyen VVC, Wills B. Dengue. N Engl J Med. 2012;366:1423–32. https://doi.org/10.1056/NEJMra1110265
2. Brady OJ, Gething PW, Bhatt S, Messina JP, Brownstein JS, Hoen AG, et al. Refining the global spatial limits of dengue virus transmission by evidence-based consensus. PLoS Negl Trop Dis. 2012;6:e1760. https://doi.org/10.1371/journal.pntd.0001760
3. Bhatt S, Gething PW, Brady OJ, Messina JP, Farlow AW, Moyes CL, et al. The global distribution and burden of dengue. Nature. 2013;496:504–7. https://doi.org/10.1038/nature12060
4. Guzman MG, Harris E. Dengue. Lancet. 2015;385:453–65. https://doi.org/10.1016/S0140-6736(14)60572-9
5. Weetman D, Kamgang B, Badolo A, Moyes CL, Shearer FM, Coulibaly M, et al. *Aedes* mosquitoes and *Aedes*-borne arboviruses in Africa: current and future threats. Int J Environ Res Public Health. 2018;15:E220. https://doi.org/10.3390/ijerph15020220
6. Lim JK, Carabali M, Lee JS, Lee KS, Namkung S, Lim SK, et al. Evaluating dengue burden in Africa in passive fever surveillance and seroprevalence studies: protocol of field studies of the Dengue Vaccine Initiative. BMJ Open. 2018;8:e017673. https://doi.org/10.1136/bmjopen-2017-017673
7. Stoler J, Al Dashti R, Anto F, Fobil JN, Awandare GA. Deconstructing "malaria": West Africa as the next front for dengue fever surveillance and control. Acta Trop. 2014;134:58–65. https://doi.org/10.1016/j.actatropica.2014.02.017
8. Fournet F, Rican S, Vaillant Z, Roudot A, Meunier-Nikiema A, Kassié D, et al. The influence of urbanization modes on the spatial circulation of flaviviruses within Ouagadougou (Burkina Faso). Int J Environ Res Public Health. 2016;13:E1226. https://doi.org/10.3390/ijerph13121226
9. Schwartz E, Meltzer E, Mendelson M, Tooke A, Steiner F, Gautret P, et al. Detection on four continents of dengue fever cases related to an ongoing outbreak in Luanda, Angola, March to May 2013. Euro Surveill. 2013;18:20488. https://doi.org/10.2807/ese.18.21.20488-en
10. Toro C, Trevisi P, López-Quintana B, Amor A, Iglesias N, Subirats M, et al. Imported dengue infection in a Spanish hospital with a high proportion of travelers from Africa: a 9-year retrospective study. Am J Trop Med Hyg. 2017;96:701–7. https://doi.org/10.4269/ajtmh.16-0335
11. Pollett S, Melendrez MC, Maljkovic Berry I, Duchêne S, Salje H, Cummings DAT, et al. Understanding dengue virus evolution to support epidemic surveillance and countermeasure development. Infect Genet Evol. 2018;62:279–95. https://doi.org/10.1016/j.meegid.2018.04.032
12. Malisheni M, Khaiboullina SF, Rizvanov AA, Takah N, Murewanhema G, Bates M. Clinical efficacy, safety, and immunogenicity of a live attenuated tetravalent dengue vaccine (CYD-TDV) in children: a systematic review with meta-analysis. Front Immunol. 2017;8:863. https://doi.org/10.3389/fimmu.2017.00863
13. Eltom K, Enan K, El Hussein ARM, Elkhidir IM. Dengue virus infection in sub-Saharan Africa between 2010 and 2020: a systematic review and meta-analysis. Front Cell Infect Microbiol. 2021;11:678945. https://doi.org/10.3389/fcimb.2021.678945
14. Vanneste K, Garlant L, Broeders S, Van Gucht S, Roosens NH. Application of whole genome data for in silico evaluation of primers and probes routinely employed for the detection of viral species by RT-qPCR using dengue virus as a case study. BMC Bioinformatics. 2018;19:312. https://doi.org/10.1186/s12859-018-2313-0
15. Sessions OM, Wilm A, Kamaraj US, Choy MM, Chow A, Chong Y, et al. Analysis of dengue virus genetic diversity during human and mosquito infection reveals genetic constraints. PLoS Negl Trop Dis. 2015;9:e0004044. https://doi.org/10.1371/journal.pntd.0004044
16. Amarasinghe A, Kuritsk JN, Letson GW, Margolis HS. Dengue virus infection in Africa. Emerg Infect Dis. 2011;17:1349–54.
17. Katzelnick LC, Coloma J, Harris E. Dengue: knowledge gaps, unmet needs, and research priorities. Lancet Infect Dis. 2017;17:e88–100. https://doi.org/10.1016/S1473-3099(16)30473-X
18. Holmes EC, Twiddy SS. The origin, emergence and evolutionary genetics of dengue virus. Infect Genet Evol. 2003;3:19–28. https://doi.org/10.1016/S1567-1348(03)00004-2
19. Usme-Ciro JA, Méndez JA, Laiton KD, Páez A. The relevance of dengue virus genotypes surveillance at country level before vaccine approval. Hum Vaccin Immunother. 2014;10:2674–8. https://doi.org/10.4161/hv.29563
20. Gonzalez JP, Du Saussay C, Gautun JC, McCormick JB, Mouchet J. Dengue in Burkina Faso (ex-Upper Volta): seasonal epidemics in the urban area of Ouagadougou [in French]. Bull Soc Pathol Exot. 1985;78:7–14.
21. Tarnagda Z, Cissé A, Bicaba BW, Diagbouga S, Sagna T, Ilboudo AK, et al. Dengue fever in Burkina Faso, 2016. Emerg Infect Dis. 2018;24:170–2. https://doi.org/10.3201/eid2401.170973
22. World Health Organization. Dengue fever—Burkina Faso. 2016 [cited 2021 Aug 25]. https://www.who.int/emergencies/disease-outbreak-news/item/18-november-2016-dengue-burkina-faso-en
23. World Health Organization. Dengue fever—Burkina Faso. 2017 [cited 2021 Aug 25]. https://www.who.int/emergencies/disease-outbreak-news/item/6-november-2017-dengue-burkina-faso-en
24. Hashimoto T, Kutsuna S, Maeki T, Tajima S, Takaya S, Katanami Y, et al. A case of dengue fever imported from

Burkina Faso to Japan in October 2016. Jpn J Infect Dis. 2017;70:675–7. https://doi.org/10.7883/yoken.JJID.2017.181
25. Baronti C, Piorkowski G, Touret F, Charrel R, de Lamballerie X, Nougairede A. Complete coding sequences of two dengue virus type 2 strains isolated from an outbreak in Burkina Faso in 2016. Genome Announc. 2017;5:e00209–17. https://doi.org/10.1128/genomeA.00209-17
26. Santiago GA, Vergne E, Quiles Y, Cosme J, Vazquez J, Medina JF, et al. Analytical and clinical performance of the CDC real time RT-PCR assay for detection and typing of dengue virus. PLoS Negl Trop Dis. 2013;7:e2311. https://doi.org/10.1371/journal.pntd.0002311
27. Johnson BW, Russell BJ, Lanciotti RS. Serotype-specific detection of dengue viruses in a fourplex real-time reverse transcriptase PCR assay. J Clin Microbiol. 2005;43:4977–83. https://doi.org/10.1128/JCM.43.10.4977-4983.2005
28. Rabaa MA, Girerd-Chambaz Y, Duong Thi Hue K, Vu Tuan T, Wills B, Bonaparte M, et al. Genetic epidemiology of dengue viruses in phase III trials of the CYD tetravalent dengue vaccine and implications for efficacy. eLife. 2017;6:e24196. https://doi.org/10.7554/eLife.24196
29. Fourié T, Luciani L, Amrane S, Zandotti C, Leparc-Goffart I, Ninove L, et al. Dengue virus type 1 infection in traveler returning from Benin to France, 2019. Emerg Infect Dis. 2020;26:1946–9. https://doi.org/10.3201/eid2608.200055
30. Santiago GA, Vázquez J, Courtney S, Matías KY, Andersen LE, Colón C, et al. Performance of the Trioplex real-time RT-PCR assay for detection of Zika, dengue, and chikungunya viruses. Nat Commun. 2018;9:1391. https://doi.org/10.1038/s41467-018-03772-1
31. Hadinegoro SR, Arredondo-García JL, Capeding MR, Deseda C, Chotpitayasunondh T, Dietze R, et al.; CYD-TDV Dengue Vaccine Working Group. Efficacy and long-term safety of a dengue vaccine in regions of endemic disease. N Engl J Med. 2015;373:1195–206. https://doi.org/10.1056/NEJMoa1506223

Address for correspondence: Andrew Letizia, PSA Sembawang, Deptford Rd. Building 7-4, 759657, Singapore; email: andrew.g.letizia.mil@mail.mil; Catherine B. Pratt, Rm 4043 Wittson Hall, 984388 Nebraska Medical Center, Omaha, NE 68198-4388, USA; email: catherine.pratt@unmc.edu; Lassana Sangaré, CHU Yalgado Ouédraogo (CHU-YO), 03 BP 7022 Ouagadougou 03, Burkina Faso; email: sangarelassana01@gmail.com

Geographic Origin and Vertical Transmission of *Leishmania infantum* Parasites in Hunting Hounds, United States

Susanne U. Franssen, Mandy J. Sanders, Matt Berriman, Christine A. Petersen,[1] James A. Cotton[1]

Vertical transmission of leishmaniasis is common but is difficult to study against the background of pervasive vector transmission. We present genomic data from dogs in the United States infected with *Leishmania infantum* parasites; these infections have persisted in the apparent absence of vector transmission. We demonstrate that these parasites were introduced from the Old World separately and more recently than *L. infantum* from South America. The parasite population shows unusual genetics consistent with a lack of meiosis: a high level of heterozygous sites shared across all isolates and no decrease in linkage with genomic distance between variants. Our data confirm that this parasite population has been evolving with little or no sexual reproduction. This demonstration of vertical transmission has profound implications for the population genetics of *Leishmania* parasites. When investigating transmission in complex natural settings, considering vertical transmission alongside vector transmission is vital.

Leishmaniasis is a disease caused by obligate intracellular protozoan parasites of the genus *Leishmania*, including *Leishmania infantum* (*1*). Zoonotic visceral leishmaniasis (ZVL) occurs in countries to which the disease is endemic and enzootic in human and animal populations. Dogs are the predominant domestic reservoir of ZVL and thus play a critical role in its ecology and control. Seropositivity is often evident in dogs before visceral leishmaniasis (VL) can be observed in humans (*2*), and dog ownership is a risk factor for human disease (*3*–*5*). As such, control measures in locations where ZVL is prominent include insecticide treatment or culling of dogs.

Although ZVL is transmitted primarily through phlebotomine sand flies (*6*), the role of other means of transmission, particularly vertical transmission, has been demonstrated (*7*–*10*). Transplacental transmission of *L. infantum* parasites can maintain infection within dog populations (*8*,*9*); pups have been shown to be infected in utero (*11*–*13*). Vertical transmission is not unique to dogs (*14*,*15*), and case reports have identified vertical transmission of VL as a cause of infant illness and death in humans (*16*,*17*). Beyond these reports, little is known about the risks of vertical transmission in dogs or humans. *Leishmania* parasites are thought to replicate exclusively clonally as intracellular amastigotes in vertebrate hosts. In contrast, in sand flies they undergo transformation into promastigotes, where they can still reproduce clonally but can also undergo meiosis to complete sexual reproduction (*18*,*19*), although sexual reproduction is not obligatory for transmission. Nothing is known about the transmission genetics of vertically transmitted *Leishmania* populations (*8*,*20*,*21*) or how the absence of vector stages affects the establishment or pathogenicity of mammalian infections.

In the United States, leishmaniasis is enzootic in hunting dogs. ZVL was first identified in 1980 in a dog with no travel outside of the United States. A large outbreak in 1999 prompted an investigation by the Centers for Disease Control and Prevention to determine the burden of disease in US hunting hounds (*22*,*23*). This investigation established the likely introduction of infected dogs from ZVL-endemic areas of Europe through the United Kingdom, but no testing of dogs outside the United States was

Author affiliations: Ludwig-Maximilians-Universität Munich, Munich, Germany (S.U. Franssen); Wellcome Sanger Institute, Hinxton, UK (S.U. Franssen, M.J. Sanders, M. Berriman, J.A. Cotton); University of Iowa College of Public Health, Iowa City, Iowa, USA (C.A. Petersen); Center for Emerging Infectious Diseases, University of Iowa, Iowa City (C.A. Petersen)

DOI: https://doi.org/10.3201/eid2806.211746

[1]These senior authors contributed equally to this article..

performed, and genomic similarity to *L. infantum* parasites from Europe and South America was not evaluated (*23*,*24*).

We subsequently established the primary route of transmission as vertical from dam to pup (*9*,*25*). Despite extensive surveillance associated with these infected dogs (*26*,*27*), no naturally *L. infantum*–infected sand fly has been found in the United States. Although vector transmission of *L. infantum* parasites from these hunting dogs has been experimentally demonstrated (*27*,*28*), it does not appear to be involved in these natural infections.

We examined whole-genome sequences of *L. infantum* parasites from canine autochthonous infection within the United States and sought to identify a likely geographic origin. We looked for evidence of recombination between these *L. infantum* isolates to test for genomic evidence of predominantly vertical transmission. Many dogs are imported from ZVL-endemic areas to non–ZVL-endemic areas; our findings highlight

Table. Summary of groups compared in analysis of geographic origin and vertical transmission of *Leishmania infantum* in hunting hounds, United States*

Group name	Sample size	Sample names	Location	Isolation year	Time span of isolations, y	Host	Disease phenotype	Source
US_d	7	foxymo_01, foxymo_02, foxymo_03, foxymo_04, foxymo_05, foxymo_06, foxymo_07	Midwestern United States	2009–2016	8	Dog	CanL	This study
BR_d	5	BR_7VLd, BR_11VLd, BR_15VLd, BR_16VLd, BR_17VLd	Rio Grande do Norte, Brazil	2010–2012	3	Dog	VL	(*43*)
IS_d	5	NT16, TH4, TH5, TH6, LRC-L1275	Israel	2005–2012	8	Dog	Unknown	(*38*)
BR_RGN_VLh	5	BR_1VLh90, BR_2VLh90, BR_3VLh90, BR_4VLh90, BR_5VLh90	Rio Grande do Norte, Brazil	1991–1993	3	Human	VL	(*43*)
BR_RGN_VLhAh	6	BR_12VLh, BR_14VLh, BR_19VLh, BR_8Ah, BR_9Ah, BR_18Ah	Rio Grande do Norte, Brazil	2011–2013	4	Human	VL or asymptomatic	(*43*)
BR_MA_VLh	6	MA01A, MA02A, MA03A, MA04A, MA05A, MA07A	Maranhão, Brazil	2005–2006	2	Human	VL	(*39*)
BR_MG_VLh	9	MG11A, MG12A, MG13A, MG14A, MG15A, MG16A, MG17A, MG18A, MG19A	Minas Gerais, Brazil	2005	1	Human	VL	(*39*)
BR_PI_VLh	11	PI01A, PI02A, PI03A, PI04A, PI05A, PI07A, PI08A, PI09A, PI10A, PI11A, PI12A	Piauí, Brazil	2005–2006	2	Human	VL	(*39*)
CH_mix	7	D_2, Peking, DOG_STRAIN, RACOON_DOG, SKIN, STRAIN_A, STRAIN_B	China	1954–1983	30	Human, dog, raccoon dog	VL, unknown	(*38*)
FR_mix	4	LEM1985, LEM3278, LPN114, RM1	France	1987–1996	10	Human, dog	CanL, unknown	(*38*)
IP_mix†	7	**NT16**, **TH4**, **TH5**, **TH6**, **LRC-L1275**, LRC-L1296, LRC-L1303	Israel/ Palestine	2005–2012	8	Human, dog	Unknown	(*38*)
IT_mix	5	ISS174, ISS2420, ISS2426, ISS2429, ISS2508	Italy	1985–2002	18	Human, dog, sand fly	VL, CanL, sand fly	(*38*)
SP_mix‡	5	LinJPCM5, BCN83, BCN87, IMT373cl1, IMT260	Spain/ Portugal	1987–2005	19	Human, dog	CL, VL, unknown	(*38, 40*),

*Samples and corresponding groups were chosen from the total of 99 isolates (Appendix 2 Figure 2, https://wwwnc.cdc.gov/EID/article/28/6/21-1746-App2.pdf) to represent geographic regions or countries with at least 5 samples available and a focus on groups with dog isolates only, humans only, and a mixture of hosts for comparison.
†Samples in groups IS_d are also part of group IP_mix and are indicated in bold.
‡The group SP_mix contains only isolates from Spain and Portugal that are in the clade of the known including several known MON-1 samples. The isolates Inf055, Inf004 from the non–MON-1 clade are not included.

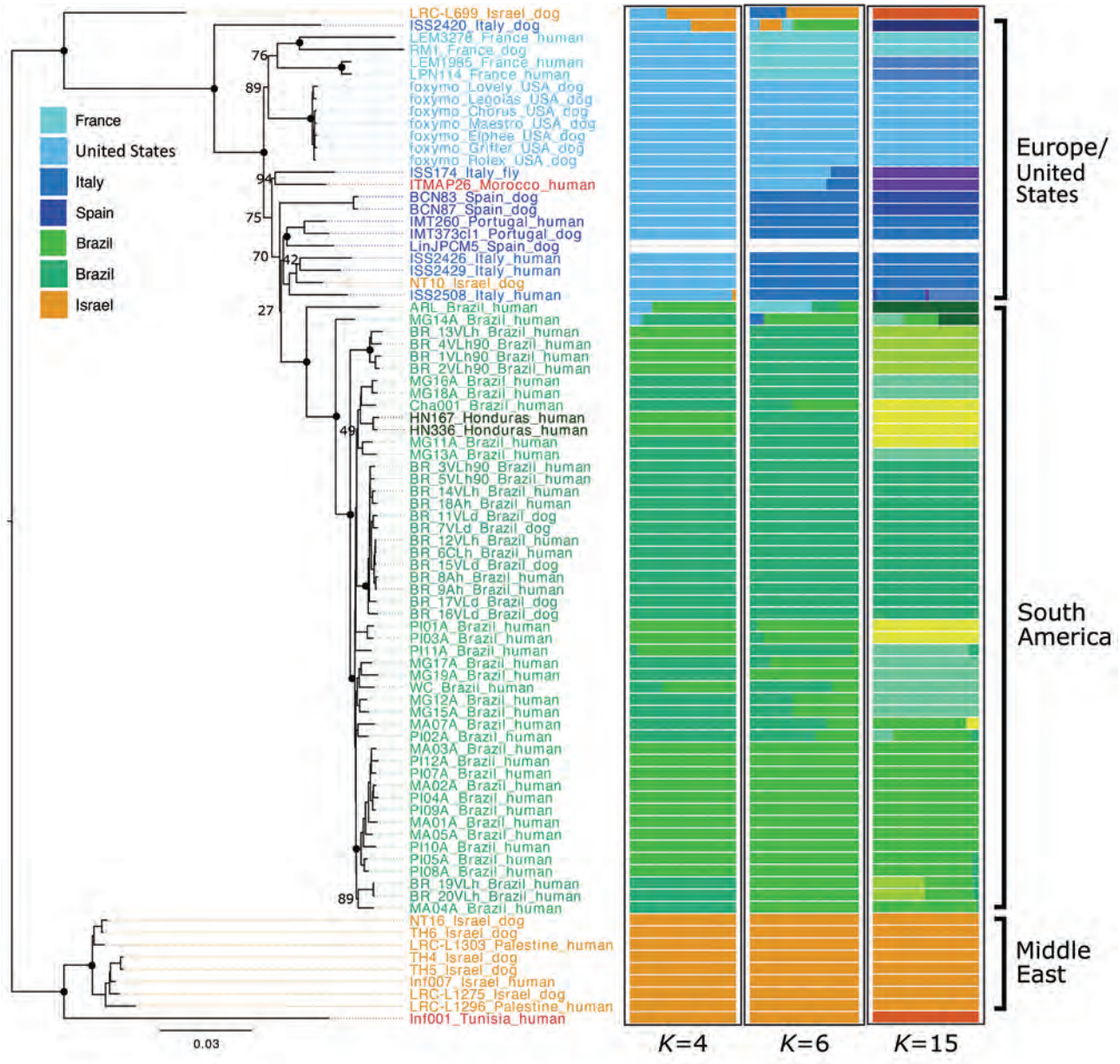

Figure 1. Neighbor-joining tree based on pairwise Nei distances demonstrating geographic origin of US hound *Leishmania* isolates. Phylogenies were reconstructed on the basis of whole-genome genotype calls of 83 parasite samples representing the dominant *L. infantum* zymodeme MON-1 from the United States, Europe, South America, and the Middle East, which were the samples most relevant in the context of the origin of the US samples (Appendix 2 Figure 2, https://wwwnc.cdc.gov/EID/article/28/6/21-1746-App2.pdf). The 2 righthand columns indicate population grouping using admixture with best fitting total number of groups (Appendix 2 Figure 1, panel A).

the need for increasing awareness and testing before import of dogs from ZVL-endemic countries (*29*).

Methods

Ethics

All dogs were enrolled with informed consent from their caretakers, and protocols followed were approved by the University of Iowa Institutional Animal Care and Use Committee. This AAALAC International–accredited institution follows the requirements for the US National Institutes of Health Office of Laboratory Animal Welfare Assurances and operates under the 2015 reprint of the Public Health service Policy on Humane Care and Use of Laboratory Animals.

Sample Collection of Parasites from US Hunting Dogs

The 7 *L. infantum* samples from US hunting dogs used in this study were identified during a retrospective cohort study of *L. infantum* infection in US hunting dogs (*26*,*27*,*30*). To identify *Leishmania*-infected dogs, an active surveillance cohort of 4 large (>50 dogs each) kennels was established from 3 different states in the midwestern United States during 2007–2017. Licensed veterinarians collected 1–5 mL whole blood and serum samples from all dogs at these kennels. Dogs were considered infected if they were positive by quantitative PCR detecting *Leishmania*-specific DNA and had *Leishmania*-specific antibodies (*31*). Parasites from the buffy coat of *Leishmania*-positive dogs were cultured in both Schneider and HOMEM media overnight at 26°C then placed onto agar slants and incubated for 3–4 weeks and observed daily for growth. Parasite cultures include 1 sibling pair (foxymo_01, foxymo_02); remaining dogs all have different grandparents. Because of the frequent exchange of hunting dogs among kennels and states, within 2 generations the ancestors of the sampled dogs came from 12 kennels and 9 different US states (Georgia, Illinois, Iowa, Kansas, Minnesota, Missouri, New Jersey, New York, and Virginia) that included the primary US locations for hunting hound breeding.

Whole-Genome Sequencing of Parasite DNA from Hunting Dogs

We used QIAamp DNA Blood Mini Kit (QIAGEN, https://www.giagen.com) according to manufacturer specifications to isolate DNA directly from primary parasite cultures. We thawed parasite cultures, counted, and placed 1 million parasites into Trizol Reagent (ThermoFisher Scientific, https://www.thermofisher.com) and extracted according to manufacturer specifications. We assessed quality and quantity of isolated DNA by using NanoDrop 2000 (ThermoFisher Scientific).

DNA Sequencing

We sheared DNA into 400–600-bp fragments by focused ultrasonication using the Covaris Adaptive Focused Acoustics technology (Covaris, https://www.covaris.com). We performed 2 methods of DNA sequencing, depending on the amount of DNA supplied, by using the NEBNext DNA Library Prep kit (New England BioLabs, https://www.neb.com). For volumes <500 ng, we amplified libraries by using KAPA HiFI DNA polymerase (Kapa Biosystems, https://kapabiosystems.com) and generated 100-bp paired-end reads on the Illumina HiSeq 2000 (Illumina, https://www.illumina.com). For volumes >500 ng, we generated amplification-free libraries and obtained 150-bp paired-end reads on the Illumina HiSeq X10 (Illumina). We performed sequencing following manufacturers' standard protocols.

Genomic Analysis Pipeline

We analyzed the genomic data of 7 *L. infantum* US hound isolates with an additional 92 publicly available *L. infantum* isolates sampled from a global distribution (Appendix 1, https://wwwnc.cdc.gov/EID/article/26/6/21-1746-App1.xlsx). For all samples, we subjected newly generated and downloaded fastq files to identical analysis pipelines. We trimmed reads using Trimmomatic version 0.39 (http://www.usadellab.org/cms/?page=trimmomatic) (parameters "ILLUMINACLIP:PE_adaptors.fa:2:30:10 TRAILING:15 SLIDINGWINDOW:4:15 MINLEN:50") and mapped them against the reference genome of JPCM5 v45 (https://tritrypdb.org) with BWA version 0.7.17 (bwa mem -M option) (*32*). Single-nucleotide polymorphisms (SNPs) were called using GATK version 4.1.2.0 (*33*): HaplotypeCaller was used with parameters "-ERC GVCF–annotate-with-num-discovered-alleles–sample-ploidy 2" to generate gvcf files for each sample, then combined using "GenomicsDBImport" and genotyped with "GenotypeGVCFs." Calls were filtered with "VariantFiltration" (filters: "QD<2.0, MQ<50.0, FS>20.0, SOR>2.5, BaseQRankSum<-3.1, ClippingRankSum<-3.1, MQRankSum<-3.1, ReadPosRankSum<-3.1and DP<6") and only polymorphic SNPs retained. We removed SNPs with >20% missing calls across samples, reducing the total number of SNPs from 43,528 to 43,336.

Phylogenetic Reconstruction and Admixture Analysis

We performed phylogenetic reconstruction by using distance-based and maximum-likelihood methods on genome-wide genotype calls. For the distance-based approach, we calculated pairwise Nei D distances and reconstructed trees by the neighbor-joining method using the R packages StAMPP version 1.6.1 (*34*) and ape version 5.4. We based bootstrap values on 100 replicates. For maximum-likelihood phylogenies, we converted the vcf file to fasta format with IUPAC codes using bcftools consensus. We estimated 1,000-bootstrap maximum-likelihood phylogenies by using RAxML-NG version 0.8.1-c1 (*35*) and the GTJC model that captures changes between heterozygous and homozygous states.

We preprocessed genome-wide SNPs for admixture analysis version 1.3.0 (*36*) only with plink version 1.90 changing the vcf format into ped and map format and removing SNPs with a missing

fraction of >0.05 and variants closer to each other than 2,000-bp with the arguments "–geno" and "–bp-space." We ran admixture for values of *K* from 1 to 20 and optimal numbers of groups (*K*) were chosen on the basis of lowest cross-validation error (Appendix 2 Figure 1, https://wwwnc.cdc.gov/EID/article/28/6/21-1746-App2.pdf). Because there was no clear number of *K* at which the cross-validation error plateaued, we present analyses with the smallest *K* at first sign of plateauing of the error and 2 larger *K*s with smaller errors.

Molecular Clock Dating

We used 2 molecular clock approaches. The first method was a simple clock model using PATHd8 (*37*) for all RAxML-NG bootstrap trees, constraining the root of the non-US New World clade to 537 years ago. The second method was a Bayesian approach that used BEAST version 1.10.4 (https://beast.community) to enable flexible modeling of rate variation with standard substitution models, a narrow uniform prior of 536.9–537.1 years for the New World clade and leaf heights set to the year of collection (Appendix 1), or constrained to 2005–2007 for samples from (*39*) and to 1900–2020 for the sample 'DOG_STRAIN' of unknown sampling date (*38*). New World and US hound clades were constrained to be monophyletic, and Bayesian Markov Chain Monte Carlo analysis was initialized with the RAxML-NG phylogeny for concatenated chromosomes. The substitution model was Hasegawa-Kishino-Yano with a 4-category gamma distribution of rate variation across sites. Results are based on 8 independent Bayesian Markov Chain Monte Carlo chains of 10 million generations, 1 million generations burn-in, and convergence checked using Tracer version 1.7.1 (https://beast.community/tracer). We accepted analyses if 6 out of 8 chains were at similar likelihoods for 2 million generations. Remaining parameters were defaults from Beauti version 1.10.4. Only results for both strict and uncorrelated gamma-distributed clocks converged and are shown.

Population Genomics Analysis

We grouped parasite samples according to geographic origin and isolated host type (Table). Groups were characterized by their number of segregating SNPs, inbreeding coefficients, and linkage decay with distance. We performed analysis in R (R Foundation for Statistical Computing, https://www.r-project.org) with the exception of R^2 estimates, which we estimated as genotype correlations with vcftools version 0.1.16 (*41*) and parameters "–geno-r2" and "–interchrom-geno-r2." We used genotype correlations because haplotypes cannot be accurately phased for our small population sets. We calculated the inbreeding coefficient F based on the formula $F = 1 - ((c_{AB}/N)/(2 \times f_A \times f_B))$, where c_{AB} represents the heterozygote count, N the group size, and f_A and f_B the frequency of alleles A and B.

Aneuploidy Estimation

We estimated sequencing coverage on the basis of sample-specific mapped bam files. For each sample, indels were determined and indel realignment was performed with the GATK version 3.6 (*33*) tools "RealignerTargetCreator" and "IndelRealigner." Quality filtering and duplicate removal was done with samtools version 1.3 using the parameters "-F 1024 -f 0x0002 -F 0x0004 -F 0x0008." Coverage was estimated with bedtools version 2.17.0 (*42*) genomecov and parameters "-d -split." For each sample, the median coverage per chromosome was assumed to represent the diploid state, so chromosome somy = (chromosome_coverage/median_coverage) × 2. Allele frequencies for isolate-specific SNPs were estimated on the basis of previous bam files and quality filtered with samtools "-q 20 -f 0x0002 -F 0x0004 -F 0x0008." Coverage by genomic position was obtained with samtools mpileup "-d 3500 -B -Q 10" and transformed into sync format with mpileup2sync "–min-qual 20" (*43*).

Results

Independent Introduction of US Hound–Derived Parasites from the Mediterranean Region

To assess the geographic origins of *L. infantum* parasites within US hunting dogs, we generated whole-genome sequence data for 7 *L. infantum* isolates from outbred hounds from 4 kennels in the midwestern United States and an ancestry tracing back to kennels in 9 US states within 2 generations with haploid coverage ranging from 29 to 78 (median 69). We compared these samples with 92 previously published *L. infantum* genome sequences of other strains from other global populations (*38*,*39*,*44*) (Appendix 1).

We constructed distance-based and ML phylogenies from whole-genome SNP variants to compare *L. infantum* genomes from US dogs to samples from *L. infantum*–endemic regions of South America and the Old World. Parasites from US hounds were monophyletic, part of the *L. infantum* MON-1 clade (*38*,*45*), and clearly distinct from *L. infantum* isolates from South America (Figure 1; Appendix 2 Figure 2). These factors suggest independent introduction to the New World. The genetically closest parasite samples were from southern Europe, but the exact origin was ambiguous. Distance-

based methods suggested 4 samples from France as genetically most closely related to US isolates (Figure 1; Figure 2, panel A). The ML phylogeny placed US parasites close to a more widespread group of MON-1 parasites (Figure 2, panel B).

To further investigate parasites' relatedness, we performed admixture analysis, which was consistent with the phylogenetic results. We applied cross validation, a standard approach in admixture to determine an optimal number of populations (*K*) that best explains the relatedness between samples. Because this process did not identify a single optimal *K* (Appendix 2 Figure 1), we considered more than 1 *K* (Figure 1; Appendix 2 Figure 2). We concentrated our analysis on 83 core samples consisting of samples from the United States and other samples from the MON-1 clade (Figures 1, 2). For *K* = 4 populations, US hound parasites were placed together with all remaining samples from Europe and single samples from Israel and Morocco (Figure 1). For *K* = 6 and *K* = 15, US samples formed a separate group, only inferred to share ancestry with one sample from Italy and one from Morocco for *K* = 6. A similar pattern was present within the total set of 99 samples. For *K* = 7, US and 2 parasites from France grouped together, and for *K* = 11, US samples only shared substantial variation with 1 sample from Italy (Appendix 2 Figure 2, panel A), which together suggested a clear origin from Mediterranean Europe but no clear country of origin.

Molecular Clock Dating Confirms Recent Divergence of US Hound–Derived Parasites

We dated the independent introduction of US hound parasites by using 2 different molecular clock approaches, relying on previously estimated introduction of *L. infantum* parasites into the New World ≈500 years ago (*46*). The first analysis using our maximum-likelihood phylogeny estimated the mean date of divergence between US parasites and relatives from Europe as 1897 (95% CI 1873–1917), whereas 2 Bayesian approaches produced estimates of 1938 (strict clock, 95% highest posterior density CI 1910–1965) and 1889 (relaxed clock, 95% CI 1689–1991) (Figure 3). Estimates across a range of approaches thus suggest that US hound parasites were introduced much more recently than *L. infantum* parasites were introduced to South America.

Patterns of Heterozygosity in US Hound Parasites Suggest Clonal Evolution

The genetic variation in a population should reflect its reproductive biology. We thus compared variation in US hound parasites with *L. infantum* populations isolated from dogs in areas where vector transmission occurs and with populations isolated from humans or a mixture of both hosts in other parts of the world (Table). Within-population diversity of the US hound parasites was intermediate between the high diversity of populations from the Old World and the low diversity of parasites from different regions within Brazil (Figure 4). For most populations, the number of polymorphic sites increased with sample size, indicating that increasing numbers of rare variants were detected with larger sample sizes. This sample size–based increase was minimal in the US hound parasite population, suggesting a large proportion of shared variation among these isolates.

To explore this shared variation further, we directly estimated population heterozygosity through the inbreeding coefficient F and the fraction of

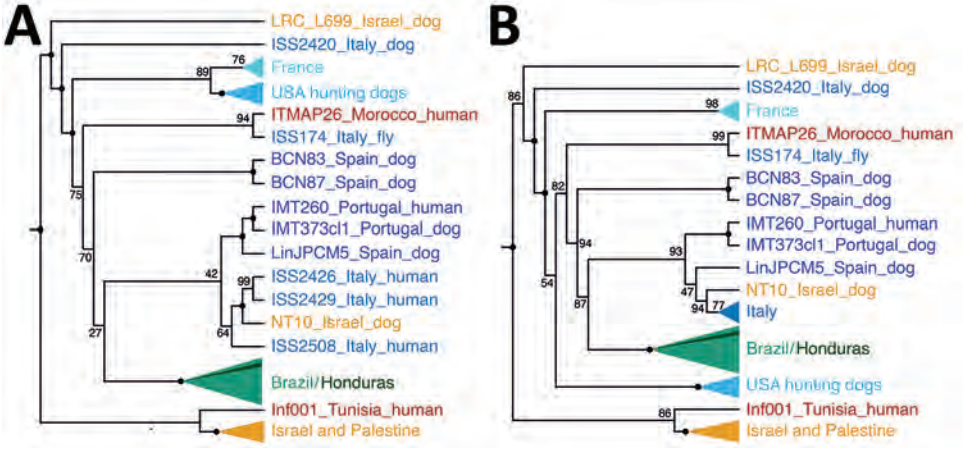

Figure 2. Geographic origin of US hound *Leishmania* isolates. A) Cladogram of the neighbor-joining tree from Figure 1 showing monophyletic groups for better visibility of evolutionary relationships of the US hound parasites. B) Cladogram of the maximum-likelihood phylogeny (Appendix 2 Figure 2, panel B, https://wwwnc.cdc.gov/EID/article/28/6/21-1746-App2.pdf). Cladograms were reconstructed on the basis of whole-genome genotype calls of 83 parasite samples representing the dominant *L. infantum* zymodeme MON-1 from the United States, Europe, South America, and the Middle East, which were the samples most relevant in the context of the origin of the US samples (Appendix 2 Figure 2). Numbers at internal nodes show bootstrap values.

population-specific polymorphic heterozygous SNP sites (Figure 5; Appendix 2 Figure 3). The inbreeding coefficient was significantly different between populations (Kruskal-Wallis test, $\chi^2 = 2843.1$, df = 12; $p<0.001$), and the US hound parasite population had exceptionally low F values compared with all other populations (Dunn test, adjusted; $p<0.001$) (Figure 5). This difference was largely caused by 79% of all polymorphic sites within US hound–derived parasites sharing the same heterozygous genotype across all 7 sampled hound isolates. This extreme excess of shared heterozygosity is present across all chromosomes and is in strong contrast to the remaining populations. Absolute numbers of heterozygous sites in the US samples were higher than in other populations (Table; Appendix 2 Figure 4, panel A). This difference could be caused by either the accumulation of mutations during a period of clonal evolution shared by these samples or a hybrid origin of the founder strain of our US samples between 2 closely related *L. infantum* populations (Appendix 2 Figure 4, panel B), because clonal propagation would maintain any heterozygosity.

No Evidence for Sexual Reproduction in *L. infantum* Isolated from US Hounds

If *L. infantum* parasite transmission in US hunting dogs occurs solely through vertical transmission, we would expect genomic signatures of sexual reproduction to be absent because sexual reproduction is thought to be limited to the vector stage (*18*). Sexual reproduction returns proportions of heterozygous and homozygous variants to the Hardy-Weinberg equilibrium. We propose that the observed extreme excess of shared heterozygous sites in US hound parasites is possible because these parasites evolve clonally for many generations with no mechanism to reduce the number of heterozygous sites through sexual reproduction. To test this proposition, we investigated whether genetic linkage between pairs of SNPs reduces as the distance between loci increases, which would be expected if recombination is occurring. Almost all global *L. infantum* populations showed this expected decay in linkage within chromosomes, except US hound–derived parasites and 2 populations from Brazil (Figure 6). The 2 populations from Brazil had too few polymorphic sites to reliably assess linkage patterns. The US hound parasites also had relatively few sites for analysis, because unphased shared heterozygous sites cannot be used for linkage estimation. However, the remaining loci showed no evidence of linkage decay with genetic distance. Pairs of variants on different chromosomes showed very similar linkage to within-chromosome comparisons (Figure 6). This finding indicates that evidence for meiotic recombination in the US dog *L. infantum* population is lacking.

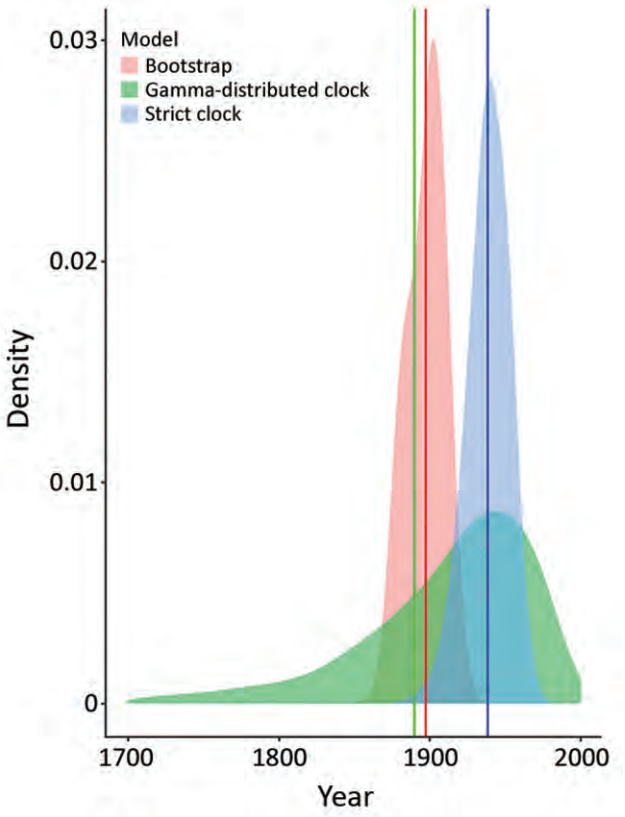

Figure 3. Molecular clock estimates of the date of the most recent common ancestor of US hound *Leishmania* samples. Shaded densities are normal kernel densities for the bootstrap estimates from PATHd8 analysis and from posterior samples for strict clock and relaxed clock with uncorrelated gamma-distributed rates in BEAST version 1.10.4 (https://beast.community). These distributions in each case represent the estimated uncertainty in the divergence date of *Leishmania infantum* isolates from US hounds and from Europe. Vertical lines in the same colors are at the means of each distribution.

Reduced Variation in Aneuploidy in Mammalian Host–Derived Parasites

Leishmania populations frequently show variation in copy number of individual chromosomes with frequent aneuploidy turnover even within a clonal population (mosaic aneuploidy). Aneuploidy variation between US isolates was largely limited to one third of the chromosomes and variation did not correlate to chromosome-specific heterozygosity, which should have been reduced if aneuploidy turnover was high (Figure 7; Appendix 2, Appendix 2 Figure 5). Although this estimate of aneuploidy variation through mean ploidy profiles between isolates is

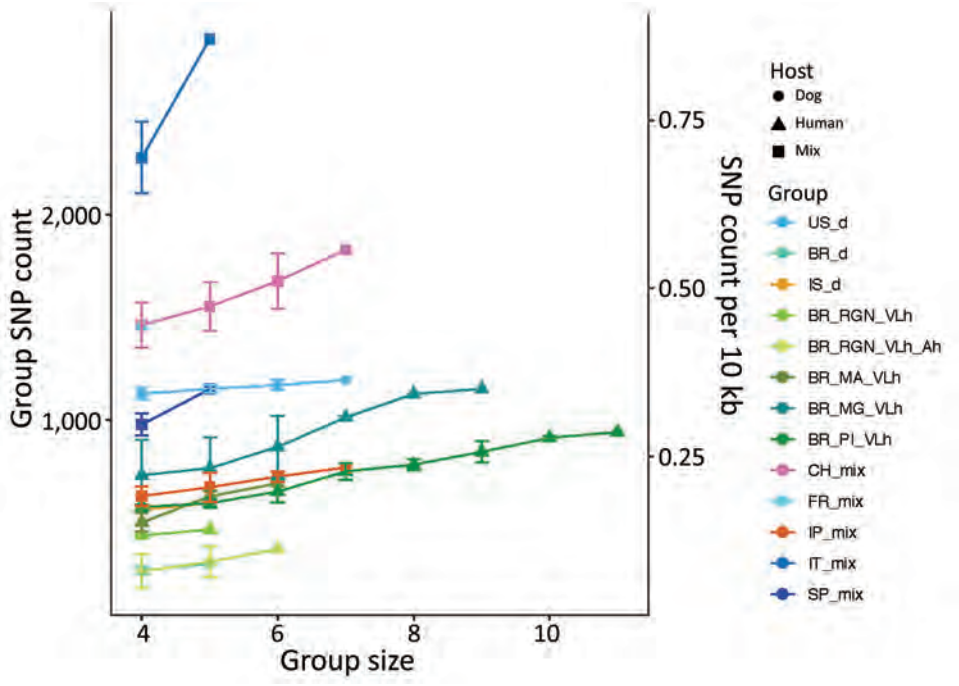

Figure 4. Number and density of segregating SNPs in each group of *Leishmania infantum* isolates by geographic region and type of host. Values are shown as both the number (left y-axis) and density (right y-axis) of segregating SNP sites in each group. Because group sizes vary, groups were subsampled in triplicate for each group size from 4 up to their respective size; means and SDs are shown. SNP, single-nucleotide polymorphism.

conservative, it supports initial findings that aneuploidy turnover might be greater in cultured promastigotes versus intra-host amastigotes (*47*,*48*).

Discussion

Our data confirm that *L. infantum* found in US hounds represents an independent introduction of *Leishmania* into the New World. Although we cannot be definitive about the precise origin of US hound *L. infantum* isolates, they form part of a MON-1 clade, associated with canine leishmaniasis throughout the Mediterranean region. Closely related MON-1 samples are from Mediterranean Europe, consistent with epidemiologic findings that deer hunting hounds imported from France may have introduced *L. infantum* parasites into the US hound population, potentially through UK breeding connections (*29*).

Molecular clock analyses suggested that US hound parasites diverged from other *L. infantum* isolates around 1900, but parasitized dogs could have entered the United States more recently. These date estimates also depend on the assumed origin of the main New World subspecies (*L. infantum* subspecies *chagasi*) 537 years ago, the central estimate from an analysis of microsatellite data, although with very wide CIs (*46*). The safest interpretation of our analysis is therefore a much

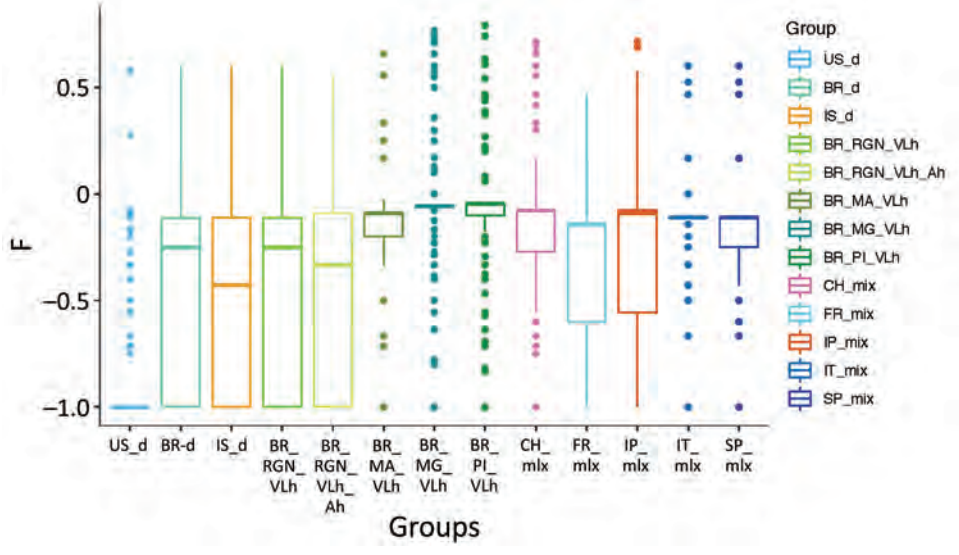

Figure 5. Extreme excess of heterozygous sites in the US hound–derived *Leishmania infantum* isolates. The group-specific inbreeding coefficient F is shown for all polymorphic sites in the respective parasite population. F measures the deviation of the frequency of heterozygotes from Hardy-Weinberg equilibrium with negative values indicating an excess and positive values a deficiency of heterozygotes over homozygotes. Horizontal lines within boxes indicate medians; box top and bottom lines indicate 25 and 75 percentiles; and error bars indicate minimum and maximum values, excluding outliers.

more recent divergence of US canine parasites from parasites in Europe than the main New World clade of *L. infantum* subsp. *chagasi*.

Our data confirmed the highly unusual genetics of the *L. infantum* population in US hounds. This parasite population demonstrated an excess of shared heterozygous loci, which could have been initiated by an already heterozygous founder strain. However, the preservation of heterozygous sites across our US samples is consistent with clonal reproduction, which is also confirmed by the absence of any signature of reduction in genetic linkage with genomic distance in this population

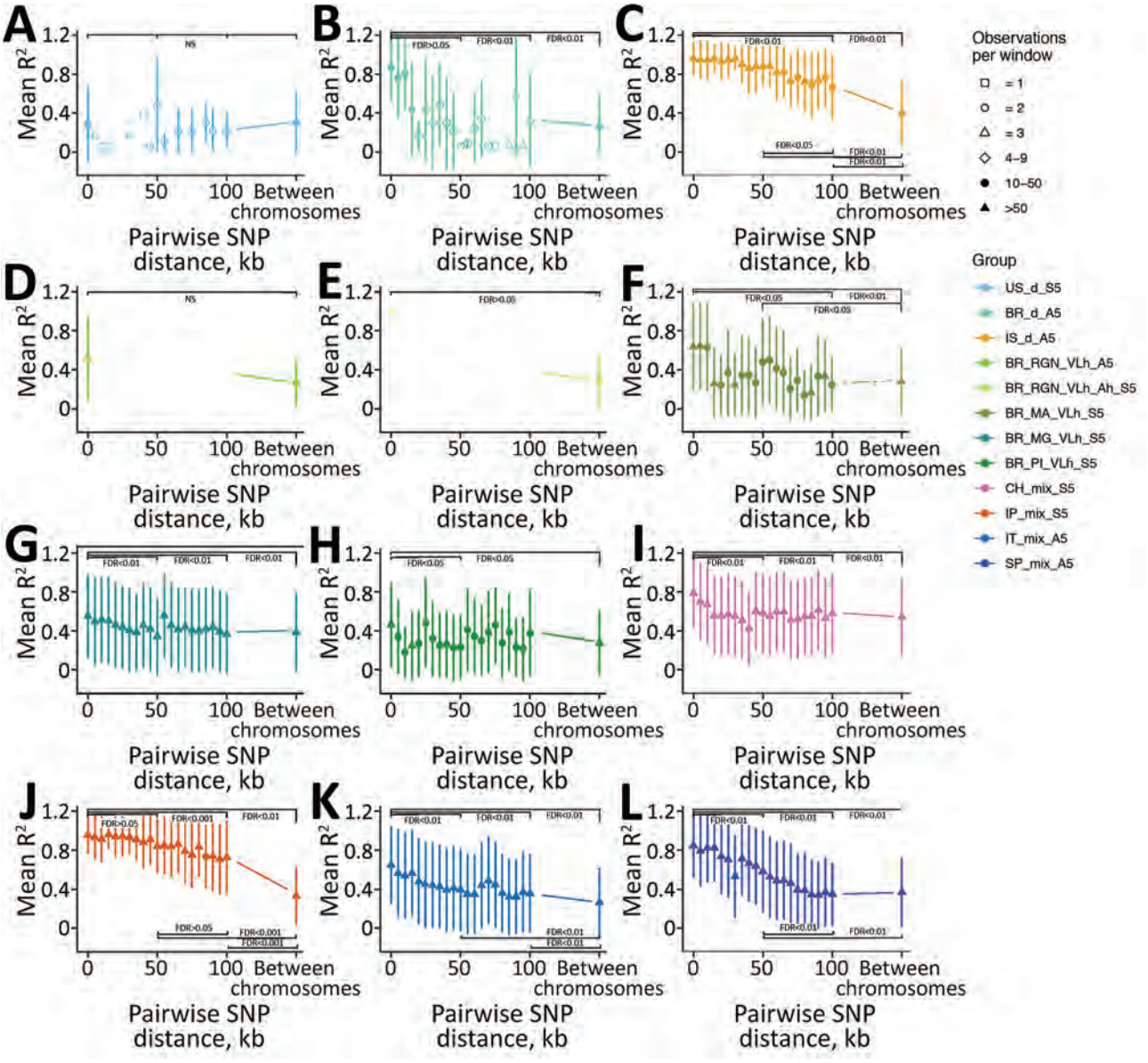

Figure 6. Decay of linkage disequilibrium with genomic distance across geographically confined groups of *Leishmania infantum* isolates. A) US_d_S5, B) BR_d_A5, C) IS_d_A5, D) BR_RGN_VLh_A5, E) BR_RGN_VLh_Ah_S5, F) BR_MA_VLh_Ah_S5, G) BR_MG_VLh_S5. H) BR_PI_VLh_S5, I) CH_mix_S5, J) IP_mix_A5, K) IT_mix_A5, L) SP_mix_A5. Long-range linkage disequilibrium was measured as R^2 for pairs of SNPs up to 100 kb apart within chromosomes and located on different chromosomes. Symbols show mean R^2 across SNP-pairs on all chromosomes, and lines show 1 SD for variants in bins of 5kb distance starting at the indicated distance. For groups with >5 samples, 5 have been randomly chosen to calculate R^2 values, indicated in group names for each subplot (S6, subsampled 5; A5, all 5 samples of the group were used). Symbol shapes indicates the number of pairwise comparisons available for each distance bin. Statistical significance of comparisons between R^2 between 4 different 5 kb windows at 0–4999 bp, 50–54.999 kb, 100–104.999 kb between SNP pairs for all between-chromosome comparisons are shown. FDR was determined based on the Kruskal-Wallis test, followed by the Dunn post hoc test when significant. For the groups in which only data for 2 of the 4 windows was present, the Mann-Whitney-Wilcoxon test was used. FDR, false discovery rate; NS, not significant; SNP, single-nucleotide polymorphism.

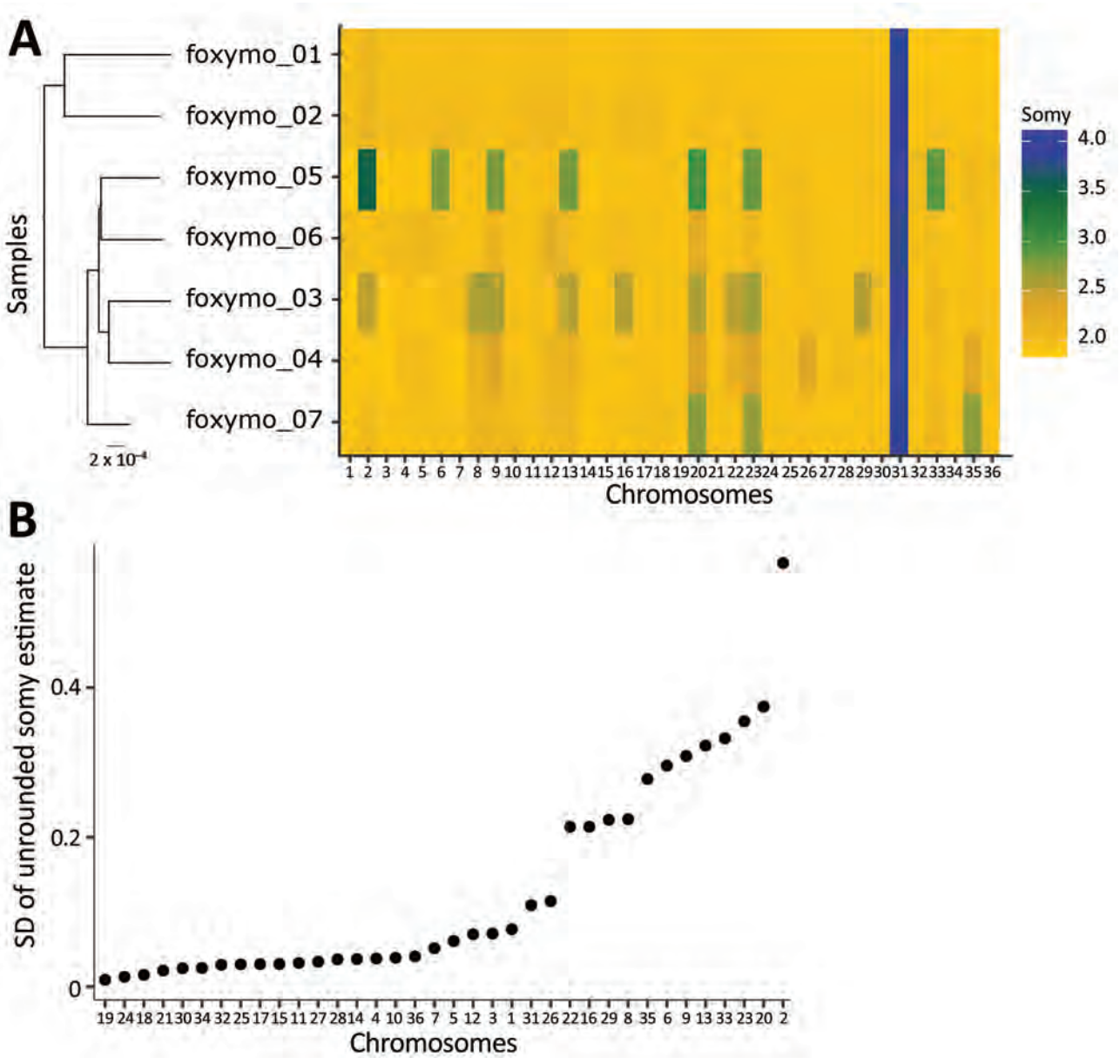

Figure 7. Aneuploidy variation of *Leishmania* isolates from US hunting hounds. A) Aneuploidy profiles, shown as a heatmap of estimated somy for each isolate and chromosome. The sample phylogeny is extracted from Figure 1. B) Chromosome-specific variation in somy across US hound isolates. Variation in somy between isolates provides a conservative estimate of somy variation, as it ignores within-isolate variation.

Without a broader sampling of parasites from US hounds, we cannot rule out that transmission via sand flies is occurring elsewhere in the United States. Similarly, we cannot quantify the amount of parasite sexual reproduction from these data and so cannot completely rule out that sexual reproduction and therefore vector transmission are occurring. However, our results are consistent with parasites replicating only clonally as amastigotes in dog phagocytes in the absence of sand fly vectors. No sand fly transmission of *L. infantum* parasites from dogs in the United States has been demonstrated (*7*,*9*,*28*), so we suspect that transmission within this population is largely occurring vertically and directly between dogs.

The population genetic signatures of vertical transmission we have found could be useful in characterizing the epidemiology of other *Leishmania* populations. The extent to which these signatures occur in more complex situations, such as with multiple introductions of parasites or mixed vertical and horizontal

transmission, remains to be established. The most direct evidence of vertical transmission would be to find that the relatedness between parasite isolates directly reflected the pedigrees of the sampled dogs, although this would be potentially complicated by horizontal transmission between dogs (e.g., through blood-blood contact during fights) (*49*). Although we have not attempted to test this possibility, parasites from the pair of siblings included here (foxymo_01 and foxymo_02) were genetically closest to each other and clearly separated from all others.

In conclusion, our data confirm the 1999–2000 outbreak investigation finding by the Centers for Disease Control and Prevention that at least 1 *L. infantum* population in US dogs was a recent introduction from Europe, distinct and much more recent than the main population of *L. infantum* in South America. This population has reproduced largely or exclusively clonally, presumably as amastigotes within canine hosts. We see no evidence of recent recombination associated with vector transmission up to the limits of our detection levels; thus, transmission has likely occurred either vertically through maternal-offspring transplacental transmission or horizontally through blood-blood contact. The absence of evidence for vector-based transmission in the northern United States makes this an unusual, and perhaps unique, ecologic system. Our findings enable the study of many aspects of *Leishmania* biology without the complication of occasional vector transmission, including adaptation of parasites to the mammal host without the additional selection pressure of vector transmissibility, mutation rates, and rates of amastigote cell division.

Acknowledgments

We thank the dog caretakers who helped us gather this data and previous members of the Petersen laboratory, who collected the samples, particularly Carolyne Bennett and staff veterinarians, who performed physical examinations, ran diagnostics, performed data entry, and ran analyses over the years. We also thank members of the Wellcome Sanger Institute DNA pipelines teams for producing and sequencing DNA libraries.

This research was funded by Wellcome (grant 206194) and the National Institutes of Health (grant R01TW010500).

About the Author

Dr. Franssen is an assistant professor in the division of evolutionary biology at the Ludwig-Maximilians-Universität in Munich, Germany. A bioinformatician by training, she has worked in evolutionary genomics and population genetics throughout her career studying evolution in a diverse range of organisms but since her postdoctorate work at the Wellcome Sanger Institute has focused on *Leishmania* and leishmaniasis.

References

1. Miró G, Petersen C, Cardoso L, Bourdeau P, Baneth G, Solano-Gallego L, et al. Novel areas for prevention and control of canine leishmaniosis [Erratum in: Trends Parasitol. 2017;33:718–30]. Trends Parasitol. 2017;33:718–30. https://doi.org/10.1016/j.pt.2017.05.005
2. Lima ID, Lima ALM, Mendes-Aguiar CO, Coutinho JFV, Wilson ME, Pearson RD, et al. Changing demographics of visceral leishmaniasis in northeast Brazil: lessons for the future. PLoS Negl Trop Dis. 2018;12:e0006164. https://doi.org/10.1371/journal.pntd.0006164
3. Gavgani ASM, Mohite H, Edrissian GH, Mohebali M, Davies CR. Domestic dog ownership in Iran is a risk factor for human infection with *Leishmania infantum*. Am J Trop Med Hyg. 2002;67:511–5. https://doi.org/10.4269/ajtmh.2002.67.511
4. Bsrat A, Berhe M, Gadissa E, Taddele H, Tekle Y, Hagos Y, et al. Serological investigation of visceral *Leishmania* infection in human and its associated risk factors in Welkait District, Western Tigray, Ethiopia. Parasite Epidemiol Control. 2018;3:13–20. https://doi.org/10.1016/j.parepi.2017.10.004
5. Lima ÁLM, de Lima ID, Coutinho JFV, de Sousa ÚPST, Rodrigues MAG, Wilson ME, et al. Changing epidemiology of visceral leishmaniasis in northeastern Brazil: a 25-year follow-up of an urban outbreak. Trans R Soc Trop Med Hyg. 2017;111:440–7. https://doi.org/10.1093/trstmh/trx080
6. Bates PA. Transmission of *Leishmania* metacyclic promastigotes by phlebotomine sand flies. Int J Parasitol. 2007;37:1097–106. https://doi.org/10.1016/j.ijpara.2007.04.003
7. Toepp AJ, Bennett C, Scott B, Senesac R, Oleson JJ, Petersen CA. Maternal *Leishmania infantum* infection status has significant impact on leishmaniasis in offspring. PLoS Negl Trop Dis. 2019;13:e0007058. https://doi.org/10.1371/journal.pntd.0007058
8. Grinnage-Pulley T, Scott B, Petersen CA. A mother's gift: congenital transmission of *Trypanosoma* and *Leishmania* species. PLoS Pathog. 2016;12:e1005302. https://doi.org/10.1371/journal.ppat.1005302
9. Boggiatto PM, Gibson-Corley KN, Metz K, Gallup JM, Hostetter JM, Mullin K, et al. Transplacental transmission of *Leishmania infantum* as a means for continued disease incidence in North America. PLoS Negl Trop Dis. 2011;5:e1019. https://doi.org/10.1371/journal.pntd.0001019
10. Petersen CA. New means of canine leishmaniasis transmission in North America: the possibility of transmission to humans still unknown. Interdiscip Perspect Infect Dis. 2009;2009:802712. https://doi.org/10.1155/2009/802712
11. da Silva SM, Ribeiro VM, Ribeiro RR, Tafuri WL, Melo MN, Michalick MSM. First report of vertical transmission of *Leishmania* (*Leishmania*) *infantum* in a naturally infected bitch from Brazil. Vet Parasitol. 2009;166:159–62. https://doi.org/10.1016/j.vetpar.2009.08.011
12. Mancianti F, Sozzi S. Isolation of *Leishmania* from a newborn puppy. Trans R Soc Trop Med Hyg. 1995;89:402. https://doi.org/10.1016/0035-9203(95)90028-4
13. Pangrazio KK, Costa EA, Amarilla SP, Cino AG, Silva TMA, Paixão TA, et al. Tissue distribution of *Leishmania chagasi* and lesions in transplacentally infected fetuses from symptomatic and asymptomatic naturally infected bitches.

Vet Parasitol. 2009;165:327–31. https://doi.org/10.1016/j.vetpar.2009.07.013
14. Masucci M, De Majo M, Contarino RB, Borruto G, Vitale F, Pennisi MG. Canine leishmaniasis in the newborn puppy. Vet Res Commun. 2003;27(Suppl 1):771–4. https://doi.org/10.1023/B:VERC.0000014268.61966.69
15. Naucke TJ, Lorentz S. First report of venereal and vertical transmission of canine leishmaniosis from naturally infected dogs in Germany. Parasit Vectors. 2012;5:67. https://doi.org/10.1186/1756-3305-5-67
16. Galindo-Sevilla N, Mancilla-Ramírez J. T-cell tolerance as a potential effect of congenital leishmaniasis on offspring immunity. Parasite Immunol. 2019;41:e12540. https://doi.org/10.1111/pim.12540
17. Adam GK, Omar SM, Ahmed MA, Abdallah TM, Ali AA. Cross-sectional study of the case-fatality rate among patients with visceral leishmaniasis infections during pregnancy in Sudan. Int J Gynaecol Obstet. 2018;140:119–20. https://doi.org/10.1002/ijgo.12332
18. Akopyants NS, Kimblin N, Secundino N, Patrick R, Peters N, Lawyer P, et al. Demonstration of genetic exchange during cyclical development of *Leishmania* in the sand fly vector. Science. 2009;324:265–8. https://doi.org/10.1126/science.1169464
19. Inbar E, Shaik J, Iantorno SA, Romano A, Nzelu CO, Owens K, et al. Whole genome sequencing of experimental hybrids supports meiosis-like sexual recombination in *Leishmania*. PLoS Genet. 2019;15:e1008042. https://doi.org/10.1371/journal.pgen.1008042
20. Figueiró-Filho EA, El Beitune P, Queiroz GT, Somensi RS, Morais NO, Dorval MEC, et al. Visceral leishmaniasis and pregnancy: analysis of cases reported in a central-western region of Brazil. Arch Gynecol Obstet. 2008;278:13–6. https://doi.org/10.1007/s00404-007-0532-0
21. Pagliano P, Carannante N, Rossi M, Gramiccia M, Gradoni L, Faella FS, et al. Visceral leishmaniasis in pregnancy: a case series and a systematic review of the literature. J Antimicrob Chemother. 2005;55:229–33. https://doi.org/10.1093/jac/dkh538
22. Anderson DC, Buckner RG, Glenn BL, MacVean DW. Endemic canine leishmaniasis. Vet Pathol. 1980;17:94–6. https://doi.org/10.1177/030098588001700110
23. Gaskin AA, Schantz P, Jackson J, Birkenheuer A, Tomlinson L, Gramiccia M, et al. Visceral leishmaniasis in a New York foxhound kennel. J Vet Intern Med. 2002;16:34–44. https://doi.org/10.1111/j.1939-1676.2002.tb01604.x
24. Owens SD, Oakley DA, Marryott K, Hatchett W, Walton R, Nolan TJ, et al. Transmission of visceral leishmaniasis through blood transfusions from infected English foxhounds to anemic dogs. J Am Vet Med Assoc. 2001;219:1076–83.
25. Gibson-Corley KN, Hostetter JM, Hostetter SJ, Mullin K, Ramer-Tait AE, Boggiatto PM, et al. Disseminated *Leishmania infantum* infection in two sibling foxhounds due to possible vertical transmission. Can Vet J. 2008;49:1005–8.
26. Duprey ZH, Steurer FJ, Rooney JA, Kirchhoff LV, Jackson JE, Rowton ED, et al. Canine visceral leishmaniasis, United States and Canada, 2000–2003. Emerg Infect Dis. 2006;12:440–6. https://doi.org/10.3201/eid1203.050811
27. Schantz PM, Steurer FJ, Duprey ZH, Kurpel KP, Barr SC, Jackson JE, et al. Autochthonous visceral leishmaniasis in dogs in North America. J Am Vet Med Assoc. 2005;226:1316–22. https://doi.org/10.2460/javma.2005.226.1316
28. Schaut RG, Robles-Murguia M, Juelsgaard R, Esch KJ, Bartholomay LC, Ramalho-Ortigao M, et al. Vectorborne transmission of *Leishmania infantum* from hounds, United States. Emerg Infect Dis. 2015;21:2209–12. https://doi.org/10.3201/eid2112.141167
29. Duthie MS, Petersen C. Could canine visceral leishmaniosis take hold in the UK? Vet Rec. 2019;184:438–40. https://doi.org/10.1136/vr.l985
30. Rosypal AC, Zajac AM, Lindsay DS. Canine visceral leishmaniasis and its emergence in the United States. [viii.]. Vet Clin North Am Small Anim Pract. 2003;33:921–37, viii. https://doi.org/10.1016/S0195-5616(03)00030-5
31. Larson M, Toepp A, Scott B, Kurtz M, Fowler H, Esfandiari J, et al.; EPID:158:001. Semi-quantitative measurement of asymptomatic *L. infantum* infection and symptomatic visceral leishmaniasis in dogs using Dual-Path Platform® CVL. Appl Microbiol Biotechnol. 2017;101:381–90. https://doi.org/10.1007/s00253-016-7925-6
32. Li H, Durbin R. Fast and accurate short read alignment with Burrows-Wheeler transform. Bioinformatics. 2009;25:1754–60. https://doi.org/10.1093/bioinformatics/btp324
33. Van der Auwera GA, Carneiro MO, Hartl C, Poplin R, Del Angel G, Levy-Moonshine A, et al. From FastQ data to high confidence variant calls: the Genome Analysis Toolkit best practices pipeline. Curr Protoc Bioinformatics. 2013;43:11.10.1–33.
34. Pembleton LW, Cogan NOI, Forster JW. StAMPP: an R package for calculation of genetic differentiation and structure of mixed-ploidy level populations. Mol Ecol Resour. 2013;13:946–52. https://doi.org/10.1111/1755-0998.12129
35. Kozlov AM, Darriba D, Flouri T, Morel B, Stamatakis A. RAxML-NG: a fast, scalable and user-friendly tool for maximum likelihood phylogenetic inference. Bioinformatics. 2019;35:4453–5. https://doi.org/10.1093/bioinformatics/btz305
36. Alexander DH, Novembre J, Lange K. Fast model-based estimation of ancestry in unrelated individuals. Genome Res. 2009;19:1655–64. PMID 19648217
37. Britton T, Anderson CL, Jacquet D, Lundqvist S, Bremer K. Estimating divergence times in large phylogenetic trees. Syst Biol. 2007;56:741–52. https://doi.org/10.1080/10635150701613783
38. Franssen SU, Durrant C, Stark O, Moser B, Downing T, Imamura H, et al. Global genome diversity of the *Leishmania donovani* complex. eLife. 2020;9:e51243. https://doi.org/10.7554/eLife.51243
39. Carnielli JBT, Crouch K, Forrester S, Silva VC, Carvalho SFG, Damasceno JD, et al. A *Leishmania infantum* genetic marker associated with miltefosine treatment failure for visceral leishmaniasis. EBioMedicine. 2018;36:83–91. https://doi.org/10.1016/j.ebiom.2018.09.029
40. Peacock CS, Seeger K, Harris D, Murphy L, Ruiz JC, Quail MA, et al. Comparative genomic analysis of three *Leishmania* species that cause diverse human disease. Nat Genet. 2007;39:839–47. https://doi.org/10.1038/ng2053
41. Danecek P, Auton A, Abecasis G, Albers CA, Banks E, DePristo MA, et al.; 1000 Genomes Project Analysis Group. The variant call format and VCFtools. Bioinformatics. 2011;27:2156–8. https://doi.org/10.1093/bioinformatics/btr330
42. Quinlan AR, Hall IM. BEDTools: a flexible suite of utilities for comparing genomic features. Bioinformatics. 2010;26:841–2. https://doi.org/10.1093/bioinformatics/btq033
43. Kofler R, Pandey RV, Schlötterer C. PoPoolation2: identifying differentiation between populations using sequencing of pooled DNA samples (Pool-Seq). Bioinformatics. 2011;27:3435–6. https://doi.org/10.1093/bioinformatics/btr589

44. Teixeira DG, Monteiro GRG, Martins DRA, Fernandes MZ, Macedo-Silva V, Ansaldi M, et al. Comparative analyses of whole genome sequences of *Leishmania infantum* isolates from humans and dogs in northeastern Brazil. Int J Parasitol. 2017;47:655–65. https://doi.org/10.1016/j.ijpara.2017.04.004
45. Kuhls K, Chicharro C, Cañavate C, Cortes S, Campino L, Haralambous C, et al. Differentiation and gene flow among European populations of *Leishmania infantum* MON-1. PLoS Negl Trop Dis. 2008;2:e261. https://doi.org/10.1371/journal.pntd.0000261
46. Leblois R, Kuhls K, François O, Schönian G, Wirth T. Guns, germs and dogs: on the origin of *Leishmania chagasi*. Infect Genet Evol. 2011;11:1091–5. https://doi.org/10.1016/j.meegid.2011.04.004
47. Dumetz F, Imamura H, Sanders M, Seblova V, Myskova J, Pescher P, et al. Modulation of aneuploidy in *Leishmania donovani* during adaptation to different *in vitro* and *in vivo* environments and its impact on gene expression. MBio. 2017;8:e00599-17. https://doi.org/10.1128/mBio.00599-17
48. Franssen SU, Takele Y, Adem E, Sanders MJ, Müller I, Kropf P, et al. Diversity and within-host evolution of *Leishmania donovani* from visceral leishmaniasis patients with and without HIV coinfection in northern Ethiopia. MBio. 2021;12:e0097121. https://doi.org/10.1128/mBio.00971-21
49. Naucke TJ, Amelung S, Lorentz S. First report of transmission of canine leishmaniosis through bite wounds from a naturally infected dog in Germany. Parasit Vectors. 2016;9:256. https://doi.org/10.1186/s13071-016-1551-0

Address for correspondence: Susanne Franssen, Wellcome Sanger Institute, Wellcome Genome Campus, Hinxton, Cambridge, CB10 1SA, UK; email: franssen@bio.lmu.de

Secondary Attack Rate, Transmission and Incubation Periods, and Serial Interval of SARS-CoV-2 Omicron Variant, Spain

Javier Del Águila-Mejía, Reinhard Wallmann, Jorge Calvo-Montes, Jesús Rodríguez-Lozano, Trinidad Valle-Madrazo, Adrian Aginagalde-Llorente

Contact tracing data of SARS-CoV-2 Omicron variant cases during December 2021 in Cantabria, Spain, showed increased transmission (secondary attack rate 39%) compared with Delta cases (secondary attack rate 26%), uninfluenced by vaccination status. Incubation and serial interval periods were also reduced. Half of Omicron transmissions happened before symptom onset in the index case-patient.

During December 2021, a total of 622 cases of SARS-CoV-2 infection compatible with the Omicron variant (BA.1/B.1.1.529) (*1*) were studied by the Contact Tracing Programe in Cantabria, Spain. A total of 1,420 close contacts (household, social, and occupational) were identified; 455 secondary cases were identified. We report the main epidemiologic characteristics of these cases, such as secondary attack rate (SAR), transmission period, incubation period, and serial interval, and compared these characteristics with those for Delta variant cases.

The Study

The Omicron cases were detected among the samples with no amplification of the spike (S) gene (non-S gene target failure) by real-time reverse transcription PCR using the TaqMan SARS-CoV-2 mutation panel (Thermo Fisher Scientific, https://www.thermofisher.com) for single-nucleotide polymorphism genotyping focused on the K417N and L452R mutations. Samples positive for the K417N mutation and negative for L452R were considered compatible with Omicron. The analysis method was validated through whole-genome sequencing of 63 samples. Libraries were constructed by using Ion AmpliSeq SARS-CoV-2 Insight Research Assay and were sequenced with Ion GeneStudio S5 system (both Thermo Fisher Scientific). Next-generation sequencing data were analyzed using Torrent suite software and were assembled by IRMA (*2*). Lineage assignment was done by Pangolin (*3*) by using consensus fasta.

We obtained data on sociodemographic characteristics (age), vaccination status (nonvaccinated or fully vaccinated), and presence or absence of symptoms, as well as symptom onset date (SOD) or diagnosis date (DD) for asymptomatic cases, from the Contact Tracing Program of Cantabria (Appendix, https://wwwnc.cdc.gov/EID/article/28/6/22-0158-App1.pdf). We obtained the same information for the 1,708 coronavirus disease cases of November 2021, when the Delta variant of SARS-CoV-2 represented 100% (1,299/1,299) of samples. We identified 12,587 close contacts and 2,201 secondary cases.

In Spain, close contacts were tested as early as 3 days and as late as 9 days after the date of last contact, depending on when the patient came into the system (*4*). We defined SAR as the proportion of secondary cases among close contacts (those who had been at a distance of <2 m for >15 min) identified through contact tracing (contact 2 days before to 10 days after index case SOD or diagnosis). We classified each relationship by the setting where it took place (household, social, or occupational). We defined global SAR as the average of secondary cases among all relationships (*5*). All SARs (with 95% CIs) are presented by index

Author affiliations: University Hospital of Móstoles, Madrid, Spain (J. Del Águila-Mejía); Public Health Observatory of Cantabria, Santander, Spain (J. Del Águila-Mejía, A. Aginagalde-Llorente); Directorate General of Public Health, Government of Cantabria, Santander (R. Wallmann); Marqués de Valdecilla University Hospital, Santander (J. Calvo-Montes, J. Rodríguez-Lozano, T. Valle-Madrazo)

DOI: https://doi.org/10.3201/eid2806.220158

Table 1. Secondary attack rates of Omicron and Delta variant of SARS-CoV-2, by setting and vaccine status of the index case-patient, Spain*

Settings	Omicron				Delta				Difference, % (95% CI)
	Index cases	Close contacts	Secondary cases	SAR, % (95% CI)	Index cases	Close contacts	Secondary cases	SAR, % (95% CI)	
Global	333	1,126	443	39.3 (36.5–42.2)	1,403	7,013	1,846	26.3 (25.3–27.4)	13† (9.9–16.1)
Unvaccinated index case-patient	210	655	269	41.1 (37.4–44.9)	535	2,876	895	31.1‡ (29.5–32.8)	10† (5.7–14.2)
Vaccinated index case-patient	111	436	159	36.5 (32.1–41.1)	829	3,904	910	23.3‡ (22–24.7)	13.2† (8.3–18)
Household	287	533	263	49.4 (54–53.6)	1,095	2,350	1,129	48 (46–50)	1.3 (−3.4 to 6)
Unvaccinated index case-patient	187	354	171	49.4 (44.2–54.7)	450	1,118	595	53.2‡ (50.3–56)	−3.8 (−9.8 to 2.2)
Vaccinated index case-patient	91	171	85	49.7 (42.3–57)	622	1,198	519	43‡ (40.5–46)	6.4 (−1.6 to 14.4)
Social	143	524	160	30.5 (26.8–34.6)	836	4,153	672	16.2 (15.1–17.3)	14.4† (10.3–18.5)
Unvaccinated index case-patient	76	283	88	31.1 (26–36.7)	315	1,640	284	17.3 (15.6–19.2)	13.8† (7.9–19.7)
Vaccinated index case-patient	61	224	64	28.6 (23.1–34)	495	2,351	368	15.7 (14.2–17.2)	12.9† (6.6–19.3)
Occupational	29	58	18	31 (20.6–43.8)	148	411	43	10.5 (7.93–13.8)	20.6† (7.3–33.8)
Unvaccinated index case-patient	14	22	8	36.4 (19.7–57)	39	97	16	16.5‡ (10.4–25.1)	20.1 (−0.04 to 44.1)
Vaccinated index case-patient	14	34	10	29.4 (16.8–46.1)	105	298	21	7‡ (4.7–10.5)	22.4† (5.1–40)

*SAR, secondary attack rate.
†p<0.001.
‡Differences between vaccinated and unvaccinated persons within same-variant context.

case-patient's vaccination status. We tested difference in SAR between Delta and Omicron and differences between SARs for vaccinated and unvaccinated persons by variant and contact setting by Pearson χ^2 test(Table 1).

Global SAR was 39% (95% CI 36.5%–42.2%) for Omicron cases and 26% (95% CI 25.3%–27.4%) for Delta, a 13-point absolute increase (9.9–16.1; p<0.0001) (Table 1). A higher SAR was also registered in social settings (30.5% for Omicron vs. 16.2% for Delta) and occupational (31% vs. 10.5%) settings but not between household close contacts (49.4% vs. 48%).

Among Delta variant cases, unvaccinated persons showed an overall increased SAR of 7.8% (95% CI 5.6%–10%; p<0.001), household SAR of 9.9% (95% CI 5.8%–14%; p<0.001), and occupational SAR of 9.5% (95% CI 0.8%–18.1%; p = 0.01) compared with vaccinated persons. In contrast, for the Omicron variant, we found no differences between vaccinated and unvaccinated persons in any of these categories.

We selected only symptomatic index cases to calculate transmission, incubation, and serial interval periods. We defined transmission period as the distribution of days from index case SOD to date of last contact with close contacts who became secondary cases. For incubation period and serial interval, we required that the secondary case-patient also be symptomatic. We defined the incubation period as the number of days between date of last contact and secondary case SOD and serial interval as the number

Table 2. Comparison of Omicron and Delta variant of SARS-CoV-2 transmission period, incubation period, and serial interval by index case-patient vaccination status, Spain*

Characteristic	Mean (SD)				Median (IQR)	
	Omicron	Delta	Difference (95% CI)†	p value	Omicron	Delta
Transmission period	0.5 (2.3)	0.8 (2.6)	−0.3 (−0.56 to −0.02)	0.04	0 (−1 to –2)	1 (−1 to 2)
Unvaccinated index case-patient	0.5 (2.3)	0.7 (2.5)	−0.2 (−0.6 to 0.14)	0.22	1 (−1 to 2)	
Vaccinated index case-patient	0.6 (2.3)	0.9 (2.7)	−0.3 (−0.7 to 0.14)	0.89	0 (−1 to 2)	
Incubation period	3.1 (2.6)	3.3 (2.7)	−0.2 (−0.6 to 0.16)	0.29	3 (1–4)	3 (1–5)
Unvaccinated index case-patient	3.1 (2.7)	3.3 (2.6)	−0.2 (−0.7 to 0.3)	0.46	3 (1–4)	
Vaccinated index case-patient	3 (2.2)	3.4 (2.9)	−0.4 (−0.9 to 0.14)	0.16	3 (2–4)	
Serial interval	4.8 (3)	5.4 (3.1)	−0.6 (−1 to −0.15)	0.008	4 (3–6)	5 (3–8)
Unvaccinated index case-patient	4.7 (3.1)	5.4 (3.1)	−0.7 (−1.3 to −0.06)	0.02		5 (3–8)
Vaccinated index case-patient	4.9 (3.1)	5.3 (3.1)	−0.4 (−1 to 0.28)	0.26		5 (3–7)

*IQR, interquartile range.
†Student t test for difference in mean of Delta and Omicron period.

of days between the index case SOD and the secondary case SOD (*6*).

For the 3 periods, we report mean (SD) and median (interquartile range [IQR]). We calculated Omicron-Delta mean differences and Student t test, 95% CI, and p values (Table 2). We constructed histograms, density plots, boxplots, and cumulative distribution functions for Omicron (Figure 1) and Delta (Appendix Figure).

The transmission period of Omicron cases was shorter (mean 0.5, median 0 days) than Delta cases (mean 0.8, median 1 day) (Figure 1, panel A) and grouped around day 0 after SOD. Mean differences between both variants were significant (−0.3 days; SD −0.56 to −0.02), and IQRs remained equal (Figure 2).

Incubation period had a median of 3 days for both variants and IQR was shorter for Omicron (Figure 1, panel B). We found no mean differences in incubation period. Finally, mean serial interval was significantly shorter for Omicron (4.8 vs. 5.4 days, SD −0.6 to −0.15; p = 0.008) (Figure 1, panel C) with a median of 4 versus 5 days. We found no differences within variants between vaccine status for any of the periods.

Conclusions

Omicron has spread quickly worldwide since its first notification on November 11, 2021 (*7*). Our findings demonstrate a significant increase in SAR for Omicron cases in Cantabria, Spain, compared with Delta in a similar period and with high vaccine coverage (>80% of target population). Global SAR and social SAR increased by ≈50% (26.3% to 39.3% for global and 16.2% to 30.5% for social), but we did not find significant differences in household SAR. By the end of December, cases increased exponentially, and the Christmas holiday could have affected the number of contacts per case in the occupational and social settings

In this study, vaccinated Omicron index case-patients seemed to have the same transmission capacity as nonvaccinated persons. We did not find this increased transmission capacity for the Delta variant, where significant differences in SAR were observed in global, household, and occupational settings (Table 1) within groups.

Omicron's increased transmissibility is consistent with the registered tendency of transmission when persons are asymptomatic or early in the symptomatic phase. SARS-CoV-2 transmission took place from day −1 to day +3 of SOD, when most secondary case contacts happen. Median day of transmission was reduced from +1 after symptom onset in Delta to day 0 (SOD) in Omicron (Table 1). Even though the incubation period did not statistically differ, serial interval was significantly decreased in Omicron (mean 4.8 vs. 5.3, median 4 vs. 5) and was again more grouped to the left (IQR 3 vs. 5). Of secondary cases, 90% had an incubation period of 6 days for Omicron and 7 days for Delta.

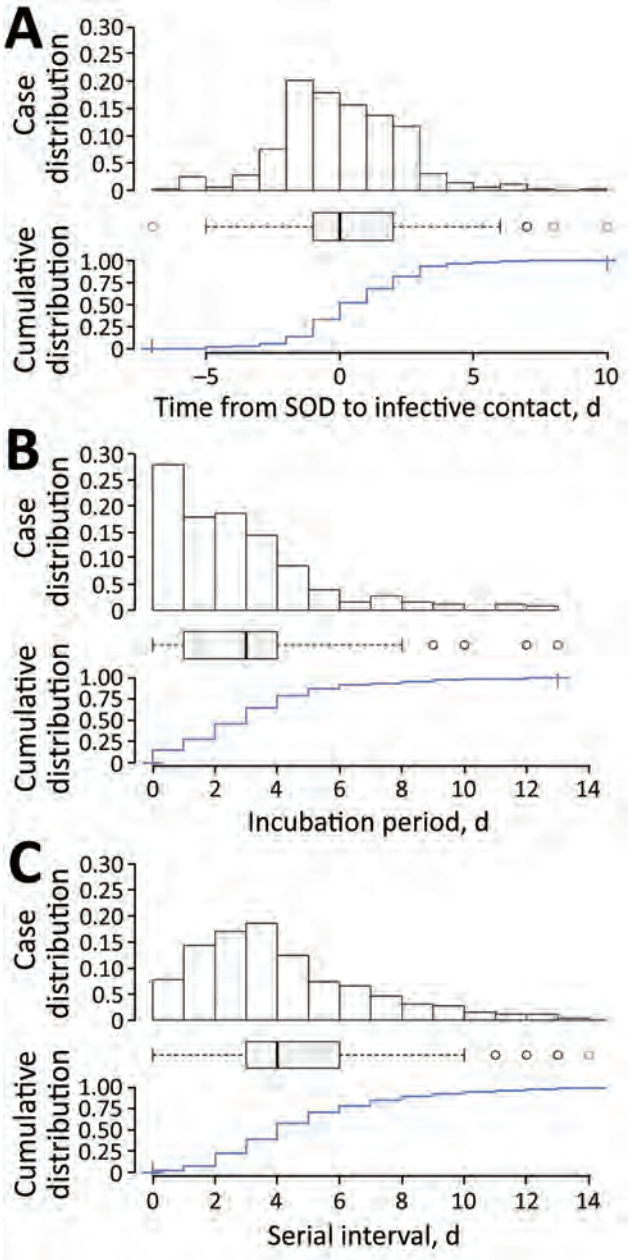

Figure 1. Distribution of Omicron variant SARS-CoV-2 cases, Cantabria, Spain, December 2021. A) Transmission period; B) incubation period; C) serial interval. Each panel shows case density over time (top), a typical boxplot (middle), and cumulative distribution for the period (bottom). For the boxplot, the center line indicates the median, the box left and right ends the interquartile range, the error bars 95% CI, and the open circles outliers. SOD, symptom onset date.

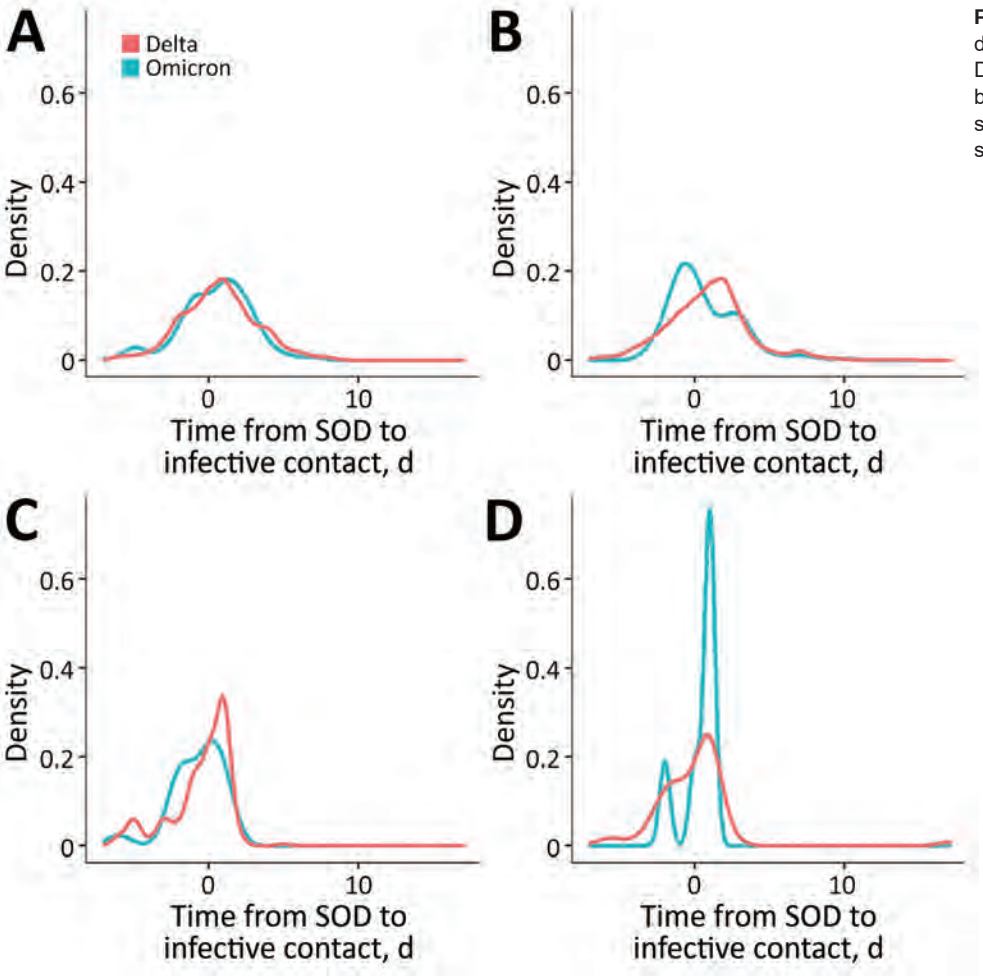

Figure 2. Transmission period distribution for Omicron and Delta variant SARS-CoV-2 cases by vaccination and symptom status, Cantabria, Spain. SOD, symptom onset date.

It has been hypothesized that Omicron's increased SAR is derived from a concentration of contagion events in the presymptomatic or paucisymptomatic period, when infected persons might be unaware of their status and containment measures such as contact-tracing, isolation, and quick testing are not possible. Half of Omicron contagion events happened before symptom onset. This finding could imply that the effectiveness of nonpharmaceutical measures targeting symptomatic cases (such as contact tracing, quick testing, and isolation) would be substantially decreased in the absence of preventive measures such as social distancing and limiting large gatherings or social meetings.

The social and economic effects of isolation and quarantine have led to continued debate regarding appropriate and adequate quarantine periods, especially in light of possible changes in disease dynamics caused by the Omicron variant (*8*–*13*). In this study, transmission for Omicron and Delta >5 days after SOD was rare, accounting for 8/356 (2%) of secondary cases in Omicron and 79/1,642 (5%) in Delta (Figure 2). This finding could potentially contribute to the debate about quarantine and isolation periods and lessening the social and economic costs of COVID-19 control measures.

This article was preprinted at https://www.researchsquare.com/article/rs-1279005/v1.

Acknowledgments

We thank all public health, health, and other workers involved in the contact tracing program of Cantabria.

About the Author

Dr. Del Águila is a resident doctor in preventive medicine and public health at University Hospital of Móstoles, Madrid, Spain. This work was done under an internship at Public Health Observatory of Cantabria, Santander, Spain. He is interested in field epidemiology, infectious diseases, and epidemics, where he focuses his research activity.

References

1. World Health Organization. Classification of Omicron (B.1.1.529): SARS-CoV-2 variant of concern [cited 2022 Jan 12]. https://www.who.int/news/item/26-11-2021-classification-of-omicron-(b.1.1.529)-sars-cov-2-variant-of-concern
2. Shepard SS, Meno S, Bahl J, Wilson MM, Barnes J, Neuhaus E. Viral deep sequencing needs an adaptive approach: IRMA, the iterative refinement meta-assembler. BMC Genomics. 2016;17:708. https://doi.org/10.1186/s12864-016-3030-6
3. O'Toole Á, Scher E, Underwood A, Jackson B, Hill V, McCrone JT, et al. Assignment of epidemiological lineages in an emerging pandemic using the pangolin tool. Virus Evol. 2021;7:veab064.
4. Directorate General of Public Health, Cantabria Health Department. Protocol for detection and management of COVID-19 cases and contacts, version 8 [in Spanish] [cited 2022 Jan 14]. https://www.scsalud.es/documents/2162705/9256837/PROTOCOLO_MANEJO+CASOS+Y+CONTACTOS_V8_221221.pdf/1f7542f9-eca4-5460-1a96-1a121bbca4f5?t=1640176144144
5. Fung HF, Martinez L, Alarid-Escudero F, Salomon JA, Studdert DM, Andrews JR, et al.; Stanford-CIDE Coronavirus Simulation Model (SC-COSMO) Modeling Group. The household secondary attack rate of severe acute respiratory syndrome coronavirus 2 (SARS-CoV-2): a rapid review. Clin Infect Dis. 2021;73(Suppl 2):S138–45. https://doi.org/10.1093/cid/ciaa1558
6. Alene M, Yismaw L, Assemie MA, Ketema DB, Gietaneh W, Birhan TY. Serial interval and incubation period of COVID-19: a systematic review and meta-analysis. BMC Infect Dis. 2021;21:257. https://doi.org/10.1186/s12879-021-05950-x
7. European Centre for Disease Prevention and Control. Assessment of the further emergence and potential impact of the SARS-CoV-2 Omicron variant of concern in the context of ongoing transmission of the Delta variant of concern in the EU/EEA, 18th update—15 December 2021. Stockholm; The Centre; 2021.
8. Centers for Disease Control and Prevention. Quarantine and isolation: COVID-19 quarantine and isolation recommendations. 2022 [cited 2022 Jan 19]. https://www.cdc.gov/coronavirus/2019-ncov/your-health/quarantine-isolation.html
9. European Centre for Disease Prevention and Control. Guidance on quarantine of close contacts to COVID-19 cases and isolation of COVID-19 cases, in the current epidemiological situation, 7 January 2022 [cited 2022 Jan 14]. https://www.ecdc.europa.eu/en/covid-19/prevention-and-control/quarantine-and-isolation
10. Ministry of Health. Quick risk assessment, SARS-CoV-2 variants in Spain: Omicron, 8th update, December 21, 2021 [in Spanish] [cited 2022 Jan 14]. https://www.sanidad.gob.es/profesionales/saludPublica/ccayes/alertasActual/nCov/documentos/20211221-ERR.pdf
11. Hay J, Kissler S, Fauver JR, Mack C, Tai CG, Samant RM, et al. Viral dynamics and duration of PCR positivity of the SARS-CoV-2 Omicron variant. 2022 [cited 2022 Jan 19]. https://dash.harvard.edu/handle/1/37370587
12. National Institute of Infectious Diseases. Active epidemiological investigation on SARS-CoV-2 infection caused by Omicron variant (Pango lineage B.1.1.529) in Japan: preliminary report on infectious period [cited 2022 Jan 19]. https://www.niid.go.jp/niid/en/2019-ncov-e/10884-covid19-66-en.html
13. Davies M, Bramwell LR, Jeffery N, Bunce B, Lee BP, Knight B, et al. Persistence of clinically relevant levels of SARS-CoV2 envelope gene subgenomic RNAs in non-immunocompromised individuals. Int J Infect Dis. 2022;116:418–25.

Address for correspondence: Adrian Aginagalde Llorente, Public Health Observatory of Cantabria, Santander, Spain. Marquis of Valdecilla Foundation, Faculty of Nursing Building 5th floor. Avda. de Valdecilla s/n 39008 Santander, Cantabria, Spain; email: director.ospc@fmdv.org

Introduction and Rapid Spread of SARS-CoV-2 Omicron Variant and Dynamics of BA.1 and BA.1.1 Sublineages, Finland, December 2021

Hanna Vauhkonen, Phuoc Truong Nguyen, Ravi Kant, Ilja Plyusnin, Mert Erdin, Satu Kurkela, Hanna Liimatainen, Niina Ikonen, Soile Blomqvist, Kirsi Liitsola, Erika Lindh, Otto Helve, Hanna Jarva, Raisa Loginov, Aino Palva, Tiina Hannunen, Sari Hannula, Mikko Parry, Paula Kauppi, Antti Vaheri, Tarja Sironen, Maija Lappalainen, Carita Savolainen-Kopra, Teemu Smura, Olli Vapalahti

Multiple introductions of SARS-COV-2 Omicron variant BA.1 and BA.1.1. lineages to Finland were detected in early December 2021. Within 3 weeks, Omicron overtook Delta as the most common variant in the capital region. Sequence analysis demonstrated the emergence and spread through community transmission of a large cluster of BA.1.1 virus.

The most recent SARS-CoV-2 variant of concern, Omicron (Pango lineage B.1.1.529), was first detected in South Africa (*1*), although it might have emerged elsewhere, and has since spread globally at an unforeseen speed. Notable examples include a superspreading event in Norway (*2*) and the rapid increase in incidence in Denmark (*3*) despite high vaccination coverage (83% of infected persons had received 2–3 vaccine doses). This rapid spread indicates the novel variant's exceptional transmissibility, as well as its potential for reinfection and vaccination breakthrough. We describe the genotypes of cases of Omicron entering Finland from their early spread up to established community transmission through the first week of January 2022. No ethics approval was needed because this study was based on routine COVID-19 surveillance data. The study regarding Helsinki University Hospital (HUH) samples was approved by the local ethical and research committee (Helsinki and Uusimaa Hospital District [HUS]; Clinical microbiology of COVID-19: diagnostics, laboratory findings and biorisks; HUS/244/2021).

Author affiliations: University of Helsinki, Helsinki, Finland (H. Vauhkonen, P. Truong Nguyen, R. Kant, I. Plyusnin, M. Erdin, A. Vaheri, T. Sironen, T. Smura, O. Vapalahti); University of Helsinki and Helsinki University Hospital, Uusimaa, Finland (S. Kurkela, H. Liimatainen, R. Loginov, M. Parry, P. Kauppi, M. Lappalainen, T. Smura, O. Vapalahti); Finnish Institute for Health and Welfare (THL), Helsinki (N. Ikonen, S. Blomqvist, K. Liitsola, E. Lindh, O. Helve, C. Savolainen-Kopra); Institute for Molecular Medicine Finland (FIMM), Helsinki (A. Palva, T. Hannunen, S. Hannula)

DOI: https://doi.org/10.3201/eid2806.220515

The Study

A total of 99,988 samples found positive for SARS-CoV-2 by reverse transcription PCR, 12.1% of 825,006 total samples tested, were detected in Finland during the study period, November 29, 2021–January 6, 2022 (Figure 1). Weekly positivity rates among persons tested rose from 6.1% of 156,077 in week 48 to 25.6% of 172,451 (3.1% of the Finnish population) in week 52 (https://sampo.thl.fi). In HUS, test positivity increased from 5.0% to 36.7% over the corresponding weeks 48–52. After a change in testing strategy favoring home antigen testing, the number of registered SARS-CoV-2 cases dropped (Appendix, https://wwwnc.cdc.gov/EID/article/28/6/22-0515-App1.pdf).

We estimated the proportions of Omicron variant lineages BA.1 and BA.1.1 within HUS by comparing PCR-based data on S-gene target failure (SGTF) to that of other circulating lineages (Figure 1; Appendix). The results showed a decrease in SGTF rates from week 24, when the proportion of the Alpha variant (B.1.1.7) was declining, to near 0 when the Delta variant (B.1.617.2) was dominant. This decrease aligns well with sequence-confirmed lineage turnover

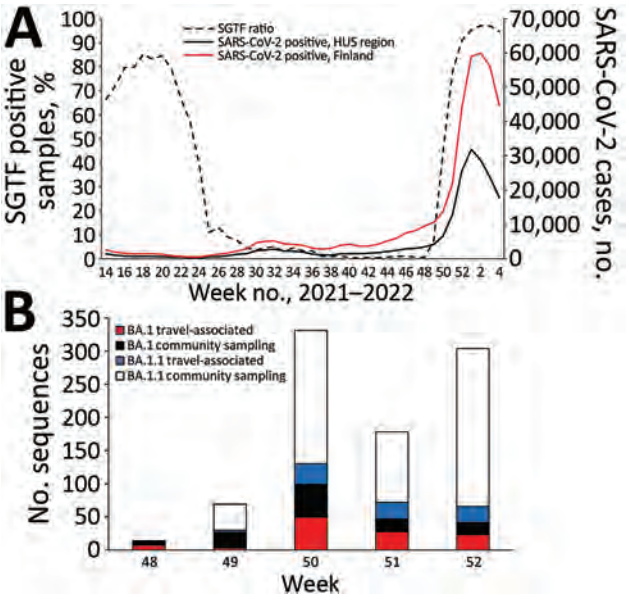

Figure 1. Introduction and spread of SARS-CoV-2 Omicron variant in Finland in late 2021–early 2022. A) Confirmed SARS-CoV-2 positives in Finland (red) and in the HUS region (black) and the proportion of SGTF measured by reverse transcription PCR–positive cases analyzed by the HUS Clinical Microbiology division (dashed line) from week 14 in 2021 through week 4 in 2022 (National Infectious Disease Registry, https://www.thl.fi/ttr/gen/rpt/tilastot.html). B) Weekly numbers of travel-associated and community sampling–derived Omicron cases (Pango lineages BA.1 and BA.1.1) for weeks 48–52, 2021. Travel-associated status was defined by either being sampled at a border or a patient record indicating most likely country of infection abroad. The lower amount of sequences obtained for week 51 originates most likely from the Christmas holiday season. Week 52 was the last full week of our study period. HUS, Helsinki and Uusimaa Hospital District; SGTF, S-gene target failure

reported elsewhere (4). Thereafter, the proportion of SGTF rose steeply from week 48 of 2021 until it reached 97% in week 2 of 2022 (Figure 1), indicating a rapid spread of the BA.1 and BA.1.1 lineages in the capital region of Finland.

The sequenced samples consisted of randomly selected population samples and samples collected at border entry (through airports, harbors, and land borders) to Finland (Table). In addition, a small proportion was preselected based on SGTF positivity (Appendix). Omicron sequence data consisted of 962 sequences, 33.4% of all sequenced samples (n = 3,100; ≈2% of all confirmed cases), during November 29, 2021–January 6, 2022. We collected 133 samples at points of border entry and recorded the number of patients in each hospital district, demographic distribution, and travel status (Table), including countries of origin for the travel-associated cases (Appendix Figure 2). In addition, we added 15 Omicron sequences obtained from hospitalized patients in HUH to the sequence dataset (Appendix Table 1).

We identified Omicron cases in 5 travelers returning to Finland from Sweden through Denmark during November 29–30, 2021. All 5 members of the travel party, who lived in 3 different hospital districts (HUS, Hospital District of Southwest Finland, and North Savo Hospital District), were found to be Omicron positive through PCR testing and sequencing. The identified sequences clustered together with reference sequences mainly from Denmark and Sweden. However, introduction from this travel party did not lead to wide community circulation.

Table. Patient data for 979 sequenced Omicron genomes in investigation of SARS-CoV-2 Omicron variant and dynamics of BA.1 and BA.1.1 sublineages, Finland, December 2021*

Variables	No. (%)†
Sex	
M	513 (52.4)
F	466 (47.6)
Travel	
Abroad	57 (5.8)
Border‡	20 (2.0)
Finland	234 (23.9)
Border‡	6 (0.6)
NA§	688 (70.3)
Border‡	107 (10.9)
Age, y	
Range	0–98
Mean	36.2
Median	34
Sample origin	
HUS	662 (79.7)
Non-HUS total¶	169 (20.3)
Non-HUS by district, no.	
Central Finland Health Care District	6
Central Ostrobothnia Hospital District	6
East Savo Hospital District	3
Hospital District of South Ostrobothnia	10
Hospital District of Southwest Finland	18
Kainuu Social and Health Care Joint Authority	5
Tavastia Proper Hospital District	3
Kymenlaakso Social and Health Services	7
Lapland Hospital District	4
North Karelia Social and Health Care Authority	17
North Ostrobothnia Hospital District	15
North Savo Hospital District	12
Pirkanmaa Hospital District	10
Päijät-Häme Hospital District	3
Satakunta Hospital District	20
South Karelia Social and Health Care District	12
South Savo Social and Health Care Authority	5
Vaasa Hospital District	6
Åland Hospital District	7
Other sample origin	
HUH	15 (1.5)
Border	133 (13.6)

*NA, not available; HUH, Helsinki University Hospital; HUS, Helsinki and Uusimaa Hospital District; Non-HUS, hospital district other than HUS.
†Unless otherwise indicated.
‡Border, samples collected from border entry (airports, harbors, and land).
§Travel data not available, probably originating from Finland.
¶Other, sample collection based on other than hospital districts.

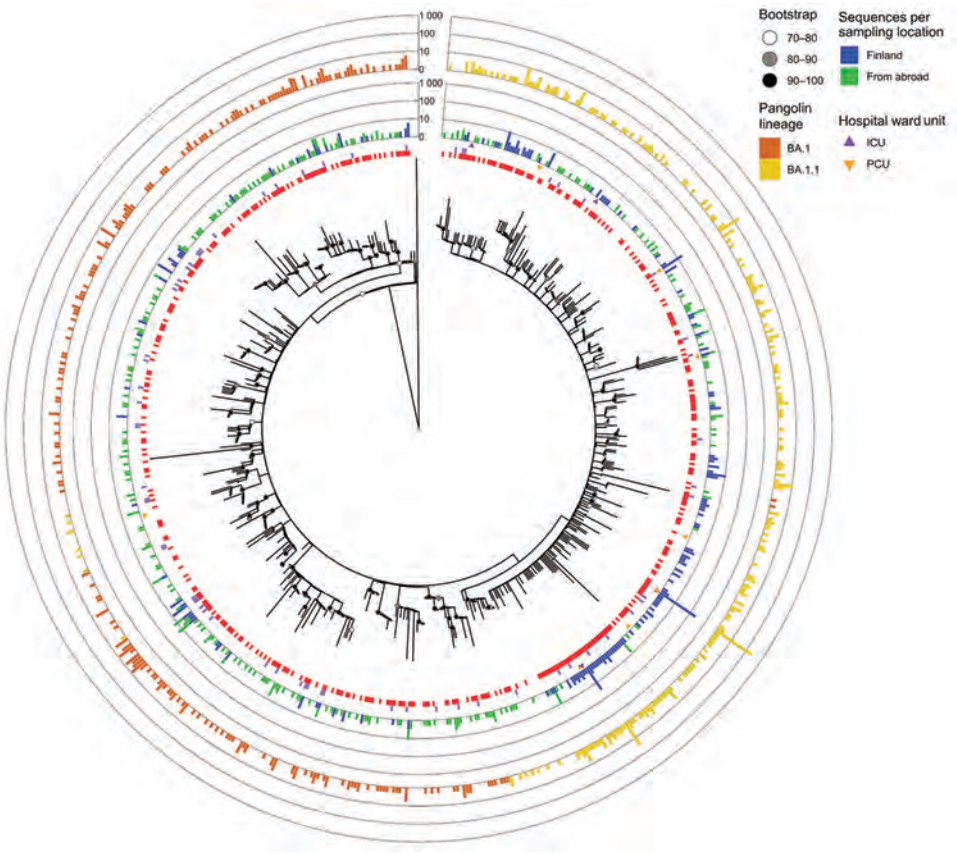

Figure 2. Clustering analysis of Omicron sequences in study of SARS-CoV-2 Omicron variant in Finland in late 2021–early 2022. The collapsed maximum-likelihood phylogenetic tree shows Omicron genomes sampled in Finland (n = 870) and reference sequences from other countries (n = 754), the reference dataset we used. The outermost bar plot shows the number of BA.1 and BA.1.1 sequences in each cluster. Purple squares indicate Omicron sequences collected from a Finland border; clusters with border samples each contain 1–9 sequences. Clustering analysis revealed that, by the beginning of January 2022, aside from 1 major BA.1.1 cluster (n = 236, 27.1% of all cases in Finland during the study period, November 29, 2021–January 6, 2022), most (n = 634, 72.8% of cases) Omicron cases in Finland were either singletons or small clusters (≤30 sequences). The tree was inferred using the IQTREE2 version 2.0.6 (http://www.iqtree.org) using ModelFinder and 1,000 bootstraps were computed with the integrated Ultrafast bootstrap algorithm and the clusters (red squares) with TreeCluster version 1.0.3 (https://github.com/niemasd/TreeCluster) using an arbitrary branch length of 0.001 and support value of 70. Triangles indicate sequences recorded from patients in the ICU or PCU. The tree is rooted to an Omicron BA.2 sequence (Genbank accession no. OV698431.1). ICU, intensive care unit; PCU, pulmonary care unit.

After the first introduction events, the number of weekly sequence-confirmed Omicron cases rose sharply during weeks 49 and 50 (Figure 1, panel B). Although weekly numbers of travel-associated (most likely imported) cases of lineage BA.1 did not differ from those for BA.1.1 ($\chi^2 = 1.03$; p = 0.5975), the proportion of BA.1.1 in the community samples was significantly higher than that of BA.1 (2-sample z-test, p = 0.0024, week 49 vs. week 50; Appendix Figure 3.). We did not detect lineage BA.2. during the study period.

Our phylogenetic and clustering analysis (Figure 2; Appendix Figure 1) inferred 80 small, highly supported lineage BA.1 subclusters that contained sequences (n = 168) from Finland, as well as 47 BA.1 sequences that were singletons or from low-support clusters. For BA.1.1 sequences, the analysis inferred 129 clusters containing BA.1.1 sequences (n = 570) from Finland and 75 singletons. Of note, among BA.1.1 clusters, 1 cluster contained 236 identical sequences, 24.5% of all Omicron sequences from Finland recorded during the study period. These sequences were also identical to isolate HKU-344 (OM212473) from Hong Kong, collected November 27, 2021. These identical sequences were detected starting December 7 through the end of the study period. Most of these cases, 197/236 (83.5%), were detected in HUS, including the first 2 cases on December 7. Eleven of the sequences from this clade were imported, with the most likely countries of infection reported as Estonia (December 9, 2021), Sweden (December 15), and the United Kingdom, Spain, or Portugal (all December 20). An additional 8 cases were sampled at the border during December 15–21; 1 originated from Sweden, but no data were available about the country of infection for the other cases. Although the analysis of imported cases suggested that a virus of identical genotype was circulating in several European countries, locally acquired infections of this genotype were detected before the documented importation events.

Altogether the results suggest widescale rapid spread of BA.1.1 in Finland. COVID-19 patients hospitalized at HUH pulmonary or intensive care units showed similar, albeit delayed, lineage turnover from Delta variant to Omicron variant (Appendix Figure 4), consistent with population-level data.

Conclusions

We characterize the rapid increase in incidence of the SARS-CoV-2 Omicron variant in Finland. Specifically, our data suggest that BA.1.1 rapidly emerged as the dominant lineage over its parent, BA.1. The BA.1.1 lineage-defining R346K substitution in the spike protein has been suspected of increasing transmission rates more than the BA.1 lineage. This substitution, which occurred convergently in the Mu variant of concern, provides evidence of positive selection (*1*,*5*) and affects antibody binding (*6*). Although this mutation might provide an additional transmission advantage through enhanced immune-escape properties in a population, alternative options such as the founder effect cannot be ruled out for explaining the rapidly established dominance of this lineage in Finland.

Overall, Finland represents one of the countries with a rapid surge of Omicron variant BA.1.1 lineage introduced into a population largely vaccinated with 2 shots and within an epidemiologic landscape of increasing Delta circulation and absent or very low BA.2 circulation. These dynamics resulted in the dominance of BA.1.1 over both the Omicron BA.1 and Delta strains. Our study exemplifies the need for genomic surveillance and rapid detection of emerging SARS-CoV-2 lineages to support public health response and mitigation efforts.

Acknowledgments

We acknowledge CSC-IT Center for Science, Finland, for providing computational resources. Sequencing was performed by the FIMM Genomics NGS sequencing unit at the University of Helsinki, supported by HiLIFE and Biocenter Finland.

This study was supported by the Academy of Finland (grant no. 336490, 339510), VEO (versatile emerging infectious disease observatory), European Union Horizon 2020 (grant no. 874735), Finnish Institute for Health and Welfare, Jane and Aatos Erkko Foundation, and Helsinki University Hospital Funds (TYH2018322 and TYH2021343).

About the Author

Dr. Vauhkonen is a laboratory coordinator at the Departmentof Virology at the University of Helsinki, Finland. Her research interests include molecular epidemiology of viral zoonoses, next-generation sequencing, and bioinformatics.

References

1. Viana R, Moyo S, Amoako DG, Tegally H, Scheepers C, Althaus CL, et al. Rapid epidemic expansion of the SARS-CoV-2 Omicron variant in southern Africa. Nature. 2022;603:679–86. https://doi.org/10.1038/s41586-022-04411-y
2. Brandal LT, MacDonald E, Veneti L, Ravlo T, Lange H, Naseer U, et al. Outbreak caused by the SARS-CoV-2 Omicron variant in Norway, November to December 2021. Euro Surveill. 2021;26:2101147. https://doi.org/10.2807/1560-7917.ES.2021.26.50.2101147
3. Espenhain L, Funk T, Overvad M, Edslev SM, Fonager J, Ingham AC, et al. Epidemiological characterisation of the first 785 SARS-CoV-2 Omicron variant cases in Denmark, December 2021. Euro Surveill. 2021;26:2101146. https://doi.org/10.2807/1560-7917.ES.2021.26.50.2101146
4. Kant R, Nguyen PT, Blomqvist S, Erdin M, Alburkat H, Suvanto M, et al. Incidence trends for SARS-CoV-2 Alpha and Beta variants, Finland, Spring 2021. Emerg Infect Dis. 2021;27:3137–41. https://doi.org/10.3201/eid2712.211631
5. Cedro-Tanda A, Gómez-Romero L, de Anda-Jauregui G, Garnica-López D, Alfaro-Mora Y, Sánchez-Xochipa S, et al. Early genomic, epidemiological, and clinical description of the SARS-CoV-2 Omicron variant in Mexico City. Viruses. 2022;14:545. https://doi.org/10.3390/v14030545
6. Greaney AJ, Starr TN, Gilchuk P, Zost SJ, Binshtein E, Loes AN, et al. Complete mapping of mutations to the SARS-CoV-2 spike receptor-binding domain that escape antibody recognition. Cell Host Microbe. 2021;29:44–57.e9. https://doi.org/10.1016/j.chom.2020.11.007

Address for correspondence: Hanna Vauhkonen, Department of Virology, University of Helsinki, Haartmaninkatu 3, 00014, Helsinki, Uusimaa, Finland; email: hanna.vauhkonen@helsinki.fi; Olli Vapalahti, Department of Virology, University of Helsinki, Haartmaninkatu 3, 00014, Helsinki, Uusimaa, Finland; email: olli.vapalahti@helsinki.fi

Rapid Increase of Community SARS-CoV-2 Seroprevalence during Second Wave of COVID-19, Yaoundé, Cameroon

Francis Ateba Ndongo, Emilande Guichet, Eric Donald Mimbé, Justin Ndié, Raphael Pelloquin, Marie Varloteaux, Livo Esemu, Mireille Mpoudi-Etame, Nadine Lamare, Ginette Edoul, Rodrigue Kamga Wouambo, Dowbiss Meta Djomsi, Marcel Tongo, Félicité Naah Tabala, Rogacien Kana Dongmo, Mamadou Saliou Kalifa Diallo, Julie Bouillin, Guillaume Thaurignac, Ahidjo Ayouba, Martine Peeters, Eric Delaporte, Anne-Cécile Zoung-Kanyi Bissek, Eitel Mpoudi-Ngolé

We conducted 2 independent population-based SARS-CoV-2 serosurveys in Yaoundé, Cameroon, during January 27–February 6 and April 24–May 19, 2021. Overall age-standardized SARS-CoV-2 IgG seroprevalence increased from 18.6% in the first survey to 51.3% in the second (p<0.001). This finding illustrates high community transmission during the second wave of COVID-19.

Since the recognition of the first cases of COVID-19 at the end of 2019 in Wuhan, China, SARS-CoV-2 has spread rapidly across the globe. By late November 2021, almost 260 million confirmed cases, including at least 5 million deaths, had been reported (*1*). Cases from Africa represent only 3.4% of those cases worldwide (*1*,*2*), but serologic surveys demonstrate that the extent of SARS-CoV-2 spread in Africa is higher (*3*). After the first pandemic wave, overall seroprevalence in Africa was estimated at ≈22%, ranging from <1% to >70% depending on country and study population (*3*). The few studies reporting data after the second wave in Africa demonstrated a rapid increase to >50% seroprevalence (*4*–*6*). Underestimation of COVID-19 cases was most likely caused by weak healthcare infrastructure, low or no access to diagnostic testing, and higher proportions of paucisymptomatic or asymptomatic disease related to younger population or cross-reactive immunity from other coronavirus infections. The overall objective of our study was to evaluate the effect of the second wave of COVID-19 on SARS-COV-2 seroprevalence in the general population of Yaoundé, the capital city of Cameroon.

Author affiliations: Ministry of Public Health of Cameroon Division of Operational Research in Health, Yaoundé, Cameroon (F. Ateba Ndongo, J. Ndié, F.N. Tabala, R.K. Dongmo, A.-C. Zoung-Kanyi Bissek); Recherches Translationnelles sur le VIH et les Maladies Infectieuses, University of Montpellier, Institut de Recherche pour le Développement, Institut National de la Santé et de la Recherche Médicale, Montpellier, France (E. Guichet, R. Pelloquin, M.S.K. Diallo, J. Bouillin, G. Thaurignac, A. Ayouba, M. Peeters, E. Delaporte); French National Agency for Research on AIDS and Infectious Diseases, Cameroon Site, Central Hospital of Yaoundé, Yaoundé (E.D. Mimbé, M. Varloteaux, A.-C. Zoung-Kanyi Bissek, E. Mpoudi-Ngolé); Centre de Recherche sur les Maladies Emergentes et Réémergentes, Yaoundé (L. Esemu, N. Lamare, G. Edoul, R. Kamga Wouambo, D. Meta Djomsi, M. Tongo, E. Mpoudi-Ngolé); Military Hospital of Yaoundé, Yaoundé (M. Mpoudi-Etame)

DOI: https://doi.org/10.3201/eid2806.212580

The Study

We conducted 2 population-based seroprevalence surveys in Yaoundé during January 27–February 6, 2021 (survey 1) and April 24–May 19, 2021 (survey 2). We adapted the study design from the World Health Organization population-based age-stratified seroepidemiologic investigation protocol for COVID-19 infection, version 2.0 (*7*). We randomly selected households in 6 of the 7 health districts in Yaoundé, with a probability of being selected proportional to the population number in each enumeration area (Appendix Figure 1, https://wwwnc.cdc.gov/EID/article/28/6/21-2580-App1.pdf). In 50% of households, we invited all residents to participate; among the remaining 50%, we invited only residents ≥40 years of age. We calculated sample size to estimate

overall seroprevalence in Yaoundé. The samples were independent for the 2 surveys. All persons belonging to the selected household were eligible. We scheduled appointments for participants who were absent during the survey. We used individual questionnaires to collect sociodemographic data, medical history associated with COVID-19 symptoms (in the 4 months before the start of the survey), contact with COVID-19 patients, and previous SARS-CoV-2 tests (recall period beginning in March 2020). We offered PCR testing to all participants who were suspected to be SARS-CoV-2–positive. We obtained written consent from all adults and written parental consent for participants <21 years of age (with children's assent when ≥10 years of age). The study was approved by the national ethics committee (approval no. 2020/10/1310/CE/CNERSH/SP).

We collected whole blood samples in EDTA tubes and as dried blood spot (DBS) samples for children and other participants who declined to provide venous blood. We eluted DBS samples and used 100 μL of diluted eluate, adjusted at a final plasma dilution of 1/200, as previously validated (Appendix Figure 2), to test for SARS-CoV-2 antibodies with a previously developed, highly sensitive, and specific multiplex assay (Luminex Corporation, https://www.luminexcorp.com) using recombinant nucleocapsid (NC) and spike (SP) SARS-CoV-2 proteins (*8*). We considered samples positive when they reacted simultaneously with NC and S proteins but considered samples reacting with only 1 antigen indeterminate because of the difficulty discriminating between antibody decline or lower specificity of single-antigen reaction, especially with samples from populations in Africa (*9*,*10*). The test was previously evaluated on 1,197 samples from Africa before the COVID-19 pandemic, including 184 from Cameroon, with 99.7% specificity (*11*).

We performed statistical analysis with Stata 16 (StataCorp, https://www.stata.com). We age-standardized the overall seroprevalence estimate on the basis of available demographic data (*12*) and tested associations between positive serologic tests and key risk factors with multivariate logistic models and likelihood ratio tests. We used the Pearson χ^2 test to compare categorical descriptive outcomes.

In the first survey, 786 (47.7%) of 1,647 eligible participants from 392 households were included. For 722 persons, we obtained sufficient sample volume for antibody testing. To improve participation for the second survey, we strengthened community mobilization, conducted surveys on the weekend, and scheduled appointments for absent participants. In the second survey, 1,234 (85.3%) of 1,447 eligible persons from 424 households were included. Serologic data were available for 1,228 persons. Distribution of sex was comparable between the surveys; the proportion of participants <20 years of age was higher but not significantly so in the second survey (Table 1). Approximately 15% of participants reported a previous diagnostic SARS-CoV-2 PCR test; only 1.3%

Table 1. Sociodemographic characteristics of participants in study of community SARS-CoV-2 seroprevalence during second wave of COVID-19 epidemic, by sex, Yaoundé, Cameroon, 2021*

	Survey 1, January 27–February 6			Survey 2, April 24–May 19		
Characteristic	Female	Male	Total	Female	Male	Total
Age group, y		n = 786			n = 1,234	
0–19	132 (28.3)	123 (37.7)	255 (32.2)	261 (36.3)	208 (40.8)	469 (38.0)
20–39	205 (44.7)	103 (31.8)	308 (39.3)	278 (38.6)	165 (32.1)	443 (35.9)
≥40	124 (27.0)	99 (30.7)	223 (28.5)	181 (25.1)	141 (27.4)	322 (26.1)
Marital status		n = 638			n = 1,216	
Single	186 (48.1)	133 (54.0)	319 (50.0)	442 (62.4)	365 (71.9)	807 (66.4)
Married or living as a couple	158 (40.8)	109 (43.4)	267 (41.9)	216 (30.5)	132 (26.0)	348 (28.6)
Divorced or separated	37 (9.6)	3 (1.2)	40 (6.3)	43 (6.1)	10 (2.0)	53 (4.4)
Widower or widow	6 (1.6)	6 (2.4)	12 (1.9)	7 (1.0)	1 (0.0)	8 (1.0)
Education		n = 681			n = 1,227	
None	26 (6.4)	11 (4.0)	37 (5.4)	75 (10.5)	45 (8.8)	120 (9.8)
Primary school	81 (19.8)	52 (19.1)	133 (19.5)	197 (27.6)	137 (26.8)	334 (27.2)
Secondary school	213 (52.1)	131 (48.2)	344 (50.5)	323 (45.2)	203 (39.7)	526 (42.9)
University	89 (21.8)	78 (28.7)	167 (24.5)	120 (16.8)	127 (24.8)	247 (20.1)
Profession		n = 620			n = 1,192	
Student	100 (26.6)	75 (30.7)	175 (28.2)	242 (34.9)	201 (40.4)	443 (37.2)
Sales or service	67 (17.8)	46 (18.9)	113 (18.2)	145 (20.9)	70 (14.1)	215 (18.0)
Women or men at home	102 (27.1)	0 (0.0)	102 (16.5)	126 (18.2)	4 (0.8)	130 (10.9)
Professional or manager	40 (10.6)	28 (11.5)	68 (11.0)	59 (8.5)	52 (10.4)	111 (9.3)
Construction	0 (0.0)	16 (6.6)	16 (2.6)	1 (0.0)	9 (1.8)	10 (0.8)
Unemployed	20 (5.3)	21 (8.6)	41 (6.6)	71 (10.2)	65 (13.1)	136 (11.4)
Other	47 (12.5)	58 (23.8)	105 (17.0)	50 (7.2)	97 (19.5)	147 (12.3)
Total	461 (58.7)	325 (41.3)	786 (100.0)	720 (58.3)	514 (41.7)	1,234 (100.0)

*Values are no. (%) participants.

Table 2. Seroprevalence of SARS-COV-2 antibodies by age, sex, and medical history in 2 consecutive population-based surveys during second wave of COVID-19, Yaoundé, Cameroon, 2021*

	Participants, survey 1, January 27–February 6				Participants, survey 2, April 24–May 19			
Characteristic	Total no.	No. positive	% Positive (95% CI)	p value	Total no.	No. positive	% Positive (95% CI)	p value
Age group, y				0.002				<0.001
0–19	236	31	13.1 (9.3–18.3)		468	200	42.7 (38.3–47.3)	
20–39	276	71	25.7 (20.8–31.4)		440	263	59.8 (55.0–64.4)	
≥40	210	48	22.9 (17.5–29.2)		320	201	62.8 (57.3–68.0)	
Sex				0.773				0.942
F	423	89	18.5 (14.8–22.9)		718	392	51.0 (47.1–54.8)	
M	299	61	19.0 (14.8–24.1)		510	272	51.6 (47.0–56.1)	
No. symptoms				0.688				0.288
0	271	70	22.5 (17.8–28.0)		776	424	51.8 (48.1–55.5)	
1–2	157	26	12.8 (7.5–21.0)		257	129	47.8 (41.6–54.0)	
3–5	134	27	22.5 (13.5–35.2)		167	92	53.9 (45.6–61.9)	
>5	68	17	18.4 (8.4–35.9)		28	19	57.5 (39.0–75.7)	
Hospitalization				0.150				0.487
Yes	28	6	10.7 (4.4–23.6)		12	8	51.0 (17.3–83.9)	
No	329	64	18.0 (12.8–24.7)		445	229	50.1 (45.1–55.2)	
Total	722	150	18.6 (15.7–21.7)		1,228	664	51.3 (48.3–54.2)	

*Overall seroprevalence estimate was age-standardized, based on available demographic data (*12*).

(1/77) reported a positive test in the first survey and 2.1% (4/194) in the second survey. In both surveys, a limited number of participants (3.3% in the first survey, 4.1% in the second) reported contact with a PCR-confirmed SARS-CoV-2–positive person.

The overall age-standardized SARS-CoV-2 IgG seroprevalence against SP and NC proteins increased from 18.6% (95% CI 15.7%–21.7%) to 51.3% (95% CI 48.3%–54.2%) (p<0.001) during the 3-month period between surveys (Table 2). In both surveys, seroprevalence remained comparable between men and women (Table 2). Seroprevalence increased in all age categories and was significantly higher among persons ≥20 years of age in both surveys (p = 0.002 for survey 1 and p<0.001 for survey 2). The proportion of persons with S protein antibodies only (29.1% vs. 16.9%) was higher than those with NC antibodies only (5.8% vs. 5.2%) (Appendix Table 1). We determined population-level distributions of median fluorescence intensity for each of the SARS-CoV-2 antigens (Appendix Figure 3). We found no association between seropositivity and history of symptoms associated with COVID-19 or hospitalization in general before the survey (Appendix Table 2).

Conclusions

In these 2 consecutive population-based SARS-CoV-2 seroprevalence studies, conducted just before the start of the second wave of COVID-19 (January–February 2021) and at its decreasing trend (April–May 2021) (Appendix Figure 4), we found extensive community transmission in Yaoundé, where seroprevalence reached up to 50%. By the end of November 2021, Cameroon reported only 106,749 cases (*2*), but seroprevalence suggests that by early May 2021, 51% of the population of Yaoundé had antibodies to SARS-CoV-2, corresponding to ≥2 million persons in the total population of Yaoundé (estimated to be ≈4.1 million). Choice of serologic tests is vital (*9*), and therefore we used strict criteria and considered seropositivity as presence of antibodies to 2 different SARS-CoV-2 antigens (*8*,*11*). We cannot exclude that a proportion of the participants with antibodies against a single antigen also had a previous SARS-CoV-2 infection or were seroconverting (*10*).

The disparity in numbers of confirmed cases and persons estimated to have SARS-CoV-2 antibodies clearly demonstrates that COVID-19 infections were mainly paucisymptomatic or asymptomatic (*1*,*2*). We also observed no association between history of symptoms or hospitalization. Moreover, few persons reported contact with confirmed SARS-CoV-2–positive persons or had received a PCR test. Similar findings were reported in other studies in Africa (*4*–*6*).

Overall, the results of the household SARS-CoV-2 serosurveys during the second COVID-19 wave in Yaoundé, Cameroon, show a high seroprevalence and rapid spread in the general population similar to that observed in other countries in Africa (*4*–*6*,*13*). The country faced additional waves, and new population-based studies to monitor the evolution of seroprevalences to the different antibodies against SARS-CoV-2 epitopes will be vital. It can also not be excluded that antigens from the different SARS-CoV-2 variants have to be included in future assays, especially against highly divergent variants as illustrated by the emergence of the Omicron variant.

Acknowledgments

We thank all the participants, the investigation teams, the community health staff, and logistical support of DROS/MINSANTE, ANRS-MIE Cameroon Site, and CREMER in the field. We are also grateful to Sébastien Awono Noah and Caroline Coulon.

This work was supported by the Agence Française de Développement and the Ministère de l'Europe et des Affaires Etrangères, France (Project ARIACOV: Appui à la riposte africaine à l'épidémie de COVID-19, https://www.ariacov.org).

About the Author

Dr. Ateba Ndongo is a medical doctor and epidemiologist affiliated at the Division of Operational Research at the Ministry of Health in Cameroon. His primary research interests are infectious diseases and management of HIV infections in children and adolescents.

References

1. World Health Organization. Coronavirus (COVID-19) dashboard [cited 2021 Nov 26]. https://covid19.who.int
2. Africa Centres for Disease Control and Prevention. Coronavirus disease 2019 (COVID-19) [cited 2021 Nov 26]. https://africacdc.org/covid-19
3. Chisale MRO, Ramazanu S, Mwale SE, Kumwenda P, Chipeta M, Kaminga AC, et al. Seroprevalence of anti-SARS-CoV-2 antibodies in Africa: a systematic review and meta-analysis. Rev Med Virol. 2022;32:e2271. https://doi.org/10.1002/rmv.2271
4. Sagara I, Woodford J, Kone M, Assadou MH, Katile A, Attaher O, et al. Rapidly increasing SARS-CoV-2 seroprevalence and limited clinical disease in three Malian communities: a prospective cohort study. Clin Infect Dis. 2022;74:1030–8. https://doi.org/10.1093/cid/ciab589
5. Fryatt A, Simms V, Bandason T, Redzo N, Olaru ID, Ndhlovu CE, et al. Community SARS-CoV-2 seroprevalence before and after the second wave of SARS-CoV-2 infection in Harare, Zimbabwe. EClinicalMedicine. 2021;41:101172. https://doi.org/10.1016/j.eclinm.2021.101172
6. Kleynhans J, Tempia S, Wolter N, von Gottberg A, Bhiman JN, Buys A, et al.; PHIRST-C Group. SARS-CoV-2 seroprevalence in a rural and urban household cohort during first and second waves of infections, South Africa, July 2020–March 2021. Emerg Infect Dis. 2021;27:3020–9. https://doi.org/10.3201/eid2712.211465
7. World Health Organization. Seroepidemiological investigation protocol for coronavirus 2019 (COVID-19) infection [cited 2021 Nov 3]. https://www.who.int/publications/i/item/WHO-2019-nCoV-Seroepidemiology-2020.2
8. Ayouba A, Thaurignac G, Morquin D, Tuaillon E, Raulino R, Nkuba A, et al. Multiplex detection and dynamics of IgG antibodies to SARS-CoV2 and the highly pathogenic human coronaviruses SARS-CoV and MERS-CoV. J Clin Virol. 2020;129:104521. https://doi.org/10.1016/j.jcv.2020.104521
9. Nkuba Ndaye A, Hoxha A, Madinga J, Mariën J, Peeters M, Leendertz FH, et al. Challenges in interpreting SARS-CoV-2 serological results in African countries. Lancet Glob Health. 2021;9:e588–9. https://doi.org/10.1016/S2214-109X(21)00060-7
10. Lumley SF, Wei J, O'Donnell D, Stoesser NE, Matthews PC, Howarth A, et al.; Oxford University Hospitals Staff Testing Group. The duration, dynamics, and determinants of severe acute respiratory syndrome coronavirus 2 (SARS-CoV-2) antibody responses in individual healthcare workers. Clin Infect Dis. 2021;73:e699–709. https://doi.org/10.1093/cid/ciab004
11. Nkuba AN, Makiala SM, Guichet E, Tshiminyi PM, Bazitama Y, Yambayamba M et al. High prevalence of anti-SARS-CoV-2 antibodies after the first wave of COVID-19 in Kinshasa, Democratic Republic of the Congo: results of a cross-sectional household-based survey. Clin Infect Dis. 2022;74:882–90. https://doi.org/10.1093/cid/ciab515
12. The World Bank. Cameroon: world development indicators. 2019 [cited 2021 Nov 26]. https://data.worldbank.org/country/cameroon
13. Mandolo J, Msefula J, Henrion MYR, Brown C, Moyo B, Samon A, et al. SARS-CoV-2 exposure in Malawian blood donors: an analysis of seroprevalence and variant dynamics between January 2020 and July 2021. BMC Med. 2021;19:303. https://doi.org/10.1186/s12916-021-02187-y

Address for correspondence: Emilande Guichet, TransVIHMI, 911 Avenue Agropolis, 34394 Montpellier, France; email: emilande.guichet@ird.fr

Dynamics of SARS-CoV-2 Antibody Response to CoronaVac followed by Booster Dose of BNT162b2 Vaccine

Marcela Helena Gambim Fonseca, Ana Carolina Matias Dinelly Pinto, Maria Francilene Souza Silva, Amanda Campelo Lima de Melo, Germana Silva Vasconcelos, Eduardo Ruback dos Santos, Fernanda Montenegro de Carvalho Araújo, Luiz Odorico Monteiro de Andrade

We evaluated the longitudinal dynamics of antibody response to the SARS-CoV-2 vaccine CoronaVac and the effect of a booster dose of BNT162b2 vaccine. We found a robust antibody response after the second dose of CoronaVac that wanes over time. The response was recovered by BNT162b2, which boosted anti-spike antibody titers.

Long-term protection against SARS-CoV-2 requires the persistence of vaccine antibodies above protective thresholds, the maintenance of immune memory cells capable of reactivation after subsequent viral exposure, or both (*1*). A decay of circulating SARS-CoV-2 antibodies over time in persons who received CoronaVac (Sinovac, http://www.sinovac.com) have been reported, suggesting the necessity of a third shot of vaccine (*2*). In Brazil, the third dose has been administered, preferably, with the BNT162b2 vaccine (Pfizer-BioNTech, https://www.pfizer.com) (*3*,*4*). Limited information is available about antibody dynamics after CoronaVac vaccine and the recent supplementing with the BNT162b2 booster. Therefore, we evaluated the longitudinal dynamics of the antibody response to CoronaVac up to 230 days after the second dose in a cohort of healthcare workers (HCWs) and evaluated the effect of a booster dose of BNT162b2 on antibody levels. The study was approved by the Ethics Committee of the Hospital Geral Dr. César Cals (Fortaleza, Brazil; approval no. CAAE 39691420.7.0000.5049). We obtained informed consent from all participants.

The Study

We included in this study 99 HCWs of both sexes, ≥18 years of age, who had received 2 doses of the CoronaVac vaccine, with an interval of 28 days between doses, and then a booster shot of BNT162b2 vaccine 8 months after the second CoronaVac dose. Blood collections and serologic tests were performed at Fundação Oswaldo Cruz (Fiocruz; Ceará, Brazil) and analyzed at 7 different timepoints: before vaccination (P1); 28 days after the first CoronaVac dose (P2); 30 (P3) 90 (P4), 180 (P5), and 230 (P6) days after the second CoronaVac dose; and 15 days after the BNT162b2 dose (P7). We monitored the HCWs for SARS-CoV-2 infection by PCR over time.

We tested all serum samples for IgG against nucleocapsid (N) and spike (S) proteins of SARS-CoV-2 by using chemiluminescent microparticle immunoassays on the ARCHITECT i2000SR equipment (Abbott, https://www.abbott.com). The cutoff value was 50 AU/mL for S antibodies and 1.4 index (S/CO) for N antibodies.

We used GraphPad Prism version 9 (https://www.graphpad.com) for statistical analyses. We describe data as median and interquartile range (IQR) or percentage. In group comparisons, we used χ^2 test to analyze the seropositivity data and Kruskal–Wallis test with subsequent Dunn's test to analyze the IgG values. We considered differences with $p<0.05$ to be statistically significant.

The cohort was 70.71% women and 29.29% men. Average age was 32.31 years (95% CI 30.3–34.3 years). The age distribution of persons was as follows: 18–30 years, 42 (42.4%); 31–45 years, 51 (51.5%); and >45 years, 6 (6.1%). Median age for each age group was as follows: 18–30 years, 23.0 years (IQR 20–27.3 years); 31–45 years, 36 years (IQR 32–39 years), >45 years, 56.50 years (IQR 52–63.3 years).

Although all HCWs completed the vaccination schedule, some HCWs were unable to give a blood sample in subsequent phases of the study. Therefore, serum samples were obtained from 99 participants in P1 and P2, 95 in P3, 94 in P4, 89 in P5, 84 in P6, and 74 in P7.

We evaluated the seropositivity and IgG levels for S and N proteins at the different timepoints

Author affiliations: Fundação Oswaldo Cruz, Eusébio, Brazil

DOI: https://doi.org/10.3201/eid2806.220061

(Figure 1). At baseline (P1), S IgG were detectable in 25.3% of HCWs, increasing to 84.9% in P2 and reaching 100% in P3. We then observed a decline in seropositivity was observed to 98.9% in P4, 94.4% in P5, and 89.3% in P6. In P7, seropositivity had recovered to 100%. N IgG was detectable in 8.1% of HCWs in P1, 19.2% in P2, and 52.6% in P3, then reduced to 29.8% in P4, 13.5% in P5, 10.7% in P6, and 12.2% in P7 (Figure 1, panel A). The seroconversion rate was 79.7% for S antibodies and 11.9% for N antibodies after the first CoronaVac dose, increasing to 100% for S antibodies and 43.6% N antibodies after the second dose.

After the first CoronaVac dose (P2), S IgG levels were significantly elevated compared with baseline values (p<0.0001) (Figure 1, panel B; Appendix Table 1, https://wwwnc.cdc.gov/EID/article/28/6/22-0061-App1.pdf). Those S IgG levels increased significantly after the second dose (P3) (p<0.0001). However, antibodies levels waned over time. The third BNT162b2 dose again significantly increased S IgG levels (p<0.0001). We observed a similar change in N IgG (Figure 1, panel C; Appendix Table 1). Median values of N IgG were significantly higher after the second CoronaVac dose (p<0.0001) and declined significantly after vaccination (p = 0.0002). In contrast, the third dose with BNT162b2 did not increase N IgG levels.

We evaluated the antibody response to the vaccine in relation to a previous SARS-CoV-2 infection. Twenty-five volunteers were seropositive in P1 and were included in the COVID-19–positive group. Eight volunteers had a positive PCR result during the study (4 in P3, 4 in P4); they were moved to the COVID-19–positive group.

The HCWs who had COVID-19 maintained the anti-S seropositivity at 100% over time. In relation to HCWs who did not have COVID-19, 79.7% of persons became seropositive to S protein in P2. The seropositivity increased to 100% in P3 but decreased in the next timepoints, recovering in P7 (Figure 2, panel A). The differences in seropositivity between the groups were statistically significant in P2 (p = 0.0145). Anti-N seropositivity was 6 (95% CI 2.7–15.1) times higher in the COVID-19–positive group in P2 compared with the COVID-19–negative group. This difference was reduced in P3, increasing in P4 and stabilizing in P5, reaching levels of 5 (95% CI 1.4–18.4) times higher in the COVID-19–positive group.

In the antibody levels analysis, antibody titers for S protein were higher in the COVID-19–positive group than for the COVID-19–negative group at all timepoints except P3 and P7 (Figure 2, panel B; Appendix Table 2). N IgG levels of COVID-19–positive persons were statistically higher than for COVID-19–negative persons at all timepoints (Figure 2, panel C; Appendix Table 2).

Conclusions

We found an antibody response to N and S protein after 2 doses of CoronaVac vaccine. However, the antibodies declined over time. After immunization, the decline of antibodies is expected because not all vaccine-induced plasmablasts commit or are maintained as long-lived memory plasma cells (*5*). Thus, the success of vaccines depends on the generation and maintenance of immunologic memory (*6*). Administration of BNT162b2 as the third vaccine dose boosted S IgG but not N IgG. The substantial increase of S IgG after

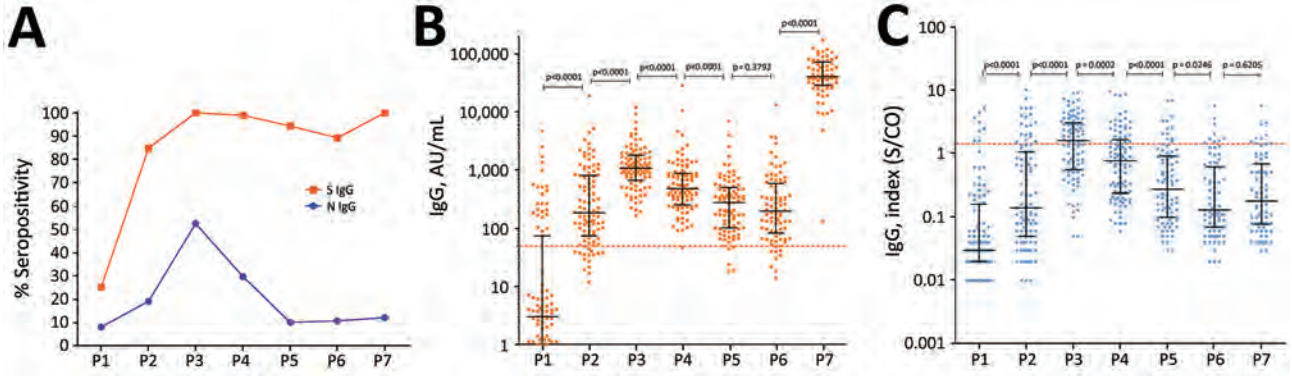

Figure 1. Antibody response over time in a cohort of healthcare workers vaccinated with 2 doses of CoronaVac vaccine (https://www.sinovac.com) followed by a BNT162b2 vaccine (Pfizer-BioNTech, https://www.pfizer.com) booster dose. A) S and N IgG seropositivity. B) S IgG levels. C) N IgG levels. Antibody responses were evaluated before vaccination (timepoint P1); 28 days after the first dose of CoronaVac vaccine (P2); 30 (P3) 90 (P4), 180 (P5), and 230 (P6) days after the second dose of CoronaVac vaccine; and 15 days after the booster dose with BNT162b2 vaccine (P7). For panels B and C, black lines indicate median levels values and error bars interquartile ranges; horizontal dotted lines indicate cutoff values. Statistical analysis performed using the Kruskal–Wallis test with subsequent Dunn's multiple testing correction. N, nucleocapsid protein; S, spike protein; S/CO, signal-to-cutoff ratio.

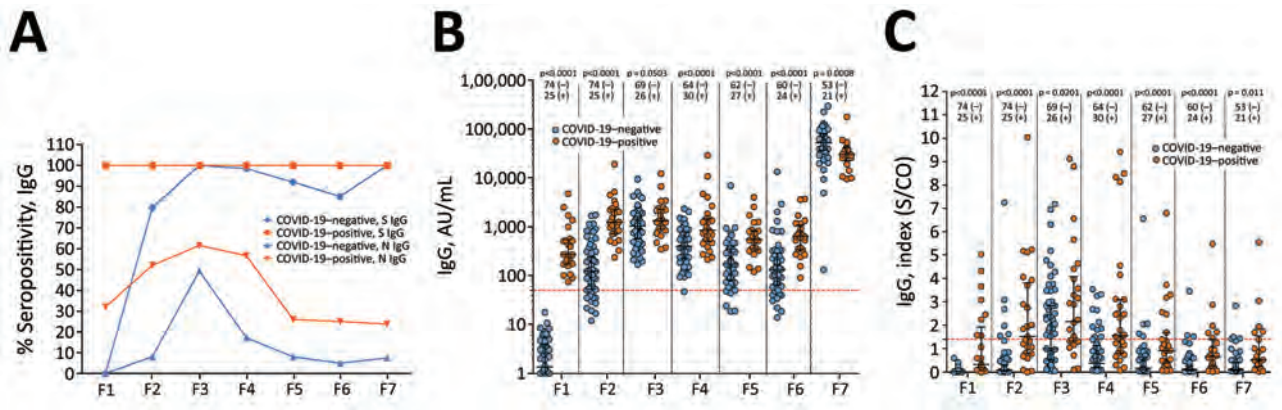

Figure 2. Comparison of antibody response over time among healthcare workers vaccinated with 2 doses of CoronaVac vaccine (https://www.sinovac.com) followed by a BNT162b2 vaccine (Pfizer-BioNTech, https://www.pfizer.com) booster dose, by COVID-19 positivity status. A) S and N IgG seropositivity. B) S IgG levels. C) N IgG levels. Antibody responses were evaluated before vaccination (timepoint P1); 28 days after the first dose of CoronaVac vaccine (P2); 30 (P3) 90 (P4), 180 (P5), and 230 (P6) days after the second dose of CoronaVac vaccine; and 15 days after the booster dose with BNT162b2 vaccine (P7). For panels B and C, black lines indicate median levels values and error bars interquartile ranges; the horizontal dotted line indicates the cutoff value of the assays. Numbers below p values indicate numbers of COVID-19–positive and COVID-19–negative persons in each timepoint. Statistical analysis performed using the Kruskal–Wallis test with subsequent Dunn's multiple testing correction. N, nucleocapsid protein; S, spike protein; S/CO, signal-to-cutoff ratio; (–), COVID-19 negative; (+), COVID-19 positive.

the booster dose suggests that CoronaVac vaccine induced immune memory. The third BNT162b2 dose did not increase the N IgG because mRNA vaccines do not induce a response to the N protein (*7*,*8*).

Previously infected participants had a significantly higher antibody level than previously uninfected participants in almost all phases of the study. In addition, we found that those without previous infection showed a faster waning of antibodies over time, a result also reported in previous studies (*9*). The antibody-making B cells multiply after each exposure, whether attributable to the infection or vaccination; therefore, antibody levels in the previously infected HCWs can reflect the sum of the antibodies produced after infection and vaccine (*10*).

In summary, a booster dose of BNT162b2 vaccine in HCWs administered 8 months after the second dose with CoronaVac vaccine recalled a specific immune response to SARS-CoV-2. That response had declined substantially 230 days after the second dose of CoronaVac vaccine, resulting in an increase of S IgG after BNT162b2 vaccination and indicating that the 2-dose CoronaVac vaccine schedule generates immune memory.

Acknowledgments

We thank the healthcare workers of COVID-19 Diagnosis Support Unit of Fiocruz, Ceará, Brazil, for participating in this study. We also thank the Paulo Goberlânio de Barros Silva for the statistical analysis.

The project is funded by Fiocruz and Ministério da Saúde, Brazil.

About the Author

Dr. Gambim Fonseca is a researcher at and coordinator of the Serology Laboratory of the COVID-19 Diagnosis Support Unit of Fiocruz Ceará, Brazil. Her primary research interests include antibodies and coronavirus disease.

References

1. Siegrist C-A. Vaccine immunology. 2018 Jan 1 [cited 2022 Mar 22]. https://www.who.int/immunization/documents/Elsevier_Vaccine_immunology.pdf
2. Sauré D, O'Ryan M, Torres JP, Zuniga M, Santelices E, Basso LJ. Dynamic IgG seropositivity after rollout of CoronaVac and BNT162b2 COVID-19 vaccines in Chile: a sentinel surveillance study. Lancet Infect Dis. 2022;22:56–63. https://doi.org/10.1016/S1473-3099(21)00479-5
3. Polack FP, Thomas SJ, Kitchin N, Absalon J, Gurtman A, Lockhart S, et al.; C4591001 Clinical Trial Group. Safety and efficacy of the BNT162b2 mRNA Covid-19 vaccine. N Engl J Med. 2020;383:2603–15. https://doi.org/10.1056/NEJMoa2034577
4. Kanno AI, Barbosa MMF, Moraes L, Leite LCC. SARS-CoV-2 vaccine development and how Brazil is contributing. Genet Mol Biol. 2021;44(Suppl 1):e20200320. https://doi.org/10.1590/1678-4685-gmb-2020-0320
5. Naaber P, Tserel L, Kangro K, Sepp E, Jürjenson V, Adamson A, et al. Dynamics of antibody response to BNT162b2 vaccine after six months: a longitudinal prospective study. Lancet Reg Health Eur. 2021;10:100208. https://doi.org/10.1016/j.lanepe.2021.100208
6. Palm AE, Henry C. Remembrance of things past: long-term B cell memory after infection and vaccination. Front Immunol. 2019;10:1787. https://doi.org/10.3389/fimmu.2019.01787
7. Mueller T. Antibodies against severe acute respiratory syndrome coronavirus type 2 (SARS-CoV-2) in individuals with and without COVID-19 vaccination: a method comparison of two different commercially available serological assays from the same manufacturer. Clin Chim

Acta. 2021;518:9–16. https://doi.org/10.1016/j.cca.2021.03.007
8. Keskin AU, Bolukcu S, Ciragil P, Topkaya AE. SARS-CoV-2 specific antibody responses after third CoronaVac or BNT162b2 vaccine following two-dose CoronaVac vaccine regimen. J Med Virol. 2022;94:39–41. https://doi.org/10.1002/jmv.27350
9. Vicenti I, Basso M, Gatti F, Scaggiante R, Boccuto A, Zago D, et al. Faster decay of neutralizing antibodies in never infected than previously infected healthcare workers three months after the second BNT162b2 mRNA COVID-19 vaccine dose. Int J Infect Dis. 2021;112:40–4. https://doi.org/10.1016/j.ijid.2021.08.052
10. Ali H, Alahmad B, Al-Shammari AA, Alterki A, Hammad M, Cherian P, et al. Previous COVID-19 infection and antibody levels after vaccination. Front Public Health. 2021;9:778243. https://doi.org/10.3389/fpubh.2021.778243

Address for correspondence: Marcela Helena Gambim Fonseca, Fundação Oswaldo Cruz, São Jose s/n, Eusebio, Ceara, Brazil; email: marcela.gambim@fiocruz.br

Outbreak of Imported Seventh Pandemic *Vibrio cholerae* O1 El Tor, Algeria, 2018

Nabila Benamrouche, Chafika Belkader, Elisabeth Njamkepo, Sarah Sihem Zemam, Soraya Sadat, Karima Saighi, Dalila Torkia Boutabba, Faiza Mechouet, Rym Benhadj-Slimani, Fatma-Zohra Zmit, Jean Rauzier, Farid Kias, Souad Zouagui, Corinne Ruckly, Mohamed Yousfi, Amel Zertal, Ramdane Chouikrat, Marie-Laure Quilici, François-Xavier Weill

After a lull of >20 years, Algeria experienced a cholera outbreak in 2018 that included 291 suspected cases. We found that outbreak isolates were *Vibrio cholerae* O1 serotype Ogawa from seventh pandemic El Tor sublineage AFR14, which corresponds to a new introduction of cholera into Africa from South Asia.

Cholera, a life-threatening diarrheal disease, is caused by *Vibrio cholerae* O1, or more rarely O139, serogroup bacteria that produce cholera toxin (CTX) and induce rapid massive loss of body fluids (*1*). Cholera has been a serious public health problem since its introduction into Africa in 1970, during the seventh cholera pandemic (*2*). This pandemic, caused by the novel *V. cholerae* O1 lineage El Tor (seventh pandemic El Tor), began in Indonesia in 1961 (*2*,*3*). After 60 years, ≈2.9 million cholera cases and ≈95,000 deaths still occur annually (*4*,*5*). During 2009–2012, nearly 60% of global cholera cases and deaths occurred in sub-Saharan Africa, but North Africa was considered cholera-free (*5*).

Algeria is a large country (2,381,741 km^2) in North Africa (*6*). The World Bank (https://www.worldbank.org) ranks Algeria as the third largest economy in the Middle East and North Africa region. In 2018, Algeria had ≈42.2 million inhabitants, ≈30.6 million of whom lived in urban areas (Macrotrends LLC, https://www.macrotrends.net).

Algeria reported cholera cases to the World Health Organization from 1971 (1,332 cases, 110 deaths) through 1994 (118 cases, 4 deaths), with a peak in 1979 (2,513 cases, 94 deaths) (Global Health Observatory, https://www.who.int/data/gho) (Figure 1). After a lull of >20 years, on August 23, 2018, the country's ministry of health announced a cholera outbreak in north Algeria (*7*). During August 7–September 27, 2018, Algeria reported 291 suspected cholera cases, including 270 persons who were hospitalized, in 7 wilayas (provinces): 6 in north-central Algeria (Bouira, Blida, Algiers, Tipaza, Aïn Defla, and Médéa) and 1 in northwest Algeria (Oran).

We used conventional microbiology and whole-genome sequencing to characterize virulence and antimicrobial resistance of clinical and environmental isolates collected during this outbreak. We also performed a phylogenomic analysis of >1,200 seventh pandemic El Tor genomes to determine whether the 2018 outbreak in Algeria was caused by a sublineage previously circulating in the country, a sublineage circulating in sub-Saharan Africa, or a new sublineage imported from elsewhere.

The Study

The Enterobacteria Laboratory of the Institut Pasteur d'Algérie performed microbial analyses for case confirmation (Appendix 1 Table 1, https://wwwnc.cdc.gov/EID/article/28/6/21-2451-App1.xlsx; Appendix 2, https://wwwnc.cdc.gov/EID/article/28/6/21-2451-App2.pdf). During August 14–September 27, 2018, this laboratory received 695 stool

Author affiliations: Institut Pasteur d'Algérie, Algiers, Algeria (N. Benamrouche, C. Belkader, S.S. Zemam, S. Sadat, D.T. Boutabba, R. Benhadj-Slimani, F. Kias); University of Algiers I, Algiers (N. Benamrouche, F. Mechouet, F.-Z. Zmit, A. Zertal); Institut Pasteur, Université Paris Cité, Paris, France (E. Njamkepo, J. Rauzier, C. Ruckly, M.-L. Quilici, F.-X. Weill); Public Hospital Establishment of Boufarik, Blida, Algeria (K. Saighi, M. Yousfi, R. Chouikrat); Specialized Hospital Establishment El Hadi Flici, Algiers (F. Mechouet, F.-Z. Zmit, A. Zertal); University Hospital of Oran and University of Oran I, Oran, Algeria (S. Zouagui)

DOI: https://doi.org/10.3201/eid2806.212451

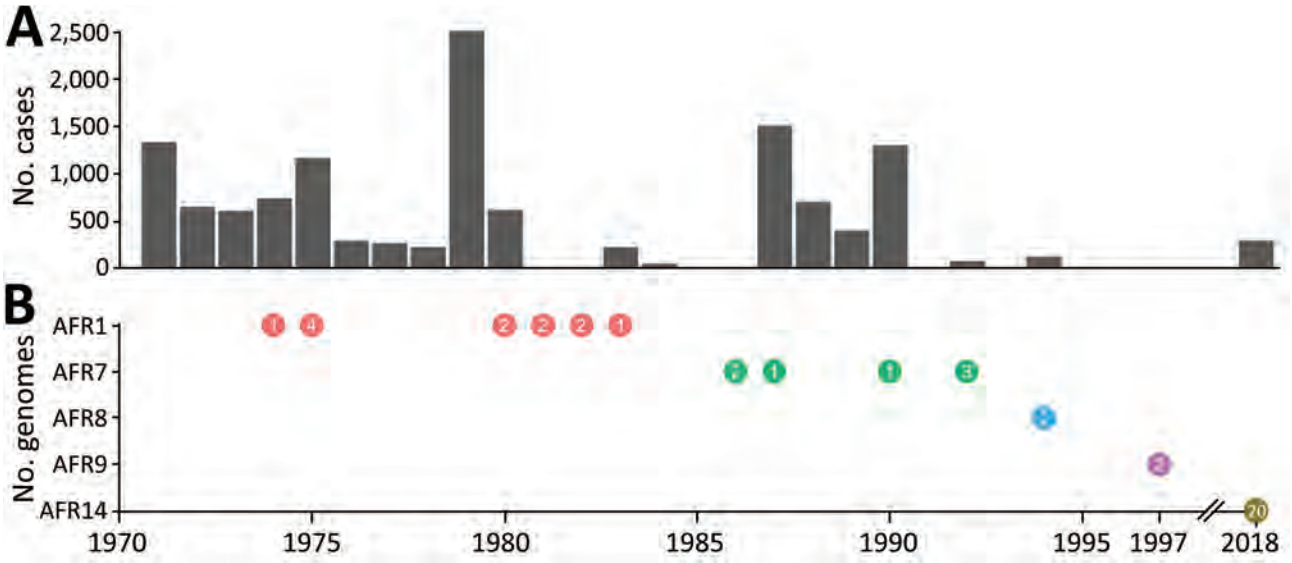

Figure 1. Cholera cases and seventh pandemic *Vibrio cholerae* O1 biotype El Tor sublineages, Algeria, 1971–2018. A) Number of cholera cases reported to the World Health Organization (WHO) by Algeria per year. For 2018, no cases were reported to WHO, but 291 suspected cases are indicated. B) Number of sequenced genomes detected from various sublineages per year of isolation. Orange circles indicate AFR1, green indicate AFR7, blue indicates AFR 8, purple AFR9, gold AFR14. Numbers in circles indicate the number of isolates.

samples from hospitals or hygiene laboratories in 7 wilayas, 277 from suspected case-patients and 418 from case-contacts, as well as 24 clinical isolates (14 from patients and 10 from case-contacts) and 5 environmental isolates (2 from wastewater, 2 from public drinking water sources, and 1 from stored water) for confirmation. In all, we confirmed 97/291 (33.3%; 95% CI 28.2%–38.9%) suspected cases as *V. cholerae* O1 El Tor serotype Ogawa carrying the *ctxA* gene and 29/428 (6.8%; 95% CI 4.8%–9.6%) case-contacts as asymptomatic carriers. Of the 5 environmental isolates, we also confirmed 2 from wastewater and 1 from stored water as serotype Ogawa.

All *V. cholerae* O1 isolates had the same antimicrobial resistance profile: resistance to streptomycin, sulfamethoxazole, trimethoprim, sulfamethoxazole/trimethoprim, nalidixic acid; decreased susceptibility to ciprofloxacin; and intermediate resistance to chloramphenicol and nitrofurantoin (Table). However, isolates were susceptible to doxycycline, azithromycin, β-lactams, and colistin.

Table. Characteristics of *Vibrio cholerae* O1 epidemic strain, Algeria, 2018*

Category	Strain characteristic
Serogroup, serotype, biotype	O1, Ogawa, El Tor
Genomic wave	3
Sublineage	Seventh pandemic *V. cholerae* O1 biotype El Tor
Genetic markers	*ctxB7*, *tcpA*^{CIRS101}, VSP-IIΔ‡
AMR profile, antimicrobial drug (MIC)†	
Streptomycin (64–128 mg/L)	Resistant
Sulfamethoxazole (1,024 mg/L)	Resistant
Trimethoprim/sulfamethoxazole (32 mg/L)	Resistant
Trimethoprim (32 mg/L)	Resistant
Chloramphenicol (16 mg/L)	Intermediate
Nalidixic acid (256 mg/L)	Resistant
Ciprofloxacin (0.25 mg/L)	Decreased susceptibility
Nitrofurantoin (64 mg/L)	Intermediate
Colistin (2 mg/L)	Susceptible
Horizontally acquired AMR elements	ICE*Vch*Ind5
Horizontally acquired AMR genes	*strAB*, *floR*, *sul2*, *dfrA1*
Chromosomal gene mutations, AMR phenotype	
*gyrA*_S83I and *parC*_S85L	Resistance to nalidixic acid; decreased susceptibility to ciprofloxacin
*nfsA*_R169C and *nfsB*_Q5Stop	Intermediate susceptibility to nitrofurantoin
*vprA*_D89N	Susceptibility to colistin

*Data were collected from 20 sequenced outbreak isolates. AMR, antimicrobial resistance; ICE*Vch*Ind5, integrative conjugative element of the SXT/R391 family; VSP-IIΔ, deletion in *Vibrio* seventh pandemic island II.
†MICs according to Clinical and Laboratory Standards Institute (https://clsi.org/media/1450/m45ed3_sample.pdf).
‡Deletion encompassing VC_0495-0512 according to GenBank accession no. AE003852.

We used whole-genome sequencing, comparative genomics, and phylogenetic analysis to characterize a selection of 20 *V. cholerae* O1 isolates, 17 clinical and 3 environmental (Appendix 1 Tables 2, 3; Appendix 2). We placed these isolates in context with a global collection of 1,265 seventh pandemic El Tor genomic sequences (Appendix 1 Table 4), including 23 isolates collected in Algeria during

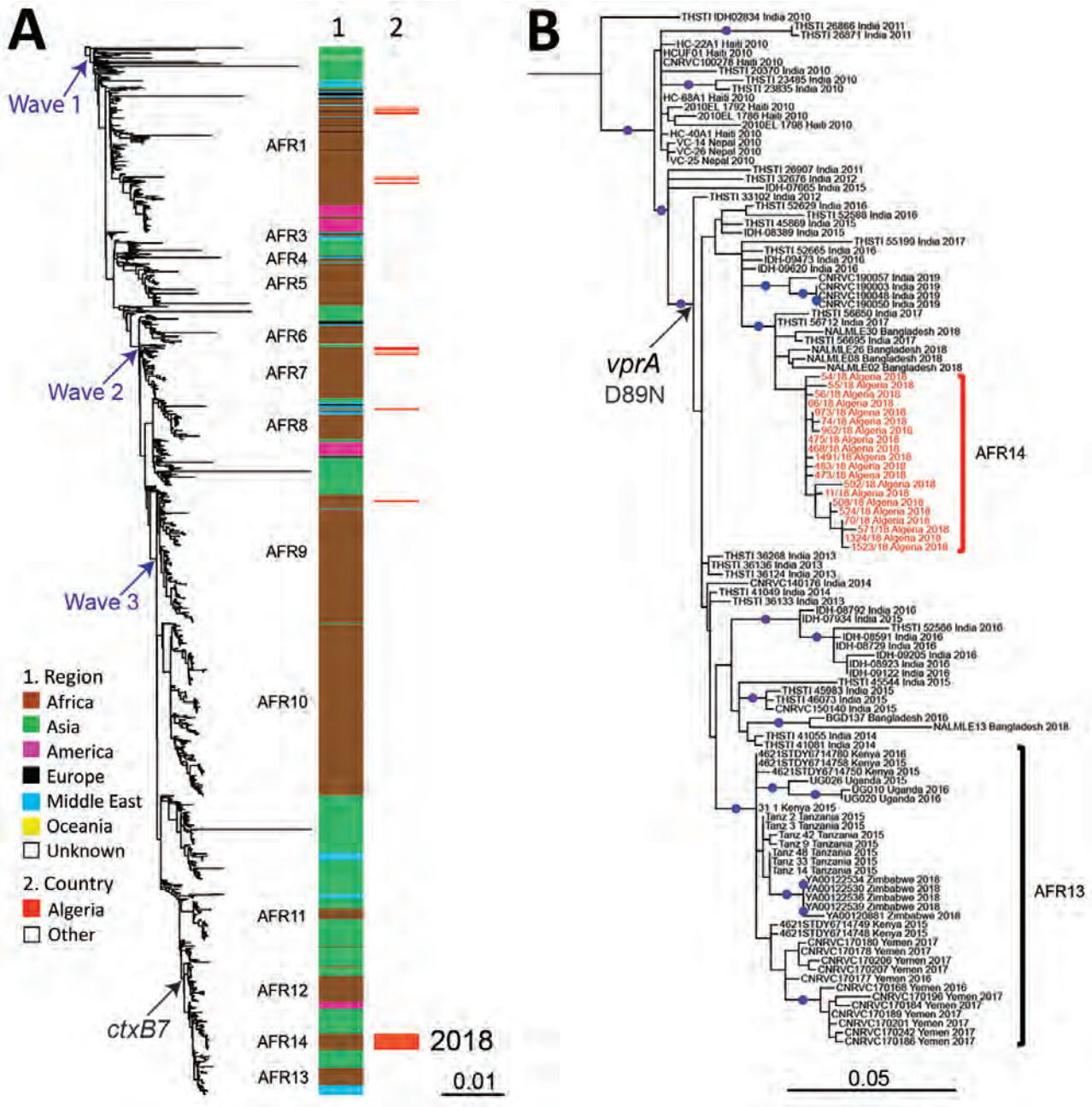

Figure 2. Phylogenomic analyses of Vibrio cholerae O1 El Tor isolates from Algeria, 2018. A) Maximum-likelihood phylogeny for 1,285 seventh pandemic V. cholerae biotype El Tor genomic sequences. A6 was used as the outgroup (Appendix 1, Table 4, https://wwwnc.cdc.gov/EID/article/28/6/21-2451-App1.xlsx). Genomic waves and acquisition of ctxB7 allele are indicated. Sublineages previously introduced into Africa (AFR1, AFR3–AFR13) are shown at the right of the tree. Column 1 indicates the geographic origins of the isolates; column 2 indicates isolates from the 2018 cholera outbreak in Algeria, all of which belong to a new seventh pandemic wave 3 sublineage AFR14. B) Maximum-likelihood phylogeny for 115 wave 3 ctxB7 isolates belonging to the distal part of the tree in panel A. N16961 was used as the outgroup (Appendix 1, Table 4). The isolates belonging to AFR14 from the 2018 cholera outbreak in Algeria are shown in red. Acquisition of the polymyxin susceptibility–associated single nucleotide variant in vprA (D89N) is indicated. Blue dots indicate bootstrap values >90%. Scale bars indicate the number of nucleotide substitutions per variable site.

1971–1997. We constructed a maximum-likelihood phylogeny of 1,285 genomes with 10,339 single-nucleotide variants (SNVs) evenly distributed over the nonrepetitive, nonrecombinant core genome. All the isolates recovered in Algeria during 2018 belonged to the seventh pandemic El Tor lineage and clustered in the wave 3 clade containing isolates carrying the *ctxB7* allele (Figure 2, panel A) (*3*). The 2018 isolates did not belong to sublineages previously found in Algeria, including AFR1, which circulated during the 1970s and early 1980s; AFR7, which circulated during the mid- to late-1980s and early 1990s; or AFR8 and AFR9, which circulated during the mid-1990s (Figures 1, 2) (*8*). The 2018 isolates also did not belong to other sublineages found in Africa, including the most recently introduced AFR13 sublineage, previously known as T13 (*8*–*11*). AFR13 has been circulating in eastern Africa since 2015 and in Yemen since 2016 (Figure 1). A second phylogeny, restricted to 115 wave 3 *ctxB7* isolates from the distal part of the global tree, showed the 2018 isolates from Algeria are closely related to isolates from South Asia collected during 2017–2018 in India and Bangladesh (Figure 2, panel B). This finding suggests the 2018 cholera outbreak in Algeria was cause by a newly imported strain (sublineage AFR14) from South Asia, rather than resurgence of any sublineage previously in Algeria or introduction of a sublineage circulating elsewhere in Africa.

The median pairwise distance between the 20 isolates recovered during the 2018 outbreak was 2.5 (range 0–8) core-genome SNVs. All 20 isolates had similar genomic features (Table), including the toxin-coregulated pilus subunit A gene variant, *tcpA*^{CIRS101}, a deletion (ΔVC_0495–0512) in the *Vibrio* seventh pandemic island II (VSP-II), and an SXT/R391 integrating conjugating element (ICE), called ICE*Vch*Ind5, encoding resistance to streptomycin (*strAB*), sulfonamides (*sul2*), trimethoprim (*dfrA1*), sulfamethoxazole/trimethoprim (*dfrA1* and *sul2*), and intermediate resistance to chloramphenicol (*floR*) (*8*). The Algeria isolates had mutations of *VC_0715*, resulting in the R169C substitution, and *VC_A0637*, resulting in the premature stop codon (Q5Stop) conferring intermediate nitrofuran resistance. Isolates also had mutations of the DNA gyrase, *gyrA* (S83I), and topoisomerase IV, *parC* (S85L), genes conferring resistance to nalidixic acid and decreased susceptibility to ciprofloxacin (*8*,*9*). In addition, isolates had a specific nonsynonymous SNV in the *vprA* gene (*VC_1320*), which resulted in the D89N substitution, conferring susceptibility to polymyxins (*9*), as reported for the AFR13 sublineage, although resistance to polymyxin B has been used as a marker of *V. cholerae* O1 biotype El Tor since the seventh pandemic began (*12*).

Conclusions

The seventh pandemic El Tor wave 3 clade, containing isolates carrying the *ctxB7* allele, emerged in South Asia earlier this century (*9*,*13*) and has been exported from Asia ≥4 times: to West Africa in 2007 (AFR12 sublineage) (*8*), Haiti in 2010 (*14*), East Africa in 2013–2015 (AFR13) (*9*,*10*), and now North Africa (AFR14). Polymyxin-susceptible seventh pandemic El Tor isolates with a *vprA* mutation encoding the D89N substitution were identified in South Asia in 2012 (*15*), spread to Eastern Africa and Yemen (AFR13) (*9*,*10*), and then spread to Algeria (AFR14).

Algeria controlled disease spread more swiftly in 2018 than during previous seventh pandemic El Tor introductions. The ministry of health led the epidemic response, initiated an emergency action plan at national and local levels, and enhanced epidemiologic surveillance and reporting. A health surveillance unit coordinated response actions and implemented recommendations. Designated hospitals managed suspected case-patients in isolation wards. Persons with suspected *V. cholerae* were hospitalized, isolated, rehydrated, and treated with doxycycline, erythromycin, azithromycin, ceftriaxone, or ciprofloxacin; patients were released only after a negative *V. cholerae* culture. Case-contacts were systematically screened, and asymptomatic carriers received chemoprophylaxis. In affected areas, the ministry of health reinforced bacteriologic monitoring of water sources, including drinking water, bore holes, wells, springs, and wadi (ravines that are dry except during rainy seasons), and took corrective action for sources with poor bacteriologic quality.

In summary, *V. cholerae* O1 isolates collected during a 2018 cholera outbreak in Algeria were a seventh pandemic El Tor sublineage, AFR14, newly introduced into Africa from South Asia. Our findings suggest that, in addition to appropriate control and prevention measures during outbreaks, such as those used in Algeria, reducing the burden of cholera in South Asia might aid in long-term control of cholera in Africa.

Acknowledgments

We thank all the participants and particularly Hamza Letlout of Public Health Facility of Tipaza and Ahlem Toua of Institut Pasteur of d'Algérie, Annex of Oran, for sending stool samples or *Vibrio cholerae* strains and Abdelali Meftah of Public Hospital Establishment of Boufarik for his assistance during this epidemic.

This work was supported by the Pasteur Institute of Algeria, Institut Pasteur, and by the French Government's Investissement d'Avenir program, Laboratoire d'Excellence, Integrative Biology of Emerging Infectious Diseases (grant no. ANR-10-LABX-62-IBEID).

About the Author

Dr. Benamrouche is a medical microbiologist, head of the Enterobacteria Laboratory at the Pasteur Institute of Algeria, Algiers, Algeria, Pasteur International Network, and a senior lecturer on the Faculty of Medicine, University of Algiers I, Algiers, Algeria. Her research interests include the surveillance and epidemiology of enteric bacterial pathogens and antimicrobial resistance.

References

1. Clemens JD, Nair GB, Ahmed T, Qadri F, Holmgren J. Cholera. Lancet. 2017;390:1539–49. https://doi.org/10.1016/S0140-6736(17)30559-7
2. Barua D, Greenough WB, editors. Cholera. New York: Plenum: 1992.
3. Mutreja A, Kim DW, Thomson NR, Connor TR, Lee JH, Kariuki S, et al. Evidence for several waves of global transmission in the seventh cholera pandemic. Nature. 2011;477:462–5. https://doi.org/10.1038/nature10392
4. World Health Organization. Cholera key facts [cited 2022 Mar 25]. https://www.who.int/news-room/fact-sheets/detail/cholera
5. Ali M, Nelson AR, Lopez AL, Sack DA. Updated global burden of cholera in endemic countries. PLoS Negl Trop Dis. 2015;9:e0003832. https://doi.org/10.1371/journal.pntd.0003832
6. United Nations. Algeria country profile [cited 2022 Mar 25]. http://data.un.org/en/iso/dz.html
7. Reliefweb. WHO: cholera—Algeria (14 September 2018) [cited 2022 Mar 25]. https://reliefweb.int/report/algeria/who-cholera-algeria-14-september-2018
8. Weill FX, Domman D, Njamkepo E, Tarr C, Rauzier J, Fawal N, et al. Genomic history of the seventh pandemic of cholera in Africa. Science. 2017;358:785–9. https://doi.org/10.1126/science.aad5901
9. Weill FX, Domman D, Njamkepo E, Almesbahi AA, Naji M, Nasher SS, et al. Genomic insights into the 2016–2017 cholera epidemic in Yemen. Nature. 2019;565:230–3. https://doi.org/10.1038/s41586-018-0818-3
10. Mashe T, Domman D, Tarupiwa A, Manangazira P, Phiri I, Masunda K, et al. Highly resistant cholera outbreak strain in Zimbabwe. N Engl J Med. 2020;383:687–9. https://doi.org/10.1056/NEJMc2004773
11. Oprea M, Njamkepo E, Cristea D, Zhukova A, Clark CG, Kravetz AN, et al. The seventh pandemic of cholera in Europe revisited by microbial genomics. Nat Commun. 2020;11:5347. https://doi.org/10.1038/s41467-020-19185-y
12. Herrera CM, Crofts AA, Henderson JC, Pingali SC, Davies BW, Trent MS. The *Vibrio cholerae* VprA-VprB two-component system controls virulence through endotoxin modification. MBio. 2014;5:e02283–14. https://doi.org/10.1128/mBio.02283-14
13. Naha A, Pazhani GP, Ganguly M, Ghosh S, Ramamurthy T, Nandy RK, et al. Development and evaluation of a PCR assay for tracking the emergence and dissemination of Haitian variant ctxB in *Vibrio cholerae* O1 strains isolated from Kolkata, India. J Clin Microbiol. 2012;50:1733–6. https://doi.org/10.1128/JCM.00387-12
14. Domman D, Quilici ML, Dorman MJ, Njamkepo E, Mutreja A, Mather AE, et al. Integrated view of *Vibrio cholerae* in the Americas. Science. 2017;358:789–93. https://doi.org/10.1126/science.aao2136
15. Samanta P, Ghosh P, Chowdhury G, Ramamurthy T, Mukhopadhyay AK. Sensitivity to polymyxin B in El Tor *Vibrio cholerae* O1 strain, Kolkata, India. Emerg Infect Dis. 2015;21:2100–2. https://doi.org/10.3201/eid2111.150762

Address for correspondence: Nabila Benamrouche, Institut Pasteur d'Algérie, Route du petit Staoueli Dely Ibrahim, 16000 Alger, Algeria; email: n_benamrouche@yahoo.fr; François-Xavier Weill, Institut Pasteur, 28 rue du Dr Roux, F-75015 Paris, France; email: francois-xavier.weill@pasteur.fr

Burkholderia pseudomallei in Environment of Adolescent Siblings with Melioidosis, Kerala, India, 2019

Praveena Bhaskaran, Vinitha Prasad, Anusha Gopinathan, Tushar Shaw, Suchitra Sivadas, Chandrasekhar Jayakumar, Soumi Chowdhury, Aparna Dravid, Chiranjay Mukhopadhyay, Anil Kumar

In 2019, *Burkholderia pseudomallei* was isolated from the backyard of 2 siblings with melioidosis in Kerala, India . This finding highlights the value of healthcare providers being aware of risk for melioidosis in febrile patients, of residents taking precautions when outside, and of increasing environmental surveillance for *B. pseudomallei* in this region.

Melioidosis is a potentially life-threatening infection caused by the soil-dwelling bacteria *Burkholderia pseudomallei*. The clinical spectrum of disease ranges from mild localized lesions to fulminant sepsis (*1*,*2*). The disease is endemic to Southeast Asia and Australia. Recently, the southern part of India has emerged as a melioidosis hot spot; infection in children accounts for 8% of infections (*2*,*3*). The risk of children acquiring infection is high because of the likelihood of environmental exposure either through wounds acquired while playing in contaminated muddy water or by inhalation of aerosols containing the bacteria during the rainy season (*4*–*6*). We report melioidosis in 2 siblings from Kerala, India, and the subsequent isolation of *B. pseudomallei* from the soil in their backyard.

The Study

In July 2019, at the onset of the monsoon season, a 15-year-old boy from southern India (patient 1) was examined because of fever for 1 week along with cough, myalgia, headache, vomiting, and diarrhea, followed by rashes over the trunk and breathlessness for 1 day. At hospital admission, the child was febrile, tachycardic, and tachypneic; his blood pressure was 85/67 mm Hg, and oxygen saturation on room air was 90%. He had a few discrete pustular lesions over the trunk (Figure 1, panel A). Chest examination revealed bilateral crackles. Initial laboratory studies showed leukocytosis; increased levels of inflammatory markers; and abnormal liver function, renal function, and coagulation profile, suggestive of multiorgan dysfunction (Table). The patient was admitted to the intensive care unit, and noninvasive ventilation and inotropic support were initiated along with empiric intravenous (IV) administration of piperacillin/tazobactam. Acute respiratory distress syndrome (Figure 1, panel B) with respiratory failure subsequently developed, and the patient was emergently intubated. Antimicrobial drugs were changed to meropenem and vancomycin. Despite these measures, the patient deteriorated rapidly, respiratory status and shock worsened, and he died within 24 hours after hospital admission.

Multiplex real-time PCR (FastTrack Diagnostics, https://www.imogena.pl) of a blood sample for common tropical diseases was positive for *Burkholderia mallei/pseudomallei*. Cultures of blood and of pus aspirated from the skin lesions yielded nonfermentative gram-negative bacilli, which the Vitek 2 system (bioMérieux, https://www.biomerieux.com) identified as *B. pseudomallei*. Isolate identity was confirmed at the Centre for Emerging and Tropical Diseases, Manipal Academy of Higher Education (Manipal, India), by monoclonal antibody–based latex agglutination test and PCR specific for the *B. pseudomallei*–specific *TTSS1* gene (*7*,*8*). Both isolates

Author affiliations: Amrita Institute of Medical Sciences and Research Centre, Amrita Vishwa Vidyapeetham, Kochi, India (P. Bhaskaran, V. Prasad, S. Sivadas, C. Jayakumar, A. Kumar); SRM Medical College Hospital and Research Centre, Chennai, India (A. Gopinathan); Ramaiah University of Applied Sciences, Bangalore, India (T. Shaw); Manipal Academy of Higher Education, Manipal, India (T. Shaw, S. Chowdhury, A. Dravid, C. Mukhopadhyay)

DOI: https://doi.org/10.3201/eid2806.211526

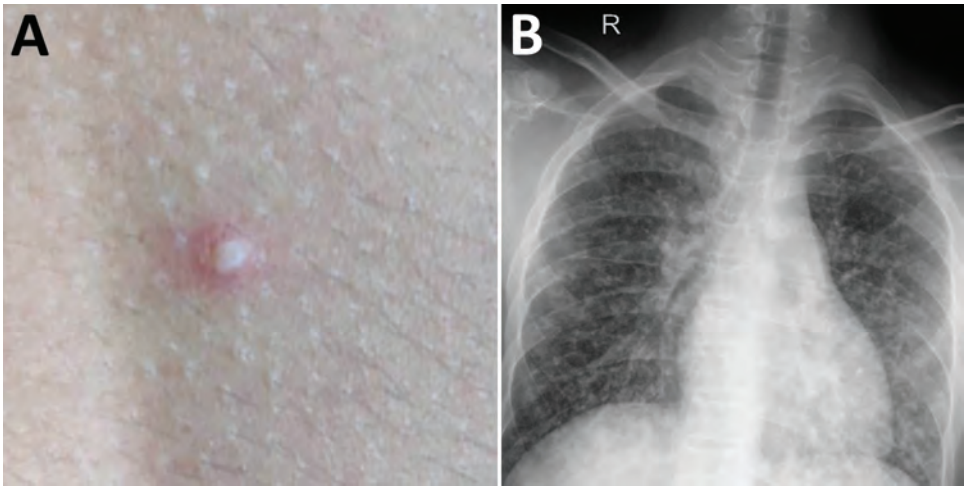

Figure 1. Images of 15-year-old boy (patient 1) with melioidosis, Kerala, India, 2019. A) Vesicular lesion on trunk. B) Chest radiograph showing diffuse heterogeneous opacities suggestive of acute respiratory distress syndrome.

were sensitive to amoxicillin/clavulanic acid, ceftazidime, cotrimoxazole, doxycycline, and meropenem.

One month later, the patient's 12-year-old brother (patient 2) was examined for fever of 3 weeks' duration along with neck swelling and sore throat of 2 weeks' duration. He received amoxicillin/clavulanate with no response. His vital signs were stable. Throat examination revealed bilateral tonsillar exudates. His left posterior cervical lymph node was 3 × 2 cm, firm, and nontender. His initial laboratory parameters were unremarkable (Table). Histopathology of the cervical node showed necrotizing lymphadenitis. Culture of lymph node tissue and throat swab grew *B. pseudomallei* with sensitivity identical to that of the isolate from his sibling. IV ceftazidime was administered, but because fever persisted, IV trimethoprim/sulfamethoxazole was added on day 5. Whole-body fluorodeoxyglucose positron emission tomography magnetic resonance imaging did not show any deep-seated abscesses. Because the fever continued to persist, ceftazidime was changed to meropenem by day 10. Fever subsided by day 14, and IV meropenem and trimethoprim/sulfamethoxazole were continued for 2 more weeks. The patient was discharged with instructions to take oral trimethoprim/sulfamethoxazole for 4 months. As of 30 months later, the child remained healthy.

Melioidosis cases among siblings within a span of 1 month suggested exposure to a common

Table. Clinical and laboratory characteristics of 2 siblings with melioidosis, Kerala, India, 2019*

Characteristic	Patient 1, 15-year-old boy†	Patient 2, 12-year-old boy‡
Clinical		
Comorbidities	None	None
Date of admission	Jul 1	Aug 8
Clinical condition	Pneumonia, ARDS, septic shock	Fever, sore throat, cervical lymphadenopathy
Laboratory		
Hemoglobin (ref 12.7–17.7), g/dL	13	13.4
Total leukocytes (ref 5,500–15,500), cells/μL	3,190	14,260
Neutrophils (ref 55–70), %	90	73.1
Thrombocytes (ref 150–400), K/μL	100	223
AST (ref 0–51), IU/L	139.4	21.2
ALT (ref 0–39), IU/L	98	16.3
Creatinine (ref 0.4–1.06), mg/dL	26.4/1.13	0.54
BUN (ref 5–20), mg/dl	26.4	14.3
Ferritin (ref 36–311), ng/mL	5,448	1374
Procalcitonin (refR <0.5), ng/mL	6.8	0.36
C-reactive protein (ref <10), mg/L)	319	16.86
Culture (source)	*Burkholderia pseudomallei* (blood, skin lesions)	*B. pseudomallei* (lymph node, throat swab)
Blood PCR	Positive for *Burkholderia mallei*/ B. *pseudomallei*	Not detected
Diagnosis (manifestations)	Melioidosis (pneumonia, ARDS, sepsis)	Melioidosis (lymphadenitis)
Treatment	Piperacillin/tazobactam, meropenem, vancomycin	Ceftazidime, meropenem, trimethoprim/sulfamethoxazole
Outcome	Died Jul 2	Discharged Sep 20

*ARDS, acute respiratory distress syndrome; ALT, alanine aminotransferase; AST, aspartate aminotransferase; ref, reference range.

environmental source. In November 2019, we sampled the patients' environment and collected 20 soil samples from an area of 1,000 square feet around the patients' house (Figure 2). We collected and processed soil dug from the flower bed and soil at 30 cm deep according to published consensus guideline for detection of *B. pseudomallei* in soil (*9*). We tested samples by culture and PCR for the presence of the bacteria. Of the 20 samples, 3 were positive for *B. pseudomallei* by culture (Figure 2) and 18 showed positive signal in the qualitative PCR targeting the *TTSS1* gene for *B. pseudomallei*. Antimicrobial susceptibility was the same for all 3 environmental isolates as for the clinical strains. Multilocus sequence typing of the clinical and environmental isolates indicated that the sequence type (ST) of the strain from the 12-year-old sibling matched that of the environmental isolates (ST 1944). The sequence type of the isolate from the 15-year-old sibling was different (ST 1556). Interview of the family indicated that both siblings had spent time playing outside the house during the rain, a known risk factor for acquiring melioidosis. The other family members were made aware of the risk factors of acquiring the disease from their environment and were advised to take preventive measures. They were asked to inform their doctor regarding the possibility of melioidosis when seeking medical care for any febrile illness or respiratory infection. However, they have remained healthy throughout the follow-up period.

Conclusion

Melioidosis is an underdiagnosed disease in India because of its diverse clinical manifestations, clinical overlap with other conditions such as tuberculosis, limited awareness by physicians and the general public, and laboratory constraints (*1*–*3*). Previous studies have reported cases from eastern, northeastern, and southern India (*3*,*10*). Both patients described in this report became ill during the monsoon season, when it rains heavily in Kerala. A recent study from southern India indicated that 90% of the children became ill during the monsoon season (*5*). Studies have shown a correlation between the disease and rainfall intensity (*3*,*11*).

A recent study from India reported frequent respiratory involvement and bacteremia in adults with acute cases (*10*). A study conducted in Southeast Asia reported that localized manifestations were more

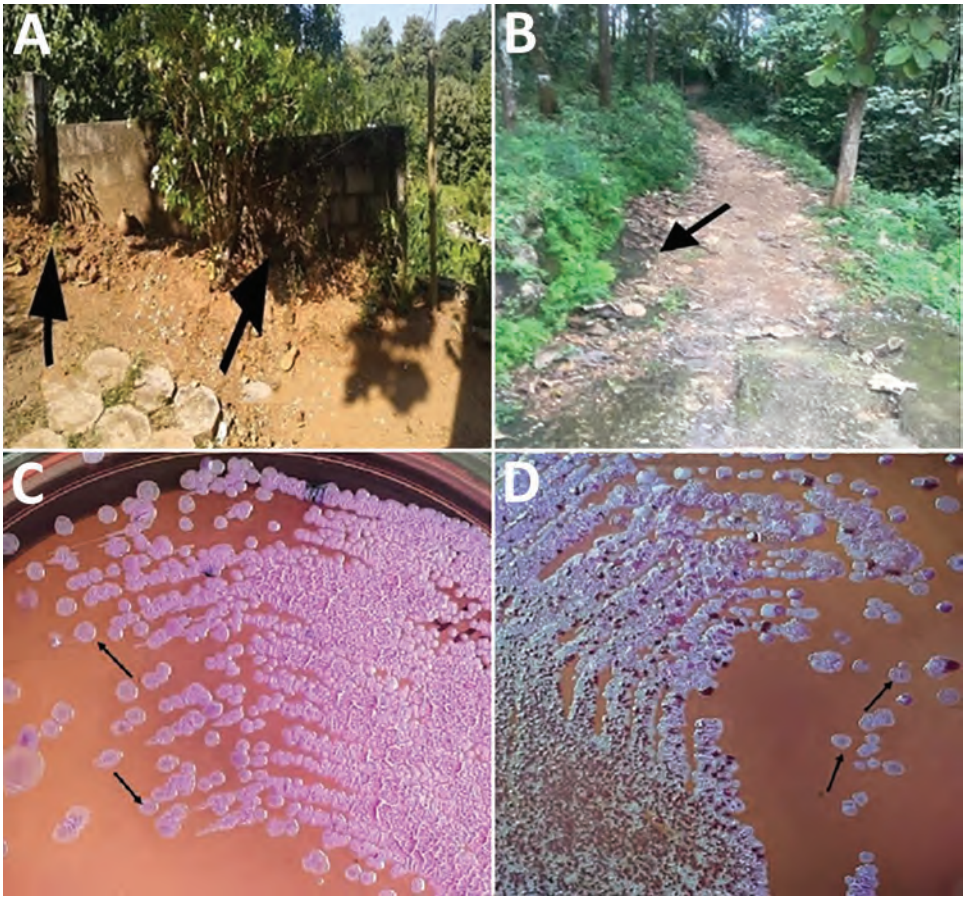

Figure 2. Cultures from environment of siblings with melioidosis, Kerala, India, 2019. A, B) Sites of soil collection (arrows) near patients' house. C, D) Ashdown agar culture showing growth of pink wrinkled colonies with metallic sheen (arrows) after 72-h incubation, typical of *Burkholderia pseudomallei*.

common in children; 46%–63% had either cutaneous lesions or lymphadenopathy (*12*). A similar study from India reported that among total cases of melioidosis, 8% were in children and the mortality rate was 9%. In that study, 54% of children had disseminated illness and 46% had localized lesions (*5*).

Fatal melioidosis in siblings and isolation of *B. pseudomallei* from their environment have been recently reported from Mexico (*13*). Cases of *B. pseudomallei* infection among siblings with cystic fibrosis have been reported from Australia (*14*). *B. pseudomallei* was also isolated from 5 of the 40 soil and water samples collected from the coastal region of Malabar, Kerala, during the 2016 rainy season (*15*). We report simultaneous isolation of *B. pseudomallei* from humans and from their immediate surrounding environment.

This study highlights the perpetual risk faced by family members of affected persons and other persons residing in a region where cases of melioidosis have been reported. It also highlights the value of seeking appropriate medical care at the onset of any febrile illness, because early diagnosis and treatment can decrease illness and death associated with the disease. Public health officials should emphasize additional precautions in melioidosis-endemic regions (e.g., not going out in the field during heavy rainfall, not walking barefoot, and not drinking water from natural reservoirs in melioidosis-endemic areas). Healthcare workers and the community should be aware of the risk for melioidosis, especially during the rainy season, and diagnostic testing should be strengthened to increase prompt identification and treatment. Furthermore, the National Centre for Disease Control should add melioidosis to the notifiable disease list in India to enable increased environmental surveillance and provide data for melioidosis risk mapping.

About the Author

Dr. Bhaskaran is a pediatric infectious diseases Fellow at Amrita Institute of Medical Sciences and Research Centre, Kochi, Kerala, India. Her primary research interests are antibiotic stewardship and neuroinfectious diseases.

References

1. Wiersinga WJ, Currie BJ, Peacock SJ. Melioidosis. N Engl J Med. 2012;367:1035–44. https://doi.org/10.1056/NEJMra1204699
2. Wiersinga WJ, Virk HS, Torres AG, Currie BJ, Peacock SJ, Dance DAB, et al. Melioidosis. Nat Rev Dis Primers. 2018;4:17107. https://doi.org/10.1038/nrdp.2017.107
3. Mukhopadhyay C, Shaw T, Varghese GM, Dance DAB. Melioidosis in South Asia (India, Nepal, Pakistan, Bhutan and Afghanistan). Trop Med Infect Dis. 2018;3:51. https://doi.org/10.3390/tropicalmed3020051
4. Sanderson C, Currie BJ. Melioidosis: a pediatric disease. Pediatr Infect Dis J. 2014;33:770–1. https://doi.org/10.1097/INF.0000000000000358
5. Mukhopadhyay C, Eshwara VK, Kini P, Bhat V. Pediatric melioidosis in Southern India. Indian Pediatr. 2015;52:711–2.
6. Pagnarith Y, Kumar V, Thaipadungpanit J, Wuthiekanun V, Amornchai P, Sin L, et al. Emergence of pediatric melioidosis in Siem Reap, Cambodia. Am J Trop Med Hyg. 2010;82:1106–12. https://doi.org/10.4269/ajtmh.2010.10-0030
7. Duval BD, Elrod MG, Gee JE, Chantratita N, Tandhavanant S, Limmathurotsakul D, et al. Evaluation of a latex agglutination assay for the identification of *Burkholderia pseudomallei* and *Burkholderia mallei*. Am J Trop Med Hyg. 2014;90:1043–6. https://doi.org/10.4269/ajtmh.14-0025
8. Novak RT, Glass MB, Gee JE, Gal D, Mayo MJ, Currie BJ, et al. Development and evaluation of a real-time PCR assay targeting the type III secretion system of *Burkholderia pseudomallei*. J Clin Microbiol. 2006;44:85–90. https://doi.org/10.1128/JCM.44.1.85-90.2006
9. Limmathurotsakul D, Dance DAB, Wuthiekanun V, Kaestli M, Mayo M, Warner J, et al. Systematic review and consensus guidelines for environmental sampling of *Burkholderia pseudomallei*. PLoS Negl Trop Dis. 2013;7:e2105. https://doi.org/10.1371/journal.pntd.0002105
10. Koshy M, Jagannati M, Ralph R, Victor P, David T, Sathyendra S, et al. Clinical manifestations, antimicrobial drug susceptibility patterns, and outcomes in melioidosis cases, India. Emerg Infect Dis. 2019;25:316–20. https://doi.org/10.3201/eid2502.170745
11. Currie BJ, Jacups SP. Intensity of rainfall and severity of melioidosis, Australia. Emerg Infect Dis. 2003;9:1538–42. https://doi.org/10.3201/eid0912.020750
12. Foong YW, Tan NW, Chong CY, Thoon KC, Tee NW, Koh MJ. Melioidosis in children: a retrospective study. Int J Dermatol. 2015;54:929–38. https://doi.org/10.1111/ijd.12837
13. Alvarez-Hernandez G, Cruz-Loustaunau D, Ibarra JA, Rascon-Alcantar A, Contreras-Soto J, Meza-Radilla G, et al. Description of two fatal cases of melioidosis in Mexican children with acute pneumonia: case report. BMC Infect Dis. 2021;21:204. https://doi.org/10.1186/s12879-021-05910-5
14. Holland DJ, Wesley A, Drinkovic D, Currie BJ. Cystic fibrosis and *Burkholderia pseudomallei* infection: an emerging problem? Clin Infect Dis. 2002;35:e138–40. https://doi.org/10.1086/344447
15. Peddayelachagiri BV, Paul S, Nagaraj S, Gogoi M, Sripathy MH, Batra HV. Prevalence and identification of *Burkholderia pseudomallei* and near-neighbor species in the Malabar coastal region of India. PLoS Negl Trop Dis. 2016;10:e0004956. https://doi.org/10.1371/journal.pntd.0004956

Address for correspondence: Anil Kumar, Amrita Institute of Medical Sciences—Microbiology, Amrita Vishwa Vidyapeetham, Amrita Lane, Ponekara Kochi, Kerala 682041, India; email: vanilkumar@aims.amrita.edu

Lizards as Silent Hosts of *Trypanosoma cruzi*

Carezza Botto-Mahan,[1] Juana P. Correa,[1] Raúl Araya-Donoso, Francisca Farías, Esteban San Juan, Nicol Quiroga, Ricardo Campos-Soto, Claudio Reyes-Olivares, Daniel González-Acuña

We assessed 4 lizard species in Chile for *Trypanosoma cruzi*, the causative agent of Chagas disease, and 1 species for its ability to transmit the protozoan to uninfected kissing bugs. All lizard species were infected, and the tested species was capable of transmitting the protozoan, highlighting their role as *T. cruzi* reservoirs.

Chagas disease is one of the most neglected vectorborne diseases, infecting 6–7 million persons worldwide; 70 million persons are at risk for infection (*1*), and the disease is a concern in several nonendemic countries (*2*). The etiologic agent is *Trypanosoma cruzi*, a zoonotic protozoan maintained in the Americas by wild and domestic mammals and transmitted by hematophagous triatomine vectors (kissing bugs) (*3*,*4*). Infection of mammals occurs by contamination of broken skin or mucous membranes with the protozoan in kissing bug feces, by congenital transmission, and orally when feeding on infected kissing bugs (or their feces) or other infected mammals (*3*,*4*). Kissing bugs become infected mainly when feeding on infected mammals (*3*).

More than 150 species of wild mammals in the Americas are naturally infected with *T. cruzi* protozoa; some of these hosts are relevant in the maintenance and interplay of the domestic and wild transmission cycles of Chagas disease (*3*,*4*). Although the role of mammals in *T. cruzi* transmission has been studied, less is known about the relevance of nonmammalian vertebrates (*5*). Reptiles have been reported as blood meal sources of kissing bugs, but their status as hosts for *T. cruzi* protozoa is not well documented (*6*).

Author affiliations: Universidad de Chile, Santiago, Chile (C. Botto-Mahan, F. Farías, E. San Juan, N. Quiroga); Universidad San Sebastián, Concepción, Chile (J.P. Correa); Arizona State University, Tempe, Arizona, USA (R. Araya-Donoso); Universidad Viña del Mar, Viña del Mar, Chile (R. Campos-Soto); Universidad Andrés Bello, Santiago (C. Reyes-Olivares); Universidad de Concepción Campus Chillán, Chillán, Chile (D. González-Acuña)

DOI: https://doi.org/10.3201/eid2806.220079

Reptiles have been described as natural hosts of some Trypanosomatid species transmitted by fly species (*7*). Although studies have shown how lizards could become experimentally infected by *T. cruzi* protozoa (*8*,*9*) and one showed an association between kissing bug infection and lizard abundance (*10*), most studies have not included reptiles as potential vertebrates involved in persistence and transmission of *T. cruzi* protozoa. To determine persistence of vectorborne infections in natural systems, it is essential to describe and characterize all host species directly (i.e., naturally infected species) or indirectly (i.e., vector blood meal sources) involved and evaluate their contribution to kissing bug infection.

We examined *T. cruzi* infection in 4 lizard species from the Pacific coast of Chile coexisting with kissing bug species. We also evaluated the competence of the most abundant lizard species to transmit *T. cruzi* protozoa to kissing bugs.

The Study

We conducted capturing and processing procedures after approval was obtained from the Institutional Committee for the Care and Use of Animals, University of Chile (permit 19275-FCS-UCH), the Agricultural and Livestock Service of Chile (permits 805/2018, 334/2019, and 4944/2019), and the National Forestry Corporation of Chile (permit 66/2018). We captured lizards at 3 sites in interior valleys and 2 Pacific islands in the arid–semiarid Mediterranean ecosystem of South America, where lizards naturally occupy the same microhabitats as kissing bugs (*Mepraia* spp.).

Depending on the species, we obtained blood from lizards in the field by using tail clipping and releasing (*Microlophus atacamensis*, Pacific Atacama racerunner) or in the laboratory by using tissue/organ extraction (*Liolaemus platei*, Plate's lizard; *Liolaemus fuscus*, dark lizard; *Garthia gaudichaudii*, Chilean marked gecko). We kept lizards for 1 week in the

[1]These authors contributed equally to this article.

Table. Lizard species from southwestern South America tested for *Trypanosoma cruzi* infection, 2011–2019*

Lizard species	Common name	No. infected/no. tested	Infected tissue or organ†	Competence (range)
Microlophus atacamensis	Pacific Atacama racerunner	11/13	Blood	ND
Liolaemus platei	Plate's lizard	18/18	Liver, spleen, stomach, intestine, lung, heart, fat, muscle, bone, gonad, blood	96.43 (50–100)
Liolaemus fuscus	Dark lizard	3/3	Liver, spleen, stomach, intestine, lung, heart, fat, muscle, bone, gonad, blood	ND
Garthia gaudichaudii	Chilean marked gecko	10/10	Liver, stomach, intestine, lung, heart, muscle, bone	ND

*Competence was assessed by real-time PCR on xenodiagnostic triatomine nymphs in *Liolaemus platei* lizard only. ND, not done.
†Not all types of organs were obtained for all sampled lizards (Appendix Table 1, https://wwwnc.cdc.gov/EID/article/28/6/22-0079-App1.pdf).

laboratory in terraria containing food, water, and light. Before processing, Plate's lizards were subjected to xenodiangoses with 3 axenic second nymph stage kissing bugs of the endemic triatomine species *Mepraia spinolai*, obtained from a laboratory colony (Faculty of Science, University of Chile, Santiago, Chile). All engorged kissing bugs were kept in vials in a climate chamber (28°C, relative humidity 75%) for 40 days to enable *T. cruzi* multiplication in instances of infection. We then froze kissing bugs for 48 hours and extracted intestines and feces. After lizards were euthanized, we extracted their tissues (blood, bone, and fat) and organs (heart, stomach, intestine, lung, liver, spleen, and gonads) when possible. We stored all samples at −20°C.

We isolated whole genomic DNA from lizard and kissing bug samples by using the DNeasy Blood and Tissue Kit (QIAGEN, https://www.qiagen.com) according to manufacturer instructions. We performed real-time PCR specific for a nuclear segment of a repetitive genomic DNA sequence of *T. cruzi* DNA by using the primers Cruzi 1 and Cruzi 2 (*11*). The reaction was performed by using the Hot FIREPol EvaGreen qPCR Mix (Solis Biodyne, https://solisbiodyne.com), 0.4 μmol/L of primers, and 5 μL of template in a final volume of 20 μL. Cycling conditions were 95°C for 15 min, followed by 50 cycles at 95°C for 15 s, 65°C for 20 s, and 72°C for 20 s, which resulted in a default melting curve. We used water as a nontemplate control and DNA from a *T. cruzi* culture (Institute of Biomedical Sciences, University of Chile, Santiago, Chile) as a positive control. Each sample was analyzed in duplicate and considered positive when ≥1 of the replicates had specific amplification and a cycle threshold (Ct) value <40.0 (*12*).

We submitted ≥1 amplicons/sampled animal that had a band visualized by electrophoresis for sequencing of both strands by Macrogen (https://www.macrogen.com). We checked quality of sequences by inspection of each chromatogram,

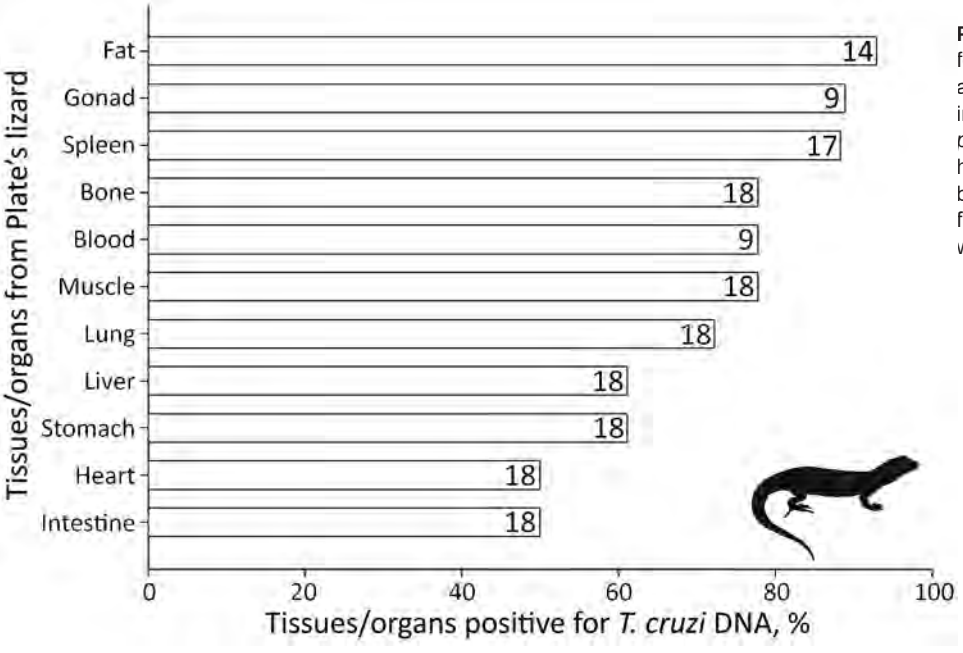

Figure 1. Tissues/organs tested for *Trypanosoma cruzi* infection and their percentages of infection in Plate's lizards (*Liolaemus platei*) in study of lizards as silent hosts of *T. cruzi*. Numbers in each bar indicate number of lizards from which a specific tissue/organ was extracted and tested.

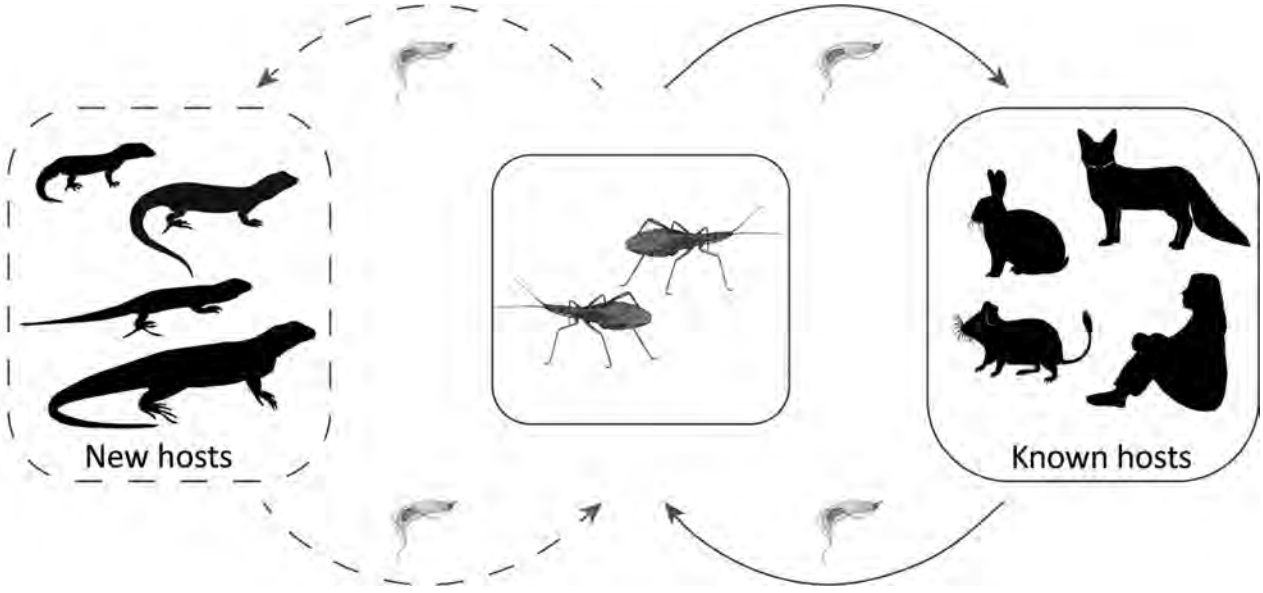

Figure 2. Transmission cycle of *Trypanosoma cruzi* parasites in the arid–semiarid Mediterranean ecosystem of South America. Solid lines indicate known *T. cruzi* transmission between mammal hosts and kissing bugs, and dashed lines indicate transmission between lizards (newly described hosts) and kissing bugs.

obtained the consensus sequence by using Bioedit 7.0.4.1 (*13*), and compared sequences with those available in GenBank. To assess if sequences were more similar to other trypanosomatid species, we compared sequences against a custom database that included other trypanosomatids with a full reference genome available (*T. brucei*, *T. conorhini*, *T. grayi*, *T. rangeli*, and *T. theileri*), excluding *T. cruzi*.

We detected *T. cruzi* infection in nearly all lizard species analyzed (Table), but not in all tested tissues or organs of *L. platei* lizards (Figure 1) and individual lizards of the other species (Appendix Table 1, https://wwwnc.cdc.gov/EID/article/28/6/22-0079-App1.pdf). We detected *T. cruzi* DNA in 11/13 blood samples from the Pacific Atacama racerunner (mean ± SD Ct 36.84 ± 1.47). All 18 Plate's lizards had *T. cruzi* DNA (Ct 34.28 ± 2.57) in blood or heart when blood was not available). All 3 Dark lizards had a *T. cruzi* infection (Ct 32.42 ± 0.90) in blood or heart when blood was not available. All 10 Chilean marked geckos had *T. cruzi* DNA (Ct 32.30 ± 1.97) in heart.

Results from standard sequencing showed all samples matched *T. cruzi* sequences (98.66% mean identity and 99.29% mean query cover). We detected no match between the samples and available reference genomes from other trypanosomatids. We submitted sequences to GenBank (access nos. OM730035–75) and compiled complete BLAST analysis results (i.e., score, query cover, percentage of identity, and GenBank access number) (Appendix Table 2).

We tested Plate's lizard competence (i.e., mean percentage of kissing bugs becoming infected after feeding on infected lizards) for 14 lizards. Nearly all (27/28) triatomine nymphs (Table) that fed on *L. platei* lizards were infected (mean ± SD Ct 33.97 ± 1.00; Appendix Table 3).

Conclusions

We show that some lizard species from southern South America can be infected by *T. cruzi*; ≥1 species is a competent host for transmitting the protozoan to kissing bugs. This reptile group is part of the transmission cycle of Chagas disease (Figure 2), highlighting the role reptiles might have in other neglected vectorborne diseases, such as leishmaniasis and African trypanosomiasis (*7*). However, it is not clear whether lizards are infected with *T. cruzi* by kissing bug consumption, vectorborne transmission, or both.

It is crucial to assess the contribution of lizards to *T. cruzi* transmission in the sylvatic and domestic cycles of Chagas disease. Lizards might not only be competent hosts transmitting the protozoan to kissing bugs but can also be part of the diet of domestic carnivores (e.g., cats and dogs) (*14*), implying that transmission could be maintained by the presence of this new group of hosts being prey for domestic animals (*15*). Determining the threats associated with new host species and vulnerability of persons living in rural areas or in low-income countries will help evaluate transmission risk to humans and generate adequate control strategies.

Acknowledgments

We thank Patricio Arroyo, Sandra Brito, Nora Peña, and Andrea Yáñez-Meza for providing field and laboratory support.

Daniel González-Acuña is deceased.

This study was supported by the Vicerrectoría de Investigación y Desarrollo of the Universidad de Chile (grant ENL01/21); grants ANID-FONDECYT 1221045 (C.B.-M. and J.P.C.) and 11181182 (J.P.C.); ANID Programa Becas - Doctorado Becas Chile 72200094 (R.A.-D.); and Universidad Viña del Mar Project FIIUVM-CTC-2211 (R.C.-S.).

About the Author

Dr. Botto-Mahan is a professor at the University of Chile, Santiago, Chile. Her major research interests are the ecology of host–vector–parasite interactions and the ecology of *T. cruzi* of the semiarid-Mediterranean ecosystem of South America.

References

1. World Health Organization. Descriptive note. Chagas disease (American trypanosomiasis). 2020 [cited 2022 Mar 28]. http://www.who.int/es/news-room/fact-sheets/detail/chagas-disease-(american-trypanosomiasis)
2. Lidani KC, Andrade FA, Bavia L, Damasceno FS, Beltrame MH, Messias-Reason IJ, et al. Chagas disease: from discovery to a worldwide health problem. Front Public Health. 2019;7:166. https://doi.org/10.3389/fpubh.2019.00166
3. Bern C, Kjos S, Yabsley MJ, Montgomery SP. *Trypanosoma cruzi* and Chagas' disease in the United States. Clin Microbiol Rev. 2011;24:655–81. https://doi.org/10.1128/CMR.00005-11
4. Telleria J, Tibayrenc M, editors. American trypanosomiasis Chagas disease. One hundred years of Research. 2nd ed. Amsterdam: Elsevier; 2017.
5. Martínez-Hernández F, Oria-Martínez B, Rendón-Franco E, Villalobos G, Muñoz-García CI. *Trypanosoma cruzi*, beyond the dogma of non-infection in birds. Infect Genet Evol. 2022; 99:105239. https://doi.org/10.1016/j.meegid.2022.105239
6. Georgieva AY, Gordon ER, Weirauch C. Sylvatic host associations of Triatominae and implications for Chagas disease reservoirs: a review and new host records based on archival specimens. PeerJ. 2017;5:e3826. https://doi.org/10.7717/peerj.3826
7. Mendoza-Roldan JA, Modry D, Otranto D. Zoonotic parasites of reptiles: a crawling threat. Trends Parasitol. 2020; 36:677–87. 10.1016/j.pt.2020.04.014 https://doi.org/10.1016/j.pt.2020.04.014
8. Ryckman RE. Epizootiology of *Trypanosoma cruzi* in southwestern North America. Part IV. lizards, laboratory hosts for *Trypanosoma cruzi* and Triatominae (Kinetoplastida: Trypanosomidae) (Hemiptera: Triatominae) (Reptilia: Squamata: Sauria: Gekkonidae, Iguanidae, Teiidae, Anguidae). J Med Entomol. 1965;2:93–5.
9. Urdaneta-Morales S, McLure I. Experimental infections in Venezuelan lizards by *Trypanosoma cruzi*. Acta Trop. 1981;38:99–105.
10. San Juan E, Araya-Donoso R, Sandoval-Rodríguez A, Yáñez-Meza A, Quiroga N, Botto-Mahan C. Lizards and rabbits may increase Chagas infection risk in the Mediterranean-type ecosystem of South America. Sci Rep. 2020;10:1853. https://doi.org/10.1038/s41598-020-59054-8
11. Piron M, Fisa R, Casamitjana N, López-Chejade P, Puig L, Vergés M, et al. Development of a real-time PCR assay for *Trypanosoma cruzi* detection in blood samples. Acta Trop. 2007; 103:195–200. https://doi.org/10.1016/j.actatropica. 2007.05.019
12. Yefi-Quinteros E, Muñoz-San Martín C, Bacigalupo A, Correa JP, Cattan PE. *Trypanosoma cruzi* load in synanthropic rodents from rural areas in Chile. Parasit Vectors. 2018;11:171. https://doi.org/10.1186/s13071-018-2771-2
13. Hall TA. BioEdit: a user-friendly biological sequence alignment editor and analysis program for Windows 95/98/NT. Nucleic Acids Symp Ser. 1999;41:95–8.
14. Doherty TS, Glen AS, Nimmo DG, Ritchie EG, Dickman CR. Invasive predators and global biodiversity loss. Proc Natl Acad Sci U S A. 2016;113:11261–5. https://doi.org/10.1073/pnas.1602480113
15. Gürtler RE, Cardinal MV. Reservoir host competence and the role of domestic and commensal hosts in the transmission of *Trypanosoma cruzi*. Acta Trop. 2015;151:32–50. https://doi.org/10.1016/j.actatropica.2015.05.029

Address for correspondence: Carezza Botto-Mahan, Laboratorio de Ecología de Interacciones, Departamento de Ciencias Ecológicas, Facultad de Ciencias, Universidad de Chile, Las Palmeras 3425, Ñuñoa, PO Box 653, Santiago, Chile; email: cbotto@uchile.cl

Public Health Response to Multistate *Salmonella* Typhimurium Outbreak Associated with Prepackaged Chicken Salad, United States, 2018

Bradford Greening, Jr., Hilary K. Whitham, Wade K. Aldous, Nancy Hall, Ann Garvey, Steven Mandernach, Emily B. Kahn, Patrick Nonnenmacher, Jason Snow, Martin I. Meltzer, Sandra Hoffmann

Quantifying the effect of public health actions on population health is essential when justifying sustained public health investment. Using modeling, we conservatively estimated that rapid response to a multistate foodborne outbreak of *Salmonella* Typhimurium in the United States in 2018 potentially averted 94 reported cases and $633,181 in medical costs and productivity losses.

The US Centers for Disease Control and Prevention estimates that 48 million illnesses, 128,000 hospitalizations, and 3,000 deaths are caused by foodborne illnesses each year in the United States (*1*). *Salmonella* alone accounts for 1.35 million illnesses, 26,600 hospitalizations, and 421 deaths in the United States annually (*2*). Although incidence of *Salmonella enterica* serotype Typhimurium has declined since 2000, infection with this serotype continues to pose a public health burden because it can result in higher rates of hospitalization and longer lengths of stay in a hospital relative to other serotypes (*3*–*6*). A subset of *Salmonella* illnesses are identified and reported as part of an outbreak (defined as ≥2 persons who become ill from the same exposure); 96% of *Salmonella* outbreaks are caused by foodborne transmission (*7*). Outbreaks provide an opportunity to identify implicated food vehicles, as well as root causes for contamination, which can in turn inform broader food safety prevention efforts. If a *Salmonella* outbreak is suspected, public health officials can limit further cases by quickly identifying the source and issuing a recall for the implicated product or making other recommendations for restricting exposure to it.

Author affiliations: Centers for Disease Control and Prevention, Atlanta, Georgia, USA (B. Greening, Jr., H.K. Whitham, E.B. Kahn, P. Nonnenmacher, J. Snow, M.I. Meltzer); State Hygienic Laboratory at the University of Iowa, Coralville, Iowa, USA (W.K. Aldous, N. Hall); Iowa Department of Public Health, Des Moines, Iowa, USA (A. Garvey); Iowa Department of Inspections and Appeals, Des Moines (S. Mandernach); US Department of Agriculture, Washington, DC, USA (S. Hoffmann)

DOI: https://doi.org/10.3201/eid2806.211633

The Study

On February 5, 2018, staff at the State Hygienic Laboratory (SHL) at the University of Iowa (Coralville, Iowa) observed a notable increase in the number of stool samples submitted for *Salmonella* testing. Whole-genome sequencing and serotyping revealed patterns of genetic similarity between isolates obtained from these samples. By completing epidemiologic interviews of affected persons and performing food sample testing on suspected food products, the Foodborne Rapid Response team of the Iowa Department of Public Health (IDPH) was able to identify the source of the outbreak as prepackaged chicken salad sold by a Midwest grocery store chain. By February 9, the grocery store chain voluntarily removed the product from all of its Iowa stores; on February 13, IDPH and the Iowa Department of Inspections and Appeals (DIA) issued a joint consumer advisory notification warning customers that the product was implicated in multiple cases of *Salmonella* illness.

Using the PulseNet national molecular subtyping network for foodborne illness surveillance (a national laboratory network that compares the DNA of bacteria from patient samples to find clusters of disease that might represent unrecognized outbreaks), we identified a total of 265 persons from 8 states with *Salmonella* Typhimurium illness as part of this outbreak. Of those, 240 were from Iowa. Ninety-four hospitalizations

Table 1. Quantitative analysis of cases averted in a multistate *Salmonella enterica* serovar Typhimurium outbreak, United States, 2018

Parameter	Value	Source
Product included in recall, lb	20,630	(*9*)
Product marked as recovered, lb (%)	5,397 (26.2)	(9)
Product available for consumption, lb	15,233	Calculated
Available product consumed, %	88.5 (82.0–94.5)	(*10,11*)
Product consumed, lb	13,481 (12,491–14,395)	Calculated
Outbreak cases reported	265	(*9*)
Cases/1,000 lb consumed	19.66 (18.41–21.22)	Calculated
Cases averted	94	Calculated
Cases averted including underdiagnosis	2,751	Calculated (*7*)
Hospitalizations averted	33	Calculated

*Values are no. (range) except as indicated.

were reported (35.5% of cases), including 1 person from Iowa who died. Decisive, cooperative actions undertaken between the Iowa SHL and IDPH, together with the Food and Consumer Safety Bureau within the Iowa DIA, resulted in the removal of contaminated product within 3 days from the initial identification of the genetically related samples, averting what could have been a larger outbreak.

Using a method reported by Scharff et al. (*8*), we estimated the number of cases of *Salmonella* Typhimurium averted by responding rapidly to this outbreak (Table 1). As a result of the alert raised by Iowa public health staff, the US Department of Agriculture (USDA) issued a recall for ≈20,630 pounds of potentially contaminated chicken salad from grocery stores in 8 states (*9*). According to USDA records, the manufacturer reported that 5,397 pounds (26.2%) of the product were recovered (*9*). Using estimates for product loss at the consumer level (10,11), we calculated that 13,481 pounds of the product were consumed, implying ≈20 confirmed cases of *Salmonella* Typhimurium per 1,000 pounds of product consumed. Assuming this rate of disease transmission also applied to the quantity of product that was successfully recalled, we conclude that ≈94 cases of *Salmonella* Typhimurium were averted through the expedient recall of the chicken salad (i.e., cases that would have been reported had the recalled product been consumed). Assuming this rate of disease transmission also applied to the quantity of product that was successfully recalled, we conclude that ≈106 (99–114) cases of *Salmonella* Typhimurium were averted through the expedient recall of the chicken salad (i.e., cases that would have been reported had the recalled product been consumed). This estimate also assumes that all reported cases of *Salmonella* infection in the outbreak resulted from consumption of the contaminated product (Appendix 1, https://wwwnc.cdc.gov/EID/article/28/6/21-1633-App1.pdf)

Our estimate does not account for potential underdiagnosis resulting from variations in medical care seeking, specimen submission, and laboratory testing. Scallan et al. (*7*) estimated that, for every reported case of nontyphoidal *Salmonella*, 29.3 (90% credible interval 21.8–38.4) cases are likely not reported; therefore, the number of cases averted due to the product recall, including underdiagnosed cases, is estimated as 2,751 (range 2,047–3,605). Those cases would have occurred had the recalled product been consumed; of those, 94 would have been reported and the rest underdiagnosed. Our results assume the middle estimate for the fraction of available product consumed, or 88.5% (Appendix 1 Table 4).

Using cost of illness estimates for nontyphoidal *Salmonella* generated by USDA/ERS (*12*), we estimated the economic costs to society averted by responding rapidly to this outbreak (Table 2). All costs are inflation-adjusted to 2018 US dollars. For our estimate of 94 cases averted, we calculated averted economic costs to society of $601,563 in direct medical costs and $31,618 in productivity losses resulting from missed working days in nonfatal cases. The total estimate of averted costs rises to $844,000 to $1 million when accounting for underdiagnosis. These numbers likely constitute an underestimate because we were conservative in selecting input parameters in cases where uncertainty or feasible ranges exist (Appendix 1). Furthermore, our analysis does

Table 2. Estimated economic impact of cases averted in a multistate *Salmonella enterica* serovar Typhimurium outbreak, United States, 2018*

Characteristic in underdiagnosis scenario	None	Low	Middle	High
Averted cases				
Underdiagnosis correction factor	0	21.8	29.3	38.4
No. cases averted	94	2,047	2,751	3,605
Economic impact of cases averted				
Medical costs, USD	$601,563	$673,626	$699,610	$731,137
Productivity loss, nonfatal cases				
Total lost working days	112.1	619.5	802.5	1,024.5
Total economic loss, USD	$31,618	$170,901	$221,123	$282,059
Total cost of illness, USD	$633,181	$844,526	$920,733	$1,013,196

*Data are for base case (middle) scenario for Fraction of Available Product Consumed. Appendix 1 Tables 5, 6 (https://wwwnc.cdc.gov/EID/article/26/6/21-1633-App1.pdf) show results using sensitivity analysis scenarios. USD, US dollars.

not consider secondary effects that could provide additional benefits, such as prevention of future potential outbreaks through providing industry with information by which to improve their processes.

Conclusions

Quantifying and communicating effects such as the amount of illness and economic costs prevented by response and prevention efforts to policymakers and other appropriate audiences using a clear and systematic approach helps to show the value in investing in a robust, responsive, and collaborative public health infrastructure. Although data from outbreak events may lack some of the information desired for a direct calculation of the effect of interventions on population health, methods do exist that aid in making conservative estimates. Routinely calculating and communicating these estimates using direct and relatable outcome indicators for a variety of public health actions helps demonstrate the importance of investing in the ability to respond to outbreaks when they occur and of sustained investment in measures that prevent these outbreaks from occurring. Future analyses could expand upon our approach by examining the sequence of public health actions in relationship to the rise and fall of daily case counts, which may provide additional useful insights into the value of timely information. Incorporating information about the distribution of product sales and recovery could yield specific knowledge for future studies.

Acknowledgments

We thank Elizabeth Allen for providing valuable feedback during the original write-up of this analysis.

The Centers for Disease Control and Prevention Epidemiology and Laboratory Capacity for Prevention and Control of Emerging Infectious Diseases provided partial support for the response actions we described through a cooperative agreement. The USDA Economic Research Service also supported this work.

About the Author

Dr. Greening is the Evaluation Team lead for the Epidemiology and Laboratory Capacity for Prevention and Control of Emerging Infectious Diseases, Division of Preparedness and Emerging Infections, Centers for Disease Control and Prevention. When this analysis was conducted, he was a health scientist and mathematical modeler in the Health Economics and Modeling Unit, Emergency Preparedness and Response Branch, Division of Preparedness and Emerging Infections at CDC. His research interests include leveraging mathematical and statistical models to improve public health emergency response and preparedness efforts.

References

1. Centers for Disease Control and Prevention. Estimates of foodborne illness in the United States. 2018 Nov 5 [cited 2019 Dec 6]. https://www.cdc.gov/foodborneburden
2. Collier SA, Deng L, Adam EA, Benedict KM, Beshearse EM, Blackstock AJ, et al. Estimate of burden and direct healthcare cost of infectious waterborne disease in the United States. Emerg Infect Dis. 2021;27:140–9. https://doi.org/10.3201/eid2701.190676
3. Jones TF, Ingram LA, Cieslak PR, Vugia DJ, Tobin-D'Angelo M, Hurd S, et al. Salmonellosis outcomes differ substantially by serotype. J Infect Dis. 2008;198:109–14. https://doi.org/10.1086/588823
4. Kennedy M, Villar R, Vugia DJ, Rabatsky-Ehr T, Farley MM, Pass M, et al.; Emerging Infections Program FoodNet Working Group. Hospitalizations and deaths due to *Salmonella* infections, FoodNet, 1996–1999. Clin Infect Dis. 2004;38(Suppl 3):S142–8. https://doi.org/10.1086/381580
5. Santos AC, Roberts JA, Cook AJ, Simons R, Sheehan R, Lane C, et al. *Salmonella* Typhimurium and *Salmonella* Enteritidis in England: costs to patients, their families, and primary and community health services of the NHS. Epidemiol Infect. 2011;139:742–53. https://doi.org/10.1017/S0950268810001615
6. Chen Y, Glass K, Liu B, Hope K, Kirk M. *Salmonella* infection in middle-aged and older adults: incidence and risk factors from the 45 and up study. Foodborne Pathog Dis. 2016;13:689–94. https://doi.org/10.1089/fpd.2016.2170
7. Scallan E, Hoekstra RM, Angulo FJ, Tauxe RV, Widdowson MA, Roy SL, et al. Foodborne illness acquired in the United States—major pathogens. Emerg Infect Dis. 2011;17:7–15. https://doi.org/10.3201/eid1701.P11101
8. Scharff RL, Besser J, Sharp DJ, Jones TF, Peter GS, Hedberg CW. An economic evaluation of PulseNet: a network for foodborne disease surveillance. Am J Prev Med. 2016;50(Suppl 1):S66–73. https://doi.org/10.1016/j.amepre.2015.09.018
9. US Department of Agriculture, Food Safety and Inspection Service. Triple T Specialty Meats Inc. recalls chicken salad products due to possible *Salmonella* contamination. 2018 Feb 21 [cited 2019 Dec 6]. https://www.fsis.usda.gov/recalls-alerts/triple-t-specialty-meats-inc.-recalls-chicken-salad-products-due-possible-salmonella
10. Muth MK, Karns SA, Nielsen SJ, Buzby JC, Wells HF. Consumer-level food loss estimates and their use in the ERS loss-adjusted food availability data. Technical bulletin no. 1927. Contract no. 59–4000–6-0121.Washington (DC): United States Department of Agriculture, Economic Research Service; 2011 Jan [cited 2019 Dec 6]. https://www.ers.usda.gov/webdocs/publications/47570/8043_tb1927.pdf
11. Food Marketing Institute; Technomic Inc. The sophistication of supermarket fresh prepared foods (but not just the food). 2016 [cited 2019 Dec 6]. https://www.fmi.org/forms/store/ProductFormPublic/sophistication-of-supermarket-fresh-prepared-foods
12. US Department of Agriculture, Economic Research Service. Cost estimates of foodborne illnesses. 2014 Oct 7 [cited 2019 Dec 6]. https://www.ers.usda.gov/data-products/cost-estimates-of-foodborne-illnesses

Address for correspondence: Bradford Greening, Centers for Disease Control and Prevention, 1600 Clifton Rd NE, MS H24-11, Atlanta GA 30329-4027, USA; email: BGreening@cdc.gov

Zoonotic Transmission of Diphtheria from Domestic Animal Reservoir, Spain

Andreas Hoefer,[1] Silvia Herrera-León,[1] Lucas Domínguez, Maria Ordobás Gavín, Beatriz Romero, Ximena Belen Araujo Piedra, Cristina Sobrino Calzada, María José Uría González, Laura Herrera-León, Case Study Investigation Group[2]

Toxigenic *Corynebacterium ulcerans* is as an emerging zoonotic agent of diphtheria. We describe the zoonotic transmission of diphtheria caused by toxigenic *C. ulcerans* from domestic animals in Spain, confirmed by core-genome multilocus sequence typing. Alongside an increasing number of recent publications, our findings highlight the public health threat posed by diphtheria reemergence.

Diphtheria has been increasing in relevance because of increasing individual travel and surges in mass relocation events of refugees, asylum seekers, and immigrants from countries where diphtheria remains endemic (*1*–*3*). These importation events, in combination with growing vaccine hesitancy in non-endemic countries, give diphtheria a high potential for reemergence.

Toxigenic *Corynebacterium ulcerans*, an agent of diphtheria, has frequently been identified in domesticated animals such as cats, dogs, and pigs in which zoonotic transmission has been demonstrated (*4*–*7*). Toxigenic *C. ulcerans* has also been identified in wild animals such as ferrets, boars, and deer (*8*). This natural reservoir of *C. ulcerans,* in both wild and domesticated animals, constitutes a major public health threat.

The Case Report

On February 23, 2019, a 60-year-old man visited the emergency department of the Hospital Universitario del Sureste in Madrid, Spain. At examination, he was found to have odynophagia, dysphonia, and a whitish membrane in the oropharynx. He visited this emergency department several times during February 26–March 5. On March 5, an emergency department doctor took a pharyngeal exudate sample and sent it to Spain's National Centre of Microbiology (CNM), and the patient was started on a course of clarithromycin on March 6.

CNM received the swab on March 7. On March 10, laboratory cultures confirmed that the throat swab contained *C. ulcerans* and was positive for the *tox* gene on PCR (*9*). The hospital then contacted the patient, who was recovering at home, and requested his immediate hospitalization for treatment and isolation. The patient complied and was started on a 12-hour course of intravenous clarithromycin. Administering antitoxin was ruled out because the patient responded well to antibiotics.

On March 11, the National Directorate of Epidemiologic Services initiated an outbreak investigation. CNM sent a culture to the Centre for Reference on Diphtheria and Streptococcal Infections (part of the United Kingdom's Health Security Agency) for toxigenicity testing, where the sample was confirmed as toxigenic by ELEK test on March 18 (*10*). Subsequent samples, taken on March 21 and 22, were negative for *C. ulcerans*, and the patient was released. While in the hospital, the patient also was revaccinated for diphtheria.

The Regional Epidemiologic Services of Madrid (RESM) conducted a survey, which confirmed that no exposure to conventional sources of infection or recent overseas travel had occurred. The case-patient

Author affiliations: European Public Health Microbiology Training Programme, Stockholm, Sweden (A. Hoefer, S. Herrera-León); Instituto de Salud Carlos III, Madrid, Spain (A. Hoefer, S. Herrera-León, L. Herrera-León); Universidad Complutense de Madrid, Madrid (L. Domínguez, B. Romero); Dirección General de Salud Pública, Madrid (M. Ordobás Gavín); Hospital Universitario del Sureste, Madrid (X.B. Araujo Piedra, C. Sobrino Calzada); Laboratorio Br Salud Ut, Madrid (M.J. Uría González)

DOI: https://doi.org/10.3201/eid2806.211956

[1]These first authors contributed equally to this article.

[2]Authors in the Case Study Investigation Group are listed at the end of this article.

and his partner live in relative isolation ≈8 km from a small urban center and are not associated with any agriculture activities. No record of a recent diphtheria booster dose was found for the case-patient or his partner. The case-patient owns 2 cats and 3 dogs, and he is known to regularly feed stray cats that frequent his estate.

RESM conducted contact tracing as indicated by national guidelines (*11*). A risk assessment identified 2 close contacts (considered high-risk) and 20 further contacts (considered moderate-risk). All 22 contacts were tested, and no *C. ulcerans* was identified. The asymptomatic household contact, the case-patient's partner, received prophylactic azithromycin, and diphtheria vaccine was administered. The second high-risk contact was the attending physician who performed the physical examination without the personal protective equipment required when treating a patient with an active case of diphtheria. The physician's vaccination history was confirmed, and prophylactic azithromycin was administered. The 20 moderate-risk contacts (including 1 domestic assistant and 19 hospital staff members) all had their vaccination coverage confirmed and were briefed on recognizing potential symptoms.

In adherence with World Health Organization and national protocols, RESM requested Animal Health Services of Madrid to investigate the animals in contact with the human case (*12*). This investigation was performed by the VISAVET Health Surveillance Centre. On March 18–19, nasal, pharyngeal, and conjunctival swabs were collected from the 2 cats (CAT1 and CAT2) and 3 dogs (DOG1, DOG2, and DOG3) that lived with the human case-patient. Three isolates from nasal swab specimens were obtained during selective culturing, 1 from CAT1, 1 from CAT2, and 1 from DOG1 (European Nucleotide Archive accession nos. ERR6177889, ERR6177890, and ERR6177890, respectively); the 2 other dogs tested negative. All isolates were identified as *tox* gene–bearing *C. ulcerans* by PCR and whole-genome sequencing. All 3 animals that had tested positive were placed in isolation by the Central Animal Shelter of the Madrid Community and treated with amoxicillin for 15 days. The animals were retested, and all the swab specimens collected were negative, at which point, the animals were returned to their owner. Workers at the animal shelter were briefed on biosafety measures and management of the infected animals. Contact tracing of the cats was performed, and 4 stray cats were captured and tested; all were negative for *C. ulcerans*. All domestic and stray animals tested were asymptomatic.

All microbiologic procedures were conducted by CNM in accordance with World Health Organization guidelines (*13*). VISAVET identified the isolates by using matrix-assisted laser desorption/ionization time-of-flight mass spectrometry.

CNM purified the genomic DNA from *C. ulcerans* isolates with the DNeasy Blood and Tissue Kit (QIAGEN, https://www.qiagen.com). Libraries were prepared by using Nextera XT DNA Library Preparation Kit and sequenced on a MiSeq platform by using version 3 reagents for 2 × 300 paired-end libraries (both from Illumina, https://www.illumina.com). Multilocus sequence typing (MLST) based on 7 housekeeping *loci* extracted from the next-generation sequencing data identified the human and animals isolates as sequence type (ST) 514 (*14*). Next-generation sequencing–derived core-genome MLST comprising 2,170 target loci revealed no allelic differences

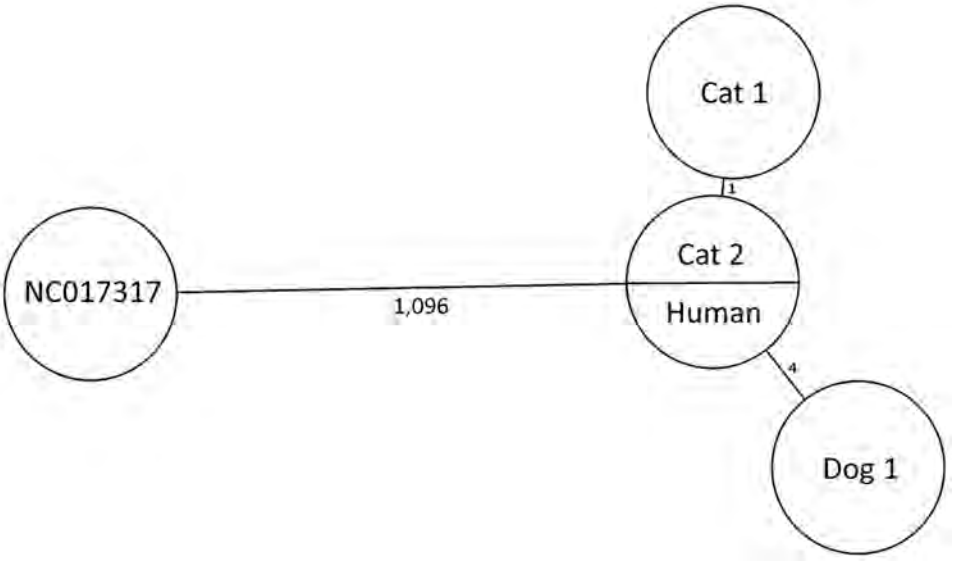

Figure. Core-genome multilocus sequence typing–based minimum spanning tree of all toxigenic *Corynebacterium ulcerans* strains associated with the zoonotic transmission of diphtheria in Spain in 2019 compared with reference strain NCTC_NC017317 from GenBank. Branches are labeled with the number of allelic differences between strains. European Nucleotide Archive accession numbers: human strain, ERR4880084; CAT1 strain, ERR6177889; CAT2 strain, ERR6177890; DOG1 strain, ERR6177891.

between the human (European Nucleotide Archive accession no. ERR4880084) and CAT2 strains, whereas CAT1 harbored 1 allelic difference (*4*). The strain from DOG1 had 4 allelic differences from the human and CAT2 strains, indicating a close relationship (*4*) (Figure). Zoonotic *C. ulcerans* collected from the human, dog, and cat exhibited a high degree of similarity, whereas epidemiologically nonrelated strains differed by thousands of single-nucleotide polymorphisms from each other (data not shown) (*6*,*8*).

Conclusions

The number of cases of diphtheria caused by toxigenic *C. ulcerans* with an epidemiologic link to domestic animals is small but rising (*4*). Under the scope of the One Health initiative, the collaboration between human and animal public health authorities was essential to identify the origin of this case. This case report highlights the sustained risk posed by zoonotic toxigenic *C. ulcerans* reservoirs in peridomestic and domestic animals. Given the high degree of conservation between the human and animal strains, a zoonotic transmission has certainly occurred in this instance. Although the captured stray cats tested negative for *C. ulcerans*, only a small portion of the stray cats in contact with the domesticated animals could be tested. The actual number of cats that were in direct contact with the domesticated animals is unknown. Currently, *C. ulcerans* is not a notifiable organism if it is detected in animals (*11*). To mitigate the future public health burden of toxigenic *C. ulcerans* from animal reservoirs, its declaration should be considered as part of the national surveillance guidelines.

Feline, canine, and porcine zoonotic transmission of toxigenic *C. ulcerans* has been previously supported by findings of the same ST (derived from MLST) in the suspected animal and the epidemiologically linked human case or cases (*7*). The ST identified in this study (ST514) was previously described in an isolate from a 59-year-old man with cutaneous lesions in France in 2005 (*14*).

Vaccinations against diphtheria are offered at 2, 4, and 11 months of age in Spain, with booster doses at 6, 14, and >65 years of age. Earlier administration of boosters may need to be considered because levels of antibodies may not be sufficient to prevent the disease in older persons who are <65 years of age (*15*).

Authors from the Case Study Investigation Group (listed alphabetically): Carmen Bárcena, Jesús Carpintero Hervás, Esther Córdoba Deorador, Fernando Fuster Loran, Marta Hernández, Beatriz Isidoro Fernández, Marta Pérez-Sancho, Elena Rodríguez Baena, Lourdes Sainz de los Terreros Soler

Acknowledgments

We thank all persons and agencies directly and indirectly involved in the effective management of this case study.

This work was partially funded by Área de Ganadería de la Dirección General de Agricultura, Ganadería y Alimentación de la Comunidad de Madrid.

About the Author

Dr. Hoefer is currently completing the European Centre for disease prevention and control Microbiology Training Programme fellowship at the National Center of Microbiology in Spain. His background is in vaccine-preventable diseases, diphtheria, and antimicrobial resistance.

References

1. Wagner KS, White JM, Lucenko I, Mercer D, Crowcroft NS, Neal S, et al.; Diphtheria Surveillance Network. Diphtheria in the postepidemic period, Europe, 2000–2009. Emerg Infect Dis. 2012;18:217–25. https://doi.org/10.3201/eid1802.110987
2. Nelson TG, Mitchell CD, Sega-Hall GM, Porter RJ. Cutaneous ulcers in a returning traveller: a rare case of imported diphtheria in the UK. Clin Exp Dermatol. 2016;41:57–9. https://doi.org/10.1111/ced.12763
3. Rahman MR, Islam K. Massive diphtheria outbreak among Rohingya refugees: lessons learnt. J Travel Med. 2019;26:26. https://doi.org/10.1093/jtm/tay122
4. Hoefer A, Pampaka D, Herrera-León S, Peiró S, Varona S, López-Perea N, et al. Molecular and epidemiological characterization of toxigenic and nontoxigenic *Corynebacterium diphtheriae*, *Corynebacterium belfantii*, *Corynebacterium rouxii*, and *Corynebacterium ulcerans* isolates identified in Spain from 2014 to 2019. J Clin Microbiol. 2021;59:59. https://doi.org/10.1128/JCM.02410-20
5. Marosevic DV, Berger A, Kahlmeter G, Payer SK, Hörmansdorfer S, Sing A. Antimicrobial susceptibility of *Corynebacterium diphtheriae* and *Corynebacterium ulcerans* in Germany 2011–17. J Antimicrob Chemother. 2020;75:2885–93. https://doi.org/10.1093/jac/dkaa280
6. Meinel DM, Margos G, Konrad R, Krebs S, Blum H, Sing A. Next generation sequencing analysis of nine *Corynebacterium ulcerans* isolates reveals zoonotic transmission and a novel putative diphtheria toxin-encoding pathogenicity island. Genome Med. 2014;6:113. https://doi.org/10.1186/s13073-014-0113-3
7. König C, Meinel DM, Margos G, Konrad R, Sing A. Multilocus sequence typing of *Corynebacterium ulcerans* provides evidence for zoonotic transmission and for increased prevalence of certain sequence types among toxigenic strains. J Clin Microbiol. 2014;52:4318–24. https://doi.org/10.1128/JCM.02291-14
8. Berger A, Dangel A, Peters M, Mühldorfer K, Braune S, Eisenberg T, et al. *Tox*-positive *Corynebacterium ulcerans* in

hedgehogs, Germany. Emerg Microbes Infect. 2019;8:211–7. https://doi.org/10.1080/22221751.2018.1562312
9. Pacheco LGC, Pena RR, Castro TLP, Dorella FA, Bahia RC, Carminati R, et al. Multiplex PCR assay for identification of *Corynebacterium pseudotuberculosis* from pure cultures and for rapid detection of this pathogen in clinical samples. J Med Microbiol. 2007;56:480–6. https://doi.org/10.1099/jmm.0.46997-0
10. Public Health England. UK standards for microbiology investigations: identification of *Corynebacterium* species. 2014 Oct 29 [cited 2021 Sep 1]. https://www.gov.uk/government/publications/smi-id-2-identification-of-corynebacterium-species
11. Centro Nacional de Epidemiología. Protocolos de la Red Nacional de Vigilancia Epidemiológica. 2015 May [cited 2021 Sep 1]. https://www.isciii.es/QueHacemos/Servicios/VigilanciaSaludPublicaRENAVE/EnfermedadesTransmisibles/Documents/PROTOCOLOS/PROTOCOLOS%20EN%20BLOQUE/PROTOCOLOS_RENAVE-ciber.pdf
12. World Health Organization. Surveillance standards for vaccine-preventable diseases, second edition. 2018 [cited 2021 Sep 1]. https://apps.who.int/iris/handle/10665/275754
13. Begg N. Manual for the management and control of diphtheria in the European region 1994 [cited 2021 Sep 1]. https://apps.who.int/iris/handle/10665/108107
14. Bolt F, Cassiday P, Tondella ML, Dezoysa A, Efstratiou A, Sing A, et al. Multilocus sequence typing identifies evidence for recombination and two distinct lineages of *Corynebacterium diphtheriae*. J Clin Microbiol. 2010;48:4177–85. https://doi.org/10.1128/JCM.00274-10
15. Limia Sánchez A, Olmedo Lucerón C. Second seroprevalence study in Spain, 2017–2018 [in Spanish]. Rev Esp Salud Publica. 2021;95:95.

Address for correspondence: Laura Herrera León, Instituto de Salud Carlos III, Ctra. de Pozuelo 28, 28222 Majadahonda, Madrid; email: lherrera@isciii.es

New Variant of *Vibrio parahaemolyticus*, Sequence Type 3, Serotype O10:K4, China, 2020

Yan Huang,[1] Yue Du,[1] Hong Wang,[1] Dongmei Tan, Airong Su, Xiugui Li, Biao Kan, Lan Lan, Cong Qu, Bo Pang,[2] Yunliang Shi,[2] Mei Lin[2]

In 2020, a new serotype of *Vibrio parahaemolyticus* O10:K4 emerged and caused several outbreaks and sporadic cases in Guangxi, China. Phylogenetic analysis indicated that those strains are new variants of the sequence type 3 pandemic clone. The new serotype may become dominant, warranting enhanced investigations and surveillance.

Vibrio parahaemolyticus is a halophilic bacterium distributed naturally in marine and estuarine environments. It is one of the most common bacterial pathogens leading to outbreaks and illness in China (*1*). In Guangxi, China, *V. parahaemolyticus* is the second most common cause of foodborne disease outbreaks.

A large proportion of the *V. parahaemolyticus* isolated during outbreaks have been O3:K6 and its serovariants, and these serovariants belonged to the pandemic clone (*2*). A total of 49 *V. parahaemolyticus* serovariants that belonged to the pandemic clone have been identified (*3*). The strains of that clone have characteristics of *tdh*+, *trh*−, *toxRS*/new+ (a unique *toxRS* sequence), and *orf8*+/− (the *orf8* sequence of f237 phage) (*2*). Furthermore, it is speculated that the appearance of derived serotypes (e.g., O4:K68, O1:K36, and O1:KUT), all of which have genetic markers and molecular profiles similar to those of the O3:K6 pandemic strains, is a selective response to host immunologic pressure of the pandemic O3:K6 serotype of V. parahaemolyticus (2,4).

In 2010, a laboratory-based foodborne disease surveillance system, which included municipal-level and prefecture-level monitoring laboratories, was established in Guangxi. Serotyping, pulse-field gel electrophoresis, and whole-genome sequencing are now routine methods used in this surveillance system when *V. parahaemolyticus* is isolated during outbreaks. In 2019, a total of 6 serotypes of *V. parahaemolyticus* were isolated and identified during outbreaks, and O3:K6 was predominant (68%, 42/62).

We report a new serotype of *V. parahaemolyticus*, O10:K4, which emerged in 2020 and caused infections in the Beibu Gulf area of Guangxi. O10:K4 has since become the predominant (71%, 20/28) *V. parahaemolyticus* serotype in Guangxi.

The Study

In August 2020, acute gastroenteritis cases were reported in coastal cities in the Beibu Gulf area in Guangxi. In early August, 10 cases of diarrhea were reported in Beihai, a coastal city of the Beibu Gulf area (Figure 1). The patients reported fever, abdominal pain, and vomiting. All patients had consumed rice noodles in the same fast-food restaurant. We obtained 7 *V. parahaemolyticus* isolates from the patients and 1 strain from a sample of instant sour bean (nonseafood) in the restaurant. Slide agglutination of the 8 *V. parahaemolyticus* isolates showed presence of the O10:K4 serotype.

At the end of August, ≈120 cases of acute gastroenteritis were reported in Fangchenggang, another coastal city in the Beibu Gulf area. Those patients also reported fever, abdominal pain, nausea, and vomiting.

Author affiliations: Guangxi Zhuang Autonomous Region for Disease Control and Prevention, Nanning, China (Y. Huang, Y. Du, H. Wang, D. Tan, A. Su, X. Li, L. Lan, C. Qu, Y. Shi, M. Lin); Guangxi Key Laboratory of Major Infectious Disease Prevention and Control and Biosafety Emergency Response, Nanning (Y. Huang, M. Lin); State Key Laboratory of Infectious Disease Prevention and Control, Beijing, China (B. Kan, B. Pang); National Institute for Communicable Disease Control and Prevention, Beijing (B. Kan, B. Pang); School of Basic Medical Sciences of Guangxi Medical University, Nanning (Y. Shi)

DOI: https://doi.org/10.3201/eid2806.211871

[1]These first authors contributed equally to this article.

[2]These senior authors contributed equally to this article.

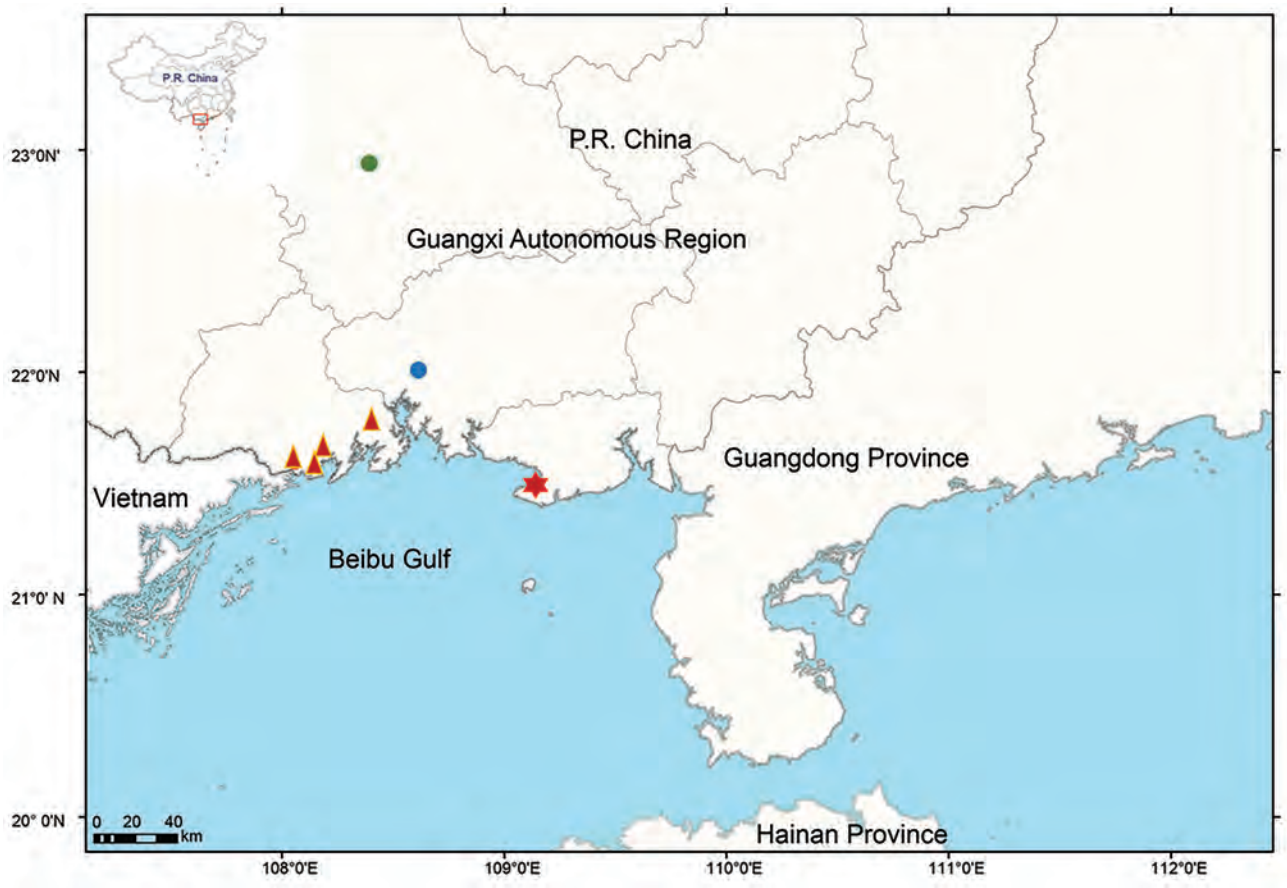

Figure 1. Geographic distribution of the new serotype of *Vibrio parahaemolyticus*, sequence type 3, serotype O10:K4, in Guangxi, China, 2020. Red star represents the outbreak site in Beihai; red triangles represent outbreak sites in Fangchenggang; blue circle represents the sporadic case in Qinzhou, and green circle represents the sporadic case in Nanning. Inset map shows study location in China.

Ten strains of serotype O10:K4 *V. parahaemolyticus* were obtained from hospitalized patients. The investigation indicated that no food had been shared by the patients, although all had consumed durians before symptom onset. The durians that these patients consumed had all been accidentally soaked in seawater. We speculate that those durians were contaminated with *V. parahaemolyticus* and that their consumption might have contributed to the infections. However, we could not isolate serotype O10:K4 *V. parahaemolyticus* from the same batch of durians that the patients consumed, although we obtained other serotype strains (O4:K13, O1:K25, O1:K33, O3:Kunk, and O4:Kunk). Follow-up surveillance detected 2 more strains of O10:K4 isolated from diarrhea patients in Qinzhou (another coastal city, on October 20, 2020) and Nanning (an inland city >200 km from the sea, on November 15, 2020) (Figure 1).

To explore the genetic position of these 20 O10:K4 isolates from persons in 4 cities, we performed whole-genome sequencing on a MiSeq platform (Illumina, https://www.illumina.com). We assembled whole-genome sequences de novo by using SPAdes v.3.12.0 (*5*) (GenBank accession nos. JAHWYL000000000, JAKJNF000000000–JAKJNW000000000) and subtyped them by using in silico multilocus sequence typing on PubMLST (https://pubmlst.org/organisms/vibrio-parahaemolyticus). All strains belonged to sequence type (ST) 3 and clonal complex 3, which is the sequence profile for most pandemic strains of *V. parahaemolyticus*.

We then integrated those genomic data with 33 various serotypes of *V. parahaemolyticus* isolated in Guangxi in recent years, as well as all 1,067 *V. parahaemolyticus* genomic sequences available in the PubMLST database (through January 14, 2022) (*6*) (additional *V. parahaemolyticus* phylogenetic information in Appendix, https://wwwnc.cdc.gov/EID/article/28/6/21-1871-App1.xlsx). We constructed a maximum-likelihood tree based on the single-nucleotide variations (SNVs) identified in the nonrepetitive and nonrecombinant core genome (Figure 2, panel A). The O10:K4 *V. parahaemolyticus* formed a unique, exclusive, and tight cluster that was most closely related to a strain isolated

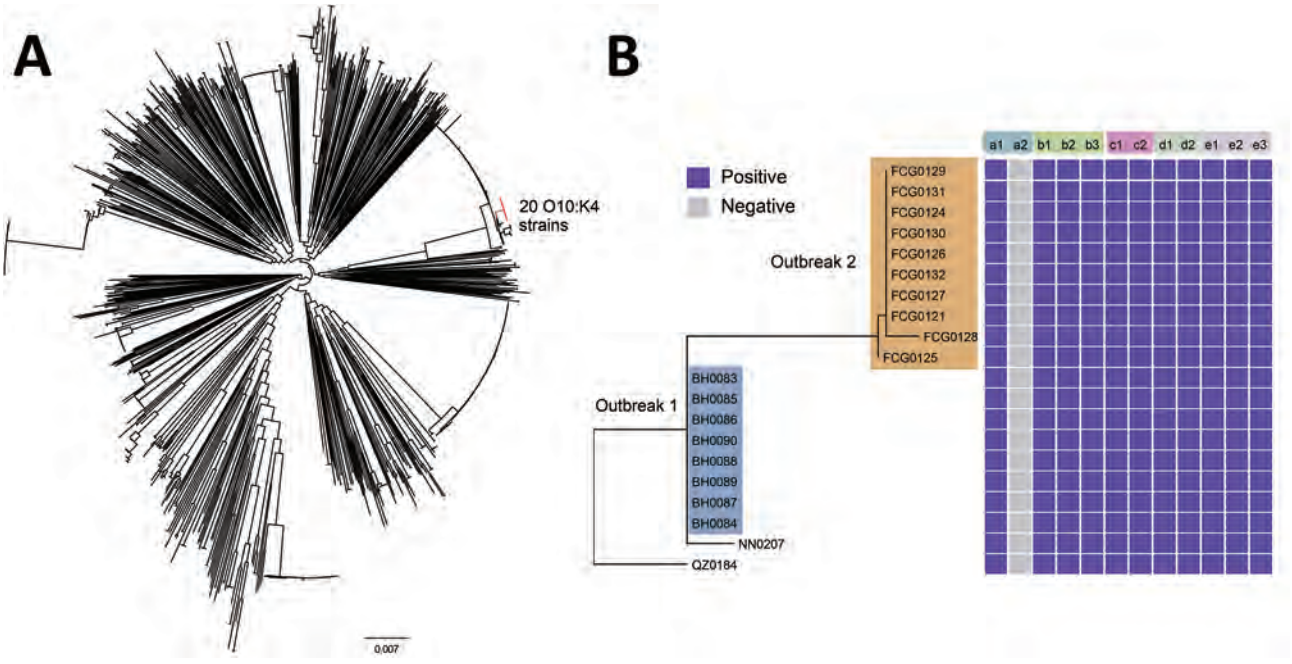

Figure 2. Phylogenetic tree based on the single-nucleotide variations in the core genomes of 1,120 *Vibrio parahaemolyticus* genomes: 20 isolates from patients in the Beibu Gulf area of Guangxi, China, 33 isolates collected in Guangxi in recent years, and all 1,067 genomic sequences available in the PubMLST database (https://pubmlst.org/organisms/vibrio-parahaemolyticus) (Appendix, https://wwwnc.cdc.gov/EID/article/28/6/21-1871-App1.xlsx). A) Maximum-likelihood tree based on the single-nucleotide variations in the nonrepetitive, nonrecombinant regions of the genomes. Branches in red indicate the O10:K4 serotype strains. Scale bar indicates frequency of single-nucleotide variations. B) Distribution of virulence genes, pathogenic islands, secretion systems, characteristic genes in pandemic clones, and antimicrobial resistance genes. a1, *tdh*; a2, *trh*; b1, VPaI-2; b2, VPaI-3; b3, VPaI-4; c1, T3SS; c2, T6SS1; d1, *orf8*; d2, *toxRS*/new; e1, tet(34); e2, tet(35); e3, *blaCARB*-22.

in China in 2016 (strain VP161407), which was also ST3. This O10:K4 cluster is part of the ST3 clade.

We next focused on the 20 O10:K4 strains and strain VP161407. We reconstructed a maximum-likelihood tree based on the SNVs determined in the core genomes of these 21 strains. We found that strain QZ0184, isolated in Qinzhou, was most closely related to strain VP161407. To further investigate the relationship between the 20 O10:K4 strains in detail, we reconstructed a maximum-likelihood tree based on the SNVs in the core genomes of the 20 strains. We found that strains isolated in Beihai and Fangchenggang formed 2 separate clusters, which indicated 2 independent outbreaks. We then detected virulence genes, pathogenic islands, and antimicrobial resistance genes in the O10:K4 strains. Analysis revealed that the characteristic genes in these O10:K4 strains were same as those in the *V. parahaemolyticus* pandemic clone: *tdh*+, *trh*–, *toxRS*/new+, and *orf8*+ (Figure 2, panel B). We also detected type 3 and type 6 secretion systems, VPaI-2, VPaI-3, and VPaI-4 in those strains (Figure 2, panel B). Moreover, we detected 3 antimicrobial resistance genes: *tet*(34), *tet*(35), and $bla_{CARB\text{-}22}$ (Figure 2, panel B).

Conclusions

The new variant of ST3 *V. parahaemolyticus* O10:K4 exhibited characteristics of the *V. parahaemolyticus* pandemic clone and caused outbreaks in the Beibu Gulf area. More recently, this variant led to cases in Nanning, which indicated transmission of this variant of *V. parahaemolyticus* from coastal areas to inland areas. The variant was also detected in several other provinces in China, which indicated its widespread nature (B. Pang, unpub. data). The emergence of serotype O10:K4 may be the response to host immunologic pressure, which was observed in serotype O4:K68 (*2*,*4*). The Beibu Gulf is also known as the Gulf of Tonkin, and Vietnam is located to its west. Therefore, similar to what was observed in a previous cholera study (*7*), the possibility remains that this variant has been circulating in the Beibu Gulf area, over time leading to infections in the countries around it.

Acknowledgments

We thank the staff at Beihai Center for Disease Control and Prevention and Fangchenggang Center for Disease Control and Prevention for their participation in the epidemiologic investigation and strain isolation.

This study was supported by Natural Science Foundation of China (grant no.81760380) and Guangxi Natural Science Foundation (grant no. 2017GXNSFAA198270).

About the Author

Dr. Huang is a researcher at Guangxi Zhuang Autonomous Region Center for Disease Control and Prevention, Guangxi, China. His research focuses on foodborne pathogens and infectious disease.

References

1. Li H, Li W, Dai Y, Jiang Y, Liang J, Wang S, et al. Characteristics of settings and etiologic agents of foodborne disease outbreaks—China, 2020. China CDC Wkly. 2021;3:889–93. https://doi.org/10.46234/ccdcw2021.219
2. Nair GB, Ramamurthy T, Bhattacharya SK, Dutta B, Takeda Y, Sack DA. Global dissemination of *Vibrio parahaemolyticus* serotype O3:K6 and its serovariants. Clin Microbiol Rev. 2007;20:39–48. https://doi.org/10.1128/CMR.00025-06
3. Han C, Tang H, Ren C, Zhu X, Han D. Sero-prevalence and genetic diversity of pandemic *V. parahaemolyticus* strains occurring at a global scale. Front Microbiol. 2016;7:567 https://doi.org/10.3389/fmicb.2016.00567
4. Chowdhury NR, Stine OC, Morris JG, Nair GB. Assessment of evolution of pandemic *Vibrio parahaemolyticus* by multilocus sequence typing. J Clin Microbiol. 2004;42:1280–2. https://doi.org/10.1128/JCM.42.3.1280-1282.2004
5. Bankevich A, Nurk S, Antipov D, Gurevich AA, Dvorkin M, Kulikov AS, et al. SPAdes: a new genome assembly algorithm and its applications to single-cell sequencing. J Comput Biol. 2012;19:455–77. https://doi.org/10.1089/cmb.2012.0021
6. Jolley KA, Bray JE, Maiden MCJ. Open-access bacterial population genomics: BIGSdb software, the PubMLST.org website and their applications. Wellcome Open Res. 2018;3:124. https://doi.org/10.12688/wellcomeopenres.14826.1
7. Pang B, Du P, Zhou Z, Diao B, Cui Z, Zhou H, et al. The transmission and antibiotic resistance variation in a multiple drug resistance clade of *Vibrio cholerae* circulating in multiple countries in Asia. PloS One. 2016;11(3):e0149742.

Address for correspondence: Mei Lin or Yunliang Shi, Guangxi Zhuang Autonomous Region Center for Disease Control and Prevention, 18 Jinzhou Rd, Nanning, Guangxi 530028, China; email: gxlinmei@126.com or syunliang2008@126.com; Bo Pang, National Institute for Communicable Disease Control and Prevention, China CDC, 155 Changbai Rd, Changping, Beijing 102206, China; email: pangbo@icdc.cn

etymologia revisited

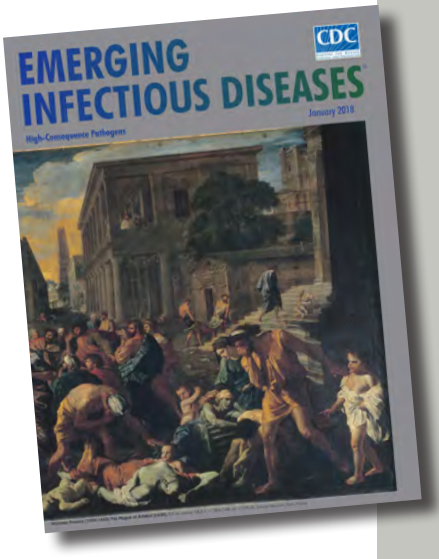

Originally published in January 2018

Plague

[plāg]

Plague (from the Latin *plaga*, "stroke" or "wound") infections are believed to have been common since at least 3000 bce. Plague is caused by the ancestor of current *Yersinia* (named for Swiss bacteriologist Alexandre Yersin, who first isolated the bacterium) *pestis* strains. However, this ancestral *Y. pestis* lacked the critical *Yersinia* murine toxin (*ymt*) gene that enables vectorborne transmission. After acquiring this gene (sometime during 1600–950 bce), which encodes a phospholipase D that protects the bacterium inside the flea gut, *Y. pestis* evolved the ability to cause pandemics of bubonic plague. The first recoded of these, the Justinian Plague, began in 541 ace and eventually killed more than 25 million persons.

Sources:

1. Alexandre Yersin BW. Etymologia: yersinia. Emerg Infect Dis. 2010;16:496.
2. Centers for Disease Control and Prevention. History of plague [cited 2017 Oct 19]. https://www.cdc.gov/plague/history/index.html.
3. Rasmussen S, Allentoft ME, Nielsen K, Orlando L, Sikora M, Sjögren K-G, et al. Early divergent strains of Yersinia pestis in Eurasia 5,000 years ago. Cell. 2015;163:571–82.

https://wwwnc.cdc.gov/eid/article/24/1/et-2401_article

Fasciolopsis buski Detected in Humans in Bihar and Pigs in Assam, India

Dipshikha Saikia,[1] Yugal K. Prasad,[1] Suman Dahal, Sudeep Ghatani

The foodborne intestinal trematode *Fasciolopsis buski* causes the neglected zoonotic disease fasciolopsiasis. We detected *F. buski* infection in 14 pediatric patients in Sitamarhi, Bihar, and in pigs in Sivasagar, Assam, India. Proper diagnostic methods and surveillance are urgently needed to accurately estimate the true burden of this disease in India.

Fasciolopsis buski is a foodborne intestinal trematode that causes the neglected zoonotic disease fasciolopsiasis in humans and pigs. *F. buski* infection is transmitted through ingestion of raw aquatic plants or water carrying encysted metacercaria. Persons with substantial worm loads can have clinical indicators, such as malnutrition, edema, malabsorption, severe diarrhea, ascites, and anemia, and might experience acute intestinal obstruction and ileus (*1*–*3*). *F. buski* worms are found mostly in Asia and the Indian subcontinent; endemicity is highest in eastern India (*4*). We previously reported multiple cases of infection with *Artyfechinostomum sufrartyfex*, an echinostome trematode, which was diagnosed in children at Shri Shubh Lal (SSL) Hospital and Research Centre in Sitamarhi, Bihar state, India (*5*). We also documented several cases of fasciolopsiasis among SSL patients during 2012–2021 and infection in pigs detected in Sivasagar district, Assam state, India during a 2019–2020 survey.

Infections with this parasite have been reported from diverse regions of India, as well as other parts of Asia (*6*–*10*). A genetic study suggested that the species found in India is different from species found in China and Vietnam (*11*). To corroborate the genetic distinctions between the strains found in India and those from China and Vietnam, we determined the complete nuclear ribosomal ITS2 and partial mitochondrial cytochrome c oxidase subunit 1 gene (cox1) sequences of *F. buski* from the samples recovered from Bihar and Assam and compared them to sequences from isolates from other regions of India, China, and Vietnam. The institutional ethics committee of Sikkim University in Gangtok, India, approved this work (SU/REG/F-1/03/2018/VOL-1/59).

The Study

During 2012–2021, a total of 14 children 3–12 years of age were brought for treatment to SSL Hospital for reported loose bowel movements, including watery feces and feces tinged with blood and mucus for >15 days, as well as vomiting, flatulence, abdominal discomfort, pain in the abdomen, fever, loss of appetite, weakness, and passage of flat reddish worms, called paterwa or lal keera in local languages. Eight patients were male and 6 female. Among the male patients, 3 were ≤5, 3 were 6–10, and 2 were >10 years of age; among the female patients, 3 were ≤5 and 3 were ≥10 years of age. All of the patients were of low socioeconomic status and resided near ponds or deep-water rice paddies contaminated with human and animal excreta and snail-infested areas. The patients were habituated to consume raw snails, contaminated water, chestnuts, and vegetables irrigated with contaminated water from nearby ditches.

On physical examination, all patients were pale and malnourished. General and systemic examination revealed persistent diarrhea, dehydration, and vomiting in most and anemia in all of the case-patients. Laboratory investigation revealed most of the patients had eosinophilia, and grade II malnutrition was associated with most patients (Table 1). All patients tested negative on tuberculin and HIV tests, and results from routine urine examination, complete blood

Author affiliations: Sikkim University, Gangtok, India (D. Saikia, S. Dahal, S. Ghatani); Shri Shubh Lal Hospital and Research Centre, Sitamarhi, India (Y.K. Prasad)

DOI: https://doi.org/10.3201/eid2806.220171

[1]These first authors contributed equally to this article.

Table 1. General and clinical symptoms for 14 patients with *Fasciolopsis buski* infections recorded in SSL Hospital, Bihar, India

Category	No. cases	Test value
Sign or symptom from general and systemic examination		
Persistent diarrhea	13	Y
Acute diarrhea	1	Y
Dehydration	12	Y
Abdomen pain	5	Y
Passage of live worms in feces or vomitus	2	Y
Passage of dead worms in feces or vomitus	12	Y
Fever	9	Y
Vomiting	12	Y
Anemia	14	10.9–14.1 g/dL*
Eosinophilia	10	50–500 eosinophils/mm^3 (1%–4%)
Total leukocyte count	7	5,000–10,000 leukocytes/μL of blood
Potassium	1	3.4–4.7 mEq/L
Malnutrition grading		
Malnutrition grade I, mild malnutrition	1	71%–80%
Malnutrition grade II, moderate malnutrition	9	61%–70%
Malnutrition grade III, severe malnutrition	4	51%–60%

*Children 3–12 years of age.

counts, serum urea, serum creatinine, serum bilirubin, and alanine aminotransferase testing were within reference ranges (Appendix 1, https://wwwnc.cdc.gov/EID/article/28/6/22-0171-App1.xlsx).

Naked eye examination of the feces revealed the presence of live parasites in 2 patients and dead parasites in 12. Two patients had mixed infection: 1 with both *F. buski* and *A. sufrartyfex* parasites and the other with *F. buski* worms and the roundworm *Ascaris lumbricoides*. On microscopic examination of feces samples, no eggs or ova of intestinal flukes were identified, except 1 sample showed fertilized roundworm ova. We isolated the recovered parasites and processed them for morphologic, anatomic, and genetic analysis. All of the patients were hospitalized and treated with praziquantel (75 mg/kg bodyweight; 3 divided doses for 2 d) and supportive measures administered for dehydration, electrolyte imbalance, and malnutrition. All patients were cured and discharged after being counseled for nutritional rehabilitation.

In 2019–2020, a survey of pigs for *F. buski* infection was performed in the Charaideo, Sivasagar, Lakhimpur, Biswanath, and Tezpur districts of Assam. A total of 128 pigs were examined; 3 in the Sivasagar district displayed evidence of parasite infection. The flukes were collected in 0.9% phosphate-buffered saline (pH 7.2) from the intestines of freshly slaughtered pigs in Sivasagar district, as well as from the feces and vomitus of SSL Hospital patients, and brought to the Sikkim University Department of Zoology for further analysis (Figure 1).

We extracted and purified genomic DNA from the flukes collected from both patients and pigs using QIAGEN DNeasy Blood and Tissue Kit (https://www.qiagen.com) according to manufacturer instructions. We performed amplification and sequencing of the complete ITS2 and partial cox1 genes using the primers 3S: 5′-GGTACCGGTGGATCACTCGGCTCGTG-3′ (forward), A28: 5′-GGGATCCTGGTTAGTTTCTTTTCCTCCGC-3′ (reverse) (*12*,*13*), and

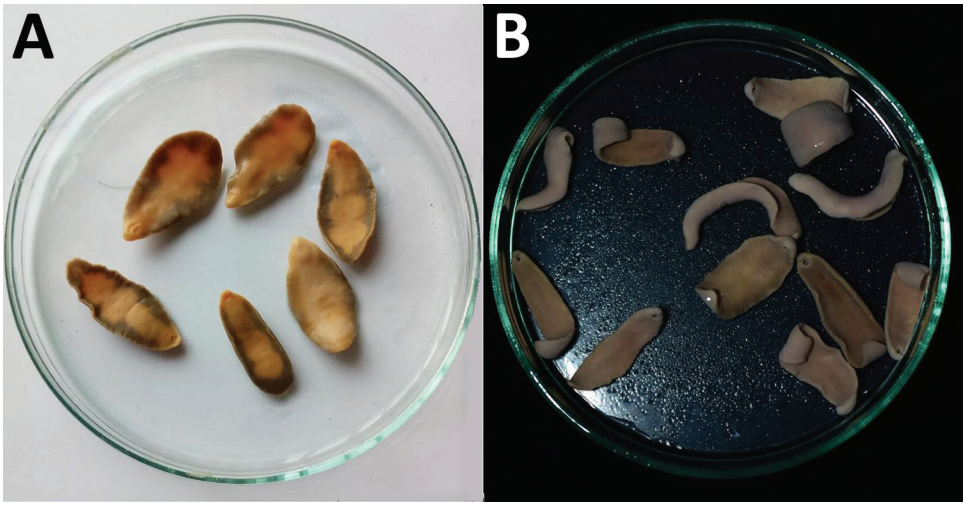

Figure 1. *Fasciolopsis buski* trematode samples preserved in absolute ethanol. A) Parasites recovered from child patients in Shri Shubh Lal Hospital and Research Centre Hospital, Sitamarhi, Bihar, India. B) Parasites isolated from the intestine of freshly slaughtered pigs in Sivasagar district of Assam.

Table 2. Genetic variations in *Fasciolopsis buski* ITS2 and COI gene regions from India and other Asian countries*

	Genetic distance					
	Among Indian isolates		From other Asian isolates†		Among other Asian isolates†	
Gene region	% Isolates	Transitions/ transversions	%	Transitions/ transversions	%	Transitions/ transversions
Nuclear ribosomal ITS2	0–0.3	1/0	7.7–8.2	12/8	0	0/0
Mitochondrial COI	0.4	1/0	12.1–12.3	36/46	0.5	3/1

*COI, cytochrome oxidase subunit 1; ITS2, internal transcribed spacer 2
†Other Asian isolates from China and Vietnam

DICE 1F: 5′-TTWCNTTRGATCATAAG, Dice 14R: 5′-CCHACMRTAAACATATGATG-3′ (reverse) (*14*). The ITS2 amplicon was ≈292 bp and the cox1, ≈784 bp. We uploaded sequences to GenBank (ITS2 accession nos. MW771525 [Sitamarhi] and MW771526 [Sivasagar]; cox1 accession nos. MW767135 [Sitamarhi] and MW767136 [Sivasagar]. We identified parasites using a BLASTn search (https://blast.ncbi.nlm.nih.gov/Blast.cgi).

The ITS2 sequences of the Sitamarhi and Sivasagar isolates were genetically similar and showed the greatest sequence similarity with previously identified *F. buski* isolates from Uttar Pradesh (GenBank accession no. KF564866) and Meghalaya, India (accession no. DQ351841), with little or no genetic variability. In contrast, *F. buski* sequences from China and Vietnam (GenBank accession nos. MN970005 and EF612489) had 7.7%–8.2% genetic difference from the isolates from India. However, the sequences from China and Vietnam were identical to each other. Similarly, the cox1 sequences from Sitamarhi and Sivasagar exhibited only 0.4% variation between each other but 12.1%–12.3% variation from sequences from Vietnam (accession no. MF287794) and China (accession no. KX169163). The sequences from China and Vietnam had only 0.5% variation from each other (Table 2; Appendix 2 Figures 1, 2, https://wwwnc.cdc.gov/EID/article/28/6/22-0171-App1.pdf).

We constructed phylogenetic trees based on the 2 gene regions using the maximum-likelihood method. Both trees clearly showed the Indian isolates forming a separate clade from the isolates from China and Vietnam (Figure 2). On the basis of our findings, we concluded that the samples collected in our study belonged to *F. buski* but that the isolates from China and Vietnam were separate taxa from those from India; however, *F. buski* samples from China and Vietnam were the same species. This discovery is consistent with the findings of a prior study in China (*11*).

Conclusions

Our study confirmed that the parasites obtained from both human patients in Sitamarhi and pigs in Sivasagar were of the *F. buski* species. However, we also corroborated that the species found in India might differ from those in China and Vietnam, and species taxonomy might need to be revised in the future (*11*).

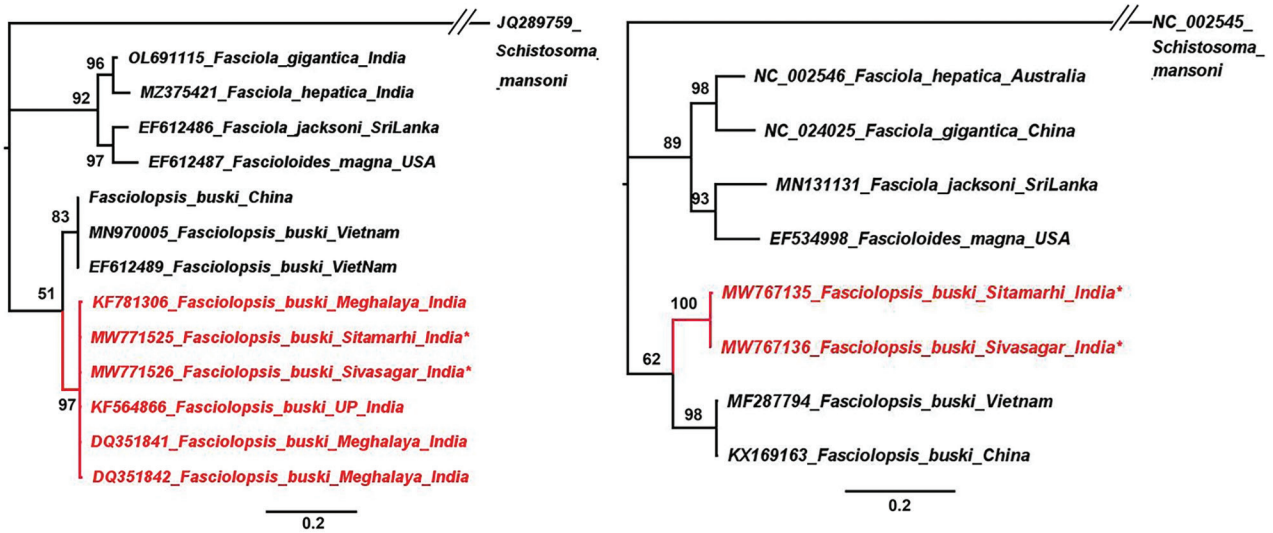

Figure 2. Phylogenetic trees for study strains of *Fasciolopsis buski*, constructed using the maximum likelihood method as implemented in MrBayes version 3.1.2 (https://bioweb.pasteur.fr/packages/pack@mrbayes@3.1.2). A) ITS2 gene tree using HKY+I model. B) Cox1 gene tree using GTR+G model. The analyses were run for 5,000,000 generations with sampling frequency of 100 and initial 25% of the trees discarded as burn-in. Node values represent Bayesian posterior probabilities. Scale bars represent branch length.

In recent years, *F. buski* infection from humans and pigs has been documented in India in the states of Assam, Bihar, Delhi, Meghalaya, and Uttar Pradesh. According to our findings, this parasite is an increasing public health threat in India, especially in remote locations and among persons from low socioeconomic backgrounds, because of the substantial risk to human and animal health it poses. Surveys are urgently needed to determine the true burden of fasciolopsiasis in the country. A lack of effective diagnostic tools for detecting neglected foodborne trematode infections, including *F. buski*, means there are no prevalence data on these infections in the country. Therefore, there is a pressing need to design and develop a rapid and easy detection tool for *F. buski* and other neglected trematode infections.

Acknowledgments

We thank CSIR and UGC, the Government of India, New Delhi, for Research Fellowship (UGC-JRF) to DS and the hospital staff at Shri Shubh Lal Hospital and Research Centre in Sitamarhi for providing help with sample collection.

We dedicate this work to the loving memory of our beloved senior colleague and coauthor of this paper, the recently deceased Dr. Yugal Kishore Prasad.

About the Author

Ms. Saikia is a PhD student in the Department of Zoology, School of Life Sciences, Sikkim University in Gangtok. Her scientific interests include helminth parasitology, particularly using the proteomics of foodborne trematodes to identify novel therapeutic targets and diagnostic markers. Dr. Prasad was director, consultant pediatrician, and neonatologist at Shri Shubh Lal Hospital and Research Centre, Sitamarhi, Bihar, India. His primary research interest was pediatric parasitology.

References

1. Achra A, Prakash P, Shankar R. Fasciolopsiasis: endemic focus of a neglected parasitic disease in Bihar. Indian J Med Microbiol. 2015;33:364–8. https://doi.org/10.4103/0255-0857.158554
2. Fried B, Graczyk TK, Tamang L. Food-borne intestinal trematodiases in humans. Parasitol Res. 2004;93:159–70. https://doi.org/10.1007/s00436-004-1112-x
3. Mas-Coma S, Bargues MD, Valero MA. Fascioliasis and other plant-borne trematode zoonoses. Int J Parasitol. 2005;35:1255–78. https://doi.org/10.1016/j.ijpara.2005.07.010
4. Ranjan S, Saurabh K, Prasad RR. Gastrointestinal manifestations of *Fasciolopsis buski* associated polyparasitism in patients of an endemic area: a hospital based study. Int J Community Med Public Health. 2017;4:1898–900. https://doi.org/10.18203/2394-6040.ijcmph20172061
5. Prasad YK, Dahal S, Saikia B, Bordoloi B, Tandon V, Ghatani S. *Artyfechinostomum sufrartyfex* trematode infections in children, Bihar, India. Emerg Infect Dis. 2019;25:1571–3. https://doi.org/10.3201/eid2508.181427
6. Prasad PK, Tandon V, Chatterjee A, Bandyopadhyay S. PCR-based determination of internal transcribed spacer (ITS) regions of ribosomal DNA of giant intestinal fluke, *Fasciolopsis buski* (Lankester, 1857) Looss, 1899. Parasitol Res. 2007;101:1581–7. https://doi.org/10.1007/s00436-007-0680-y
7. Jha AK, Jha SK. Endoscopic diagnosis of *Fasciolopsis buski*: revisited (with video). JGH Open. 2019;4:284–6. https://doi.org/10.1002/jgh3.12187
8. Mahajan RK, Duggal S, Biswas NK, Duggal N, Hans C. A finding of live *Fasciolopsis buski* in an ileostomy opening. J Infect Dev Ctries. 2010;4:401–3. https://doi.org/10.3855/jidc.235
9. Swargiary A, Roy B, Giri BR, Ronghang B. A comparative study on the anthelmintic efficacy of some medicinal plants of North-East India: alteration in the glycolytic enzymes of *Fasciolopsis buski*, a giant intestinal fluke. Asian Pac J Trop Med. 2013;6:412–20.
10. Singh UC, Kumar A, Srivastava A, Patel B, Shukla VK, Gupta SK. Small bowel stricture and perforation: an unusual presentation of *Fasciolopsis buski.* Trop Gastroenterol. 2011;32:320–2.
11. Ma J, Sun MM, He JJ, Liu GH, Ai L, Chen MX, et al. *Fasciolopsis buski* (Digenea: Fasciolidae) from China and India may represent distinct taxa based on mitochondrial and nuclear ribosomal DNA sequences. Parasit Vectors. 2017;10:101. https://doi.org/10.1186/s13071-017-2039-2
12. Bowles J, Blair D, McManus DP. A molecular phylogeny of the human schistosomes. Mol Phylogenet Evol. 1995;4:103–9. https://doi.org/10.1006/mpev.1995.1011
13. Blair D, Agatsuma T, Watanobe T, Okamoto M, Ito A. Geographical genetic structure within the human lung fluke, *Paragonimus westermani*, detected from DNA sequences. Parasitology. 1997;115(Pt 4):411–7. https://doi.org/10.1017/S0031182097001534
14. Moszczynska A, Locke SA, McLaughlin JD, Marcogliese DJ, Crease TJ. Development of primers for the mitochondrial cytochrome c oxidase I gene in digenetic trematodes (Platyhelminthes) illustrates the challenge of barcoding parasitic helminths. Mol Ecol Resour. 2009;9(Suppl s1):75–82. https://doi.org/10.1111/j.1755-0998.2009.02634.x

Address for correspondence: Sudeep Ghatani, Assistant Professor, Department of Zoology, School of Life Sciences, Sikkim University, 5th Mile, Tadong, Gangtok 737102, Sikkim, India; email: sghatani@cus.ac.in

Identification of Human Case of Avian Influenza A(H5N1) Infection, India

Varsha Potdar, Megha Brijwal, Rakesh Lodha, Pragya Yadav, Santosh Jadhav, Manohar Lal Choudhary, Aashish Choudhary, Veena Vipat, Nivedita Gupta, Ashok Kumar Deorari, Lalit Dar, Priya Abraham

A 11-year-old boy with acute myeloid leukemia was brought for treatment of severe acute respiratory infection in the National Capital Region, New Delhi, India. Avian influenza A(H5N1) infection was laboratory confirmed. Complete genome analysis indicated hemagglutinin gene clade 2.3.2.1a. We found the strain to be susceptible to amantadine and neuraminidase inhibitors.

Avian influenza viruses remain major threats worldwide, responsible for multiple outbreaks among poultry and episodes of transmission to humans. During January 2003–February 3, 2022, there were 862 reported cases of human infection with avian influenza A(H5N1) virus in 18 countries, resulting in a 53% case-fatality rate (https://www.who.int/docs/default-source/wpro---documents/emergency/surveillance/avian-influenza/ai-20220401.pdf).

The first outbreak of highly pathogenic avian influenza H5N1 in poultry in India, which occurred in January 2006 in Maharashtra, was caused by clade 2.2 (*1*); subsequent yearly outbreaks reported in poultry across the country were caused by newer clades 2.3.2.1 and 2.3.2.1c (*2*–*4*). Avian influenza surveillance in poultry revealed the presence of low-pathogenicity H9N2 and H4N6 viruses (*5*). On March 15, 2019, a human case of low-pathogenicity avian influenza A(H9N2) was detected in India (*6*). To date, 371 H5N1 and H5N8 avian influenza outbreaks in domestic or wild birds have been recorded in 15 of 28 states in India (https://empres-i.apps.fao.org/diseases). The first outbreaks of highly pathogenic avian influenza H5N8 in Europe were reported in August 2020 and since have been reported in poultry and wild birds in several countries in Europe, Asia, and Africa (https://web.oie.int/downld/SG/2021/A_88SG_2.pdf).

Author affiliations: ICMR National Institute of Virology, Pune, India (V. Potdar, P. Yadav, S. Jadhav, M.L. Choudhary, V. Vipat, P. Abraham); All India Institute of Medical Sciences, New Delhi, India (M. Brijwal, R. Lodha, A. Choudhary, A.K. Deorari, L. Dar); Indian Council of Medical Research, New Delhi (N. Gupta)

DOI: https://doi.org/10.3201/eid2806.212246

The Study

An 11-year old boy who had acute myeloid leukemia diagnosed in June 2021 in the department of pediatrics at the All India Institute of Medical Sciences (AIIMS) in New Delhi was brought in for treatment of fever, cough, coryza, and breathing difficulty in the first week of July 2021. The patient was a resident of Gurugram, National Capital Region (Delhi), India. His clinical work-up showed febrile neutropenia with pneumonia and shock, which progressed to acute respiratory distress syndrome, so he was mechanically ventilated. He then developed multiorgan dysfunction, which ultimately resulted in his death on July 12, 2021. An in-depth interview with family members indicated that the patient often frequented a family-owned poultry business and may have been exposed to birds with undetected infection, although no infected domestic or wild avian sources or any environmental contamination had been reported in or around the residence of the child.

Staff in the AIIMS department of pediatrics referred nasopharyngeal (NP) swab specimens collected on July 7 and bronchoalveolar lavage (BAL) fluid collected on July 11 to the department of microbiology for respiratory virus testing, which used a Fast Track Diagnostics Respiratory Pathogens 21 kit and real-time PCR for influenza (https://www.siemens-healthineers.com) for diagnosis. Both BAL and NP samples tested positive for influenza A and influenza B Victoria lineage. Influenza A type could not be determined, so we referred samples to the National Influenza Centre at the Indian Council of Medical Research of the National Institute of Virology (Pune, India) for differential influenza diagnosis. The real-time reverse transcription PCR for avian influenza

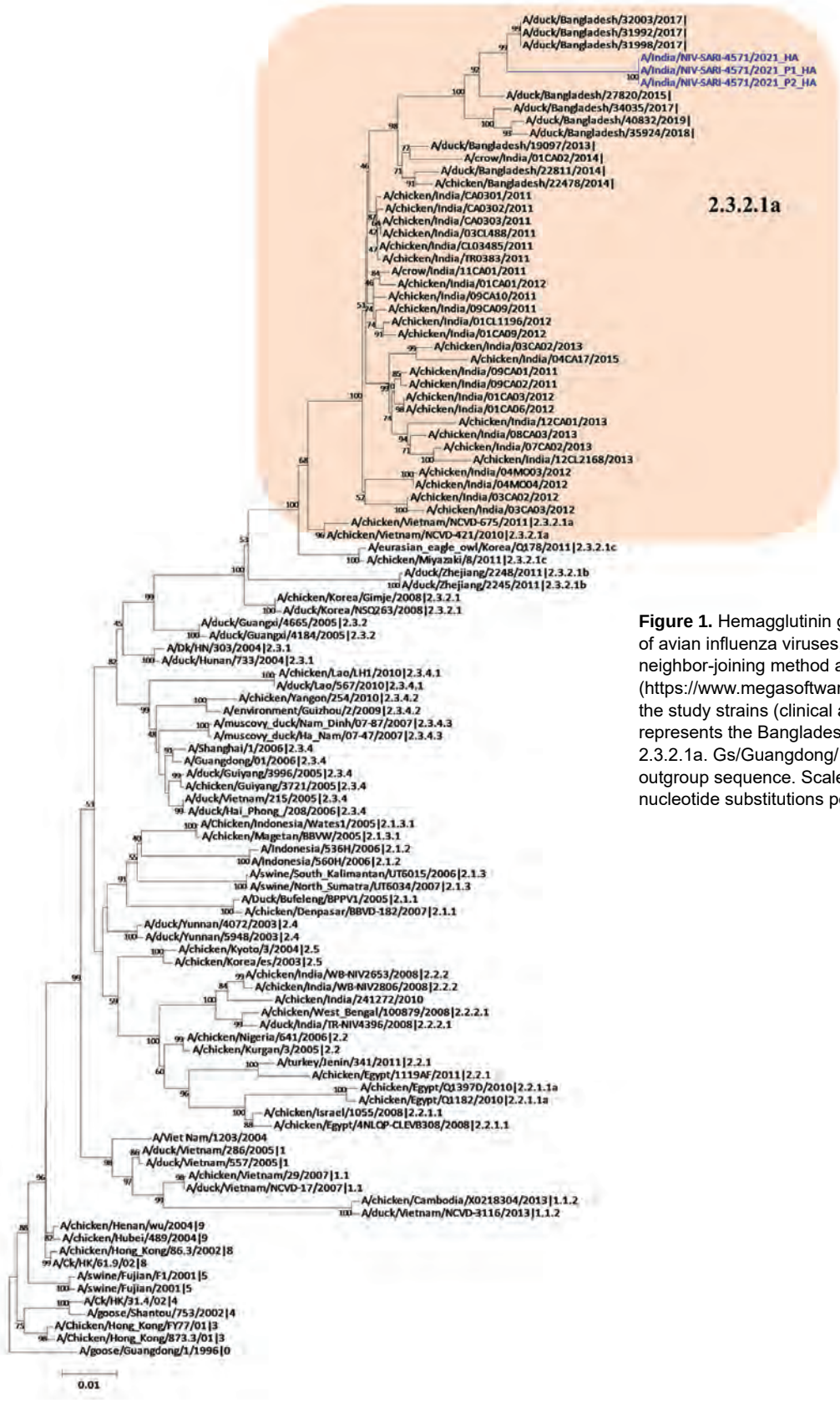

Figure 1. Hemagglutinin gene phylogenetic tree of avian influenza viruses, constructed using the neighbor-joining method as implemented in MEGA 7 (https://www.megasoftware.net). Blue text indicates the study strains (clinical and isolate); shaded area represents the Bangladesh and India strains in clade 2.3.2.1a. Gs/Guangdong/1/96 was used as the outgroup sequence. Scale bar indicates number of nucleotide substitutions per site.

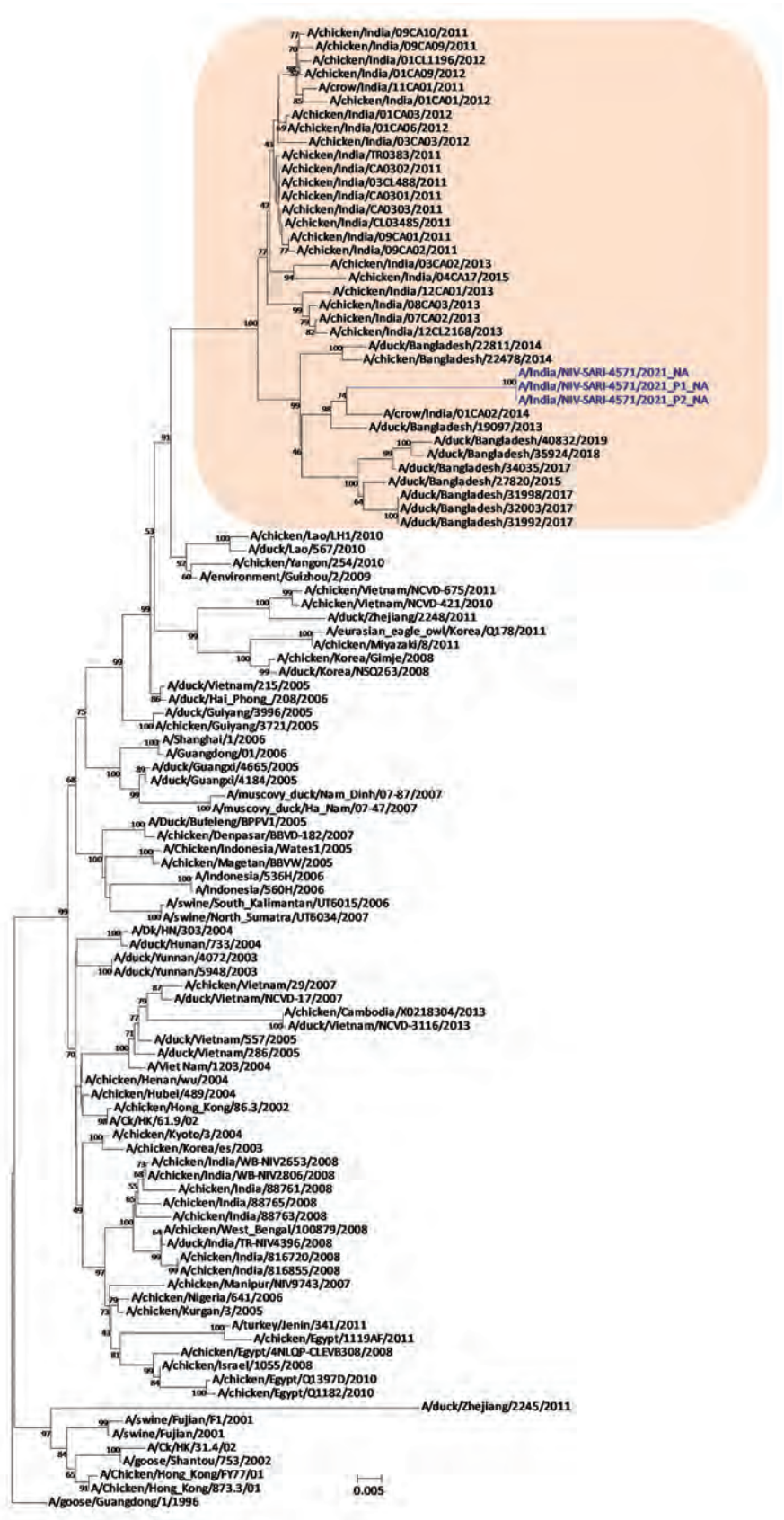

Figure 2. Neuraminidase gene phylogenetic tree constructed using the neighbor-joining method as implemented in MEGA 7 (https://www.megasoftware.net). Blue text indicates the study strains (clinical and isolate); shaded area represents the Bangladesh and India strains in clade 2.3.2.1a. Gs/Guangdong/1/96 was used as the outgroup sequence. Scale bar indicates number of nucleotide substitutions per site.

viruses H5Nx, H7N9, H9N2, and H10N8 was performed as documented elsewhere (*7*,*8*); results were positive for an H5Nx virus (cycle threshold value for H5 was 25). To confirm the subtype A/H5 identity, short fragments of multiple genes were sequenced: 230-bp matrix, 400-bp hemagglutinin (HA), 600-bp neuraminidase (NA), 600-bp nonstructural), and the influenza B HA gene, and results were analyzed using BLAST (https://blast.ncbi.nlm.nih.gov/Blast.cgi). We isolated and identified strain A/India/NIV-SARI-4571/2021 (H5N1) at a Biosafety Level 4 laboratory using MDCK cells.

We then generated whole-genome sequences from the original clinical NP samples and BAL-and MDCK-grown for passages 1 and 2 isolates using the Miniseq NGS Platform (Illumina, https://www.illumina.com) and a de-novo assembly program using QIAGEN CLC Genomics software 10.1.1 (https://www.quiagen.com). We constructed phylogenetic trees for 8 genes of A/India/NIV-SARI-4571/2021 (H5N1) virus using the neighbor-joining model with a Tamura-Nei nucleotide substitution performing 1,000 replicates of bootstrap support implemented in MEGA 7 (https://megasoftware.net) software. We submitted sequences to GenBank (accession nos. OL311384–91).

The sequences generated for the original clinical sample and the passaged virus were identical, suggesting no passage-induced mutations. We performed BLAST analysis of all 8 genes of A/India/NIV-SARI-4571/2021. The HA gene showed 97% identity with A/duck/Bangladesh/32003/2017 (H5N1). The polymerase basic (PB) 1 and nonstructural genes showed 97% nucleotide similarity to the avian influenza A/duck/Mongolia/729/2019 (H4N6) virus, suggesting probable reassortment.

Phylogenetic analysis of the HA gene demonstrated that the virus belonged to clade 2.3.2.1a (Figure 1) and clustered with the A/duck/Bangladesh 2017 (H5N1)–like strain. Clade 2.3.2.1a has a H9N2-like PB1 gene and is the dominant clade in poultry in many countries, including Vietnam (*9*), India (*3*), Bangladesh, Bhutan, and Nepal (*10*). The NA gene clustered with an A/crow/India/01CA02/2014 (H5N1)–like strain (Figure 2). Phylogenetic trees indicate locations for the other 6 genes of the study strain (Appendix Figure 1).

Using the WHO/CDC H5N1 inventory (*11*), we reviewed potential markers for the newly identified A/India/NIV-SARI-4571/2021 strain. The HA protein (H5) possessed a multiple basic amino acid cleavage site motif (PQRERRRKR*G), resulting in a highly pathogenic strain of clade 2.3.2.1 viruses. The sequence of the 220-loop receptor-binding site between amino acids Q222 and G224 remains conserved for the avian α 2–3 receptor.

We did not observe the NA and matrix 2 gene mutations responsible for neuraminidase inhibitors and amantadine resistance in the study strain. The virus remains purely avian-adapted, and we observed no markers for adaptation in mammals or pathogenicity for humans (Appendix Figure 2). We also did not observe PB2 hallmark mutations E627K and D701N, responsible for host adaptation and virulence in mammals in the study strain (*12*). The PDZ ligand domain (ESEV) at the C terminus remained conserved. We observed further compensatory mutations during the adaptation of H5N1 in mice, L89V, G309D, T339K, R477G, and I495V of PB2 (*13*) in the study strain. However, further studies are required to understand their role.

No evidence of H5 antibodies was detected in 18 close contacts of the deceased child. Available information and initial field investigations revealed that no additional cases were detected, indicating low human-to-human transmission. However, unreported high-pathogenicity avian influenza virus continues to exist in traded poultry in India, constituting a substantial risk for further human exposure (https://www.who.int/emergencies/disease-outbreak-news/item/human-infection-with-avian-influenza-a(h5n1)-%EF%BD%B0-india). Although widespread avian influenza outbreaks have been documented globally, only a limited number have shown transmission of avian influenza viruses to humans (*14*). The severe immunocompromised status of the child in this study may have made him vulnerable, and direct exposure to infected poultry might have been the source of infection. Influenza B virus, simultaneously detected with influenza A in this case-patient, is known to persist in such cases and might have been identified because of a prior infection (*15*).

Conclusions

In December 2020 and early 2021, outbreaks of avian influenza H5N1 and H5N8 were reported in poultry in 15 states in India; the National Capital Region, Maharashtra, Punjab, and Kerala, in particular, were severely affected. The whole-genome sequencing of A/India/NIV-SARI-4571/2021 (H5N1) virus in our study provides valuable insight into the absence of hallmark mutations responsible for adaptation and virulence in mammals. The strain remained sensitive to amantadine and neuraminidase inhibitors. However, identification of a human H5N1 case in India highlights the need for systemic surveillance at the human–animal interface level.

Acknowledgments

The authors acknowledge the National Centre for Disease Control, Delhi, for field investigation and Chakradhar Tosh from the Indian Council of Agricultural Research–National Institute of High Security Animal Diseases for sharing the serum samples of close contacts of the case. The authors from the National Institute of Virology, Pune, acknowledge Shailesh Pawar for sharing the serological protocols, the National Influenza Centre team for diagnosis, and the biosafety level 4 laboratory for sequencing and virus isolation and serology testing. The authors from AIIMS acknowledge the Department of Health Research and the Indian Council of Medical Research, Government of India, for supporting the virology laboratory as a regional laboratory under the Virus Research and Diagnostic Laboratory network.

Financial support was provided by the Indian Council of Medical Research, Department of Health Research, New Delhi.

About the Author

Dr. Potdar is senior scientist heading the National Influenza Centre at the National Institute of Virology, Pune, India. Her primary research interest is molecular characterization of influenza, SARS-CoV-2, and other respiratory viruses.

References

1. Ray K, Potdar VA, Cherian SS, Pawar SD, Jadhav SM, Waregaonkar SR, et al. Characterization of the complete genome of influenza A (H5N1) virus isolated during the 2006 outbreak in poultry in India. Virus Genes. 2008;36:345–53. https://doi.org/10.1007/s11262-007-0195-8
2. Chakrabarti AK, Pawar SD, Cherian SS, Koratkar SS, Jadhav SM, Pal B, et al. Characterization of the influenza A H5N1 viruses of the 2008-09 outbreaks in India reveals a third introduction and possible endemicity. PLoS One. 2009;4:e7846. https://doi.org/10.1371/journal.pone.0007846
3. Nagarajan S, Tosh C, Smith DK, Peiris JSM, Murugkar HV, Sridevi R, et al. Avian influenza (H5N1) virus of clade 2.3.2 in domestic poultry in India. PLoS One. 2012;7:e31844. https://doi.org/10.1371/journal.pone.0031844
4. Tosh C, Nagarajan S, Kumar M, Murugkar HV, Venkatesh G, Shukla S, et al. Multiple introductions of a reassortant H5N1 avian influenza virus of clade 2.3.2.1c with PB2 gene of H9N2 subtype into Indian poultry. Infect Genet Evol. 2016;43:173–8. https://doi.org/10.1016/j.meegid.2016.05.012
5. Pawar SD, Kale SD, Rawankar AS, Koratkar SS, Raut CG, Pande SA, et al. Avian influenza surveillance reveals presence of low pathogenic avian influenza viruses in poultry during 2009-2011 in the West Bengal State, India. Virol J. 2012;9:151. https://doi.org/10.1186/1743-422X-9-151
6. Potdar V, Hinge D, Satav A, Simões EAF, Yadav PD, Chadha MS. Laboratory-confirmed avian influenza A(H9N2) virus infection, India, 2019. Emerg Infect Dis. 2019;25:2328–30. https://doi.org/10.3201/eid2512.190636
7. Kreman T. Capacity building for avian influenza H5N1. Centers for Disease Control and Prevention training presentation; October 6–10, 2007; Pune, India.
8. World Health Organization. WHO information for molecular diagnosis of influenza virus—update. 2014. [cited on 2015 Nov 24] https://cdn.who.int/media/docs/default-source/influenza/global-influenza-surveillance-and-response-system/related-documents/molecular_diagnosis_influenza_virus_humans_update_201403.pdf
9. Nguyen T, Rivailler P, Davis CT, Hoa T, Balish A, Dang NH, et al. Evolution of highly pathogenic avian influenza (H5N1) virus populations in Vietnam between 2007 and 2010. Virology. 2012;432:405–16. https://doi.org/10.1016/j.virol.2012.06.021
10. Marinova-Petkova A, Franks J, Tenzin S, Dahal N, Dukpa K, Dorjee J, et al. Highly pathogenic reassortant avian influenza A(H5N1) virus clade 2.3.2.1a in poultry, Bhutan. Emerg Infect Dis. 2016;22:2137–41. https://doi.org/10.3201/eid2212.160611
11. Centers for Disease Control and Prevention. H5N1 genetic changes inventory: a tool for international surveillance 2021 [cited on 2021 Jul 29]. https://www.cdc.gov/flu/avianflu/h5n1-genetic-changes.htm
12. Long JS, Howard WA, Núñez A, Moncorgé O, Lycett S, Banks J, et al. The effect of the PB2 mutation 627K on highly pathogenic H5N1 avian influenza virus is dependent on the virus lineage. J Virol. 2013;87:9983–96. https://doi.org/10.1128/JVI.01399-13
13. Li J, Ishaq M, Prudence M, Xi X, Hu T, Liu Q, et al. Single mutation at the amino acid position 627 of PB2 that leads to increased virulence of an H5N1 avian influenza virus during adaptation in mice can be compensated by multiple mutations at other sites of PB2. Virus Res. 2009;144:123–9. https://doi.org/10.1016/j.virusres.2009.04.008
14. Adlhoch C, Fusaro A, Gonzales JL, Kuiken T, Marangon S, Niqueux É, et al.; European Food Safety Authority; European Centre for Disease Prevention and Control and European Union Reference Laboratory for Avian Influenza. Avian influenza overview December 2020 - February 2021. EFSA J. 2021;19:e06497.
15. Verma N, Pooniya V, Kumar A. Clinical profile and outcome of influenza A/H1N1 in pediatric oncology patients during the 2015 outbreak: a single center experience from northern India. J Pediatr Hematol Oncol. 2017;39:e357–8. https://doi.org/10.1097/MPH.0000000000000962

Address for correspondence: Priya Abraham, ICMR-National Institute of Virology, Department of Health Research, Ministry of Health & Family Welfare, 20-A Dr. Ambedkar Road, Pune 411001, India; email: priya.abraham@icmr.gov.in; Lalit Dar, All India Institute of Medical Sciences, Ansari Nagar East, Gautam Nagar, New Delhi, Delhi 110029, India; email: lalitdaraiims@gmail.com

Serum Neutralization of SARS-CoV-2 Omicron BA.1 and BA.2 after BNT162b2 Booster Vaccination

Rune M. Pedersen, Line L. Bang, Lone W. Madsen, Thomas V. Sydenham, Isik S. Johansen, Thøger G. Jensen, Ulrik S. Justesen, Thomas E. Andersen

Authors affiliation: University of Southern Denmark, Odense, Denmark

DOI: https://doi.org/10.3201/eid2806.220503

The SARS-CoV-2 Omicron variant BA.2 sublineage is rapidly replacing earlier Omicron lineages, suggesting BA.2 has increased vaccine evasion properties. We measured neutralization titers of authentic BA.1 and BA.2 isolates in serum samples from persons who received the BNT162b2 booster vaccine. All samples neutralized BA.1 and BA.2 at equal median values.

The emergence of the SARS-CoV-2 Omicron variant BA.1 (B.1.1.529) in late 2021 caused immediate apprehension because it readily outcompeted the already highly transmissible Delta variant. The high number of spike mutations and indications of substantial vaccine evasion properties prompted the World Health Organization to designate BA.1 a variant of concern on November 26, 2021 (*1*). Recently, a large-scale epidemiologic study addressed concerns about BA.1 vaccine evasion by showing that 2-dose vaccination and an mRNA vaccine booster dose provides at least temporary protection against this variant (*2*).

Surveillance data from countries where Omicron was initially detected indicate that BA.1 is a transient lineage that is rapidly replaced by the Omicron sublineage BA.2 (D. Yamasoba et al., unpub data, https://doi.org/10.1101/2022.02.14.480335). By now, the BA.2 sublineage is dominant in ≥18 countries and is progressing in the United States, where cases are doubling weekly (*3*). The higher transmissibility of this sublineage in countries with high vaccination rates could indicate that BA.2 escapes vaccines even better than BA.1.

We investigated BA.2 vaccine escape in vitro by directly comparing the neutralization of authentic BA.1 and BA.2 strains in serum samples from persons who had received 2 doses of the BNT162b2 Pfizer-BioNTech (https://www.pfizer.com) mRNA vaccine and 1 booster dose. We analyzed serum samples collected during January 26–28, 2022, from 20 (8 male, 12 female) immunocompetent SARS-CoV-2–naive participants by using a 90% plaque reduction neutralization test ($PRNT_{90}$), as previously described (*4*). Median age among participants was 57 years (interquartile range [IQR] 50–60 years). We performed whole-genome sequencing by using a MinION (Oxford Nanopore Technologies, https://nanoporetech.com) sequencing instrument to identify the clinical isolates used for $PRNT_{90}$. We obtained lineage and mutation calls by using Pangolin version 3.1.17 with pangoLEARN database 06–12–2021 and Nextclade version 0.14.4 (*5*,*6*). Viral genome sequences are available on GenBank (accession nos. ON055855 for the ancestral strain, ON055874 for BA.1, and ON055857 for BA.2). We analyzed all serum samples for antibodies by using the Liaison TrimericS IgG Quantitative immunoassay (DiaSorin, https://www.diasorin.com). Participants signed informed consent forms, and the study was approved by the Regional Committees on Health Research Ethics for Southern Denmark (no. S-20210007C). Experiments with live SARS-CoV-2 were conducted in approved Biosafety Level 3 facilities (license no. 20200016905/5).

Among vaccinated participants, the median time between the first and second BNT162b2 dose was 35 (IQR 34–36) days; median time between the second and booster doses was 168 (IQR 154–174) days. The median time between the booster dose and serum sampling was 42 (IQR 40–42) days. The median $PRNT_{90}$ toward the ancestral SARS-CoV-2 strain was 320 (IQR 160–480), whereas the median $PRNT_{90}$ toward BA.1 and BA.2 was 40 (IQR 20–80) for both. All neutralization titers measured for BA.1 and BA.2 were above the threshold limit (Figure). Using the Wilcoxon signed-rank test, we assessed differences between the neutralization titers of the ancestral strain and the 2 Omicron strains and found statistically significant differences for both strains (BA.1, $p<0.0001$; BA.2, $p<0.0001$), whereas the difference between BA.1 and BA.2 was not statistically significant ($p = 0.1953$). The median antibody level measured by Liaison immunoassay was 4,115 (IQR 2,675–6,000) binding antibody units/mL. We used the Spearman coefficient (ρ) to correlate the neutralization titers toward the ancestral strain (ρ 0.8073; $p<0.0001$), BA.1 (ρ 0.7396; $p = 0.0002$), and BA.2 (ρ 0.7496; $p = 0.0002$) (Appendix Figure (Appendix Figure, https://wwwnc.cdc.gov/EID/article/28/6/22-0503-App1.pdf).).

Although vaccine evasion appears to be a key feature of both BA.1 and the emerging BA.2 strain, according to our results, BA.2 does not evade the humoral immune response induced by the BNT162b2 vaccine better than BA.1 does. Thus, the current surge of BA.2 seems to occur as a result of mechanisms of transmissibility other than antibody escape.

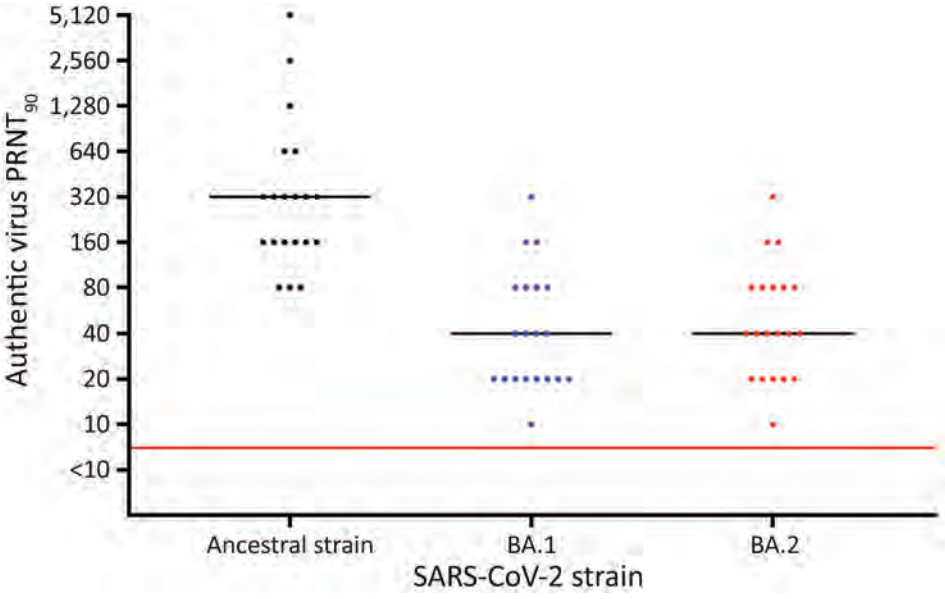

Figure. Results of $PRNT_{90}$ of serum against SARS-CoV-2 ancestral strain and Omicron sublineages BA.1 and BA.2 after BNT162b2 (Pfizer-BioNTech, https://www.pfizer.com) booster vaccination, Denmark. Serum samples were collected from 20 SARS-CoV-2–naive participants who received 2 BNT162b2 doses and a booster BNT162b2 dose. Viral genome sequences are available in GenBank (accession nos. ON055855 for the ancestral strain, ON055874 for BA.1, and ON055857 for BA.2). Red line indicates neutralization threshold; black lines indicate median neutralization titers for each strain. $PRNT_{90}$, 90% plaque reduction neutralization test.

At the time of this submission, J. Yu et al. (*7*) had published data from serum neutralization of lentivirus constructs that express the spike proteins of BA.1 and BA.2. Our authentic virus results are in accordance with theirs; Yu et al. found that BA.1 and BA.2 pseudoviruses were neutralized equally and at median values ≈8 times lower than the ancestral strain. In addition, our $PRNT_{90}$ results showed that all serum samples neutralized the Omicron variants at or above the neutralization threshold value of 10 at the 6-week post-booster time point (Figure). This finding is in accordance with the epidemiologic results on BA.1–specific vaccine effectiveness reported by N. Andrews et al. (*2*), which showed that 2 doses and a booster of BNT162b2 provides a certain degree of protection against symptomatic BA.1 infection. Assuming that the neutralization data of BA.2 also reflects vaccine effectiveness, our results indicate that at 6 weeks after a booster dose persons should at least be temporarily protected against mild disease with this sublineage. Health agencies should continue to encourage booster vaccination for persons who have received 2 doses of BNT162b2.

About the Author

Dr. Pedersen is a clinical microbiologist at Odense University Hospital, Odense, Denmark. His research interests include viral infections, gastrointestinal infections, and vaccine studies.

References

1. World Health Organization. Classification of omicron (B.1.1.529): SARS-CoV-2 variant of concern. November 26, 2021 [cited 2022 Mar 18]. https://www.who.int/news/item/26-11-2021-classification-of-omicron-(b.1.1.529)-sars-cov-2-variant-of-concern
2. Andrews N, Stowe J, Kirsebom F, Toffa S, Rickeard T, Gallagher E, et al. Covid-19 vaccine effectiveness against the Omicron (B.1.1.529) variant. N Engl J Med. 2022 Mar 2 [Epub ahead of print]. https://doi.org/10.1056/NEJMoa2119451
3. Centers for Disease control and Prevention. COVID data tracker: variant proportions [cited 2022 March 9]. https://covid.cdc.gov/covid-data-tracker/#variant-proportions
4. Pedersen RM, Bang LL, Tornby DS, Kierkegaard H, Nilsson AC, Johansen IS, et al. The SARS-CoV-2-neutralizing capacity of kidney transplant recipients 4 weeks after receiving a second dose of the BNT162b2 vaccine. Kidney Int. 2021;100:1129–31. https://doi.org/10.1016/j.kint.2021.09.006
5. O'Toole Á, Scher E, Underwood A, Jackson B, Hill V, McCrone JT, et al. Assignment of epidemiological lineages in an emerging pandemic using the pangolin tool. Virus Evol. 2021;7:b064. https://doi.org/10.1093/ve/veab064
6. Hadfield J, Megill C, Bell SM, Huddleston J, Potter B, Callender C, et al. Nextstrain: real-time tracking of pathogen evolution. Bioinformatics. 2018;34:4121–3. https://doi.org/10.1093/bioinformatics/bty407
7. Yu J, Collier AY, Rowe M, Mardas F, Ventura JD, Wan H, et al. Neutralization of the SARS-CoV-2 Omicron BA.1 and BA.2 variants. N Engl J Med. 2022 Mar 16 [Epub ahead of print]. https://doi.org/10.1056/NEJMc2201849

Address for correspondence: Thomas Emil Andersen, Department of Clinical Microbiology, Odense University Hospital, University of Southern Denmark, J.B. Winsløws Vej 21, 2nd Fl, 5000 Odense C, Denmark; email: thandersen@health.sdu.dk

Recombinant BA.1/BA.2 SARS-CoV-2 Virus in Arriving Travelers, Hong Kong, February 2022

Haogao Gu, Daisy Y.M. Ng, Gigi Y.Z. Liu, Samuel S.M. Cheng, Pavithra Krishnan, Lydia D.J. Chang, Sammi S.Y. Cheuk, Mani M.Y. Hui, Tommy T.Y. Lam, Malik Peiris, Leo L.M. Poon

Author affiliations: The University of Hong Kong, Hong Kong, China (H. Gu, D.Y.M. Ng, G.Y.Z. Liu, S.S.M. Cheng, P. Krishnan, L.D.J. Chang, S.S.Y. Cheuk, M.M.Y. Hui, T.T.Y. Lam, M. Peiris, L.L.M. Poon); Centre for Immunology & Infection, Hong Kong (T.T.Y. Lam, M. Peiris, L.L.M. Poon); HKU-Pasteur Research Pole, Hong Kong (M. Peiris, L.L.M. Poon)

DOI: https://doi.org/10.3201/eid2806.220523

We studied SARS-CoV-2 genomes from travelers arriving in Hong Kong during November 2021–February 2022. In addition to Omicron and Delta variants, we detected a BA.1/BA.2 recombinant with a breakpoint near the 5′ end of the spike gene in 2 epidemiologically linked case-patients. Continued surveillance for SARS-CoV-2 recombinants is needed.

The SARS-CoV-2 Omicron variant (Pango lineage B.1.1.529) emerged in November 2021. Within a few weeks, subvariants BA.1, BA.1.1, and BA.2 were detected in varying proportions on different continents, but BA.1 initially was dominant (*1*). By March 2022, these 3 subvariants accounted for >95% of sequences submitted to GISAID (https://www.gisaid.org). We previously demonstrated the feasibility of testing incoming travelers for SARS-CoV-2 genomic surveillance (*2*). We report detecting a BA.1/BA.2 recombinant SARS-CoV-2 subvariant in travelers arriving in Hong Kong, China.

Using our previously described next-generation sequencing method (*2*), we analyzed 198 (25%) of 793 SARS-CoV-2 reverse transcription PCR (RT-PCR)–positive samples collected from travelers arriving in Hong Kong during November 15, 2021–February 4, 2022 (Appendix Table 1, https://wwwnc.cdc.gov/EID/article/28/6/22-0523-App1.pdf). We randomly selected samples with cycle thresholds <30 and successfully deduced near-full genome sequences from 180 samples (mean coverage 97.6%; depth ≥100). Deduced genomes predominantly were Delta (n = 58) and Omicron (BA.1 = 66, BA.1.1 = 28, and BA.2 = 26) variants (Appendix Figures 1, 2). Time distribution of these variants agrees with global surveillance data submitted to GISAID, confirming that travel hubs are useful sentinel sites to monitor SARS-CoV-2 circulation (*2*). Of note, the BA.2 cases we detected predominantly were imported from the Philippines and Nepal, indicating this subvariant might have become established in these countries before detection in Hong Kong.

In our phylogenetic analysis, 2 additional nearly identical sequences formed a distinct branch in the Omicron clade (Appendix Figure 2). We detected these sequences from 2 epidemiologically linked cases, patients 1 and 2, who were work colleagues and traveled together to Hong Kong on February 1, 2022, from Germany via the Netherlands. They tested SARS-CoV-2–positive by RT-PCR at the airport upon arrival (cycle thresholds 27 and 22). Patient 1 reported having a sore throat and cough since January 28, but patient 2 was asymptomatic. Both patients had received 2 doses of Pfizer-BioNTech COVID-19 vaccine (Pfizer Inc., https://www.pfizer.com); patient 1 received the second dose on November 1, 2021, and patient 2 received the second dose on June 22, 2021.

The distinct topology of viral sequences from these patients suggested that they were infected by a recombinant virus. To test that hypothesis, we used previously reported BA.1- and BA.2-defining single-nucleotide polymorphisms (SNPs) to analyze the genomes (Appendix). We found that the 5′ end sequences (nucleotide region 1–20055) from the 2 cases only contained BA.1-specific SNPs (Figure, panel A). By contrast, the corresponding 3′ end sequences only contained BA.2-specific SNPs. We further conducted a recombination analysis and confirmed that only 1 breakpoint was located within nucleotide positions 20055–21618 (Appendix Figure 3). The nucleotide 5′ end of the sequences is phylogenetically similar to authentic BA.1 and the 3′ end similar to BA.2 sequences at this breakpoint (Figure, panel B). The breakpoint identified in this recombinant virus is near the 5′ end open reading frame of the spike gene. Recombinant viruses, including B.1.1.7/B1.177 and Delta/BA.1, with a breakpoint in this region have been reported (*3*; P. Colson et al., unpub. data, https://www.medrxiv.org/content/10.1101/2022.03.03.22271812v2; T. Peacock, unpub. data, https://github.com/cov-lineages/pango-designation/issues/441).

We further examined our sequence data to exclude the possibility of coinfection or contamination (*4*). We noted that the minor allele frequencies at these BA.1- and BA.2-defining SNP positions were extremely low (mean 0.5%, median 0.06%) (Figure, panel A), indicating these samples contained only 1

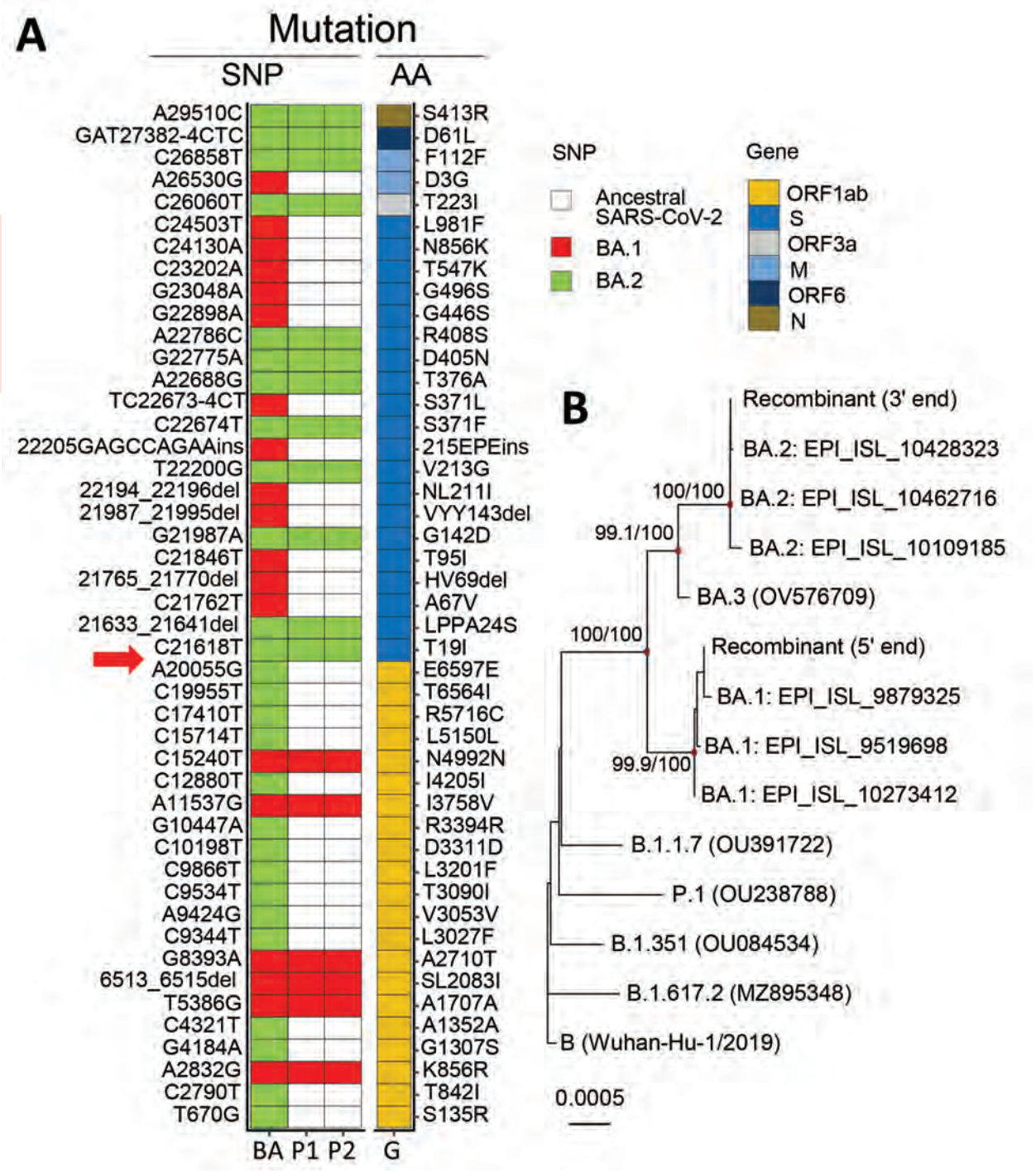

Figure. Detection of recombinant BA.1/BA.2 SARS-CoV-2 virus in arriving travelers, Hong Kong, China, February 2022. A) Mapping of BA.1- and BA.2-specific SNPs against the reference sequence genome (Genbank accession no. MN908947.3). Red boxes indicate BA.1-specific SNPs and green boxes indicate BA.2-specific SNPs found in samples from P1 and P2; the corresponding AA changes of these SNPs also are indicated. Red arrow indicates the putative breaking point. B) Phylogeny of viral RNA sequences at the 5′ and 3′ ends to the putative breakpoint. The maximum-likelihood tree was generated by using IQ-TREE (http://www.iqtree.org) and the transition plus empirical base frequencies plus proportion of invariable site nucleotide substitution model with Wuhan-Hu-1 (GenBank accession no. MN908947.3) as the outgroup. References sequences are shown with GISAID (https://www.gisaid.org) or GenBank accession numbers. Red node points show strongly supported branches as detected by SH-aLRT and ultrafast bootstrap values. Scale bar indicates nucleotide substitutions per site. AA, amino acid; BA, BA.1/BA.2 recombinant; G, gene; M, membrane; N, nucleocapsid; ORF, open reading frame; P1, patient 1; P2, patient 2; S, spike; SNP, single-nucleotide polymorphism.

virus population. We used the patient 2 sample to clone an RT-PCR product (≈2.2 kbp) spanning the recombination breakpoint. We detected BA.1-specific (19955C/20055A) and BA.2-specific (21618T/21633–21641del/21762C) SNPs in the same plasmid clone, confirming the 2 patients were infected by a BA.1/BA.2 recombinant virus.

We found no similar BA.1/BA.2 recombinant sequences in GISIAD or GenBank (as of March 7, 2022), suggesting a novel recombinant. The BA.1 region of this recombinant virus is genetically close to 3 BA.1 sequences detected in Europe and the United States (Figure, panel B), whereas its BA.2 region is identical to 19,555 BA.2 sequences from multiple continents. Because global cocirculation of BA.1 and BA.2 subvariants is high, pinpointing the geographic location where this recombination event occurred would be difficult.

Emerging Omicron subvariants could allow vaccine breakthrough and widespread reinfection. Previous studies reported detection of SARS-CoV-2 interlineage recombinants at the same time as different SARS-CoV-2 lineages were cocirculating (*3*; D. VanInsberghe et al., unpub. data, https://doi.org/10.1101/2020.08.05.238386; P. Colson et al., unpub. data; T. Peacock, unpub. data). The high transmissibility of Omicron (*5*,*6*) has led to wide cocirculation of BA.1 and BA.2 subvariants in many regions, which might provide ample opportunities to generate novel recombinants among these or other variants via coinfection events. Although current global surveillance data suggest that our recombinant might only be a sporadic case, the potential effects of novel recombinants should not be underestimated. Of note, homologous recombination is common in animal and other human coronaviruses (*7*), and some recombination events could generate recombinants with enhanced virulence (*8*,*9*). Long-term global SARS-CoV-2 genomic surveillance will be needed to monitor for possible more virulent or transmissible strains.

Acknowledgments

We gratefully thank the staff from the originating laboratories for obtaining the specimens and from the submitting laboratories for generating genomic data and sharing via GISAID (Appendix Table 2). We thank colleagues from the Centre for PanorOmic Sciences of the University of Hong Kong for providing technical support. We also thank the Centre for Health Protection of the Department of Health for providing epidemiological data for the study.

This work is supported by Research Grants Council of Hong Kong theme-based research schemes (no. T11-705/21-N) and the Health and Medical Research Fund (no. COVID190205).

About the Author

Dr. Gu is a postdoctoral fellow at The University of Hong Kong, Hong Kong, China. His research interests focus on bioinformatics and virus evolution.

Reference

1. World Health Organization. Statement on Omicron sublineage BA.2 [cited 2022 Feb 22]. https://www.who.int/news/item/22-02-2022-statement-on-omicron-sublineage-ba.2
2. Gu H, Cheng SSM, Krishnan P, Ng DYM, Chang LDJ, Liu GYZ, et al. Monitoring international travelers arriving in Hong Kong for genomic surveillance of SARS-CoV-2. Emerg Infect Dis. 2022;28:247–50. https://doi.org/10.3201/eid2801.211804
3. Jackson B, Boni MF, Bull MJ, Colleran A, Colquhoun RM, Darby AC, et al.; COVID-19 Genomics UK (COG-UK) Consortium. Generation and transmission of interlineage recombinants in the SARS-CoV-2 pandemic. Cell. 2021;184:5179–5188.e8. https://doi.org/10.1016/j.cell.2021.08.014
4. Heguy A, Dimartino D, Marier C, Zappile P, Guzman E, Duerr R, et al. Amplification artifact in SARS-CoV-2 Omicron sequences carrying P681R mutation, New York, USA. Emerg Infect Dis. 2022;28:881–3. https://doi.org/10.3201/eid2804.220146
5. Fonager J, Bennedbæk M, Bager P, Wohlfahrt J, Ellegaard KM, Ingham AC, et al. Molecular epidemiology of the SARS-CoV-2 variant Omicron BA.2 sub-lineage in Denmark, 29 November 2021 to 2 January 2022. Euro Surveill. 2022;27. https://doi.org/10.2807/1560-7917.ES.2022.27.10.2200181
6. Eggink D, Andeweg SP, Vennema H, van Maarseveen N, Vermaas K, Vlaemynck B, et al. Increased risk of infection with SARS-CoV-2 Omicron BA.1 compared with Delta in vaccinated and previously infected individuals, the Netherlands, 22 November 2021 to 19 January 2022. Euro Surveill. 2022;27:2101196. https://doi.org/10.2807/1560-7917.ES.2022.27.4.2101196
7. Su S, Wong G, Shi W, Liu J, Lai ACK, Zhou J, et al. Epidemiology, genetic recombination, and pathogenesis of coronaviruses. Trends Microbiol. 2016;24:490–502. https://doi.org/10.1016/j.tim.2016.03.003
8. Terada Y, Matsui N, Noguchi K, Kuwata R, Shimoda H, Soma T, et al. Emergence of pathogenic coronaviruses in cats by homologous recombination between feline and canine coronaviruses. PLoS One. 2014;9:e106534. https://doi.org/10.1371/journal.pone.0106534
9. Wang L, Junker D, Collisson EW. Evidence of natural recombination within the S1 gene of infectious bronchitis virus. Virology. 1993;192:710–6. https://doi.org/10.1006/viro.1993.1093

Address for correspondence: Leo Poon, School of Public Health, The University of Hong Kong, 21 Sassoon Road, Hong Kong 999077, China; email: llmpoon@hku.hk

SARS-CoV-2 Breakthrough Infections among US Embassy Staff Members, Uganda, May–June 2021

Julie R. Harris, Daniel Owusu, Kevin O'Laughlin, Adam L. Cohen, Amen Ben Hamida, Jaymin C. Patel, Molly M. Freeman, Thomas Nsibambi, Rebecca Nieves, Barbara J. Marston, Samuel Wasike, Jennifer S. Galbraith, Amy L. Boore, Lisa J. Nelson, Sarah Anne J. Guagliardo, John D. Klena, Ketan Patel, Marek Ma

Author affiliations: Centers for Disease Control and Prevention, Kampala, Uganda (J.R. Harris, T. Nsibambi, S. Wasike, J.S. Galbraith, A.L. Boore, L.J. Nelson); Centers for Disease Control and Prevention, Atlanta, Georgia, USA (D. Owusu, K. O'Laughlin, A.L. Cohen, A.B. Hamida, J.C. Patel, M.M. Freeman, B.J. Marston, S.A.J. Guagliardo, J.D. Klena, K. Patel); US Department of State, Kampala (R. Nieves, M. Ma)

DOI: https://doi.org/10.3201/eid2806.220427

The SARS-CoV-2 Delta variant emerged shortly after COVID-19 vaccines became available in 2021. We describe SARS-CoV-2 breakthrough infections in a highly vaccinated, well-monitored US Embassy community in Kampala, Uganda. Defining breakthrough infection rates in highly vaccinated populations can help determine public health messaging, guidance, and policy globally.

Breakthrough infections after vaccination are a known phenomenon, but the expected rate of such infections for SARS-CoV-2 was unknown in mid-2021. This uncertainty was compounded by the emergence of the SARS-CoV-2 Delta variant, initially recognized in India in October 2020 (*1*) and identified in the United States in March 2021 (*2*).

During February–June 2021, the US Embassy in Kampala, Uganda, offered COVID-19 vaccinations to the US mission community, including US citizens working at the US Embassy (14%), their eligible family members (11%), locally employed staff (i.e., Ugandan citizens working at the US Embassy) (64%), and other eligible persons. Of the 833 persons eligible for vaccination through the US Embassy, 94% were fully vaccinated by April 18, 2021, and 97% were fully vaccinated by May 23, 2021. By May 2021, Uganda was entering its second major wave of SARS-CoV-2 infections, dominated by the Delta variant (*3*). Throughout the pandemic, mission community members were required to report SARS-CoV-2 infections and symptoms suggestive of infection, and free SARS-CoV-2 testing was available at the US Embassy.

During May 24–June 26, 2021, a total of 20 PCR-confirmed SARS-CoV-2 infections were reported to the health unit at the US Embassy in Kampala among the mission community and in 1 US government staff member temporarily stationed in Uganda for work, an attack rate of 2.3% (Figure). Among 19 infected persons who consented to use of their data, 8 (42%) were female; mean age was 40 (range 18–63) years. Ten (53%) persons identified as Black African, 6 (32%) as White American, 2 (11%) as Asian American, and 1 (5%) as Black American. Thirteen (68%) persons were symptomatic, and 4 (21%) cases were identified through travel-related testing. Nine (47%) of the infected persons had contact with a person with confirmed SARS-CoV-2 infection before their symptom onset; 3 of the contacts were also fully vaccinated, 2 with Moderna (https://www.modernatx.com) and 1 with AstraZeneca (https://www.astrazeneca.com) vaccines. Four persons had underlying conditions, including diabetes, hypertension, chronic hepatitis B virus infection, and pregnancy. No infected persons were seriously ill or required hospitalization.

All infected persons were fully vaccinated at the time of symptom onset or positive SARS-CoV-2 test results. Seventeen infected persons had received 2 doses of the Moderna vaccine at the US Embassy, and all 17 received the second dose during March 27–April 23, 2021 (Figure). Two persons had received vaccines outside the US Embassy: 1 person received 2 Moderna doses in the United States, the second of which they received on February 22; the other person received an initial Pfizer-BioNTech (https://www.pfizer.com) vaccine dose in Uganda and a second dose in the United States on May 1. The mean time between first and second dose for all 19 patients was 28.9 (range 21–35) days. The mean time between second dose and positive SARS-CoV-2 test was 66 (range 47–107) days.

Although breakthrough infections are expected with any vaccine, the rate of SARS-CoV-2 breakthrough infections, and the potential for transmission from fully vaccinated persons, was not clear at the time we began our investigation. An article describing breakthrough infections in the United States during January–April 2021, immediately before the Delta wave in the United States, stated that only a small fraction of vaccinated persons experience breakthrough infections and that these persons account for a small percentage of all COVID-19 cases (*4*). Those authors reported ≈10,000 breakthrough cases, which were passively reported from states, in a population

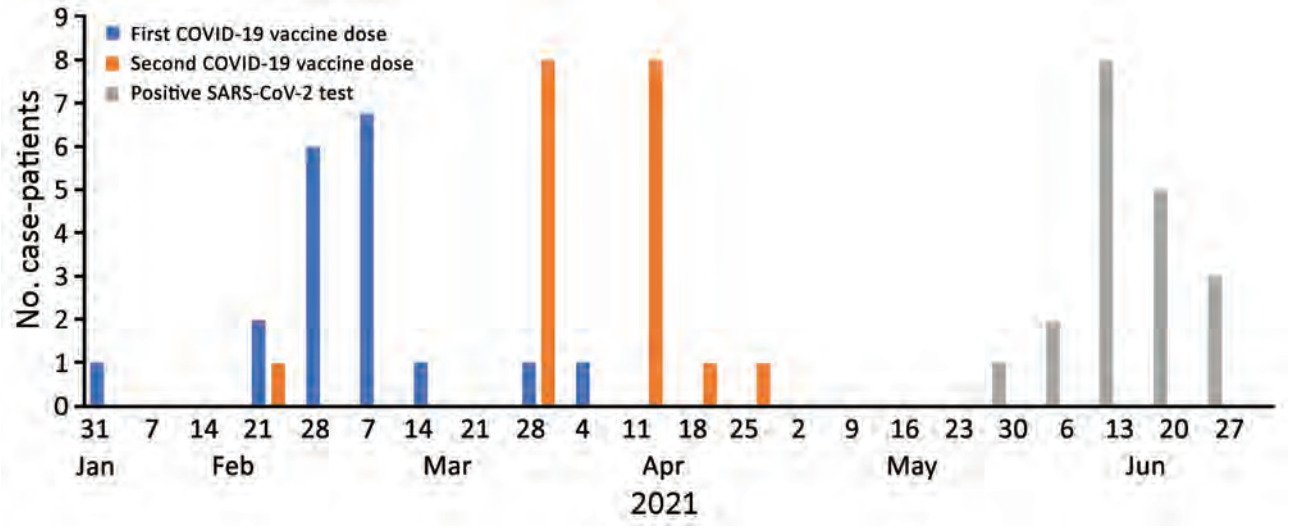

Figure. Dates of first COVID-19 vaccine dose, second vaccine dose, and positive SARS-CoV-2 test among 19 staff, family members, and visiting US government staff with identified postvaccination SARS-CoV-2 infection, US Embassy, Kampala, Uganda, 2021. Among 20 persons with breakthrough infections, 19 consented to have their data included.

of 101 million vaccinated persons, a breakthrough rate of 0.01%. Although the authors acknowledged those findings were certainly an undercount, identifying true rates of breakthrough infections in terms of vaccination status and reporting rates in an extremely large and diverse population is difficult, if not impossible. Our findings showed that breakthrough infections could be expected early after SARS-CoV-2 vaccines became available, even in highly vaccinated populations, when community transmission is high and provided early suggestive evidence of transmission from fully vaccinated, infected persons. Because new variants of concern can rapidly emerge, evaluation of closely monitored populations with known, consistently recorded vaccination histories and rapid access to diagnostic testing, such as embassy communities, could be useful for determining health messaging and preventive measures in areas that do not yet have exposure to the variants. Instances of well-described sentinel populations are rare but can be highly informative (*5*).

We shared our experience in real time with other embassies in the region to help examine common experiences and guide expectations. As future SARS-CoV-2 variants emerge, identifying novel, rapid approaches to monitor breakthrough infection rates continually and systematically is critical to determining vaccine effectiveness and the need for additional interventions to reduce disease spread. Well-delineated populations with relatively homogeneous vaccination practices and clear documentation of vaccination histories, such as overseas US Embassy staff or similar populations, could be a useful source of data for public health prevention and control efforts during pandemics.

About the Author

Dr. Harris is the resident advisor for Uganda with the Field Epidemiology Training Program (FETP) at the US Centers for Disease Control and Prevention, Atlanta, Georgia, USA. Her primary research interests include epidemiology and mathematical modeling.

References

1. Dhar MS, Marwal R, Vs R, Ponnusamy K, Jolly B, Bhoyar RC, et al.; Indian SARS-CoV-2 Genomics Consortium (INSACOG). Genomic characterization and epidemiology of an emerging SARS-CoV-2 variant in Delhi, India. Science. 2021;374:995–9. https://doi.org/10.1126/science.abj9932
2. Centers for Disease Control and Prevention. COVID data tracker: variant proportions [cited 2022 Mar 22]. https://covid.cdc.gov/covid-data-tracker/#variant-proportions
3. World Health Organization. WHO coronavirus (COVID-19) dashboard [cited 2021 Nov 2]. https://covid19.who.int/table
4. Birhane M, Bressler S, Chang G, Clark T, Dorough L, Fischer M, et al.; CDC COVID-19 Vaccine Breakthrough Case Investigations Team. COVID-19 vaccine breakthrough infections reported to CDC—United States, January 1–April 30, 2021. MMWR Morb Mortal Wkly Rep. 2021;70:792–3. https://doi.org/10.15585/mmwr.mm7021e3
5. Farinholt T, Doddapaneni H, Qin X, Menon V, Meng Q, Metcalf G, et al. Transmission event of SARS-CoV-2 delta variant reveals multiple vaccine breakthrough infections. BMC Med. 2021;19:255. https://doi.org/10.1186/s12916-021-02103-4

Address for correspondence: Julie Harris, US Embassy Kampala, 1577 Ggaba Road, Kampala 10102, Uganda; email: ggt5@cdc.gov

Multistate Outbreak of Infection with SARS-CoV-2 Omicron Variant after Event in Chicago, Illinois, USA, 2021

Hillary Spencer, Richard A. Teran, Hannah J. Barbian, Sarah Love, Rachel Berg, Stephanie R. Black, Isaac Ghinai,[1] Janna L. Kerins[1]

Author affiliations: Centers for Disease Control and Prevention, Atlanta, Georgia, USA (H. Spencer, R.A. Teran); Chicago Department of Public Health, Chicago, Illinois, USA (H. Spencer, R.A. Teran, S. Love, R. Berg, S.R. Black, I. Ghinai, J.L. Kerins); Rush University, Chicago (H.J. Barbian)

DOI: https://doi.org/10.3201/eid2806.220411

Bars and restaurants are high-risk settings for SARS-CoV-2 transmission. A multistate outbreak after a bar gathering in Chicago, Illinois, USA, highlights Omicron variant transmissibility, the value of local genomic surveillance and interstate coordination, vaccination value, and the potential for rapid transmission of a novel variant across multiple states after 1 event.

Settings in which adherence to mask wearing and physical distancing is challenging, such as bars and restaurants, pose a risk for transmission of SARS-CoV-2 (*1*). Superspreading events in bars have been linked to subsequent community transmission (*2*,*3*). In early December 2021, the Chicago Department of Public Health was alerted to SARS-CoV-2 infection caused by the Omicron variant (B.1.1.529) in a Louisiana, USA, resident who had attended a party in Chicago, Illinois, USA, over the Thanksgiving weekend (November 2021). The party was held in a large bar that also served walk-in patrons. Many party attendees also attended a dinner at a private event space; the first confirmed Omicron case-patient in Chicago had attended both the bar party and the dinner. We investigated the COVID-19 outbreak after confirmation of infections caused by the Omicron variant in multiple party attendees.

We defined a confirmed SARS-CoV-2 case-patient as a person who tested positive for the virus by molecular or antigen testing of a specimen collected November 25–December 11, 2021, and who had attended the bar event, the dinner, or both on November 27. Probable case-patients were persons experiencing COVID-19-like symptoms (https://ndc.services.cdc.gov/case-definitions/coronavirus-disease-2019-2021) who had attended either gathering but who had no confirmatory testing performed or tested negative. The initial case-patient was interviewed, and additional cases were identified through tracing of household and social gathering contacts; infected persons not associated with the invitation-only events were identified through routine case investigation, in which places of possible transmission are elicited. Contacts were persons who attended either event or both events and had neither confirmed nor probable case status. We verified testing results and vaccination status in reportable disease databases and vaccine registries when possible (vaccination status was self-reported by 2 persons). Available clinical remnant specimens from patients with confirmed cases were submitted to a reference laboratory for whole-genome sequencing. Persons were interviewed by their respective local health departments. We assigned virus lineages by using the PANGO Lineage Assigner (pangolin v3.1.19, pangoLEARN v1/20/22, scorpio v0.3.16; https://cov-lineages.org) and assembled a phylogenetic tree by using PhyML v3.3 (*4*). Our investigation was reviewed by the Centers for Disease Control and Prevention and conducted in accordance with its policies and applicable federal law (45 C.F.R. part 46.102(l)(2), 21 C.F.R. part 56; 42 U.S.C. §241(d); 5 U.S.C. §552a; 44 U.S.C. §3501 et seq).

We identified 15 cases (14 confirmed and 1 probable with negative test results) across 5 states (Figure, panel A); 7 (47%) isolates were sequenced and all were Omicron (B.1.1.529, sublineage BA.1) and closely phylogenetically related (Figure, panel B). Nearly all (14/15, 93%) infected persons had visited the bar, 1 (7%) had attended dinner only, and 1 (7%) had attended both events. Median patient age was 27 (range 23–37) years; 73% were women. Most interviewed persons (86%, 12/14) reported being symptomatic. Of the 11 who reported symptoms and completed the interview, the most common signs/symptoms were cough (82%), fatigue (82%), fever or chills (64%), congestion (64%), and myalgias (55%). None reported loss of smell or taste. In addition, none reported visiting an emergency department and none were hospitalized or died.

Most (80%, 12/15) persons were fully vaccinated (i.e., ≥14 days after receiving 2 doses of the Pfizer-BioNTech [https://www.pfizer.com] or Moderna mRNA vaccine [https://www.moderna.com] or 1 dose of the Johnson & Johnson/Janssen vaccine [https://www.jnj.com]). Of those, 25% (3/12) had received a booster 13–32 days before the event). Median time since receipt of most recent vaccine among

[1]These authors are co-senior authors.

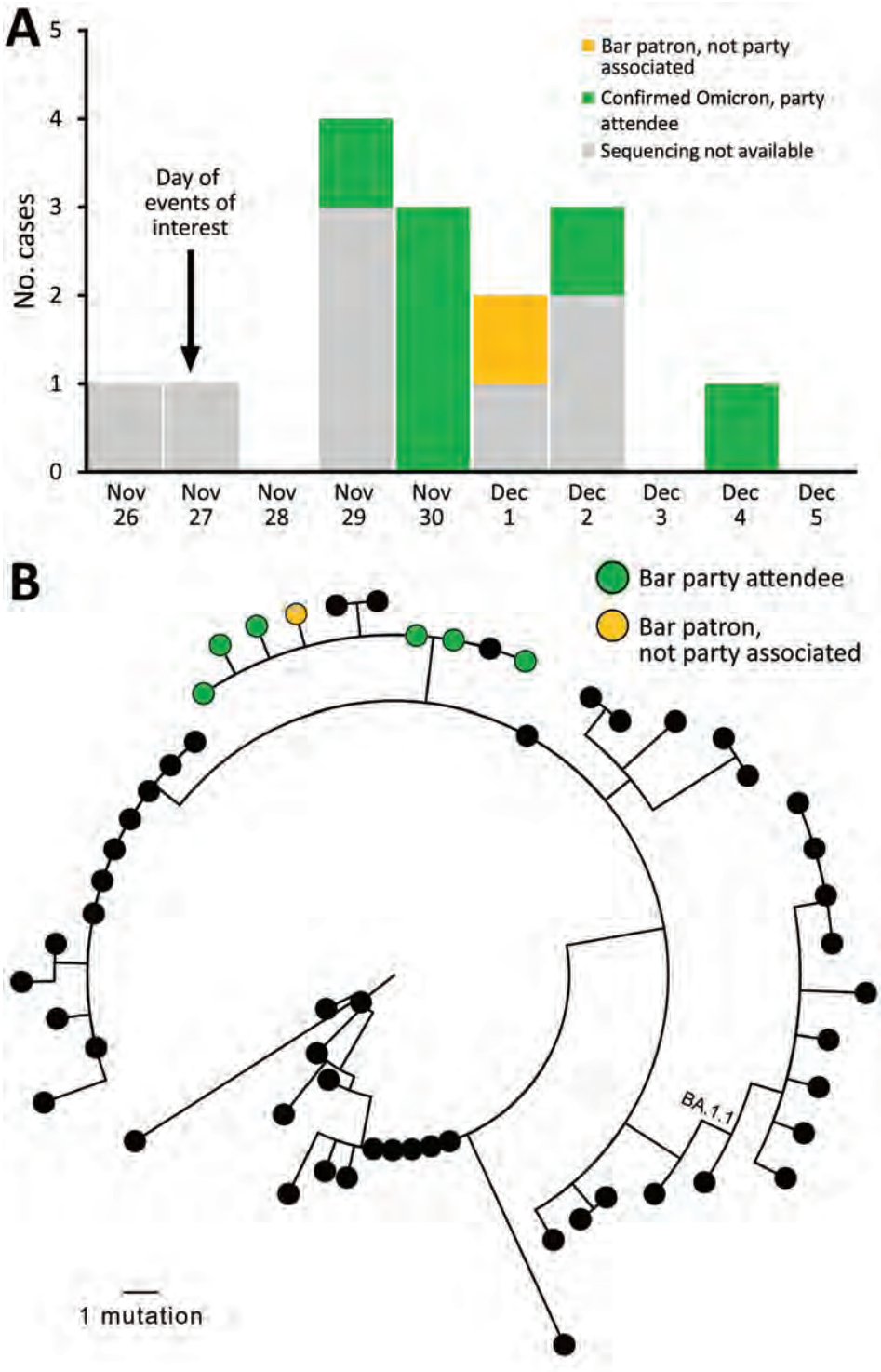

Figure. Cases in multistate (Colorado, Illinois, Louisiana, Missouri, Michigan) outbreak of infection with severe acute respiratory syndrome 2 Omicron variant after event in Chicago, Illinois, USA, November–December 2021. A) Cases over time. Sequencing results are shown, if available. B) Genetic relatedness of viruses isolated. Maximum-likelihood phylogeny of 7 sequenced Omicron samples in bar-associated outbreak (green and yellow) with 50 contextual sequences (black). Contextual sequences are a random sample of Omicron BA.1 and BA.1.1 sequences selected from all Omicron sequences in GISAID (https://www.gisaid.org) that were collected in the United States or before December 11, 2021, and had >90% genome coverage. Random selection was performed by using CLC Genomics Workbench (QIAGEN, https://www.qiagen.com). No contextual sequences were from Illinois. GISAID accession numbers for all included sequences are listed in the Appendix (https://wwwnc.cdc.gov/EID/article/28/6/22-0411-App1.xlsx). One outbreak-associated specimen was sequenced by a private laboratory and not uploaded to GISAID. Full-genome sequences were used for PhyML phylogenetic analysis (*4*), excluding 250 bp from genome ends and an error-prone region (reference positions 21492–21935). Outbreak sequences were identical to each other or contained a single-nucleotide substitution (T12000C, T22813G, T25414C) and clustered (with 3 contextual sequences) in a clade diverged by 2 nts from the closest other sequences. The 2 nt substitutions that defined the outbreak branch (C11950T, C28472T) were present in just 5.2% of contemporaneous Omicron sequences from the United States available on GISAID, indicating that all available outbreak sequences were closely genetically related.

9 persons fully vaccinated but not boosted was 258 (interquartile range 209–279) days. Two infected persons had prior SARS-CoV-2 infection (113 and 468 days since previous infection); both were fully vaccinated (1 before and 1 after infection). Three (20%) infected persons were either unvaccinated or partially vaccinated. Five infected persons visited the bar as members of the public (not party attendees); of those 5, Omicron was confirmed in the 1 specimen that was available for sequencing. Identifying this variant at a

time when it was not widely circulating prompted interstate notification for this out-of-state person.

This outbreak involving transmission in a bar between close social contacts and non–party-associated bar patrons demonstrates the high potential for Omicron transmission in indoor settings for which consistent mask use and distancing are challenging. Although no persons in this outbreak experienced severe disease, most were young and fully vaccinated. Local capacity for genomic sequencing, conducted across 7 laboratories in 5 states (Colorado, Illinois, Louisiana, Missouri, Michigan), enabled identification of linked case-patients beyond invited attendees who may have been excluded from traditional epidemiologic investigations.

Outbreak investigation limitations include incomplete identification of, or nonresponse from, dinner and party attendees; limited availability of clinical remnant specimens; and inability to estimate attack rates among persons in the bar. This outbreak highlights Omicron transmissibility; the value of local genomic surveillance capacity and interstate coordination; the value of vaccination for reducing the likelihood of severe disease; and the potential for rapid, widespread transmission of a novel variant across multiple states from 1 event over a holiday weekend.

Acknowledgements

We thank Sarah Patrick, Judy Kauerauf, Ann Wiringa, Ishani Doshi, Shirley Morales, Rachel Rubin, Matthew Sinn, Pauline Harrington, Heather Blankenship, Julie Hand, Christine Record, Alexis Burakoff, Christopher Grano, Carla Barrios, Christine Roloff, and Ashley Becht for their assistance with this study.

About the Author

Dr. Spencer is a pediatric infectious diseases physician and Epidemic Intelligence Service officer assigned to the Chicago Department of Public Health Bureau of Communicable Diseases and Bureau of Maternal, Infant, Child, and Adolescent Health. Her research interests include antimicrobial stewardship and infectious diseases in children.

References

1. Fisher KA, Tenforde MW, Feldstein LR, Lindsell CJ, Shapiro NI, Files DC, et al.; IVY Network Investigators; CDC COVID-19 Response Team. Community and close contact exposures associated with COVID-19 among symptomatic adults ≥18 years in 11 outpatient health care facilities—United States, July 2020. MMWR Morb Mortal Wkly Rep. 2020;69:1258–64. https://doi.org/10.15585/mmwr.mm6936a5
2. Sami S, Turbyfill CR, Daniel-Wayman S, Shonkwiler S, Fisher KA, Kuhring M, et al. Community transmission of SARS-CoV-2 associated with a local bar opening event—Illinois, February 2021. MMWR Morb Mortal Wkly Rep. 2021;70:528–32. https://doi.org/10.15585/mmwr.mm7014e3
3. Majra D, Benson J, Pitts J, Stebbing J. SARS-CoV-2 (COVID-19) superspreader events. J Infect. 2021;82:36–40. https://doi.org/10.1016/j.jinf.2020.11.021
4. Guindon S, Dufayard JF, Lefort V, Anisimova M, Hordijk W, Gascuel O. New algorithms and methods to estimate maximum-likelihood phylogenies: assessing the performance of PhyML 3.0. Syst Biol. 2010;59:307–21. https://doi.org/10.1093/sysbio/syq010

Address for correspondence: Hillary Spencer, Chicago Department of Public Health, Rm 200, 333 S State St, Chicago, IL 60604, USA; email: rhq6@cdc.gov or hillary.spencer@cityofchicago.org

Molecular Diagnosis of *Pseudoterranova decipiens* Sensu Stricto Infections, South Korea, 2002–2020

Hyemi Song,[1] Seungwan Ryoo,[1] Bong-Kwang Jung, Jaeeun Cho, Taehee Chang, Sooji Hong, Hyejoo Shin, Woon-Mok Sohn, Jong-Yil Chai

Author affiliations: Korea Association of Health Promotion, Seoul, South Korea (H. Song, S. Ryoo, B.-K. Jung, J. Cho, T. Chang, S. Hong, H. Shin); Gyeongsang National University College of Medicine, Jinju, South Korea (W.-M. Sohn); Seoul National University College of Medicine, Seoul (J.-Y. Chai)

DOI: https://doi.org/10.3201/eid2806.212483

Human *Pseudoterranova decipiens* larval infections were diagnosed by molecular analysis of mitochondrial *cox*1 and *nd*1 genes in 12 health check-up patients in South Korea during 2002–2020. Based on high genetic identity (99.3%–100% for *cox*1 and 96.7%–98.0% for *nd*1), we identified all 12 larvae as *P. decipiens* sensu stricto.

Human anisakiasis, which is caused by infection with larvae of the family Anisakidae after consuming infested marine fish or squids, is one of the most serious foodborne zoonotic diseases (*1*). Several species of *Anisakis* (*A. simplex* sensu stricto,

[1]These authors contributed equally to this article.

A. physeteris, and *A. pegreffii*) (*1*–*3*), *Pseudoterranova* (*P. decipiens* sensu stricto, *P. azarasi*, and *P. cattani*) (*4*–*6*), and *Contracecum* (*C. osculatum*) (*7*) nematodes have been reported to cause human infections.

Human anisakiasis was reported in the Netherlands during 1960 and has been found to occur in various parts of the world, including Japan and South Korea (*1*). Most human case-patients were infected with larvae of *A. simplex* s.s. (*1*). However, after 1999, a considerable number of cases infected with *A. pegreffii* nematodes (a sibling species of *A. simplex* s.s.) were diagnosed in Italy, Japan, and South Korea on the basis of molecular analysis of the larvae (*2*,*3*). Compared with *Anisakis* spp. nematodes, human infections with *Pseudoterranova* spp. nematodes have been relatively rare in Asia (*1*,*4*–*6*). In South Korea, among 645 anisakidosis cases recorded after 1971 until 2015, only ≈11.8% were infected with *Pseudoterranova* larvae (*8*). However, all of these *Pseudoterranova* infections were diagnosed on the basis of only the morphology of the larvae (*8*).

Within the genus *Pseudoterranova*, 8 species have been validated on the basis of molecular and morphologic/biologic characteristics: *P. decipiens* s.s., *P. kogiae*, *P. ceticola*, *P. azarasi*, *P. krabbei*, *P. bulbosa*, *P. decipiens* E, and *P. cattani* (*9*). Among those, 6 species (*P. decipiens* s.s., *P. krabbei*, *P. bulbosa*, *P. azarasi*, *P. decipiens* E, and *P. cattani*) are morphologically and biologically related to each another and designated as the *P. decipiens* species complex or *P. decipiens* sensu lato (*9*). These species can be discriminated by allozyme or molecular genetic analyses (*10*).

In our study, 12 human pseudoterranoviasis cases were found among patients who visited health check-up centers or hospitals in South Korea during 2002–2020 because of vague abdominal discomfort. Larvae were extracted by using gastrointestinal endoscopy (11 case-patients) or colonoscopy (1 case-patient). The larvae were confirmed to be *P. decipiens* s.s. by sequence analysis of the mitochondrial cytochrome *c* oxidase 1 (*cox*1) and NADH dehydrogenase subunit 1 (*nd*1) genes.

The patients consisted of 5 men (41–55 years of age) and 7 women (29–59 years of age). A total of 12 larvae (1 larva from each patient) were collected from the stomach (11 patients) or cecum (1 patient) (Appendix Table 1, https://wwwnc.cdc.gov/EID/article/28/6/21-2483-App1.pdf) and were processed for sequencing of 2 mitochondrial genes (Appendix).

Sequences of the *cox*1 (141 bp) (samples nos. OK539788–OK539799) and *nd*1 (153 bp) genes (OK539800–OK539807) showed high homologies with the sequences of *P. decipiens* s.s. (GenBank accession

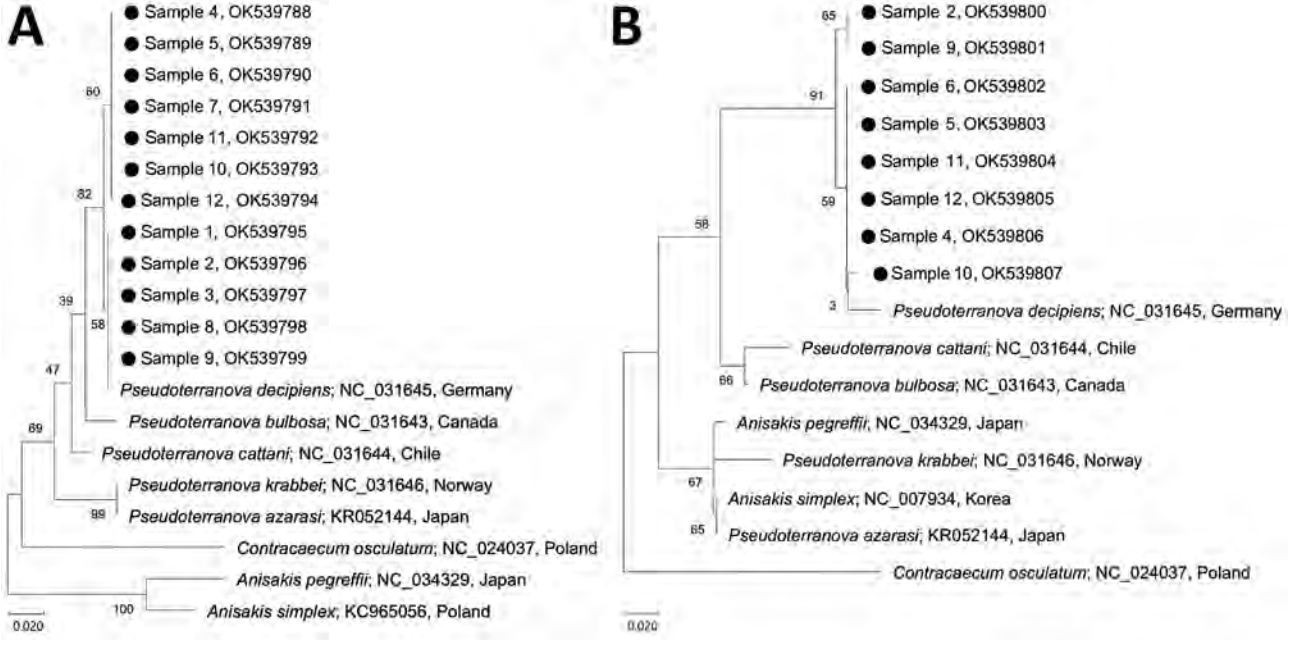

Figure. Phylogenetic analyses of *Pseudoterranova* nematode larvae extracted from 12 health check-up patients in South Korea, 2002–2020 (black dots), in comparison with other anisakid species. A) mitochondrial cytochrome oxidase c gene sequences; B) mitochondrial NADH dehydrogenase gene sequences. Trees were constructed by using the neighbor-joining method based on the Kimura 2-parameter model of nucleotide substitution with 1,000 bootstrap replications and viewed by using MEGA-X (https://www.megasoftware.net). GenBank accession numbers and country of origin are provided for reference sequences. Details of patient information for the 12 samples from this study are provided in Appendix Table 1 (https://wwwnc.cdc.gov/EID/article/28/6/21-2483-App1.pdf). Numbers along branches are bootstrap values. Scale bars indicate nucleotide substitutions/site.

no. NC_031645 for *cox*1 and *nd*1). The homology between samples from this study and *P. decipiens* s.s. was 99.3%–100% for *cox*1 and 97.4%–98.0% for *nd*1 (Appendix Tables 1–3).

The phylogenetic tree for *cox*1 showed that the 12 study samples were tightly clustered with *P. decipiens* s.s. reported from Germany but separate from *P. bulbosa* from Canada, *P. cattani* from Chile, *P. krabbei* from Norway, and *P. azarasi* from Japan (Figure). The phylogenetic tree for *nd*1 showed that 8 study samples were closely aligned with *P. decipiens* s.s. reported from Germany but clearly separated from *P. cattani* from Chile, *P. bulbosa* from Canada, *P. krabbei* from Norway, and *P. azarasi* from Japan (Figure). We also determined genetic distances between the study specimens and *P. decipiens*, *P. azarasi*, *P. bulbosa*, *P. cattani*, and *P. krabbei* for *cox1* (Appendix Table 2) and *nd*1 (Appendix Table 3).

For the specific diagnosis of anisakid larvae, analysis of the larval morphology is highly useful. However, extracting a fully intact larva from human patients for high-quality morphologic analysis is usually difficult. In such instances, molecular analysis of the larvae is helpful and essential for obtaining a specific diagnosis. Analyses of the internal transcribed spacer region and partial 28S rDNA could discriminate *P. decipiens* s.s. from *P. bulbosa*, *P. krabbei*, *P. cattani*, and possibly *P. decipiens* E (*10*). However, great sequence similarity was observed between *P. decipiens* s.s. and *P. azarasi*. Thus, it was difficult to distinguish them by using nuclear genes (*10*). Some investigators used mitochondrial genes, including *cox*1, *cox*2, and *nd*1, to distinguish them (*4*,*5*).

In our study, we used 2 mitochondrial genes, *cox*1 and *nd*1, to distinguish the species of *Pseudoterranova*. Our results showed that the nematode specimens from these patients nested within *P. decipiens* s.s. but were clearly separated from *P. azarasi*, *P. bulbosa*, *P. cattani*, and *P. krabbei* samples available in GenBank. Molecular analysis of larvae will be useful for obtaining specific diagnoses of infection.

Acknowledgments

We thank the endoscopy doctors and staff in the branch offices of the Korea Association of Health Promotion for assistance in collecting *P. decipiens* sensu stricto larval specimens from 12 health check-up patients, and members of the Institute of Parasitic Diseases, Korea Association of Health Promotion for assistance in processing the specimens for morphologic and molecular studies.

About the Author

Dr. Song is a research scientist at the Institute of Parasitic Diseases at Korea Association of Health Promotion, Seoul, South Korea. Her primary research interests are molecular aspects of parasites and parasitic diseases.

References

1. Sohn WM, Chai JY. Anisakiosis (Anisakidosis). In: Palmer SR, Soulsby L, Torgerson PR, Brown DW, editors. Oxford textbook of zoonoses. Oxford (UK): Oxford University Press; 2011. p. 774–6.
2. Lim H, Jung BK, Cho J, Yooyen T, Shin EH, Chai JY. Molecular diagnosis of cause of anisakiasis in humans, South Korea. Emerg Infect Dis. 2015;21:342–4. https://doi.org/10.3201/eid2102.140798
3. Mattiucci S, Fazii P, De Rosa A, Paoletti M, Megna AS, Glielmo A, et al. Anisakiasis and gastroallergic reactions associated with *Anisakis pegreffii* infection, Italy. Emerg Infect Dis. 2013;19:496–9. https://doi.org/10.3201/eid1903.121017
4. Nordholm A, Kurtzhals JA, Karami AM, Kania PW, Buchmann K. Nasal localization of a *Pseudoterranova decipiens* larva in a Danish patient with suspected allergic rhinitis. J Helminthol. 2020;94(E187):e187. https://doi.org/10.1017/S0022149X20000681
5. Arizono N, Miura T, Yamada M, Tegoshi T, Onishi K. Human infection with *Pseudoterranova azarasi* roundworm. Emerg Infect Dis. 2011;17:555–6. https://doi.org/10.3201/eid1703.101350
6. Weitzel T, Sugiyama H, Yamasaki H, Ramirez C, Rosas R, Mercado R. Human infections with *Pseudoterranova cattani* nematodes, Chile. Emerg Infect Dis. 2015;21:1874–5. https://doi.org/10.3201/eid2110.141848
7. Schaum E, Müller W. Heterocheilidiasis: human infection with fish ascarides [in German]. Dtsch Med Wochenschr. 1967;92:2230–3. https://doi.org/10.1055/s-0028-1106122
8. Sohn WM, Na BK, Kim TH, Park TJ. Anisakiasis: report of 15 gastric cases caused by *Anisakis* type I larvae and a brief review of Korean anisakiasis cases. Korean J Parasitol. 2015;53:465–70. https://doi.org/10.3347/kjp.2015.53.4.465
9. Mattiucci S, Nascetti G. Advances and trends in the molecular systematics of anisakid nematodes, with implications for their evolutionary ecology and host-parasite co-evolutionary processes. Adv Parasitol. 2008;66:47–148. https://doi.org/10.1016/S0065-308X(08)00202-9
10. Nadler SA, D'Amelio S, Dailey MD, Paggi L, Siu S, Sakanari JA. Molecular phylogenetics and diagnosis of *Anisakis, Pseudoterranova*, and *Contracaecum* from northern Pacific marine mammals. J Parasitol. 2005;91:1413–29. https://doi.org/10.1645/GE-522R.1

Address for correspondence: Jong-Yil Chai, Department of Tropical Medicine and Parasitology, Seoul National University College of Medicine, Seoul 03080, South Korea; email: cjy@snu.ac.kr

Experimental Infection of Mink with SARS-COV-2 Omicron Variant and Subsequent Clinical Disease

Jenni Virtanen,[1] Kirsi Aaltonen,[1] Kristel Kegler, Vinaya Venkat, Thanakorn Niamsap, Lauri Kareinen, Rasmus Malmgren, Olga Kivelä, Nina Atanasova, Pamela Österlund, Teemu Smura, Antti Sukura, Tomas Strandin, Lara Dutra, Olli Vapalahti, Heli Nordgren, Ravi Kant, Tarja Sironen

Author affiliations: University of Helsinki, Helsinki, Finland (J. Virtanen, K. Aaltonen, K. Kegler, V. Venkat, T. Niamsap, L. Kareinen, R. Malmgren, O. Kivelä, N. Atanasova, T. Smura, A. Sukura, T. Strandin, L. Dutra, O. Vapalahti, H. Nordgren, R. Kant, T. Sironen); Finnish Meteorological Institute, Helsinki (N. Atanasova); Finnish Institute for Health and Welfare, Helsinki (P. Österlund); Helsinki University Hospital, Helsinki (O. Vapalahti)

DOI: https://doi.org/10.3201/eid2806.220328

We report an experimental infection of American mink with SARS-CoV-2 Omicron variant and show that mink remain positive for viral RNA for days, experience clinical signs and histopathologic changes, and transmit the virus to uninfected recipients. Preparedness is crucial to avoid spread among mink and spillover to human populations.

SARS-CoV-2 has been detected in farmed and feral American mink (*Neovison vison*) in multiple countries, and extensive environmental contamination and human-to-mink and mink-to-human transmission has been documented (*1*–*5*). These factors have led to strict measures in mink farms and mink-farming countries to prevent the spread of the disease. In late 2021, a new SARS-CoV-2 variant (Omicron), characterized by possibly milder symptoms and more efficient human-to-human transmission, was detected, but its infectivity and spread in American mink is unknown (*6*,*7*).

We tested the response of American mink to the Omicron variant by infecting 3 male mink intranasally with 4×10^5 plaque-forming units of the virus (Appendix, https://wwwnc.cdc.gov/EID/article/28/6/22-0328-App1.pdf). We conducted follow-up on infected mink for 7 days and performed histopathologic evaluation of upper and lower respiratory tracts on the last day of follow-up. We sampled saliva daily.

All experimentally infected mink showed mild to moderate signs of illness, including lethargy, anorexia, diarrhea, nasal and lacrimal discharge, and sneezing. Consistent with earlier experiments with other variants (*8*; D. Adney et al., unpub. data, https://www.biorxiv.org/content/10.1101/2022.01.20.477164v1), saliva samples tested PCR-positive 1 day postinfection (dpi) and remained that way throughout follow-up (Table; Appendix). Infectious virus was cultured 1–3 dpi. Even though some of the clinical signs could be caused by other factors, such as stress from the change of environment, their consistency with signs seen in studies of other variants, combined with PCR results, demonstrate that the Omicron variant also causes clinical disease in mink.

To study whether mink can transmit the virus, we placed 2 uninfected indirect contact mink in separate cages 10–20 cm from the cages of the infected mink and followed their progress for 10 days. Similar signs to the experimentally infected mink developed in both initially uninfected mink, and they were consistently PCR-positive from day 3 onward (Table), indicating mink-to-mink transmission. Infectious virus was detected in cell culture even before it was detected by PCR. Even though no evidence of mink-to-human transmission of the Omicron variant exists, it seems possible on the basis of our results and the information from studies of other variants.

Gross findings in the nasal cavity and lungs were subtle in both experimentally infected and recipient mink and consisted of hyperemia of respiratory mucosa with small amounts of viscous exudate and noncollapsed, dark-red, and wet pulmonary lobes. All mink showed histopathologic changes in the upper and lower respiratory tracts (Figure). We observed multifocal degeneration and loss of respiratory epithelium with variable mucosal and submucosal neutrophilic infiltration in the nose. The lumen contained sloughed epithelial cells, mucinous material, and degenerated neutrophils (Figure, panels A, C). Viral nucleoprotein was widely distributed beyond intact cells, within sloughed cells, and in mucosal respiratory epithelium (Figure, panels B, D). The olfactory epithelium was inconsistent and mildly affected with only focal viral antigen detection. Unlike in some experimental infections reported in rodents, clear pathology was observed in the lungs (*9*). In 2 inoculated and both recipient mink, pulmonary lesions (Figure, panels E, G) were associated with viral antigen expression (Figure, panels F, H) and characterized by multifocal to coalescing alveolar damage with degeneration or necrosis of alveolar septa, infrequent hyalin membrane formation, and variable proliferation

[1]These authors contributed equally to this article.

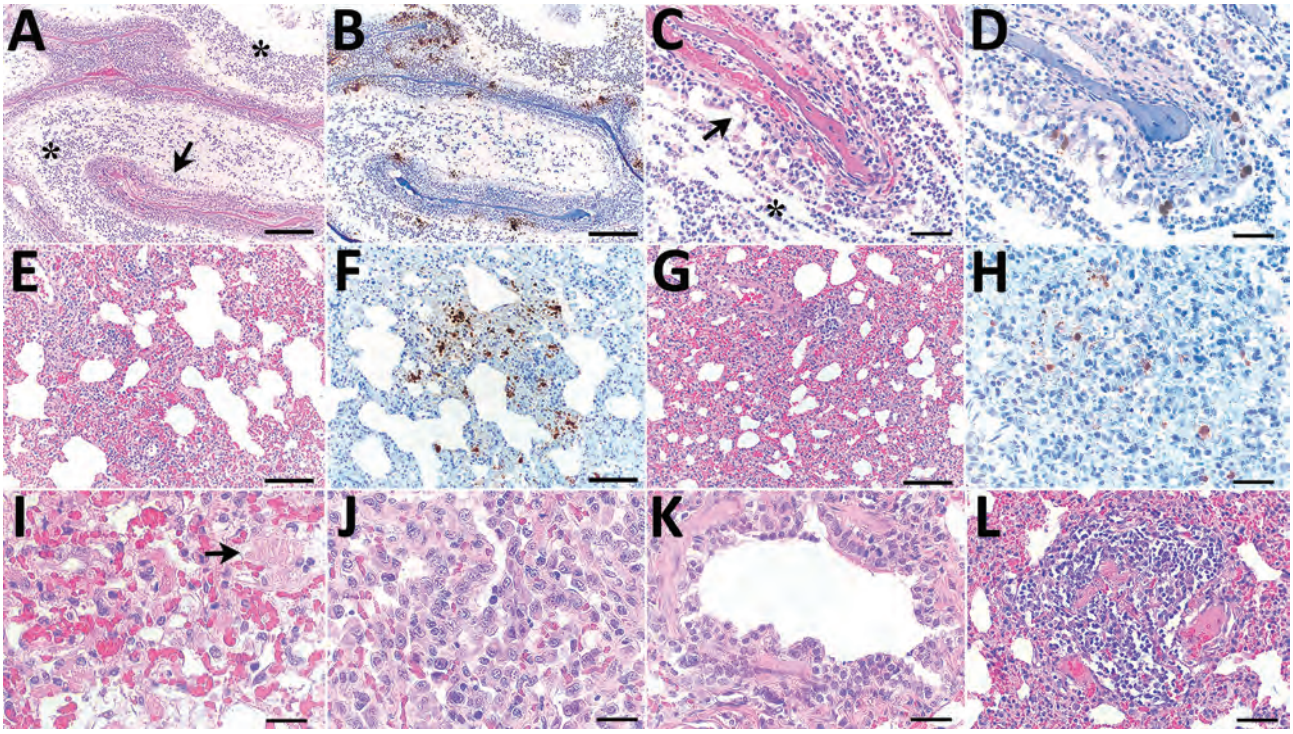

Figure. Histopathologic changes and SARS-CoV-2 expression in the upper and lower respiratory tracts of mink experimentally infected with Omicron variant at 7 days postinfection and recipient mink after 10 days of follow-up. A) Respiratory segment of the nose from an intranasally infected mink showing luminal accumulation of exudate (asterisks) and degeneration of mucosal epithelium (arrow) Scale bar indicates 500 µm. B) Viral antigen widely detected within nasal lumen and respiratory epithelium. Scale bar indicates 500 µm. C, D) Respiratory epithelium from a recipient mink depicting marked degeneration and loss (arrow in panel C) and intraluminal accumulation of sloughed cells and neutrophils (asterisk in pane C), and intraepithelial viral expression (panel D). Scale bars indicate 50 µm. E–H) Lungs from intranasally infected (E, F) and recipient (G, H) mink showing alveolar damage with intralesional presence of viral nucleoprotein. Scale bars indicate 200 µm in panels E–G and 50 µm in panel H. I, J) Marked degeneration and necrosis of alveolar septa and focal hyalin membrane (arrow in panel I) and prominent proliferation of type II pneumocytes (panel J) in an intranasally infected mink. Scale bars in indicate 25 µm). K, L) Recipient mink showing bronchiolar epithelial degeneration and hyperplasia (K) and vasculitis (L) with complete destruction of blood vessel wall and mononuclear cell infiltration. Scale bar indicates 50 µm in panel K and 100 µm in panel L. Hematoxylin and esosin stain and immunohistochemistry, hematoxylin counterstain.

of type II pneumocytes (Figure, panels I, J). Alveolar spaces contained macrophages, sloughed cells, edema, and hemorrhage. Bronchiolar epithelial degeneration and hyperplasia were variably present (Figure, panel K), and the lumen filled with few sloughed cells and neutrophils. Bronchi were lined by hyperplastic epithelium with increased numbers of goblet cells. Other consistent findings were vasculitis (Figure, panel L), perivasculitis, and perivascular and peribronchial edema. In 1 inoculated mink, we observed markedly thickened alveolar septa by mononuclear cells, marked proliferation of type II pneumocytes,

Table. Results of PCR and cell culture testing for SARS-CoV-2 Omicron variant in saliva samples from 3 experimentally infected mink and 2 uninfected recipient mink*

Mink ID	1 dpi	2 dpi	3 dpi	4 dpi	5 dpi	6 dpi	7 dpi	8 dpi	9 dpi	10 dpi
Infected mink										
451	+/ND	+/+	+/−	+/−	+/−	+/−	+/−			
453	+/(+)	+/−	+/−	+/−	+/−	+/−	+/ND			
455	+/−	+/−	+/(+)	+/−	+/−	+/−	+/−			
Recipient mink										
452	(+)/+	−/−	+/ND	+/−	+/−	+/+	+/−	+/−	+/−	(+)/−
454	-/+	−/+	(+)/−	+/−	+/−	+/ND	+/ND	+/−	+/−	+/−

*Plus sign alone indicates signal detected with both primers of Luna SARS-CoV-2 reverse transcription quantitative PCR Multiplex Assay Kit (New England BioLabs Inc., https://www.neb.com) and cycle threshold value from cell culture media was >5 cycles lower than that of the original saliva sample. Plus symbol in parentheses indicates signal detected only with 1 of 2 primers and cycle threshold value from cell culture media was 1–5 cycles lower than that of the original saliva sample. Minus sign indicates no signal with either of the primers and no cytopathic effect was detected in cell culture or cycle threshold value from the culture media was the same or higher than that of the original sample. dpi, days postinfection; ID, identification; ND, not done.

intra-alveolar macrophages, few syncytial cells, bronchi and bronchiolar epithelial cell hyperplasia, vasculitis, and perivasculitis. We could not detect viral antigen in this mink. Strikingly, all evaluated mink lacked viral antigen in the epithelium of bronchi and bronchioles.

The Omicron variant is different from other variants in its more efficient spread, primarily attributable to immune escape and likely milder symptoms in humans (*6*,*7*). These factors make preventing virus introduction into mink farms through asymptomatic humans more difficult, creating a more substantial risk for the formation of virus reservoirs among farmed or feral mink. This study shows that mink can be infected by Omicron and, crucially, efficiently transmit the virus to other mink. Despite the reports of lower virulence of Omicron, mink experience clinical disease and nasal and pulmonary microscopic lesions that closely resemble infection with previously reported variants in mink and humans (*8*). Clarifying the clinical signs will help detect the virus among mink earlier. Questions remain about the risks that the spread of this easily transmitted variant among mink would create for public health, including transmission to humans and emergence of mink-specific mutations, followed by their spillover to human population.

This article was preprinted at https://www.biorxiv.org/content/10.1101/2022.02.16.480524v2.

Acknowledgments

We thank Jari Elemo, Mari Elemo, and other animal caretakers for handling the animals and assessing their health and Esa Pohjalainen, Sanna Mäki, Tiina Sihvonen, Johanna Rintamäki, Hanna Valtonen, Marika Skön, Larissa Laine, and Elina Väisänen for technical assistance. We thank Kati Kuipers, Anne Kujanpää, Laura Vähälä, and the Finnish Centre for Laboratory Animal Pathology (FCLAP) for expert technical help, as well as Johanna Korpela and Jussi Peura from Finnish Fur Breeders Association and Jan Segervall and Maarit Mohaibes from the Kannus Research Farm Luova Ltd. for providing the animals. We also thank E3 Excellence in Pandemic Response and Enterprise Solutions coinnovation project and all its parties.

This study was supported by the Academy of Finland (grant no. 336490, 339510), VEO–European Union's Horizon 2020 (grant no. 874735), Business Finland E3 (4917/31/2021), Finnish Institute for Health and Welfare, and the Jane and Aatos Erkko Foundation.

About the Author

Ms. Virtanen is a PhD student at the University of Helsinki in the field of clinical microbiology. Her research interests include zoonotic viruses and pathogens in human-animal interface.

References

1. Aguiló-Gisbert J, Padilla-Blanco M, Lizana V, Maiques E, Muñoz-Baquero M, Chillida-Martínez E, et al. First description of SARS-CoV-2 infection in two feral American mink (*Neovison vison*) caught in the wild. Animals (Basel). 2021;11:1422. https://doi.org/10.3390/ani11051422
2. Oreshkova N, Molenaar RJ, Vreman S, Harders F, Oude Munnink BB, Hakze-van der Honing RW, et al. SARS-CoV-2 infection in farmed minks, the Netherlands, April and May 2020 [Erratum in: Euro Surveill. 2021; 26:210325c]. Euro Surveill. 2020;25. https://doi.org/10.2807/1560-7917.ES.2020.25.23.2001005
3. Rabalski L, Kosinski M, Mazur-Panasiuk N, Szewczyk B, Bienkowska-Szewczyk K, Kant R, et al. Zoonotic spill-over of SARS-CoV-2: mink-adapted virus in humans. Clin Microbiol Infect. 2021.
4. Rabalski L, Kosinski M, Smura T, Aaltonen K, Kant R, Sironen T, et al. Severe acute respiratory syndrome coronavirus 2 in farmed mink (*Neovison vison*), Poland. Emerg Infect Dis. 2021;27:2333–9. https://doi.org/10.3201/eid2709.210286
5. Hammer AS, Quaade ML, Rasmussen TB, Fonager J, Rasmussen M, Mundbjerg K, et al. SARS-CoV-2 transmission between mink (*Neovison vison*) and humans, Denmark. Emerg Infect Dis. 2021;27:547–51. https://doi.org/10.3201/eid2702.203794
6. Viana R, Moyo S, Amoako DG, Tegally H, Scheepers C, Althaus CL, et al. Rapid epidemic expansion of the SARS-CoV-2 Omicron variant in southern Africa. Nature. 2022;603:679–86. https://doi.org/10.1038/s41586-022-04411-y
7. Wolter N, Jassat W, Walaza S, Welch R, Moultrie H, Groome M, et al. Early assessment of the clinical severity of the SARS-CoV-2 Omicron variant in South Africa: a data linkage study. Lancet. 2022;399:437–46. https://doi.org/10.1016/S0140-6736(22)00017-4
8. Song Z, Bao L, Deng W, Liu J, Ren E, Lv Q, et al. Integrated histopathological, lipidomic, and metabolomic profiles reveal mink is a useful animal model to mimic the pathogenicity of severe COVID-19 patients. Signal Transduct Target Ther. 2022;7:29. https://doi.org/10.1038/s41392-022-00891-6
9. Halfmann PJ, Iida S, Iwatsuki-Horimoto K, Maemura T, Kiso M, Scheaffer SM, et al.; Consortium Mount Sinai Pathogen Surveillance (PSP) study group. SARS-CoV-2 Omicron virus causes attenuated disease in mice and hamsters. Nature. 2022;603:687–92. https://doi.org/10.1038/s41586-022-04441-6

Address for correspondence: Jenni Virtanen, Department of Veterinary Biosciences, Faculty of Veterinary Medicine, University of Helsinki, Agnes Sjöbergin katu 2, 00790, Helsinki, Finland; email: jenni.me.virtanen@helsinki.fi

Horse-Specific *Cryptosporidium* Genotype in Human with Crohn's Disease and Arthritis

Żaneta Zajączkowska, Anna Baštýřová Brutovská, Katarzyna Akutko, John McEvoy, Bohumil Sak, Andrzej B. Hendrich, Błażej Łukianowski, Martin Kváč, Marta Kicia

Author affiliations: Wroclaw Medical University, Wroclaw, Poland (Ż. Zajączkowska, K. Akutko, A.B. Hendrich, B. Łukianowski, M. Kicia); Czech Academy of Sciences, České Budějovice, Czech Republic (A. Baštýřová Brutovská, B. Sak, M. Kváč); North Dakota State University, Fargo, North Dakota, USA (J. McEvoy); University of South Bohemia, České Budějovice (M. Kváč)

DOI: https://doi.org/10.3201/eid2806.220064

We identified an unusual subtype of a *Cryptosporidium* sp. horse genotype as the cause of cryptosporidiosis in a 13-year-old girl in Poland who was undergoing immunosuppressive treatment for juvenile rheumatoid arthritis and Crohn's disease. The same subtype was identified in a horse the girl had ridden.

Cryptosporidium spp. causes diarrheal disease that can become chronic and life-threatening in persons who have an immature or malfunctioning immune system. Humans are primarily infected with *C. hominis* and *C. parvum* (*1*), but can also be infected with other species and genotypes, including *Cryptosporidium* sp. horse genotype, which primarily infects horses and donkeys.

Molecular studies targeting the polymorphic 60-kD glycoprotein (*gp60*) gene have shown that humans and horses/donkeys are infected with different subtypes of the *Cryptosporidium* sp. horse genotype (*2*–*4*). We identified an unusual subtype of the *Cryptosporidium* sp. horse genotype as the cause of cryptosporidiosis in a 13-year-old girl receiving immunosuppressive treatment for juvenile rheumatoid arthritis and Crohn's disease.

The Human Research Ethics Committee of Wroclaw Medical University approved use of diagnostic samples and corresponding patient data for this study (permit No. KB-24/2014). Written consent was provided by the parents of the child involved in the study.

The girl was being treated at the Wroclaw Medical University (Wroclaw, Poland) since 2009. On the basis of recommended criteria, she was given a diagnoses of rheumatoid arthritis when she was 3 years of age and Crohn's disease when she was 5 years of age (*5*,*6*). She had received the immunosuppressant adalimumab since her rheumatoid arthritis diagnosis; that treatment continued after diagnosis of Crohn's disease because of frequent relapses and lesions in the large bowel. In 2018, she was hospitalized because of recurrent gastrointestinal relapses, including diarrhea, fever (temperature >38.5°C), and abdominal cramps. Initial therapy included entocort (9 mg/d) and mesalizine (2,000 mg/d).

We tested stool samples for a panel of gastrointestinal bacteria (*Salmonella*, *Shigella*, *Campylobacter*, *Yersinia*, and *Clostridium difficile*). We also tested for parasitic protists, including microsporidia (*Encephalitozoon* spp., *Enterocytozoon bieneusi*), *Cryptosporidium* spp., *Giardia intestinalis*, and *Cyclospora cayetanensis*. Examination of stool showed *Cryptosporidium* oocysts (20,000–60,000 oocysts/gram of stool (*7*). Test results for other gastrointestinal pathogens (bacteria and other parasitic protists) were negative.

We used the small ribosomal subunit rRNA and *gp60* genes (*8*), respectively, to identify *Cryptosporidium* to the species/genotype and subgenotype levels. We purified amplicons (QIAquickR; QIAGEN, https://www.qiagen.com) and directly sequenced them in both directions (SeqMe, https://www.seqme.eu). We repeated amplification and sequencing of each locus 3 times. We aligned nucleotide sequences by using references from GenBank and MAFFT version 7 (http://mafft.cbrc.jp/alignment/software) and performed phylogenetic analysis by using the maximum-likelihood method in MEGAX (https://www.megasoftware.net). Phylogenetic analyses of small ribosomal subunit rRNA and *gp60* showed a *Cryptosporidium* sp. horse genotype belonging to the subtype family VIaA15G4 (Figure).

A follow-up medical interview showed that the patient rode a horse once per week at a riding stable; therefore, we collected fecal samples from all 10 horses at the stable and analyzed them for *Cryptosporidium* spp. None of the examined horses shed microscopically detectable *Cryptosporidium* oocysts or showed signs of cryptosporidiosis.

However, a horse ridden by the patient was PCR positive for a *Cryptosporidium* sp. horse genotype that had 100% identity with the isolate from the patient (GenBank accession nos. MK779952, MK784560, MZ255144, and MZ269096). The patient stopped attending the stable after the diagnosis, and symptoms resolved within 2 weeks without specific *Cryptosporidium* treatment. *Cryptosporidium* was not detectable in the patient 2 months after the diagnosis, and no

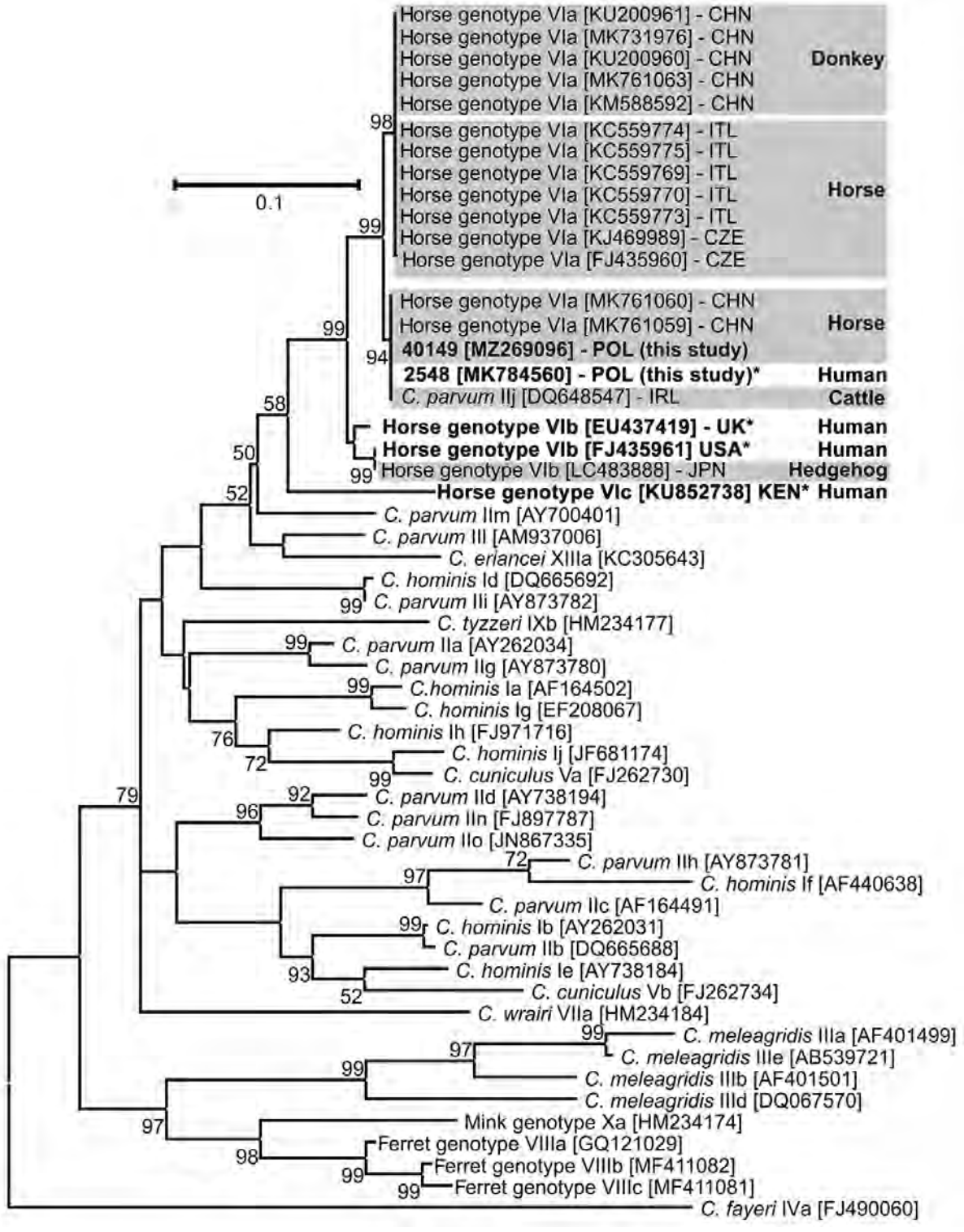

Figure. Maximum-likelihood tree based on partial sequences of 60-kD glycoprotein of *Cryptosporidium* spp. from a 13-year-old immunocompromised girl and a horse she rode in Poland (and reference sequences. Bold and asterisks indicate isolates reported from humans; gray shading indicates isolates reported from animals. The general time reversible model was applied using a discrete gamma distribution. Robustness of the phylogeny was tested with 1,000 bootstraps. Values along the branches indicate bootstrap values with >50% support. GenBank accession number are indicated in brackets. Country of origin of *Cryptosporidium* sp. horse genotype isolates is indicated by 3-letter International Organization for Standardization country abbreviation. Scale bar indicates nucleotide substitutions per site.

exacerbations of underlying disease were observed during the 1-year follow-up period.

Documentation of direct animal-to-human transmission of *Cryptosporidium* spp. is rare. In most cases of infection by animal-specific *Cryptosporidium*, patients did not report direct contact with the host suspected of being the source of infection. Our findings demonstrate horse-to-human transmission of the *Cryptosporidium* sp. horse genotype VIa family, a subtype previously believed to be specific to horses and donkeys.

Crohn's disease pathophysiology is closely linked to perturbations of the gut microbiome, but this disease and its causes remain poorly understood. Because of unexplained etiology, there is no specific treatment; immunosuppressive drugs are used to reduce inflammation, achieve remission, or prevent exacerbation. Immunosuppressive therapies cause increased susceptibility to opportunistic pathogens, such as *Cryptosporidium* spp., and limited data suggest that *Cryptosporidium* infection in inflammatory bowel disease (IBD) patients is not rare (*9*), despite protists being frequently overlooked in diagnostic testing. Manifestation of intestinal cryptosporidiosis might be confused with symptoms of Crohn's disease and other IBD relapses.

The condition of the immune system is a critical determinant of the clinical course of *Cryptosporidium* infection. Despite immunosuppressive therapy, we observed complete clearance of the *Cryptosporidium* infection without specific treatment. In this regard, the infection was more similar to a case of self-limiting diarrhea in an immunocompetent person than to a chronic and life-threatening disease that is frequently associated with immunocompromised persons (*10*). Our findings suggest that the combination of Crohn's disease and rheumatoid arthritis and immunomodulatory treatment might increase likelihood of infection with *Cryptosporidium* spp. that are not commonly infectious for humans.

In summary, we show the need for considering atypical sources of *Cryptosporidium* infection in persons with IBD who are undergoing immunosuppressive therapy. A necessary first step is to expand diagnostic testing of IBD patients to include opportunistic protists, such as *Cryptosporidium* spp. Once diagnosis is confirmed, genotyping of isolates can be used to help identify the source of infection, which is critical to preventing disease recurrence.

This study was supported by a Ministry of Health subvention (grant STM.A060.20.105) from the IT Simple System of Wroclaw Medical University and the Czech Science Foundation (grant 21-23773S).

About the Author

Dr. Zajączkowska is a research scientist in the Department of Biology and Medical Parasitology at Wroclaw Medical University, Wroclaw, Poland. Her primary research interests are opportunistic parasites, including microsporidia, *Cryptosporidium* spp., and *Pneumocystis jirovecii*, in humans and animals.

References

1. Xiao L. Molecular epidemiology of cryptosporidiosis: an update. Exp Parasitol. 2010;124:80–9. https://doi.org/10.1016/j.exppara.2009.03.018
2. Jian F, Liu A, Wang R, Zhang S, Qi M, Zhao W, et al. Common occurrence of *Cryptosporidium hominis* in horses and donkeys. Infect Genet Evol. 2016;43:261–6. https://doi.org/10.1016/j.meegid.2016.06.004
3. Robinson G, Elwin K, Chalmers RM. Unusual *Cryptosporidium* genotypes in human cases of diarrhea. Emerg Infect Dis. 2008;14:1800–2. https://doi.org/10.3201/eid1411.080239
4. Xiao L, Hlavsa MC, Yoder J, Ewers C, Dearen T, Yang W, et al. Subtype analysis of *Cryptosporidium* specimens from sporadic cases in Colorado, Idaho, New Mexico, and Iowa in 2007: widespread occurrence of one *Cryptosporidium hominis* subtype and case history of an infection with the *Cryptosporidium* horse genotype. J Clin Microbiol. 2009; 47:3017–20. https://doi.org/10.1128/JCM.00226-09
5. Levine A, Koletzko S, Turner D, Escher JC, Cucchiara S, de Ridder L, et al.; European Society of Pediatric Gastroenterology, Hepatology, and Nutrition. ESPGHAN revised porto criteria for the diagnosis of inflammatory bowel disease in children and adolescents. J Pediatr Gastroenterol Nutr. 2014;58:795–806. https://doi.org/10.1097/MPG.0000000000000239
6. Aletaha D, Neogi T, Silman AJ, Funovits J, Felson DT, Bingham III CO, et al. 2010 Rheumatoid arthritis classification criteria: an American College of Rheumatology/European League Against Rheumatism collaborative initiative. Arthritis Rheum. 2010;62:2569–81. https://doi.org/10.1002/art.27584
7. Kvác M, Ondrácková Z, Kvetonová D, Sak B, Vítovec J. Infectivity and pathogenicity of *Cryptosporidium andersoni* to a novel host, southern multimammate mouse (*Mastomys coucha*). Vet Parasitol. 2007;143:229–33. https://doi.org/10.1016/j.vetpar.2006.08.031
8. Alves M, Xiao L, Sulaiman I, Lal AA, Matos O, Antunes F. Subgenotype analysis of *Cryptosporidium* isolates from humans, cattle, and zoo ruminants in Portugal. J Clin Microbiol. 2003; 41:2744–7. https://doi.org/10.1128/JCM.41.6.2744-2747.2003
9. Colussi O, Rouen A, Seksik P, Cosnes J, Beaugerie L, Sokol H. Acute cryptosporidiosis as a cause of sudden recurrence of digestive symptoms in patients with Crohn's disease. J Crohns Colitis. 2010;4:669–70. https://doi.org/10.1016/j.crohns.2010.05.008
10. Hunter PR, Hadfield SJ, Wilkinson D, Lake IR, Harrison FCD, Chalmers RM. Subtypes of *Cryptosporidium parvum* in humans and disease risk. Emerg Infect Dis. 2007;13:82–8. https://doi.org/10.3201/eid1301.060481

Address for correspondence: Żaneta Zajączkowska, Department of Biology and Medical Parasitology, Wroclaw Medical University, ul J. Mikulicza-Radeckiego 9, Wrocław, Dolnoslaskie 50-367 Poland; email: zaneta.kopacz@umw.edu.pl

Lyme Disease, Anaplasmosis, and Babesiosis, Atlantic Canada

Ziyad O. Allehebi, Farhan M. Khan, Mark Robbins, Elizabeth Simms, Richard Xiang, Allam Shawwa, L. Robbin Lindsay, Antonia Dibernardo, Clarice d'Entremont, Alex Crowell, Jason J. LeBlanc, David J. Haldane

Author affiliations: Dalhousie University, Halifax, Nova Scotia, Canada (Z.O. Allehebi, F.M. Khan, M. Robbins, E. Simms, J.J. LeBlanc, D.J. Haldane); Nova Scotia Health, Halifax (Z.O. Allehebi, F.M. Khan, R. Xiang, A. Shawwa, J.J. LeBlanc, D.J. Haldane); Public Health Agency of Canada National Microbiology Laboratory, Winnipeg, Manitoba, Canada (L.R. Lindsay, A. Dibernardo); Yarmouth Regional Hospital, Yarmouth, Nova Scotia, Canada (C. d'Entremont, A. Crowell); Nova Scotia Provincial Public Health Laboratory Network, Halifax (D.J. Haldane)

DOI: http://doi.org/10.3201/eid2806.220443

In July 2021, a PCR-confirmed case of locally acquired *Babesia microti* infection was reported in Atlantic Canada. Clinical features were consistent with babesiosis and resolved after treatment. In a region where Lyme disease and anaplasmosis are endemic, the occurrence of babesiosis emphasizes the need to enhance surveillance of tickborne infections.

Babesiosis is an emerging infectious disease caused by a zoonotic hemoprotozoan parasite of the genus *Babesia*, which consists of ≈100 species (*1*–*4*). Human disease in North America is primarily attributed to *Babesia microti*, and clinical features range from asymptomatic infection to severe disease or death (*1*–*6*). A small number of cases of locally acquired human *B. microti* infections in Central and Western Canada have been described (*3*–*6*). We report a confirmed case of babesiosis from Atlantic Canada in an area where Lyme disease and anaplasmosis are endemic (*7*–*9*). All clinical features and laboratory findings were consistent with babesiosis (*4*).

A 58-year-old immunocompetent man sought care at a hospital in southwest Nova Scotia, Canada, in July 2021 for a 3-day history of nonspecific symptoms (headache, photophobia, fatigue, general weakness, and fever up to 40°C). The patient's most recent travel was to Maine (USA) 25 years prior. He did not recall any recent tick bites; however, he had been treated for Lyme disease 3 times since 2019.

At admission, laboratory results were unremarkable aside from elevated C-reactive protein (164 mg/L [reference range ≤8 mg/L]) and high lactate dehydrogenase (372 U/L [reference range 120–230 U/L]). Leukocyte counts were normal except for a new onset of thrombocytopenia (platelet count 73 × 10^9/L). Wright-stained peripheral blood smears revealed intra-erythrocytic ring forms and extracellular merozoites (Figure). Parasitemia was estimated at 2.3%. Results of BinaxNow malaria testing was negative (Abbott Laboratories, https://www.globalpointofcare.abbott). *B. microti*–specific PCR performed on whole blood at the National Microbiology Laboratory (Winnipeg, Manitoba, Canada) was positive.

On day 7 after symptom onset, the patient's condition worsened, and parasitemia increased to 6.6%. Bloodwork showed increased C-reactive protein (298 mg/L), decreased platelets (56 × 10^9/L), anemia (122 × 10^{12} erythrocytes/L), and increased liver enzymes (aspartate aminotransferase 76 IU/L [reference range 5–45 U/L], alanine aminotransferase 69 IU/L [reference range 0–54 U/L], and alkaline phosphatase 120 IU/L [reference range 38–150 U/L]). The patient was treated with atovaquone (750 mg orally 2×/d) and with azithromycin (500 mg orally 1×/d) for 10 days, along with doxycycline for 14 days for possible Lyme disease co-infection. Over the next 7 days, parasitemia gradually decreased to undetectable levels; the patient improved clinically and was discharged.

B. microti is primarily transmitted through feeding of infected nymphal and adult female ticks (*1*–*3*). In Atlantic Canada, the vector (*Ixodes scapularis* blacklegged ticks) and reservoir (the white-footed mouse *Peromyscus leucopus*) for *B. microti* are the same as those for *Borrelia burgdorferi* (*7*). Locally acquired *B. microti* infections are thought to be rare in Canada; previous cases were reported only recently from Central and Western Canada (*3*–*6*), and only rare occurrences are described in previous surveillance in human, animal, and ticks (*6*,*10*). Climate change and other environmental factors are now known to influence the abundance, range, and activity of ticks and reservoirs, as well as the risks for human exposure to tickborne pathogens (*1*,*10*). As seen with the increasing spread of *Ixodes ricinus* ticks in Europe (*1*), a northward expansion of blacklegged ticks is occurring in the southern parts of central and western Canada and in the Atlantic provinces, along with a concomitant rise in reported cases of Lyme disease (*10*). Compared with other provinces of Canada, Nova Scotia has the highest incidence of Lyme disease, increasing from 1.7 to 26.1 cases/100,000 population during 2009–2015 (*7*). Recently, increasing reports of ticks

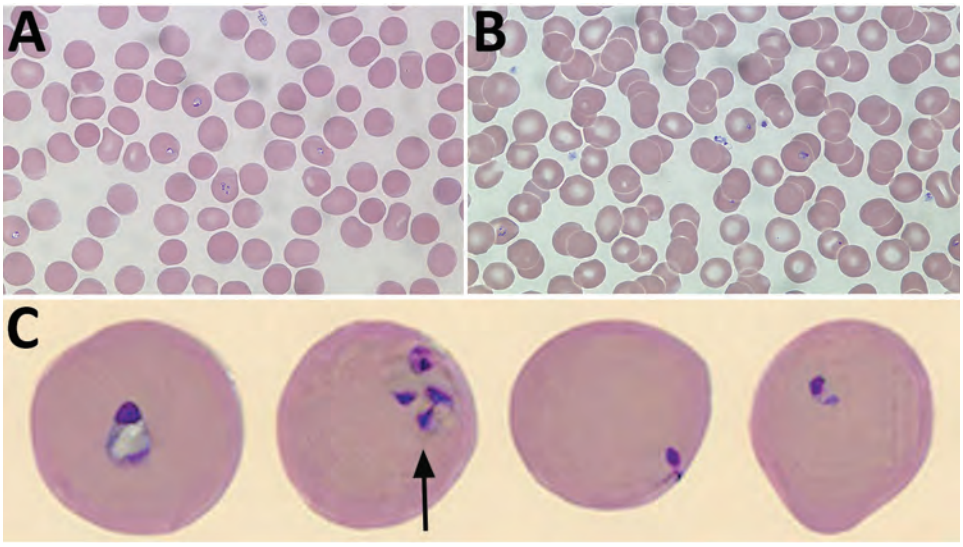

Figure. *Babesia microti* detected on Wright-stained peripheral blood smears from a 58-year-old man, southwest Nova Scotia, Canada, July 2021. Some typical features of *B. microti* infection include multiple ring forms present in erythrocytes (A), extracellular ring forms (B), and ring forms of various shapes and sizes (C), including the pathognomonic finding of merozoites arranged in a tetrad formation resembling a Maltese cross (arrow). Images in panels A and B obtained by using Wright's stain (original magnification ×100), For panel C, the CellaVision DM96 system (https://www.cellavision.com) and the Cellavision Remote Review Software version 6.0.1 build 7 were used to capture and display cells with abnormalities.

infected with *Anaplasma phagocytophilum* and cases of human granulocytic anaplasmosis also have been documented in Nova Scotia (*8*,*9*). This case of locally acquired *B. microti* infection adds another item to the menu of tickborne diseases in that Atlantic province. In absence of transovarial transmission in ticks with *B. microti*, expansion of the vector alone is unlikely to increase babesiosis cases unless sufficient amplification of the parasite is occurring in natural reservoirs. In northeast sections of North America, human infections caused by *B. microti* appear to be limited to the white-footed mouse, short-tailed shrew (*Blarina* spp.), and chipmunks (*Tamia striatus*) (*1*). Ongoing surveillance of tickborne disease in Atlantic Canada should include monitoring for *B. microti* in humans, ticks, and small mammals.

The discovery of *B. microti* infection in Atlantic Canada is important for multiple reasons. From a clinical perspective, physicians should be aware of the possibility of babesiosis occurring in the region, be able to recognize compatible symptoms, and be prepared to trigger proper investigations and implement therapeutic options when warranted. Because Lyme disease and anaplasmosis are already endemic in Nova Scotia, co-infections also should be considered if *B. microti* is detected; however, without evidence supporting the reciprocal conclusion, treatment of *B. microti* infection in cases of Lyme disease should only be considered if compatible with the clinical context (*8*,*9*). Ongoing surveillance, increased awareness, and education should be encouraged to better define and understand the changing epidemiology of tickborne diseases in Atlantic Canada.

Acknowledgments

We thank Jessica Lin for her technical expertise in conducting the PCR testing for this investigation.

About the Author

Dr. Allehebi is a 4th-year medical microbiology resident at Dalhousie University in Halifax.

References

1. Gray JS, Ogden NH. Ticks, human babesiosis and climate change. Pathogens. 2021;10:1430. https://doi.org/10.3390/pathogens10111430
2. Gray EB, Herwaldt BL. Babesiosis surveillance—United States, 2011–2015. MMWR Surveill Summ. 2019;68:1–11. https://doi.org/10.15585/mmwr.ss6806a1
3. Scott JD. First record of locally acquired human babesiosis in Canada caused by *Babesia duncani*: a case report. SAGE Open Med Case Rep. 2017;5:2050313X17725645.
4. Yang J, Smith C, Battad A. *Babesia microti* acquired in Canada. CMAJ. 2021;193:E1213–7. https://doi.org/10.1503/cmaj.201983
5. Bullard JM, Ahsanuddin AN, Perry AM, Lindsay LR, Iranpour M, Dibernardo A, et al. The first case of locally acquired tick-borne *Babesia microti* infection in Canada. Can J Infect Dis Med Microbiol. 2014;25:e87–9. https://doi.org/10.1155/2014/209521
6. Drews SJ, Van Caeseele P, Bullard J, Lindsay LR, Gaziano T, Zeller MP, et al. *Babesia microti* in a Canadian blood donor and lookback in a red blood cell recipient. Vox Sang. 2021.
7. Gasmi S, Ogden NH, Lindsay LR, Burns S, Fleming S, Badcock J, et al. Surveillance for Lyme disease in Canada: 2009–2015. Can Commun Dis Rep. 2017;43:194–9. https://doi.org/10.14745/ccdr.v43i10a01
8. Chase B, Bonnar P. A walk through the tall grass: a case of transaminitis, thrombocytopenia, and leukopenia resulting from an emerging zoonotic infection in Nova Scotia. J Assoc Med Microbiol Infect Dis Canada. 2018;3:247–50. https://doi.org/10.3138/jammi.2018-08.07.2

9. Guillot C, Badcock J, Clow K, Cram J, Dergousoff S, Dibernardo A, et al. Sentinel surveillance of Lyme disease risk in Canada, 2019: results from the first year of the Canadian Lyme Sentinel Network (CaLSeN). Can Commun Dis Rep. 2020;46:354–61. https://doi.org/10.14745/ccdr.v46i10a08
10. Bouchard C, Dibernardo A, Koffi J, Wood H, Leighton PA, Lindsay LRN. N Increased risk of tick-borne diseases with climate and environmental changes. Can Commun Dis Rep. 2019;45:83–9. https://doi.org/10.14745/ccdr.v45i04a02

Address for correspondence: David J. Haldane, Division of Microbiology, Department of Pathology and Laboratory Medicine Nova Scotia Health, 326A MacKenzie Building, 5788 University Ave, Halifax, NS B3H 1V8, Canada; email: david.haldane@nshealth.ca

Viral Zoonoses in Small Wild Mammals and Detection of Hantavirus, Spain

Silvia Herrero-Cófreces, François Mougeot, Tarja Sironen, Hermann Meyer, Ruth Rodríguez-Pastor, Juan José Luque-Larena

Author affiliations: Universidad de Valladolid, Palencia, Spain (S. Herrero-Cófreces, R. Rodríguez-Pastor, J.J. Luque-Larena); Instituto de Investigación en Recursos Cinegéticos, Ciudad Real, Spain (F. Mougeot); University of Helsinki, Helsinki, Finland (T. Sironen); Bundeswehr Institute of Microbiology, Munich, Germany (H. Meyer)

DOI: https://doi.org/10.3201/eid2806.212508

We screened 526 wild small mammals for zoonotic viruses in northwest Spain and found hantavirus in common voles (*Microtus arvalis*) (1.5%) and high prevalence (48%) of orthopoxvirus among western Mediterranean mice (*Mus spretus*). We also detected arenavirus among small mammals. These findings suggest novel risks for viral transmission in the region.

Wildlife viromes harbor potentially threatening zoonoses for humans that require increased effort in identification and surveillance (*1*). Rodents are considered main reservoirs of emerging zoonoses (*2*), and the large population fluctuations of reservoir species play a key role in modulating infection risk (*3*). Anthropogenic land-use changes, agricultural intensification, and irrigation also favor rodent invasions and risk for pathogen spillover (*4*). The common vole (*Microtus arvalis*) is a widespread rodent inhabiting intensified farming landscapes in northwestern Spain, where population numbers and pathogen prevalence lead to spillover of zoonotic bacteria such as *Francisella tularensis* and *Bartonella* spp. (*5*).

We report the prevalence of rodent-borne zoonotic viruses in Europe (i.e., hantavirus, arenavirus [lymphocytic choriomeningitis virus (LCMV)], and orthopoxvirus) (*6*) among the small mammals inhabiting farming landscapes. We also report the effect of natural fluctuations of common vole numbers on viral prevalence (phase dependence). Our study was conducted in intensively farmed landscapes, in the Tierra de Campos region of Castilla-y-León, northwestern Spain (*7*), where the small mammal population is mainly composed of 4 species: common vole, long-tailed field mouse (*Apodemus sylvaticus*), western Mediterranean mouse (*Mus spretus*), and greater white-toothed shrew (*Crocidura russula*) (*7*).

We live-trapped small mammals during March 2013–March 2019. We collected samples from blood, spleen, liver, and lungs by using standard protocols and stored them at –23°C until molecular analysis could be performed (Appendix, https://wwwnc.cdc.gov/EID/article/28/6/21-2508-App1.pdf). We owned all necessary licenses and permits for conducting this study.

We detected specific hantavirus, LCMV, and orthopoxvirus IgG in serum samples by using immunofluorescence assay. We used fluorescein isothiocyanate (FITC) anti-IgG as a secondary antibody and evaluated all slides under a fluorescence microscope. For molecular analysis, we isolated RNA from liver and lung tissues and DNA from a mix of liver and spleen. We performed single-step reverse transcription PCR (RT-PCR) for LCMV detection in the liver, nested reverse transcription PCR for hantavirus detection in lung samples, and conventional pan-poxvirus PCR method followed by an additional orthopoxvirus-specific PCR for orthopoxvirus detection in the mix samples. We used generalized linear models to test variations of prevalence between species and calculate prevalence in common voles according to host sex (male or female), trapping month (March, July, or November), and population density phase (increase, peak, or crash).

We screened 526 individual animals from 4 species for the presence of 3 viruses (Table; Appendix). We found evidence of hantavirus infection only in

Table. Prevalence of hantavirus, arenavirus (LCMV), and orthopoxvirus in 4 small mammal species from the Tierra de Campos region, Castilla-y-León, northwest Spain, 2013–2019*

Species	Common name	Virus	Prevalence		
			Screening method	No. positive/screened	% Positive (95% CI)
Apodemus sylvaticus	Long-tailed field mouse	LCMV	IFA	2/34	5.9 (0.7–19.7)
			PCR	0/2	Not tested
		Hantavirus	IFA	0/34	Not tested
			PCR	Not tested	Not tested
		Orthopoxvirus	IFA	0/34	Not tested
			PCR	Not tested	Not tested
Crocidura russula	Greater white-toothed shrew	LCMV	IFA	0/7	Not tested
			PCR	1/9	11.1 (0.3–48.2)
		Hantavirus	IFA	0/7	Not tested
			PCR	0/9	Not tested
		Orthopoxvirus	IFA	0/7	Not tested
			PCR	Not tested	Not tested
Microtus arvalis	Common vole	LCMV	IFA	8/382	2.1 (0.9–4.1)
			PCR	2/89	2.2 (0.3–7.9)
		Hantavirus	IFA	3/382	0.8 (0.2–2.3)
			PCR	4/62	6.5 (1.8–15.7)
		Orthopoxvirus	IFA	5/382	1.3 (0.4–3.0)
			PCR	0/243	Not tested
Mus spretus	Western Mediterranean mouse	LCMV	IFA	0/25	Not tested
			PCR	Not tested	Not tested
		Hantavirus	IFA	0/25	Not tested
			PCR	Not tested	Not tested
		Orthopoxvirus	IFA	12/25	48.0 (27.8–68.7)
			PCR	Not tested	Not tested
All hosts		LCMV	All tests	13/526	2.5 (1.3–4.2)
		Hantavirus	All tests	7/458	1.5 (0.6–3.1)
		Orthopoxvirus	All tests	17/510	3.3 (2.0–5.3)

*LCMV, lymphocytic choriomeningitis virus.

common voles, at an average prevalence of 1.6% (95% CI 0.6%–3.3%; 7/438). Positive results for LCMV infection (either by immunofluorescence assay or PCR) were detected in 5.9% (95% CI 0.7%–19.7%) of long-tailed field mice (2/34, 11.1% (95% CI 0.7%–48.2%) of shrews (1/9), and 2.2% (95% CI 1.1%–4.0%) of common voles (10/458). Orthopoxvirus IgG was present in 1.3% (95% CI 0.4%–3.0%) of common voles (5/382) and in 48% (95% CI 27.8%–68.7%) of western Mediterranean mice (12/25), and we observed significant differences between both species (χ^2 = 59.643, d.f. = 3; p < 0.001). In long-tailed field mice, we only detected LCMV during summer (July). In common voles, we found no effect of cycle phase or month on virus prevalence (Appendix), but LCMV prevalence differed between sexes (χ^2 = 5.189, d.f. = 1; p = 0.023) and was higher in males (3.7%; 95% CI 1.6%–7.1%) than in females (0.8%; 95% CI 0.1%–0.3%).

Recent surveys of viral zoonoses in Spain have shown low antibody prevalence of LCMV (1.7%) (*8*) and hantavirus (0.06%) (*9*) among humans. Hantavirus antibodies were detected in red foxes (*Vulpes vulpes*) (*10*), and LCMV antibodies were detected in long-tailed field mice and red foxes (*8*,*10*). Our study detected hantavirus in a wild rodent reservoir in Spain. The reported prevalence was low (1.6%) and did not differ between the phases of the common vole population cycle. However, the cyclic dynamic of this rodent host, which harbored all 3 virus species screened, may influence the risks associated with contact with infected rodents. Common voles can reach densities of up to 1,000 per hectare during population peaks, so the infected proportion may become a considerable public health concern. Orthopoxvirus infection risk is of growing concern in Europe because of the absence of smallpox vaccination among the human population <45 years of age (*6*). Because half of all the western Mediterranean mice analyzed were positive for orthopoxvirus, the potential transmission risk for the virus from this rodent to humans should be considered and further confirmed with larger sample sizes.

Further investigation is required regarding the molecular nature and infectivity of the hantavirus and orthopoxvirus detected, as well as their circulation pathways, which will help to uncover possible transmission routes and determine more precisely the level of infection risk to human populations. Our results can be used by local authorities to refine virus surveillance, including clinical diagnosis of new viruses, and improve public health strategies to prevent and minimize zoonotic risks for persons living in areas recurrently affected by outbreaks linked to common voles.

Acknowledgments

We thank Hussein Alburkat for helping with immunologic assays and the Instituto de Salud Carlos III for collaborating with DNA extraction.

This work was funded by the projects ECOTULA (grant no. CGL2015-66962-C2-1-R) and BOOMRAT (grant no. PID2019-109327RB-I00) funded by the Government of Spain, and GESINTTOP, co-funded by Instituto Tecnológico Agrario de Castilla-y-León–Junta de Castilla-y-León, Diputación Provincial de Palencia, and Diputación Provincial de Valladolid. S.H.C. was supported by a Ph.D. studentship from Junta de Castilla-y-León (co-funded by the European Social Fund) and an Erasmus+ Mobility grant. R.R.P. was supported by a PhD studentship from the University of Valladolid (co-funded by Banco Santander).

About the Author

Ms. Herrero-Cófreces is a biologist and doctoral student in the Department of Agroforestry Sciences at the University of Valladolid in Palencia, Spain. Her primary research interests include rodents, rodent-borne diseases, and ecology of zoonoses.

References

1. Carroll D, Daszak P, Wolfe ND, Gao GF, Morel CM, Morzaria S, et al. The global virome project. Science. 2018;359:872–4. https://doi.org/10.1126/science.aap7463
2. Han BA, Schmidt JP, Bowden SE, Drake JM. Rodent reservoirs of future zoonotic diseases. Proc Natl Acad Sci U S A. 2015;112:7039–44. https://doi.org/10.1073/pnas.1501598112
3. Cavanagh RD, Lambin X, Ergon T, Bennett M, Graham IM, van Soolingen D, et al. Disease dynamics in cyclic populations of field voles (*Microtus agrestis*): cowpox virus and vole tuberculosis (*Mycobacterium microti*). Proc R Soc London Ser B Biol Sci. 2004;271:859–67.
4. Faust CL, McCallum HI, Bloomfield LSP, Gottdenker NL, Gillespie TR, Torney CJ, et al. Pathogen spillover during land conversion. Ecol Lett. 2018;21:471–83. https://doi.org/10.1111/ele.12904
5. Herrero-Cófreces S, Mougeot F, Lambin X, Luque-Larena JJ. Linking zoonosis emergence to farmland invasion by fluctuating herbivores: common vole populations and tularemia outbreaks in NW Spain. Front Vet Sci. 2021;8:698454. https://doi.org/10.3389/fvets.2021.698454
6. Kallio-Kokko H, Uzcategui N, Vapalahti O, Vaheri A. Viral zoonoses in Europe. FEMS Microbiol Rev. 2005;29:1051–77. https://doi.org/10.1016/j.femsre.2005.04.012
7. Rodríguez-Pastor R, Luque-Larena JJ, Lambin X, Mougeot F. "Living on the edge": the role of field margins for common vole (*Microtus arvalis*) populations in recently colonised Mediterranean farmland. Agric Ecosyst Environ. 2016;231:206–17. https://doi.org/10.1016/j.agee.2016.06.041
8. Lledó L, Gegúndez MI, Saz JV, Bahamontes N, Beltrán M. Lymphocytic choriomeningitis virus infection in a province of Spain: analysis of sera from the general population and wild rodents. J Med Virol. 2003;70:273–5. https://doi.org/10.1002/jmv.10389
9. Lledó L, Klingström J, Gegúndez MI, Plyusnina A, Vapalahti O, Saz JV, et al. Hantavirus infections in Spain: analysis of sera from the general population and from patients with pneumonia, renal disease and hepatitis. J Clin Virol. 2003;27:296–307. https://doi.org/10.1016/S1386-6532(02)00228-7
10. Lledó L, Serrano JL, Giménez-Pardo C, Gegúndez I. Wild red foxes (*Vulpes vulpes*) as sentinels of rodent-borne hantavirus and lymphocytic choriomeningitis virus in the province of Soria, northern Spain. J Wildl Dis. 2020;56:658–61. https://doi.org/10.7589/2019-09-239

Address for correspondence: Silvia Herrero-Cófreces, Departamento de Ciencias Agroforestales, Escuela Técnica Superior de Ingenierías Agrarias, Universidad de Valladolid, Avenida de Madrid 50, Palencia, E-34004, Spain; email: silvia.herrero.cofreces@uva.es

Detecting SARS-CoV-2 Omicron B.1.1.529 Variant in Wastewater Samples by Using Nanopore Sequencing

Lasse D. Rasmussen, Stine R. Richter, Sofie E. Midgley, Kristina T. Franck

Author affiliation: Statens Serum Institut, Copenhagen, Denmark

DOI: https://doi.org/10.3201/eid2806.220194

We report wastewater surveillance for SARS-CoV-2 variants of concern by using mutation-specific, real-time PCR and rapid nanopore sequencing. This surveillance might be useful for an early warning in a scenario in which a new variant is emerging, even in areas that have low virus incidences.

To limit spread of novel SARS-CoV-2 variants such as Omicron B.1.1.529, early detection is crucial. Wastewater surveillance has been suggested as an early warning system for SARS-CoV-2 spread in low-prevalence areas or communities where human testing is limited (*1*).

We provide a method to rapidly determine the presence of Omicron in wastewater samples that have low viral load, in which the Omicron genome

represents a minor fraction of the total SARS-CoV-2 genomes. Unlike previously published methods relying on time-consuming, full-genome sequencing and complex variant analysis (2), we used a metagenomics approach of long reads containing all differentiating mutations.

For the wastewater surveillance system in Denmark, 24-hour composite samples are collected 3 times/week at the inlet of wastewater treatment plants (WWTPs) throughout the country. Initial RNA purification and real-time quantitative reverse transcription PCR (RT-PCR) analysis is performed by a commercial laboratory (Eurofins Environment Testing Denmark, https://www.eurofins.com), and RNA from SARS-CoV-2–positive wastewater samples is sent to Statens Serum Institut (SSI) for variant analysis.

On November 26, 2021, the Word Health Organization declared Omicron to be a variant of concern (3). On November 29, the commercial laboratory initiated prescreening of wastewater samples for Omicron by using a real-time quantitative RT-PCR targeting the K417N amino acid substitution. Based on the mutation scheme reported by the World Health Organization on November 26, K417N was present in Omicron but absent in Delta, the predominant variant in Denmark at the time (4). K417N has been detected in 69.3% of Omicron overall but in 94.9% of the dominant sublinage in Denmark, BA.2 (5).

On November 30, samples from 3 WWTPs showed weak positive signals for the K417N mutation; cycle threshold values were 38.6 for WWTP1, 37.2 for WWTP2, and 39.9 for WWTP2. Cycle threshold values from the K417R assay were 32.1 for WWTP1, 32.5 for WWTP2, and 36.8 for WWTP2. A quantitative RT-PCR targeting the RNA dependent RNA polymerase gene determined viral loads for the 3 samples to be 5,400 genomes/L for WWTP1, 5,800 genomes/L for WWTP2, and 3,000 genomes/L for WWTP3. Only WWTP2 had suspected infection with Omicron among persons living in the catchment area (based on a spike gene dropout PCR performed at the Danish National COVID Test Center). For WWTP1 and WWTP3, the closest suspected case-patients resided 20 km from the catchment area.

Because Delta cases that have the K417N aa substitution have been detected sporadically in Denmark, in addition to the limitations mentioned above, the K417N variant PCR is not sufficient to confirm the presence of Omicron in wastewater samples. Therefore, purified RNA from K417N positive samples was transported to SSI by courier for confirmation by sequencing. A metagenomics approach was used, amplifying a 1,049-nt fragment of the spike gene, including part of the receptor-binding domain (nt 22799–23847 [GenBank accession no. NC_045512.2_Wuhan-Hu-1], aa 412–761).

We used a modification of a protocol developed for Sanger sequencing (6). In brief, we used a Superscript IV One-Step PCR (Invitrogen, https://www.thermofisher.com). The PCR mixture contained 10 μL Platinum SuperFi RT-PCR Master Mix, 1 μL each of primers nCoV-2019_76_LEFT_alt3 and nCoV-2019_78_RIGHT (final concentration 0.4 μmol/L) artic primers v3 (7), 0.5 μL SuperScript IV RT Mix, 1.5 μL nuclease-free water, and 5 μL 5× diluted RNA from wastewater samples. PCR conditions were as reported (5). PCR products were bead purified before library preparation using Agencourt AMPure XP (Beckman Coulter, https://www.beckmancoulter.com).

We prepared libraries by using the Rapid Barcoding Sequencing Kit (Oxford Nanopore Technologies, https://nanoportech.com) according to the manufacturer's protocol and omitting optional steps. Libraries were loaded onto R9.4.1 flow cells (Oxford Nanopore Technologies). We performed sequencing on a GridION (Oxford Nanopore Technologies) by using high-accuracy basecalling. We analyzed generated reads continuously every hour for the first 3 hours and mapped reads against references, including the Delta and Omicron variants. We performed mapping and consensus extractions by using CLC Genomics Workbench version 21.0.4 (Long Read Support [β] plugin; QIAGEN, https://www.qiagen.com). We used

Table. Results of read mapping and consensus sequence analysis for detection of SARS-CoV-2 Omicron B.1.1.529 variant in 2 wastewater treatment plants, Denmark*

Sequencing Time, hours	Wastewater treatment plant 1			Wastewater treatment plant 2		
	Mapped reads		Omicron mapping consensus mutations	Mapped reads		Omicron mapping consensus mutations
	Delta	Omicron		Delta	Omicron	
1	17122	783	T23104A, **C23202A, C23525T, C23604A**	21743	1292	**C23202A, C23525T, C23604A**
2	30980	1446	**T23075C, C23202A, C23525T, C23604A**	40040	2326	C22971T, **T23075C, C23202A, C23525T, C23604A**
3	41320	1967	**T23075C, C23202A, C23525T, C23604A**	58254	3453	G22992C, **C22995A, T23075C, C23202A, C23525T, C23604A**

*Boldface indicates Omicron-specific mutations. Mutation A23403G was omitted because it is present in Delta and Omicron, but it was present in all consensus sequences.

NextClade (*8*) for typing consensus sequences and mutation detection (Table).

At every analysis point, 4.5% of reads mapped as Omicron at WWTP1 and 5.6% at WWTP2. Few (<100) reads from WWTP3 mapped to any SARS-CoV-2 references, probably because of low viral load. Within 1 hour of sequencing (≈3 hours after RNA samples arrived at SSI and 9 hours after wastewater sample collection), 3 identical Omicron-specific mutations (C23202A, C23525T, and C23604A) were detected in the consensus sequences of WWTP1 and WWTP2 (Table). After 2 hours, a single additional Omicron mutation was found in both WWTPs. For WWTP2, one additional mutation was detected after 3 hours (Table). Omicron confirmed by whole-genome sequencing was detected in humans in the catchment areas of WWTP1 on December 12 and WWTP2 December 6. Our results show that this rapid metagenomics-like method can detect SARS-CoV-2 variants n a small fraction of the population, even at low viral loads.

In conclusion, we have demonstrated wastewater surveillance for SARS-CoV-2 variants by using a setup combining mutation-specific, real-time PCR and rapid nanopore sequencing. This surveillance might serve as an early warning system in a scenario in which a known variant is emerging, even in areas with low incidence.

Acknowledgments

We thank Cecilie Muss and Tina Christoffersen for providing excellent technical assistance, Louise S. Nørgaard for collaborating in implementation of the prescreening PCR at Eurofins, and the Danish COVID-19 Genome Consortium for providing sequences from the human cases in the catchment areas.

About the Author

Dr. Rasmussen is a molecular biologist and a senior scientist at Statens Serum Institut, Copenhagen, Denmark. His primary research interests are emerging viruses and monitoring of SARS-CoV-2 in Denmark.

References

1. Farkas K, Hillary LS, Malham SK, McDonald JE, Jones DL. Wastewater and public health: the potential of wastewater surveillance for monitoring COVID-19. Curr Opin Environ Sci Health. 2020;17:14–20. https://doi.org/10.1016/j.coesh.2020.06.001
2. Izquierdo-Lara R, Elsinga G, Heijnen L, Munnink BB, Schapendonk CM, Nieuwenhuijse D, et al. Monitoring SARS-CoV-2 circulation and diversity through community wastewater sequencing, the Netherlands and Belgium. Emerg Infect Dis. 2021;27:1405–15. https://doi.org/10.3201/eid2705.204410
3. World Health Organization. Enhancing readiness for Omicron (B.1.1.529): technical brief and priority actions for member state [cited 2022 Mar 30]. https://www.who.int/news/item/26-11-2021-classification-of-omicron-(b.1.1.529)-sars-cov-2-variant-of-concern
4. Danish COVID-19 Genome Consortium. Genomic overview of SARS-CoV-2 in Denmark [cited 2022 Mar 30]. https://www.covid19genomics.dk/statistics
5. Outbreak information. A standardized, open-source database of COVID-19 resources and epidemiologic data [cited 2022 Mar 17], https://outbreak.info
6. Jørgensen TS. 2021. Sanger sequencing of a part of the SARS-CoV-2 spike protein [cited 2022 Mar 30]. https://doi.org/10.17504/protocols.io.bsbdnai6
7. Github. ARTIC nanopore protocol for nCoV2019 novel coronavirus [cited 2022 Mar 30]. https://github.com/artic-network/artic-ncov2019/blob/master/primer_schemes/nCoV-2019/V3/nCoV-2019.tsv
8. Aksamentov I, Roemer C, Hodcroft EB, Neher RA. Nextclade: clade assignment, mutation calling and quality control for viral genomes. J Open Source Softw. 2021;6:3773. https://doi.org/10.21105/joss.03773

Address for correspondence: Lasse D. Rasmussen, Statens Serum Institut, Artillerivej 5, DK-2300 Copenhagen S, Denmark; email: lara@ssi.dk

Identifying Japanese Encephalitis Virus Using Metatranscriptomic Sequencing, Xinjiang, China

Yi Yan,[1] Rongjiong Zheng,[1] Haizhou Liu, Zhiyong Wu, Mengchan Hao, Li Ma, Liying Wang, Jie Gao, Yining Yang, Di Liu, Xiaobo Lu

Author affiliations: Wuhan Institute of Virology, Wuhan, China (Y. Yan, H. Liu, Z. Wu, M. Hao, L. Ma, L. Wang, J. Gao, D. Liu); University of Chinese Academy of Sciences, Beijing, China (Y. Yan, Z. Wu, M. Hao, L. Ma, L. Wang, D. Liu); First Affiliated Hospital of Xinjiang Medical University, Urumqi, China (R. Zheng, Y. Yang, D. Liu, X. Lu); People's Hospital of Xinjiang Uygur Autonomous Region, Urumqi (Y. Yang).

DOI: https://doi.org/10.3201/eid2806.210616

[1]These authors contributed equally to this article.

The treat of infectious disease epidemics has increased the critical need for continuous broad-ranging surveillance of pathogens with outbreak potential. Using metatranscriptomic sequencing of blood samples, we identified several cases of Japanese encephalitis virus infection from Xinjiang Uyghur Autonomous Region, China. This discovery highlights the risk for known viral diseases even in nonendemic areas.

Epidemics of infectious viral diseases seriously threaten human health and safety as well as social stability and development. In recent years, outbreaks of diseases such as influenza A(H7N9) (*1*), Ebola disease (*2*), and COVID-19 (*3*) have emphasized the need to continuously monitor potential pathogens in nature and pathogens known to circulate in human populations. Metagenomic sequencing (mNGS), because of its simplicity, low cost, and unbiased screening qualities, has been widely applied to identify pathogens for diagnosis and research. mNGS can simultaneously sequence multiple isolates, so it does not require anticipation of a specific disease cause, unlike conventional targeted-pathogen detection methods. mNGS can also analyze host immune response and the existence of antimicrobial resistance genes (*4*).

We used mNGS for routine screening for tick-related pathogens in Xinjiang Province, China. We tested 10/25 retained blood samples collected from previously infected patients who had been bitten by ticks. Using Kraken2 (*5*), we preliminarily identified abundant amounts of 7 pathogens potentially associated with human disease: Proteus virus Isfahan, Japanese encephalitis virus (JEV), *Mycobacterium tuberculosis*, *Clostridium tetani*, hepatitis C virus (HCV), *Streptacidiphilus bronchialis*, and *Staphylococcus aureus* (Appendix Figure 1, https://wwwnc.cdc.gov/EID/article/28/6/21-0616-App1.pdf). At the same time, a de novo assembly used with BLAST-based methodology (https://blast.ncbi.nlm.nih.gov/Blast.cgi) found several human disease–related viruses: JEV, HCV, Crimean-Congo hemorrhagic fever virus, and human gammaherpesvirus 4.

After we observed JEV and HCV in results from both methods, we confirmed presence of the 2 viruses based on results from a mapping-based method using Bowtie2 (*6*). The average coverage of JEV genome in 8 samples was 59.3%, and the coverage in sample 6 (GenBank accession no. MW766363) reached 99.5% (Appendix Figure 2). HCV was mapped only in sample 8 (GenBank accession no. MW766365). The results of JEV and HCV genome mapping were highly consistent with those using mNGS and the de novo assembly.

Because of some inconsistent etiologic findings, we used different approaches to validate the presence of the other pathogens. Coverage of Crimean-Congo hemorrhagic fever virus reached an average of 15.6%, but the concentrated regions were highly homologous to human-sorting nexin 10. Coverage of human gammaherpesvirus 4 was negligible, <0.15%. Although Proteus virus Isfahan was abundant in reads, the signals detected were concentrated in regions 13608–13909 and 39231–39841, which had high similarity with human long noncoding RNA LHRI_lnC2063.9. As for the other 4 bacteria, we identified almost no homologous contigs by assembly, and the only contig related to *Staphylococcus aureus* in sample 10 was completely consistent with the origin sequence of *Homo sapiens* isolate CHM13 chromosome 21. The mapping approach showed <0.001 coverage of all 4 genomes and genome distribution was very scattered and low in depth (usually <10×) and showed no active expression of any specific genes.

After gradual analysis and verification, we confirmed that there were JEV nucleic acids in some of these samples. Although confirming infection using JEV-specific antibody testing would have been ideal, extensive hemolysis of the samples precluded this testing. We reviewed the clinical manifestations of these patients, some of whom had fever, headache, and other signs and symptoms consistent only with mild JEV infections.

Phylogenetic analysis of the JEV envelope gene showed that the viruses belonged to the G3 genotype (Figure), not G1, which has dominated epidemics since the 1950s (*7*). Because we did not rule out the history of vaccination among these patients and there is no JEV vaccination policy in Xinjiang, the genetic similarity between these strains and the G3 vaccine strain SA 14-14-2 suggested that vaccinated travelers might have imported (*7*) and shed the virus. Large numbers of imported JEV cases in nonendemic areas have been reported elsewhere (*8*).

These overlapping or inconsistent results might indicate some limitations in the use of a single method for metagenomic analysis, suggesting that although mNGS has been widely used, careful judgments are still necessary to avoid clinical misdiagnosis. In particular, when co-infection exists, such as JEV and HCV co-infection noted in this study, clinically misdiagnosing any pathogen might lead to serious medical consequences. Introducing unbiased mNGS testing into clinical practice should improve the rigor of analysis.

Our study could not accurately determine the source or vectors of these JEV infections; ticks are

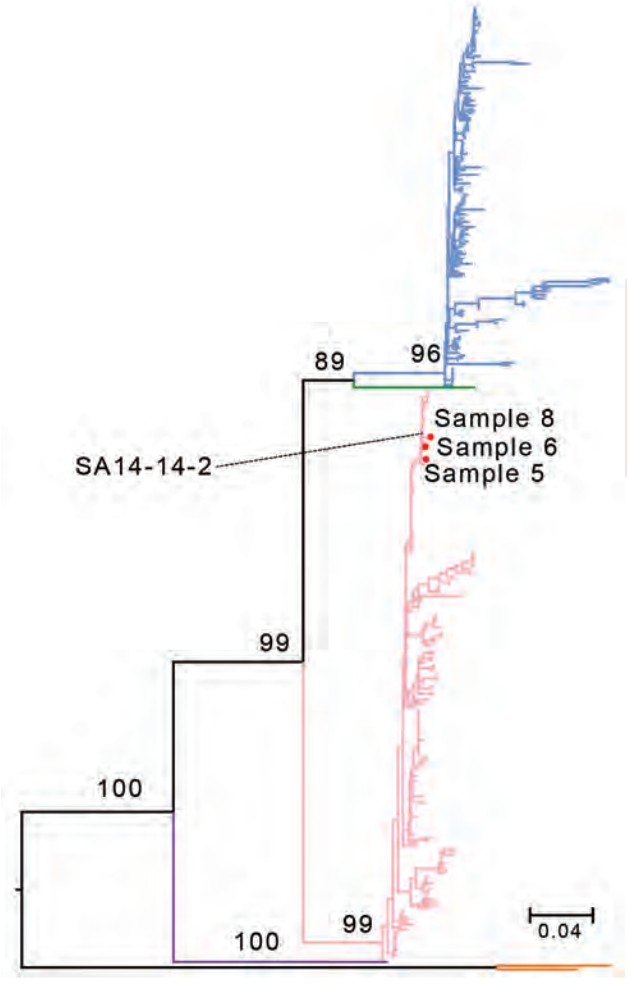

Figure. Maximum-likelihood tree based on the nucleic acid sequences of the Japanese encephalitis virus (JEV) envelope gene for 3 samples from persons in Xinjiang, Uyghur Autonomous Region, China (samples 5, 6, and 8), and reference sequences. SA 14-14-2 is the JEV vaccine strain. The branch colors represent different JEV genotypes: blue branches indicate genotype 1; green, genotype 2; pink, genotype 3; purple, genotype 4; and orange, genotype 5. Values at nodes are bootstrap values supporting the branch. Scale bar indicates the substitution rate of equal-length branches.

not JEV hosts (*9*), and no mosquito species known to transmit JEV has been reported in Xinjiang (*10*). Despite our lack of information on the sources in these cases, our findings prompt us to strongly recommend strengthening surveillance for JEV and other emerging and reemerging pathogens in this region to prevent and neutralize the threat from pathogens before they cause public health incidents.

Acknowledgments

We thank Lei Zhang of the core facility and technical support at Wuhan Institute of Virology for assistance with experimental platform.

The work was supported by grants nos. 31970548, 91631110, and 82060115 from the National Natural Science Foundation of China.

About the Author

Dr. Yan is a PhD student at the Key Laboratory of Special Pathogens and Biosafety, Wuhan Institute of Virology, Center for Biosafety Mega-Science, Chinese Academy of Sciences. Her research interests focus mainly on detecting unknown pathogens and metagenomics.

References

1. Wang X, Jiang H, Wu P, Uyeki TM, Feng L, Lai S, et al. Epidemiology of avian influenza A H7N9 virus in human beings across five epidemics in mainland China, 2013–17: an epidemiological study of laboratory-confirmed case series. Lancet Infect Dis. 2017;17:822–32. https://doi.org/10.1016/S1473-3099(17)30323-7
2. Ni M, Chen C, Qian J, Xiao H-X, Shi W-F, Luo Y, et al. Intra-host dynamics of Ebola virus during 2014. Nat Microbiol. 2016;1:16151. https://doi.org/10.1038/nmicrobiol.2016.151
3. Zhou P, Yang X-L, Wang X-G, Hu B, Zhang L, Zhang W, et al. A pneumonia outbreak associated with a new coronavirus of probable bat origin. Nature. 2020;579:270–3. https://doi.org/10.1038/s41586-020-2012-7
4. Lu B, Yan Y, Dong L, Han L, Liu Y, Yu J, et al. Integrated characterization of SARS-CoV-2 genome, microbiome, antibiotic resistance and host response from single throat swabs. Cell Discov. 2021;7:19. https://doi.org/10.1038/s41421-021-00248-3
5. Wood DE, Salzberg SL. Kraken: ultrafast metagenomic sequence classification using exact alignments. Genome Biol. 2014;15:R46. https://doi.org/10.1186/gb-2014-15-3-r46
6. Langmead B, Salzberg SL. Fast gapped-read alignment with Bowtie 2. Nat Methods. 2012;9:357–9. https://doi.org/10.1038/nmeth.1923
7. Wu R, Wang Q, Liu H, Chai C, He B, Huang X, et al. Phylogenetic analysis reveals that Japanese encephalitis virus genotype III is still prevalent in swine herds in Sichuan province in China. Arch Virol. 2016;161:1719–22. https://doi.org/10.1007/s00705-016-2814-y
8. Tiwari S, Singh RK, Tiwari R, Dhole TN. Japanese encephalitis: a review of the Indian perspective. Braz J Infect Dis. 2012;16:564–73. https://doi.org/10.1016/j.bjid.2012.10.004
9. Misra UK, Kalita J. Overview: Japanese encephalitis. Prog Neurobiol. 2010;91:108–20. https://doi.org/10.1016/j.pneurobio.2010.01.008
10. Xia H, Wang Y, Atoni E, Zhang B, Yuan Z. Mosquito-associated viruses in China. Virol Sin. 2018;33:5–20.

Address for correspondence: Xiaobo Lu, Xinjiang Medical University Affiliated First Hospital, Li Yu Shan South Road No.137, Urumqi, 830000, China; email: xjykdluxiaobo@126.com; Di Liu, Wuhan Institute of Virology, Chinese Academy of Sciences, Xiao Hong Shan No. 44, Wuchang District, Wuhan, 430071, China; email: liud@wh.iov.cn.

Expansion of L452R-Positive SARS-CoV-2 Omicron Variant, Northern Lombardy, Italy

Federica Novazzi, Andreina Baj, Angelo Genoni, Daniele Focosi, Fabrizio Maggi

Author affiliations: Azienda Socio Sanitaria Territoriale, Sette Laghi, Varese, Italy (F. Novazzi, A. Baj, A. Genoni, F. Maggi); University of Insubria, Varese (F. Novazzi, A. Baj, A. Genoni, F. Maggi); Pisa University Hospital, Pisa, Italy (D. Focosi).

DOI: https://doi.org/10.3201/eid2806.220210

We report 25 cases of infection with SARS-CoV-2 Omicron variant containing spike protein L452R mutation in northern Lombardy, Italy. Prevalence of this variant was >30% in this region, compared with <0.5% worldwide. Many laboratories are using previously developed L452R-specific PCRs to discriminate Omicron from Delta mutations, but these tests may be unreliable.

According to PANGOlin phylogeny, the SARS-CoV-2 Omicron variant of concern (VOC) consists of B.1.1.529 sublineages BA.1, in which there are 36 further sublineages; BA.2, sometimes called stealth Omicron or Omicron 2, with 3 further sublineages), and BA.3. As of April 2, 2022, among the ≈2 million Omicron sequences deposited in GISAID, spike mutation L452R (S:L452R) had been reported at <0.5% prevalence in BA.1 (425 cases), BA.1.1 (1,441), BA.1.17 (630), BA.1.15 (1,848), BA.1.1.15 (67), BA.1.15.1 (571), BA.1.14 (123), BA.1.1.1 (150), BA.1.1.2 (30), BA.1.16 (116), BA.1.1.14 (138), BA.1.1.13 (107), BA.1.1.16 (40), BA.1.1.11 (117), BA.1.13 (38), BA.1.1.12 (11), BA.1.9 (430), BA.1.12 (73), BA.1.9 (430), BA.1.12 (73), BA.1.1.10 (11), B.1.13.1 (5), BA.1.1.4 (1), BA.1.1.8 (24), BA.1.1.3 (6), BA.1.3 (3), BA.1.5 (1), BA.1.1.7 (8), BA.1.6 (4), BA.1.1.5 (1), BA.1.2 (3), BA.1.4 (1), BA.1.16.1 (1), BA.2 (125), and BA.2.3 (22).

The microbiology laboratory at Azienda Socio Sanitaria Territoriale (ASST), Sette Laghi (Territorial Social Health Authority of the Seven Lakes; Varese, Italy), which serves a wide area of the northern Lombardy region of Italy, has started a whole-genome next-generation sequencing (NGS) program for SARS-CoV-2–positive patients who seek care at emergency departments, as well as healthcare workers and patients in selected wards at 5 referral hospitals. During December 3, 2021–January 27, 2022, we identified 301 patients who tested positive by qualitative real-time reverse transcription PCR, then had blood samples undergo NGS; 220 samples were positive for Delta VOC and 81 for Omicron VOC. Among the Omicron cases, 25 were positive for spike mutation L452R (S:L452R) (Table). Of the sequences that we deposited in the GISAID database (https://www.gisaid.org), 17 belonged to PANGOlin sublineage BA.1, 3 to BA.1.1, 2 to BA.3, and 3 to undetermined sublineages. This proportion corresponded to a L452R prevalence of

Table. Patient demographics and SARS-CoV-2 phylogeny for 25 patients who tested positive for L452R-positve Omicron variant infection, northern Lombardy, Italy*

Patient no.	Date	Age, y/sex	Symptoms	NextStrain	PANGOlin	GISAID accession no.
1	2021 Dec 3	41/F	NA	21K	BA.1	EPI_ISL_9319568
2	2022 Jan 3	80/M	Fever	21K	BA.1	EPI_ISL_9306683
3	2022 Jan 3	43/F	Chest pain, diarrhea	21K	BA.1	EPI_ISL_9306774
4	2022 Jan 3	64/M	Fever and dyspnea	21K	BA.1	EPI_ISL_9319248
5	2022 Jan 3	52/F	NA	21K	BA.1	EPI_ISL_9306775
6	2022 Jan 3	55/M	Syncope (multiple sclerosis)	21K	BA.1	EPI_ISL_9306776
7	2022 Jan 3	65/F	NA	21K	BA.1	EPI_ISL_9322734
8	2022 Jan 3	48/F	Headache	21M	None	EPI_ISL_9323426
9	2022 Jan 3	31/F	NA	21M	None	EPI_ISL_9319319
10	2022 Jan 3	37/M	NA	21K	BA.1	EPI_ISL_9319384
11	2022 Jan 3	14/M	NA	21K	BA.1	EPI_ISL_9323297
12	2022 Jan 3	53/M	NA	21K	BA.1	EPI_ISL_9323497
13	2022 Jan 3	73/M	NA	21M	BA.3	EPI_ISL_9324184
14	2022 Jan 3	78/M	None	21K	BA.1	EPI_ISL_9306777
15	2022 Jan 3	82/F	None	21K	BA.1	EPI_ISL_9307474
16	2022 Jan 12	70/F	Dyspnea	21K	BA.1	EPI_ISL_9319456
17	2022 Jan 17	87/M	Right pneumonia	21K	BA.1	EPI_ISL_9324185
18	2022 Jan 19	92/M	NA	21K	BA.1	EPI_ISL_9323128
19	2022 Jan 19	2/F	NA	21K	BA.1.1	EPI_ISL_9309942
20	2022 Jan 19	47/F	NA	21K	BA.1.1	EPI_ISL_9323348
21	2022 Jan 19	45/M	NA	21M	BA.1	EPI_ISL_9324374
22	2022 Jan 19	26/M	NA	21M	None	EPI_ISL_9324445
23	2022 Jan 24	23/M	Fever (multiple sclerosis)	21K	BA.1.1	EPI_ISL_9310402
24	2022 Jan 24	22/F	NA	21K	BA.1	EPI_ISL_9323222
25	2022 Jan 24	1/F	Cough	20B	BA.3	EPI_ISL_9324518

*NA, not available.

31% (25 of 81 Omicron-positive participants in our study), compared with <0.5% worldwide. The wide heterogeneity in viral sequences excluded the likelihood of local transmission chains and supported the hypothesis of multiple introductions and convergent gene evolution.

The Omicron VOC leads to lower hospitalization and intensive care unit admission rates than some other VOCs, although it is resistant to most spike monoclonal antibodies (A. Peralta-Santos, unpub. data, https://doi.org/10.1101/2022.01.20.477163). To be effective, sotrovimab and small chemical antivirals have to be administered in the first days after onset of symptoms (D.K. Rai, unpub. data, https://www.biorxiv.org/content/10.1101/2022.01.17.476644v1), a timeframe not compatible with that needed to perform and receive results from spike or whole-genome NGS.

Attempts are underway to develop Omicron-specific PCRs, but in the interim, many laboratories are exploiting previously developed, commercially available, variant-specific PCRs to more promptly discriminate Omicron from Delta variants, an approach that relies on identifying the S: L452R mutation. Convergent evolution has led S: L452 mutations to occur in time across many different variants of interest (e.g., L452R in SARS-CoV-2 Iota and Epsilon and L452Q in Lambda), accounting for an overall 60% prevalence among SARS-CoV-2 isolates deposited in GISAID as of January 30, 2022. However, under the current simplified understanding of the variant landscape, it had been supposed that L452R mutations occurred in nearly all Delta samples across hundreds of AY sublineages, but not in Omicron samples. Our data clearly show that the approaches now being use currently are at risk of becoming unreliable for identifying variants because of gaps in knowledge.

Of note, L452R has been associated not only with resistance to some monoclonal antibodies (*1*) but also with T-cell immunity escape (N. Le Bert, unpub. data, https://doi.org/10.1101/2022.01.20.477163). The population of the northern Lombardy area has 80% coverage for 2-dose/single vaccine and 56% of residents have received an additional booster (*2*). Under such heavy selective pressure from vaccine-elicited immunity, it is not surprising that Omicron mutations leading to T-cell escape have a fitness advantage, and hence their prevalence should continue to increase.

D.F. wrote the first draft; A.G. performed sequencing; A.B. and F.N. provided data curation; F.M. conceived the study and revised the manuscript.

About the Author

Dr. Novazzi is a research scientist at University of Insubria, Varese, Italy. Her research interests include emerging viral infections.

References

1. Starr TN, Greaney AJ, Dingens AS, Bloom JD. Complete map of SARS-CoV-2 RBD mutations that escape the monoclonal antibody LY-CoV555 and its cocktail with LY-CoV016. Cell Rep Med. 2021;2:100255. https://doi.org/10.1016/j.xcrm.2021.100255
2. Regione Lombardia. Territorial vaccine coverage [in Italian] [cited on 2022 Jan 29] https://www.regione.lombardia.it/wps/portal/istituzionale/HP/vaccinazionicovid/dashboard-vaccini-territorio

Address for correspondence: Andreina Baj, University of Insubria, Via Dunant 5, Varese 21100, Italy; email: andreina.baj@uninsubria.it

Association of Healthcare and Aesthetic Procedures with Infections Caused by Nontuberculous Mycobacteria, France, 2012–2020

Kiara X. McNamara, Joseph F. Perz, Kiran M. Perkins

Author affiliation: Centers for Disease Control and Prevention, Atlanta, Georgia, USA

DOI: https://doi.org/10.3201/eid2806.220520

To the Editor: Daniau et al. (*1*) described extrapulmonary nontuberculous mycobacteria (NTM) infections associated with medical procedures in France, highlighting the need for timely case reporting and genomic analysis to identify outbreak causes and prevent infections. On the basis of our experience investigating NTM healthcare-associated infections (HAIs) and outbreaks, we believe that an enhanced approach toward NTM that recognizes early signals of potential outbreaks and promptly uses the skills and investigative expertise of public health professionals is integral to mitigating disease spread. NTM pose substantial costs and burdens for patients, contributing to more hospitalizations and deaths than other waterborne pathogens (*2*). Among Centers for Disease Control and Prevention consultations for waterborne HAI outbreaks, 30% were caused by NTM, accounting for 40% of cases and further substantiating need to prevent transmission in healthcare facilities (*3*). Extrapulmonary NTM infections can be challenging to detect because of their long incubation period and nonspecific signs and symptoms, which raises concern that many healthcare-associated cases are unidentified (*4*).

Clinical vigilance and systematic surveillance for extrapulmonary NTM HAIs are urgently needed to detect cases, assist public health investigations, and reduce patient illness and death (*4*). Surveillance signals should trigger robust investigations, inclusive of active case-finding efforts, such as notification of potentially exposed patients, which has previously led to discovery of multiple additional cases (*3*). Investigating NTM HAIs may point to upstream causes of infection in the healthcare delivery process, such as contaminated medical products or poor infection control practices, requiring elimination of sources and appropriate interventions (*4*). Recommendations from experts and scientific evidence suggest that even a single extrapulmonary NTM HAI should prompt additional investigation (*5*). NTM HAIs are an emerging threat to patients and carry serious consequences for patient safety. Comprehensive NTM case investigations with public health engagement are needed to inform best practices and minimize infection burdens for patients and healthcare facilities.

References

1. Daniau C, Lecorche E, Mougari F, Benmansour H, Bernet C, Blanchard H, et al. Association of healthcare and aesthetic procedures with infections caused by nontuberculous mycobacteria, France, 2012–2020. Emerg Infect Dis. 2022;28:518–26. https://doi.org/10.3201/eid2803.211791
2. Collier SA, Deng L, Adam EA, Benedict KM, Beshearse EM, Blackstock AJ, et al. Estimate of burden and direct healthcare cost of infectious waterborne disease in the United States. Emerg Infect Dis. 2021;27:140–9. https://doi.org/10.3201/eid2701.190676
3. Perkins KM, Reddy SC, Fagan R, Arduino MJ, Perz JF. Investigation of healthcare infection risks from water-related organisms: summary of CDC consultations, 2014-2017. Infect Control Hosp Epidemiol. 2019;40:621–6. https://doi.org/10.1017/ice.2019.60
4. Crist MB, Perz JF. Modern healthcare versus nontuberculous mycobacteria: who will have the upper hand? Clin Infect Dis. 2017;64:912–3.
5. The Council for Outbreak Response: Healthcare-Associated Infections (HAIs) and Antimicrobial-Resistant Pathogens. Proposed investigation/reporting thresholds and outbreak definition for extrapulmonary nontuberculous mycobacteria [cited 2022 Mar 22]. https://www.corha.org/wp-content/uploads/2019/09/CORHA-Proposed-NTM-Thresholds-and-Definition-08-19.pdf

Address for correspondence: Kiara X. McNamara, Centers for Disease Control and Prevention, 1600 Clifton Rd NE, Atlanta, GA 30329-4027, USA; email: rhv0@cdc.gov

In Response: We thank McNamara and colleagues for their commentary (*1*) on our article (*2*). We agree that early recognition of potential outbreaks of healthcare-acquired infections (HAIs) caused by nontuberculous mycobacteria (NTM) is crucial for controlling the spread of those diseases that pose human and financial burdens. Because NTM are not transmissible from human to human and are not on the list of highly pathogenic bacteria, reporting of NTM infections is not mandatory. Consequently, specific reporting methods are needed to organize this information. In France, we had the opportunity to combine the national early warning response system (EWRS) for HAIs diagnosed in healthcare facilities, computerized since 2011, and the networking of clinical microbiologists with the National Reference Centre for Mycobacteria and Resistance of Mycobacteria to Anti-Tuberculosis Agents (CNRMyRMA). In addition,

the French Public Health Agency, which receives data and coordinates the response in the EWRS, directly communicates with the CNRMyRMA, and they can make decisions in common with other professionals and health authorities involved. For each notified case of NTM HAI (from EWRS or from an isolate sent to CNRMyRMA), active research of other previous cases is recommended. However, it is often not easy, because of diagnosis and notification delays, to investigate associated practices and potential environmental sources. After 2 cases are reported in EWRS, investigations can be focused on common expositions or procedures, leading to targeted environmental specimens.

We believe that underestimations of the number of cases in France can be improved by increasing awareness of healthcare professionals through publications describing the risk factors associated with NTM HAI and by triggering clinical and microbiological vigilance through networks and registers. We hope that our article (*2*) together with this comment will help emphasize the value of the public health approach to NTM infections.

Côme Daniau, Anne Berger-Carbonne, Emmanuelle Cambau

Author affiliations: Santé Publique France, Saint-Maurice, France (C. Daniau, A. Berger-Carbonne); Assistance Publique Hôpitaux de Paris, Centre National de Référence des Mycobactéries et de la Résistance des Mycobactéries aux Antituberculeux, Paris, France (E. Cambau)DOI: https://doi.org/10.3201/eid2806.220686

References

1. McNamara KX, Perz JF, Perkins KM. Association of healthcare and aesthetic procedures with infections caused by nontuberculous mycobacteria, France, 2012–2020. Emerg Infect Dis. 2022 Jun [*date* cited]. https://doi.org/10.3201/eid2806.220520
2. Daniau C, Lecorche E, Mougari F, Benmansour H, Bernet C, Blanchard H, et al. Association of healthcare and aesthetic procedures with infections caused by nontuberculous mycobacteria, France, 2012–2020. Emerg Infect Dis. 2022;28:518–26. https://doi.org/10.3201/eid2803.211791

Address for correspondence: Côme Daniau, Unité Infections Associées aux Soins et Résistance aux Antibiotiques, Direction de Maladies Infectieuses, Santé Publique France, 12 Rue du Val d'Osne, 94410 Saint-Maurice, France; email: come.daniau@santepubliquefrance.fr

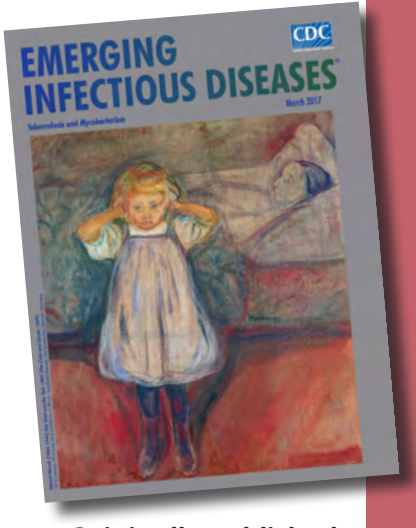

Originally published in March 2017

etymologia revisited

Mycobacterium chimaera

[mi'ko-bak-tēr'e-əm ki-mēr'ə]

Formerly an unnamed *Mycobacterium* sequevar within the *M. avium–M. intracellulare–M. scrofulaceum* group (MAIS), *M. chimaera* is an emerging opportunistic pathogen that can cause infections of heart valve prostheses, vascular grafts, and disseminated infections after open-heart surgery. Heater–cooler units used to regulate blood temperature during cardiopulmonary bypass have been implicated, although most isolates are respiratory. In 2004, Tortoli et al. proposed the name M. chimaera for strains that a reverse hybridization–based line probe assay suggested belonged to MAIS but were different from *M. avium, M. intracellulare*, or *M. scrofulaceum*. The new species name comes from the chimera, a mythological being made up of parts of 3 different animals.

Sources:

1. Schreiber PW, Kuster SP, Hasse B, Bayard C, Rüegg C, Kohler P, et al. Reemergence of *Mycobacterium chimaera* in heater–cooler units despite intensified cleaning and disinfection protocol. Emerg Infect Dis. 2016;22:1830–3.
2. Struelens MJ, Plachouras D. *Mycobacterium chimaer*a infections associated with heater-cooler units (HCU): closing another loophole in patient safety. Euro Surveill. 2016;21:1–3.
3. Tortoli E, Rindi L, Garcia MJ, Chiaradonna P, Dei R, Garzelli C, et al. Proposal to elevate the genetic variant MAC-A, included in the *Mycobacterium avium* complex, to species rank as *Mycobacterium chimaera* sp. nov. Int J Syst Evol Microbiol. 2004;54:1277–85.

https://wwwnc.cdc.gov/eid/article/23/3/et-2303_article

The New Microbiology: From Microbiomes to CRISPR

Pascale Cossart; ASM Press, Washington DC, USA, 2018; ISBN: 978-1-683-67010-0; Pages: 200; Price: US $30.00

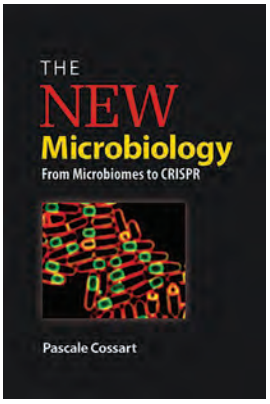

Infections, diseases, epidemics, and pandemics are some of the words that come to mind when one hears the word "microbes." Although microbes, including bacteria and viruses, are responsible for many infections, they are beneficial for maintaining good health and environmental stability. The quest to understand the interaction between microorganisms and the environment led microbiologists to major discoveries of the 20th century, including DNA, microbiomes, and clustered regularly interspaced short palindromic repeats (CRISPR).

The New Microbiology: From Microbiomes to CRISPR by Pascale Cossart, a microbiologist at the Institut Pasteur (Paris, France), presents an engaging background of revolutionary discoveries and advances in microbiology. The author uses her extensive knowledge of bacteriology to offer a succinct and compelling narrative on the evolution of microbiology over the centuries.

Each of the 4 parts of this book details certain advances in microbiology. In the first part (New Concepts in Microbiology), Cossart presents a broad and informative discussion that covers bacteria–host interaction, contributions to the ecosystem, and survival mechanisms in the environment. The CRISPR and CRISPR/Cas9 systems used for genome modification in prokaryotes and eukaryotes is a notable discovery detailed by the author. In the second section (Sociomicrobiology: the Social Lives of Bacteria), the author describes how bacteria can exist as either single species or multispecies in communities called biofilms that are formed through adherence to surfaces. Her discussion includes how these biofilms form, how bacteria can communicate through specific signals, and different methods by which some bacteria thrive. For example, she notes that "*Bdellovibrio* can invade other bacteria and multiply, causing the host bacteria to explode," but also points out that some other microbial communities in specific environments, known as microbiotas, "produce innumerable compounds that benefit its inhabitants."

Cossart explores the discovery and pathogenicity of different disease-causing bacteria in the book's third section (The Biology of Infections). She details historical plagues such as the bubonic plague, caused by *Yersinia pestis* bacteria, and other bacterial diseases, including pertussis and diphtheria. She describes the evolution of other bacteria that are either foodborne, sexually transmitted, or pathogenic to insects and plants. In the book's conclusion (Bacteria as Tools), she elucidates ways bacteria are being used as tools for research in different contexts. Cossart thoroughly highlights the most revolutionary discoveries in microbiology, including PCR technology that detects and amplifies DNA fragments from small sample and the CRISPR/Cas9 system, a genome modification and editing technology that "could generate bacteria capable of synthesizing medicines or their precursors on a massive scale."

This book provides a straightforward, in-depth assessment of microbiology concepts. Readers will be fascinated with the detailed description of microbial evolution and the connection between old and new concepts. Although considerable advances have occurred in microbiology, such as the use of novel molecular tools to clarify mechanisms underlying bacteria–host interaction, the author offers compelling arguments that show microbiology will continue to evolve and that new discoveries are on the horizon. Cossart provides convincing evidence that some of these discoveries will enable us to evaluate the role of different microbiotas in host defense, whereas other discoveries will uncover ways to protect the environment from imminent dangers, including those associated with climate change.

Tomi Obe, Nikki W. Shariat

Author affiliation: University of Georgia, Athens, Georgia, USA

DOI: http://doi.org/10.3201/eid2806.212085

Address for correspondence: Tomi Obe, University of Georgia, 953 College Station Rd, Athens GA 30602, USA; email: tomi.obe@uga.edu

William C. Campbell (1930–), *Tapeworm Enigma*, 2020 (detail). Acrylic with supplemental gel on canvas, 14 in x 18 in/35.6 cm x 45.7 cm. Personal Collection, Tom and Bev Kennedy, Waunakee, Wisconsin, USA. Digital image by Tim Fitch Photography.

Tapeworm Enigma

Byron Breedlove and Richard Bradbury

Among the parasitic organisms that can transmit infections to humans are about 300 species of helminths (parasitic worms). In his book *People, Parasites, and Plowshares,* Columbia University parasitologist Dickson Despommier notes, "These are the most underappreciated of our parasites that have for centuries kept a low profile, cruising just under the radar screen of the world's health agencies."

Helminths of three main groups—cestodes (tapeworms), trematodes (flatworms, or flukes), and roundworms (nematodes)—are human parasites responsible for an enormous burden of disease. A number of helminthic infections are designated as neglected tropical diseases. Among those diseases are lymphatic filariasis, caused by threadlike worms spread by mosquitoes; onchocerciasis or river blindness, caused by the parasitic worm *Onchocerca volvulus* and transmitted from

Author affiliations: Centers for Disease Control and Prevention, Atlanta, Georgia, USA (B. Breedlove); Federation University Australia, Berwick, Victoria, Australia (R. Bradbury)

DOI: https://doi.org/10.3201/eid2806.AC2806

bites by black flies; and dracunculiasis, commonly called Guinea worm disease, transmitted by ingestion of water fleas.

A trio of soil-transmitted helminths—intestinal roundworms (*Ascaris lumbricoides*), whipworms (*Trichuris trichiura*), and hookworms (*Necator americanus*, *Ancylostoma duodenale*, and *Ancylostoma ceylanicum*)—are dubbed the "unholy trinity." Those helminths infect humans via ingestion of food or water contaminated with soil containing their eggs or larvae or, in the case of hookworms, may infect by direct passage of their larvae through the skin. According to the Centers for Disease Control and Prevention, a large portion of the world's population is infected with one or more of those parasitic worms: 807–1,121 million people with roundworms, 604–795 million with whipworms, and 576–740 million with hookworms.

In his book, Despommier explains that tapeworms, among the most well-known parasitic helminths, "get their common name from their off-putting resemblance to a white cloth tape measure." He adds that "judging by the global distribution of tapeworm infections, and the number of different host species that harbor them, parasitologists now consider the cestodes to be among the most successful of the worm infections."

The most common way that humans acquire taeniasis—intestinal infection with tapeworms of the genus *Taenia* and caused by worms of three species, *Taenia solium* (pork tapeworm), *Taenia saginata* (beef tapeworm), and *Taenia asiatica* (Asian tapeworm)—is by eating raw or undercooked pork or beef containing tapeworm cysts. According to the World Health Organization, among those tapeworms, the most debilitating health problems are caused by *T. solium*.

This month's cover art, *Tapeworm Enigma*, is one of a number of paintings created by Irish-American biologist and parasitologist William C. Campbell. Campbell studied at Trinity College at the University of Dublin and the University of Wisconsin, Madison, Wisconsin, USA. After graduating, he joined the Merck Institute for Therapeutic Research in New Jersey, where he worked for the next 33 years, also holding adjunct professorships at the University of Pennsylvania, New York Medical College, and Drew University.

Campbell's research on ivermectin as an antihelmintic treatment for animals led to the discovery that this agent would also be effective in treating onchocerciasis. As a result, in 2015 half of the Nobel Prize in Physiology or Medicine was awarded jointly to Campbell and Satoshi Ōmura for their co-discovery of ivermectin, currently widely used against nematode parasites, including the etiologic agents of river blindness, elephantiasis, and strongyloidiasis. (Although other applications for ivermectin are being applied in many parts of the world, the focus of this essay is parasitic diseases and the use of ivermectin as an antihelmintic drug.)

Campbell is also a poet and a painter. His persistent curiosity and extensive knowledge about parasitic worms are apparent in his artistic endeavors. In a 2019 newspaper interview, Campbell explained, "Some people focus on one subject and then have a hobby to sort of escape from their main subject. I don't look at it that way at all. I'm not painting pictures to escape from the science that I do. I want to bring the science with me into the painting and bring the two together."

Tapeworm Enigma exemplifies his surrealistic approach to painting. A moment is needed for the viewer to realize that the segmented strands of green, blue, yellow, and orange that cover the vibrant red background indeed represent tapeworms. A purple rostellum, streaked with white and black, seems disturbingly agile, all too eye-catching. At the bottom left of the painting is the orange segmented body of a *Dibothriocephalus latus* worm tapering into the unsegmented neck and terminating in its distinctive scolex, with a slit-like groove for attachment to the intestine. The light blue profile of a human face juxtaposed with the dark blue scolex of a *T. saginata* tapeworm in the center of the painting invariably forces the viewer to pause and contemplate, possibly while also squirming a bit, the parasite–host relationship.

Campbell (pers. comm., email, 2022 April 7) explained that "The painting features the attachment-organ of the beef tapeworm of humans (dark blue and highly textured). Adjacent to it is a human profile that gives way to a tapeworm (light blue) that disintegrates, as tapeworms do, as it gets beyond maturity. In upper left is a stylized *'en face'* view of the pork tapeworm. Elsewhere are stretches of nondescript tapeworms. Less easily found is a larval stage (hexacanth embryo) of a tapeworm, as well as suggestions of the fish tapeworm of humans."

Exercising his prerogative as an artist, Campbell concludes, "The 'meaning' of the picture must remain cryptic!" Perhaps, though, he offered a clue in a 2017 interview in the *Irish America Magazine*: "I consider them [parasitic worms] beautiful," he said. "They are just doing their own thing and not meaning to be destructive. And I have said in some recent papers that the objective is not to get rid of parasitic worms, the objective is to get rid of parasitic diseases."

Bibliography

1. Campbell WC. William C. Campbell: biographical. [cited 2022 Apr 22]. https://www.nobelprize.org/prizes/medicine/2015/campbell/biographical
2. Centers for Disease Control and Prevention. About parasites [cited 2022 Apr 19]. https://www.cdc.gov/parasites/about.html
3. Centers for Disease Control and Prevention. Parasites-taeniasis [cited 2022 Apr 19]. https://www.cdc.gov/parasites/taeniasis/index.html
4. Cox FE. History of human parasitology. Clin Microbiol Rev. 2002;15:595–612. https://doi.org/10.1128/CMR.15.4.595-612.2002
5. Despommier DD. People, parasites, and plowshares: learning from our body's most terrifying invaders. New York: Columbia University Press; 2013. https://doi.org/10.7312/columbia/9780231161947.003.0006
6. Doyle J. Love of art and learning. Foster's Daily Democrat [cited 2022 Apr 8]. https://www.fosters.com/story/news/education/2019/02/19/nobel-prize-winner-shares-love-of-art-and-learning/5903432007
7. Haque R. Human intestinal parasites. J Health Popul Nutr. 2007;25:387–91.
8. Harty P. Hall of fame: Dr. William C. Campbell. Irish America Magazine. April/May 2017 [cited 2022 Apr]. https://www.irishamerica.com/2017/03/hall-of-fame-dr-william-c-campbell-2
9. Kuchta R, Radačovská A, Bazsalovicsová E, Viozzi G, Semenas L, Arbetman M, et al. Host switching of zoonotic broad fish tapeworm (*Dibothriocephalus latus*) to salmonids, Patagonia. Emerg Infect Dis. 2019;25:2156–8. https://doi.org/10.3201/eid2511.190792
10. Mathison BA, Sapp SG. An annotated checklist of the eukaryotic parasites of humans, exclusive of fungi and algae. ZooKeys. 2021;1069:1–313. https://doi.org/10.3897/zookeys.1069.67403
11. Van Voorhis WC, Hooft van Huijsduijnen R, Wells TN. Profile of William C. Campbell, Satoshi Ōmura, and Youyou Tu, 2015 Nobel laureates in physiology or medicine. Proc Natl Acad Sci U S A. 2015;112:15773–6. https://doi.org/10.1073/pnas.1520952112
12. World Health Organization. Taeniasis/cysticercosis: key facts [cited 2022 Apr 19]. https://www.who.int/news-room/fact-sheets/detail/taeniasis-cysticercosis

Address for correspondence: Byron Breedlove, EID Journal, Centers for Disease Control and Prevention, 1600 Clifton Rd NE, Mailstop H16-2, Atlanta, GA 30329-4027, USA; email: wbb1@cdc.gov

etymologia revisited

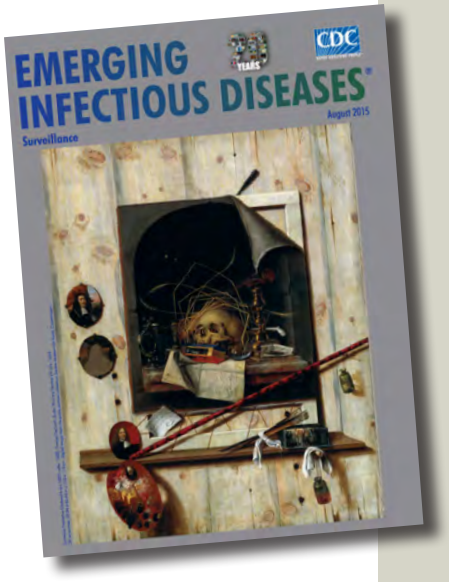

Originally published in August 2015

Escherichia coli

[esh"ə-rik'e-ə co'lī]

A gram-negative, facultatively anaerobic rod, *Escherichia coli* was named for Theodor Escherich, a German-Austrian pediatrician. Escherich isolated a variety of bacteria from infant fecal samples by using his own anaerobic culture methods and Hans Christian Gram's new staining technique. Escherich originally named the common colon bacillus *Bacterium coli commune*. Castellani and Chalmers proposed the name *E. coli* in 1919, but it was not officially recognized until 1958.

Sources:

1. Oberbauer BA. Theodor Escherich—Leben und Werk. Munich: Futuramed-Verlag; 1992.
2. Shulman ST, Friedmann HC, Sims RH. Theodor Escherich: the first pediatric infectious diseases physician? Clin Infect Dis. 2007;45:1025–9 .

https://wwwnc.cdc.gov/eid/article/21/8/et-2108_article

EMERGING INFECTIOUS DISEASES®

Upcoming Issue

- Self-Reported and Physiologic Reactions to Third BNT162b2 mRNA COVID-19 (Booster) Vaccine Dose
- Epidemiologic, Clinical, and Genetic Characteristics of Human Infections with Influenza A(H5N6) Viruses, China
- Nipah Virus Detection at Bat Roosts after Spillover Events, Bangladesh, 2012–2019
- Model of Basic Reproduction Number to Assess Effects of Nonpharmaceutical Interventions on Nosocomial SARS-CoV-2 Transmission
- Analyzing and Modeling the Spread of SARS-CoV-2 Omicron Lineages BA.1 and BA.2, France, September 2021–February 2022
- One Health Genomic Analysis of Extended-Spectrum β-Lactamase–Producing *Salmonella enterica*, Canada, 2012–2016
- Effect of Returning University Students on COVID–19 Infections in England, 2020
- Outbreak of IncX8 Plasmid–Mediated KPC-3–Producing *Enterobacterales*, China
- Targeted Screening for Chronic Q Fever, the Netherlands
- Novel *Mycobacterium tuberculosis* Complex Ecotype Related to *M. caprae*
- Potential Human Health Threats from Eurasian Avian-Like Swine Influenza A(H1N1) Virus and Its Reassortant Viruses
- Isolation and Characterisation of Novel Reassortant H10N7 Influenza A Virus in Harbor Seal in British Columbia, Canada
- Chronic Pulmonary Disease Caused by *Tsukamurella toyonakaense*
- Detection of Highly Pathogenic Avian Influenza A(H5N8) Clade 2.3.4.4b Virus in Dust Samples from Poultry Farms, France, 2021
- SARS-CoV-2 Delta–Omicron Recombinant Viruses, United States
- Multisystem Inflammatory Syndrome after Breakthrough SARS-CoV-2 Infection in 2 Immunized Adolescents
- Identifying Aortic Aneurysms Using Focused Detection of *Helicobacter cinaedi*
- Genetically Diverse Highly Pathogenic Avian Influenza A(H5N1/H5N8) Viruses among Wild Waterfowl and Domestic Poultry, Japan, 2021
- Suspected Cat-to-Human Transmission of SARS-CoV-2
- Type 1 Diabetes Mellitus Associated with Nivolumab after Second SARS-CoV-2 Vaccination, Japan

Complete list of articles in the July issue at https://wwwnc.cdc.gov/eid/#issue-290

Earning CME Credit

To obtain credit, you should first read the journal article. After reading the article, you should be able to answer the following, related, multiple-choice questions. To complete the questions (with a minimum 75% passing score) and earn continuing medical education (CME) credit, please go to http://www.medscape.org/journal/eid. Credit cannot be obtained for tests completed on paper, although you may use the worksheet below to keep a record of your answers.

You must be a registered user on http://www.medscape.org. If you are not registered on http://www.medscape.org, please click on the "Register" link on the right hand side of the website.

Only one answer is correct for each question. Once you successfully answer all post-test questions, you will be able to view and/or print your certificate. For questions regarding this activity, contact the accredited provider, CME@medscape.net. For technical assistance, contact CME@medscape.net. American Medical Association's Physician's Recognition Award (AMA PRA) credits are accepted in the US as evidence of participation in CME activities. For further information on this award, please go to https://www.ama-assn.org. The AMA has determined that physicians not licensed in the US who participate in this CME activity are eligible for AMA PRA Category 1 Credits™. Through agreements that the AMA has made with agencies in some countries, AMA PRA credit may be acceptable as evidence of participation in CME activities. If you are not licensed in the US, please complete the questions online, print the AMA PRA CME credit certificate, and present it to your national medical association for review.

Article Title

Cross-Sectional Study of Clinical Predictors of Coccidioidomycosis, Arizona, USA

CME Questions

1. Your patient is a 29-year-old man with suspected coccidioidomycosis (CM). According to the analysis by Ramadan and colleagues of ≈400 participants with suspected CM prospectively enrolled in 2019, which of the following statements about clinical predictors of CM in outpatient and inpatient settings is correct?

A. Compared with participants without CM, participants with CM were more likely to be older and White
B. Participants with vs without CM were more likely to have immunocompromised conditions
C. Participants with vs without CM were more likely to have fatigue and shortness of breath and less likely to have rash
D. Hemoglobin ($p = 0.008$), platelet count ($p = 0.01$), eosinophilic count ($p<0.001$), and total protein ($p = 0.04$) levels were higher in participants with vs without CM

2. According to the analysis of ≈400 participants with suspected CM prospectively enrolled in 2019 by Ramadan and colleagues, which of the following statements about prediction models for CM for outpatient and inpatient settings is correct?

A. Rash was a robust predictive marker of CM in outpatients and inpatients
B. Eosinophilic count was predictive only in outpatient settings.
C. The findings suggest preliminary support for the development of a CM prediction model for use in the clinical setting
D. Inpatient univariable models showed that muscle aches and immunocompromised status were positively associated with CM

3. According to analysis of ≈400 participants with suspected CM prospectively enrolled in 2019 by Ramadan and colleagues, which of the following statements about clinical and public health implications of clinical predictors of CM and prediction models for CM for outpatient and inpatient settings is correct?

A. Prediction models may guide clinical decision making to test for CM, expedite identification of more serious CM complications, and reduce unnecessary use of tests or antimicrobial agents
B. The models developed in this study have excellent accuracy
C. Patients with features negatively associated with CM (PCT, muscle aches, or shortness of breath) should not undergo CM testing
D. Current public health recommendations do not address testing for CM among patients presenting with pneumonia-like symptoms

Earning CME Credit

To obtain credit, you should first read the journal article. After reading the article, you should be able to answer the following, related, multiple-choice questions. To complete the questions (with a minimum 75% passing score) and earn continuing medical education (CME) credit, please go to http://www.medscape.org/journal/eid. Credit cannot be obtained for tests completed on paper, although you may use the worksheet below to keep a record of your answers.

You must be a registered user on http://www.medscape.org. If you are not registered on http://www.medscape.org, please click on the "Register" link on the right hand side of the website.

Only one answer is correct for each question. Once you successfully answer all post-test questions, you will be able to view and/or print your certificate. For questions regarding this activity, contact the accredited provider, CME@medscape.net. For technical assistance, contact CME@medscape.net. American Medical Association's Physician's Recognition Award (AMA PRA) credits are accepted in the US as evidence of participation in CME activities. For further information on this award, please go to https://www.ama-assn.org. The AMA has determined that physicians not licensed in the US who participate in this CME activity are eligible for AMA PRA Category 1 Credits™. Through agreements that the AMA has made with agencies in some countries, AMA PRA credit may be acceptable as evidence of participation in CME activities. If you are not licensed in the US, please complete the questions online, print the AMA PRA CME credit certificate, and present it to your national medical association for review.

Article Title

Antimicrobial-Resistant *Shigella* spp. in San Diego, California, USA, 2017–2020

CME Questions

1. Which of the following statements regarding *Shigella* spp. is most accurate?

A. They are anaerobic, gram-positive bacilli
B. ≥10,000 organisms are required to cause infection
C. They are transmitted via the fecal-oral route or in contaminated food and water
D. *S. flexneri* is more common than S. sonnei in the United States

2. Which of the following characteristics of patients with *Shigella* spp. infections was noted in the current study?

A. Cases were fairly equally divided between women and men
B. 23% of the cohort were unhoused
C. The rate of HIV infection was <10%
D. Sexual orientation was not a risk factor for infection

3. According to the current study, what was the rate of resistance to fluoroquinolones among *Shigella* spp.?

A. 7%
B. 23%
C. 59%
D. 81%

4. Which of the following variables in the current study was associated with a higher rate of resistance of *Shigella* spp. to at least 2 antibiotics?

A. HIV infection
B. Being unhoused
C. History of amphetamine use
D. Foreign travel

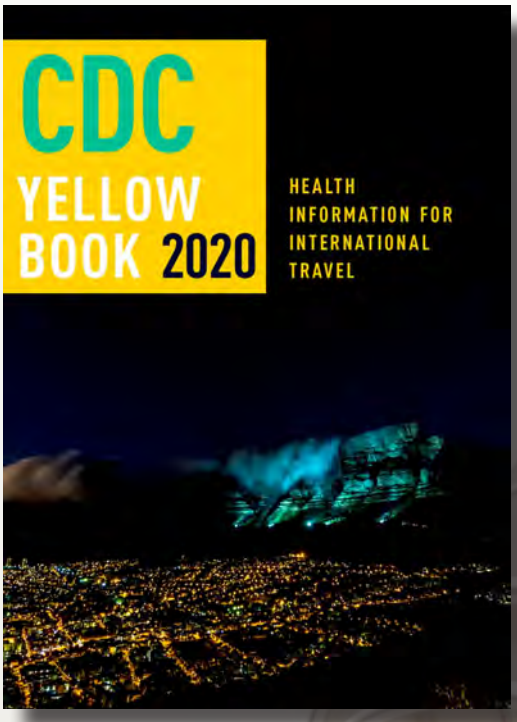

Available Now
Yellow Book 2020

The fully revised and updated CDC Yellow Book 2020: Health Information for International Travel codifies the US government's most current health guidelines and information for clinicians advising international travelers, including pretravel vaccine recommendations, destination-specific health advice, and easy-to-reference maps, tables, and charts.

ISBN: 978-0-19-006597-3 | $115.00 | May 2019 | Hardback | 720 pages

ISBN: 978-0-19-092893-3 | $55.00 | May 2019 | Paperback | 687 pages

Yellow Book 2020 includes important travel medicine updates

- **The latest information on emerging infectious disease threats, such as Zika, Ebola, and henipaviruses**
- **Considerations for treating infectious diseases in the face of increasing antimicrobial resistance**
- **Legal issues facing clinicians who provide travel health care**
- **Special considerations for unique types of travel, such as wilderness expeditions, work-related travel, and study abroad**

OXFORD
UNIVERSITY PRESS

Order your copy at:
www.oup.com/academic